

UNIVERSITY of CALIFORNIA

Santa Barbara

**Microbial Membrane Modification through Rational Design, Synthesis, and
Implementation of Conjugated Oligoelectrolytes**

A dissertation submitted in partial satisfaction of the requirements for the degree

Doctor of Philosophy in Chemistry

by

Alex Sajovic Moreland

Committee in charge:

Professor Guillermo C. Bazan, Chair

Professor Bradley F. Chmelka

Professor Kevin W. Plaxco

Professor Javier Read de Alaniz

March 2020

The dissertation of Alex Sajovic Moreland is approved.

Professor Bradley F. Chmelka

Professor Kevin W. Plaxco

Professor Javier Read de Alaniz

Professor Guillermo C. Bazan, Committee Chair

December 2019

**Microbial Membrane Modification through Rational Design, Synthesis, and
Implementation of Conjugated Oligoelectrolytes**

Copyright © 2020

by

Alex Sajovic Moreland

*dedicated to friends and family who have supported me,
colleagues who have guided and challenged me,
and all those who share a passion for science*

Acknowledgements

First and foremost, I would like to thank my family. For as long as I can remember, my parents have actively supported my academic endeavors and career aspirations. Their interest and excitement in whatever I happen to be working on at any given time has always inspired me to keep at it. It goes without saying that their guidance has shaped who I am today and has played a major part in each of my achievements. I would also like to acknowledge all the other members of my family, both close and distant, who have always expressed an interest in my work and applauded my efforts. Knowing how many people I have in my corner has always kept me motivated. Additionally, I would like to thank many of my longtime friends who constantly joke that I will be in school forever. The support and the japing have been equally motivational.

My first opportunity to work in a lab came in my first quarter as an undergraduate student. Dr. Bob Miller in Dr. Hunter Lenihan's lab hired me to work on a project assessing the impacts of metal nanoparticles on marine phytoplankton. After a few months working with Bob, I was given some freedom to think about my own research under his guidance. This exposure to the scientific process of identifying a problem and designing experiments to investigate it is what sparked my passion for working in the lab. Bob's three years of guidance put me on the path to become the lab rat that I am today.

While taking organic chemistry lab, my TA, Dr. Karl Voigtritter, recruited me to Professor Bruce Lipshutz's lab. In addition to starting my work as a synthetic chemist, this opportunity was also what prompted me to add chemistry as a second

major. Bruce, who in one of our first meetings told me that organic chemistry was only for those who are willing to get up after being continually knocked down by their work, deserves many thanks for converting me into an organic chemist. My first graduate student mentor, Dr. Alex Abela, taught me the (dark) artistic side of organic chemistry, such as how to recrystallize products and properly run a flash column. After Alex completed his degree, Karl took over as my mentor. Over the next year, I learned from Karl how to really think about synthesis instead of simply following a prep. In addition to being an excellent mentor, Karl became a great friend and we continued to talk about science and life long after I completed my undergraduate studies.

While working in the Lipshutz Lab, I had the great fortune of sharing an office (and a hood for a few months) with one of the most creative and “cowboy” organic chemists I have met, Dr. Roscoe Linstadt. We both started in the group as undergraduates and luckily for us all, Roscoe stayed in the group to continue his work as a grad student. Roscoe had as much influence on my style as an organic chemist as anyone else and he was always the first person I turned to for advice when I returned to UCSB. His partner in crime, Dr. Dan Lippincott, who took over my vacated hood next to Roscoe’s, was equally as important in my continued development as an organic chemist. Both Dan and Roscoe provided countless pieces of invaluable knowledge to get me over a number of synthetic hurdles. Dan and Roscoe also became great friends – I still miss spending my breaks in their lab while working late into the night.

Although unrelated to the work in this dissertation, my time at Raytheon Vision Systems was immensely important in my development as a scientist and engineer. I first need to thank Brad Eachus, who was also a longtime roommate of mine and all-around great guy, for referring me when RVS was looking for a chemist. I learned from a fantastic group of people including Paul Goetz, Sean Harris, Borys Kolasa, Tami Knudson, Dr. Bengi Hanyaloglu, Jim Bangs, and Dr. Andreas Hampp. In particular, I need to thank Andreas for using me as a Swiss Army knife working in various labs on a number of projects. I found that being exposed to so many different tasks made learning each new skill progressively easier. This ability to pick up new things will undoubtedly be a vital skill for the rest of my career. In addition, I need to thank my RVS family for the number of friendships I gained and for their support of my decision to return to school. In fact, it was a collaboration with Dr. Dan Morse in the ICB that eventually led me to Dr. Gui Bazan's Lab.

When I joined Gui's group, my plan was to combine my backgrounds in chemistry and engineering to work on organic electronics. Among the many things I need to thank Gui for, the first is for pushing me back into synthesis. I had nearly forgotten how much I enjoy the creative aspect of designing a pathway, the day-to-day labwork, and even the frustrating difficulties associated with making and breaking bonds. I also need to thank Gui for all the opportunities he provided to me as a grad student – perusing new ideas, acting as a mentor to undergraduate students, working with and visiting our collaborators at the Army Research Labs, and taking on various responsibilities within the group.

There are many current and former members of our group, as well as CPOS as a whole, who deserve thanks. In particular, Dr. Zach Rengert, my first labmate in Gui's group, helped me through the first couple years of my graduate studies. He taught me a lot about chemistry as well as the research and workings of the group. We had numerous discussions about our sometimes-similar and sometimes-opposing views on chemistry and life. Many of my most-memorable experiences at my hood, both good and bad, involve working alongside Zach. I would also like to thank two other former chemists in our group, Dr. Cheng-Kang Mai and Dr. Ming Wang, for all of the time they spent answering my synthesis questions. Additionally, I would like to thank Dr. Bing Wang for countless insightful conversation on biology and chemistry, Dr. Chenyao Nie for her amazing contributions to our antibiotics program, Zichao Zhang for her breakthroughs that led to that program, and all three for the ongoing friendships that we have.

Of the people who I have worked directly with, Sam Holton is particularly deserving of recognition. Sam worked with me during his last two years as an undergrad student and for another year as a tech. He was a part of nearly everything I worked on during that time and was a major component of our lab. Even before starting his own graduate studies at UC Davis, he was helping to train our new grad students on various techniques. His interest in all fields of science and his never-ending enthusiasm led to numerous discussions on everything from reaction mechanisms to Klein bottles. I hope Sam got as much from working in our lab as our lab got from having him. I was lucky enough to have a second outstanding undergraduate, Amoge Ezike, for a few months through the ICB SABRE program.

Amoge's ability to think critically and her attention to detail made her immediately valuable to our group. In only a couple weeks, she was able to organize and conduct her own experiments, the data from which are included as part of Chapter 2 of this dissertation. In addition to her skill in the lab, Amoge's positive and warm demeanor was uplifting to everyone in the group.

Within my cohort, there are three fellow students that I want to thank – Dr. Martin Seifrid, Dr. Brett Yurash, and (soon to be Dr.) Evan Landstrom. In addition to the various useful technical discussions, Martin, Brett, and Evan helped me navigate the graduate program. All three are excellent scientists and have been great friends through this often-painful process.

I want to thank the ICB for supporting my graduate studies and in particular for the opportunity to work with the Army Research Labs. During two visits to Dr. Jim Sumner's lab at the ARL, I had a great experience working with Dr. Justin Jahnke, Dr. Deborah Sarkes, and a number of other excellent engineers and scientists. Jim and his group were very welcoming and incredibly helpful in my research. Working in an unfamiliar lab can be daunting and frustrating but they made it enjoyable and fruitful.

The amazing shared facilities at UCSB deserve credit for much of the successful research conducted on campus. Since arriving at UCSB in 2008 as an undergraduate student, I have been fortunate enough to learn from the numerous experts that run these labs. As such, there is a long list of people who deserve to be acknowledged for their contributions to the work in this dissertation as well as their impacts on me as a scientist in general: Dr. Hongjun Zhou, Dr. James Pavlovich, Dr.

Dmitriy Uchenik, and Dr. Alexander Mikhailovsky (DCB); Dr. Rachel Behrens and Dr. Amanda Strom (MRL); Dr. Mary Raven and Dr. Ben Lopez (NRI); Dr. Mark Cornish, Dr. Stephan Kraemer, Dr. Tom Mates, Dr. Jerry Hu, and Shamon Walker (CNSI); and Dr. Jen Smith (BNL).

Chemists have a strong, almost fanatical connection to their glassware. At UCSB we are fortunate to have our own master glassblower, Richard Bock, to make any piece of glassware we can image. Additionally, his necromancy-like ability to bring back to life our most-beloved pieces of glassware when they meet untimely ends has saved all of us at one point or another. Nearly every reaction that will be detailed in this dissertation involved at least one piece of glassware made by Richard.

The DCB Machine Shop, run by Bruce Dunson and more recently by Roger Green, is another vital resource. Whether it's lending tools, repairing or modifying equipment, or building something from scratch, the machine shop is always there to keep our research moving smoothly.

The list of critical DCB staff who support our research would not be complete without Cabe Fletcher, Adrian Shelor, and Trevor Bellefeuille. Maintaining PPE, shipping/receiving, stocking up on supplies, moving and servicing equipment, and everything else related to lab management runs through these guys. When everything is running as it should and their services are not immediately needed, they are always available for light-hearted conversations about fishing in Mammoth or how Apeel is taking over Santa Barbara.

Thank you to everyone who has directly or indirectly contributed to this dissertation.

Curriculum Vitae

EDUCATION

Bachelor of Science in Chemistry and **Bachelor of Science in Biological Science**,
University of California, Santa Barbara, June 2012

Doctor of Philosophy in Chemistry, University of California, Santa Barbara, December
2019 (expected)

RESEARCH and INDUSTRY EXPERIENCE

Graduate Student Researcher – Department of Chemistry and Biochemistry, University of
California, Santa Barbara (Bazan Lab, Fall 2014 – present).

Graduate Student Mentor – UCSB Materials Department RISE Program (mentee: Samuel
Holton, 2015-2017).

Graduate Student Mentor – UCSB Institute for Collaborative Biotechnologies SABRE
Program (mentee: Amoge Ezike, Summer 2017).

Multidiscipline Engineer – Raytheon Vision Systems, Goleta, California (2012-2014).

Undergraduate Student Researcher – Department of Chemistry and Biochemistry,
University of California, Santa Barbara (Lipshutz Lab, 2010-2012).

Undergraduate Student Researcher – Bren School of Environmental Science &
Management, University of California, Santa Barbara (Lenihan Lab, advised by Dr. Robert
Miller, 2008-2011).

PUBLICATIONS

1. *Structural Optimization of Conjugated Oligoelectrolytes for use as Membrane Permeabilizing Agents* **A. S. Moreland**, S. J. Holton, A. Ezike, G. C. Bazan, submitted to *Angew. Chem.*
2. *Self-Assembled Monolayers of Conjugated Oligoelectrolytes as Interlayers for Enhanced Biotic-Abiotic Interfaces* **A. S. Moreland**, J. P. Jahnke, S. J. Holton, J. J. Sumner, G. C. Bazan, submitted to *ACS Appl. Mater. Inter.*
3. *Optimization of Conjugated Oligoelectrolytes to Enhance Selectivity toward Bacterial Cells* J. Limwongyut, C. Nie, **A. S. Moreland**, G. C. Bazan, submitted to *Angew. Chem.*
4. *Photoswitchable Conjugated Oligoelectrolytes for Light-Induced Change of Membrane Morphology* D. Leifert, **A. S. Moreland**, J. Limwongyut, A. A. Mikhailovsky, G. C. Bazan, submitted to *Angew. Chem.*

5. Bioelectronic Composites Using Conjugated Polyelectrolytes: New Living Materials for Harnessing Bioelectrochemical *Pathways* S. R. McCuskey, Y. Su, D. Leifert, **A.S. Moreland**, G. C. Bazan, submitted to *Adv. Mater.*
6. *Tuning Geobacter sulfurreducens biofilm with conjugated polyelectrolyte for increased performance in bioelectrochemical system* L. Ren, S. R. McCuskey, **A. S. Moreland**, G. C. Bazan, T.-Q. Nguyen, *Biosens. Bioelectron.* 2019, 114, 111630.
7. *A Chain-Elongated Oligophenylenevinylene Electrolyte Increases Microbial Membrane Stability* C. Zhou, G. W. N. Chia, J. C. S. Ho, **A. S. Moreland**, T. Seviour, B. Liedberb, A. N. Parikh, S. Kjelleberg, J. Hinks, G. C. Bazan *Adv Mater*, 2019, 31 (18), e1808021

PATENTS

1. "Short Conjugated Oligoelectrolytes and Uses Thereof," Application: PCT/US19/23411, Filing: March 21, 2019.

Abstract

Demarcating the boundary between bacterial cells and the external environment, the membrane provides a selective barrier for the flux of chemical entities into- and out of- the cells. As such, membrane properties have significant implications in a number of technologies. In whole-cell biocatalysis and bioenergy production, for example, the barrier imposed by the membrane limits efficient flow of substrates, products, and electrical current. This barrier is also partly responsible for the difficulties in treating certain infections by preventing antibiotics from reaching their targets within cells. Additionally, the membrane functions to guide the physical interactions of cells with other biotic and abiotic components of their environment. Thus, the selective modulation of membrane properties represents a powerful tool that can benefit numerous microbe-based technologies.

Conjugated oligoelectrolytes (COEs) are a class of compounds defined by a π -delocalized backbone consisting of a discrete number of repeat units and pendant ionic functionalities. Specific subsets of COEs possess the proper distribution of charge and hydrophobic/hydrophilic balance to permit spontaneous intercalation into model- and natural- membranes. The consequences of COE intercalation into membranes are variable and highly dependent on molecular structure. In this work, we will probe the structure-activity relationships that govern COE effects on membranes. Additionally, the strategic design and synthesis of COEs to achieve specific effects on membranes will be described.

In one study, a homologous series of COEs will be employed to elucidate how structural elements direct antimicrobial and membrane-permeabilizing properties.

Through careful examination of independent structural components, an improved understanding of COE structure-property relationships will be developed and applied in subsequent studies. In a separate effort, the design of a COE photo-actuator for on-demand membrane permeabilization will be described and its activity will be demonstrated in model-membrane vesicles as well as living cells. A novel class of asymmetric COEs bearing functional handles will be discussed with an emphasis on design and synthesis. The use of one such compound as an interlayer for improved biotic-abiotic interfaces in bioelectronic applications will be described in detail. Additional representative compounds of this class will be investigated as “membrane-anchors” for the localization of small molecules and proteins to the surface of cells as well as a means to direct cell-surface and cell-cell interactions. Finally, preliminary studies into the potential for COEs to represent a new class of antibiotics will be presented with a focus on structural optimization for improved selectivity toward bacterial cells.

Contents

I. Introduction	xxii
I.1. Lipid membranes, their function in cells, and the challenges and opportunities they present.....	xxii
I.2. Conjugated Oligoelectrolytes as modulators of membrane properties	xxiv
I.3. Overview and Objectives	xxvii
Chapter 1: Self-Assembled Monolayers of COEs for Improved Biotic-Abiotic Interfaces	1
1.1 Introduction.....	1
1.2 Design and synthesis of a gold-binding COE	3
1.3 Intercalation of COE-SH into Microbial Membranes and the effect on Bacterial Growth.....	6
1.4 Formation and characterization of COE-SH Monolayers.....	7
1.5 Application of COE-SH Functionalized Anodes in Microbial Fuel Cells.....	9
1.6 Additional Experiments and Calculations	10
1.6.1 Surface coverage calculated from XPS spectrum	10
1.6.2 Calculation of first-atomic-layer contribution to Au 4f XPS signal.....	11
1.6.3 Surface coverage calculated by reductive desorption	13
1.6.4 Cell density on electrodes assessed by SEM.....	14
1.6.5 Control MFCs with thermally-deactivated cells.....	14
1.6.6 2-step SAM formation via click chemistry	15
1.7 Conclusions	19
1.8 Experimental methods	20
1.9 Synthetic methods for the preparation of COE-SH.....	24
Chapter 2: Structure-Property Relationships Pertaining to COE Antimicrobial and Membrane-Permeabilizing Effects	40
2.1 Introduction.....	40
2.2 Design and Synthesis of a Series of COEs for Probing Structure-Property Relationships.....	43
2.3 Effect of COE Structure on the Ability to Associate with <i>E. coli</i> cells.....	46
2.4 Quantification of COE Effects on Lipid Ordering by Electron Paramagnetic Resonance Spectroscopy.....	47
2.5 Effect of COE Structure on Antimicrobial Properties	50
2.6 Effect of COE Structure on Microbial Membrane Permeability	52

2.6.1	ONPG Assay as a Measure of COE-mediated OM Permeability	52
2.6.2	Nile Red as a Probe for COE-Mediated Membrane Permeability of Hydrophobic Compounds	55
2.7	Conclusions	57
2.8	Experimental Methods	60
2.9	Synthetic Methods	65
Chapter 3: Light-Actuated Membrane Permeabilization by a COE Photoswitch		91
3.1	Introduction	91
3.2	Design and synthesis of a photo-isomerizable COE	92
3.3	Photophysical Properties of DSAzB	94
3.4	DSAzB-Mediated Photo-Triggered Calcein Release from Liposomes	97
3.5	Effect of DSAzB Isomerization on Lipid Ordering	103
3.6	Photo-triggered Permeabilization of Live Bacterial Cells by DSAzB	104
3.6.1	Propidium iodide influx a metric for DSAzB-induced permeability.....	104
3.6.2	Bacterial growth inhibition and bactericidal activity of DSAzB.....	106
3.7	Conclusions	108
3.8	Experimental methods	110
Chapter 4: COEs as membrane anchors for bioconjugation		116
4.1	Introduction	116
4.2	Copper-Catalyzed Azide-Alkyne Cycloaddition in Membrane Engineering	117
4.2.1	Design and Synthesis of Alkyne- and Azide-bearing COEs for CuAAC-based Membrane Engineering.....	119
4.2.2	COE-Alkyne as a Membrane Anchor for the CuAAC-Promoted Attachment of Azide-Containing Molecules	122
4.2.3	COE-Alkyne as a Membrane Anchor for Attaching Cells to Azide- Functionalized Surfaces.....	127
4.2.4	COE-mediated cell-cell interactions	130
4.3	Introduction to the NiNTA/His-tag System	131
4.3.1	Design and Synthesis of a NiNTA-Bearing COE for the Localization of His- Tagged Peptides or Proteins to Membrane Surfaces	132
4.3.2	Analysis of COE-NTA mediated YPet binding by flow cytometry	134
4.3.3	COE-NTA mediated membrane localization of a peptide bearing a His-Tag and a fluorescent probe	137
4.4	Conclusions	139

4.5	Experimental Methods	140
4.6	Synthetic Methods	144
4.6.1	COE-azide and COE-alkyne.....	144
4.6.2	COE-NTA	155
Chapter 5:	Antibiotics	165
5.1	Introduction.....	165
5.1.1	Antimicrobial Resistance and the Threat it poses to Humanity	165
5.1.2	The Membrane as a Target for Antibiotics	166
5.2	Design of a COE antibiotic – our initial “hit” compound	167
5.3	The effect of pendant and terminal alkyl chain lengths on antimicrobial and cytotoxic properties.....	171
5.4	Multi-functional end groups and their effect on COE antimicrobial activity.....	179
5.5	Conclusions	183
5.6	Synthetic Methods	186
Chapter 6:	Additional Experiments and Supporting Information	204
6.1	Interactions of COEs with Lipopolysaccharide	204
6.2	Effect of COEs on lipid phase transitions and lipid segregation as measured by differential scanning calorimetry	210
6.3	EPR order parameter and correlation time calculations	214
	Summary and outlook	219
	Bibliography	221
	NMR Spectra	244
	Chapter 1	244
	Chapter 2.....	254
	Chapter 4.....	282
	Chapter 5.....	298

List of Figures

Figure 1-1 Depiction of a surface-binding COE	2
Figure 1-2 Derivatization of COE2-4C to design a gold-binding analogue, COE-SH	3
Figure 1-3 Synthetic preparation of COE-SH.....	4
Figure 1-4 Confocal fluorescence micrographs of <i>E. coli</i> stained with COE-SH.....	6
Figure 1-5 XPS spectra confirming the formation of COE-SH SAMs.....	8
Figure 1-6 COE-SH anode functionalization impacts on voltage, power density, and time to reach peak power in U-tube MFCs.	10
Figure 1-7 Probability of photoelectron escape from bulk gold based on depth below the surface	12
Figure 1-8 Reductive desorption cyclic voltammogram and quantification of COE-SH SAM surface coverage.....	13
Figure 1-9 SEM micrographs of COE-SH treated and control gold anodes from MFCs.....	14
Figure 1-10 MFC performance using COE-SH functionalized anodes with live or thermally-deactivated <i>E. coli</i>	15
Figure 1-11 Synthesis of alkyne-containing COE-CH for use in copper-catalyzed azide-alkyne cycloaddition	16
Figure 1-12 2-step formation of COE SAMs on gold via copper-catalyzed azide-alkyne cycloaddition “click” reaction.	17
Figure 1-13 Method to functionalize silica particles with COE-CH via copper-catalyzed azide-alkyne cycloaddition “click” reaction.....	18
Figure 2-1 The influence of COE molecular structure on inactivation or substrate-dependent permeabilization of bacteria.	41
Figure 2-2 Homologous series of COEs designed and synthesized for the purpose of elucidating structure-property relationships related to permeability and antimicrobial activity	43
Figure 2-3 Synthetic route used to access COEs with variable core and alkyl chain lengths	45
Figure 2-4 Impact of COE structure on membrane affinity.....	46
Figure 2-5 Changes in lipid order parameter as a function of COE structure	49
Figure 2-6 Minimum inhibitory concentration of a series of COEs against <i>E. coli</i> as a function of total length.....	50
Figure 2-7 Graphical depiction of the ONPG assay used to assess COE permeabilization of the OM.	52
Figure 2-8 Relative ONPG turnover after treatment with various COEs	53

Figure 2-9 Comparison of permeabilizing abilities of COE2-2C-C10 and Triton X-100	55
Figure 2-10 Graphical depiction of the Nile Red uptake assay used to assess COE permeabilization of the OM	56
Figure 2-11 Nile Red emission from <i>E. coli</i> membranes as a function of COE structure.....	57
Figure 3-1 Depiction of light-activated membrane permeabilization mediated by the photoisomerization of the novel conjugated oligoelectrolyte, DSAzB.	92
Figure 3-2 Rational design of a COE photoswitch based on our well-studied COE2-4C framework.	93
Figure 3-3 Synthetic preparation of the photoisomerizable COE, “DSAzB.”	94
Figure 3-4 Kinetic absorption spectra of DSAzB and its neutral analogue during <i>E</i> -to- <i>Z</i> photoisomerization in various solvents.	95
Figure 3-5 Kinetic absorption measurements of DSAzB during <i>E</i> -to- <i>Z</i> photoisomerization, <i>Z</i> -to- <i>E</i> thermal isomerization, <i>Z</i> -to- <i>E</i> photoisomerization, and thermodynamic equilibrium.	96
Figure 3-6 Comparison of DSAzB and COE2-4C response to irradiation at 405 nm.....	97
Figure 3-7 Temperature-dependence of DSAzB photo-actuation of liposome permeabilization as measured by calcein release.	98
Figure 3-8 Effect of light dose on DSAzB photo-actuated liposome permeabilization	100
Figure 3-9 DSAzB photo-actuated liposome permeabilization – effect of DSAzB concentration and comparison to the non-isomerizing analogue, COE2-4C.	101
Figure 3-10 Effect of DSAzB isomerization on correlation time T_{2B} for 16-SASL in 20:80 DMPG:DMPC liposomes.....	103
Figure 3-11 DSAzB photo-actuation of <i>S. epidermidis</i> membrane permeability as measured by PI influx.....	106
Figure 3-12 Bactericidal activity of 405 nm irradiation, DSAzB, and a combination of both against <i>S. epidermidis</i>	107
Figure 3-13 A potential mechanism for DSAzB-mediated photo-actuation of membrane permeability.....	110
Figure 4-1 COE-mediated membrane engineering via CuAAC reactions.....	118
Figure 4-2 Synthetic route used to access COE-azide and COE-alkyne.....	120
Figure 4-3 Synthetic route used to access the CuAAC ligand BTTPS.....	121
Figure 4-4 Experimental procedure used to investigate the ability of COE-alkyne to act as membrane-anchor for subsequent CuAAC-mediated functionalization.	123
Figure 4-5 Absorption spectra of supernatants demonstrating the removal of FITC-azide from solution through CuAAC with membrane-intercalated COE-alkyne.....	124

Figure 4-6 Calculated and measured amounts of FITC-azide that were attached to <i>E. coli</i> cells via CuAAC with membrane intercalated COE-alkyne.....	125
Figure 4-7 Absorption and fluorescence spectra of COE-alkyne and FITC-azide with or without copper demonstrating an undesirable interaction between the two compounds that results in suppression of fluorescence.....	126
Figure 4-8 Fluorescence confocal micrographs demonstrating the ability of COE-alkyne to “click” <i>E. coli</i> cells to an azide-functionalized surface	128
Figure 4-9 Fluorescence micrograph of optimized conditions for COE-alkyne-mediated bacteria-surface conjugation via CuAAC	129
Figure 4-10 Fluorescence micrographs of cell-cell interactions mediated by COE-alkyne and COE-azide.....	130
Figure 4-11 Synthetic pathway used to access COE-NTA	133
Figure 4-12 Labelling bacterial membranes with YPet by surface display through peptide-protein interactions and with the novel COE-NTA system through Ni-NTA/His-tag interactions.....	135
Figure 4-13 Flow cytometry measurements of Ypet-labelled cells through induction of the eCPX scaffold or introduction of Ni-NTA moieties by staining with COE-NTA.....	136
Figure 4-14 Fluorescence confocal micrographs demonstrating COE-NTA-mediated surface decoration of <i>E. coli</i> cells with a dye-labelled, His-tagged peptide	138
Figure 5-1 Derivatization of COE2-2C to produce a COE with improve antimicrobial activity through increased affinity for bacteria – COE2-2hexyl.....	168
Figure 5-2 Generic structure of COEs used for preliminary antimicrobial/cytotoxicity SAR studies.....	172
Figure 5-3 Four COEs designed to test the effects of multiple short terminal chains relative to a single long terminal chain.....	175
Figure 5-4 Correlation of MIC values for COEs against various gram-negative strains.....	178
Figure 5-5 Comparison of MIC values against <i>A. baumannii</i> vs. <i>E. cloacae</i> , <i>P. aeruginosa</i> , and <i>E. coli</i> K12	179
Figure 5-6 Synthetic routes used to access COEs with complex end groups.....	180
Figure 5-7 Association of “COE2-3C-C3propy-“ family of COEs with <i>E. coli</i> K12.....	182
Figure 6-1 Structures of three COEs used to investigate the effects of COE-intercalation on the release of LPS from <i>E. coli</i> cells	205
Figure 6-2 SDS-PAGE gels for quantification of LPS in <i>E. coli</i> K12 supernatants following treatment with COEs or EDTA	206
Figure 6-3 Absorbance and emission spectra of DSSN as a function of LPS concentration	210

Figure 6-4 DSC traces of the gel-to-liquid transition in DMPC liposomes stained with different concentrations of DSBN and DSSN.....	212
Figure 6-5 Values extracted from EPR spectra to calculate order parameter and effective correlation times.....	218
Figure 6-6 Example spectra from time-course EPR measurements with correctly identified maxima and minima.....	218
Figure 6-7 Example output of order parameter and correlation time from a time-course EPR experiment.	218

List of Tables

Table 1-1 Calculation of COE-SH surface coverage by XPS.....	11
Table 2-1 Correlation (R) and significance (p) values between COE structural parameters and observed effects on microbes or model membranes	58
Table 5-1 Comparison of antimicrobial activity of COE2-2hexyl and azithromycin.....	169
Table 5-2 IC ₅₀ values for COE2-2hexyl against various cell lines.....	170
Table 5-3 Antimicrobial activity, cytotoxicity, and selectivity of thirteen COEs containing variable structural parameters.....	172
Table 5-4 MIC values for ten COEs against ESKAPE pathogens tested at Emery Pharma as well as two <i>E. coli</i> strains.	174
Table 5-5 Antimicrobial activity and cytotoxicity of COEs as a function of pendant chain structure.	176
Table 5-6 Antimicrobial susceptibility tests of COEs containing complex terminal chains..	181
Table 5-7 Comparison of antimicrobial activity and cytotoxicity/hemolysis of COE2-3C-C3butyl and COE2-3C-C3propyl-NH ₂	183
Table 6-1 Quantitative comparison of the effects of three COEs and EDTA on the release of LPS from <i>E. coli</i> cells. Relative optical density of LPS bands in SDS-PAGE gels.....	207

I. Introduction

I.1. Lipid membranes, their function in cells, and the challenges and opportunities they present

Lipid membranes demarcate the interface between living cells and their immediate external environment. Although their presence was first hypothesized in the 17th century,¹ it was not until 1972 that the modern fluid mosaic model of their structure was proposed by Singer and Nicolson.² Our understanding of biological membranes and the myriad of functions they serve continues to expand. Beyond providing a selective permeability barrier, the lipids, proteins, and other components of the membrane have roles in signaling, adhesion,³ responding to- and evading environmental stresses, energy generation in the form of ATP synthesis,⁴ and potentially even the origins of Life itself.⁵ Modulation of membrane properties thus provides a powerful tool for investigating and harnessing numerous cellular processes.

Contained within membranes of unicellular organisms is all the biological machinery necessary to sustain life, with each cell functioning as an independent, microscopic “factory”. Microbes, particularly fungi, have been used by humans for thousands of years to preserve food through fermentation.^{6, 7} While fermentation typically relies on the innate abilities of microbes, “engineered” cells are used today to perform a variety of functions from pharmaceutical manufacturing⁸ to environmental remediation.^{9, 10} In addition to now-routine genetic engineering

techniques, materials approaches can be used to enhance desirable functions of microbes or impart additional functions *de novo*. Such chemical modifications of microbes often rely on modulation of membrane properties or the introduction of specific functionalities to the membrane surface. In many applications, such as whole-cell biocatalysis,^{11, 12} the membrane actually presents a barrier that must be overcome in order for the technology to be successful.

Bioelectronics, broadly defined as the interconversion of electrical and biochemical signals,¹³ is one such field where the inherent properties of the natural microbial membrane limit practical utility.^{14, 15} In certain bacteria, evolution has provided the means to transport electrons through the membrane, either via a direct route utilizing proteins or appendages that act as electrical conduits^{16, 17} or by the release of soluble redox-active molecules that can function as electron shuttles.^{18, 19} Harnessing this ability with systems such as seafloor microbial fuel cells (MFCs)^{20, 21} has been investigated as a possible energy source for low power devices like remote sensors.^{22, 23} However, the electrical and ionic conduction barrier imposed by the membrane presents a major obstacle for the broader realization of microbe-powered devices.

Bacterial membranes, although a barrier to traditional antibiotics,^{24, 25} are themselves a proven target for antimicrobial agents.^{26, 27} Antimicrobial peptides (AMPs), which act through membrane interactions, are present in all living organism and have likely been part of the innate immune response since the first cellular forms of life.^{28, 29} AMP activity is selective for bacteria,³⁰ or even particular species of bacteria,^{31, 32} over mammalian cells based on differences in membrane composition.

Significant efforts to use AMPs, both natural and synthetic, as therapeutic agents have yielded mixed results.³³⁻³⁵ Lessons learned from these successes and failures have been applied to membrane-active small molecule antibiotics.³⁶ With the impending antimicrobial-resistance (AMR) crisis,³⁷ antibiotics which act through interactions with microbial membranes are likely to represent a key component of our therapeutic arsenal.

I.2. Conjugated Oligoelectrolytes as modulators of membrane properties

Conjugated oligoelectrolytes (COEs) are a class of compounds defined by a π -delocalized backbone adorned with ionic pendant functionalities. In contrast to conjugated polyelectrolytes (CPEs), COEs have monodisperse molecular weight and generally contain only a limited number of repeat units (~ 5 at most). A subset of these compounds, sometimes referred to as membrane-intercalating COEs (“MICOEs”), possess the appropriate distribution of hydrophobic and hydrophilic domains to permit the association within lipid bilayers. For the remainder of this dissertation, the term “COE” will be used to mean those structures which possess this membrane-intercalating ability. An idealized representation of such a structure embedded within a membrane is depicted in Figure I-1.

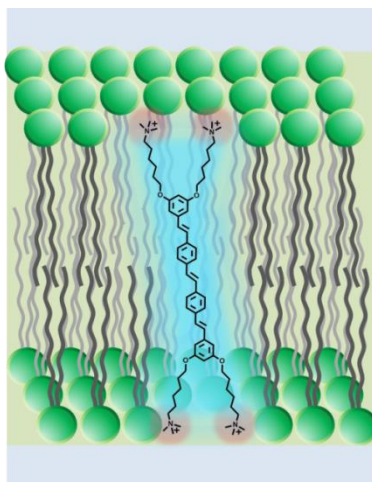


Figure I-1 Depiction of a membrane-intercalating COE embedded within a lipid bilayer.

Although not originally intended as membrane-active compounds,³⁸ our group now has a successful history designing and applying COEs as modulators of membrane properties. In 2010, the pioneers of this work within our group demonstrated that DSSN+, which has since become our most well-studied COE, was able to intercalate into model lipid membranes as well as live yeast cells.³⁹ Furthermore, it was shown that intercalation of DSSN+ could facilitate transmembrane electron transport across supported bilayer membranes and greatly improve yeast MFC voltage production. DSSN+, as well as subsequent derivatives have now been applied to various bioelectronic and bioelectrochemical systems utilizing a variety of bacteria and fungi.⁴⁰⁻⁴⁵ The initial hypothesis that these COEs could act as “molecular wires” for transmembrane electron transport was eventually replaced by the idea that intercalation caused increased membrane permeability.⁴² This conclusion represented a point of divergence for the program, from which two separate directions were pursued – the design and synthesis of true “molecular wire” COEs and utilization of COE-induced membrane permeability for other applications.

By including a redox-active ferrocene moiety within the core, Dr. Zach Rengert synthesized a COE which could directly transport electrons through the membrane of *S. oneidensis*.⁴⁶ DSFO, as it was named, was even able to act a “prosthetic” for *S. oneidensis* knockouts that lacked their native machinery for exoelectrogenesis (constituents of the *Mtr* pathway). Zach’s subsequent structural derivatives, DVFBO and F4-DVFBO, were also proven to act as molecular wires. Samantha McCuskey demonstrated that the ability to increase current extraction from *S. oneidensis* by these compounds was dependent on the poised potential within the system – the increase was only observed above the specific redox potential for each of the two compounds.⁴⁷

On a separate front, Dr. Chelsea Catania began to investigate the potential utility of COEs as general membrane permeabilizing agents with potential applications in whole-cell biocatalysis.⁴⁸ She found that COE intercalation into *E. coli* membranes permitted the diffusion of a small molecule (ONPG) across the outer membrane. Additionally, she found that the periplasmic protein alkaline phosphatase (ALP) was released to the extracellular media following treatment with COEs. Furthermore, the magnitude of the permeabilizing effect was found to be dependent on molecular structure. Subsequently, Dr. Stephanie Fronk and coworkers demonstrated that COEs could sufficiently permeabilize yeast without toxic effects to accelerate the intracellular biotransformation of fumaric acid to L-malic acid.⁴⁹ Through modification of the structural topology, Jakkarin Limwongyut was able to create a COE with reduced microbial toxicity that retained membrane permeabilizing effects.⁵⁰

Through the course of designing new COEs for bioelectronics and biosynthesis applications, a number of structures were found to be toxic to microbes. Dr. Hengjing Yan screened a variety of these COEs, along with non-toxic analogues, in order to begin to understand structure-property relationships that govern antimicrobial properties.⁵¹ She found that shorter compounds were generally more damaging to bacteria – a result which was also predicted by a molecular dynamics model that suggested a membrane “pinching” mechanism was responsible for cell damage and increased permeability.⁵² To produce antimicrobial action by an “active” mechanism, Dr. Bing Wang synthesized PTTP, a COE with a modified core to promote highly-efficient singlet oxygen generation.⁵³ Following intercalation into microbial membranes, PTTP did not inactivate bacteria until it was irradiated with low light doses at 540 nm. Bing also synthesized two COEs with near infrared absorption that were shown to kill bacteria via photothermal conversion.⁵⁴ In both systems it can be assumed that the photo-activated antimicrobial effects of the COEs are magnified by the fact that they are localized to the bacterial membranes.

I.3. Overview and Objectives

As the barrier between cells and the environment, membranes provide an ideal target for materials-based approaches to utilize or combat bacteria. To this point, our group has demonstrated the utility of COE-mediated membrane tuning for applications in bioelectronics, biocatalysis, and antimicrobials. The intent of the research described in this dissertation is to use rational synthetic design to probe

structure-property relationships of COE-membrane interactions and explore additional functions of COEs as membrane modifiers. With the exception of Chapter 5, the applications discussed for COEs are merely examples and are not meant to constrain potential utility. Modulation of membrane properties, or the imparting of new functions altogether, shall take precedent over specific applications. Moreover, the creative rational design and synthesis of tailor-made COEs will be the common motif connecting each of the chapters.

Figure I-2 depicts the diverse functions of COEs designed by our group. This dissertation will cover all of these systems except photothermal/phodynamic antimicrobial COEs^{53, 54} which was work by Dr. Bing Wang and redox-active COEs for transmembrane electron transport^{46, 47} which was work by Dr. Zach Rengert, Dr. Nate Kirchhofer, and Samantha McCuskey (and Luana Llanes is continuing this effort).

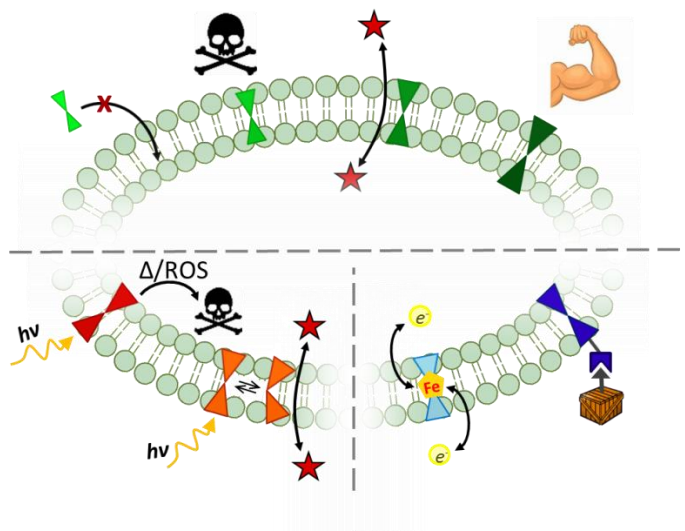


Figure I-2 Graphical illustration of various COE-mediated processes studied by our group. The upper hemisphere indicates the “size-dependent” effects of COEs on microbes. The lower-left quadrant highlights light-induced effects of COEs. The lower-right quadrant depicts COEs with particular structural units that provide specific functionality.

Figure I-3 depicts one of our well-studied molecules, COE2-4C, as a composition of various “blocks”, each of which is meant to represent a particular structural component. The red and blue blocks represent the interior and exterior portions of the conjugated backbone, respectively. The green blocks represent the pendant alkyl chains that connect the conjugated core to the ionic functionalities. The ionic functionalities, as well as any additional functionalities that exist beyond the charged groups, are represented by the yellow blocks. The chapters of this dissertation are depicted by the particular block changes that will be described therein.

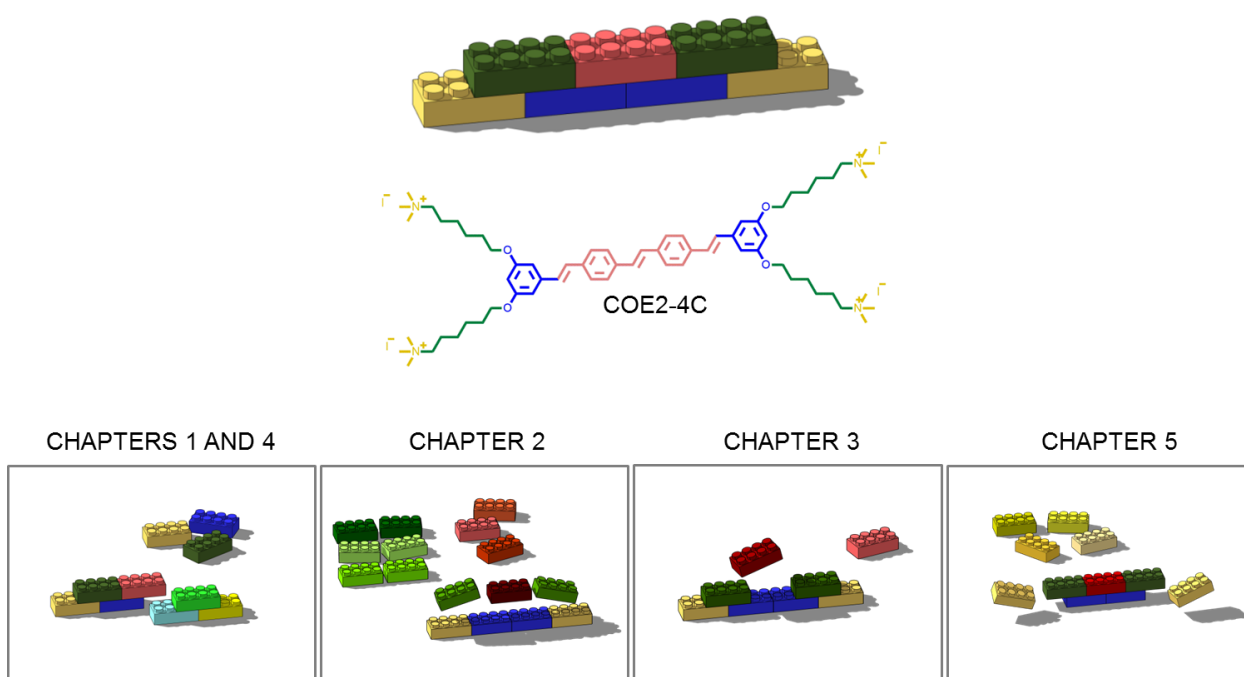


Figure I-3 The structural “building blocks” of COEs. Chapters of this dissertation will focus on tailoring the composition of these blocks in a specific manner in order to achieve the desired function.

In Chapters 1 and 4, the design and synthesis of a new structural class of COEs will be described. Unlike previous COEs synthesized by our group, this new

class possesses an asymmetric framework and reactive functionalities. Using COE2-4C as a parent structure, asymmetry was introduced by changing one of the exterior phenyl rings (blue block) from a 3,5-dialkoxy to a 4-alkoxy substitution pattern. The modified synthetic route additionally allowed for the inclusion of different linker (green) and terminal functionalities (yellow) on either side of the molecule. In this manner, a single occurrence of a reactive functional group was installed on the 4-alkoxy substituted side of the COE. In Chapter 1, the key structure includes a thiol which facilitates self-assembled monolayer formation on gold electrodes. The benefits of localizing the COE to the biotic-abiotic interface in bioelectronic devices will be discussed in relation to previous work within the group utilizing COEs to enhance electron transport in these devices. In Chapter 4, COEs will be used to introduce specific reactive functionalities to the surface of microbial membranes. Specifically, COEs bearing alkyne or azide groups will present those functionalities on the periphery of bacterial cells for use in subsequent “click” reactions. Additionally, a COE containing a nitrilotriacetic acid moiety will be used to localize peptides and proteins to the surface of bacterial cells. The potential utility of these functions will be described within the context of membrane bioconjugation.

In Chapter 2, a homologous series of twelve COEs will be used to determine structure-activity relationships pertaining to the antimicrobial and membrane-permeabilizing actions of COEs. Again, using COE2-4C as a parent structure, this new series of COEs maintains the same exterior phenyl rings (blue) and terminal groups (yellow) while modulating the lengths of the interior core (red) and linker (green). The role of different blocks on the COE-induced effects on bacteria will be

described in detail. The results of this analysis show that the ability of COEs to permeabilize membranes is not intrinsically correlated to antimicrobial activity. Unlike surfactants, COEs are thus able to significantly increase permeability well below bactericidal concentrations, suggesting that COEs may represent superior membrane permeabilizing agents. Additionally, the fact that the antimicrobial action of COEs is not dependent on non-specific surfactant-like membrane permeabilization provides optimism that COEs could be developed as a novel class of antibiotics.

In Chapter 3, the stilbene interior core (red) of COE2-4C will be substituted for an azobenzene moiety. This minor structural modification – switching the two central carbons for nitrogens – yields a photo-isomerizable COE. It will be demonstrated that, unlike the parent structure, this new COE is able to produce on-demand photo-actuated membrane permeabilization. Similar to the findings in Chapter 2, it will be shown that increased membrane permeability as a result of COE photo-isomerization is not correlated to antimicrobial action. Thus, a case will be made that this new structure can function as a benign membrane-permeabilizing agent which has the potential for spatial and temporal control.

In Chapter 5, the conclusions of Chapter 2 will be utilized in the design of COEs will enhanced antimicrobial activity. Modification of the terminal groups (yellow) will be investigated as a means to control selectivity for bacteria over mammal cells. The potential for our COEs to represent a novel antibiotic platform will be explored.

Chapter 6 includes additional information in support of the preceding chapters as well as further studies into COE-membrane and COE-microbe interactions. A

summary of the dissertation will be provided, followed by a list of references and NMR spectra of pertinent intermediates and final products.

Chapter 1: Self-Assembled Monolayers of COEs for Improved Biotic-Abiotic Interfaces

1.1 Introduction

The field of bioelectronics can roughly be defined as the conversion of electrical signals to biochemical signals or vice versa.¹³ Advances in specific bioelectronic technologies have the potential to radically change energy production,⁵⁵ biosynthesis,⁵⁶ sensing,^{57, 58} medicine,^{59, 60} agriculture,⁶¹ and many other high-impact fields. As the cornerstone of bioelectronics research, producing a seamless mechanical and electronic interface between abiotic and biotic components represents a persistent challenge.^{13, 62, 63} In the case of living systems, including those that are microbe-based, this interface has the additional requirement that it not damage the function of cells or tissues. Advances in these interfaces come from both biological^{64, 65} and materials^{41, 66} perspectives.

Exoelectrogenic bacteria, or those with the innate ability to respire on solid-state conductors, are particularly well-suited for bioelectronic applications. Evolution has resulted in only a few strongly-exoelectrogenic species – a fact which limits the scope of their utility.¹⁴ Rather than try to force these bacteria to perform under unfavorable conditions, enhancing the abilities of weakly-electrogenic bacteria (which include many model organisms such as *E. coli*) may prove more fruitful. Addition of redox mediators, either to the media^{67, 68} or to the electrode,^{69, 70} is a well-documented and successful method for pushing the limits of these bacteria, particularly in the case of microbial fuel cells. This enhancement can also be

achieved through biological approaches, such as the expression of recombinant proteins that act as both physical tethers and electrical conduits between bacterial membranes and electrode surfaces.⁷¹

Our group has demonstrated that COEs present an alternative method for improving the exoelectrogenic behavior of bacteria. Depending on chemical structure, COEs either act as direct redox mediators^{46, 47} or through non-redox mechanisms.^{40, 44, 45} In the case of the COEs which cannot act as redox mediators, the enhanced electronic communication at the biotic-abiotic interface is likely due to favorable changes in membrane properties such as increased permeability.^{42, 49, 72} The work described in this chapter is an effort to address some of the practical concerns with using COEs as soluble additives in bioelectronic by instead tethering the COE directly to the electrode surface. Figure 1-1 shows an idealized case of a surface-bound COE intercalated into a membrane without taking into consideration the possible effects of membrane proteins or the LPS layer.

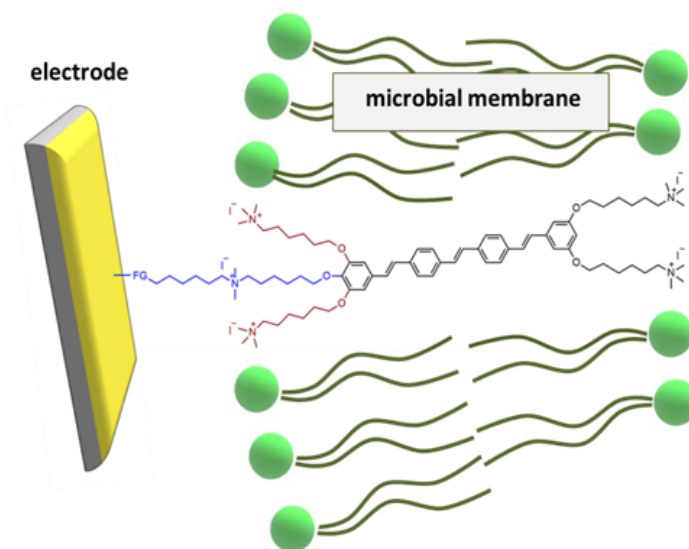


Figure 1-1 Cartoon representation of a surface-binding COE (blue) as a structural analogue of a previously-described COE (red).

1.2 Design and synthesis of a gold-binding COE

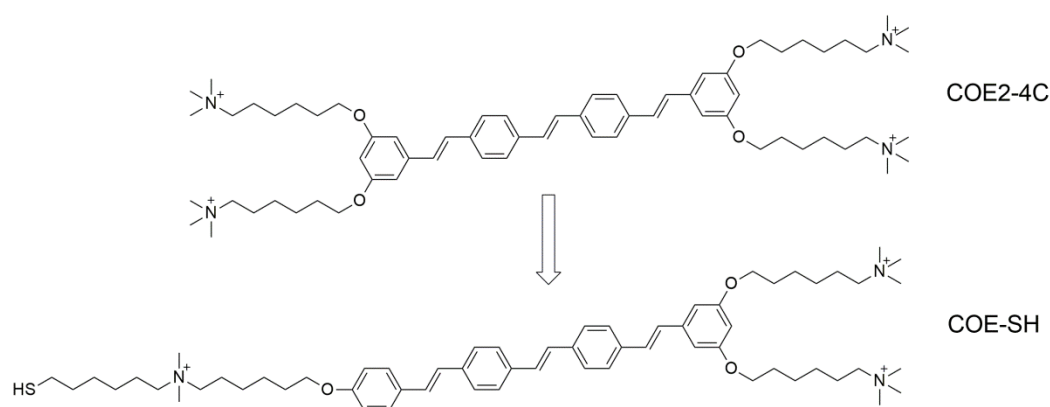


Figure 1-2 Derivatization of COE2-4C to design a gold-binding analogue, COE-SH.

In designing a new COE with the ability to form SAMs on gold surfaces, we used the previously-described COE2-4C as a parent structure (Figure 1-2) due to its ideal combination of low antimicrobial activity⁷³ and significant improvement in bioelectronic devices.⁷⁴ The new structure, COE-SH, was designed to contain a single thiol functionality so that each molecule would be tethered to a gold surface by one gold-sulfur bond. This was expected to simplify characterization of the resulting SAMs and reduce the likelihood of any residual free thiols in the system. To maintain a similar distribution of charges, COE-SH was designed to contain a quaternary amine at an intermediate position along the tether containing the thiol group. It was believed that directly replacing the ammonium groups on one side of the molecule for a single thiol would affect the new COE's ability to intercalate into membranes (or result in undesirable interactions with microbes such as higher antimicrobial activity). It is also likely that without this third ammonium group, the COE would have had minimal aqueous solubility.

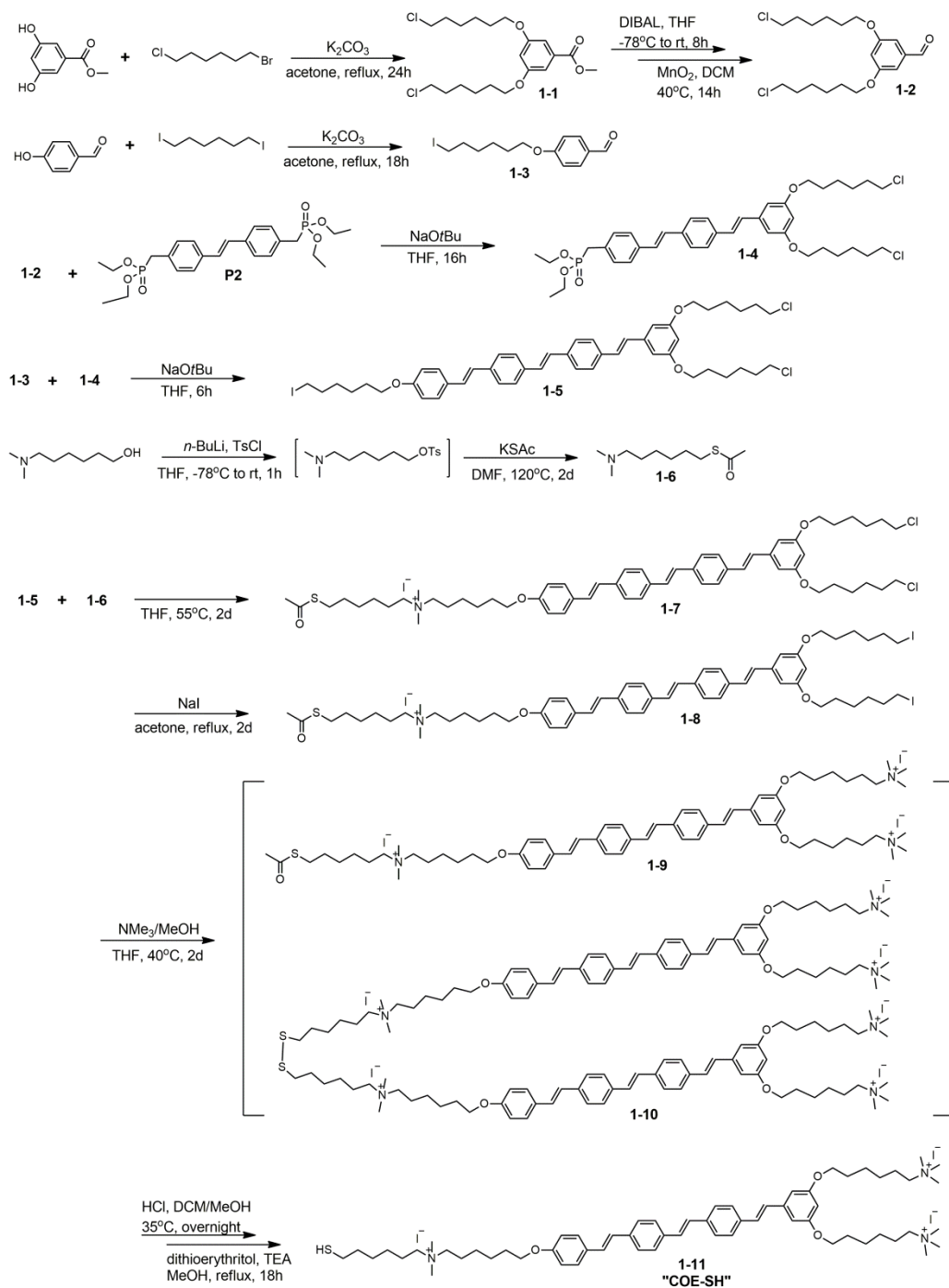


Figure 1-3 Synthetic preparation of COE-SH.

The synthetic route for preparing COE-SH, shown in Figure 1-3, begins in a similar manner as the routes of our previously-described COEs. The key alteration in

the route occurs at the first Horner-Wadsworth-Emmons (HWE) reaction which yields intermediate **1-4**. In the case of symmetrical 4-ring COEs, the Horner-Wadsworth-Emmons (HWE) reaction would have required two equivalents of **1-2** for one equivalent of **P2**. In the case of the present route, only 0.85 equivalents of **1-2** were used in the preparation of **1-4** (note: a similar intermediate was described for the preparation of COEs containing five aromatic rings⁷³). Another critical component of the asymmetry was the use of alkyl chlorides in **1-2** rather than bromides or iodides as used in our previous COEs. The importance of this will become apparent in the following paragraph.

The second HWE reaction, between **1-3** and **1-4**, resulted in the key asymmetric intermediate **1-5**. This intermediate will be described again for its use in preparation of other COEs in Section 1.6 and Chapter 4. The utility of this compound lies in the differential reactivities of the alkyl chlorides and alkyl iodide. Due to the significantly-higher reactivity of the iodide, quaternization with a tertiary amine can be achieved selectively, allowing for the chlorides to eventually be substituted for different ammonium groups (by way of first converting to iodides). The reaction yielding **1-7** illustrates how this process was used to introduce a thiol functionality (protected as the thioacetate) to only the desired position. By replacing **1-6** with a different amine, a single occurrence of a desired functional group can be introduced into the COE structure.

Conversion of the alkyl chlorides of **1-7** to iodides using sodium iodide (Finkelstein reaction) and subsequent treatment with trimethylamine was expected to afford **1-9**. However, ¹H NMR spectroscopy confirmed the additional presence of

1-10, formed during the quaternization reaction through deprotection of the thioacetate and oxidation of the resulting thiol to disulfide. The mixture of **1-9** and **1-10** was converted exclusively to the desired product **1-11** in a two-step process, first deprotecting the thioacetate with HCl and then reducing the disulfide with dithioerythritol. Detailed synthetic methods for the preparation of COE-SH can be found in Section 1.9.

1.3 Intercalation of COE-SH into Microbial Membranes and the effect on Bacterial Growth

The ability of COE-SH to intercalate into microbial membranes was assessed by confocal microscopy. The observation of fluorescence localized to the periphery of the cells is routinely used in our group to confirm COE interactions with membranes. As shown in Figure 1-4, COE-SH appears to exclusively interact with the membrane of *E. coli*. While this experiment does not guarantee that COE-SH can intercalate into membranes following attachment to a surface, it does demonstrate that the structural modifications do not prevent it from interacting with membranes.

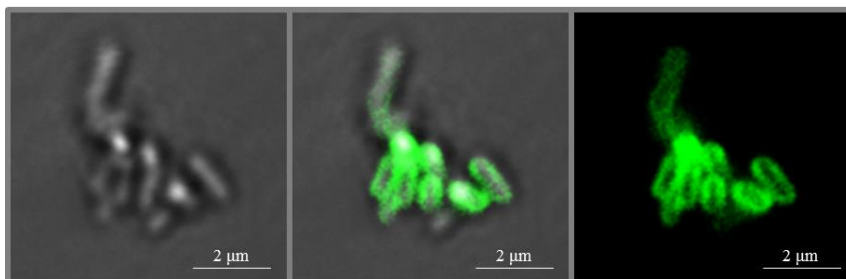


Figure 1-4 Confocal fluorescence micrographs of *E. coli* stained with COE-SH – bright field (left), fluorescence (right), and overlay (center). Localization of fluorescence to the periphery of cells indicates that COE-SH is intercalated in the membranes.

The antimicrobial activity of COE-SH was tested by standard broth microdilution with *E. coli* K12. Partial inhibition of growth was observed beginning at 64 μM but 90% inhibition was not observed even at the highest test concentration (1024 μM). While COE-SH does seem to inhibit bacterial growth to a greater extent than the related COE2-4C,⁷³ the concentration required for significant inhibition is higher than what is likely to be applied in MFC devices.

1.4 Formation and characterization of COE-SH Monolayers

The defining structural feature of COE-SH is the gold-binding thiol functionality. Before testing whether COE-SH was able to act as an effective interlayer at the biotic-abiotic interface, it was necessary to determine appropriate conditions for SAM formation. Planar gold films on silicon substrates were submerged in degassed 1 mM aqueous solutions of COE-SH for 24 hours. X-ray photoelectron spectroscopy (XPS) was used to confirm and quantify the resulting SAMs. Figure 1-5 shows a full spectrum and high resolution scan centered on the sulfur S 2p region. The single spin-orbit coupled doublet at 161.9 eV is characteristic of a thiolate-gold bond.⁷⁵ It is important to note that no free thiol (~160 eV) or higher oxidation state sulfur species (162-164 eV) are observed. Insufficient rinsing or use of ethanol instead of water during SAM-formation resulted in significant amounts of free thiol, indicating the presence of physically adsorbed COE-SH. Additionally, minimal thiolate-gold bond formation was observed when using ethanol.

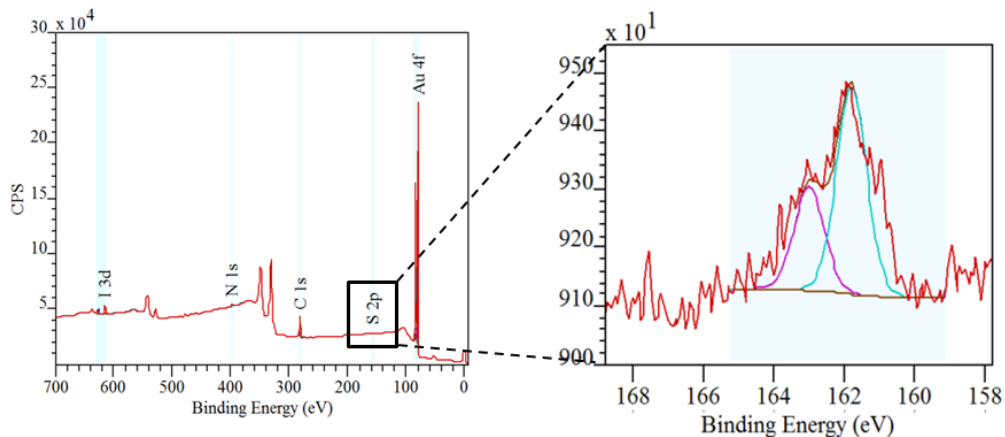


Figure 1-5 XPS spectra confirming the formation of COE-SH SAMs. The binding energy of the S 2p peak is characteristic of a thiolate-gold bond.

Surface coverage on the planar gold films was estimated to be 26% using the XPS survey spectrum (calculation described in Sections 1.6.1 and 1.6.2). To confirm this result, coverage was also calculated reductive desorption.^{76, 77} A detailed description of this experiment can be found in Section 1.6.3 but an overview will be provided here. Cyclic voltammetry was used to calculate the number of electrons required to reduce the SAM and the number of available gold atoms was estimated from the surface area of the electrode. By dividing the number of injected electrons by the number of gold atoms, it was determined that 35% of the gold surface was functionalized with COE-SH. This is in good agreement with the XPS calculation, with both methods suggesting the functionalization of approximately 1/3 of the surface gold atoms. Based on the large size and significant charge of COE-SH, this result seems reasonable as an upper limit of surface coverage. A method for increased COE SAM surface coverage (with a modified COE structure) is described in Section 1.6.6.

1.5 Application of COE-SH Functionalized Anodes in Microbial Fuel Cells

To assess the ability of COE-SH SAMs to facilitate more intimate electronic coupling between microbes and electrodes, we applied the well-established U-tube MFC system. *E. coli* K12 was used as a model weakly-electrogenic organism due to its ease-of-use and the significant body of work our group has conducted using it in the past. In this study we used carbon felt air-cathodes and gold wire anodes, either bare or functionalized with COE-SH. Figure 1-6a shows the potential output through time for the control and functionalized-anode devices. For the first hour of operation, there is little difference between the two systems. Over the next hour, the output of the devices containing COE-SH SAMs increases to a maximum of 50 mV, twice that of the control. Following this rapid increase, the output of the COE-SH devices begins to decline until it returns to a similar level as the control devices (around 5 hours of operation). Although we did not determine the cause of this decline in output, it is feasible that the gold-sulfur bond was not stable under the conditions in the reactor.

Power density curves were measured to further investigate the effects of COE-SH SAMs on the electrical connection between cells and electrode. Figure 1-6b shows the power density curves for control and COE-SH devices after approximately two hours of operation. Functionalized anodes provided twice the peak power as controls. As both sets of devices had approximately the same internal resistance (~7 M Ω), this difference was most likely due to a reduced activation barrier in the case of the functionalized anodes. In addition to achieving twice the peak potential and

power, COE-SH functionalization of anodes resulted in a ~50 % reduction in time to reach peak potential relative to controls (Figure 1-6c). While “turn-on” time is not a typical figure of merit for MFCs, it is an important metric in other microbe-based bioelectronic technologies such as sensing applications.

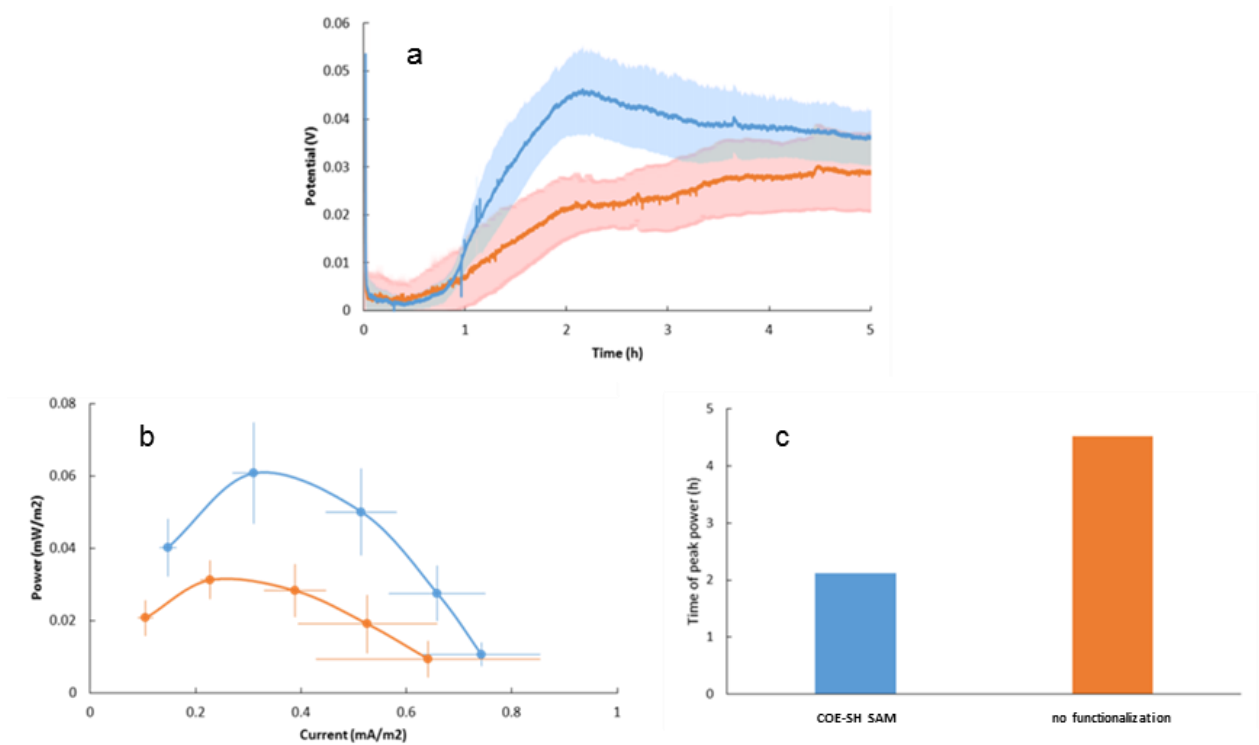


Figure 1-6 COE-SH anode functionalization impacts on voltage, power density, and time to reach peak power in U-tube MFCs – potential output through time (a), power density curve after 2 hours of operation (b), and time to reach peak power (c).

1.6 Additional Experiments and Calculations

1.6.1 Surface coverage calculated from XPS spectrum

The calculation of surface coverage from the XPS spectrum is summarized in Table 1-1. Peak areas (Au 4f and S 2p) were measured directly from the spectrum (using CASA-XPS) and were divided by empirically-derived relative sensitivity factors. The resulting “corrected area” was used to determine the relative atomic ratio. Since

much of the Au 4f signal comes from gold atoms in the bulk film, the gold atomic ratio was further corrected by calculating the contribution from the first atomic layer (Section 1.6.2). The results indicate that there is 1 sulfur atom per every 3.89 gold atoms on the surface (i.e. 25.7% of surface gold atoms are bound to a sulfur).

Table 1-1 Calculation of COE-SH surface coverage by XPS.

	Au 4f	S 2p
Peak Area	374083	1486
Relative Sensitivity Factor	17.4	1.68
Corrected Area	21499	885
Relative Atomic Ratio	24.31	1.00
Surface Contribution	0.16	1
Corrected Relative Atomic Ratio	3.89	1.00
Calculated % Coverage	-	25.7

1.6.2 Calculation of first-atomic-layer contribution to Au 4f XPS signal

As the Au 4f signal includes contributions from the bulk gold, it was critical to first calculate the amount of signal which originated from only the first atomic layer. This was done by using Equation 1

$$P(d) = \exp(-d/\lambda) \quad \text{Equation 1-1}$$

where $P(d)$ is the probability of a photoelectron escaping from depth d and λ is the mean free path (MFP) of an electron through a specific material.⁷⁸ For an Au 4f

electron through bulk gold, the MFP is ~ 1.6 nm.⁷⁹ Assuming a lattice parameter of ~ 0.4 nm for face-center cubic Au,⁸⁰ one atomic layer represents 0.25 MFP ($0.4/1.6$). The following calculation, also shown in Figure 1-7, results in an estimated 16% of the total Au 4f signal originating from the first atomic layer of gold (plotting and integration using Wolfram Mathematica 10.4). The area under the curve from $d = 0$ to $d = 0.25$ MFP is 0.23 (“first” in the calculation below) and the area under the curve from $d = 0$ to $d = 3.5$ MFP (truncated) is 1.42 (“total” in the calculation below). Dividing the first area by the total area yields the fraction of total Au 4f signal that originates from atoms in the first atomic layer (i.e the first 0.4 nm or the first 0.25 MFP).

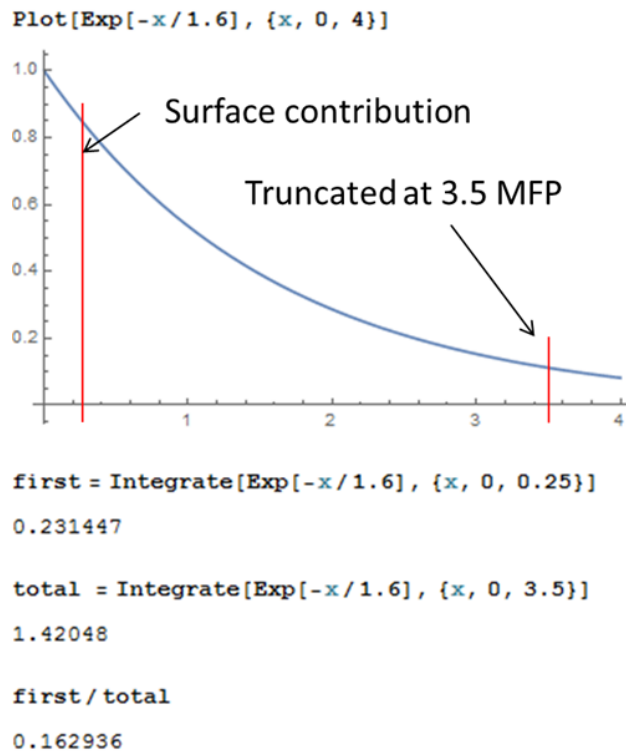


Figure 1-7 Probability of photoelectron escape from bulk gold based on depth below the surface (mean free path).

1.6.3 Surface coverage calculated by reductive desorption

SAMs were formed by immersing coiled gold wires (1 cm² surface area) in 1 mM aqueous solutions of COE-SH. Gold-sulfur bonds were reduced using cyclic voltammetry by sweeping the voltage between 0 and -1.4 V at 100 mV/s and measuring current. The area under the curve (peak centered at ~-1 V) was measured, converted to Coulombs, and multiplied by the inverse of the elementary charge to determine the number of electrons used in the process. The number of gold atoms in the first atomic layer was estimated based on 1 cm² total surface area and a lattice parameter of 0.4 nm.⁸⁰ As reduction of gold-sulfur bonds is a one-electron process, the number of electrons injected was directly divided by the number of surface gold atoms to yield an approximate surface coverage of 35%. The voltammogram and calculation (Wolfram Mathematica 10.4) are shown in Figure 1-8.

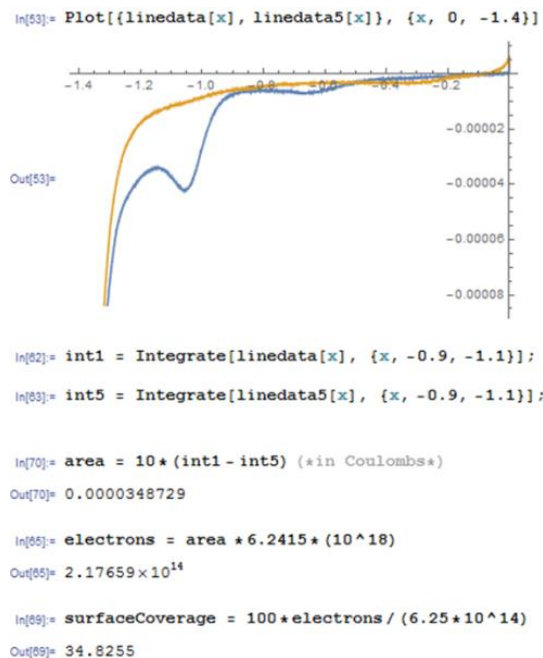


Figure 1-8 Reductive desorption cyclic voltammogram and quantification of COE-SH SAM surface coverage.

1.6.4 Cell density on electrodes assessed by SEM

To assess whether COE-SH SAMs allowed for increased electrode colonization, anodes were removed from MFCs post-run, sputtered with gold, and imaged using scanning electron microscopy. As shown in Figure 1-9, no discernable difference in cell densities is observed between control (B) and COE-SH treated anodes (A). While the cell densities seem to be similar at the end of the experiment, we did not rule out the possibility that COE-SH SAMs increase the rate of colonization. It is conceivable that such an effect could be responsible for the shortened time to reach peak power observed in the COE-SH SAM devices.

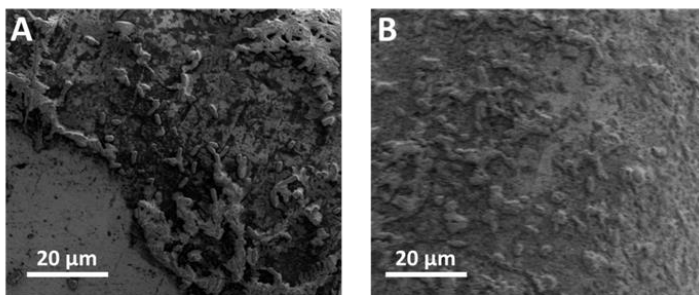


Figure 1-9 SEM micrographs of COE-SH treated (A) and control (B) gold anodes from MFCs (post-run).

1.6.5 Control MFCs with thermally-deactivated cells

To ensure that the rapid increase in potential of COE-SH SAM devices was directly related to microbial metabolism, we added thermally-deactivated *E. coli* to reactors with functionalized anodes. No significant output was recorded from these MFCs, suggesting that the measured potential was in fact related to microbial metabolism and not some spurious effect such as capacitive discharge. This thermally-deactivated cell control (green) is shown along with the functionalized anode device data (blue) using live cells in Figure 1-10.

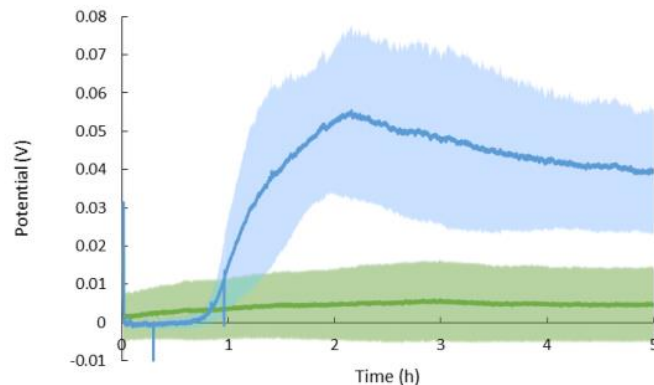


Figure 1-10 MFC performance using COE-SH functionalized anodes with live (blue) or thermally-deactivated (green) *E. coli*.

1.6.6 2-step SAM formation via click chemistry

During the course of optimizing SAM-formation conditions, it became apparent that high surface coverage with COE-SH would be challenging. In fact, early attempts to form monolayers from solutions in ethanol yielded little more than physically adsorbed COE-SH on the gold surface. In the event that we would be unable to find appropriate conditions using COE-SH, a second method for making COE SAMs was devised. Instead of forming the monolayer by directly functionalizing a gold surface with a COE, we hypothesized that utilizing “click” chemistry could allow for better SAM formation. As such, we designed and synthesized the alkyne-containing COE-CH as shown in Figure 1-11.

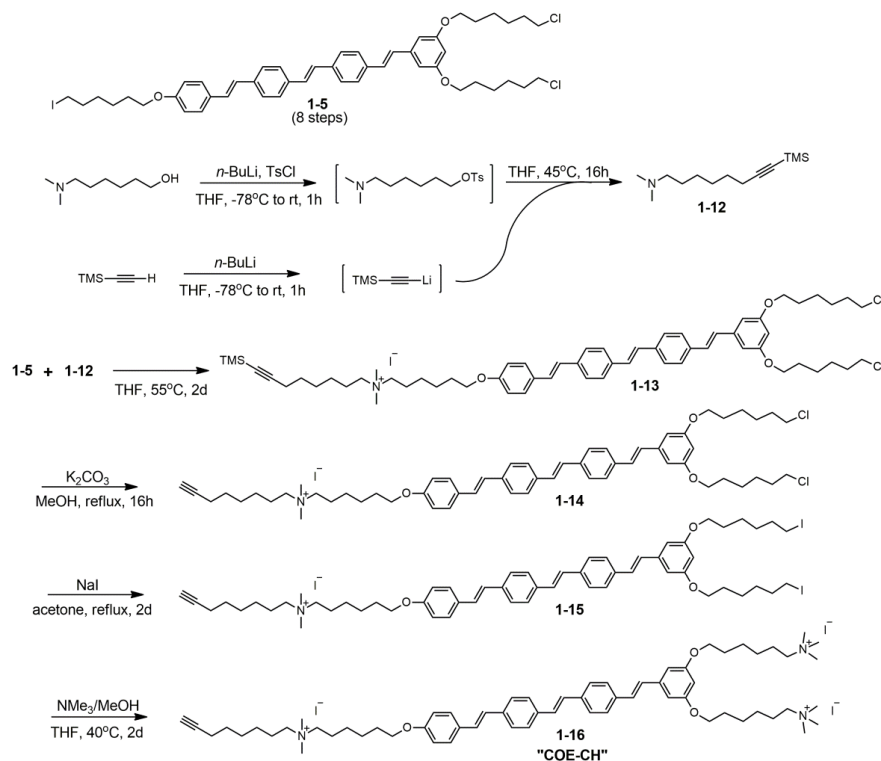


Figure 1-11 Synthesis of alkyne-containing COE-CH for use in copper-catalyzed azide-alkyne cycloaddition.

As outlined below in Figure 1-12, gold surfaces were first functionalized with 6-azidohexane-1-thiol to introduce azide functionalities to the surface. SAM formation with this compound was facile and efficient, as evident by the $\sim 80\%$ coverage calculated by XPS. Reaction of the surface-tethered azide groups with the alkyne on the COE was achieved under standard copper-catalyzed cycloaddition conditions (sodium ascorbate, copper sulfate). XPS of the resulting monolayers indicated that the conversion of azides to triazoles was highly efficient. Under these conditions it was possible to achieve significantly higher surface coverages ($\sim 80\%$) than even the eventual optimal conditions for COE-SH.

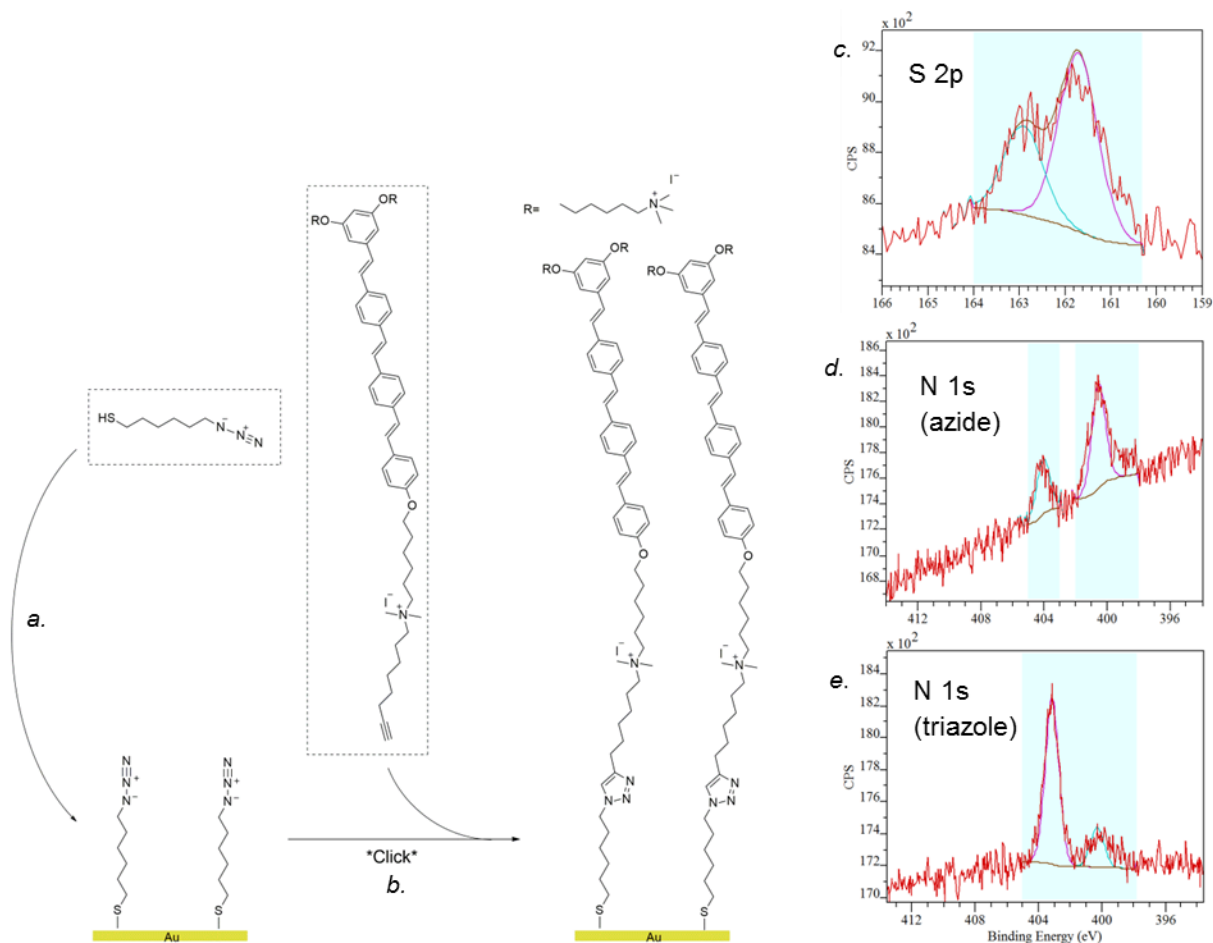


Figure 1-12 2-step formation of COE SAMs on gold via copper-catalyzed azide-alkyne cycloaddition "click" reaction. (a) gold substrate initially functionalized with 6-azido-1-hexanethiol. (b) subsequent cycloaddition reaction with COE-CH using sodium ascorbate and copper sulfate. XPS spectra following step "a" indicating the presence of thiolate-gold (c) and azide (d). (e) XPS N 1s spectrum indicative of triazole following "click" reaction in step "b".

While this two-step method to monolayer formation was not used in subsequent MFC tests, it did provide a generalized method for extending COE surface functionalization to materials other than gold (without having to synthesize a new COE for each new material). As an example, silica gel was functionalized by the same general protocol (Figure 1-13).

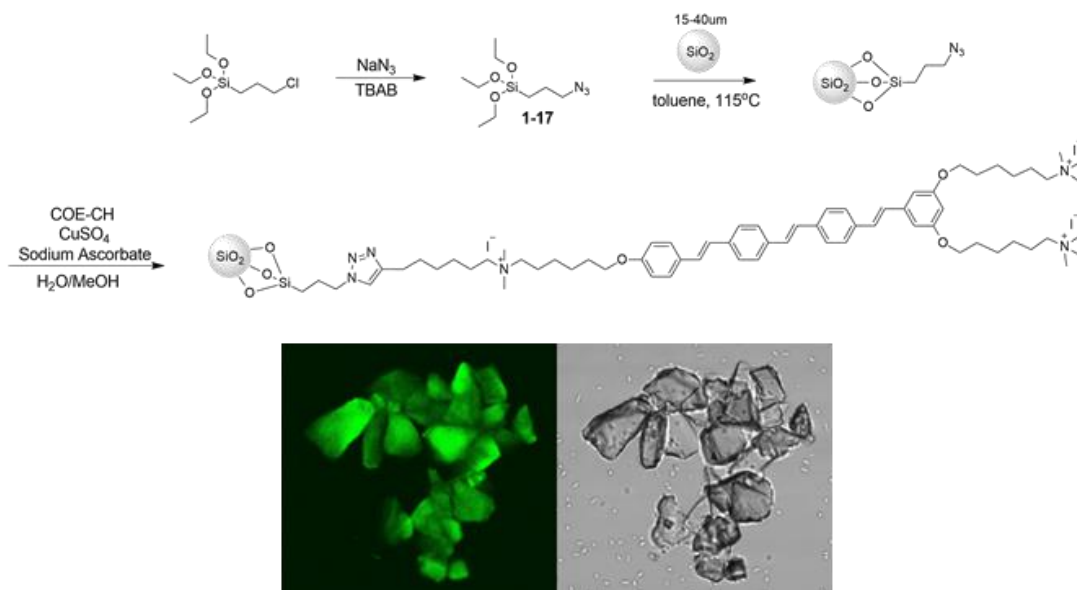


Figure 1-13 Method to functionalize silica particles with COE-CH via copper-catalyzed azide-alkyne cycloaddition “click” reaction (top). Laser scanning confocal micrographs of COE-functionalized silica particles and *E. coli* K12 cells (epifluorescence, bottom left; bright field, bottom right). (Scale: 60x60 μM).

An attempt was made to use functionalized silica particles to demonstrate that surface-bound COEs were still able to intercalate into microbial membranes. While this experiment was not able to confirm intercalation of the COE into the bacterial membranes, it did suggest that COE-functionalized silica provides a surface which is amenable to attachment by microbes (a number of cells can be observed on the silica particles in the bright field image). This method for functionalizing surfaces with COEs could prove useful in future studies such as the application of COEs to solid-supports for whole-cell flow biocatalysis. Related COE systems will be discussed in Chapter 4 as “anchors” for membrane bioconjugation.

1.7 Conclusions

In conclusion, a COE was designed with the specific intent of investigating how COE SAMs influence the biotic-abiotic interface in bioelectronic systems. This novel structure was roughly based on previous compounds synthesized by our group with the addition of a thiol moiety at one end to allow for SAM formation on gold surfaces. Favorable interactions with microbes (membrane intercalation, low antimicrobial activity) were confirmed, COE monolayers on gold were characterized by XPS and CV (reductive desorption), and effects on the biotic-abiotic interface were investigated. While not meant to be the exclusive target application of this technology, MFCs were used to demonstrate that COE SAMs provide an improved interface for bioelectronic devices. The improvements in device performance are in line with previous experiments in our group using solutions of COEs to stain cells in suspension. The approach described here has the benefit of localizing the COE to the electrode surface, resulting in lower material consumption (by nearly 3 orders of magnitude) and the possibility of re-use. Stability of this particular system may be insufficient for “recycling” anodes but this does not represent an insurmountable challenge for future efforts.

In addition to the specific goals set forth at the outset of this study, a significant synthetic hurdle was addressed in the process. For the first time, our group designed and synthesized an asymmetric COE structure with a reactive chemical moiety for a specific application. Utilizing the synthetic methods derived for COE-SH, an analogous structuring bearing an alkyne in the place of the thiol was synthesized

(COE-CH). This structure was shown to be amenable to copper-catalyzed azide-alkyne cycloaddition (“click”) and was utilized in the formation of SAMs on azide-functionalized gold and silica. The synthetic route for the preparation of these two COEs produced a key intermediate for subsequent asymmetric COEs with specific functionalities that will be described in Chapter 4.

1.8 Experimental methods

Materials and Instrumentation

Solvents and reagents for synthetic preparations were purchased from Fisher Scientific, Alfa Aesar, Acros, Sigma Aldrich, and Tokyo Chemical Industry. *Escherichia coli* ATCC 10798 was purchased from American Type Culture Collection (Manassas, VA). Inhibitor-free anhydrous solvents were prepared using packed alumina columns under argon in a solvent purification system. EMD Millipore Analytical Chromatography aluminum-backed plates (Silica gel 60 F254) were used for thin layer chromatography and separation was visualized with UV light (254/366 nm). Silicycle SiliaFlash P60 silica gel was used for flash chromatography under positive air pressure. Optical density measurements for MIC studies were conducted on a Tecan M220 Infinite Pro. ^1H NMR (400 MHz, 500 MHz) and ^{13}C NMR (101 MHz and 126 MHz) were measured on actively-shielded Agilent Technologies 400-MR DDR2 400 MHz or Varian Unity Inova 500 MHz spectrometers. Multiplicity of signals was described by s (singlet), d (doublet), t (triplet), and m (multiplet). Chemical shifts (δ in ppm) were referenced to residual solvent peaks of Chloroform-*d* (^1H NMR δ =

7.26 and ^{13}C NMR $\delta = 77.0$) or DMSO- d_6 (^1H NMR $\delta = 2.50$ and ^{13}C -NMR $\delta = 39.52$). HRMS (m/z) measurements were performed on a Waters GCT Premier time-of-flight mass spectrometer. Spectral confocal microscopy was conducted on an Olympus Fluoview 1000. XPS spectra were collected on a Kratos Axis Ultra with a monochromated Al source.

Strain and Culture Conditions

Escherichia coli K12 (ATCC #10798, ATCC, VA) was grown under aerobic conditions in Luria-Bertani (LB) broth (10 g/L bactotryptone, 5 g/L yeast extract, 10 g/L NaCl) overnight at 37 °C with orbital shaking (250 rpm). Cells were collected by centrifugation and resuspended in fresh Luria-Bertani broth (for MIC and MFC experiments) or washed 2x with 150 mM phosphate-buffered saline (PBS) before resuspending in PBS (confocal microscopy experiments).

Minimum Inhibitory Concentration

Following overnight growth, collection, and resuspension in fresh LB, cells were diluted to 1 OD₆₀₀. Stock bacteria solutions were prepared by further 1:1000 dilution in LB. COE-SH stock solution was prepared in LB media at a concentration of 2.048 mM. Bacteria stock solution was added to a serial dilution of COE-SH stock on a 96-well plate to achieve final concentrations from 2- to 1024 μM . Plates were incubated overnight at 37 °C with orbital shaking (250 rpm) and optical density was recorded at 600 nm.

Spectral Confocal Microscopy

E. coli cells (1 O.D.) were treated with COE-SH (10 μ M) for an hour and diluted to 0.1 O.D. Samples were prepared by depositing 4 μ L of the cell solution on a pre-cleaned microscope slide and gently placing a cover slip on top. To prevent drying, nail polish was used to seal the edge of the cover slip to the slide. Concurrent bright field and epifluorescence (excitation: 405nm, detection: 415-425nm) images were collected. Images were processed using Fiji.

X-Ray Photoelectron Spectroscopy (XPS)

Survey scans were collected with pass energy of 40 kV, step size of 0.5 keV, and dwell time of 250 ms. High resolution scans were collected with pass energy of 20 kV, steps size of 0.05 keV, and dwell time of 1200 ms. Spectra were processed using CASA-XPS.

SAM Preparation

Self-assembled monolayers were formed by submerging gold films or gold wires in degassed COE-SH solutions in MiliQ water for 24 hours. Substrates were washed with copious amounts of MiliQ water and sonicated in MiliQ water. Three rounds of rinsing and sonicating was sufficient to remove adsorbed COE-SH as evident by XPS data. Following the final MiliQ wash, substrates were rinsed with isopropyl alcohol and blown dry with a stream of argon.

For preparation of COE SAMs on gold films via “click” chemistry, azide groups were introduced by immersing films overnight in degassed ethanol solutions

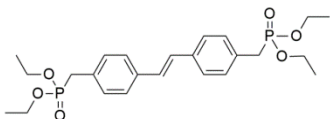
containing 1 mM 6-azidohexane-1-thiol. Substrates were rinsed thoroughly with ethanol and isopropyl alcohol before drying under a stream of argon. The “click” reaction was performed by immersing the azide-functionalized gold films in degassed aqueous solutions containing 0.5 mM COE-CH, 0.02 mM copper (II) sulfate, and 1 mM sodium ascorbate for 24 hours. Substrates were subjected to three rounds of rinsing and sonicating in MiliQ water, rinsed once with isopropyl alcohol, and blown dry with a stream of argon before collecting XPS spectra.

For preparation of COE SAMs on silica gel particles via “click” chemistry, the silica gel was first treated with Piranha (3:1 concentrated sulfuric acid and 30% hydrogen peroxide) for 15 minutes. Azide groups were introduced by stirring the silica particles with (3-azidopropyl)triethoxysilane in toluene at 110°C overnight. The silica particles were collected by centrifugation and were washed with toluene and diethyl ether before drying under vacuum. The “click” reaction was performed by stirring the azide-functionalized silica particles in water with 0.5 mM COE-CH, 0.02 mM copper (II) sulfate, and 1 mM sodium ascorbate for 24 hours. The particles were again collected by centrifugation and washed multiple times with water until it was evident that all the COE-CH had been removed (i.e. the rinse water was no longer fluorescent).

1.9 Synthetic methods for the preparation of COE-SH

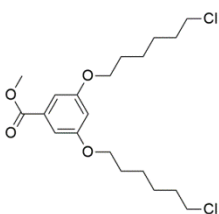
(E)-tetraethyl ((ethene-1,2-diylbis(4,1-phenylene))bis(methylene))bis(phosphonate)

(P2)



Intermediate **P2** was synthesized in two steps according to literature procedures.³⁹

methyl 3,5-bis((6-chlorohexyl)oxy)benzoate (1-1)



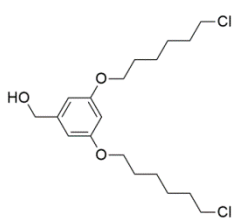
To a 100 mL round bottom flask were added 4 g (23.8 mmol) 3,5-dihydroxy methylbenzoate and 6.74 g (28.8 mmol) potassium carbonate. Acetone (50 mL) followed by 10 g (50 mmol) 1-bromo-6-chlorohexane were added to the reaction vessel. A reflux condenser was installed and the mixture was stirred for 24 hours at reflux. After cooling, the contents were partitioned between ethyl acetate and water. The aqueous phase was separated and washed twice with ethyl acetate. The combined organic phase was washed twice with water, dried over MgSO₄, and concentrated by rotary evaporation. Column chromatography (1:10 ethyl acetate:hexanes, *r_f* = 0.25) afforded the product as a clear oil (8.2 g, 85%)

¹H NMR (400 MHz, CDCl₃): δ 7.15 (s, 2H), 6.62 (s, 1H), 3.97 (t, *J* = 6.4 Hz, 4H), 3.89 (s, 3H), 3.55 (t, *J* = 6.7 Hz, 4H), 1.80 (m, 8H), 1.50 (m, 8H).

¹³C NMR (126 MHz, CDCl₃): δ 166.88, 160.04, 131.87, 107.64, 106.56, 68.03, 52.17, 44.94, 32.49, 29.00, 26.60, 25.37, 25.25.

ESI/TOF-MS: 427.1 [M+Na]⁺

(3,5-bis((6-chlorohexyl)oxy)phenyl)methanol (1-1b)

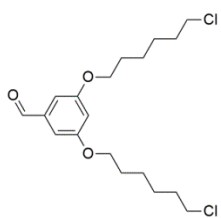


To a dry 50 mL round bottom flask was added 5.3 g (13.07 mmol) **1-1**. After three cycles of evacuation and argon backfilling, dry THF was cannulated into the reaction vessel under an argon atmosphere. The reaction vessel was cooled to -78 °C and 4.65 g (32.68 mmol) diisobutylaluminum hydride was added slowly via syringe. The mixture was stirred and allowed to warm to room temperature. After 8 hours, the mixture was cooled to 0 °C and quenched by the sequential, slow addition of 5 mL Et₂O, 0.25 mL H₂O, 0.5 mL 2 M NaOH, and 2.5 mL H₂O. The mixture was again allowed to warm to room temperature and MgSO₄ was slowly added. Stirring was continued for 15 minutes before solids were removed over a pad of celite. Concentration of the filtrate afforded the product as a clear oil which was used without further purification (4.6 g, 93%).

¹H NMR (500 MHz, CDCl₃): δ 6.49 (s, 2H), 6.36 (s, 1H), 4.60 (s, 2H), 3.94 (t, *J* = 6.4 Hz, 4H), 3.54 (t, *J* = 6.7 Hz, 4H), 1.74-1.84 (m, 8H), 1.45-1.54 (m, 8H).

¹³C NMR (126 MHz, CDCl₃): δ 160.41, 143.26, 105.07, 100.55, 67.78, 65.35, 44.98, 32.50, 29.08, 26.61, 25.40, 25.39.

3,5-bis((6-chlorohexyl)oxy)benzaldehyde (1-2)



To a solution of intermediate **1-1b** (4.2 g, 11.14 mmol) in DCM (50 mL) was added 14.5 g MnO₂ (167 mmol). The heterogeneous mixture was stirred at 40 °C for 14 hours. After cooling to room temperature, the mixture was filtered through a pad of celite and concentrated. The

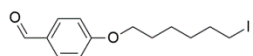
product was obtained as a clear oil and was used without further purification (4.1 g, 98%).

^1H NMR (400 MHz, CDCl_3): δ 9.89 (s, 1H), 6.98 (s, 2H), 6.69 (s, 1H), 3.99 (t, J = 6.7 Hz, 4H), 3.55 (t, J = 6.7 Hz, 4H), 1.81 (m, 8H), 1.51 (m, 8H)

^{13}C NMR (126 MHz, CDCl_3): δ 191.96, 160.66, 138.33, 107.99, 107.60, 68.15, 44.93, 32.47, 28.95, 26.58, 25.36.

ESI/TOF-MS: 397.1 $[\text{M}+\text{Na}]^+$

4-((6-iodohexyl)oxy)benzaldehyde (**1-3**)



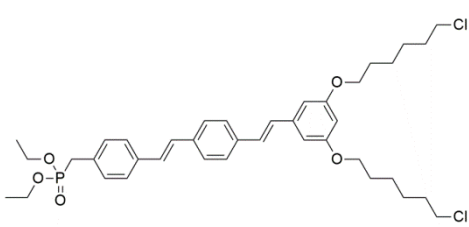
3-hydroxybenzaldehyde (800 mg, 6.55 mmol), 1,6-diiodohexane (8.9 g, 26.2 mmol), potassium carbonate (1.08 g, 7.86 mmol), and acetone (50 mL) were added to a 100 mL round bottom flask. A reflux condenser was installed and the mixture was refluxed under inert atmosphere for 18 hours. After cooling to room temperature, the mixture was portioned between ethyl acetate and brine. The aqueous phase was subsequently washed two additional times with ethyl acetate. The combined organic phase was washed two times with brine, dried over Na_2SO_4 , filtered through celite, and concentrated to give a yellowish oil. Column chromatography (1:10 ethyl acetate: hexanes, r_f = 0.25) afforded the pure product as a white solid (1.65 g, 76%).

^1H NMR (600 MHz, CDCl_3): δ 9.88 (s, 1H), 7.83 (d, J = 8.8 Hz, 2H), 6.99 (d, J = 8.6 Hz, 2H), 4.04 (t, J = 6.4 Hz, 2H), 3.21 (t, J = 6.9 Hz, 2H), 1.80-1.89 (m, 4H), 1.46-1.53 (m, 4H).

^{13}C NMR (126 MHz, CDCl_3): δ 190.74, 164.11, 131.96, 129.83, 114.72, 77.19, 76.98, 76.77, 68.11, 33.28, 30.15, 28.85, 24.97, 6.78.

ESI/TOF-MS: 355.0 $[\text{M}+\text{Na}]^+$

Diethyl 4-((E)-4-((E)-3,5-bis((6-chlorohexyl)oxy)styryl)styryl)benzylphosphonate (1-4)



Compound **P2** (5.41 g, 11.267 mmol) was added to a dry 250 mL round bottom flask which was subsequently evacuated and backfilled with argon. Dry THF (75 mL) was added and the

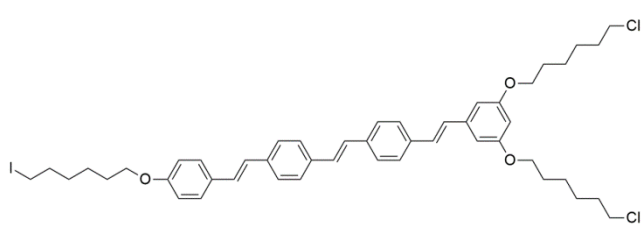
vessel was cooled to 0 °C. In a separate dry vessel, sodium *tert*-butoxide (920 mg, 9.58 mmol) was dissolved in dry THF (20 mL). The solution of sodium *tert*-butoxide was slowly added to **P2** via syringe. Intermediate **1-2** (3.52 g, 9.39 mmol) was added to a third dry vessel, dissolved with 25 mL dry THF, and added to the reaction vessel slowly via syringe. The reaction was allowed to proceed under inert atmosphere for 16 hours at room temperature. Upon completion of the reaction, the contents were partitioned between ethyl acetate and brine. The aqueous layer was washed with three portion of ethyl acetate. The organic layers were combined, washed with two portions of water, dried over MgSO_4 and concentrated by rotary evaporation. The product was purified by column chromatography (1:6 ethyl acetate: hexanes, $r_f = 0$ and 1:1:1 ethyl acetate: dichloromethane: hexanes, $r_f = 0.25$) to afford a green semisolid (3.0 g, 45%).

^1H NMR (400 MHz, CD_2Cl_2): δ 7.46-7.51 (m, 6H), 7.30 (dd, $J = 8.3, 2.5$ Hz, 2H), 7.09 (s, 2H), 7.05 (d, $J = 4.7$ Hz, 2H), 6.66 (d, $J = 2.2$ Hz, 2H), 6.38 (m, 1H), 3.97-4.07 (m,

8H), 3.56 (t, $J = 6.7$ Hz, 4H), 3.19 (s, 1H), 3.14 (s, 1H), 1.82 (m, 8H), 1.52 (m, 8H), 1.26 (t, $J = 7.1$ Hz, 6H)

^{13}C NMR (126 MHz, CDCl_3): δ 160.40, 139.24, 136.72, 136.53, 135.97, 130.08, 128.63, 128.13, 126.86, 126.79, 126.63, 105.14, 100.97, 67.81, 62.19, 44.99, 32.51, 29.13, 26.64, 25.44, 16.35

1,3-bis((6-chlorohexyl)oxy)-5-((E)-4-((E)-4-((E)-4-((6-iodohexyl)oxy)styryl)styryl)styryl)benzene (1-5)



Intermediate **1-4** (2.75 g, 3.73 mmol) was added to a dry 100 mL round bottom flask which was subsequently evacuated and backfilled with argon.

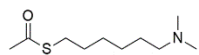
Dry THF (30 mL) was added and the vessel was cooled to 0 °C. In a separate dry vessel, sodium *tert*-butoxide (366 mg, 3.81 mmol) was dissolved in dry THF (10 mL). The solution of sodium *tert*-butoxide was slowly added to **1-4** via syringe. Intermediate **1-3** (1.2 g, 9.39 mmol) was added to a third dry vessel, dissolved with 10 mL dry THF, and added to the reaction vessel slowly via syringe. The reaction was allowed to proceed under inert atmosphere for 6 hours at room temperature. Upon completion of the reaction, the contents were partitioned between ethyl acetate and brine. The aqueous layer was washed with three portion of ethyl acetate. The organic layers were combined, washed with two portions of water, dried over MgSO_4 and concentrated by rotary evaporation. The product was purified by

column chromatography (dichloromethane, $r_f = 0.4$) to afford a green solid (2.9 g, 88%).

^1H NMR (400 MHz, CD_2Cl_2): δ 7.55 – 7.43 (m, 10H), 7.14 – 6.86 (m, 8H), 6.66 (d, $J = 2.2$ Hz, 2H), 6.38 (m, 1H), 3.99 (m, 6H), 3.56 (t, $J = 6.7$ Hz, 4H), 3.21 (t, $J = 7.0$ Hz, 2H), 1.77-1.90 (m, 12H), 1.48-1.57 (m, 12H)

^{13}C NMR (126 MHz, CDCl_3): δ 160.43, 158.84, 139.27, 137.10, 136.85, 136.46, 136.19, 129.98, 128.66, 128.59, 128.29, 128.21, 127.82, 127.75, 126.92, 126.86, 126.84, 126.59, 126.04, 114.72, 105.16, 101.00, 67.83, 67.79, 45.03, 33.41, 32.55, 30.28, 29.17, 29.09, 26.68, 25.47, 25.08, 6.99.

S-(6-(dimethylamino)hexyl) ethanethioate (**1-6**)



To a dry 250 mL round bottom flask under inert atmosphere was added 6-(dimethylamino)hexane-1-ol (2.64 g, 18.2 mmol) and 100 mL of dry THF. After cooling this reaction vessel to -78 °C, *n*-butyl lithium (17.34 mmol) was added dropwise via syringe as a 1.6 M solution in hexane. The reaction was allowed to proceed for five minutes and then the vessel was warmed to 0 °C. In a separate flask, *p*-toluenesulfonyl chloride (3.37 g, 17.69 mmol) was dissolved in 20 mL of dry THF under inert atmosphere. This solution was cooled to 0 °C and transferred to the reaction vessel via cannula. The reaction was allowed to proceed for one hour at room temperature. Upon completion, the reaction mixture was concentrated under reduced pressure by rotary evaporation. To this mixture was added potassium thioacetate (2.08 g, 17.69 mmol) and DMF (50 mL). The resulting solution was transferred to a 100 mL round bottom flask equipped with a reflux

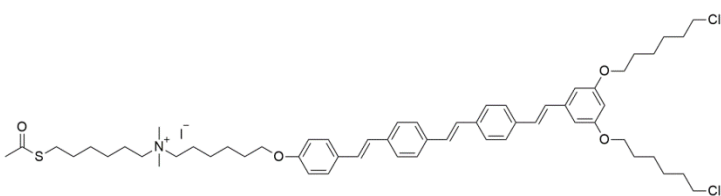
condenser and was refluxed under inert atmosphere for two days. After cooling to room temperature, the contents of the reaction were partitioned between ethyl acetate and 2 M lithium chloride solution. The aqueous layer was separated and washed with another portion of ethyl acetate. The organic layers were combined and subsequently washed five times with 2 M lithium chloride solution followed by once with water. The organic layer was dried over MgSO₄ and concentrated by rotary evaporation to yield a mixture of reddish liquid and solid. Two portions of 10 mL hexanes were added to this mixture, decanted, and concentrated to afford the product as a pale reddish oil.

¹H NMR (400 MHz, CD₂Cl₂): δ 2.84 (t, *J* = 7.3 Hz, 2H), 2.29 (s, 3H), 2.21 (t, *J* = 7.3 Hz, 2H), 2.16 (s, 6H), 1.25-1.59 (m, 8H)

¹³C NMR (126 MHz, CDCl₃): δ 195.85, 59.53, 45.21, 30.57, 29.40, 29.00, 28.67, 27.30, 26.90

ESI/TOF-MS: 204.1 [M+H]⁺

6-(acetylthio)-N-(6-(4-((E)-4-((E)-4-((E)-3,5-bis((6-chlorohexyl)oxy)styryl)styryl)styryl)phenoxy)hexyl)-N,N-dimethylhexan-1-aminium iodide (1-7)



A 25 mL round bottom flask was flame dried and cooled under inert atmosphere. Intermediates **1-5** (700 mg,

0.796 mmol) and **1-6** (350 mg, 1.72 mmol) were added to the reaction vessel and dissolved in 12 mL dry THF. The reaction was heated 55 °C and allowed to proceed

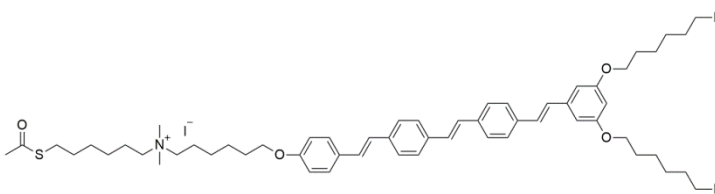
for two days under inert atmosphere. Following completion of the reaction, the volatiles were removed under reduced pressure by rotary evaporation. The resulting green solid was washed a number of times with hexane to afford the pure product (810 mg, 0.748 mmol, 94%)

^1H NMR (400 MHz, CD_2Cl_2): δ 7.55 – 7.40 (m, 10H), 7.13 – 6.86 (m, 8H), 6.66 (d, J = 2.2 Hz, 2H), 6.38 (m, 1H), 3.99 (m, 6H), 3.49-3.60 (m, 8H), 3.31-3.37 (m, 6H), 2.84 (t, J = 7.3 Hz, 2H), 2.32 (s, 3H), 1.42-1.89 (m, 32H)

^{13}C NMR (126 MHz, CDCl_3): δ 198.41, 160.41, 139.26, 136.48, 130.08, 128.64, 128.58, 128.25, 128.07, 127.76, 127.71, 126.89, 126.84, 126.81, 126.79, 126.57, 126.16, 114.76, 114.72, 109.99, 105.14, 67.82, 67.53, 64.28, 51.36, 45.00, 32.51, 30.68, 29.18, 29.13, 28.93, 28.63, 28.59, 27.97, 26.64, 25.89, 25.70, 25.47, 25.43, 25.41, 22.76, 22.52.

ESI/TOF-MS: 954.5 $[\text{M}]^+$

6-(acetylthio)-N-(6-(4-((E)-4-((E)-4-((E)-3,5-bis((6-iodohexyl)oxy)styryl)styryl)styryl)phenoxy)hexyl)-N,N-dimethylhexan-1-aminium iodide (1-8)



A 25 mL two-neck flask was fitted with a reflux condenser and flame-dried under inert atmosphere. Intermediate **1-7**

(400 mg, 0.369 mol), sodium iodide (1.73 g, 11.5 mmol), and 12.5 mL of acetone were added to the reaction vessel. The mixture was refluxed under inert atmosphere for three days. After cooling to room temperature, the contents of the reaction were

partitioned between dichloromethane and brine. The aqueous phase was removed and the organic phase was washed with two more portions of brine followed by one of water. The organic phase was dried over MgSO_4 and concentrated under reduced pressure by rotary evaporation. The resulting green solid was dissolved in minimal dichloromethane and precipitated into diethyl ether. The solids were collected by centrifugation and the supernatant was decanted. Residual volatiles were removed under reduced pressure and the desired product was afforded as a green solid (455 mg, 0.359 mmol, 97%).

^1H NMR (400 MHz, CD_2Cl_2): δ 7.55 – 7.40 (m, 10H), 7.13 – 6.86 (m, 8H), 6.66 (d, J = 2.2 Hz, 2H), 6.38 (m, 1H), 3.99 (m, 6H), 3.46-3.60 (m, 4H), 3.31-3.37 (m, 6H), 3.22 (t, J = 6.9 Hz, 4H), 2.84 (t, J = 7.3 Hz, 2H), 2.32 (s, 3H), 1.41-1.93 (m, 32H)

^{13}C NMR (126 MHz, CDCl_3) δ 196.71, 160.30, 158.72, 158.59, 139.20, 136.94, 136.74, 136.39, 136.18, 136.13, 130.03, 128.57, 128.48, 128.15, 127.99, 127.78, 127.70, 127.66, 126.84, 126.78, 126.75, 126.51, 126.06, 114.67, 105.12, 103.73, 100.96, 67.82, 67.55, 64.35, 64.30, 51.19, 49.40, 49.23, 49.05, 48.88, 48.71, 33.31, 30.53, 30.15, 29.58, 29.08, 28.98, 28.86, 28.57, 27.90, 25.84, 25.58, 25.43, 24.99, 22.60, 22.39, 6.97.

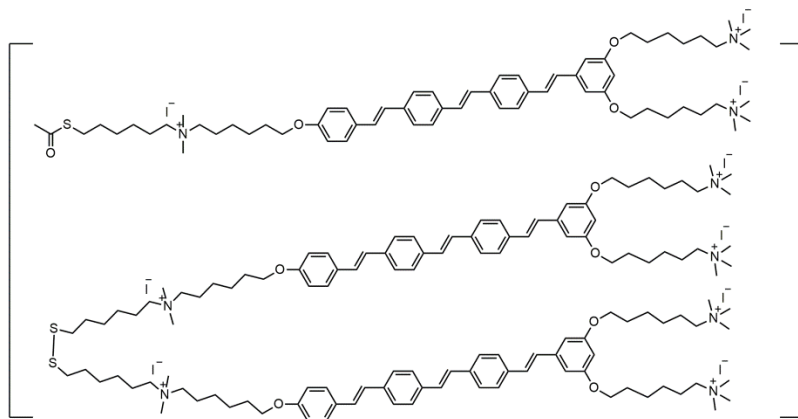
ESI/TOF-MS: 1138.4 [M-I]⁺

Inseparable mixture of

6,6'-((5-((E)-4-((E)-4-((E)-4-((6-((6-(acetylthio)hexyl)dimethylammonio)hexyl)oxy)styryl)styryl)styryl)-1,3-phenylene)bis(oxy))bis(N,N,N-trimethylhexan-1-aminium) iodide (**1-9**)

and

6,6',6'',6'''-((((1E,1'E)-(((1E,1'E)-(((1E,1'E)-((((disulfanediy)bis(hexane-6,1-diyl))bis(dimethylammonionediyl))bis(hexane-6,1-diyl))bis(oxy))bis(4,1-phenylene))bis(ethene-2,1-diyl))bis(4,1-phenylene))bis(ethene-2,1-diyl))bis(4,1-phenylene))bis(ethene-2,1-diyl))bis(benzene-5,3,1-triyl))tetrakis(oxy)) tetrakis(N,N,N-trimethylhexan-1-aminium) iodide (**1-10**)

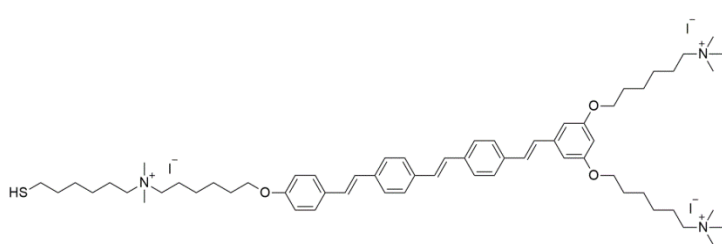


A 10 mL gas-tight reaction tube was flame dried and cooled under argon atmosphere. Intermediate **1-8** (350 mg, 0.276 mmol), dry

tetrahydrofuran (3 mL), and methanol (0.5 mL) were added to this vessel and stirred under argon until **10a** was completely dissolved. Trimethylamine was added via syringe as a 3.2 M solution in methanol (0.43 mL, 1.38 mmol). The screw-cap was fitted and the mixture heated to 40 °C overnight at which point a yellow precipitate was observed. Additional methanol was added (~1mL) until the solid was completely dissolved. The mixture was allowed to stir for an additional 12 hours at 40 °C. Tetrahydrofuran, methanol, and trimethylamine were removed under reduced

pressure. The resulting green semisolid was dissolved in a minimal amount of methanol and precipitated into diethyl ether to afford a yellow solid. ^1H NMR analysis revealed a ~1:1 mixture of compounds **1-9** and **1-10**.

6,6'-((5-((E)-4-((E)-4-((E)-4-((6-((6-mercaptohexyl)dimethylammonio)hexyl)oxy)styryl)styryl)styryl)-1,3-phenylene)bis(oxy))bis(N,N,N-trimethylhexan-1-aminium) iodide (**1-11**, "COE-SH")



Intermediates **1-9** and **1-10** were both converted to the final product through two steps to remove the acetate protecting

group and reduce the disulfide bonds.

Step 1: 104 mg of the **1-9/1-10** mixture was added to a 50 mL round bottom flask. 15 mL of methanol and 5 mL of dichloromethane were added and the mixture was stirred until all solids were dissolved. 2 mL of concentrated hydrochloric acid was slowly added to the reaction vessel. The mixture was heated to 35 °C overnight. After cooling to room temperature, the mixture was slowly added to 30 mL diethyl ether in a 50 mL centrifuge tube. The yellow precipitate was centrifuged and the supernatant decanted. The solid was dissolved in methanol and precipitated in diethyl ether two additional times (99 mg recovered).

Step 2: 56 mg of the yellow solid from Step 1 and dithioerythritol (14mg, 0.09 mmol) were added to a 5 mL round bottom which was subsequently evacuated and

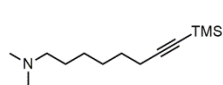
backfilled with argon five times. To this flask was added 2.5 mL of a 16:1 mixture of methanol and triethylamine via syringe. The flask was fitted with a reflux condenser and the mixture was refluxed for 18 hours. After cooling to room temperature, the mixture was added to 20 mL of diethyl ether. The yellow precipitate was collected by centrifuging and decanting. The solid was dissolved in methanol and precipitated in diethyl ether three additional times.

^1H NMR (500 MHz, Methanol- d_4) δ 7.58 – 7.46 (m, 10H), 7.21 – 6.99 (m, 6H), 6.91 (d, J = 8.2 Hz, 2H), 6.73 (d, J = 2.4 Hz, 2H), 6.39 (s, 1H), 4.08 – 4.00 (m, 6H), 3.44 – 3.32 (m, 8H), 3.14 (d, J = 3.3 Hz, 18H), 3.07 (s, 6H), 2.52 (t, J = 7.0 Hz, 2H), 1.90 – 1.23 (m, 58H).

^{13}C NMR (126 MHz, DMSO- d_6) δ 160.48, 158.85, 139.56, 137.25, 137.03, 136.70, 136.41, 130.48, 130.07, 128.97, 128.81, 128.51, 128.29, 128.12, 127.38, 127.31, 127.00, 126.13, 115.14, 105.41, 101.18, 67.83, 67.80, 65.70, 63.35, 52.65, 52.62, 50.41, 37.99, 28.92, 28.72, 27.67, 25.94, 25.83, 25.55, 25.52, 22.49, 22.46, 22.12.

ESI/TOF-MS: 543.8 [M-2I] $^{2+}$, 320.2 [M-3I] $^{3+}$

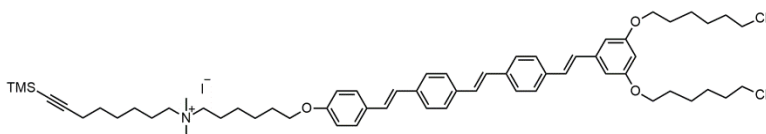
N,N-dimethyl-8-(trimethylsilyl)oct-7-yn-1-amine (**1-12**)



To a flame-dried 25 mL round bottom flask (A) equipped with a stir bar was added 6-(dimethylamino)hexane-1-ol (440 mg, 3.03 mmol) and anhydrous THF (8 mL) under inert atmosphere. The vessel was cooled to -78 °C and *n*-butyl lithium (1.6 M in hexane, 1.9 mL, 3.03 mmol) was added slowly. The reaction was maintained at -78 °C for 15 minutes, at which point *p*-toluenesulfonyl chloride (590 mg, 3.1 mmol) was added as a solution in THF (5 mL). The vessel was

allowed to warm room temperature slowly over 1 hour. Concurrently, a separate flame-dried 50 mL round bottom flask (B) equipped with a stir bar was charged with trimethylsilylacetylene (313 mg, 3.19 mmol) and anhydrous THF (8 mL) under inert atmosphere. This vessel was cooled to -78 °C and *n*-butyl lithium (1.6 M in hexane, 1.9 mL, 3.03 mmol) was added slowly. After 5 minutes, vessel B was also allowed to warm to room temperature slowly. After 1 hour, both vessels were cooled to 0 °C and the contents of vessel A were slowly transferred via cannula to vessel B. Vessel B was then moved to an oil bath and heated to 45 °C for 16 hours under inert atmosphere. After cooling to room temperature, the contents of the reaction were partitioned between water and diethyl ether. The organic layer was collected and the aqueous layer was extracted with five additional portions of diethyl ether. The organic layers were combined, dried over MgSO₄, filtered, and concentrated under reduced pressure to afford a light amber oil (300 mg, 44%). The product was used without further purification.

N-(6-(4-((*E*)-4-((*E*)-4-((*E*)-3,5-bis((6-chlorohexyl)oxy)styryl)styryl)styryl)phenoxy)hexyl)-*N,N*-dimethyl-8-(trimethylsilyl)oct-7-yn-1-aminium iodide (**1-13**)

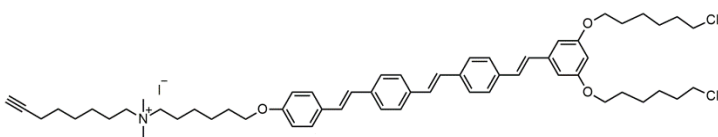


To a 5 mL round bottom flask equipped with a stir bar was added **1-5** (130 mg, 0.148), **1-12** (53 mg, 0.235 mmol), and anhydrous THF (2.5 mL). The reaction vessel was sealed and heated to 55 °C for 3 days. After cooling to room

temperature, volatiles were removed under reduced pressure. The green semi-solid residue was dissolved in DCM with a small amount of methanol and precipitated into diethyl ether in a centrifuge tube. The contents were centrifuged and the supernatant discarded. The resulting green solid was washed multiple times with diethyl ether to afford the pure product (155 mg, 95 %).

^1H NMR (400 MHz, Chloroform-*d*) δ 7.53 – 7.42 (m, 10H), 7.10 – 6.86 (m, 8H), 6.64 (d, J = 2.2 Hz, 2H), 6.37 (t, J = 2.2 Hz, 1H), 3.97 (t, J = 6.3 Hz, 6H), 3.55 (t, J = 6.7 Hz, 6H), 3.49 – 3.43 (m, 4H), 3.37 – 3.26 (m, 6H), 2.22 (t, J = 6.3 Hz, 2H), 1.76-1.68 (m, 16H), 1.65 – 1.43 (m, 16H) 0.13 – 0.09 (m, 9H).

N-(6-(4-((*E*)-4-((*E*)-4-((*E*)-3,5-bis((6-chlorohexyl)oxy)styryl)styryl)styryl)phenoxy)hexyl)-*N,N*-dimethyloct-7-yn-1-aminium iodide (**1-14**)



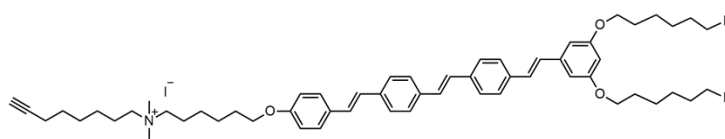
To a 5 mL round bottom flask equipped with a stir bar and reflux condenser was added **1-**

13 (80 mg, 0.072 mmol), potassium carbonate (3 mg, 0.0217 mmol), and methanol (2.5 mL). The mixture was heated to reflux for 16 hours. After cooling to room temperature, volatiles were removed under reduced pressure. The residue was dissolved in DCM and subsequently extracted with water 3 times. The organic layer was dried over MgSO₄, filtered, and partially concentrated (to ~5 mL) under reduced pressure. The solution was added to a 20 mL of diethyl ether in a centrifuge tube. The solids were recovered by centrifugation and the supernatant discarded. The

greenish solid was washed multiple times with diethyl ether to afford the pure product (70 mg, 94%).

^1H NMR (500 MHz, Methanol- d_4) δ 7.60 – 7.48 (m, 10H), 7.20 – 6.90 (m, 8H), 6.73 (d, J = 2.1 Hz, 2H), 6.39 (t, J = 1.9 Hz, 1H), 4.04 (t, J = 6.2 Hz, 6H), 3.55 – 3.34 (m, 14H), 3.10 – 3.08 (m, 1H), 2.52 (t, J = 7.0 Hz, 2H), 1.81-1.68 (m, 16H), 1.66 – 1.58 (m, 8H), 1.53 – 1.46 (m, 8H).

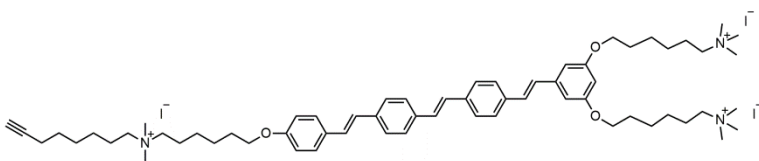
N-(6-(4-((*E*)-4-((*E*)-4-((*E*)-3,5-bis((6-iodohexyl)oxy)styryl)styryl)styryl)phenoxy)hexyl)-*N,N*-dimethyloct-7-yn-1-aminium iodide (**1-15**)



To a 10 mL round bottom flask equipped with a stir bar and fitted with a reflux condenser was added **1-14** (30 mg, 0.029 mmol), sodium iodide (109 mg, 0.726 mmol), and acetone (6 mL). The mixture was heated to reflux under inert atmosphere for 3 days. After cooling to room temperature, the contents were portioned between DCM and water. The organic layer was collected, extracted two additional times with water, dried over MgSO_4 , filtered, and concentrated under reduced pressure. The resulting greenish solid (35 mg, 99%) was used without further purification.

^1H NMR (500 MHz, Methanol- d_4) δ 7.61 – 7.48 (m, 10H), 7.21 – 6.91 (m, 8H), 6.73 (d, J = 2.1 Hz, 2H), 6.39 (t, J = 1.9 Hz, 1H), 4.02 (t, J = 6.2 Hz, 6H), 3.49 – 3.34 (m, 10H), 3.21 (t, J = 6.9 Hz, 4H), 3.10 – 3.08 (m, 1H), 2.52 (t, J = 7.0 Hz, 2H), 1.79-1.69 (m, 16H), 1.66 – 1.41 (m, 16H).

6,6'-((5-((E)-4-((E)-4-((E)-4-((6-(dimethyl(oct-7-yn-1-yl)ammonio)hexyl)oxy)styryl)styryl)styryl)-1,3-phenylene)bis(oxy))bis(N,N,N-trimethylhexan-1-aminium) iodide (**1-16**, "COE-CH")



To a 5 mL round bottom flask equipped with a stir bar was added **1-15** (35 mg,

0.029 mmol), trimethylamine (3.2 M in methanol, 0.05 mL, 0.16 mmol), anhydrous THF (2.5 mL) and a small amount of chloroform (~0.5 mL). The vessel was sealed and stirred at room temperature overnight. A small amount of methanol was added (~ 1 mL) to dissolve the precipitates that had formed and the mixture was stirred for an additional 1 day at room temperature. The solution was diluted with a sufficient amount of methanol to dissolve the precipitates. The solution was then added to 20 mL of diethyl ether in a centrifuge tube. Precipitates were centrifuged and the supernatant was discarded. The product was obtained as a greenish solid (37 mg, 96%) following multiple washes with diethyl ether.

¹H NMR (500 MHz, DMSO-d₆) δ 7.71 – 7.40 (m, 10H), 7.40 – 7.03 (m, 6H), 6.93 (d, J = 8.3 Hz, 2H), 6.82 – 6.73 (m, 2H), 6.44 – 6.34 (m, 1H), 4.03 – 3.95 (m, 6H), 3.37 – 3.24 (m, 8H), 3.12 – 3.04 (m, 18H), 3.01 (s, 6H), 2.76 (t, J = 2.7 Hz, 1H), 2.15 (td, J = 6.9, 2.6 Hz, 2H), 1.77 – 1.30 (m, 32H).

¹³C NMR (126 MHz, DMSO-d₆) δ 160.49, 158.86, 137.28, 136.43, 130.10, 128.84, 128.83, 128.53, 128.31, 128.14, 127.39, 127.32, 127.01, 126.15, 115.16, 105.43, 101.12, 84.90, 71.77, 67.82, 65.66, 63.37, 52.60, 50.40, 45.88, 32.47, 28.92, 28.12, 28.07, 26.51, 25.95, 25.71, 25.56, 25.31, 22.50, 22.14, 18.04.

Chapter 2: Structure-Property Relationships Pertaining to COE Antimicrobial and Membrane-Permeabilizing Effects

2.1 Introduction

The asymmetric outer membrane (OM) of gram-negative bacteria presents a formidable barrier to diffusion of polar and nonpolar molecules alike. Lipopolysaccharide (LPS), which generally accounts for ~75% of the outer leaflet in the OM,^{81, 82} is particularly well suited for preventing hydrophobic compounds from entering the cell.^{83, 84} Compounds that are able to transverse the LPS must then pass through the hydrophobic bilayer domain of the OM in order to reach the periplasmic space. This exceptional barrier, which allows gram-negative bacteria to withstand harsh environmental conditions, has important ramifications in topics including whole-cell biocatalysis,^{11, 12} genetic engineering,⁸⁵ bioenergy production,^{86, 87} and antibiotic resistance.^{24, 25}

Amphiphilic compounds are routinely used to increase the permeability of various molecules across the gram-negative OM.^{85, 88} Mismatches in spontaneous curvature, with surfactants possessing positive curvature and membrane lipids possessing slightly-negative curvature,⁸⁹⁻⁹¹ can result in disruption, poration, or micellation of membranes.^{92, 93} While some level of these effects can be tolerated by a cell, sufficient perturbation eventually results in cell death or lysis. The cell-destroying and cell-permeabilizing effects of surfactants are thus based on the same underlying mechanism of membrane disruption, albeit to differing degrees. This has

obvious consequences in situations where it is desirable to permeabilize the OM without killing the cells, such as the reuse of whole-cell biocatalysts.^{94, 95}

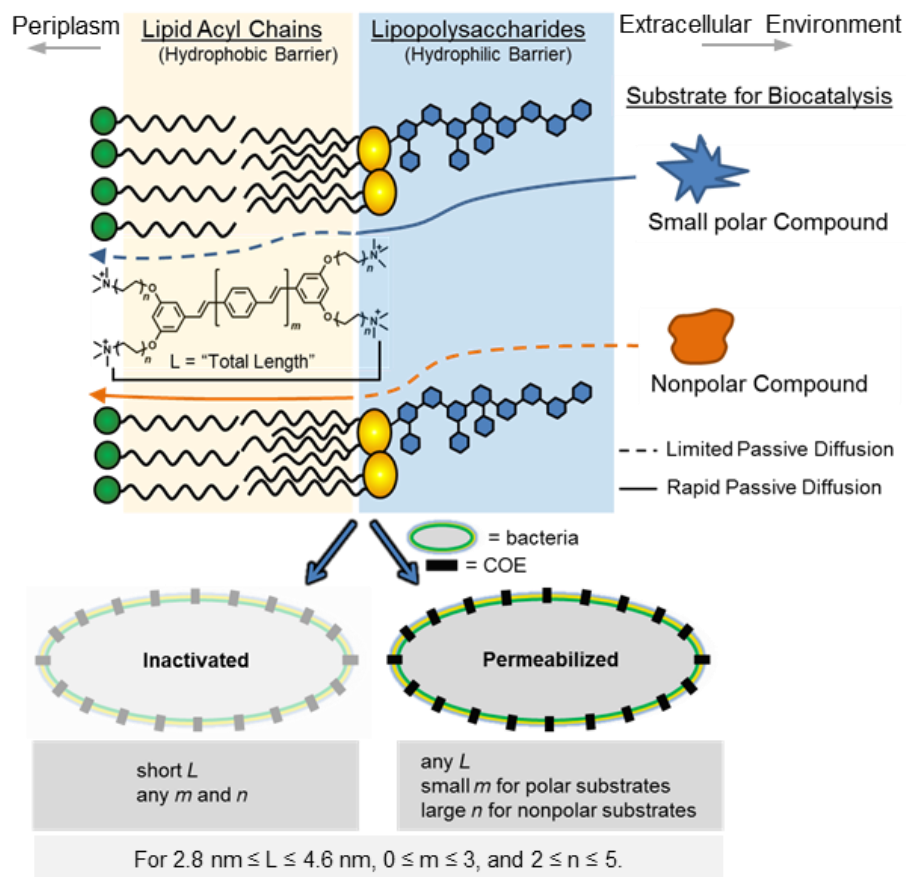


Figure 2-1 The influence of COE molecular structure on inactivation or substrate-dependent permeabilization of bacteria. Parameters L , m , and n determine the nature of COE-induced effects within the constraints set by the series of compounds used in this study.

Membrane-intercalating COEs, although also amphiphilic, may have effects on membranes that differ from those of surfactants due to their differential distribution of polar and nonpolar domains. These COEs generally possess little-to-no intrinsic curvature and span the entire membrane rather than interdigitating into a single leaflet. Our group has demonstrated that the addition of COEs to bacteria can increase membrane permeability at concentrations well below what is required to

inhibit growth.⁴⁸ Furthermore, we have shown that certain COEs are able to increase the stability of microbial membranes during bio-butanol production.⁹⁶ The observation that the modulation of membrane permeability/stability may be functionally different from antimicrobial action presents the possibility for tuning membrane properties without reducing the viability of cells. Previous COEs developed in our group tend to show correlation between increasing permeability and inhibiting bacterial growth,⁷³ although the relationship is not expected to be causative. The focus of this chapter will be the design, synthesis, and application of a homologous series of COEs with the intent to decouple antimicrobial and permeabilizing effects. Furthermore, the structural components of COEs that govern these different effects will be elucidated (Figure 2-1). Specifically, the effects of parameters m and n (within the bounds set by the compounds selected for this study) will be shown to dictate permeability for substrates of different polarities. Parameter L will be shown to be inversely correlated to the antimicrobial activity but a lower limit of L will be described (this limit will be overcome by other structural modifications in Chapter 5).

2.2 Design and Synthesis of a Series of COEs for Probing Structure-Property Relationships

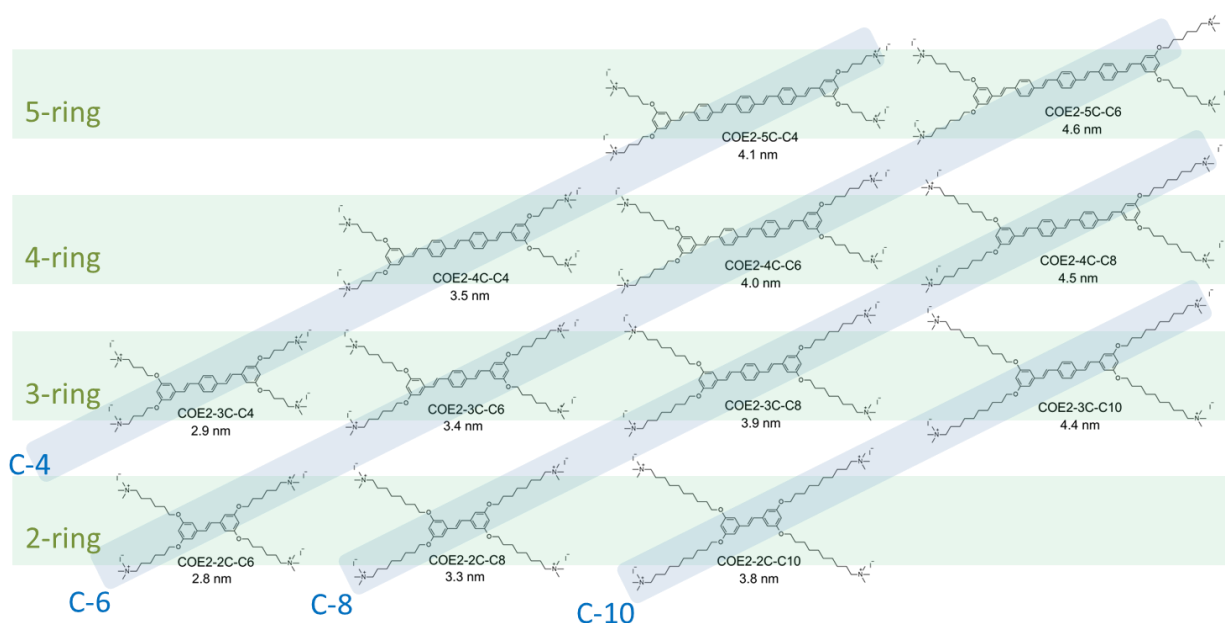


Figure 2-2 Homologous series of COEs designed and synthesized for the purpose of elucidating structure-property relationships related to permeability and antimicrobial activity. Structures are grouped in rows (green) according to number of aromatic rings and along the bottom-left to top-right diagonal (blue) according to number of carbons in the pendant chains (blue). Structures in the same column have similar length (as measured by the distance between ammonium groups on opposite ends of the molecule).

Prior to this work, phenylenevinylene-based COEs developed by our group contained between two and five aromatic rings with two pendant chains of six carbons each on either side (connected via 4-amino- or 3,5-dialkoxy- linkages to the core). The general synthetic route for the compounds described in this chapter is derived from previously-reported methods by our group.^{38, 39, 44} Figure 2-2 includes four of these previously-described structures across the “C-6” diagonal. The other eight COEs in Figure 2-2 are structural analogues that were synthesized specifically to determine how changes in the number of core repeat units, pendant chain

lengths, and overall length of the compound affect interactions with membranes. COEs are grouped in rows based on number of aromatic rings and columns based on similar total length. Compounds with the same pendant chain length fall along the same diagonal from bottom-left to top-right. Naming convention for these structures is as follows: "COE2" is a reference to a prior convention within our group where this class of COEs contains 3,5-dialkoxy linkages between the core and pendant chains; "#C" has been used in our group to represent the core of the compound where # indicates the number of aromatic rings; "C#" describes the pendant chains where # represents the number of carbons in each of the equivalent four pendants. For example, COE2-3C-C8 contains 3,5-dialkoxy linkages between a core of three rings and pendants of eight carbons.

A general overview of the synthetic route to all twelve COEs used in this study is depicted below in Figure 2-3. Note that the letters "a", "b", "c", and "d" in the names of intermediates correspond to values of n equal to 2, 3, 4, and 5 respectively. The first step in the synthesis of each structure was the reaction of 3,5-dihydroxybenzaldehyde with a dibromoalkane of the desired linker length (four, six, eight, or ten carbons). In the case of the COEs with two rings in the core, the resulting benzaldehyde derivatives **2-1** were converted to the styryl derivatives **2-3** via the Wittig Reaction and subsequently coupled via metathesis using Grubbs Catalyst 2nd Generation (**2-4**). The bromides of **2-4** were converted to iodides (**2-5**) with sodium iodide in refluxing acetone. In the case of COEs with greater than 2 rings in the core, the benzaldehyde derivatives **2-1** were converted from bromides to the analogous iodides **2-2**. For three-ring and four-ring compounds, intermediates **2-**

2 (2 equivalents) were reacted with phosphonates **P1** or **P2** respectively via the Horner-Wadsworth-Emmons (HWE) reaction. In the case of COEs with five rings in the core, one equivalent of the benzaldehyde **2-2** was reacted with phosphonate **P1**, yielding intermediates **2-8** which were subsequently subjected to another HWE to afford intermediate **2-9**. Intermediates **2-5**, **2-6**, **2-7**, and **2-9** were reacted with trimethylamine to afford the final products. Detailed synthetic methods are presented in Section 2.9.

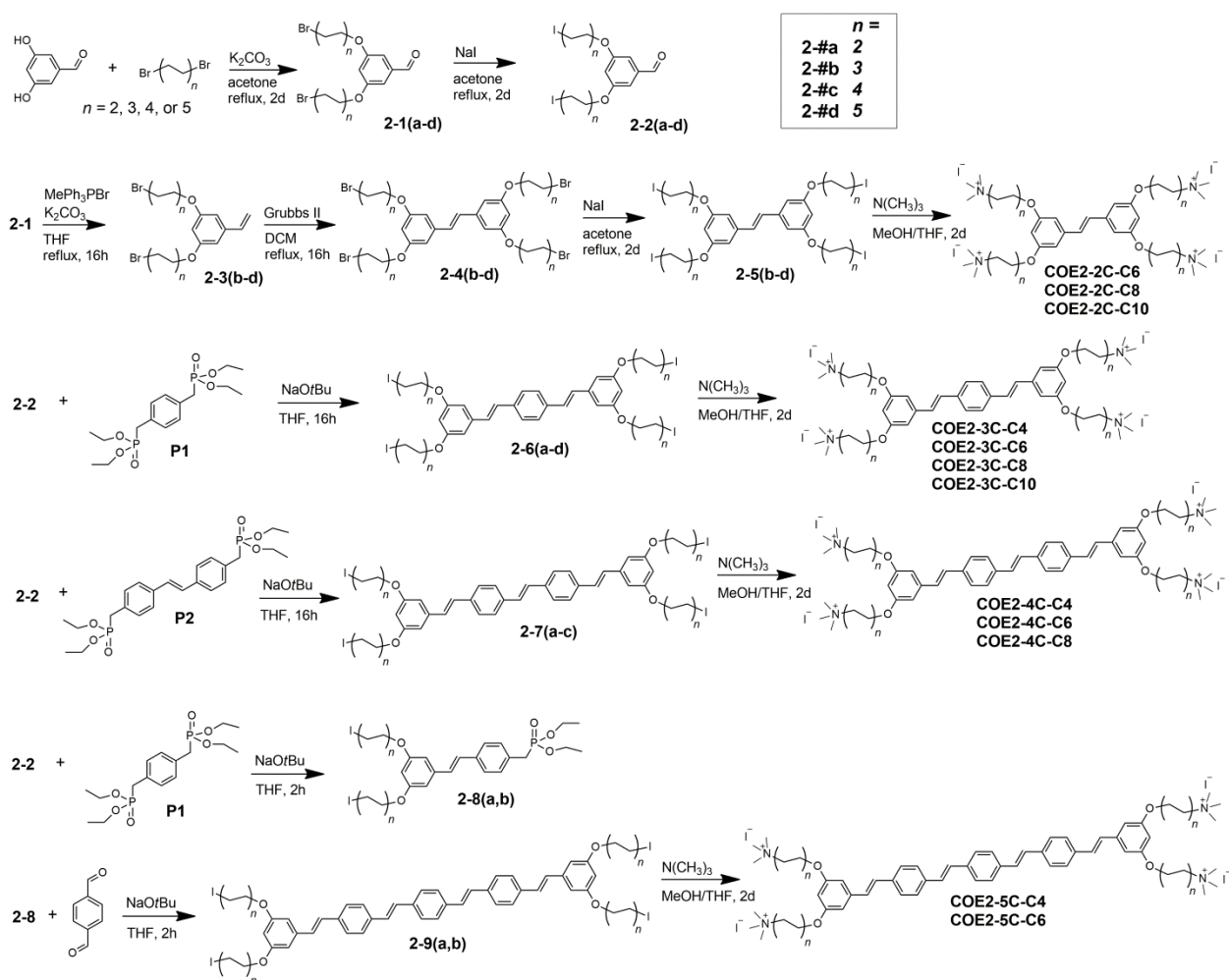


Figure 2-3 Synthetic route used to access COEs with variable core and alkyl chain lengths.

2.3 Effect of COE Structure on the Ability to Associate with *E. coli* cells

In order to assess the effects of COEs on bacterial cells, it was first necessary to determine the extent to which chemical structure affects the ability of COEs to interact with microbial membranes. Previous investigations in our group have demonstrated that shorter COEs, such as COE2-2C-C6, have a significantly-reduced propensity to intercalate into membranes when compared to longer COEs.⁷³ For the purpose of this study, solutions of all twelve COEs were made in 50 mM PBS buffer (10-120 μM COE). COE solutions were mixed 1:1 v/v with *E. coli* K12 suspensions in 50 mM PBS such that the final bacteria concentration was 1 OD₆₀₀. These solutions were centrifuged and the supernatant removed to a 96-well plate. Residual COE in the supernatant was determined by absorbance at the appropriate wavelength for the particular compound. The amount of COE associated with bacteria was calculated as the initial (“staining”) amount minus the residual amount.

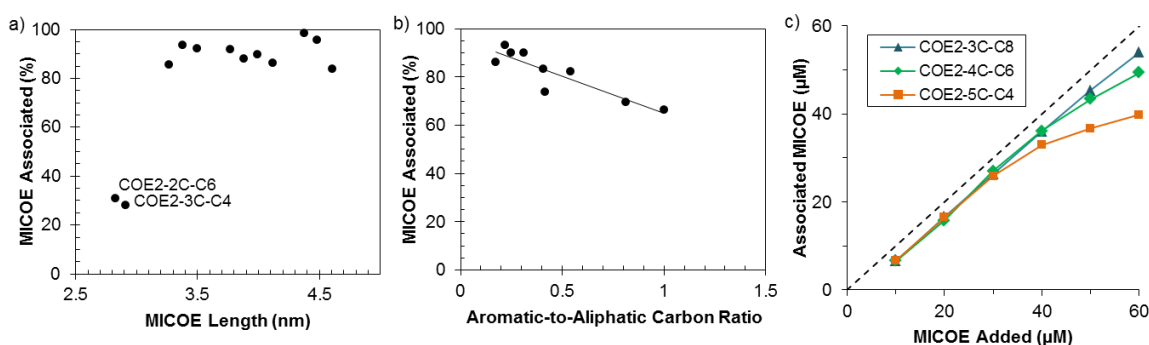


Figure 2-4 Impact of COE structure on membrane affinity. (a) Percent of the added 10 μM COE that becomes associated with bacteria as a function of COE length – of particular note is the difference between the two shortest COEs and the other ten. (b) Percent of the added 60 μM COE that becomes associated as a function of aromatic and aliphatic content. (c) Concentration of COE associated vs. COE added for three COEs of similar total length – the dashed line represents “100 associated.”

Figure 2-4a illustrates the marked effect that COE total length has on the ability of the COEs to intercalate (10 μ M COE, 1 OD₆₀₀ *E. coli* K12). The two shortest COEs, COE2-2C-C6 and COE2-3C-C4 largely remain in solution (~30% associated), while all other COEs associate with cells to a high degree (80-100% associated). This result is in agreement with previous findings.⁷³ If the concentration of COE is increased to 60 μ M per 1 OD₆₀₀ of cells, a secondary trend is observed (Figure 2-4b and Figure 2-4c) – COEs with fewer rings in the core or longer pendant alkyl chains have a higher affinity for cells than those with more rings and shorter pendants. While beyond the scope of this investigation, there is evidence that this trend may be due to aggregation of the COEs with extended conjugated cores.⁹⁷ It is conceivable that an increased propensity to aggregate reduces the driving force to intercalate, assuming that COE aggregates are unable to interact with membranes. It is worth noting that this trend is only apparent at relatively high COE concentrations, below which it appears that the association of all the COEs (excluding COE2-2C-C6 and COE2-3C-C4) approaches 100%.

2.4 Quantification of COE Effects on Lipid Ordering by Electron Paramagnetic Resonance Spectroscopy

Electron paramagnetic resonance (EPR) spectroscopy is routinely used to measure the intermolecular ordering of lipids and proteins in cell membranes or model bilayer systems.⁹⁸⁻¹⁰⁰ In much the same way that nuclear magnetic resonance (NMR) spectroscopy probes the effects of an applied field on nuclear spins, EPR can be used to understand the nature and local environment of paramagnetic species

through their response to an applied field.¹⁰¹ The unpaired electron of nitroxide radicals, such as TEMPO, were some of the earliest paramagnetic species used as EPR probes in biological systems and are still commonly used today.^{102, 103} A particularly useful feature of the nitroxide radical is the coupling between the unpaired electron and the spin-active nitrogen nucleus. This results in the splitting of the signal into three lines, the anisotropy of which can be used to determine preferential orientation or rotational motion of the radical.¹⁰⁴

In this study, we used EPR to investigate the effects that COEs have on the physical properties of model membranes – specifically, the ordering of lipids as measured by the rotational freedom of a spin probe within the membrane. Large unilamellar vesicles of *E. coli* total lipid extract and 1 mole % of the radical probe 16-DOXYL-stearic acid (16-SASL) were formed by extrusion¹⁰⁵ and subsequently stained with each of the twelve COEs. EPR spectra were used to calculate order parameter (*S*) and correlation times according to published methods (see section 6.3 for full details).¹⁰⁶⁻¹¹⁰ Figure 2-5 shows the relative COE-induced effects on lipid ordering, from which the conclusion can be made that “short” COEs decrease lipid order (negative change in *S*) while “long” COEs increase it (positive change in *S*). This trend is observed for COEs with different core lengths (Figure 2-5a) and for COEs with different alkyl chain lengths (Figure 2-5b). In fact, the only structural parameter that correlates with the changes in lipid order is the total length of the COE (see Table 2-1 in Section 2.7).

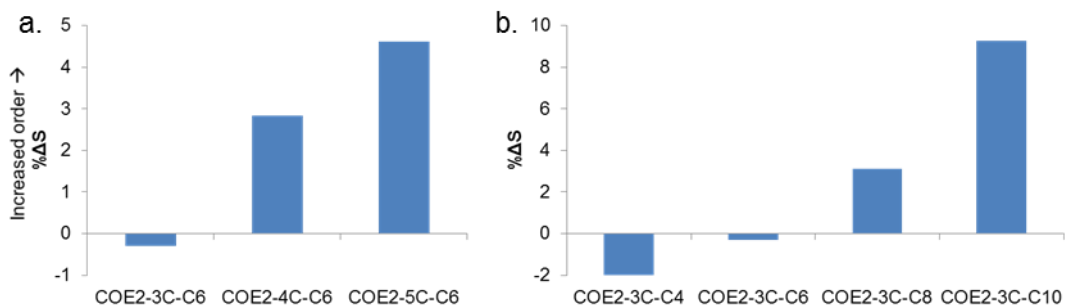


Figure 2-5 Changes in order parameter as a function of COE structure. (a) Three COEs containing different core lengths but the same alkyl chain length. (b) Four COEs with 3-ring cores but alkyl chains of increasing length.

The dependence of S on COE total length is in good agreement with the computational model previously used to describe COE interactions with membranes.⁵² Specifically, the “membrane pinching” effect of short COEs that was observed *in silico* is supported by the reduction in S determined by EPR. It bears noting that a similar trend has been observed for polar carotenoids of different lengths – induced negative strain led to reduced order, while induced positive strain increased order.¹¹⁰ Surfactants, on the other hand, generally reduce lipid order when they are added in sufficient concentration to increase membrane permeability.¹¹¹ While the extent of surfactant-mediated disordering does not seem to correlate with biocidal activity, it has been hypothesized that significant increases in lipid order is at least part of the mechanism of action of antimicrobial peptides (AMPs).¹¹²⁻¹¹⁴ Based on the relationship between COE length and lipid ordering, it appears that COEs behave more like polar carotenoids than either surfactants or AMPs.

2.5 Effect of COE Structure on Antimicrobial Properties

The structure-dependent antimicrobial properties of the twelve COEs were determined by serial broth microdilution. The minimum inhibitory concentration (MIC) is defined as the lowest concentration of compound that is required to inhibit overnight growth of liquid culture bacteria by 90%. In the case of the present study, *E. coli* K12 was used as the model organism. Due to the solubility constraints of the largest COEs, all compounds were tested in a range from 512 μM to 1 μM (log-2 dilution). The results are shown in Figure 2-6, with the COEs ordered by total length along the x-axis.

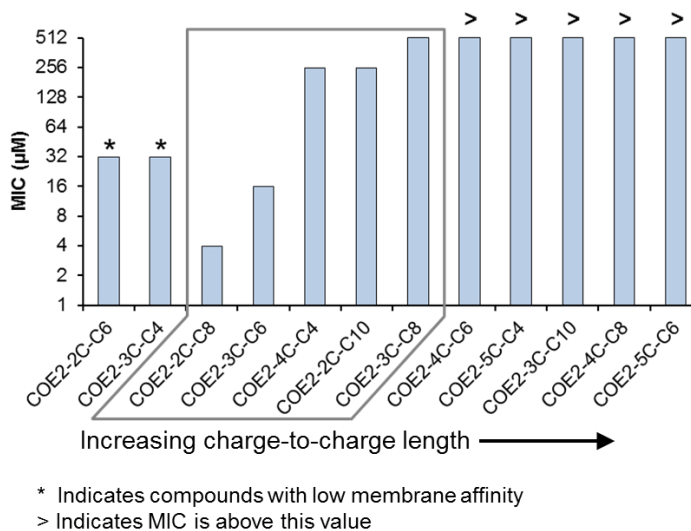


Figure 2-6 Minimum inhibitory concentration of a series of COEs against *E. coli* as a function of total length.

Previous studies of COEs with C-6 pendant chains by our group had found that shorter COEs tended to produce lower MICs.⁷³ For example, COE2-3C-C6 was shown to possess greater antimicrobial properties than COE2-4C-C6. Additionally,

this trend was only broken by the shortest compound in the C-6 pendant family, COE2-2C-C6. It was suggested that the higher-than-expected MIC for COE2-2C-C6 could be explained by its limited propensity to associate with bacteria cells. As described above in Section 2.3.1, the limited cell association of COE2-2C-C6 was confirmed and it was found that the slightly-longer COE2-3C-C4 shared this property. Both of these COEs were also found to have relatively high MICs, confirming that limited association is a likely explanation for the deviation from the length-MIC relationship.

Of the remaining 10 COEs (all of which associate with cells to a high degree), the longest five must be excluded from further analysis as their MIC values approach/exceed their limits of solubility. Within the remaining set of five COEs (bound by the box in Figure 2-6), an obvious dependence on length is observed. As previous studies in the group had only considered COEs with C-6 pendant chains, it was impossible to determine whether the core length or total length was the defining feature. It was hypothesized, however, that COEs of shorter total length would induce more severe membrane “pinching” and that this effect was responsible for the antimicrobial properties. The results presented here support this hypothesis by demonstrating that MIC correlates strongly with total length but not pendant length or core length (see Table 2-1 in Section 2.7 for summary of correlation R and significance p-values).

2.6 Effect of COE Structure on Microbial Membrane Permeability

2.6.1 ONPG Assay as a Measure of COE-mediated OM Permeability

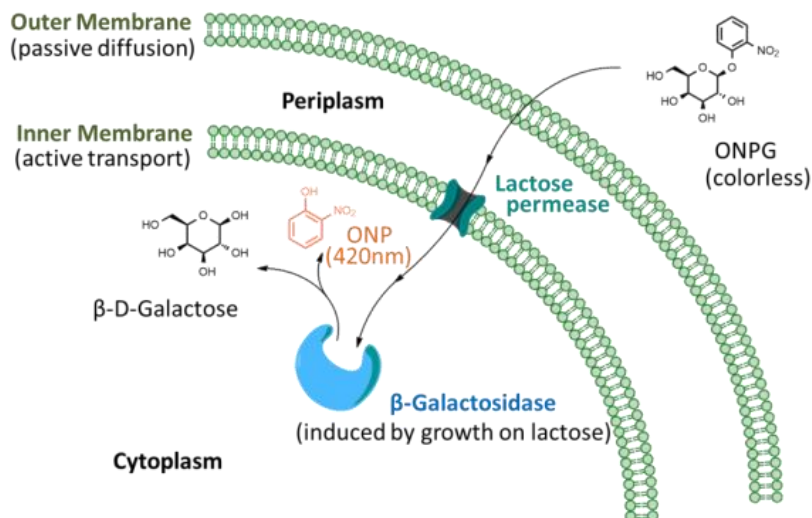


Figure 2-7 Graphical depiction of the ONPG assay used to assess COE permeabilization of the OM. Colorless ONPG traverses the OM (rate-limiting step), is transported through the IM by lactose permease, and is cleaved by β -galactosidase into β -D-galactose and ONP. OM permeability is determined by measuring the production of ONP (absorption at 420 nm).

Effects on OM permeability are routinely investigated using the well-established ONPG Assay.^{87, 115} This colorimetric assay relies on the enzymatic cleavage of colorless ortho-nitrophenyl- β -D-galactopyranoside (ONPG) into galactose and ortho-nitrophenol (ONP, $\lambda_{\text{max, absorption}} = 420 \text{ nm}$) by cytosolic β -galactosidase, a constituent of the *lac* operon. Lactose permease within the inner membrane allows for transport of ONPG from the periplasm to the cytoplasm. Permeation through the OM is the rate-limiting step and thus the rate of ONP production is directly related to OM permeability. This process is depicted in Figure 2-7 for reference.

Previous studies within our group had led to the hypothesis that COE total length, in addition to determining antimicrobial properties, determines the extent of membrane permeabilization.^{52, 73} As only C-6 pendant structures were considered, no assumptions were made about the role of core or pendant lengths independently. To probe the relationship between COE structural elements and their ability to permeabilize the OM, the ten longest COEs (i.e. those with high affinity for microbes) were tested in the ONPG assay. The results of this experiment, plotted as the ONPG turnover rate of COE-treated *E. coli* relative to an untreated control, are presented in Figure 2-8.

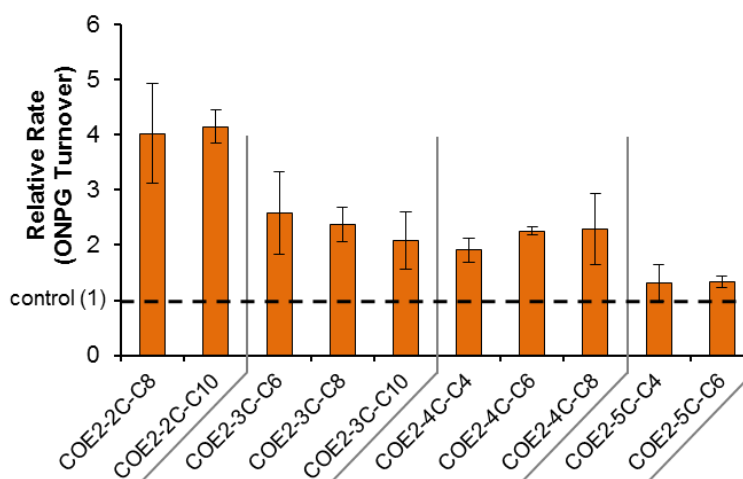


Figure 2-8 Relative ONPG turnover after treatment with 10 $\mu\text{M}/\text{OD}_{600}$ COE (grouped by core length).

Unlike the dependence of MIC on COE total length described in Section 2.5, the results of the ONPG assay suggest that membrane permeability does not correlate to this structural feature. Instead, the only structural parameter with significant effect on ONPG turnover rate was found to be the core length, with shorter cores resulting in more significant permeabilization. To highlight this trend, the relative ONPG

turnover rates in Figure 2-8 were grouped according to core length. In general, 5-ring COEs increased turnover by ~25%, 4-ring COEs increased turnover by ~100%, 3-ring COEs increased turnover by ~125%, and 2-ring COEs increased turnover by ~300%.

The decoupling of antimicrobial and membrane permeabilizing effects is exemplified by the example of COE2-2C-C10. While this compound shows the greatest increase in ONPG turnover, it has limited antimicrobial properties (MIC = 256 μ M). COE2-2C-C8 has a similar effect on permeability but a significantly lower MIC (4 μ M). COE2-3C-C6 has less impact on permeability yet is more harmful to bacteria (MIC = 16 μ M). With the ideal combination of limited antimicrobial properties and significant membrane permeabilizing ability, COE2-2C-C10 was chosen for a direct comparison against the standard permeabilizing surfactant, Triton X-100.¹¹⁶⁻¹¹⁸ ONPG turnover following the addition of different concentrations of both agents is shown in Figure 2-9. Consistent with literature,¹¹⁷ Triton X-100 was found to have a maximal effect at 0.2% v/v, above which it is likely that cell damage begins to limit the enzymatic process. While Triton X-100 was able to increase turnover by a factor of two, COE2-2C-C10 (40 μ M/OD₆₀₀) increased turnover to a rate of 11-times that of control. It is worth noting that this massive increase in turnover rate is achieved at a concentration well below the MIC (256 μ M).

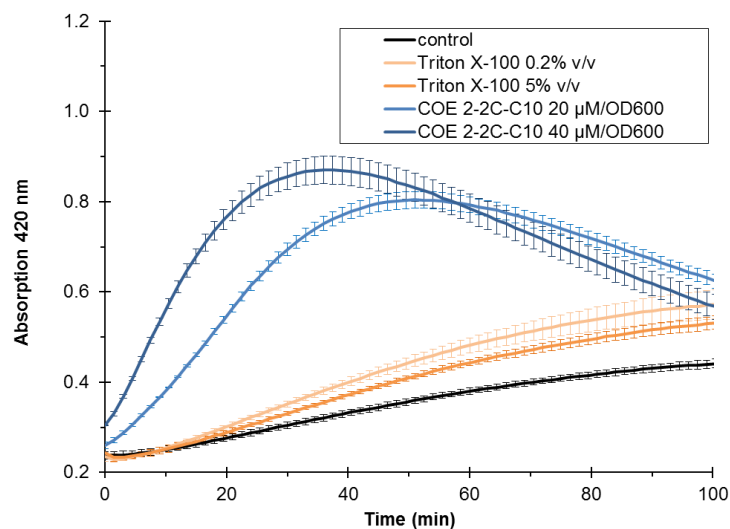


Figure 2-9 Comparison of permeabilizing abilities of COE2-2C-C10 and Triton X-100.

2.6.2 Nile Red as a Probe for COE-Mediated Membrane Permeability of Hydrophobic Compounds

As discussed in Section 2.1, the OM provides orthogonal barriers to permeation of both polar and nonpolar compounds. In Section 2.6.1, the structure-property relationship pertaining to ability of COEs to increase the permeation of a polar molecule (ONPG) was explored. In this section, the membrane association of a hydrophobic dye, Nile Red (NR), will be used to determine if permeation of nonpolar molecules is governed by the same structural parameters. N-phenyl-naphthylamine (NPN) is traditionally used in this assay^{119, 120} but spectral overlap with certain COEs precluded its usage in this study. NR, similar to NPN and other solvatochromic dyes, experiences a blue-shift in photoluminescence (PL) and an increase in fluorescence quantum yield upon intercalating into hydrophobic lipid bilayers.¹²¹ These changes in spectral properties are shown in Figure 2-10.

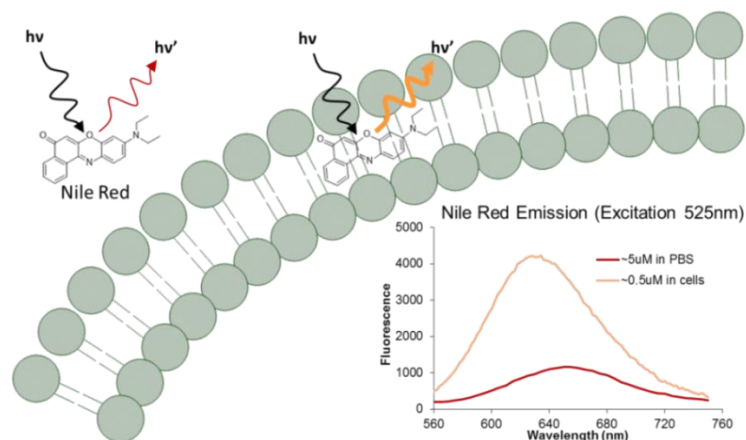


Figure 2-10 Graphical depiction of the Nile Red uptake assay used to assess COE permeabilization of the OM.

In the present study, NR was allowed to intercalate into the membranes of COE-treated *E. coli* cells for 75 minutes. Figure 2-11 shows the PL intensity (630 nm) of NR from *E. coli* cells stained with each of the ten COEs with high affinity for bacteria. Relative to the untreated control, all COE-treated samples show increased PL from NR. Surprisingly, the data indicate that the ability of NR to intercalate is not dictated by the core length (as was observed for ONPG) but rather the length of the pendant chain. For example, all three COEs with C-6 pendants seem to increase NR PL to the same degree (~2x relative to control). Within each core-length subfamily of COEs, PL increases concomitantly with pendant length. This unexpected result suggests that COE-mediated permeation through the hydrophilic and hydrophobic barriers of the OM are dependent on separate COE structural components. While COE2-2C-C10 was found to be the ideal structure for OM permeabilization toward polar compounds, the NR assay suggests that COE2-3C-C10 may be superior for nonpolar compounds (slightly higher NR PL intensity and >2x higher MIC). In a situation where permeation of both hydrophilic and hydrophobic molecules is

desired, COE2-2C-C10 possess the best composition of structural features (long total length for low antimicrobial action, short core for increased permeability of polar compounds, and long pendant chains for increased permeability of nonpolar compounds).

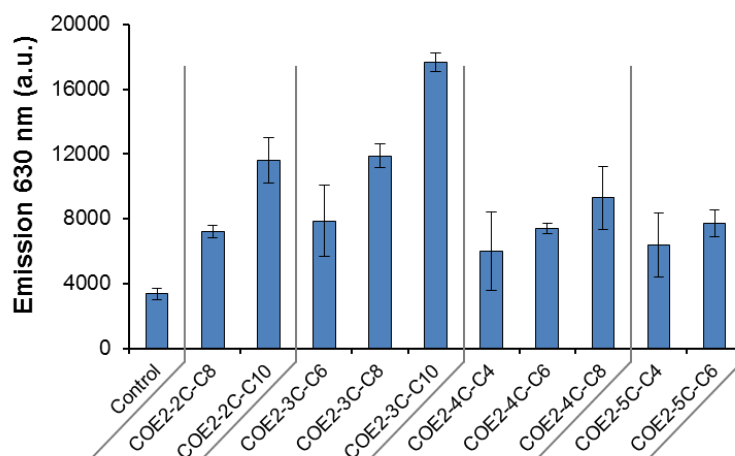


Figure 2-11 Nile Red emission (630 nm) from *E. coli* membranes as a function of COE structure.

2.7 Conclusions

In summary, we designed, synthesized, and tested a homologous series of COEs with the intent of determining structure-function relationships pertaining to antimicrobial action and membrane permeabilization. The correlation R and significance p-value for each pairwise comparison of structure and function is summarized in Table 2-1. In addition to gaining insight into which components of the COE structure dictate effects on bacteria cells, we identified a privileged structure

with high membrane association, low antimicrobial activity, and excellent permeabilizing action.

Table 2-1 Correlation (R) and significance (p) values between COE structural parameters and observed effects on microbes or model membranes

		Length (L)	Core (<i>m</i>)	Pendant (<i>n</i>)	Ratio (<i>m/n</i>)
Association	R	-0.255	-0.805	0.773	-0.833
	p	0.4765	0.0049	0.0088	0.0028
MIC	R	0.916	0.292	0.152	0.076
	p	0.0287	0.6334	0.8067	0.9035
ONPG turnover	R	-0.503	-0.909	0.546	-0.749
	p	0.1146	0.0001	0.0821	0.0080
Nile Red uptake	R	0.468	-0.246	0.832	-0.571
	p	0.1248	0.4412	0.0008	0.0524
Order Parameter <i>S</i>	R	0.589	0.336	0.250	0.165
	p	0.0439	0.2850	0.4326	0.6065
Correlation time τ_{2b}	R	0.603	0.289	0.327	-0.071
	p	0.0381	0.3622	0.2988	0.8264
Correlation time τ_{2c}	R	0.721	0.387	0.341	-0.070
	p	0.0081	0.2138	0.2786	0.9827

While the primary goal of this work was to decouple antimicrobial and permeabilizing properties of COEs, further insights into the various effects of COEs were uncovered. For example, EPR demonstrated that COEs with longer total length significantly increase lipid order. This result provides an explanation for the observation that long COEs can increase the robustness of microbial membranes against the disrupting effects of *n*-butanol.⁹⁶ With regard to the supposition that membrane “pinching” is directly related to antimicrobial properties of COEs, the

strong correlation between MIC and total length seems to lend credence to our original hypothesis. The fact that MIC is only correlated to total length may allow for rational design of COEs with enhanced antimicrobial activity (further discussion in Chapter 5). Similarly, better permeabilizing agents can be developed based on singular correlation with either core or pendant length depending on the nature of the intended substrate.

One final consideration is the mechanism of antimicrobial and permeabilizing effects of COEs. Unlike traditional surfactants, permeabilizing effects of COEs do not appear to be related to decreased lipid order. Unlike AMPs, increased lipid order does not appear to be part of the antimicrobial mechanism of action of COEs – in fact, COEs which increase order to the greatest extent are the least toxic to cells and can even increase membrane robustness. Based on similarities in chemical topology (size, charge distribution, etc.) between COEs and polar carotenoids, it is not surprising that similar effects on lipid order are observed in the two classes of molecules. While this study indicates that COEs do not permeabilize in the same fashion as surfactants or kill bacteria in the same fashion as AMPs, further structure-property studies are required in order to truly elucidate the mechanisms of action of COEs.

2.8 Experimental Methods

Materials and Instrumentation

Solvents and reagents for the preparation of the COEs were purchased from Fisher Scientific, Alfa Aesar, Acros, Sigma Aldrich, and Tokyo Chemical Industry. *E. coli* total lipid extract was purchased from Avanti Polar Lipids. 2-nitrophenyl β -*D*-galactopyranoside (ONPG) and the radical probe 16-DOXYL-stearic acid (16-SASL) were purchased from Sigma-Aldrich. *Escherichia coli* ATCC 10798 was purchased from American Type Culture Collection (Manassas, VA). Inhibitor-free anhydrous solvents were prepared using packed alumina columns under argon in a solvent purification system. EMD Millipore Analytical Chromatography aluminum-backed plates (Silica gel 60 F254) were used for thin layer chromatography and separation was visualized with UV light (254/366 nm). Silicycle SiliaFlash P60 silica gel was used for flash chromatography. Measurements for MIC, ONPG, NR and association studies were conducted on a Tecan M220 Infinite Pro. Continuous wave X-Band EPR spectra were collected on a Bruker EMXplus Spectrometer. ^1H NMR (400 MHz, 500 MHz, 600 MHz) and ^{13}C NMR (101 MHz and 126 MHz) were measured on an Agilent Technologies 400-MR DDR2 400 MHz, a Varian Unity Inova 500 MHz, or a Varian VNMRS 600 MHz spectrometer. Multiplicity of signals was described by s (singlet), d (doublet), t (triplet), and m (multiplet). Chemical shifts (δ in ppm) were referenced to residual solvent peaks of Chloroform-*d* (^1H NMR δ = 7.26 and ^{13}C NMR δ = 77.0) or DMSO-*d*₆ (^1H NMR δ = 2.50 and ^{13}C -NMR δ = 39.52). HRMS

(m/z) measurements were performed on a Waters GCT Premier time-of-flight mass spectrometer.

Strain and Culture Conditions

Escherichia coli K12 (ATCC #10798, ATCC, VA) was grown under aerobic conditions in Luria-Bertani (LB) broth (10 g/L bactotryptone, 5 g/L yeast extract, 10 g/L NaCl) overnight at 37 °C with orbital shaking (250 rpm). Cell cultures for ONPG turnover were supplemented with 2 g/L for the induction of *lacZ*. Cells were collected by centrifugation and either resuspended in fresh Luria-Bertani broth (for MIC) or washed 2x with M9 minimal media (6.8 g/L Na₂HPO₄, 3 g/L KH₂PO₄, 1 g/L NH₄Cl, 0.5 g/L NaCl) before resuspending in M9.

Minimum Inhibitory Concentration

Following overnight growth, collection, and resuspension in fresh LB, cells were diluted to 1 OD₆₀₀. Stock bacteria solutions were prepared by further 1:1000 dilution in LB. For COEs with sufficient solubility, stock solutions of 5.12 mM were prepared in 150 mM PBS before further diluting in LB to a final concentration of 1.024 mM. For COEs with lower solubility (both 5-ring compounds, and all with C8 or C10 chains), stock solutions were prepared directly in LB at 1.024 mM. 100 µL of 1.024 mM stock COE solutions were transferred to the first column of 96-well plates (in triplicate), and serially diluted across the next nine columns in LB (50 µL each well, concentrations from 2 µM to 1024 µM). The 11th column received 50 µL of LB, and the 12th column 100 µL of LB (LB sterility control). 50 µL of the bacteria stock was

added to columns 1 through 11 to give final COE concentrations from 1 μM to 512 μM . Plates were incubated overnight at 37 °C with orbital shaking (250 rpm). Optical density at 600 nm was measured on a Tecan plate reader. MIC was determined as the lowest concentration to give $\text{OD} < 0.1 \text{OD}_{\text{control}}$.

COE Association with Bacteria

Following overnight growth, collection, washing and resuspension in M9, cells were diluted to 2 OD_{600} . COE stock solutions of 120, 100, 80, 60, 40, and 20 μM were made in M9. 100 μL of stock cell solution was mixed with 100 μL of stock COE solution in microfuge tubes (triplicate) to give final concentrations of 1 OD_{600} cells and 60, 50, 40, 30, 20, or 10 μM COE. After 30 minute incubation at room temperature, all samples were centrifuged and 100 μL of supernatants removed to a 96-well plate. COE in the supernatant was quantified by optical absorption (310 nm for 2-ring compounds, 365 nm for 3-ring compounds, 385 nm for 4-ring compounds, and 400 nm for 5-ring compounds) on a Tecan plate reader. Calibration curves were made using COE solutions in M9 from 5 μM to 60 μM . Cell-associated COE was calculated by subtracting the supernatant concentration from the original concentration in the cell/COE mixture.

ONPG Assay

Overnight liquid cultures of *E. coli* (ATTC #10798, ATCC, VA) in Luria Bertani broth were supplemented with 2% lactose for the induction of *lacZ*. Cells were washed 2 times with M9 (6.8 g/L Na_2HPO_4 , 3 g/L KH_2PO_4 , 1 g/L NH_4Cl , 0.5 g/L NaCl) and left

at room temperature for 1 hour before staining with COEs (10 $\mu\text{M}/\text{OD}_{600}$) for 1 hour. Excess COE was removed by washing cells once with M9 before resuspending to 0.6 OD_{600} . Stained and control samples (100 μL) were transferred to a 96-well plate in triplicate. Absorption measurements at 420 nm were commenced immediately following the addition of 3.9 mM ONPG (50 μL) to each well. Turnover rate was measured as the slope of the line during the linear regime.

Nile Red Association

Overnight liquid cultures of *E. coli* were washed three times with PBS before staining with COEs (10 $\mu\text{M}/\text{OD}_{600}$) for 1 hour. Cells were washed one time with PBS and resuspended to 0.25 OD_{600} . 300 μL aliquots of cell suspensions were mixed with 3 μL of NR stock solution (50 μM in 25% ethanol:water). After incubating at 30°C for 75 minutes, NR fluorescence was recorded (excitation: 525 nm, emission: 630 nm).

EPR Experiments

Stock solutions of 10 mg/mL *E. coli* total lipid extract and 0.05 mg/mL 16-DOXYL-stearic acid were prepared in chloroform. 1 mL aliquots of this stock were concentrated in 2 Dr. vials under reduced pressure by rotary evaporation. Large unilamellar vesicles were formed by extrusion (10 mg/mL lipids in 50 mM PBS).¹⁰⁵ These vesicles were then diluted to ~2 mM and mixed 1:1 v/v with 20 μM COE solutions in 50 mM PBS. Following incubation at room temperature for 1 hour, ~5 μL samples were transferred to quartz capillaries. Continuous wave X-band EPR spectra were collected used to calculate order parameter (S) and correlation times

according to published methods.¹⁰⁶⁻¹¹⁰ See section 6.6 for sample spectra and a complete description of the calculations.

Correlation and Significance

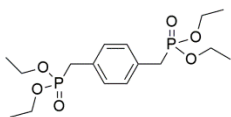
Correlation (R) and significance (p) values were calculated in MATLAB 2016b by using the *corrcoef* function in the form of [R,P] = corrcoef(matrix) where “matrix” was derived from a table of structural parameters and experimental data. The first column was the length as measured between the two furthest ammonium nitrogens. The second and third columns were the number of rings (2-5) and number of carbons on a single alkyl chain (4-10), respectively. The fourth column was the aromatic:aliphatic ratio, calculated as the number of total carbons in the aromatic core divided by the total aliphatic carbons in all four pendant chains. For association, the percent associated when stained with 60 $\mu\text{M}/\text{OD}_{600}$ was used to calculate correlation with the structural parameters (COE2-2C-C6 and COE2-3C-C4 were excluded as described in Section 2.3). For MIC, the MIC value was used (again, COE2-2C-C6 and COE2-3C-C4 were excluded). For ONPG, the relative turnover rate (as shown in Figure 2-8) was used. For Nile Red association, the emission value was used (arbitrary units, as shown in Figure 2-11). For order parameter and correlation times, values calculated from EPR spectra (see Chapter 6.3 for details about these calculations) were used. The MATLAB function returns two matrices, the first for R and the second for p. Target values for each output occur at the position with column # = column # of dependent variable in *matrix* and row # = column # of each structural parameter in *matrix*.

2.9 Synthetic Methods

The synthesis of COE2-2C-C6, COE2-3C-C6, COE2-4C-C6, and COE2-5C-C6 have been described in literature.^{44, 73} Note that these structures were previously referred to as COE2-2C, COE2-3C, COE2-4C, and COE2-5C.

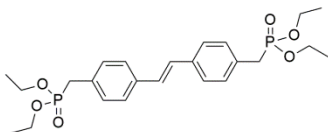
Phosphonates **P1** and **P2** made according to literature³⁹

tetraethyl (1,4-phenylenebis(methylene))bis(phosphonate) (**P1**)



(E)-tetraethyl ((ethene-1,2-diylbis(4,1-phenylene))bis(methylene))bis(phosphonate)

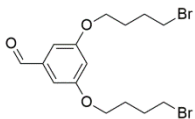
(P2)



General Procedure for alkylations of 3,5-dihydroxybenzaldehyde:

3,5-dihydroxybenzaldehyde, the appropriate dibromoalkane (10 eq), and potassium carbonate (2.5 eq) were refluxed in acetone for two days. Following aqueous workup, products were purified by flash chromatography.

3,5-bis((4-bromobutyl)oxy)benzaldehyde (**2-1a**)



3,5-dihydroxybenzaldehyde (800 mg, 1 eq), 1,4-dibromobutane (12.5 g, 10 eq), potassium carbonate (2 g, 2.5 eq), and acetone (40 mL)

were added to a 100 mL flame-dried two-neck flask equipped with a

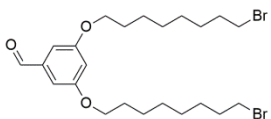
stir bar and fitted with a reflux condenser. The mixture was refluxed for two days under inert atmosphere. After cooling to room temperature, the mixture was portioned between ethyl acetate and brine. The aqueous layer was removed and extracted three additional times with ethyl acetate. The combined organic layers were dried with MgSO₄, filtered and concentrated under reduced pressure to leave a slightly yellow oil (note: most of the excess 1,4-dibromobutane was removed during concentration). The pure product was obtained as a white solid (1.3 g, 56%) following flash chromatography (2 CV hexanes followed by 1:5 ethyl acetate/hexanes).

¹H NMR (600 MHz, Chloroform-*d*) δ 9.89 (s, 1H), 6.99 (d, *J* = 2.3 Hz, 2H), 6.69 – 6.67 (m, 1H), 4.03 (t, *J* = 6.1 Hz, 4H), 3.49 (t, *J* = 6.6 Hz, 4H), 2.10 – 2.04 (m, 4H), 1.99 – 1.93 (m, 4H).

¹³C NMR (151 MHz, Chloroform-*d*) δ 191.81, 160.48, 138.39, 107.96, 107.68, 67.30, 33.21, 29.36, 27.74.

HRMS (ESI-TOF): 462.9893 [M+Na+CH₃OH]⁺

3,5-bis((8-bromooctyl)oxy)benzaldehyde (2-1c)



3,5-dihydroxybenzaldehyde (800 mg, 1 eq), 1,8-dibromooctane (15.8 g, 10 eq), potassium carbonate (2 g, 2.5 eq), and acetone (40 mL) were added to a 100 mL flame-dried two-neck

flask equipped with a stir bar and fitted with a reflux condenser. The mixture was refluxed for two days under inert atmosphere. After cooling to room temperature, the mixture was portioned between ethyl acetate and brine. The aqueous layer was

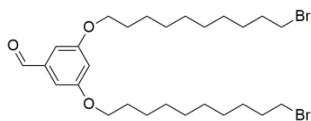
removed and extracted three addition times with ethyl acetate. The combined organic layers were dried with MgSO₄, filtered and concentrated under reduced pressure to leave a clear oil. The pure product was obtained as a white solid (2 g, 67%) following flash chromatography (3 CV hexanes, 1 CV 1:20 ethyl acetate/hexanes, 1:9 ethyl acetate/hexanes).

¹H NMR (500 MHz, Chloroform-*d*) δ 9.89 (s, 1H), 6.98 (d, *J* = 2.3 Hz, 2H), 6.69 (t, *J* = 2.3 Hz, 1H), 3.99 (t, *J* = 6.5 Hz, 4H), 3.41 (t, *J* = 6.8 Hz, 4H), 3.38 (d, *J* = 6.6 Hz, 4H), 1.93 – 1.83 (m, 4H), 1.84 – 1.74 (m, 4H), 1.52 – 1.40 (m, 8H), 1.43 – 1.29 (m, 8H).

¹³C NMR (500 MHz, Chloroform-*d*) δ 192.02, 160.71, 138.31, 108.01, 107.58, 68.33, 33.91, 32.74, 29.11, 29.05, 28.64, 28.05, 25.88.

HRMS (ESI-TOF): 543.0891 [M+Na]⁺

3,5-bis((10-bromodecyl)oxy)benzaldehyde (2-1d)



3,5-dihydroxybenzaldehyde (800 mg, 1 eq), 1,10-dibromodecane (17.4 g, 10 eq), potassium carbonate (2 g, 2.5 eq), and acetone (40 mL) were added to a 100 mL flame-

dried two-neck flask equipped with a stir bar and fitted with a reflux condenser. The mixture was refluxed for two days under inert atmosphere. After cooling to room temperature, the mixture was portioned between ethyl acetate and brine. The aqueous layer was removed and extracted three addition times with ethyl acetate. The combined organic layers were dried with MgSO₄, filtered and concentrated under reduced pressure to leave a clear, viscous oil. Excess 1,10-dibromodecane

was removed by vacuum distillation. The pure product was obtained as a white solid (2.2 g, 66%) following flash chromatography (1.5 CV hexanes, 1:25 ethyl acetate/hexanes).

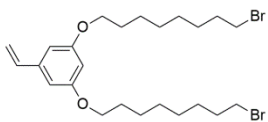
^1H NMR (500 MHz, Chloroform-*d*) δ 9.89 (s, 1H), 6.98 (d, J = 2.3 Hz, 2H), 6.69 (t, J = 2.3 Hz, 1H), 3.99 (t, J = 6.5 Hz, 4H), 3.41 (t, J = 6.9 Hz, 4H), 1.90 – 1.74 (m, 8H), 1.50 – 1.29 (m, 24H).

^{13}C NMR (126 MHz, Chloroform-*d*) δ 192.22, 160.89, 138.45, 108.17, 107.73, 77.16, 68.55, 34.17, 32.96, 29.56, 29.49, 29.42, 29.26, 28.88, 28.30, 26.12.

General Procedure for Wittig Reaction:

Benzaldehyde derivatives **2-1c** and **2-1d** were converted to the analogous styrene derivatives **2-3c** and **2-3d** with the Wittig reagent methyl triphenylphosphonium bromide (1.1 eq) in the presence of potassium carbonate (1.1 eq). Reactions were refluxed in anhydrous THF overnight. Following aqueous workup, products were purified by flash chromatography.

1,3-bis((8-bromooctyl)oxy)-5-vinylbenzene (2-3c)



2-1c (300 mg, 1.0 eq), methyl triphenylphosphonium bromide (227 mg, 1.1 eq), and potassium carbonate (88 mg, 1.1 eq)

were added to a flame dried 15 mL round bottom flask equipped with a stir bar and reflux condenser. 7 mL of anhydrous THF was added via cannula. The reaction mixture was heated to reflux overnight under inert atmosphere. After cooling to room temperature, the reaction mixture was diluted with 25 mL of

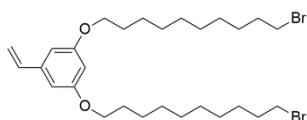
dichloromethane and transferred to a separatory funnel. The organic layer was extracted three times with brine, dried over Na₂SO₄, and concentrated via rotary evaporation. The product was isolated as a white solid (220 mg, 73%) following flash chromatography (1:15 ethyl acetate/hexane).

¹H NMR (400 MHz, Chloroform-*d*) δ 6.61 (dd, *J* = 17.5, 10.8 Hz, 1H), 6.53 (d, *J* = 2.3 Hz, 2H), 6.35 (t, *J* = 2.3 Hz, 1H), 5.69 (d, *J* = 17.5 Hz, 1H), 5.21 (d, *J* = 10.8 Hz, 1H), 3.92 (t, *J* = 6.5 Hz, 4H), 3.39 (t, *J* = 6.8 Hz, 4H), 1.84 (p, *J* = 6.9 Hz, 4H), 1.75 (p, *J* = 6.7 Hz, 4H), 1.50 – 1.37 (m, 16H).

¹³C NMR (126 MHz, Chloroform-*d*) δ 160.35, 139.47, 136.92, 114.11, 104.83, 100.96, 67.93, 33.97, 32.77, 29.21, 29.16, 28.68, 28.08, 25.95.

HRMS (ESI-TOF): 519.1297 [M+H]⁺

1,3-bis((10-bromodecyl)oxy)-5-vinylbenzene (2-3d)



2-1d (140 mg, 1.0 eq), methyl triphenylphosphonium bromide

(96 mg, 1.1 eq), and potassium carbonate (37 mg, 1.1 eq)

were added to a flame dried 10 mL round bottom flask equipped with a stir bar and reflux condenser. 5 mL of anhydrous THF was added via cannula. The reaction mixture was heated to reflux overnight under inert atmosphere. After cooling to room temperature, the reaction mixture was diluted with 25 mL of dichloromethane and transferred to a separatory funnel. The organic layer was extracted three times with brine, dried over Na₂SO₄, and concentrated via rotary evaporation. The product was isolated as a white solid (99 mg, 71%) following flash chromatography (1:15 ethyl acetate/hexane).

^1H NMR (500 MHz, Chloroform-*d*) δ 6.63 (dd, $J = 17.5, 10.8$ Hz, 1H), 6.55 (d, $J = 2.2$ Hz, 2H), 6.38 (t, $J = 2.2$ Hz, 1H), 5.72 (dd, $J = 17.5, 0.9$ Hz, 1H), 5.23 (dd, $J = 10.8, 0.8$ Hz, 1H), 3.95 (t, $J = 6.5$ Hz, 4H), 3.41 (t, $J = 6.9$ Hz, 4H), 1.86 (p, $J = 7.1$ Hz, 4H), 1.77 (p, $J = 7.1$ Hz, 4H), 1.50 – 1.27 (m, 24H).

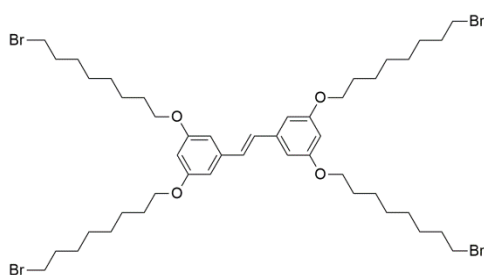
^{13}C NMR (126 MHz, Chloroform-*d*) δ 160.37, 139.44, 136.94, 114.08, 104.81, 100.97, 67.99, 34.02, 32.81, 29.42, 29.34, 29.30, 29.25, 28.73, 28.15, 26.02.

HRMS (ESI-TOF): 575.1878 [M+H] $^+$

General Procedure for Metathesis Reactions:

Styrene derivatives **2-3c** and **2-3d** were converted to the analogous stilbene derivatives using Grubbs 2nd Generation (0.01 eq). Reactions were heated to 50°C in dry DCM under inert atmosphere for 16 hours. Products were purified by flash chromatography.

(E)-1,2-bis(3,5-bis((8-bromooctyl)oxy)phenyl)ethene (**2-4c**)



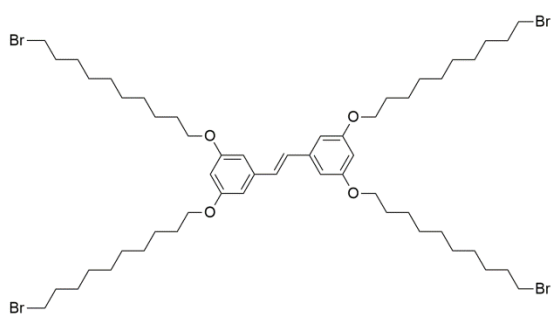
2-3c (125 mg, 1.0 eq) was added to a flame dried microwave tube equipped with a stir bar and septum. Grubbs Catalyst 2nd Generation (2 mg, 0.01 eq) was transferred to a small vial under inert atmosphere. 1 mL of dry DCM was added to the catalyst and the solution was transferred via syringe to the reaction vessel. The reaction mixture was heated to 50°C under inert atmosphere for 16 hours with most of the microwave tube above the oil to prevent the reaction from drying out. After cooling to room temperature the

reaction mixture was directly purified by flash chromatography (5:7 chloroform/hexane) to afford the product as a white solid (101 mg, 83%).

^1H NMR (500 MHz, Chloroform-*d*) δ 6.99 (s, 2H), 6.64 (d, J = 2.2 Hz, 4H), 6.39 (t, J = 2.2 Hz, 2H), 3.98 (t, J = 6.5 Hz, 8H), 3.42 (t, J = 6.8 Hz, 8H), 1.87 (p, J = 7.3 Hz, 8H), 1.79 (p, J = 6.6 Hz, 8H), 1.57 – 1.31 (m, 32H).

^{13}C NMR (126 MHz, Chloroform-*d*) δ 160.44, 139.08, 129.11, 105.14, 103.73, 100.97, 67.98, 33.97, 32.78, 29.23, 29.16, 28.68, 28.09, 25.97.

(E)-1,2-bis(3,5-bis((10-bromodecyl)oxy)phenyl)ethene (**2-4d**)



2-3d (85 mg, 1.0 eq) was added to a flame dried microwave tube equipped with a stir bar and septum. Grubbs Catalyst 2nd Generation (1.3 mg, 0.01 eq) was transferred to a small vial under inert

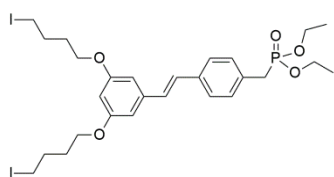
atmosphere. 1 mL of dry DCM was added to the catalyst and the solution was transferred via syringe to the reaction vessel. The reaction mixture was heated to 50°C under inert atmosphere for 16 hours with most of the microwave tube above the oil to prevent the reaction from drying out. After cooling to room temperature the reaction mixture was directly purified by flash chromatography (5:7 chloroform/hexane) to afford the product as a white solid (60 mg, 73%).

^1H NMR (500 MHz, Chloroform-*d*) δ 6.98 (s, 2H), 6.64 (d, J = 2.1 Hz, 4H), 6.39 (t, J = 2.2 Hz, 2H), 3.97 (t, J = 6.5 Hz, 8H), 3.41 (t, J = 6.9 Hz, 8H), 1.86 (p, J = 7.1 Hz, 8H), 1.79 (p, J = 7.6 Hz, 8H), 1.51 – 1.28 (m, 48H).

^{13}C NMR (126 MHz, Chloroform-*d*) δ 160.45, 139.07, 129.10, 105.12, 100.96, 68.03, 34.03, 32.82, 29.43, 29.35, 29.32, 29.28, 28.74, 28.15, 26.04.

Procedures for Horner-Wadsworth-Emmons Reactions for 5-ring Compounds:

(E)-diethyl 4-(3,5-bis(4-iodobutoxy)styryl)benzylphosphonate (**2-8a**)



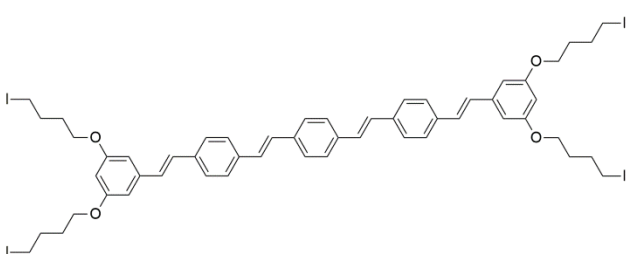
2-2a (300 mg, 1.1 eq) and anhydrous THF (4 mL) were added to a flame-dried 10 mL round bottom flask. **P1** (216 mg, 1.05 eq) and anhydrous THF (4 mL) were added under inert atmosphere to a flame-dried 25 mL round bottom flask equipped with a stir bar. The solution was cooled to 0°C and sodium *tert*-butoxide (52.2 mg, 1 eq) was added as a solution in anhydrous THF (5 mL). After 15 minutes, the solution of **2-2a** was added in a single portion via syringe under inert atmosphere. The reaction was maintained at 0°C for 1 hour. The contents were portioned between water and DCM. The organic layer was removed and the aqueous layer was extracted with DCM an additional 3 times. The organic layers were combined, dried over Na_2SO_4 , filtered, and concentrated under reduced pressure. The pure product (150 mg, 38%) was obtained as a yellowish oil following flash chromatography (9:1 DCM/ethyl acetate).

^1H NMR (400 MHz, Chloroform-*d*) δ 7.44 (d, J = 7.9 Hz, 2H), 7.29 (dd, J = 8.2, 2.5 Hz, 2H), 7.10 – 6.94 (m, 2H), 6.64 (d, J = 2.2 Hz, 2H), 6.35 (t, J = 2.2 Hz, 1H), 4.10 –

3.96 (m, 8H), 3.27 (t, $J = 6.8$ Hz, 4H), 3.16 (d, $J = 21.8$ Hz, 2H), 2.09 – 1.98 (m, 4H), 1.96 – 1.86 (m, 4H), 1.25 (t, $J = 7.0$ Hz, 6H).

^{13}C NMR (126 MHz, Chloroform- d) δ 160.23, 139.34, 135.80, 135.77, 131.20, 131.12, 130.14, 130.09, 128.81, 128.79, 128.48, 128.46, 126.73, 126.71, 105.20, 100.90, 66.73, 62.21, 62.16, 30.18, 30.14, 16.43, 16.38, 6.42.

1,4-bis((E)-4-((E)-3,5-bis(4-iodobutoxy)styryl)styryl)benzene (2-9a)



2-8a (43 mg, 2.2 eq), terephthalaldehyde (3.6 mg, 1 eq), and anhydrous THF (3 mL) were added to a flame-dried 10 mL round

bottom flask equipped with a stir bar. The solution was cooled to 0°C under inert atmosphere. Sodium *tert*-butoxide (5.4 mg, 2.1 eq) was added as a solution in anhydrous THF (2 mL) via syringe slowly over 5 minutes. The reaction was maintained at 0°C for 1 hour and then partitioned between DCM and water. The organic layer was removed and the aqueous layer was extracted with DCM an additional 3 times. The organic layers were combined, dried over Na_2SO_4 , filtered, and concentrated under reduced pressure. The pure product (20 mg, 58%) was obtained as a bright yellow solid following flash chromatography (2:1 DCM/hexanes).

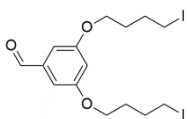
^1H NMR (400 MHz, Chloroform- d) δ 7.57 – 7.47 (m, 12H), 7.20 – 6.96 (m, 8H), 6.66 (d, $J = 2.2$ Hz, 4H), 6.37 (t, $J = 2.2$ Hz, 2H), 4.02 (t, $J = 6.0$ Hz, 8H), 3.28 (t, $J = 6.8$ Hz, 8H), 2.14 – 1.99 (m, 8H), 1.98 – 1.87 (m, 8H).

^{13}C NMR (126 MHz, Chloroform-*d*) δ 160.26, 139.39, 136.86, 136.74, 136.51, 128.83, 128.49, 128.25, 128.16, 126.95, 126.90, 126.88, 105.23, 100.95, 66.75, 30.19, 30.15, 6.41.

General Procedure for Halogen Exchange (Finkelstein reaction):

All final products were prepared directly from alkyl iodide intermediates via quaternization with trimethylamine but the conversion from alkyl bromide to iodide occurred at different stages depending on the particular COE. In all cases, alkyl bromides were converted to analogous iodides via refluxing for ~2 days in acetone in the presence of sodium iodide. Some compounds were directly used following aqueous workup while others were purified as described below.

3,5-bis((4-iodobutyl)oxy)benzaldehyde (2-2a)

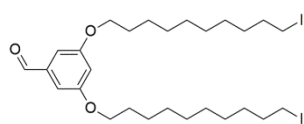


2-1a (678 mg, 1 eq), sodium iodide (7.22 g, 25 eq), and acetone (15 mL) were combined in a 25 mL round bottom flask equipped with a stir bar and fitted with a reflux condenser. The mixture was refluxed for 2 days under inert atmosphere. After cooling, the mixture was portioned between ethyl acetate and brine. The aqueous layer was discarded and the organic layer was extracted 2 additional times with brine, once with saturated sodium thiosulfate, and once with water. The organic layer was dried over Na_2SO_4 , filtered, and concentrated via rotary evaporation. No further purification was necessary. (810 mg, 97%)

^1H NMR (500 MHz, DMSO- d_6) δ 9.90 (s, 1H), 7.05 (d, J = 2.3 Hz, 2H), 6.82 (t, J = 2.3 Hz, 2H), 4.06 (t, J = 6.3 Hz, 5H), 3.35 (t, J = 6.9 Hz, 5H), 1.93 (p, J = 6.9 Hz, 6H), 1.80 (p, J = 6.4 Hz, 6H).

^{13}C NMR (151 MHz, Chloroform- d) δ 191.82, 160.47, 138.37, 107.96, 107.68, 67.09, 30.06, 29.98, 6.11.

3,5-bis((10-iododecyl)oxy)benzaldehyde (2-2c)

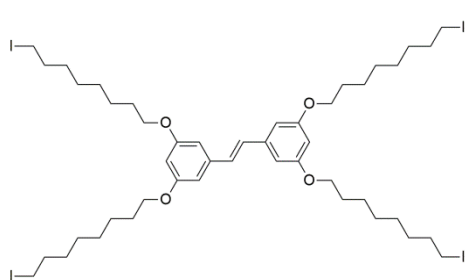


2-1c (650 mg, 1 eq), sodium iodide (4.7 g, 25 eq), and acetone (15 mL) were combined in a 25 mL round bottom flask equipped with a stir bar and fitted with a reflux condenser. The mixture was refluxed for 2 days under inert atmosphere. After cooling, the mixture was portioned between ethyl acetate and brine. The aqueous layer was discarded and the organic layer was extracted 2 additional times with brine, once with saturated sodium thiosulfate, and three times with water. The organic layer was dried over Na_2SO_4 , filtered, and concentrated via rotary evaporation. No further purification was necessary. (718 mg, 95%)

^1H NMR (500 MHz, Chloroform- d) δ 9.89 (s, 1H), 6.98 (d, J = 2.3 Hz, 2H), 6.69 (t, J = 2.3 Hz, 1H), 3.98 (t, J = 6.5 Hz, 4H), 3.19 (t, J = 7.0 Hz, 4H), 1.90 – 1.72 (m, 8H), 1.49 – 1.20 (m, 24H).

^{13}C NMR (151 MHz, Chloroform- d) δ 191.82, 160.48, 138.38, 107.95, 107.68, 67.30, 33.21, 30.45, 29.36, 29.25, 29.09, 28.48, 27.74, 25.95, 7.26.

(E)-1,2-bis(3,5-bis((8-iodooctyl)oxy)phenyl)ethene (**2-5c**)

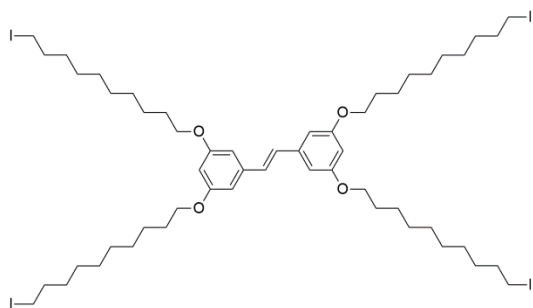


2-4c (47 mg, 1 eq), sodium iodide (105 mg, 15 eq), and acetone (1mL) were added to a microwave tube equipped with a stir bar. The vessel was placed in a 70°C oil bath such that headspace within the vessel remained above the oil level. The reaction was allowed to proceed for 2 days under inert atmosphere. After cooling to room temperature, the mixture was diluted in 10 mL of dichloromethane. The mixture was extracted once with saturated sodium thiosulfate and five times with water. The organic layer was then dried over Na₂SO₄, filtered, and concentrated via rotary evaporation. No further purification was necessary. (50 mg, 89%)

¹H NMR (500 MHz, Chloroform-*d*) δ 6.99 (s, 2H), 6.64 (d, *J* = 2.2 Hz, 4H), 6.39 (t, *J* = 2.2 Hz, 2H), 3.98 (t, *J* = 6.5 Hz, 8H), 3.20 (t, *J* = 7.0 Hz, 8H), 1.91 – 1.75 (m, 16H), 1.54 – 1.31 (m, 32H).

¹³C NMR (151 MHz, Chloroform-*d*) δ 160.46, 139.07, 129.10, 105.12, 100.97, 68.02, 33.50, 30.48, 29.43, 29.27, 28.45, 25.99, 7.26.

(E)-1,2-bis(3,5-bis((10-iododecyl)oxy)phenyl)ethene (**2-5d**)



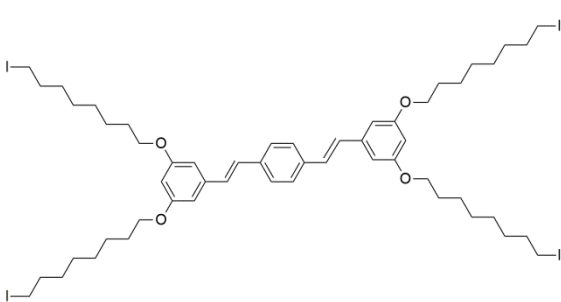
2-4d (40 mg, 1 eq), sodium iodide (54 mg, 10 eq), and acetone (1mL) were added to a microwave tube equipped with a stir bar. The vessel was placed in a 70°C oil bath such that only the part containing the reaction

mixture was submerged. The reaction was allowed to proceed for 2 days under inert atmosphere. After cooling to room temperature, the mixture was diluted in 10 mL of dichloromethane. The mixture was extracted once with saturated sodium thiosulfate and five times with water. The organic layer was then dried over Na₂SO₄, filtered, and concentrated via rotary evaporation. The resulting orange solid was passed through a silica plug with 1:8 ethyl acetate/hexane to afford the product as a white solid (42 mg, 90%).

¹H NMR (600 MHz, Chloroform-*d*) δ 7.00 (s, 2H), 6.66 (d, *J* = 2.2 Hz, 4H), 6.40 (t, *J* = 2.3 Hz, 2H), 3.99 (t, *J* = 6.5 Hz, 8H), 3.21 (t, *J* = 7.0 Hz, 8H), 1.88 – 1.77 (m, 16H), 1.53 – 1.45 (m, 8H), 1.44 – 1.34 (m, 40H).

¹³C NMR (151 MHz, Chloroform-*d*) δ 160.47, 139.08, 129.11, 105.14, 100.98, 68.04, 33.54, 30.48, 29.44, 29.33, 29.31, 29.28, 28.51, 26.04, 7.29.

1,4-bis((E)-3,5-bis((8-iodooctyl)oxy)styryl)benzene (2-6c)



2-6cBr (not shown in Figure 2-3, see below) (400 mg, 1 eq), sodium iodide (1.35 g, 25 eq), and acetone (5 mL) were combined in a 10 mL round bottom flask equipped with a stir bar and fitted with a

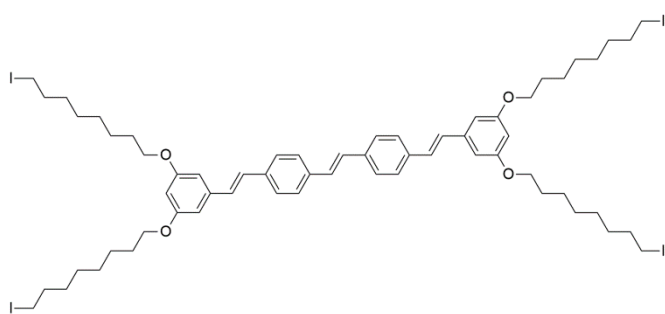
reflux condenser. The mixture was refluxed for 2 days under inert atmosphere. After cooling to room temperature, the mixture was partitioned between dichloromethane and saturated sodium thiosulfate. The organic layer was discarded and the organic layer was extracted with water three times. The organic layer was then dried over

Na₂SO₄, filtered, and concentrated via rotary evaporation. The resulting pinkish solid was passed through a silica plug with 1:8 ethyl acetate/hexane to afford the product as a white solid (420 mg, 90%).

¹H NMR (600 MHz, Chloroform-*d*) δ 7.49 (s, 4H), 7.10 – 7.01 (m, 4H), 6.66 (d, *J* = 2.1 Hz, 4H), 6.39 (t, *J* = 2.2 Hz, 2H), 3.98 (t, *J* = 6.5 Hz, 8H), 3.20 (t, *J* = 7.0 Hz, 8H), 1.88 – 1.74 (m, 16H), 1.52 – 1.32 (m, 32H).

¹³C NMR (151 MHz, Chloroform-*d*) δ 160.60, 139.33, 136.76, 128.86, 128.71, 127.01, 105.27, 101.14, 68.14, 33.65, 30.56, 29.39, 29.30, 28.61, 26.13, 7.38.

(E)-1,2-bis(4-((*E*)-3,5-bis((8-iodooctyl)oxy)styryl)phenyl)ethene (**2-7c**)



2-7cBr (not shown in Figure 2-3, see below) (220 mg, 1 eq), sodium iodide (680 mg, 25 eq), and acetone (5 mL) were combined in a 10 mL round bottom flask equipped

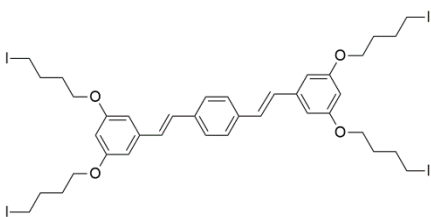
with a stir bar and fitted with a reflux condenser. The mixture was refluxed for 2 days under inert atmosphere. After cooling to room temperature, the mixture was partitioned between dichloromethane and saturated sodium thiosulfate. The organic layer was discarded and the organic layer was extracted an additional time with saturated sodium thiosulfate and with water three times. The organic layer was then dried over Na₂SO₄, filtered, and concentrated via rotary evaporation. No further purification was necessary to obtain the pure product as a white solid (420 mg, 90%).

^1H NMR (600 MHz, Chloroform-*d*) δ 7.50 (d, J = 2.2 Hz, 8H), 7.12 (s, 2H), 7.11 – 7.01 (m, 4H), 6.66 (d, J = 2.0 Hz, 4H), 6.41 – 6.37 (m, 2H), 3.98 (t, J = 6.5 Hz, 8H), 3.20 (t, J = 6.9 Hz, 8H), 1.82 (dq, J = 25.4, 7.2 Hz, 16H), 1.51 – 1.32 (m, 32H).

^{13}C NMR (126 MHz, Chloroform-*d*) δ 160.46, 139.20, 136.73, 136.58, 128.70, 128.57, 128.15, 126.91, 126.86, 105.12, 100.99, 68.00, 33.53, 30.46, 29.28, 29.20, 28.50, 26.01, 7.34.

General Procedure for Horner-Wadsworth-Emmons Reactions for 3-ring and 4-ring Compounds:

1,4-bis((E)-3,5-bis(4-iodobutoxy)styryl)benzene (2-6a)



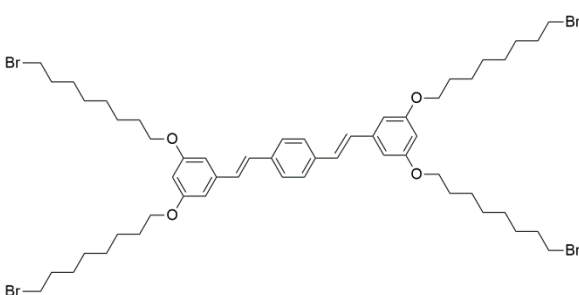
2-2a (200 mg, 1 eq) and anhydrous THF (1 mL) were added to a flame-dried 2 Dr vial under inert atmosphere. **P1** (79 mg, 0.525 eq) and anhydrous THF (2 mL) were added to a flame-dried 10 mL round bottom flask equipped with a stir bar under inert atmosphere. This mixture was cooled to 0°C before adding sodium *tert*-butoxide (38 mg, 1 eq) as a solution in anhydrous THF (2 mL). The temperature was maintained at 0°C for 15 minutes, at which point the solution of **2-2a** was added slowly via syringe. After an additional 2 hours at 0°C, the mixture was portioned between dichloromethane and water. The organic layer was collected and the aqueous layer was extracted with an additional portion of dichloromethane. The combined organic layers were dried over Na_2SO_4 ,

filtered, and concentrated via rotary evaporation. The pure product was obtained as a white solid (148 mg, 69%) by flash chromatography (2:5 DCM/hexanes).

^1H NMR (500 MHz, Chloroform-*d*) δ 7.54 – 7.45 (m, 4H), 7.11 – 6.98 (m, 4H), 6.66 (d, J = 2.2 Hz, 4H), 6.37 (t, J = 2.2 Hz, 2H), 4.02 (t, J = 6.1 Hz, 8H), 3.28 (t, J = 6.9 Hz, 9H), 2.10 – 2.01 (m, 8H), 1.95 – 1.87 (m, 9H).

^{13}C NMR (126 MHz, cdcl_3) δ 160.25, 139.36, 136.61, 128.79, 128.56, 126.93, 105.24, 100.96, 66.75, 30.19, 30.15, 6.44.

1,4-bis((E)-3,5-bis((8-bromooctyl)oxy)styryl)benzene (2-6cBr)



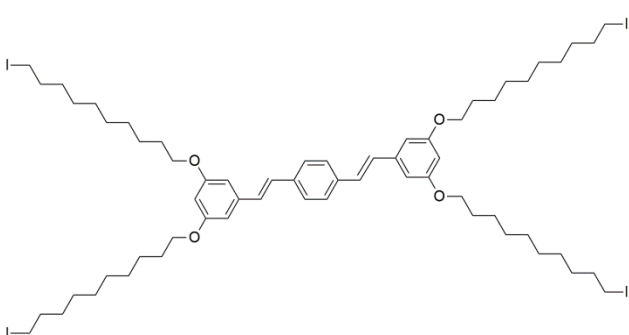
2-1c (500 mg, 2 eq) and **P1** (191 mg, 1.05 eq) were added to a flame-dried 10 mL round bottom flask equipped with a stir bar. Anhydrous THF (2 mL) was added via syringe under inert atmosphere. The mixture was cooled to 0°C. In a separate flame-dried flask, a solution of sodium *tert*-butoxide (97 mg, 2.1 eq) was prepared in anhydrous THF (3 mL). The entirety of the sodium *tert*-butoxide solution was added to the reaction flask via syringe slowly. The mixture was left in the ice bath and allowed to warm to room temperature overnight. The contents were partitioned between dichloromethane and water. The organic layer was separated and the aqueous layer was extracted with three additional portions of dichloromethane. The organic layers were combined, back-extracted with an additional portion of water, dried over Na_2SO_4 , filtered, and

concentrated via rotary evaporation. The pure product was obtained as a white solid (415 mg, 78%) following flash chromatography (1:8 ethyl acetate/hexanes).

^1H NMR (600 MHz, Chloroform-*d*) δ 7.49 (s, 4H), 7.10 – 7.00 (m, 4H), 6.66 (d, J = 1.9 Hz, 4H), 6.39 (t, J = 2.2 Hz, 2H), 3.98 (t, J = 6.5 Hz, 8H), 3.42 (t, J = 6.8 Hz, 8H), 1.87 (p, J = 7.0 Hz, 8H), 1.79 (d, J = 6.9 Hz, 8H), 1.52 – 1.33 (m, 32H).

^{13}C NMR (151 MHz, Chloroform-*d*) δ 160.46, 139.19, 136.62, 128.71, 128.55, 126.87, 105.12, 100.99, 67.99, 33.98, 32.80, 29.26, 29.19, 28.70, 28.11, 25.99.

1,4-bis((E)-3,5-bis((10-iododecyl)oxy)styryl)benzene (2-6d)



2-2d (200 mg, 1 eq) and anhydrous THF (1 mL) were added to a flame-dried 2 Dr vial under inert atmosphere. **P1** (52 mg, 0.525 eq) and anhydrous THF (2 mL) were added to a flame-

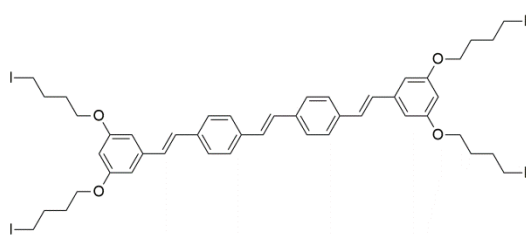
dried 10 mL round bottom flask equipped with a stir bar under inert atmosphere. This mixture was cooled to 0°C before adding sodium *tert*-butoxide (31 mg, 1.05 eq) as a solution in anhydrous THF (2 mL). The temperature was maintained at 0°C for 15 minutes, at which point the solution of **2-2d** was added slowly via syringe. After an additional 2 hours at 0°C, the mixture was portioned between dichloromethane and water. The organic layer was collected and the aqueous layer was extracted with an additional portion of dichloromethane. The combined organic layers were dried over Na_2SO_4 , filtered, and concentrated via rotary evaporation. The pure product was

obtained as a white solid (154 mg, 74%) by flash chromatography (1:9 ethyl acetate/hexanes).

^1H NMR (600 MHz, Chloroform-*d*) δ 7.48 (s, 4H), 7.08 – 7.02 (m, 4H), 6.66 (s, 4H), 6.39 (s, 2H), 3.98 (t, J = 6.5 Hz, 8H), 3.19 (t, J = 7.0 Hz, 8H), 1.86 – 1.75 (m, 16H), 1.50 – 1.25 (m, 48H).

^{13}C NMR (151 MHz, Chloroform-*d*) δ 160.48, 139.17, 136.62, 128.73, 128.54, 126.85, 105.11, 101.00, 68.05, 33.54, 30.47, 29.43, 29.32, 29.30, 29.27, 28.50, 26.03, 7.26.

(E)-1,2-bis(4-((*E*)-3,5-bis(4-iodobutoxy)styryl)phenyl)ethene (**2-7a**)



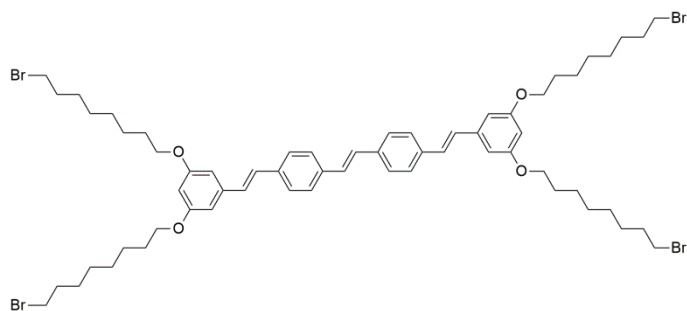
2-2a (100 mg, 1 eq) and anhydrous THF (1 mL) were added to a flame-dried 2 Dr vial under inert atmosphere. **P2** (62 mg, 0.525 eq) and anhydrous THF (2 mL) were added to a flame-dried 10 mL round bottom flask equipped with a stir bar under inert atmosphere. This mixture was cooled to 0°C before adding sodium *tert*-butoxide (24 mg, 1 eq) as a solution in anhydrous THF (2 mL). The temperature was maintained at 0°C for 15 minutes, at which point the solution of **2-2a** was added slowly via syringe. After an additional 4 hours at 0°C, the mixture was portioned between dichloromethane and water. The organic layer was collected and the aqueous layer was extracted with an additional portion of dichloromethane. The combined organic layers were dried over Na_2SO_4 , filtered, and concentrated via rotary evaporation.

The pure product was obtained as a bright yellow solid (95 mg, 66%) by flash chromatography (1 CV hexanes, 1:8 ethyl acetate/hexanes).

^1H NMR (600 MHz, Chloroform-*d*) δ 7.53 – 7.48 (m, 8H), 7.13 (s, 2H), 7.11 – 7.01 (m, 4H), 6.66 (s, 4H), 6.37 (s, 2H), 4.02 (t, $J = 6.1$ Hz, 4H), 3.28 (t, $J = 6.9$ Hz, 4H), 2.10 – 1.99 (m, 4H), 1.95 – 1.89 (m, 4H).

^{13}C NMR (151 MHz, Chloroform-*d*) δ 160.24, 141.61, 136.82, 136.52, 128.81, 128.49, 128.21, 126.92, 126.86, 105.24, 101.86, 66.74, 30.18, 30.13, 6.35.

(E)-1,2-bis(4-((*E*)-3,5-bis((8-bromooctyl)oxy)styryl)phenyl)ethene (**2-7cBr**)



2-1c (500 mg, 2 eq) and **P2** (252 mg, 1.05 eq) were added to a flame-dried 10 mL round bottom flask equipped with a stir bar. Anhydrous THF (2 mL) was

added via syringe under inert atmosphere. The mixture was cooled to 0°C. In a separate flame-dried flask, a solution of sodium *tert*-butoxide (97 mg, 2.1 eq) was prepared in anhydrous THF (3 mL). The entirety of the sodium *tert*-butoxide solution was added to the reaction flask via syringe slowly. The mixture was left in the ice bath and allowed to warm to room temperature overnight. The contents were partitioned between dichloromethane and water. The organic layer was separated and the aqueous layer was extracted with three additional portions of dichloromethane. The organic layers were combined, back-extracted with an additional portion of water, dried over Na_2SO_4 , filtered, and concentrated via rotary

evaporation. The pure product was obtained as a white solid (419 mg, 72%) following flash chromatography (2 CV 1:10 ethyl acetate/hexanes, 1:5:5 ethyl acetate/hexanes/DCM).

^1H NMR (600 MHz, Chloroform-*d*) δ 7.50 (s, 8H), 7.15 – 6.99 (m, 6H), 6.67 (d, J = 2.2 Hz, 4H), 6.40 (t, J = 2.2 Hz, 2H), 3.98 (t, J = 6.5 Hz, 8H), 3.42 (t, J = 6.8 Hz, 8H), 1.87 (p, J = 6.9 Hz, 8H), 1.80 (p, J = 6.6 Hz, 8H), 1.53 – 1.34 (m, 32H).

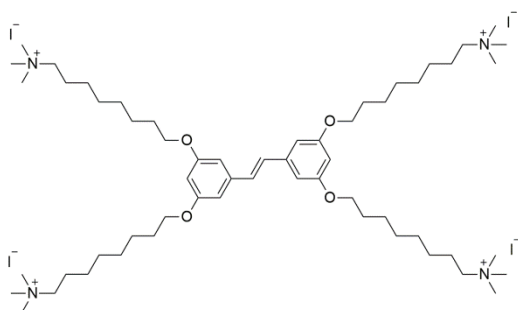
^{13}C NMR (151 MHz, Chloroform-*d*) δ 160.48, 139.21, 136.74, 136.58, 128.70, 128.56, 128.14, 126.92, 126.88, 105.14, 101.01, 68.00, 34.04, 32.83, 29.31, 29.24, 28.74, 28.15, 26.03.

General Procedure for Quaternization Reactions:

Final target compounds were prepared by quaternization of alkyl iodide intermediates with trimethylamine. In all cases, intermediates were dissolved in anhydrous tetrahydrofuran and trimethylamine (20 eq) was added as a 3.2 M solution in methanol. All reactions were allowed to run for 2 days at room temperature under inert atmosphere in sealed 1 Dr vials. During the course of the reaction, methanol was added whenever insoluble material was observed (dropwise until solids dissolved). Following the reaction, mixtures were transferred to 50 mL centrifuge tubes and 10-20 mL of diethyl ether was added to precipitate the final target compounds. Suspensions were centrifuge and the supernatant decanted. The solids were dissolved in methanol and again precipitated with diethyl ether, centrifuged, and decanted. The centrifuge tubes were placed within glass containers and left under vacuum overnight. Solids were then dissolved in water, filtered

through 0.45 μM PTFE syringe filters, and lyophilized to provide the final products as fluffy solids (white or bright yellow depending on the conjugated core length). All reactions were quantitative.

(E)-8,8',8'',8'''-((ethene-1,2-diylbis(benzene-5,3,1-triyl))tetrakis(oxy))tetrakis(*N,N,N*-trimethyloctan-1-aminium) iodide (**COE2-2C-C8**)



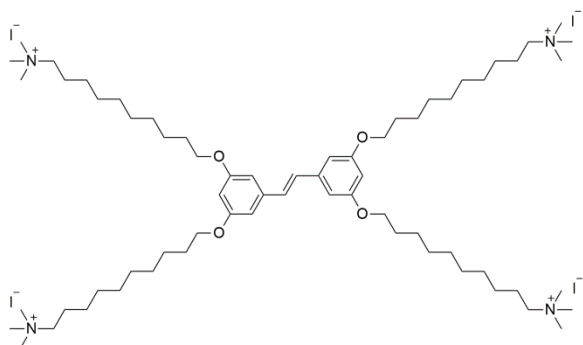
From **2-5c**

^1H NMR (500 MHz, $\text{DMSO-}d_6$) δ 7.16 (s, 2H), 6.73 (d, $J = 2.2$ Hz, 4H), 6.37 (t, $J = 2.3$ Hz, 2H), 3.96 (t, $J = 6.4$ Hz, 8H), 3.26 (ddd, $J = 10.7, 6.2, 2.3$ Hz, 8H), 3.03 (s, 36H), 1.75 – 1.62 (m, 16H), 1.45 – 1.24 (m, 32H).

^{13}C NMR (126 MHz, $\text{DMSO-}d_6$) δ 160.48, 139.38, 129.31, 105.39, 101.15, 67.94, 65.75, 52.61, 29.20, 29.06, 28.95, 26.20, 25.94, 22.49.

HRMS (ESI-TOF): 589.3229 $[\text{M}-2\text{I}]^{2+}$

(*E*)-10,10',10'',10'''-(((ethene-1,2-diylbis(benzene-5,3,1-triyl))tetrakis(oxy))tetrakis(*N,N,N*-trimethyldecan-1-aminium) iodide (**COE2-2C-C10**)



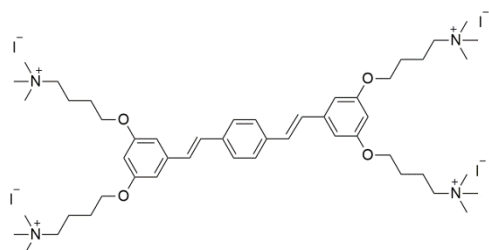
From **2-5d**

^1H NMR (600 MHz, DMSO- d_6) δ 7.17 (s, 2H), 6.74 (d, $J = 2.1$ Hz, 4H), 6.37 (t, $J = 2.2$ Hz, 2H), 3.97 (t, $J = 6.5$ Hz, 8H), 3.30 – 3.24 (m, 8H), 3.04 (s, 36H), 1.75 – 1.62 (m, 16H), 1.46 – 1.38 (m, 8H), 1.37 – 1.24 (m, 40H).

^{13}C NMR (151 MHz, DMSO- d_6) δ 160.49, 139.40, 129.32, 105.42, 101.19, 67.96, 65.77, 52.63, 29.39, 29.25, 29.23, 28.96, 26.21, 26.02, 22.50.

HRMS (ESI-TOF): 645.3853 [$\text{M}-2$] $^{2+}$

4,4',4'',4'''-(((1*E*,1'*E*)-1,4-phenylenebis(ethene-2,1-diyl))bis(benzene-5,3,1-triyl))tetrakis(oxy))tetrakis(*N,N,N*-trimethylbutan-1-aminium) iodide (**COE2-3C-C4**)



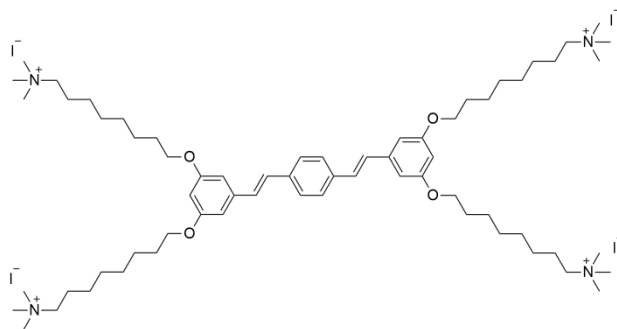
From **2-6a**

^1H NMR (600 MHz, DMSO- d_6) δ 7.60 (s, 4H), 7.25 (dd, $J = 36.5, 15.9$ Hz, 4H), 6.81 (s, 4H), 6.44 (s, 2H), 4.05 (t, $J = 6.2$ Hz, 8H), 3.43 – 3.37 (m, 8H), 3.10 – 3.04 (m, 32H), 1.90 – 1.79 (m, 8H), 1.74 (p, $J = 6.8$ Hz, 8H).

^{13}C NMR (126 MHz, DMSO- d_6) δ 160.27, 139.60, 136.82, 129.03, 128.81, 127.38, 105.66, 101.43, 67.32, 65.47, 52.72, 26.08, 19.69.

HRMS (ESI-TOF): 528.2205 [M-2] $^{2+}$

8,8',8'',8'''-(((1E,1'E)-1,4-phenylenebis(ethene-2,1-diyl))bis(benzene-5,3,1-triyl))tetrakis(oxy)) tetrakis(N,N,N-trimethyloctan-1-aminium) iodide (COE2-3C-C8)



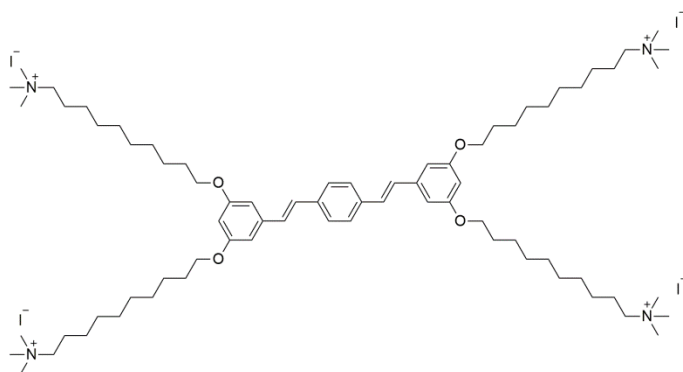
From **2-6c**

^1H NMR (500 MHz, DMSO- d_6) δ 7.60 (s, 4H), 7.33 – 7.14 (m, 4H), 6.77 (s, 4H), 6.39 (s, 2H), 3.99 (s, 8H), 3.35 – 3.22 (m, 8H), 3.04 (s, 36H), 1.80 – 1.59 (m, 16H), 1.51 – 1.20 (m, 32H).

^{13}C NMR (151 MHz, DMSO- d_6) δ 160.35, 139.50, 136.60, 128.94, 128.65, 127.41, 105.35, 101.25, 68.20, 66.30, 52.80, 28.79, 28.74, 28.62, 25.81, 25.64, 22.41.

HRMS (ESI-TOF): 640.3478 [M-2] $^{2+}$

10,10',10'',10'''-((((1E,1'E)-1,4-phenylenebis(ethene-2,1-diyl))bis(benzene-5,3,1-triyl))tetrakis(oxy))tetrakis(N,N,N-trimethyldecan-1-aminium) iodide (**COE2-3C-C10**)



From **2-6d**

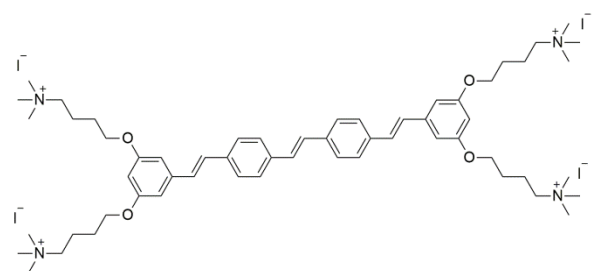
^1H NMR (600 MHz, DMSO- d_6) δ
 7.60 (s, 4H), 7.23 (dd, $J = 32.2$,
 16.3 Hz, 4H), 6.75 (s, 4H), 6.37 (s,

2H), 3.97 (t, $J = 6.3$ Hz, 8H), 3.31 – 3.15 (m, 8H), 3.03 (s, 36H), 1.90 – 1.54 (m, 16H), 1.49 – 1.37 (m, 8H), 1.34 – 1.20 (m, 40H).

^{13}C NMR (126 MHz, DMSO- d_6) δ 160.49, 139.48, 136.82, 128.88, 127.33, 105.39, 101.13, 67.96, 65.80, 52.64, 39.88, 29.38, 29.24, 29.22, 29.19, 28.94, 26.17, 26.01, 22.50.

HRMS (ESI-TOF): 696.4102 [M-2I] $^{2+}$

4,4',4'',4'''-((((1E,1'E)-((E)-ethene-1,2-diylbis(4,1-phenylene))bis(ethene-2,1-diyl))bis(benzene-5,3,1-triyl))tetrakis(oxy))tetrakis(N,N,N-trimethylbutan-1-aminium) iodide (**COE2-4C-C4**)



From **2-7a**

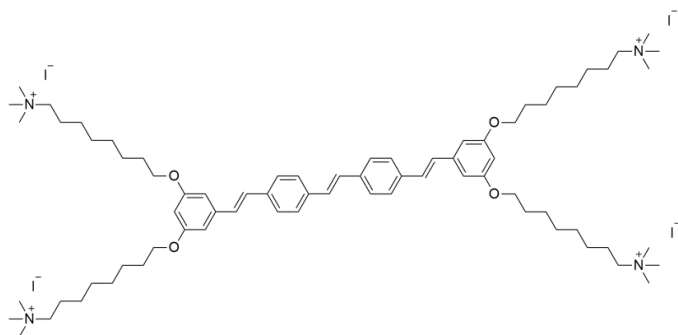
^1H NMR (600 MHz, DMSO- d_6) δ 7.63 (q,
 $J = 8.3$ Hz, 8H), 7.32 – 7.20 (m, 8H), 6.82

(s, 4H), 6.45 (s, 2H), 4.07 (t, $J = 6.2$ Hz, 8H), 3.41 – 3.37 (m, 8H), 3.08 (s, 36H), 1.90 – 1.83 (m, 8H), 1.79 – 1.73 (m, 8H).

^{13}C NMR (126 MHz, DMSO- d_6) δ 160.29, 139.63, 137.04, 136.74, 129.08, 128.79, 128.50, 127.38, 105.63, 105.00, 101.44, 67.28, 65.47, 52.70, 40.30, 40.13, 39.96, 39.80, 39.63, 26.11, 19.70.

HRMS (ESI-TOF): 579.2454 [M+H] $^+$

8,8',8'',8'''-((((1E,1'E)-((E)-ethene-1,2-diylbis(4,1-phenylene))bis(ethene-2,1-diyl))bis(benzene-5,3,1-triyl))tetrakis(oxy))tetrakis(N,N,N-trimethyloctan-1-aminium) iodide (COE2-4C-C8)



From **2-7c**

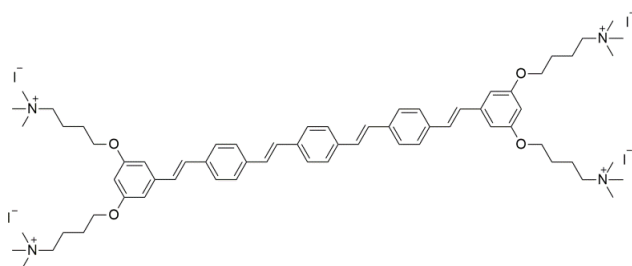
^1H NMR (600 MHz, Chloroform- d)
 δ 7.66 – 7.59 (m, 8H), 7.36 – 7.16

(m, 6H), 6.77 (s, 4H), 6.39 (s, 2H), 3.99 (t, $J = 6.5$ Hz, 8H), 3.28 (dd, $J = 10.7, 6.4$ Hz, 8H), 3.04 (s, 36H), 1.75 – 1.65 (m, 16H), 1.48 – 1.25 (m, 32H).

^{13}C NMR (126 MHz, DMSO- d_6) δ 160.51, 139.52, 136.97, 136.80, 128.90, 128.46, 127.34, 105.39, 101.16, 67.93, 65.76, 52.61, 39.98, 29.18, 29.03, 28.94, 26.19, 25.94, 22.49.

HRMS (ESI-TOF): 691.3712 [M-2I] $^{2+}$

4,4',4'',4'''-((((1E,1'E)-(((1E,1'E)-1,4-phenylenebis(ethene-2,1-diyl))bis(4,1phenylene))bis(ethene-2,1-diyl))bis(benzene-5,3,1-triyl))tetrakis(oxy))tetrakis(N,N,N-trimethylbutan-1-aminium) iodide (**COE2-5C-C4**)



From **2-9a**

¹H NMR (500 MHz, DMSO-*d*₆) δ 7.67 – 7.59 (m, 12H), 7.33 – 7.17 (m, 8H),

6.82 (d, *J* = 2.1 Hz, 4H), 6.45 (t, *J* = 2.1 Hz, 2H), 4.07 (t, *J* = 6.1 Hz, 8H), 3.45 – 3.36 (m, 8H), 3.09 (s, 36H), 1.92 – 1.83 (m, 8H), 1.81 – 1.72 (m, 8H).

¹³C NMR (126 MHz, DMSO-*d*₆) δ 160.30, 139.66, 137.09, 136.96, 136.72, 129.11, 128.57, 128.45, 127.39, 105.64, 101.46, 67.29, 65.48, 52.71, 40.50, 40.33, 40.17, 40.00, 39.83, 39.66, 39.50, 26.13, 19.72.

HRMS (ESI-TOF): 630.2702 [M-2I]²⁺

Chapter 3: Light-Actuated Membrane Permeabilization by a COE Photoswitch

3.1 Introduction

The first example of photo-activated release of the internal contents within liposomes was in 1977 when rhodopsin was shown to allow rapid permeation of inorganic cations through phosphatidylcholine membranes following exposure to light.¹²² This observation was attributed to membrane disruption caused by the *cis* to *trans* isomerization of retinal, the chromophore of rhodopsin. The concept of on-demand release of solutes from within a liposome is still an active area of research today, particularly in the development of drug delivery systems.¹²³⁻¹²⁵ While various stimuli such as temperature,^{126, 127} pH,^{128, 129} ultrasound,^{130, 131} and magnetism,¹³² have been employed to induce solute release from liposomes, light remains an ideal option due to the possibility for high temporal and spatial control.¹³³

Light-activated release from liposomes can be achieved by chemical cross-linking,¹³⁴ cleaving bonds within lipids,¹³⁵ or, as in the case of the rhodopsin example, isomerization. Various photo-isomerizable chromophores have been investigated including retinoyl,¹³⁶ spiropyran,¹³⁷ stilbene,¹³⁸ and azobenzene.¹³⁹ Specific additives, such as cholesterol, have been used to enhance these systems through direct effects on the photoswitch unit (i.e. red-shifted absorption)¹⁴⁰ or by promoting the formation of photoswitch-rich domains within the bilayer.¹⁴¹ The incorporation of azobenzene groups into designer surfactants has emerged as a common method to localize the isomerizable component within the bilayer.¹⁴²⁻¹⁴⁴ In

this chapter, the design, synthesis, and application of the first COE photo-actuator system will be described (Figure 3-1). A number of beneficial attributes of COEs, such as the ability to spontaneously intercalate into membranes and the compatibility with living systems, will be leveraged to improve upon prior surfactant-based technologies.

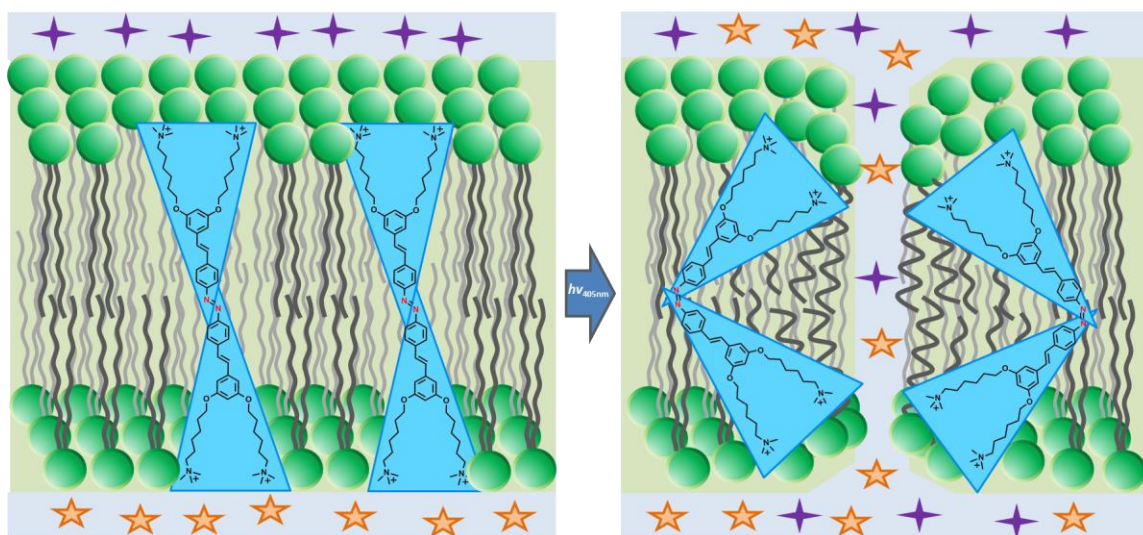


Figure 3-1 Cartoon schematic of light-activated membrane permeabilization mediated by the photoisomerization of the novel conjugated oligoelectrolyte, DSAzB.

3.2 Design and synthesis of a photo-isomerizable COE

As a parent structure for the design of a photo-isomerizable COE, we selected the well-studied COE2-4C (“COE2-4C-C6” in Chapter 2). As previously described, COE2-4C associates well with bacterial and model membranes but does not have significant antimicrobial activity. Furthermore, it was shown in Chapter 2 that this structure does not cause significant membrane permeabilization. In order to demonstrate the greatest difference in permeabilizing ability between Z and E

isomers, it is important that the E isomer not cause significant effects on permeability. It is also beneficial that this parent structure contains three internal olefins, allowing for the central stilbene unit to be replaced with azobenzene while maintaining the rest of the symmetrical structure. The same cannot be said for the 3- and 5-ring analogous (with two or four ethynylene groups, respectively, there is no “central” olefin). This simple substitution would also be possible in the 2-ring analogue but the 4-ring structure has a number of predicted benefits: higher degree of association with membranes, lower antimicrobial activity, lower probability of permeabilizing effect of the E isomer, and red-shifted absorbance. The structures of the parent COE2-4C and the two isomers of the photoswitch COE, DSAzB, are shown below in Figure 3-2.

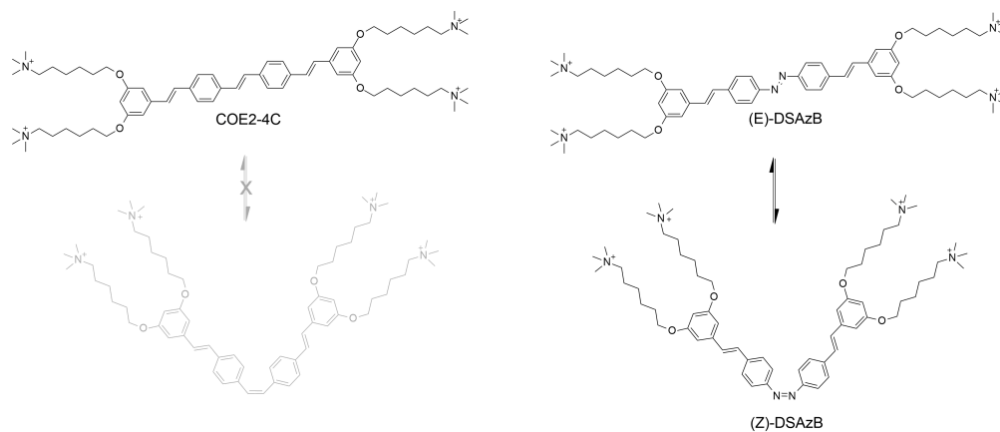


Figure 3-2 Rational design of a COE photoswitch based on our well-studied COE2-4C framework.

DSAzB was prepared as shown in Figure 3-3 in collaboration with Dr. Dirk Leifert, a postdoc in our group. P-toluidine was first converted to the nitroso analogue (**3-1**), which was then reacted with another equivalent of p-toluidine to afford **3-2**. Radical bromination and the Arbuzov reaction were used to form **3-5**. This intermediate was

reacted with benzaldehyde derivative **3-4** (prepared following published protocol)⁴⁴ to afford the final neutral intermediate **3-6**. The target compound (**3-7**), “DSAzB,” was formed by quaternization with trimethylamine.

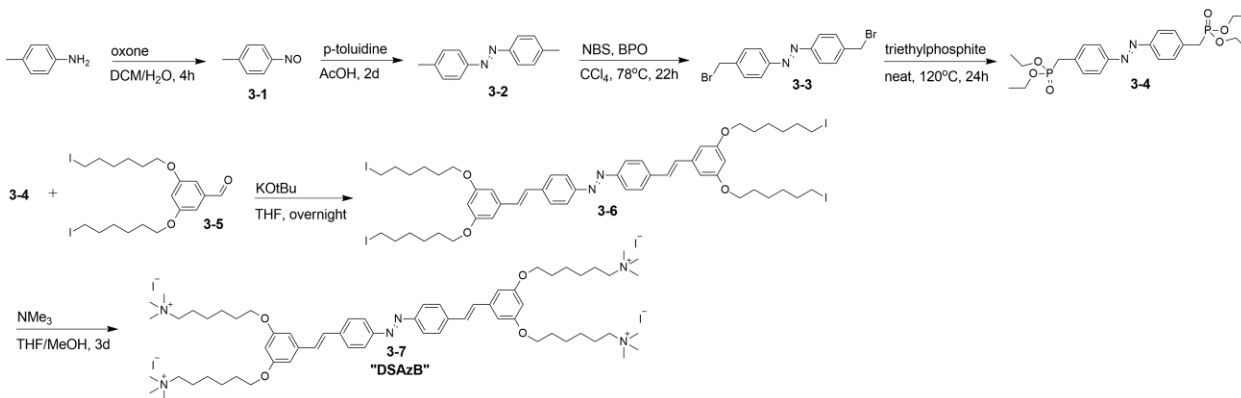


Figure 3-3 Synthetic preparation of the photoisomerizable COE, “DSAzB.”

3.3 Photophysical Properties of DSAzB

Characteristics of the DSAzB photo-isomerization process were measured by continuously exposing samples to 405 nm light (LED, 3.75 mW/cm²) while collecting sequential absorbance spectra (320-580 nm, CCD). Samples were prepared in water, 50 mM PBS, or *E. coli* total lipid extract (ECE) (Avanti Polar Lipids). Additionally, the isomerization process of the neutral analogue **3-6** was measured in the same manner in toluene. The spectra in Figure 3-4 show the dynamics of the isomerization process over two minutes.

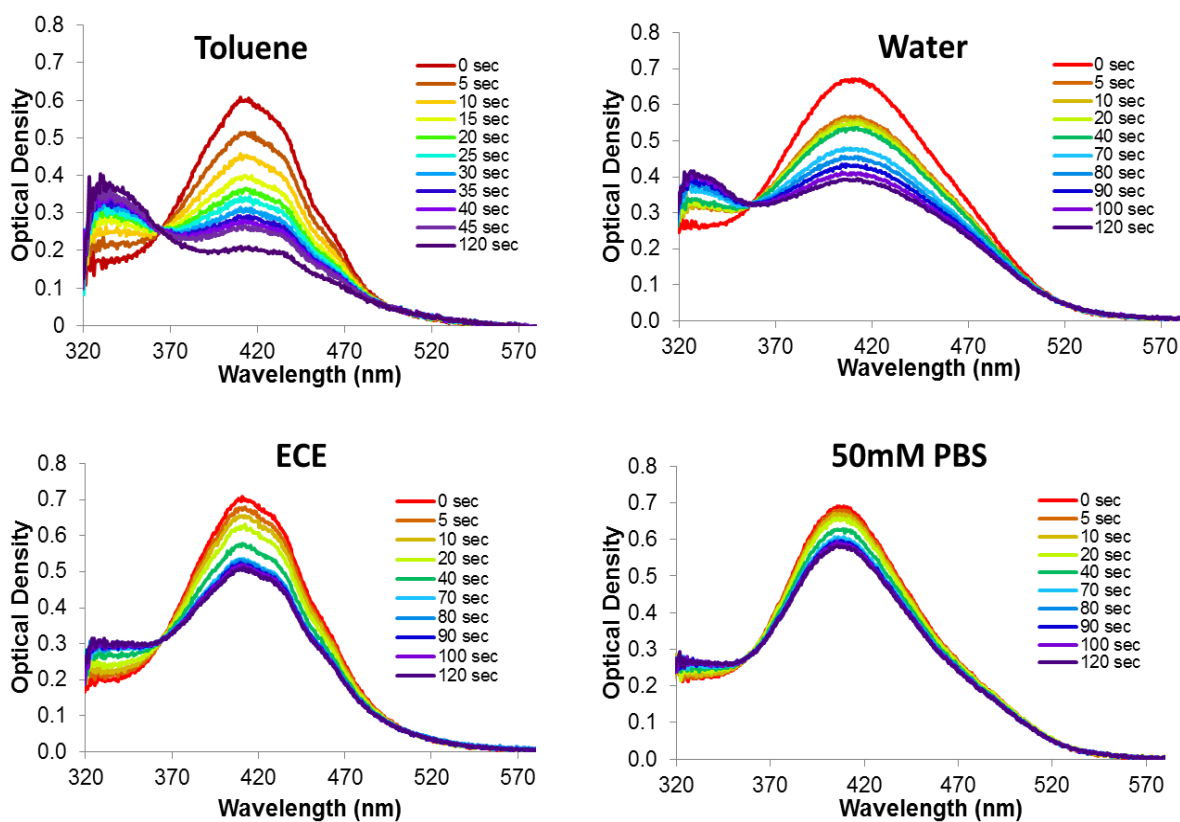


Figure 3-4 Kinetic absorption spectra of DSAzB and its neutral analogue during *E*-to-*Z* photoisomerization in various solvents.

The similarity of the spectra in ECE to those in toluene (and not those in aqueous media), specifically the position of λ_{\max} and the occurrence of vibronic peaks, indicate that DSAzB in the ECE sample is residing in a non-polar environment. This is strong evidence that the COE is intercalated within the lipid bilayer.

One observation from these data is that the isomerization process is more efficient in less-polar media, a result that is consistent with the literature on substituted azobenzene compounds.¹⁴⁵ It is interesting to note, however, that the process is less efficient than expected once intercalated in ECE liposomes. Based on the similarity of polarity, it would be expected that isomerization in ECE

liposomes would reflect that of toluene (and certainly be more efficient than in water). The fact that isomerization is less efficient than anticipated simply based on polarity of the environment suggests that interactions with the membrane present an additional barrier to forming a large population of the Z isomer. This could either be due to a higher activation barrier or a relatively higher energy of the Z isomer relative to the E isomer (i.e. the isomerization back to E might be faster). As the photophysical properties of DSAzB were not the main focus of this effort, we did not explore this phenomenon further.

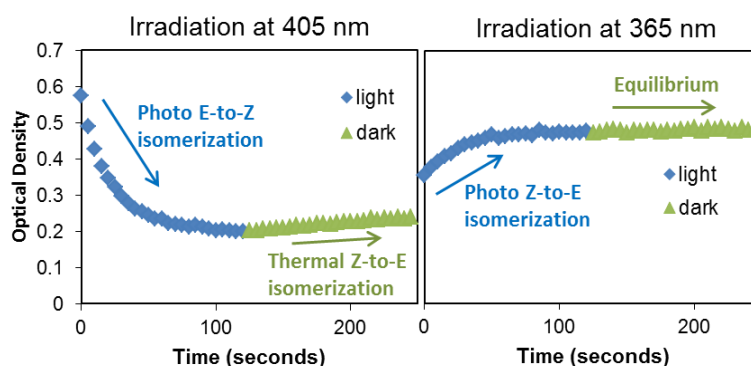


Figure 3-5 Kinetic optical density (405 nm) measurements of DSAzB during *E*-to-*Z* photoisomerization, *Z*-to-*E* thermal isomerization, *Z*-to-*E* photoisomerization, and thermodynamic equilibrium.

With an understanding of the local-environment effects on Z-to-E isomerization, we set out to explore the kinetics of thermal- and photo-isomerization from the E isomer to the Z isomer. Figure 3-5 shows the absorption of DSAzB at 405 nm during irradiation at 405 nm followed by isomerizing back to the E isomer, first in the dark and then under irradiation at 365 nm (the approximate λ_{\max} of the Z isomer). The initial isomerization process appeared to saturate after ~100 seconds of irradiation.

Thermal isomerization back to the E isomer occurred slowly after irradiation was ended. Irradiation with 365 nm light resulted in a rapid Z-to-E transition that reached equilibrium after ~30 seconds. This equilibrium condition remained unchanged once irradiation was ended. It is worth noting that the E/Z ratio in this final state is lower than the original state.

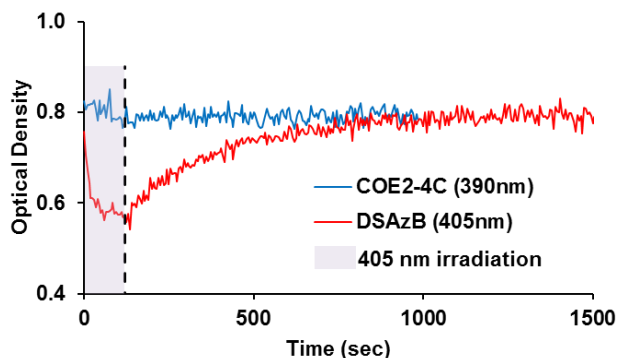


Figure 3-6 Comparison of DSAzB and COE2-4C response to irradiation at 405 nm.

As we intended to use COE2-4C as a non-isomerizable control COE in subsequent experiments, it was necessary to demonstrate that no isomerization was observed under the conditions which lead to isomerization of DSAzB. Figure 3-6 shows the absorption of COE2-4C ($\lambda_{\text{max}} = 390 \text{ nm}$) and DSAzB during and after 405 nm irradiation for 120 seconds. No detectable change in the absorption of COE2-4C is observed, indicating that no isomerization occurred under these conditions.

3.4 DSAzB-Mediated Photo-Triggered Calcein Release from Liposomes

To examine the ability of DSAzB to act as a photo-actuator for liposome permeabilization, we used the standard calcein release assay.¹⁴² When calcein is

loaded in high concentration in liposomes, self-quenching limits fluorescence. Upon release to bulk solution, fluorescence intensity increases. To minimize the complexity of the system, we used unilamellar vesicles of 20:80 DMPG:DMPC in place of the ECE vesicles used in the previous section. Liposomes were prepared by extrusion¹⁰⁵ in the presence of 20 mM calcein and purified by size-exclusion chromatography (Sephadex G50) to remove extraliposomal calcein. After staining calcein-loaded liposomes with 1 mol % DSAzB, fluorescence was measured for 14 minutes in the dark at various temperatures. The samples were irradiated at 405 nm at an intensity of 15 mW/cm² for 1 minute. Fluorescence measurements were continued for an additional 10 minutes. The resulting data are presented in Figure 3-7.

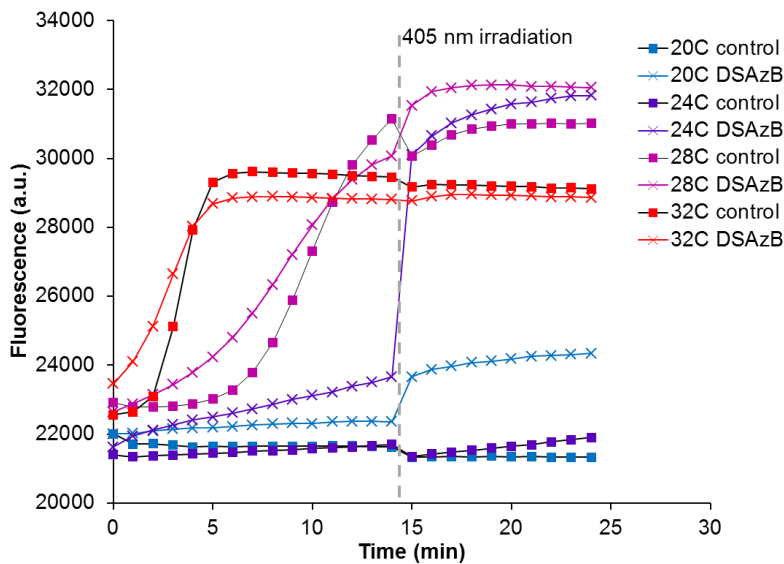


Figure 3-7 Temperature-dependence of DSAzB photo-actuation of liposome permeabilization as measured by calcein release. Assuming the T_m of the liposomes is similar to DMPG or DMPC independently ($\sim 24^\circ\text{C}$), DSAzB was able to increase permeability above and below T_m .

At 20°C, the lowest temperature tested, minimal calcein release was observed before irradiation for either the control or DSAzB-stained samples. Following irradiation, the fluorescence of the control sample decreased slightly, indicating some level of calcein photobleaching. The DSAzB sample, on the other hand, showed a significant increase in fluorescence as the isomerization process allowed for calcein to leak from the liposomes. A similar result was observed for the samples at 24°C with the effect of DSAzB being more pronounced. At 28°C, the control and DSAzB-stained liposomes were both permeable before irradiation and much of the calcein escaped the liposomes in the first 14 minutes (although a small spike in fluorescence was still observed in the DSAzB sample). It is known that liposomes are most permeable at their lipid transition temperature (T_m) due to the simultaneous presence of multiple phases which gives rise to grain boundaries.^{146, 147} Given that the T_m for DMPC and DMPG are 24°C and 23°C (Avanti Polar Lipids), respectively, it is conceivable that the T_m of this system was near 28°C. A similar observation was made for the samples at 32°C but the leakage appeared to plateau after 5 minutes. A full description of the experiment can be found in section 3.8 but a description of the heating may be warranted for the present discussion. All samples in this experiment were loaded onto 96-well plates and placed in a plate reader at room temperature (~22°C). The entire system was then heated to the indicated temperature, all the while taking fluorescence measurements. In general, samples took ~5-10 minutes to reach the set temperature (hence the 14 minute period before irradiation). Assuming the T_m is at or around 28°C, the 32°C samples would have passed through T_m after a few minutes. This may explain the plateau in leakage in

the 32°C samples that was observed earlier and at a lower level of fluorescence than for the 28°C samples. Despite the confounding effects of passing through T_m during heating, this experiment proved that DSAzB can act as a photo-actuator to release solutes within liposomes. Furthermore, it appeared that DSAzB could have this effect below, at, or above the T_m .

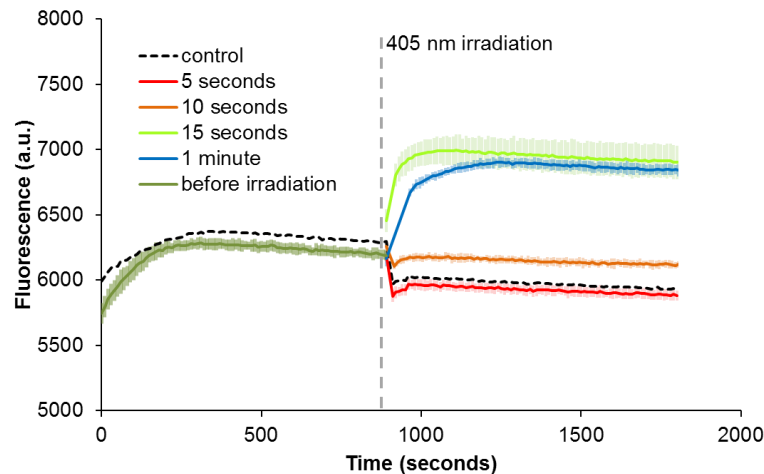


Figure 3-8 Effect of light dose on DSAzB photo-actuated liposome permeabilization. The significant difference between 10 and 15 seconds of irradiation suggests permeability does not increase linearly with the amount of DSAzB that isomerizes. Instead there appears to be a “tipping point.”

We next modified our experimental protocol to better investigate the effects of DSAzB above T_m . Rather than slowly allowing the samples to equilibrate to a set temperature, we quickly pre-warmed the calcein-loaded liposomes to 30°C before adding DSAzB. Once the samples were warmed, DSAzB was added and the fluorescence measurements initiated. The results of this modified experiment are shown in Figure 3-8. In the first 14 minutes (pre-irradiation), both the control and DSAzB-stained samples experience a brief period of calcein leakage before stabilizing. Irradiation with 405 nm light at 15 mW/cm² was again used to isomerize

DSAzB but the exposure time was varied. Samples that received only 5 seconds of irradiation were nearly indistinguishable from the control. Increasing the exposure to 10 seconds resulted in a small increase in fluorescence relative to control (although the effect of calcein photobleaching was stronger than that of increased permeability). Samples that were exposed for 15 seconds showed a massive increase in fluorescence. Further increasing the exposure to 1 minute did not result in a further increase in fluorescence but did seem to cause more photobleaching. There are two significant observations to be made from this data. First, DSAzB is able to effectively produce light-activated release of solutes from liposomes above their T_m . The second observation is that there appears to be a “tipping-point” in exposure time which may indicate a cooperative mechanism for the effects of DSAzB. A similar observation of cooperative action was made previously for an azobenzene-surfactant system.¹⁴⁸

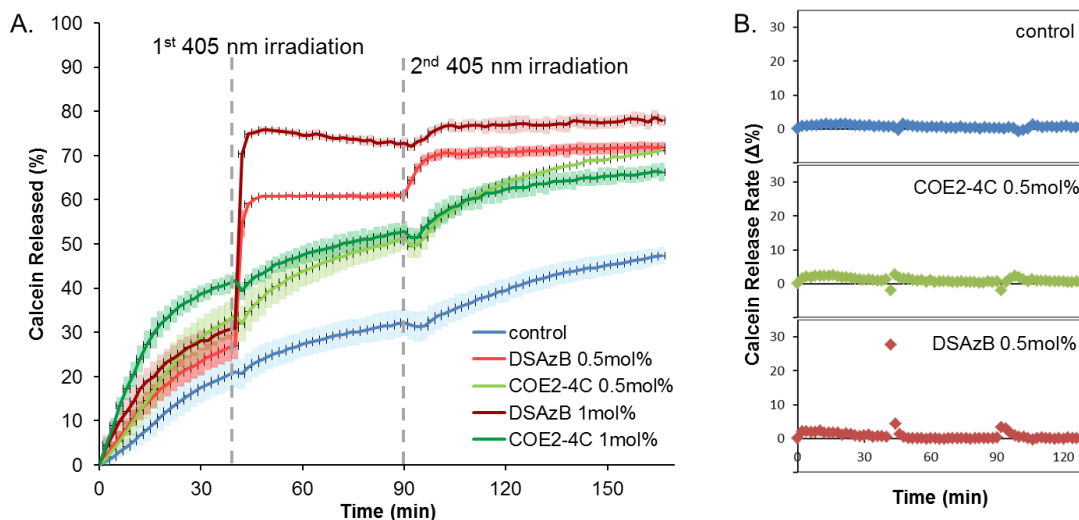


Figure 3-9 DSAzB photo-actuated liposome permeabilization – effect of DSAzB concentration and comparison to the non-isomerizing analogue, COE2-4C.

In our final calcein release study, we wanted to determine what percentage of total calcein was released, what effect COE concentration had, how the non-isomerizable COE2-4C compared to DSAzB in permeabilizing ability, and if sequential irradiations could result in multiple permeabilization events. As shown in Figure 3-9A, a single irradiation of 30 seconds allowed for the release of >30% of the calcein within the liposomes stained with 0.5 mol % DSAzB. Twice as much DSAzB resulted in slightly higher permeability both before and after irradiation. As expected, COE2-4C increased permeability before irradiation to approximately the same degree as DSAzB but irradiation had no effect. A second irradiation event was able to release an additional 10% of calcein from liposomes with 0.5 mol % DSAzB. The rapid recovery from a permeable to a less-permeable state following irradiation was observed in all of the calcein release studies but is highlighted in Figure 3-9B. An explanation of this phenomenon will be ventured later in this chapter but its potential utility will be discussed here. This rapid switching, coupled with the ability to produce multiple permeabilization events, is ideal for precise spatial and temporal control in a dynamic system. For example, consider the use of such a system in treating malignant tumors. If the area immediately around a tumor was irradiated (please excuse the obvious shortcomings of the present system based on the required wavelength of light), DSAzB-stained liposomes containing a therapeutic agent through the blood would release their cargo only when they passed through the target area. As the liposomes circulate through the blood around healthy tissues, the cargo would remain inside the liposomes until they again pass near the tumor.

3.5 Effect of DSAzB Isomerization on Lipid Ordering

To investigate how the isomerization of DSAzB affects the physical properties of bilayers, we used a time-course EPR spectroscopy experiment to track the dynamics of lipid order. 20:80 DMPG:DMPC unilamellar vesicles were prepared with 2 mole % DSAzB and 1 mole % of the spin label 16-SASL. One side of the resonant cavity of the spectrometer was uncovered such that the samples could be irradiated during the experiment. Spectra were collected every minute for 15 minutes. After the fourth measurement, irradiation of the sample was initiated while continuing to collect spectra every minute. After the seventh measurement, irradiation was stopped and spectra were collected for nine more minutes.

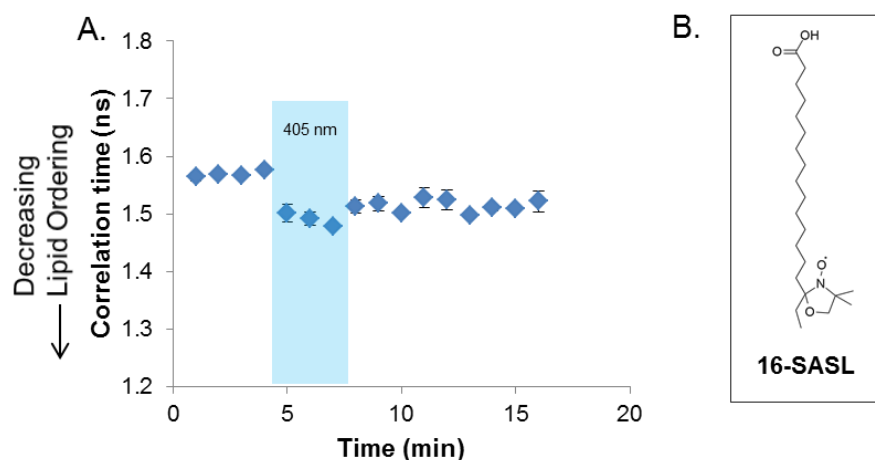


Figure 3-10 (A) Effect of DSAzB isomerization on correlation time T_{2B} for 16-SASL in 20:80 DMPG:DMPC liposomes. Irradiation of the sample resulted in decreased T_{2B} , indicating that lipid order was reduced as a result of DSAzB isomerization. (B) Structure of the spin label 16-SASL used in this study.

As shown in Figure 3-10, isomerization of DSAzB resulted in a reduced correlation time (T_{2B}), indicating the lipids became less ordered. In Chapter 2 it was shown that the total length of COEs govern their effects on lipid order, with short COEs reducing order and long COEs increasing order. The observation that the Z-isomer of DSAzB resulted in reduced order relative to the E-isomer is in agreement with this prior conclusion. It was also shown in Chapter 2 that changes in lipid order cannot explain changes in permeability. This appears to be the case for the isomers of DSAzB as well. After irradiation was stopped, the correlation time increased slowly, likely as a result of DSAzB thermal isomerization back to the E-isomer. Based on the calcein release studies in Section 3.4, the rate at which correlation time returns to the initial value is much slower than the rate at which the low-permeability state is restored. While lipid order seems to be determined by the shape of DSAzB, it does not appear to play a role in permeability. This suggests that increased permeability is not a direct result of membrane disruption and supports the idea of a cooperative effect involving many DSAzB molecules (one possible mechanism will be suggested in Section 3.7).

3.6 Photo-triggered Permeabilization of Live Bacterial Cells by DSAzB

3.6.1 Propidium iodide influx a metric for DSAzB-induced permeability

Given the positive results in the liposome permeability experiments, it was reasonable to assume that DSAzB could act as a permeability actuator in living systems as well. Unlike many photo-activated systems for increasing membrane

permeability, DSAzB has the advantage of being able to spontaneously intercalate into pre-formed lipid bilayers (such as biological membranes). To determine if the isomerization of DSAzB can lead to bacterial membrane permeabilization, we monitored the influx of propidium iodide (PI) into *S. epidermidis* cells. PI is routinely used as a “dead stain” in bacterial viability assays due to its inability to cross intact membranes.¹⁴⁹ More recently, PI influx into cells has been used to assess membrane integrity.^{150, 151} This process can be measured in real time due to the red-shift in PI emission following interaction with intracellular RNA and DNA. In this experiment, *S. epidermidis* cells were stained with either DSAzB or COE2-4C or left untreated. Fluorescence from PI (excitation – 525 nm, emission – 620 nm) was recorded through time, before and after irradiating the samples with 405 nm light. The results, shown in Figure 3-11, demonstrate that isomerization of membrane-intercalated DSAzB can act as a permeability photo-actuator in live bacteria. Before irradiation, cells stained with 2.5 μ M DSAzB or COE2-4C resisted the uptake of PI (similar to control). While irradiation did not increase PI influx in COE2-4C or control samples, a spike in fluorescence was observed in the DSAzB samples immediately following the first and second irradiation events (30 seconds each).

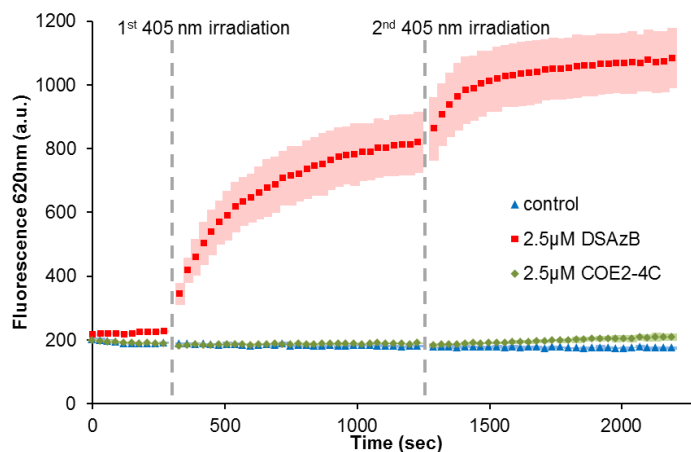


Figure 3-11 DSAzB photo-actuation of *S. epidermidis* membrane permeability as measured by PI influx. Similar to the calcein release studies, irradiation of DSAzB-stained cells increases membrane permeability while irradiation of control or COE2-4C-stained cells has no effect on permeability.

3.6.2 Bacterial growth inhibition and bactericidal activity of DSAzB

To better understand the effect of DSAzB on microbes, we measured its ability to inhibit *S. epidermidis* growth using standard broth microdilution. Cells were diluted to $OD_{600} = 0.002$ and exposed to COE2-4C or DSAzB over the concentration range 0.25-128 μM . The MICs (defined as the lowest concentration that resulted in a 90% reduction of growth in overnight culture) for COE2-4C and DSAzB were 2 μM and 1 μM , respectively. It bears noting that the initial cell density in this experiment was $\sim 1/500^{\text{th}}$ of the density used in the PI influx experiment above. As such, it is unlikely that the 2.5 μM used in the previous experiment would have negatively impacted the growth of the cells.

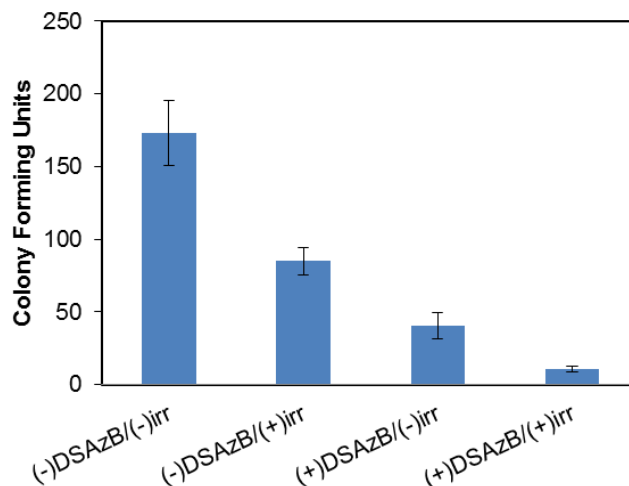


Figure 3-12 Bactericidal activity of 405 nm irradiation, DSAzB, and a combination of both against *S. epidermidis*. The bactericidal activity of DSAzB and irradiation appears to be an additive effect of the two treatments applied independently.

In addition to growth inhibition, we assessed the bactericidal activity of DSAzB with- and without-irradiation. *S. epidermidis* cells ($OD_{600} = 1.0$) were treated with 2.5 μM DSAzB in 150 mM PBS to mimic the conditions of the PI influx assay. Control and DSAzB samples were either kept in the dark or exposed to 30 seconds of 405 nm irradiation. All samples were then diluted to approximately 1×10^4 CFUs/mL (assuming 100% survival) in BHI media. 10 μL of these samples were spread on BHI agar plates and incubated overnight at 37°C. The number of colonies that grew for each treatment group is shown in Figure 3-12. Both DSAzB and irradiation were able to reduce CFUs independently (~75% and ~50% reduction, respectively). Samples that received the combined treatment of DSAzB and irradiation experienced approximately 1 \log_{10} reduction in viable cells, indicating that the effects of the two treatments are essentially additive. This suggests that under these particular conditions, the isomerization process does not have significant bactericidal effects.

Furthermore, these results indicate that the increased PI influx observed in Section 3.6.1 was not a result of killing the bacteria. Neither irradiation nor DSAzB alone was able to increase PI influx but both were shown to be slightly bactericidal. Additionally, the instantaneous increase in PI influx following isomerization of DSAzB is likely too fast of a process to be explained by bactericidal activity.

3.7 Conclusions

In conclusion, we designed and synthesized a novel COE (DSAzB) that functions as a light-activated membrane permeabilizing agent for model- and biological-membranes. By replacing the central olefin of the well-studied COE2-4C with an azo functionality, we introduced a photo-switch into the conjugated core of the structure. Relative to azobenzene, DSAzB has a red-shifted absorption, allowing for photo-isomerization with visible light (405 nm). Similar to others COEs developed in our group, DSAzB spontaneously intercalates into lipid bilayers. Intercalation of the E-isomer decreases lipid order (as demonstrated by EPR) but does not impact permeability of liposomes or bacteria. Photo-isomerization of DSAzB within a membrane results in increased permeability as evident by calcein release from liposomes or PI influx into live *S. epidermidis*. In both cases it was shown that increased permeability can be triggered multiple times. EPR experiments demonstrated that the kinetics of effects on lipid order are comparable to isomerization rates, both of which are slower than the permeability on/off switching rate. These results suggest that lipid disorder as a result of DSAzB isomerization is

not directly responsible for the observed permeability increase (consistent with results presented in Chapter 2). The fact that liposome permeability is not linearly related to light dose is another indication that the mechanism is related to something other than lipid order. Section 3.4 describes an apparent threshold dose, below which there is little effect on permeability. Cooperative effects of other photoactuators have been hypothesized previously¹⁴⁸ and may be important in the present system as well. If a cooperative effect is required for “turning on” permeability, it is reasonable to image that “turning off” permeability is also dependent on groups of molecules rather than the effects of each single molecule. For example, DSAzB may form rich- and poor- domains within the liposome (see Section 6.2 for a discussion of COE aggregation and domain formation). During isomerization, a critical point could be reached where a sufficient population of (Z)-DSAzB is present in the rich domains to cause membrane disruptions such as pores^{152, 153} or phase boundaries,^{115, 154, 155} both of which are known mechanisms of permeabilization. These (Z)-DSAzB rich domains, which would have formed when DSAzB was primarily in the E-form, may not be thermodynamically favorable following isomerization. Dissipation of the domains to form a more homogenous COE-lipid mixture could cause permeability to “turn off”, even though the individual DSAzB molecules would still be in the Z-form. A schematic depiction of this process is present in Figure 3-13. While only a hypothesis, a number of observations hint to a mechanism of this nature and there is no data to the contrary. Studies of how COEs increase permeability are ongoing and future discoveries are expected to increase our understanding of the DSAzB photo-actuator system.

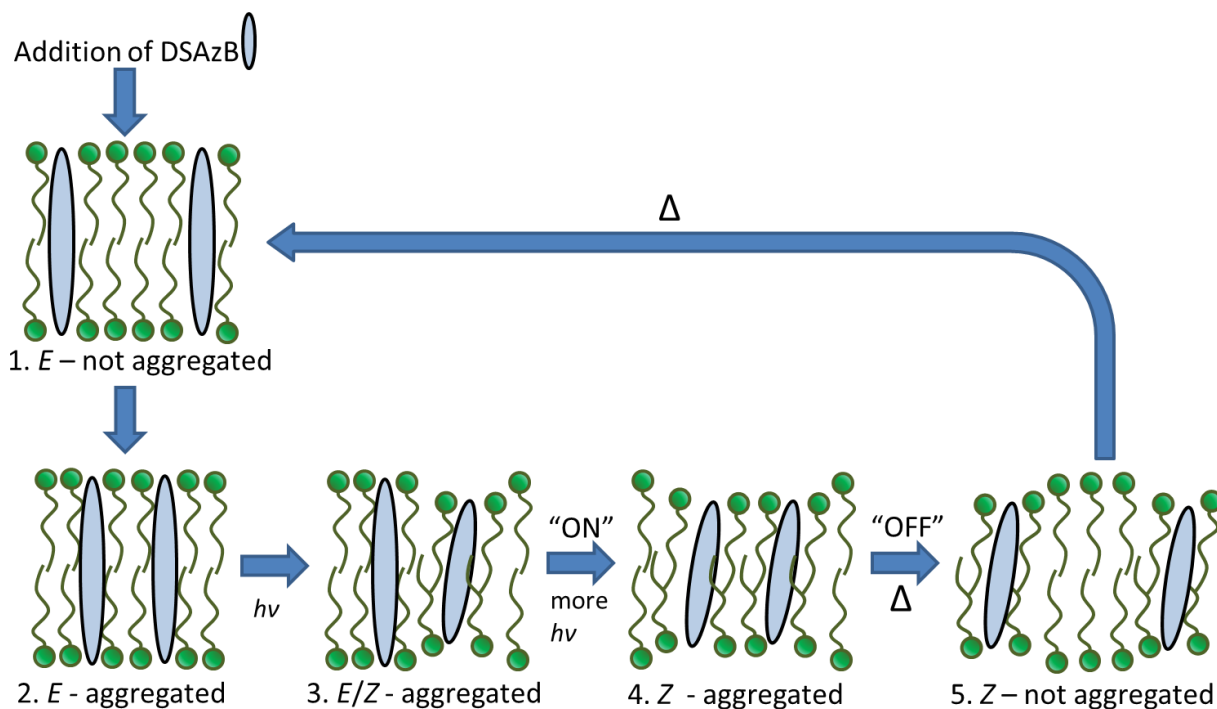


Figure 3-13 A potential mechanism for DSAzB-mediated photo-actuation of membrane permeability. (1) Following the addition of DSAzB to liposomes or cells, DSAzB spontaneously intercalates within the lipid bilayer. (2) Domains of high DSAzB concentration are formed. (3) Irradiation results in the isomerization of some fraction of DSAzB but no increase in membrane permeability is observed. (4) Continued irradiation causes the concentration of the Z-isomer to reach a tipping-point, resulting in increased membrane permeability. (5) Domains rich in the Z-isomer are unstable and thus DSAzB de-aggregates to form a more-homogenous mixture within the lipid bilayer, resulting in a loss of membrane permeability. (5 to 1) DSAzB slowly isomerizes back to the E-isomer, returning the system to the original state.

3.8 Experimental methods

Materials and Instrumentation

Solvent and reagents for the synthesis of DSAzB were purchased from common suppliers such as Sigma Aldrich, Acros Organics, Fisher Scientific, Alfa Aesar, Ark Pharm, and TCI and were used as received. Lipids (DMPC, DMPG, and *E. coli* total lipid extract) were purchased from Avanti Polar Lipids. The spin probe 16-SASL was purchased from Sigma Alrich. Dry and inhibitor-free THF was dispensed under

argon from a solvent purification system using packed alumina columns. Throughout the preparation of DSAzB, flash chromatography was carried out on Silicycle SiliaFlash P60 silica gel under positive Argon pressure. For thin layer chromatography, EMD Millipore Analytical Chromatography TLC Silica gel 60 F254 with aluminum backing was used with UV light (254/366 nm) for detection. Synthetic intermediates were characterized by $^1\text{H-NMR}$ (400 MHz and 500 MHz) and $^{13}\text{C-NMR}$ (101 MHz and 126 MHz) using an Agilent Technologies 400-MR DDR2 400 MHz or a Varian Unity Inova 500 MHz spectrometer. The multiplicity of all signals was described by s (singlet), d (doublet), t (triplet) and m (multiplet). Chemical shifts (δ in ppm) were referenced to the solvent residual peak of CDCl_3 ($^1\text{H-NMR}$: $\delta = 7.26$; $^{13}\text{C-NMR}$: $\delta = 77.0$) or DMSO-d_6 ($^1\text{H-NMR}$: $\delta = 2.50$; $^{13}\text{C-NMR}$: $\delta = 39.52$). Additionally, high-resolution mass spectrometry was used to confirm the identity of the compounds (Waters GCT Premier time-of-flight mass spectrometer). Size exclusion chromatography (SEC) for calcein release experiments was carried out on Sephadex G50 (50-150 μm), preequilibrated and eluted with 50 mM phosphate buffer saline. Calcein release and MIC experiments were conducted using a Tecan M200 plate reader. VitrotubesTM quartz capillaries (0.60 mm ID X 0.84 mm OD) were used for EPR experiments. Capillaries were sealed using Leica CRITOSEAL[®]. Continuous wave X-Band EPR spectra were collected on a Bruker EMXplus Spectrometer. The resonant chamber (Bruker ER 4119HS-LC) was equipped with an optical window to facilitate photoisomerization experiments.

Calcein Release Studies

Lipid films (10 mg, 20:80 DMPG:DMPC) were prepared in 2 Dr vials by concentrating chloroform solutions (10 mg/mL) using rotary evaporation. Films were re-hydrated with a 20mM calcein solution (1 mL). Large unilamellar liposomes were formed by extrusion¹⁰⁵ through 200nm and 100nm filters at 45 °C. Calcein-loaded liposomes were separated from free calcein by size exclusion chromatography (Sephadex G50, 50 mM PBS). Liposome solutions were diluted to 4 mM (total lipid content) with 50 mM PBS and mixed 1:1 v/v with solutions of DSAzB or COE2-4C in 50 mM PBS. 100 μ L aliquots of the resulting solutions were immediately transferred to a 96-well plate. Time-course measurements of calcein release were conducted on a plate reader with excitation at 495 nm and emission measurements at 520 nm. Isomerization of DSAzB was achieved by ejecting plates from the reader and irradiated with a 405 nm LED (15 mW/cm²). For studies where calcein leakage is listed as a percent of the total calcein content (instead of fluorescence intensity), control samples without COE were treated with Triton X-100 (2 % v/v final concentration) in order to lyse the liposomes and release the entire calcein content. Fluorescence intensity of these samples was set to equal 100% calcein release and all other samples were reported as a percentage of this intensity.

EPR Spectroscopy Experiments

Stock solutions of DMPG (10 mg/mL), DMPC (10 mg/mL), and 16-SASL (1 mg/mL) were prepared in chloroform. These stocks were mixed such that the final composition was 20:80 DMPG:DMPC and 1% 16-SASL. Aliquots (1 mL) of this

solution were transferred to 2 Dr vials and the solvent was evaporated under reduced pressure. Lipid films were further dried under high vacuum overnight. Lipid films (10 mg) were reconstituted in 0.74 mL of water to achieve ~20 mM total lipid and sequentially extruded through 200 nm and 100 nm filters. Liposome solutions were mixed 1:1 v/v with either water or 0.2 mM aqueous solution of DSazB. Approximately 5 μ L of samples were wicked into quartz capillaries, which were then sealed and inserted into 3 mm quartz EPR tubes. On the spectrometer, the cover over the optical window of the resonant chamber was removed. A 405 nm LED was positioned ~50 cm away from the resonant chamber such that the beam would be centered on the optical window. Spectra were collected every minute for four minutes without irradiation, every minute for four minutes with irradiation (~15 mW/cm²), and then every minute for eight minutes without irradiation. EPR spectra were processed in MATLAB R2016b (academic license). A detailed description of the processing and calculations can be found in Section 6.6. Briefly, effective correlation times were calculated according to published methods as follows¹⁰⁶⁻¹⁰⁹:

$$\tau_{2B} = 6.51 \times 10^{-10} \Delta H_0 [(h_0/h_-)^{1/2} - (h_0/h_+)^{1/2}]s \quad \text{Equation 2-1}$$

$$\tau_{2C} = 6.51 \times 10^{-10} \Delta H_0 [(h_0/h_-)^{1/2} + (h_0/h_+)^{1/2} - 2]s \quad \text{Equation 2-2}$$

where the values for ΔH_0 (width of central line in gauss), h_+ (height of low field peak), h_0 (height of central peak), and h_- (height of high field peak) were extracted directly from the spectra.

Minimum Inhibitory Concentration

A single colony of *S. epidermidis* was picked from an agar plate and inoculated into Brain Heart Infusion (BHI) medium. The broth culture were incubated at 37°C overnight with constant shaking. The resulting cell suspension was diluted in fresh BHI medium to an optical density of 0.002 at 600 nm. Log-2 dilutions of DSAzB and COE2-4C in BHI (0.25 μ M to 128 μ M) were prepared on a 96-well plate. The cell suspension added to the wells containing COE solutions as well as control wells without COE. The plate was incubated at 37°C overnight with 200 rpm shaking. The growth of the bacteria was measured by optical density at 600 nm. The minimum inhibitory concentration (MIC) was defined as the concentration of COE that inhibited at least 95% of bacterial growth relative to control. The experiments were performed in triplicate.

Propidium Iodide Influx Experiment

A single colony of *S. epidermidis* was inoculated in BHI medium overnight at 37 °C with shaking. The overnight broth culture was centrifuged (7000 rpm, 4 min) and the cell pellet was washed with 50 mM PBS. Cells were resuspended with 50 mM PBS such that a further 2-fold dilution would produce an optical density of 1 at 600 nm.

In microfuge tubes, 500 μ L of the cell suspension was mixed and incubated with 500 μ L of DSAzB or COE2-4C (5 μ M and 10 μ M) for 30 minutes (final OD₆₀₀ = 1 and final COE concentrations of 2.5 μ M and 5 μ M). After the incubation, cell suspensions were centrifuged (7000 rpm, 4 min) and the supernatant was discarded. Cell pellets were then resuspended in 1 mL of 150 mM PBS to achieve an optical density of 1.

100 μ L of cell suspensions were transferred onto a 96-well plate and 100 μ L of 5 μ M propidium iodide (PI) was added to each well and mixed thoroughly. PI fluorescence (excitation = 525 nm and emission = 620 nm) was measured on a plate reader for 10 minutes. The entire plate was then subjected to an irradiation at 405 nm for 30 seconds before continuing fluorescence measurement for an additional 15 minutes. To illustrate that DSAzB has a capability to repeatedly permeabilize cell membranes, the plate was irradiated for a second time (same conditions) and fluorescence was measured for an additional 15 minutes. Fluorescence signals were measured every 30 seconds during all measurements and the experiment was performed in triplicate.

Bactericidal activity of DSAzB and irradiation at 405 nm

S. epidermidis cells were treated with 2.5 μ M DSAzB at an optical density of 1 at room temperature for 30 minutes. The cells were pelleted (7000 rpm, 4 min), the supernatant was discarded, and the cell pellet was resuspended to an optical density of 1 in 150 mM PBS. In a 96-well plate, 100 μ L of cell suspensions (with or without DSAzB) and 100 μ L PBS were mixed together and the wells were irradiated at 405 nm for 30 seconds. After irradiation, the cell suspensions were diluted in BHI to approximately 1×10^4 cfu/mL. Control and DSAzB-stained cells which had been kept in the dark were similarly diluted in BHI. The diluted suspensions were then aliquoted (10 μ L) and spread on BHI agar plates. The plates were incubated at 37 $^{\circ}$ C overnight and the colonies grew on the plates were counted manually. Plates for each test group were prepared in triplicate.

Chapter 4: COEs as Membrane Anchors for Bioconjugation

4.1 Introduction

Bioconjugation, in the most basic sense, is the chemical coupling of biological and synthetic entities. The biological components are typically proteins, DNA, RNA, or carbohydrates while the synthetic component provides additional functionality such as fluorescence or specific surface reactivity.¹⁵⁶ Downstream applications of bioconjugation include everything from nanomedicine¹⁵⁷ to sensing and imaging.¹⁵⁸ Given the breadth of this field, it should come as no surprise that an equally extensive set of specific chemistries have been developed for the purpose of bioconjugation.¹⁵⁹⁻¹⁶²

Cell surface engineering, which often involves bioconjugation techniques, is the study and manipulation of the interface between cells and their environment.¹⁶³ Recombinant DNA methods have facilitated membrane surface display of proteins for applications such as antibody fragment screening,^{164, 165} whole-cell bioremediation,^{9, 10} biofuel¹⁶⁶ and bioenergy¹⁶⁷ production, biocatalysis,¹⁶⁸ and biosensing.^{169, 170} However, only the chemistry available in the canonical amino acids is accessible through surface display alone. The ability to introduce unnatural chemical functionalities onto the surface of cells represented a major advancement in cell surface engineering and whole-cell bioconjugation technology.^{163, 171} In addition to the incorporation of non-canonical amino acids into surface-displayed proteins, there are two additional routine methods for introducing new functionalities

on the surface of cells – relying on metabolic pathways to “accidentally” introduce non-native substrates in the membrane and direct chemical modification of native biomolecules at the cell surface.^{172, 173}

Modified lipids have been successfully used to introduce reactive functionalities to the surface of cells through liposome-cell fusion.^{174, 175} With their strong propensity for spontaneous intercalation into membranes, it seemed that COEs could function as facile, expedient delivery systems for the introduction of functional chemical handles to membrane surfaces. In addition to ease-of-use considerations relative to liposome fusion systems, COE systems also provide a means for tracking the attached “cargo” by monitoring COE fluorescence.

4.2 Copper-Catalyzed Azide-Alkyne Cycloaddition in Membrane Engineering

Ideal bioconjugation reactions are facile, fast, selective, and simple.¹⁷⁶ As such, copper-catalyzed azide-alkyne cycloaddition reactions (CuAAC), often simply referred to as “click”, have been utilized heavily in bioconjugation.^{161, 177} Although [3+2] azide-alkyne cycloaddition was first described by Huisgen in 1963,¹⁷⁸ it was not until 2002 that the labs of Sharpless and Meldal developed Cu-catalyzed systems that could proceed at biologically-relevant temperatures.^{179, 180} The primary drawback of CuAAC as a bioorthogonal reaction is the very fact that it relies on copper which is known to be harmful to cells.¹⁸¹ To avoid the use of copper, the Bertozzi group applied the knowledge that cyclooctyne reacts violently with phenylazide¹⁸² to develop strain-assisted [3+2] azide-alkyne cycloadditions as

bioorthogonal reactions.¹⁸³ Since this initial discovery, various Cu-free cycloaddition reactions have been developed for bioconjugation.¹⁷⁷ The necessary reactivity of the functional groups, however, can pose problems for synthesis and application. CuAAC is still widely used and represents a simpler system, albeit with obvious disadvantages. To limit the negative effects of the copper catalyst, new ligands have been developed to reduce the required loading and limit interactions with cells.^{184, 185} As a model system, CuAAC utilizing such a ligand was chosen as the ideal starting point for developing COEs as membrane anchors for cell surface engineering.

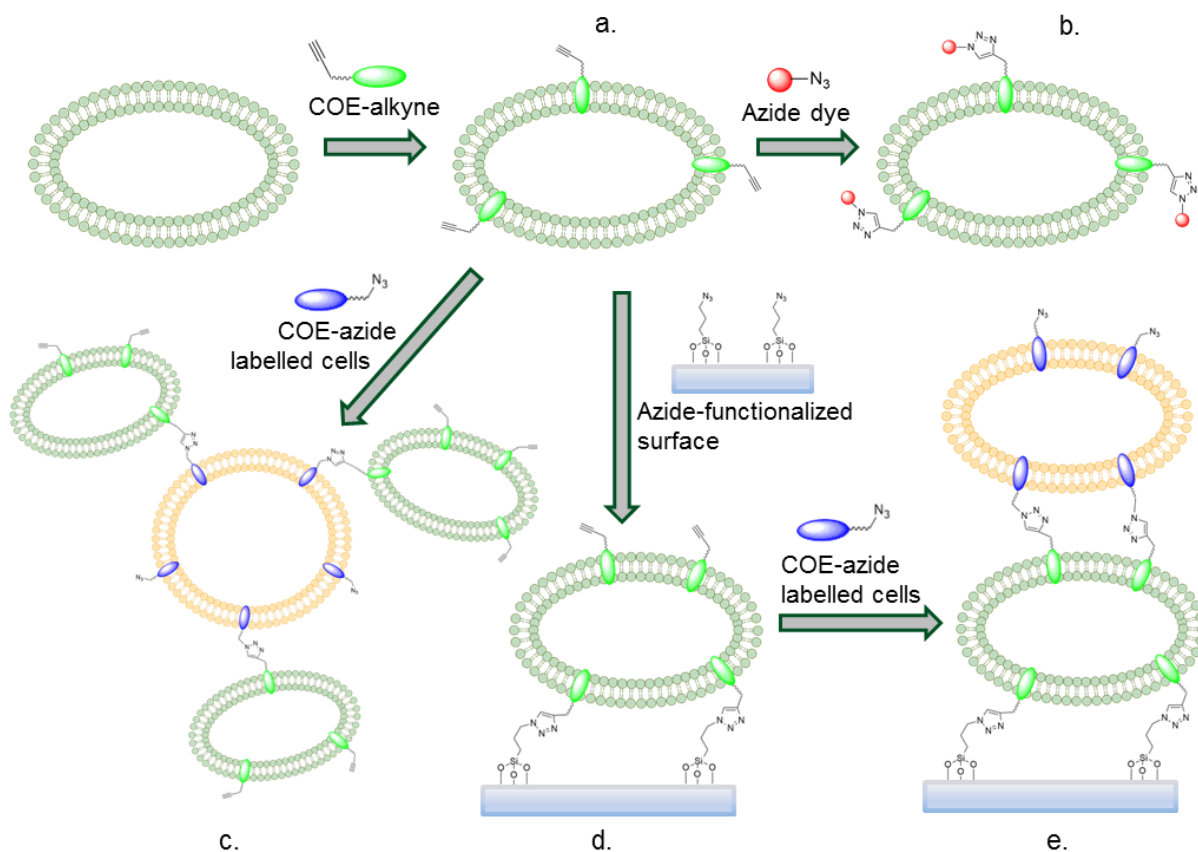


Figure 4-1 COE-mediated membrane engineering via CuAAC reactions. (a) Following intercalation of an alkyne-bearing COE (green oval), the functional handle could be used to (b) attach small molecules or dyes to the membrane surface, (c) facilitate cell-cell interactions using an azide-bearing COE (blue oval), (d) attach cells to an azide-functionalized surface, (e) or produce a biofilm in a layer-by-layer fashion.

Figure 4-1 depicts a number of experiments designed to probe the ability of azide- or alkyne-bearing COEs to facilitate CuAAC reactions at the surface of cells. Cells will first be stained with COE-alkyne to introduce alkyne functionalities to the membrane surface (Figure 4-1a). COE-alkyne incorporation can be quantified using the absorption of the residual COE in the supernatant after centrifuging the cell (as previously described, such as in Section 2.3). Azide-bearing optical probes can then be used to assess the ability of the alkyne groups to participate in CuAAC reactions (Figure 4-2b). For example, 3-azido-(diethylamino)coumarin has been used to analyze the incorporation and localization of alkyne-bearing lipids within cells.¹⁸⁶

To investigate the ability of COEs to direct cell-cell and cell-surface interactions via CuACC, cells stained with COE-alkyne can be mixed with either COE-azide labelled cells (Figure 4-1c) or azide-functionalized surfaces (Figure 4-1d). A combination of both approaches (sequentially) could allow for the formation of a “biofilm” in a layer-by-layer fashion (Figure 4-1e). The design and synthesis of COE-alkyne and COE-azide, as well as their application in various CuACC reactions will be discussed in the following sections.

4.2.1 Design and Synthesis of Alkyne- and Azide-bearing COEs for CuAAC-based Membrane Engineering

The design and synthetic route to access COE-azide and COE-alkyne were based on the successful COE-SH discussed in Chapter 1. Intermediate **1-5** in Figure 4-2 was originally designed as an asymmetric scaffold to allow for the introduction of a single thiol group. In the cases of COE-azide and COE-alkyne, a short oligomer of ethylene glycol was included between the ammonium group and the terminal

functional groups (azide or alkyne in this case). The purpose of this was to act as a hydrophilic spacer between the ammonium group, which is expected to be near the lipid headgroups following intercalation, and the reactive groups. Relative to the hydrophobic hexyl chain between the ammonium and thiol groups of COE-SH, it was expected that the oligo ethylene glycol chain would be more likely to present the reactive groups to the extracellular media.

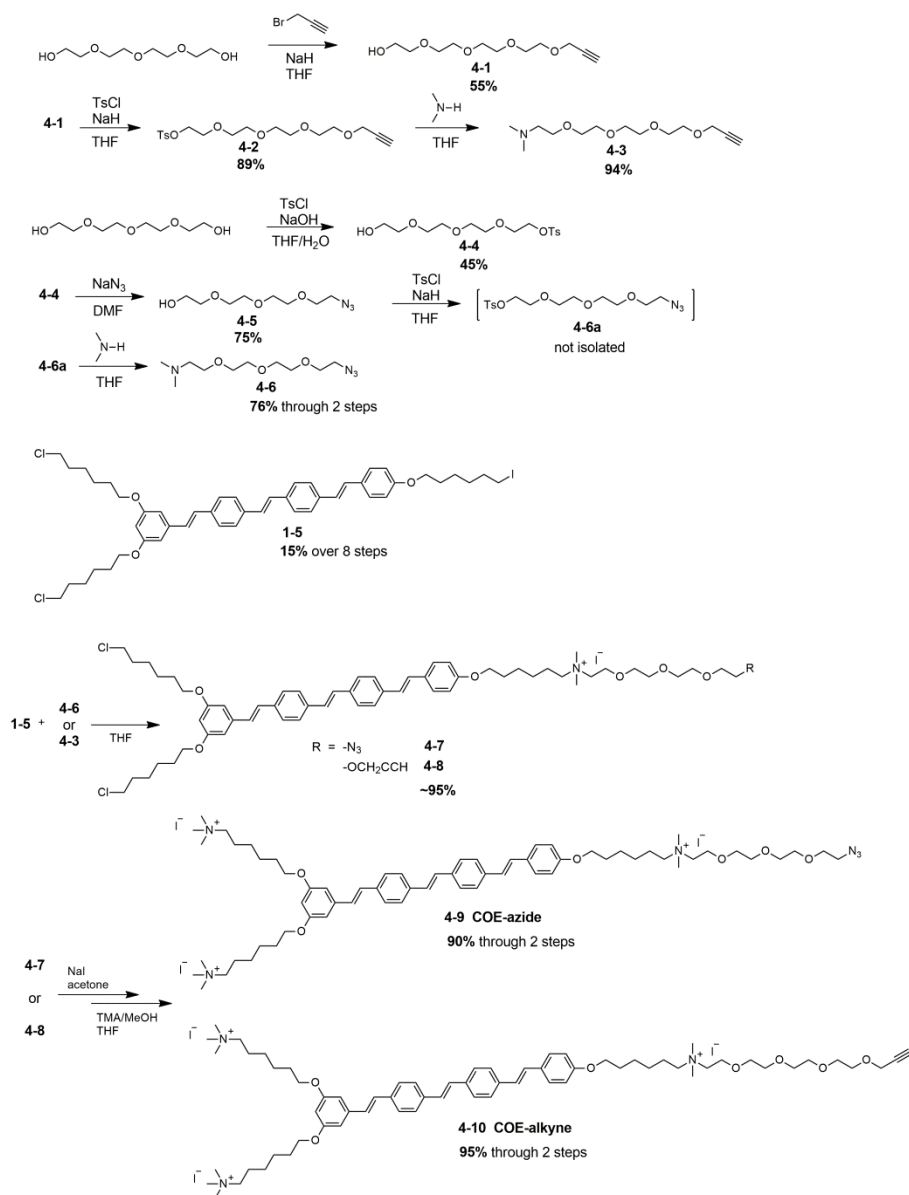


Figure 4-2 Synthetic route used to access COE-azide and COE-alkyne.

As shown in Figure 4-2, the synthesis of both COE-azide and COE-alkyne started with tetraethylene glycol. In the case of COE-alkyne, the alkyne functionality was introduced by reaction with propargyl bromide (**4-1**). The second alcohol group was subsequently tosylated (**4-2**) and substituted by dimethylamine to afford intermediate **4-3**. In the case of COE-azide, tetraethylene glycol was first mono-tosylated (**4-4**) and subsequently reacted with sodium azide (**4-5**). The second alcohol was then tosylated and substituted with dimethylamine (2-step-1-pot) to afford intermediate **4-6**. Intermediates **4-3** and **4-6** were reacted with **1-5** to introduce the alkyne or azide functionalities to the COE scaffold (intermediates **4-7** and **4-8**). Conversion of alkyl chlorides to iodides and subsequent quaternization with trimethylamine afforded COE-azide (**4-9**) or COE-alkyne (**4-10**).

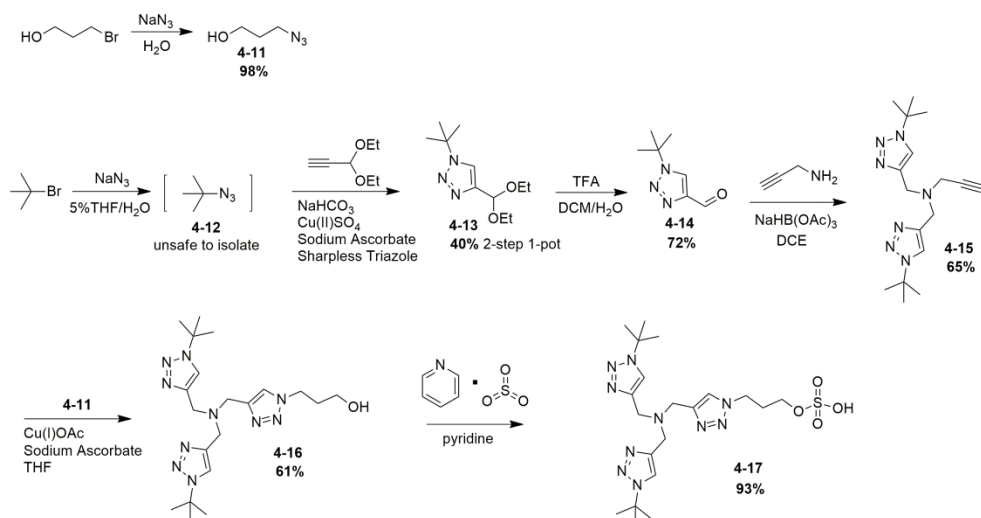


Figure 4-3 Synthetic route used to access the CuAAC ligand BTTPS.

The synthesis of the tristriazolamine ligand BTTPS was carried out according to literature¹⁸⁷ with some modifications (Figure 4-3). 3-bromo-propane-1-ol was converted to the analogous azide by reaction with sodium azide (**4-11**). In a similar

fashion, *tert*-butylbromide was converted to *tert*-butylazide (**4-12**), which was not isolated. The choice of solvent in this reaction was key to the safe handling of the volatile azide product. As the starting bromide is denser than water, it formed the bottom layer during the biphasic reaction (with THF as a phase-transfer catalyst). The resulting azide product is less dense than water and thus formed the top layer following the reaction. This top layer was simply transferred directly to the next step with THF as the only impurity. Under CuAAC conditions, this azide was reacted with 3,3-diethoxy-1-propyne to form the triazole intermediate **4-13**. The diethyl acetal was converted to the corresponding aldehyde using trifluoroacetic acid (**4-14**). Two equivalents of this intermediate were reacted with propargyl amine via reductive amination to afford intermediate **4-15**. A second CuAAC reaction was used to introduce the third triazole unit (**4-16**). The alcohol group was then converted to sulfate using sulfur trioxide pyridine complex to afford the final target **4-17** (BTTPS).

4.2.2 COE-Alkyne as a Membrane Anchor for the CuAAC-Promoted Attachment of Azide-Containing Molecules

The ability to attach an azide-dye to the membrane of bacteria was used as an initial investigation into whether COEs could act as attachment points for membrane decoration. A fluorescein-based dye (“FITC-azide”) was made specifically for this purpose by reacting fluorescein isothiocyanate with 3-azido-1-propanamine (procedure not described). A diagrammatic explanation of this experiment is presented in Figure 4-4. *E. coli* cells were stained with COE-alkyne to introduce alkyne functionalities to the membrane surface. FITC-azide was added to the cells along with CuSO₄, BTTPS, and sodium ascorbate. The samples were centrifuged

and the supernatant and pellet (after resuspending) were separately transferred to a 96-well plate. Copper-free and COE-free controls were also prepared in the same fashion. Absorption and fluorescence measurement were used to calculate the amount of FITC-azide that was bound to cells via reaction with COE-alkyne.

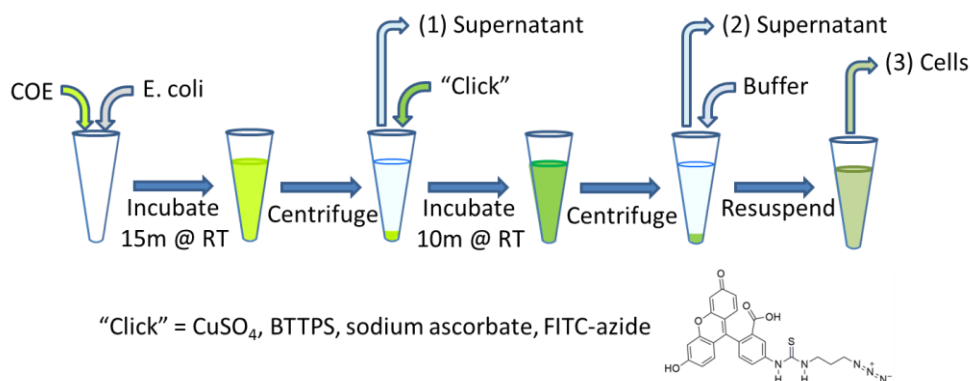


Figure 4-4 Experimental procedure used to investigate the ability of COE-alkyne to act as membrane-anchor for subsequent CuAAC-mediated functionalization. Supernatants removed for calculating the association of COE-alkyne (1) and FITC-azide that had been clicked to the cells (2). (3) Cells sampled in order to confirm results from (1) and (2).

As shown by the absorption spectra in Figure 4-5, the supernatants of samples that included both COE-alkyne and copper contain less FITC-azide than either copper-free or COE-free controls. Supernatants from both control samples contained approximately 50 $\mu\text{M}/\text{OD}_{600}$ FITC-azide (which was the initial concentration). That neither control showed a reduction in FITC-azide indicates that both COE-alkyne and copper were required for attachment of FITC-azide to cells. Furthermore, the amount of FITC-azide that was "missing" from the supernatant was proportional to the amount of COE-alkyne used. Together, these results indicate that membrane-

intercalated COE-alkyne was able to act as an alkyne-display system for bioorthogonal CuAAC with FITC-azide.

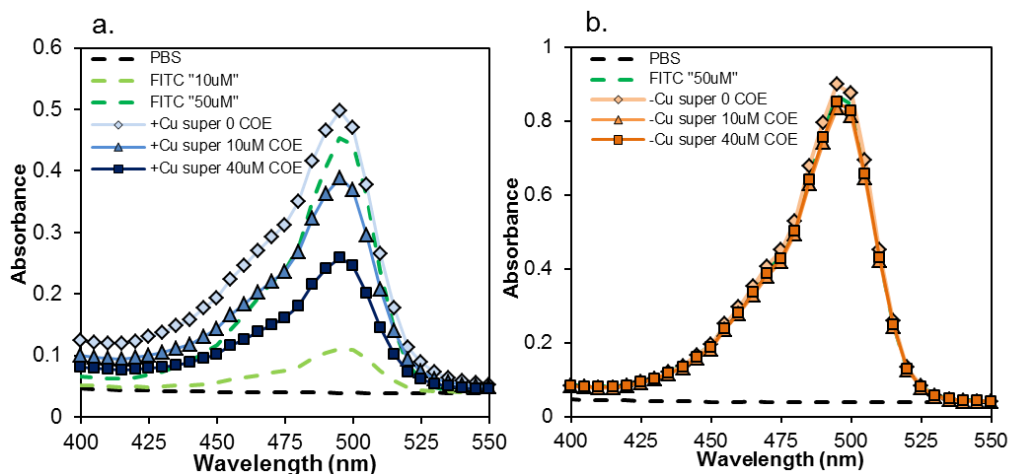


Figure 4-5 Absorption spectra of supernatants demonstrating the removal of FITC-azide from solution through CuAAC with membrane-intercalated COE-alkyne. (a) Samples containing both COE-alkyne and copper show reduced levels of FITC-azide in the supernatant as a function of COE concentration. FITC-azide was not removed from the supernatant in the absence of COE-alkyne. (b) Samples that did not include copper show that FITC-azide remained in the supernatant (i.e. FITC-azide was not “clicked” to the cells).

All FITC-azide that was removed from the supernatant would be expected to be present in the cell pellet. The supernatant absorption at 495 nm (FITC-azide maximum, as shown in Figure 4-5) was used to calculate the amount of FITC-azide that became attached to cells (initial amount added minus the residual amount in the supernatant). Figure 4-6 shows the results of this calculation along with the measured absorption of the resuspended cells. As described above, copper-free or COE-free controls appeared to have essentially no cell-bound FITC-azide. Additionally, the amount of FITC-azide bound to cells in the samples including both COE-alkyne and FITC-azide was found to be dependent on the amount of COE-alkyne. These results were expected based on the analysis of the supernatants and

further support the finding that membrane-intercalated COE-alkyne was able to “click” FITC-azide to the cell surface.

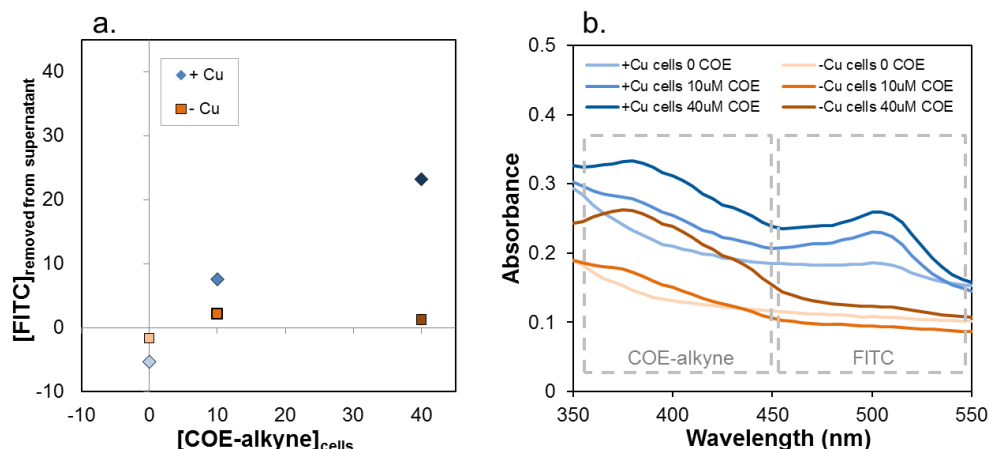


Figure 4-6 Calculated and measured amounts of FITC-azide that were attached to *E. coli* cells via CuAAC with membrane intercalated COE-alkyne. **(a)** Calculated amounts of FITC-azide attached to cells based on the initial amount and the amount that remained in the supernatant. **(b)** Absorption spectra of cell solutions with or without COE-alkyne or copper. The presence of FITC-azide is only observed in cells treated with both COE-alkyne and copper.

While the absorption measurements provided evidence that this system functions as intended, fluorescence measurements suffered from an unexpected (and unexplained) photo-physical phenomenon. Despite the obvious presence of FITC-azide in cell suspensions containing COE-alkyne and copper, hardly any FITC-azide fluorescence was observed (data not shown). In addition, no COE-alkyne fluorescence was observed in these samples. Other than the two samples where the “click” reaction was expected to have occurred, all samples displayed reasonable COE-alkyne and/or FITC-azide fluorescence. To determine if the unexpected absence of fluorescence was a direct result of the “click” reaction, a similar experiment was conducted in solution without cells. Figure 4-7 shows the absorption

and fluorescence spectra of COE-alkyne, FITC-azide, and a mixture of the two, both in the presence and the absence of copper.

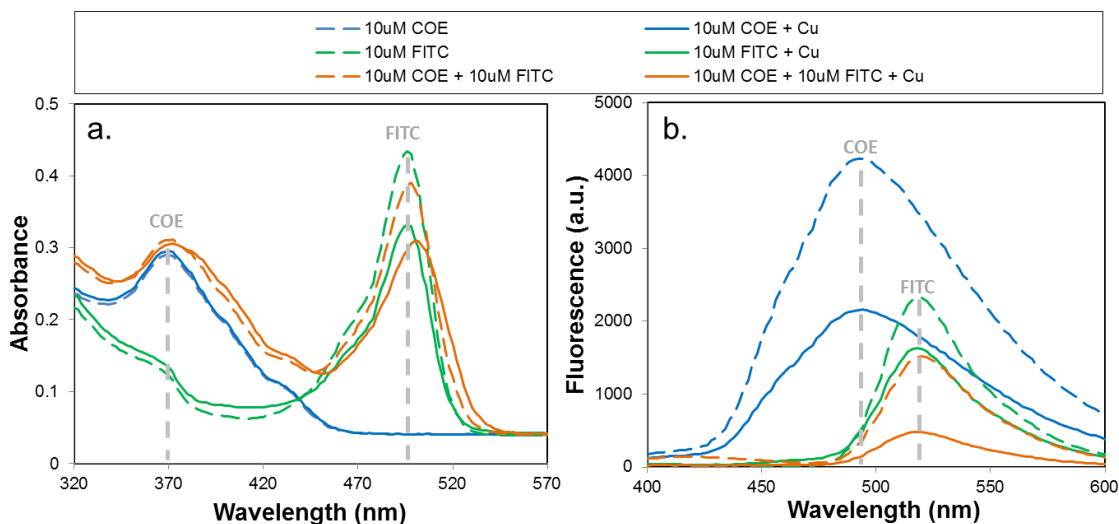


Figure 4-7 (a) Absorption and (b) fluorescence (excitation: 380 nm) spectra of COE-alkyne and FITC-azide with (solid lines) or without copper (dashed lines) demonstrating an undesirable interaction between the two compounds that results in suppression of fluorescence.

As expected, the absorbance spectra in Figure 4-7a shows that the COE-alkyne/FITC-azide mixture (orange) is essentially the sum of the two individual components (blue and green for COE-alkyne and FITC-azide, respectively). Some level of quenching by copper was observed in the fluorescence measurements of both COE-alkyne and FITC-azide but not enough to explain the results in the previous experiment. Interestingly, COE-alkyne fluorescence was completely suppressed in the samples that contained FITC-azide, regardless of the presence or absence of copper (Figure 4-7b, orange lines). FITC-azide fluorescence was also reduced in the mixture, especially in the case where copper was also present. As COE-alkyne and FITC-azide are oppositely charged, it is possible that coulombic

interactions brought them into close proximity leading to some manner of quenching. The addition of copper and resulting “click” only exacerbated the issue. Although absorption data sufficiently demonstrated the attachment of FITC-azide to cells, the apparent photo-physical incompatibility of COE-alkyne and FITC-azide precludes the use of fluorescence confocal microscopy to show co-localization at the membrane. This experiment would have otherwise been used to unequivocally show that FITC-azide had “clicked” to the membrane surface (as opposed to entering cell by way of COE-induced membrane permeability). The fact that COE-alkyne and FITC-azide fluorescence was suppressed in the *E. coli* “click” samples (and not in copper-free samples) does suggest that they are in close proximity (i.e. the observation of quenching suggests co-localization at the membrane). Efforts to find a system without this unexpected quenching phenomenon are ongoing.

4.2.3 COE-Alkyne as a Membrane Anchor for Attaching Cells to Azide-Functionalized Surfaces

To assess the ability of COE-alkyne to “click” cells to surfaces, azide-functionalized quartz slides were prepared using (3-azidopropyl)triethoxysilane (see Section 1.6.4 for the preparation of this compound). A solution containing CuSO₄, BTTPS, and sodium ascorbate was added to *E. coli* cells with or without COE-alkyne. These solutions were immediately placed on azide-functionalized or unfunctionalized quartz slides. After 15 minutes, unattached or loosely-attached cells were removed by rinsing gently and the slides were imaged by confocal laser scanning microscopy. As shown in Figure 4-8A, cells that were not treated with COE-alkyne did not readily adhere to the functionalized substrate. Cells that were treated with COE-alkyne

showed a similar inability to adhere to the unfunctionalized substrate (Figure 4-8B). Only when COE-alkyne treated cells were placed on a treated substrate was significant adhesion observed (approximately 10-times more adhered cells than either of the two controls), demonstrating that COE-alkyne can be used to “click” bacteria to an azide-functionalized surface (Figure 4-8C).

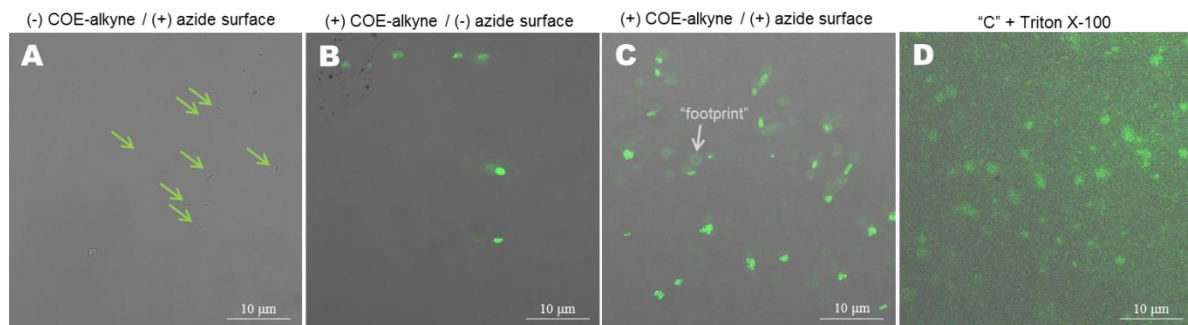


Figure 4-8 Fluorescence confocal micrographs demonstrating the ability of COE-alkyne to “click” *E. coli* cells to an azide-functionalized surface.

A number of large (~1-5 µm), fluorescent patches were observed on the “click” sample described above (arrow in Figure 4-8C). It was hypothesized that these “footprints” arose when cells that had been “clicked” to the surface were removed, potentially during the wash step. To investigate this further, the “click” sample was treated with Triton X-100 and sonicated to remove the adhered cells (Figure 4-8D). No cells were observed on the substrate but the “footprints” remained. It is unclear whether these patches contain cell fragments or not but their size suggests that they indicate where cells or groups of cells had been “clicked” to the surface. While it is beyond the scope of this project, it would be interesting to investigate whether these fluorescent areas do contain remnants of bacterial membranes. This could

potentially have some utility in the study of membrane-proteins as a method for attaching microbial membrane fragments to a surface.

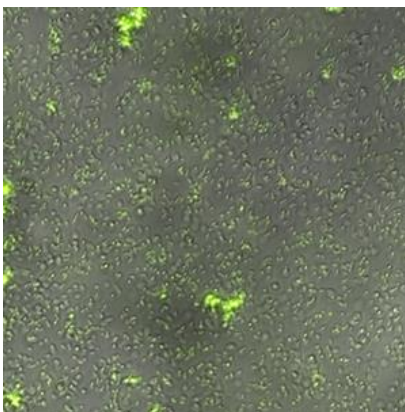


Figure 4-9 Fluorescence micrograph of optimized conditions for COE-alkyne-mediated bacteria-surface conjugation via CuAAC (scale: 100x100 μ M).

We further optimized the conditions for “clicking” COE-alkyne stained cells to azide-functionalized quartz and other materials (such as cellulose nanofibrils – data not shown). Instead of pre-mixing the stained bacteria with CuSO_4 , BTTSPS, and sodium ascorbate, the stained cells were first added to the substrate. After allowing the cells to settle on the surface for 30 minutes, the “click” reagents were added. In this manner, we were able to achieve up to ~50% surface coverage (Figure 4-9). We also found that higher COE concentrations (10 $\mu\text{M}/\text{OD}_{600}$ or more) resulted in more “footprints” and fewer intact cells. By imaging the samples before washing, we found that COE-alkyne was able to induce aggregation of the cells at higher concentrations. Our hypothesis is that cell clusters cause increased strain on “clicked” cells at the surface, leading to the destruction of these cells and removal of the entire cell cluster during the wash step. Once an area of the surface has reacted with COE-alkyne, no new cells can be attached at that location (this is supported by

the fact that we never observed cells adhered directly on top of the “footprints”). The best surface coverage can thus be achieved by avoiding amounts of COE-alkyne that are sufficiently high to cause cell aggregation.

4.2.4 COE-mediated cell-cell interactions

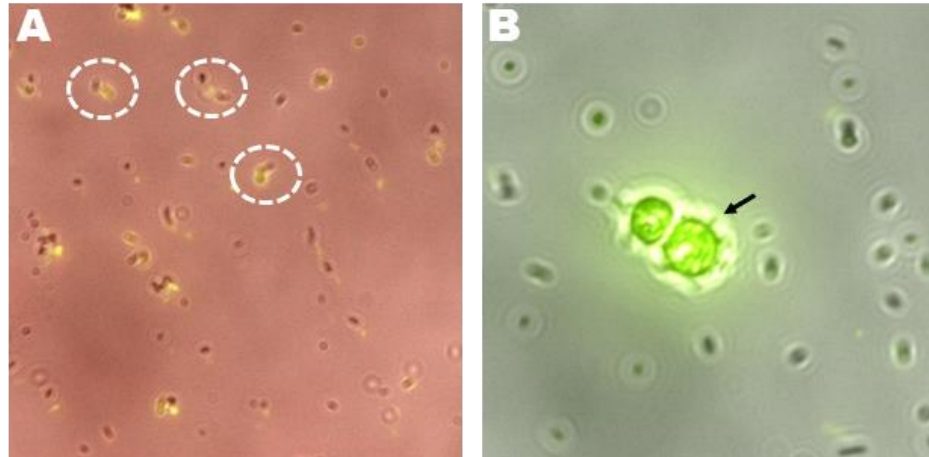


Figure 4-10 Fluorescence micrographs of cell-cell interactions mediated by COE-alkyne and COE-azide. (A) *E. coli* cells stained with COE-alkyne (non-emissive) and COE-azide/DSSN (emissive – yellow; fluorescence from DSSN). (B) *B. subtilis* stained with COE-alkyne and *S. cerevisiae* stained with COE-azide.

Preliminary attempts to direct physical cell-cell interactions via “click” reactions using COE-alkyne and COE-azide were conducted in collaboration with the Army Research Laboratory (ARL). Figure 4-10 demonstrates two systems in which suggest that cells stained with the two COEs were brought in close contact through CuAAC. In Figure 4-10A, separate cultures of *E. coli* were stained with either COE-alkyne or COE-azide and DSSN³⁹ (to allow for differentiation based on fluorescence) before mixing the two cultures in the presence of copper. Cell aggregates, three of which are indicated by the dashed ovals, were found to contain mixtures of cells from the two cultures. No aggregates were observed where any cell’s nearest

neighbor did not originate from the opposite culture. In Figure 4-10B, *B. subtilis* stained with COE-alkyne are shown attached to the surface of *S. cerevisiae* stained with COE-azide (one of the fungi-associated bacteria is indicated by the black arrow; DSSN was not used in this case as differential staining is not required to distinguish between the two cell types). These un-optimized experiments suggest that COE-alkyne and COE-azide facilitate cell-cell interactions between orthogonally-stained cells of the same- or different- species.

4.3 Introduction to the NiNTA/His-tag System

Immobilized metal ion affinity chromatography (IMAC) is a mainstay of protein purification. Originally, proteins were separated based on their natural affinities for the solid-supported metal ions.¹⁸⁸ The discovery that multiple histidine residues at the N- or C-terminus can greatly increase affinity of recombinant proteins has led to the heavily-utilized “His-tag” system.¹⁸⁹ Many of the modern commercial resins for His-tagged protein isolation rely on Ni(II)-NTA¹⁹⁰ to separate the target protein from complex mixtures. The tetradentate nitrilotriacetic acid moiety strongly chelates Ni²⁺ and allows for reversible attachment of His-tagged proteins. Decreasing the pH of the eluent, adding imidazole, or a combination of both can be used to disrupt or compete with the His-tag interaction with the metal ion.¹⁹¹

The Ni-NTA/His-tag system has been widely applied as a bioconjugation technique where one of the components is a recombinant protein. For example, Ni-NTA-functionalized surfaces have been used to adhere and orient proteins for

atomic force microscopy measurements.¹⁹² The Ni-NTA structure has also been incorporated into lipids in order to allow for liposome surface engineering with proteins.^{193, 194} These systems have found utility in such applications as nano-carrier targeting (particularly for cancer therapy),¹⁹⁵⁻¹⁹⁷ CRISPR/Cas9 complex delivery,¹⁹⁸ biosensors and biocatalysts,¹⁹⁹⁻²⁰¹ development of vaccines,²⁰² and the study of viral penetration into cells.²⁰³ These systems are so widely used that Ni-NTA-lipids are now commercially available, such as DOGS-NTA-Ni from Avanti Polar Lipids. As described in Section 4.2, COEs have tangible advantages over lipids as membrane anchors for functional handles. In this section, the design, synthesis, and membrane-protein-conjugation ability of a NTA-bearing COE (“COE-NTA”) will be described.

4.3.1 Design and Synthesis of a NiNTA-Bearing COE for the Localization of His-Tagged Peptides or Proteins to Membrane Surfaces

The design of COE-NTA follows that of the two COEs described in Section 4.2. Specifically, the same neutral intermediate (**1-5** in the scheme below) served as the core scaffold and an amine derivate of tetraethylene glycol was used to introduce the function handle (NTA in this case). The synthesis of the NTA-containing fragment was inspired by various literature procedures²⁰⁴⁻²⁰⁶ that utilized a protected lysine derivative as the starting material. The synthetic route to prepare COE-NTA is shown below in Figure 4-11. N-epsilon-CBz-lysine and bromoacetic acid were used to prepare **4-18**, NTA with an amine-terminated appendage originating at the alpha-position of one of the carboxyl groups. The carboxylic acids were then protected as

ethyl esters (**4-19**), both to prevent functional group incompatibilities and to increase solubility. Pd/C and H₂ were used to remove the CBz protecting group (**4-20**) before

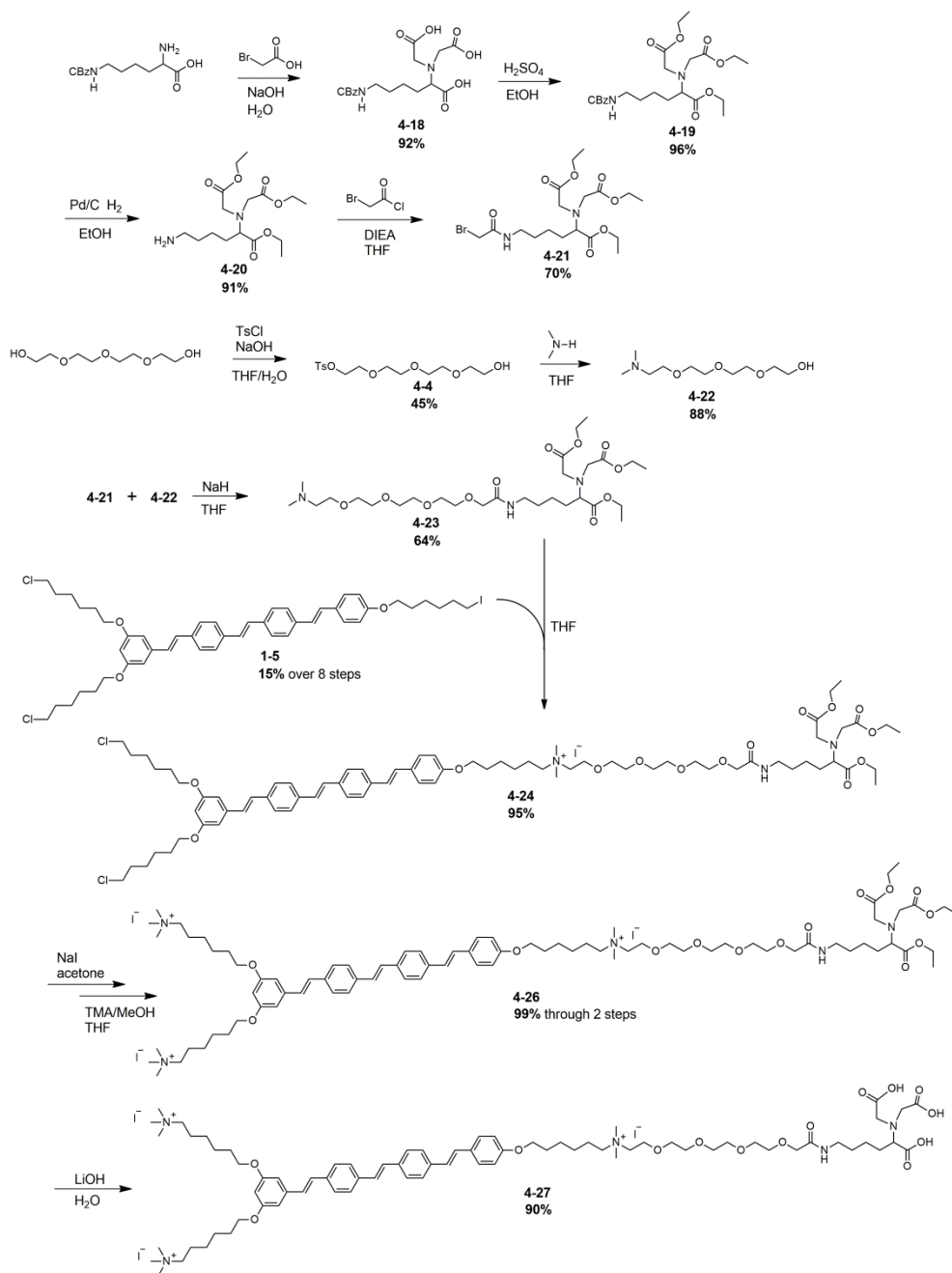


Figure 4-11 Synthetic pathway used to access COE-NTA.

reacting with bromoacetyl chloride (**4-21**). Mono-tosylation of tetraethylene glycol afforded **4-4** (previously described in the preparation of COE-azide in Section 4.2.1) and subsequent substitution with dimethylamine afforded the dimethylamino-derivative **4-22** that would serve to bridge the COE core and the NTA moiety. The alcohol of **4-22** was selectively used for the nucleophilic attack of the bromoacetyl group of **4-21** to afford **4-22** and the tertiary amine was subsequently used to quaternize with the alkyl iodide of **1-5** to afford **4-24**. The alkyl chlorides of **4-24** were converted to iodides before quaternizing with trimethylamine (**4-26**) as described previously for COE-alkyne and COE-azide. The ethyl protecting groups were removed with LiOH to afford the final un-metallated compound **4-27** (note: ethyl- was specifically chosen as a protecting group to facilitate mild deprotection at the last step). Chelation of nickel (II) (not shown) was achieved by mixing 1 mM **4-27** and 20 mM Ni(NO₃)₂ in DI water in a 1:1 mole ratio and heating to 45°C for 1 hour. COE-NTA was thus prepared in 20 total steps with an overall yield of 1.8%.

4.3.2 Analysis of COE-NTA mediated YPet binding by flow cytometry

The following work was conducted in collaboration with Dr. Deborah Sarkes, Dr. Justin Jahnke, and Dr. James Sumner at ARL. To determine if membrane-intercalated COE-NTA was able to localize His-tagged proteins to the surface of cells, we used flow cytometry to measure the fluorescence of YPet-Mona (a modified and His-tagged Yellow Fluorescent Protein derivative; hereafter referred to as “YPet”). YPet was previously used by our collaborators at ARL to quantify the expression and surface display of a recombinant protein.²⁰⁷ The employed eCPX

surface display scaffold, which is a modified OmpX system, presents both the N- and C-termini toward the extracellular space.^{208, 209} Our collaborators used this system to display gold-binding peptide sequences at the N-terminus and the P2X peptide sequence at the C-terminus. P2X has a strong affinity for YPet and thus induction of eCPX could be quantified by labeling with YPet.²⁰⁷ This process and the novel COE-NTA protein-membrane conjugation system are depicted in Figure 4-12 (top and bottom pane, respectively).

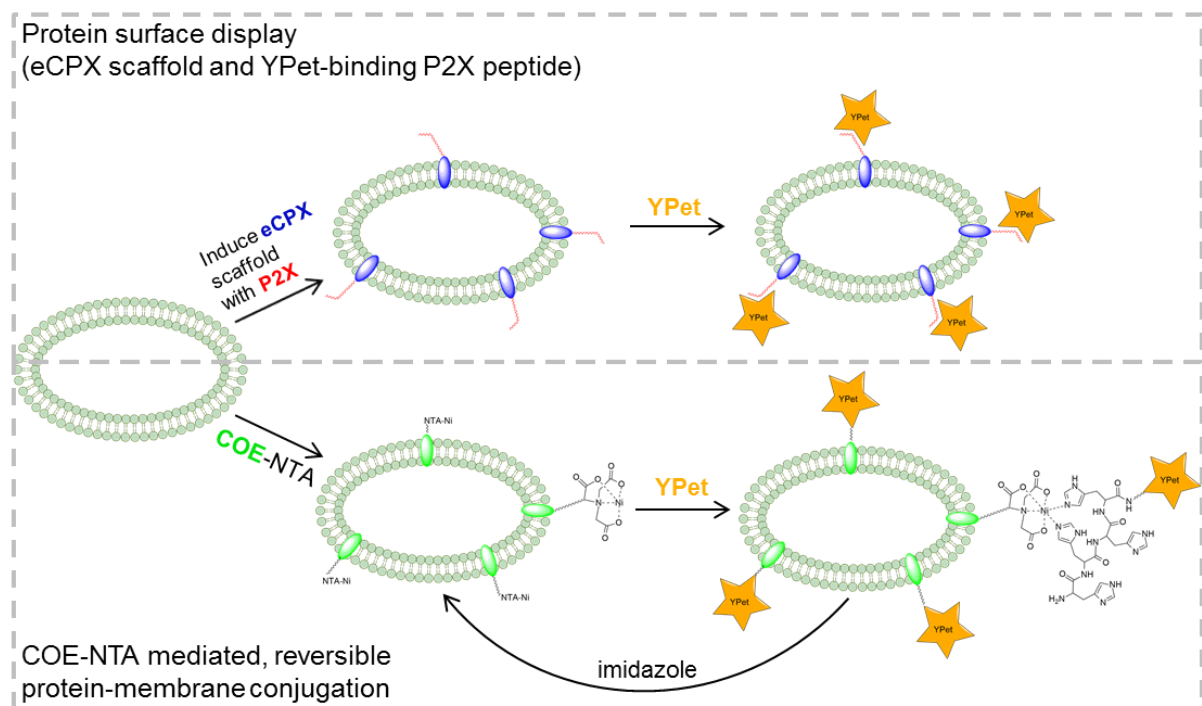


Figure 4-12 Labelling bacterial membranes with YPet by surface display (top pane) through peptide-protein interactions and with the novel COE-NTA system (bottom pane) through Ni-NTA/His-tag interactions.

We used this prior experience to test the protein-localizing ability of COE-NTA relative to recombinant surface display techniques (Figure 4-13). Flow cytometry was employed so that the fluorescence from individual cells could be measured. As a baseline, untreated *E. coli* cells were measured on the FITC-channel (which is

optimal for measuring YPet fluorescence) and were found to produce negligible fluorescence (Figure 4-13a). Addition of 5 $\mu\text{M}/\text{OD}_{600}$ COE-NTA to *E. coli* resulted in slight aggregation of cells (as evident in the forward-scatter profile) but did not significantly increase fluorescence (Figure 4-13b). When the P2X-containing eCPX complex was induced and the cells were labelled with YPet, a fluorescence intensity of 4×10^3 was achieved at the maximum of the count distribution (Figure 4-13c). A similar fluorescence intensity was observed at the maximum of the count distribution for cells stained with COE-NTA and subsequently incubated with YPet (Figure 4-13d).

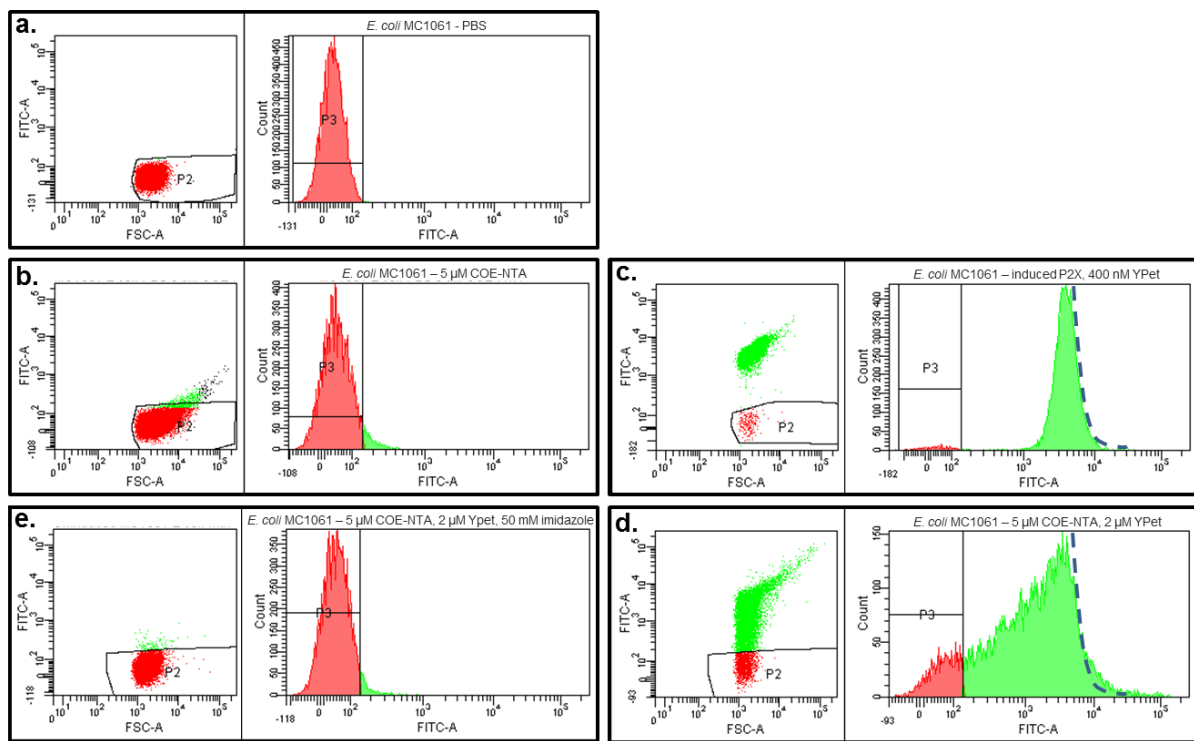


Figure 4-13 Flow cytometry measurements of Ypet-labelled cells through induction of the eCPX scaffold or introduction of Ni-NTA moieties by staining with COE-NTA. (a) Untreated cells. (b) COE-NTA stained cells. (c) YPet-labelled cells following eCPX induction. (d) YPet-labelled cells following treatment with COE-NTA. (e) YPet-“unlabeled” cells following imidazole treatment of YPet/COE-NTA treated cells (i.e. pane “d”).

That both systems showed approximately the same intensity indicates that COE-NTA is able to achieve a similar maximum level of Ypet labelling. The broader distribution seen with COE-NTA is most likely a result of the low Ni-NTA/His-tag affinity relative to the interaction between P2X and Ypet (the protein-protein interaction is likely to be much stronger). These results indicate that COE-NTA could serve as an efficient method for directing His-tagged proteins to the surface of cells.

To determine if COE-NTA could function in a reversible manner, we assessed the ability of imidazole to disrupt the interaction with the His-tag and release YPet from the surface of cells. After treating *E. coli* (labelled with 5 μ M COE-NTA and 5 μ M Ypet) with 50 mM imidazole for 12 minutes, cells were centrifuged, the supernatant was discarded, and cells were resuspended in fresh buffer. As shown in Figure 4-13e, imidazole treatment reduced the fluorescence to the level of COE-NTA stained cells without YPet (i.e. Figure 4-13b). Imidazole-treated cells were re-cultured and showed similar growth after 4 hours to untreated cells. To the best of our knowledge, reversible surface display has not been demonstrated for any recombinant protein-based systems. These results demonstrate the potential future utility of COE-NTA for situations where it is desirable to have reversible protein-membrane interactions.

4.3.3 COE-NTA mediated membrane localization of a peptide bearing a His-Tag and a fluorescent probe

The experiments described above provide strong evidence that COE-NTA can localize His-tagged proteins to the surface of living bacteria. In particular, the imidazole-based reversibility of the process indicates that cell-protein association is mediated by the Ni-NTA functional group of the COE. To provide additional support

to this finding, an experiment was designed to explicitly demonstrate co-localization of COE-NTA and its bound protein/peptide to the membrane. A His-tagged and Cy5-labeled peptide (Nur77) was added to *E. coli* cells stained with either COE-NTA or COE-alkyne (as a control for the importance of Ni-NTA). Fluorescence scanning confocal microscopy was used to image the location of the COEs and the peptide. To highlight the speed at which COEs can be used to introduce functional handles to the surface of cells, the entire staining and labelling process was limited to less than fifteen minutes (see Section 4.5 for details).

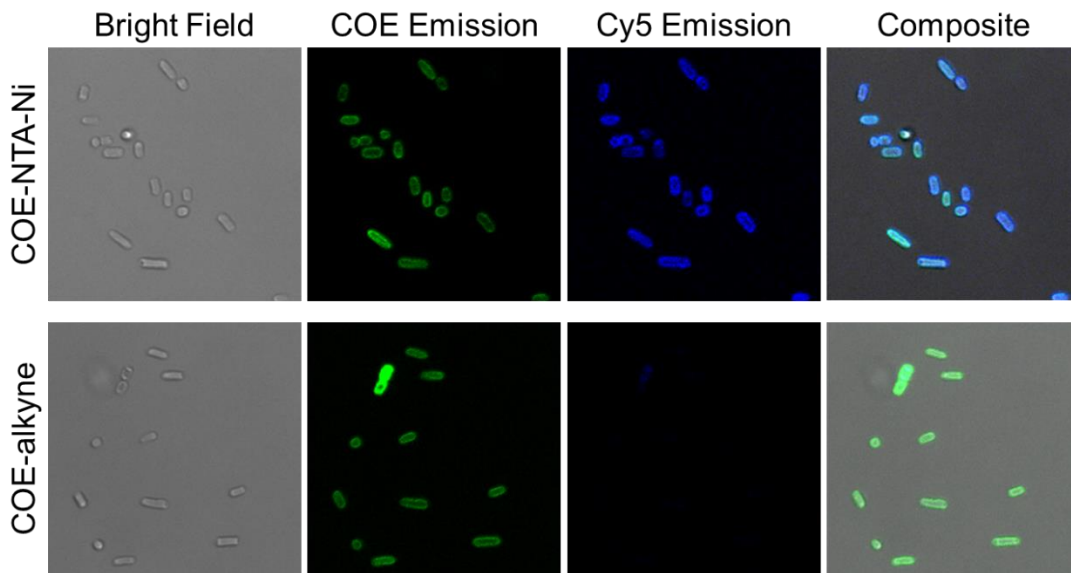


Figure 4-14 Fluorescence confocal micrographs demonstrating COE-NTA-mediated surface decoration of *E. coli* cells with a dye-labelled, His-tagged peptide (scale: 15x15 μM).

As shown in Figure 4-14, Cy5 fluorescence was observed in samples containing COE-NTA but not in samples containing COE-alkyne. Furthermore, Cy5 emission was co-localized with COE-NTA emission, originating exclusively from the membrane. No Cy5 fluorescence was observed within the cells, indicating that COE-NTA does not sufficiently disrupt membranes to allow the passage of

peptides/proteins. Association of His-tagged peptides/proteins with COE-NTA labelled cells is thus exclusively a result of COE-mediated protein-membrane conjugation.

4.4 Conclusions

In conclusion, a new family of COEs was designed specifically to introduce functional handles to the membranes of cells. Three members of this new family were synthesized and tested. COE-alkyne and COE-azide were used for the facile and expedient display of alkyne- or azide- functional groups at the cell surface. These “click” functional groups were utilized in CuAAC reactions to attach an azide-dye to the membrane of cells stained with COE-alkyne, attach cells to functionalized surfaces, and promote physical interactions between cells stained with the orthogonal COEs. COE-NTA was designed with the specific intent of decorating the surface of cells with His-tagged peptides or proteins. Flow cytometry and confocal microscopy were used to demonstrate that COE-NTA is able to mediate peptide/protein conjugation with cell membranes exclusively through the Ni-NTA/His-tag interaction. The results of both systems demonstrate the potential utility of COEs as a means to introduce specific functionalities to cell surfaces that can be used to modulate interactions with small molecules, biomolecules, surfaces, and other cells.

4.5 Experimental Methods

Materials and Instrumentation

Solvents and reagents for synthetic preparations were purchased from Fisher Scientific, Alfa Aesar, Acros, Sigma Aldrich, and Tokyo Chemical Industry. *Escherichia coli* ATCC 10798 was purchased from American Type Culture Collection (Manassas, VA). Inhibitor-free anhydrous solvents were prepared using packed alumina columns under argon in a solvent purification system. EMD Millipore Analytical Chromatography aluminum-backed plates (Silica gel 60 F254) were used for thin layer chromatography and separation was visualized with UV light (254/366 nm). Silicycle SiliaFlash P60 silica gel was used for flash chromatography under positive air pressure. Pre-packed Biotage C18 columns were used for RP chromatography on a Biotage Isolera One. Optical density measurements for MIC studies were conducted on a Tecan M220 Infinite Pro. ^1H NMR (400 MHz, 500 MHz) and ^{13}C NMR (101 MHz and 126 MHz) were measured on actively-shielded Agilent Technologies 400-MR DDR2 400 MHz or Varian Unity Inova 500 MHz spectrometers. Multiplicity of signals was described by s (singlet), d (doublet), t (triplet), q (quartet), p (pentet) and m (multiplet). Chemical shifts (δ in ppm) were referenced to residual solvent peaks of Chloroform-*d* (^1H NMR δ = 7.26 and ^{13}C NMR δ = 77.0) or DMSO-*d*₆ (^1H NMR δ = 2.50 and ^{13}C -NMR δ = 39.52). Scanning laser confocal microscopy was conducted on a Leica SP8 and fluorescence microscopy on a Nikon Eclipse TE2000-E. A BD FACS Aria was used for flow cytometry experiments.

“Click” with FITC-azide

Single colonies of *E. coli* ATCC 10798 were picked from a plate and cultured in LB overnight at 37°C. After centrifuging and resuspending in PBS, cells were stained with 10 or 40 $\mu\text{M}/\text{OD}_{600}$ COE-alkyne to introduce alkyne functionalities to the membrane surface. Cells were pelleted and the supernatant was removed to a 96-well plate to measure the residual amount of COE-alkyne. FITC-azide (50 $\mu\text{M}/\text{OD}_{600}$) was added to the cells along with CuSO_4 , BTTPS, and sodium ascorbate. After 10 minutes, the samples were centrifuged and the supernatant and pellet (after resuspending) were separately transferred to the 96-well plate. Copper-free and COE-free controls were also prepared in the same fashion. Absorption (350-500 nm) and fluorescence (excitation: 380 nm, emission: 400-600 nm) measurements were collected on a plate reader at room temperature.

“Click” Cells to Surfaces

15x15 mm quartz slides were treated Piranha (3:1 concentrated sulfuric acid and 30% hydrogen peroxide) for 15 minutes. Azide functional groups were introduced by immersing the slides in toluene containing 10 mM (3-azidopropyl)triethoxysilane (see Section 1.6.4 for the preparation of this compound) at 100°C overnight. Overnight cultures of *E. coli* ATCC 10798 were washed and resuspended in PBS before staining with 10 $\mu\text{M}/\text{OD}_{600}$ COE-alkyne. A solution containing CuSO_4 , BTTPS, and sodium ascorbate was added to *E. coli* cells with or without COE-alkyne. 100 μL aliquots of these solutions were placed on functionalized or unfunctionalized quartz slides. After 15 minutes, the slides were rinsed multiple times with 150 mM PBS.

The slides were immersed in 150 mM PBS to prevent desiccation of the cells and imaged (confocal) within 1 hour.

Higher surface coverage was achieved by altering the order of addition, concentrations, and time at each step. ~50% coverage was achieved by first adding cells stained with 2 $\mu\text{M}/\text{OD}_{600}$ COE-alkyne to the quartz slides. After allowing the cells to settle on the slide for 30 minutes (taking care to prevent the sample from drying), a solution containing CuSO_4 , BTTPS, and sodium ascorbate was added. After 10 minutes, the slides were gently washed with PBS and imaged (fluorescence microscope).

Attachment of YPet to *E. coli* Using COE-NTA

E. coli MC1061 was grown for four hours in LB at 37°C. Cells for control using the eCPX display system were cultured for another hour in the presence of 0.04% w/v L-arabinose to induce expression. All cells were washed and resuspended in PBS. Un-induced cells were stained with 5 $\mu\text{M}/\text{OD}_{600}$ COE-NTA for 15 minutes, pelleted, and resuspended in fresh PBS. YPet (prepared previously at ARL²⁰⁷) was added to COE-NTA stained cells and induced cells for 15 minutes. Cells were pelleted and resuspended in FACSFlow solution (BD) for flow cytometry analysis. Untreated cells were gated according to a scatterplot of forward-scatter (FSC) and fluorescence on the FITC channel. Samples were analyzed for YPet content using the FITC channel (10^4 events were recorded in each sample).

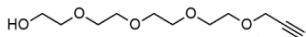
Attachment of a Dye-Labelled Peptide to *E. coli* Using COE-NTA

E. coli ATCC 10798 was cultured in LB for 6 hours at 37°C. Cells were pelleted and resuspended in PBS at a density twice that of $OD_{600} = 1$. Cells were stained with COE-NTA or COE-alkyne (as a control) at a final concentration of $5 \mu\text{M}/OD_{600}$. After ten minutes of incubation with the COEs, cells were pelleted and the supernatants were discarded. Samples were resuspended in PBS to a density of $OD_{600} = 1$. A solution of Nur77 (Cy5-labelled at one terminus and His-tagged at the other) was added such that the final concentration was $500 \text{ nM}/OD_{600}$. After incubation for 1 minute, the cells were pelleted and the supernatant was discarded. Cells were resuspended in PBS to a density of $OD_{600} = 0.2$ and $10 \mu\text{L}$ aliquots were transferred to glass slides for confocal microscopy analysis. Fluorescence for both COEs was measured on one channel (ex: 405 nm, em: 460-480 nm) and Cy5 on a separate channel (ex: 640 nm, em: 660-680 nm). Images were processed using ImageJ.

4.6 Synthetic Methods

4.6.1 COE-azide and COE-alkyne

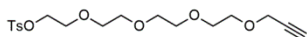
3,6,9,12-tetraoxapentadec-14-yn-1-ol (**4-1**)



To a 50 mL flame-dried round bottomed flask equipped with a stir bar was added sodium hydride (257 mg, 60 wt%, 6.7 mmol) and anhydrous THF (20 mL). The suspension was cooled to 0°C and stirred under inert atmosphere. In a separate flame-dried flask, tetraethylene glycol (1.94 g, 10 mmol) was dissolved in 5 mL anhydrous THF and transferred (fast addition via syringe) to the vessel containing sodium hydride. This mixture was allowed to stir for 30 minutes at 0°C, at which point propargyl bromide (0.65 mL, 9.2 M, 6 mmol) was added slowly via syringe. The temperature was maintained for an additional 30 minutes before allowing the solution to warm to room temperature. After 14 hours, the solution was filtered through a pad of celite using dichloromethane and concentrated under reduced pressure. The pure product (1.27 g, 55%, clear oil) was afforded following flash chromatography (1:5 acetone/DCM).

^1H NMR (500 MHz, Chloroform-*d*) δ 4.20 (d, $J = 2.4$ Hz, 2H), 3.77 – 3.64 (m, 14H), 3.64 – 3.57 (m, 2H), 2.56 – 2.48 (m, 1H), 2.42 (t, $J = 2.4$ Hz, 1H).

3,6,9,12-tetraoxapentadec-14-yn-1-yl 4-methylbenzenesulfonate (**4-2**)

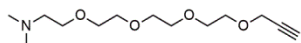


A suspension of sodium hydride (43 mg, 60 wt%, 1.08 mmol) in 2 mL of anhydrous THF was prepared in a 5 mL round bottom flask equipped with a stir bar. After cooling to 0°C under inert atmosphere, a solution of **4-1** (250 mg, 1.08 mmol) in 1 mL was added slowly via syringe and the mixture was allowed to stir for 30 minutes. A solution of p-toluenesulfonyl chloride (205 mg, 1.3 mmol, 3 mL anhydrous THF) was then added via syringe. The mixture was allowed to warm to room temperature and stirring was continued under inert atmosphere overnight. Solvent was removed under reduced pressure and the residue was resuspended in diethyl ether. Solids were removed by filtration and the solvent was again removed under reduced pressure. The pure product (370 mg, 89%, clear oil) was obtained by flash chromatography (1:9 acetone/DCM, *r_f* = 0.7).

¹H NMR (500 MHz, Chloroform-*d*) δ 7.80 (d, *J* = 8.3 Hz, 2H), 7.34 (d, *J* = 7.8 Hz, 2H), 4.19 (d, *J* = 2.4 Hz, 2H), 4.17 – 4.14 (m, 2H), 3.71 – 3.58 (m, 14H), 2.44 (s, 3H), 2.42 (t, *J* = 2.4 Hz, 1H).

¹³C NMR (126 MHz, Chloroform-*d*) δ 144.77, 133.05, 129.81, 127.98, 79.67, 74.49, 70.75, 70.60, 70.54, 70.41, 69.24, 69.12, 68.68, 58.39, 21.63.

N,N-dimethyl-3,6,9,12-tetraoxapentadec-14-yn-1-amine (**4-3**)

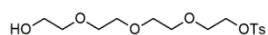


To a flame-dried 25 mL flask equipped with a stir bar was added **4-2** (250 mg, 0.65 mmol) and anhydrous THF (5 mL). A solution of dimethylamine in THF (10 mL, 2 M, 20 mmol) was added via syringe. The flask was sealed by covering the needle hole in the septum with electrical tape.

The mixture was heated to 40°C and stirred overnight. Volatiles were removed under reduced pressure and the residue was partitioned between ethyl acetate and water (pH = 4). The organic layer was removed and discarded. The aqueous layer was adjusted to pH = 10 and extracted 5 times with DCM. The combined organic layers were dried over sodium sulfate, filtered, and concentrated to afford the product (158 mg, 94%, yellowish oil).

^1H NMR (500 MHz, Chloroform-*d*) δ 4.21 (d, J = 2.4 Hz, 2H), 3.71 – 3.60 (m, 12H), 3.58 (t, J = 5.9 Hz, 2H), 2.52 (t, J = 5.9 Hz, 2H), 2.43 (t, J = 2.4 Hz, 1H), 2.27 (s, 6H).

2-(2-(2-(2-hydroxyethoxy)ethoxy)ethoxy)ethyl 4-methylbenzenesulfonate (**4-4**)

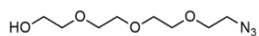


To a 50 mL round bottom flask equipped with a stir bar was added tetraethylene glycol (5 g, 26 mmol) and THF (5 mL). This solution was cooled to 0°C before adding sodium hydroxide as an aqueous solution (1.24 g, 5.15 mL, 6 M, 31 mmol). A solution of p-toluenesulfonyl chloride (4.9 g, 26 mmol) in THF (15 mL) was added slowly at 0°C. The mixture was allowed to warm to room temperature and stirred overnight. The reaction was partitioned between between 10 mL of water and 100 mL of DCM. The organic layer was collected and the aqueous layer was extracted 3 additional times with DCM. The combined organic layers were dried over sodium sulfate and concentrated under reduced pressure. The residue was purified by flash chromatography (1:5 acetone/DCM) to yield the pure product (4.04 g, 45%, clear oil).

^1H NMR (500 MHz, Chloroform-*d*) δ 7.80 (d, J = 8.3 Hz, 2H), 7.34 (d, J = 7.9 Hz, 2H), 4.18 – 4.15 (m, 2H), 3.73 – 3.58 (m, 14H), 2.45 (s, 3H).

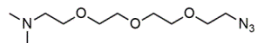
^{13}C NMR (126 MHz, cdcl_3) δ 144.81, 133.00, 129.83, 127.97, 72.46, 70.73, 70.65, 70.47, 70.33, 69.25, 68.70, 61.73, 21.63.

2-(2-(2-(2-azidoethoxy)ethoxy)ethoxy)ethanol (**4-5**)



To flame-dried 15 mL round bottom flask equipped with a stir bar was added **4-4** (750 mg, 2.15 mmol), sodium azide (210 mg, 3.23 mmol), and anhydrous DMF (2 mL). The mixture was heated to 50°C and stirred under inert atmosphere overnight. After cooling to room temperature, the reaction was partitioned between diethyl ether and a saturated lithium chloride solution. The organic layer was collected and the aqueous layer was extracted 3 additional times with diethyl ether. The combined organic layers were washed 3 times with saturated lithium chloride, dried over sodium sulfate, and concentrated under reduced pressure to afford the pure product (405 mg, 86%).

2-(2-(2-(2-azidoethoxy)ethoxy)ethoxy)-N,N-dimethylethanamine (**4-6**)

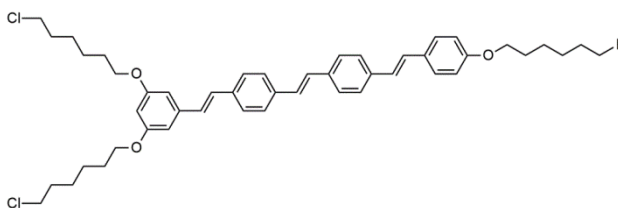


To a flame-dried 5 mL round bottom flask equipped with a stir bar was added sodium hydride (37 mg, 60 wt%, 0.91 mmol) and anhydrous THF (1 mL). This suspension was cooled to 0°C and a solution of **4-5** (200 mg, 0.91 mmol, 2 mL THF) was added slowly via syringe. The mixture was stirred for 30 minutes at 0°C under inert atmosphere before adding a solution of p-toluenesulfonyl chloride (191 mg, 1.0 mmol, 2 mL THF) cannula. The mixture was allowed to warm to room temperature and stirred for 2 hours under inert atmosphere, at which TLC was used to confirm the reaction was complete.

Dimethylamine in THF (2.3 mL, 2 M, 4.6 mmol) was then added via syringe and the vessel was sealed with electrical tape. After stirring overnight at room temperature, volatiles were removed under reduced pressure. The residue was partitioned between DCM and water (pH 11). The organic layer was removed and the aqueous layer was extracted with three more portions of DCM. The combined organic layers were dried over sodium sulfate and concentrated under reduced pressure. The residue was loaded on a long pad of silica gel and 1.5 CVs of chloroform were passed through the pad. The pure product (170 mg, 76% through two steps, yellowish oil) was eluted with 1.5 CVs of methanol.

^1H NMR (400 MHz, Chloroform-*d*) δ 3.69 – 3.61 (m, 10H), 3.58 (t, J = 5.9 Hz, 2H), 3.39 (t, J = 5.1 Hz, 2H), 2.53 (t, J = 5.8 Hz, 2H), 2.28 (s, 6H).

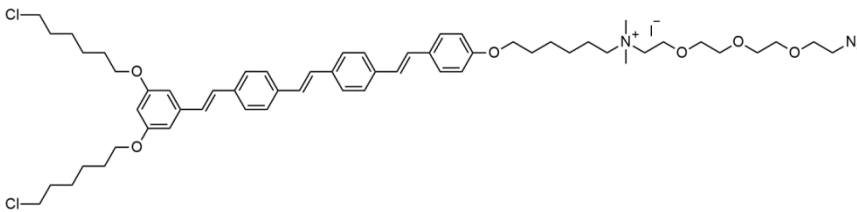
1,3-bis((6-chlorohexyl)oxy)-5-((E)-4-((E)-4-((E)-4-((6-iodohexyl)oxy)styryl)styryl)styryl)benzene (**1-5**)



See Section 1.9

15% over 8 steps, yellow-green solid

N-(2-(2-(2-(2-azidoethoxy)ethoxy)ethoxy)ethyl)-6-(4-((E)-4-((E)-4-((E)-3,5-bis((6-chlorohexyl)oxy)styryl)styryl)styryl)phenoxy)-N,N-dimethylhexan-1-aminium (**4-7**)



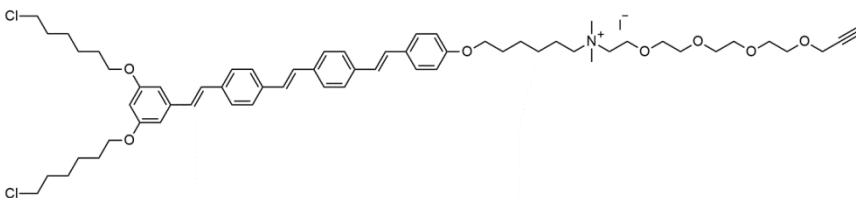
To a flame-dried 5 mL gas-tight flask equipped with a stir bar was added **4-6**

(13.5 mg, 0.048 mmol), **1-5** (46 mg, 0.045 mmol), and 2.5 mL anhydrous THF. The mixture was stirred for two days at 60°C under inert atmosphere. After cooling to room temperature, the mixture was partitioned between DCM and water. The aqueous layer was discarded and the organic layer was washed two additional times with water. The organic layer was dried over sodium sulfate, filtered, and concentrated under reduced pressure. The residue was tritiated with diethyl ether to leave the pure product (55 mg, 92%, green semisolid).

^1H NMR (500 MHz, Chloroform-*d*) δ 7.60 – 7.41 (m, 10H), 7.14 – 6.85 (m, 8H), 6.67 (d, $J = 2.1$ Hz, 2H), 6.39 (t, $J = 2.5$ Hz, 1H), 4.07 – 3.95 (m, 8H), 3.89 (s, 2H), 3.74 – 3.61 (m, 12H), 3.57 (t, $J = 6.7$ Hz, 4H), 3.48 – 3.32 (m, 8H), 1.92 – 1.76 (m, 12H), 1.66 – 1.45 (m, 12H).

^{13}C NMR (126 MHz, cdCl_3) δ 160.44, 158.74, 139.27, 137.05, 136.83, 136.50, 136.27, 130.07, 128.66, 128.61, 128.26, 128.13, 127.89, 127.78, 126.93, 126.87, 126.84, 126.60, 126.14, 114.77, 105.15, 101.00, 70.67, 70.50, 70.35, 70.04, 67.84, 67.58, 66.20, 65.03, 63.40, 52.10, 50.73, 45.03, 32.53, 29.15, 28.97, 26.66, 25.91, 25.70, 25.45, 22.84.

N-(6-(4-((E)-4-((E)-4-((E)-3,5-bis((6-chlorohexyl)oxy)styryl)styryl)styryl)phenoxy)hexyl)-N,N-dimethyl-3,6,9,12-tetraoxapentadec-14-yn-1-aminium iodide (**4-8**)



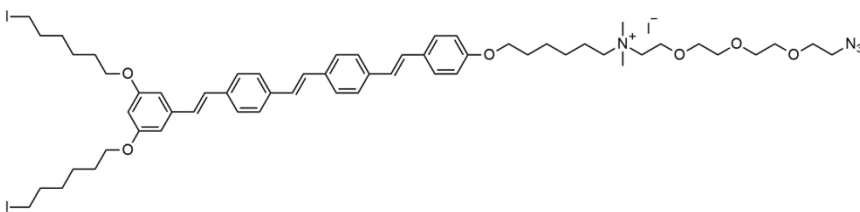
To a flame-dried 10 mL gas-tight flask equipped with a stir bar was added **4-3**

(40 mg, 0.154 mmol), **1-5** (113 mg, 0.128 mmol), and 2.5 mL anhydrous THF. The mixture was stirred for two days at 60°C under inert atmosphere. After cooling to room temperature, the mixture was partitioned between DCM and water. The aqueous layer was discarded and the organic layer was washed two additional times with water. The organic layer was dried over sodium sulfate, filtered, and concentrated under reduced pressure. The pure product (66 mg, 43%, green semisolid) was obtained by C18 reverse phase chromatography (methanol).

^1H NMR (500 MHz, Chloroform-*d*) δ 7.46 – 7.34 (m, 10H), 7.05 – 6.78 (m, 8H), 6.59 (d, $J = 2.2$ Hz, 2H), 6.31 (t, $J = 2.2$ Hz, 1H), 4.12 (d, $J = 2.4$ Hz, 2H), 3.95 – 3.87 (m, 8H), 3.84 – 3.79 (m, 2H), 3.63 – 3.52 (m, 14H), 3.49 (t, $J = 6.7$ Hz, 4H), 3.31 (s, 6H), 2.43 (t, $J = 2.4$ Hz, 1H), 1.80 – 1.69 (m, 12H), 1.54 – 1.37 (m, 12H).

^{13}C NMR (126 MHz, CDCl_3) δ 160.43, 158.73, 139.27, 137.06, 136.84, 136.50, 136.27, 130.08, 128.66, 128.27, 128.13, 127.79, 126.93, 126.85, 126.60, 126.15, 114.76, 105.14, 101.00, 74.96, 74.91, 70.61, 70.47, 70.39, 70.17, 69.33, 67.83, 67.57, 66.26, 58.49, 52.11, 45.04, 32.54, 29.15, 28.98, 26.67, 25.91, 25.72, 25.46, 22.84.

N-(2-(2-(2-(2-azidoethoxy)ethoxy)ethoxy)ethyl)-6-(4-((E)-4-((E)-4-((E)-3,5-bis((6-iodohexyl)oxy)styryl)styryl)styryl)phenoxy)-N,N-dimethylhexan-1-aminium iodide (**4-9a**)

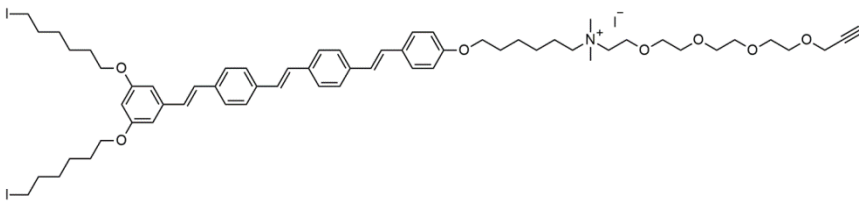


To a 5 mL gas-tight flask equipped with a stir bar was added **4-7** (28 mg, 0.028

mmol), sodium iodide (42 mg, 0.28 mmol) and acetone (3 mL). The flask was sealed and heated to 75°C for two days. After cooling to room temperature, volatiles were removed under reduced pressure. The residue was partitioned between water and dichloromethane. The organic layer was collected and the aqueous layer was extracted with two more portions of dichloromethane. The combined organic layers were dried over sodium sulfate, filtered, and concentrated under reduced pressure to afford the desired product as a green solid (33 mg, 98%).

¹H NMR (500 MHz, Chloroform-*d*) δ 7.53 – 7.41 (m, 10H), 7.13 – 6.86 (m, 8H), 6.67 (d, *J* = 2.2 Hz, 2H), 6.39 (t, *J* = 2.2 Hz, 1H), 4.03 – 3.93 (m, 8H), 3.90 – 3.83 (m, 2H), 3.70 – 3.62 (m, 12H), 3.39 (s, 8H), 3.22 (t, *J* = 7.0 Hz, 4H), 1.92 – 1.76 (m, 12H), 1.61 – 1.44 (m, 12H).

N-(6-(4-((E)-4-((E)-4-((E)-3,5-bis((6-iodohexyl)oxy)styryl)styryl)styryl)phenoxy)hexyl)-N,N-dimethyl-3,6,9,12-tetraoxapentadec-14-yn-1-aminium iodide (**4-10a**)

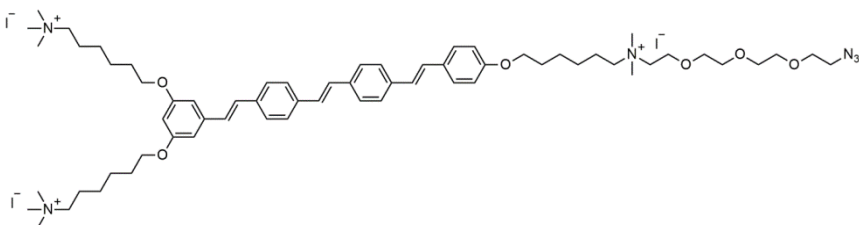


To a 5 mL gas-tight flask equipped with a stir bar was added **4-8** (45 mg, 0.040

mmol), sodium iodide (60 mg, 0.40 mmol) and acetone (3 mL). The same procedure was used as above for **4-9a**. (50 mg, 96%).

^1H NMR (500 MHz, Chloroform-*d*) δ 7.54 – 7.44 (m, 10H), 7.15 – 6.88 (m, 9H), 6.68 (d, J = 2.2 Hz, 2H), 6.40 (t, J = 2.2 Hz, 1H), 4.21 (d, J = 2.4 Hz, 2H), 4.05 – 3.98 (m, 8H), 3.94 – 3.89 (m, 2H), 3.71 – 3.63 (m, 12H), 3.40 (s, 6H), 3.23 (t, J = 7.0 Hz, 4H), 2.51 (t, J = 2.4 Hz, 1H), 1.93 – 1.77 (m, 12H), 1.57 – 1.48 (m, 12H).

6,6'-((5-((E)-4-((E)-4-((E)-4-((1-azido-12,12-dimethyl-3,6,9-trioxa-12-azaoctadecan-12-ium-18-yl)oxy)styryl)styryl)styryl)-1,3-phenylene)bis(oxy))bis(N,N,N-trimethylhexan-1-aminium) iodide (**4-9**)



To a 1 Dr vial equipped with a stir bar was added **4-9a** (18 mg, 0.015 mmol),

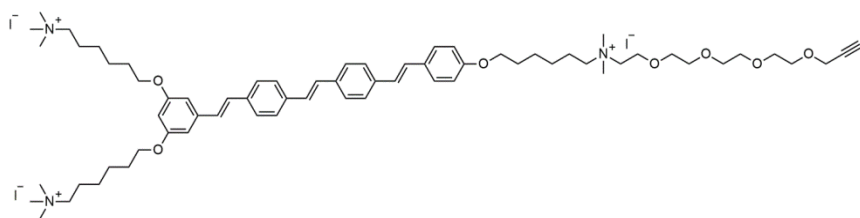
trimethylamine (0.05 mL, 3.2 M in methanol, 0.16 mmol), and anhydrous THF (1 mL). The reaction was stirred at room temperature for 2 days. Volatiles were removed, first by sparging with argon and then under reduced pressure. The residue

was dissolved in minimal methanol and precipitated in diethyl ether. The solid was collected by centrifugation and washed with additional diethyl ether to afford the desired product at a yellow-green solid (19 mg, 96%).

^1H NMR (400 MHz, $\text{DMSO-}d_6$) δ 7.67 – 7.47 (m, 10H), 7.32 – 6.86 (m, 8H), 6.75 (d, $J = 2.1$ Hz, 2H), 6.36 (t, $J = 2.1$ Hz, 1H), 4.04 – 3.91 (m, 6H), 3.83 – 3.76 (m, 2H), 3.58 – 3.47 (m, 12H), 3.36 (t, $J = 4.9$ Hz, 2H), 3.31 – 3.24 (m, 6H), 3.03 (s, 24H), 1.81 – 1.58 (m, 12H), 1.52 – 1.39 (m, 6H), 1.37 – 1.25 (m, 6H).

^{13}C NMR (126 MHz, $\text{DMSO-}d_6$) δ 160.02, 158.40, 139.11, 136.61, 136.24, 135.97, 129.64, 128.51, 128.36, 128.11, 128.06, 127.83, 127.67, 126.90, 126.85, 126.54, 125.69, 114.67, 104.93, 100.72, 69.71, 69.70, 69.55, 69.47, 69.23, 67.36, 65.25, 64.09, 63.90, 62.23, 52.18, 50.80, 49.97, 28.46, 28.42, 25.50, 25.11, 25.09, 22.03, 21.77.

6,6'-((5-((E)-4-((E)-4-((E)-4-((16,16-dimethyl-4,7,10,13-tetraoxa-16-azadocos-1-yn-16-ium-22-yl)oxy)styryl)styryl)styryl)-1,3-phenylene)bis(oxy))bis(N,N,N-trimethylhexan-1-aminium) iodide (**4-10**)



To a 1 Dr vial equipped with a stir bar was added **4-10a** (30 mg, 0.023 mmol),

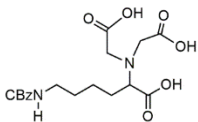
trimethylamine (0.035 mL, 3.2 M in methanol, 0.113 mmol), and anhydrous THF (1 mL). The same procedure was used as above for **4-9**. (31 mg, 95%).

^1H NMR (500 MHz, DMSO- d_6) δ 7.69 – 7.51 (m, 10H), 7.32 – 7.07 (m, 6H), 6.95 (d, J = 8.3 Hz, 2H), 6.78 (d, J = 2.1 Hz, 2H), 6.39 (t, J = 2.7 Hz, 1H), 4.14 (d, J = 2.6 Hz, 2H), 4.01 (t, J = 7.1 Hz, 6H), 3.83 (t, J = 4.5 Hz, 2H), 3.60 – 3.49 (m, 14H), 3.44 (t, J = 2.2 Hz, 1H), 3.34 – 3.26 (m, 6H), 3.06 (s, 24H), 1.79 – 1.67 (m, 12H), 1.54 – 1.43 (m, 6H), 1.40 – 1.31 (m, 6H).

^{13}C NMR (126 MHz, DMSO- d_6) δ 160.03, 158.41, 139.12, 136.83, 136.24, 135.97, 129.65, 128.52, 128.37, 128.12, 128.07, 127.84, 127.68, 126.91, 126.86, 126.55, 125.69, 114.68, 104.94, 100.71, 80.33, 77.17, 69.78, 69.70, 69.50, 69.45, 68.54, 67.36, 65.26, 64.13, 63.89, 62.25, 57.51, 52.19, 50.83, , 28.47, 28.42, 25.50, 25.11, 25.10, 22.03, 21.78.

4.6.2 COE-NTA

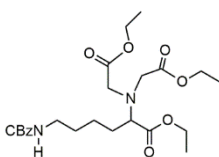
2,2'-((5-(((benzyloxy)carbonyl)amino)-1-carboxypentyl)azanediyl)diacetic acid (**4-18**)



To a 50 mL round bottom flask equipped with a stir bar was added bromoacetic acid (2.08g, 15 mmol) and 7 mL 2 M sodium hydroxide.

This solution was stirred and cooled to 0°C. In a separate vessel, N-epsilon-CBz-lysine (2 g, 7.13 mmol) was dissolved in 11 mL 2 M sodium hydroxide and slowly added to the cooled solution. The mixture was stirred at 0°C for two hours, room temperature overnight, and at 50°C for two hours. At 50°C, 22 mL 1 M hydrochloric acid was added slowly. The solution was then cooled to room temperature and the white solid product was collected by filtration. The product was used without further purification (2.6 g, 92%, no characterization).

diethyl 2,2'-((6-(((benzyloxy)carbonyl)amino)-1-ethoxy-1-oxohexan-2-yl)azanediyl) diacetate (**4-19**)



To a 10 mL round bottom flask equipped with a stir bar and reflux condenser was added **4-18** (0.75 g, 1.73 mmol), ethanol (5 mL), and a drop of sulfuric acid. The mixture was refluxed overnight,

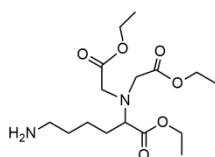
cooled to room temperature, and transferred to a separatory funnel. Aqueous sodium bicarbonate was added until ~pH = 7 followed by DCM. The organic layer was collected and the aqueous layer was extracted with 4 more portions of DCM. The combined organic layers were dried with sodium sulfate, filtered, and

concentrated under reduced pressure to yield the product (0.77 g, 96%) which was used without further purification.

^1H NMR (500 MHz, Chloroform-*d*) δ 7.40 – 7.30 (m, 5H), 5.10 (s, 2H), 4.18 – 4.10 (m, 6H), 3.62 (s, 4H), 3.41 (t, $J = 7.6$ Hz, 1H), 3.24 – 3.17 (m, 2H), 1.75 – 1.64 (m, 2H), 1.58 – 1.38 (m, 4H), 1.29 – 1.21 (m, 9H).

ethyl 6-amino-2-((2-ethoxy-2-oxoethyl)(2-methoxy-2-oxoethyl)amino)hexanoate

(4-20)

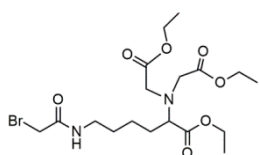


To a 10 mL round bottom flask equipped with a stir bar was added **4-19** (500 mg, 1.08 mmol), ethanol (5 mL), and a small portion of 10 wt% palladium on carbon (tip of a small spatula). The solution

was sparged with argon for 15 minutes followed by hydrogen for 2 minutes. The hydrogen atmosphere was maintained using a balloon attached to the flask via a syringe and needle through a septum. The heterogeneous mixture was stirred at 65°C for 6 hours. After cooling to room temperature, the solution was sparged with argon for 5 minutes. Solids were removed by filtering through a pad of celite using a large volume of ethyl acetate to wash the pad. Concentration under reduced pressure afforded the desired product (343 mg, 91%).

^1H NMR (500 MHz, Chloroform-*d*) δ 4.13 (q, $J = 7.2$ Hz, 6H), 3.63 (s, 4H), 3.40 (t, $J = 7.5$ Hz, 1H), 2.70 – 2.66 (m, 2H), 1.75 – 1.63 (m, 2H), 1.49 – 1.33 (m, 4H), 1.25 (t, $J = 7.1$ Hz, 9H).

diethyl 2,2'-((6-(2-bromoacetamido)-1-ethoxy-1-oxohexan-2-yl)azanediyl)diacetate

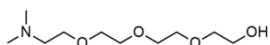


(4-21)

A flame-dried 10 mL round bottom flask equipped with a stir bar was charged with 2 mL anhydrous THF and 53 μ L bromoacetyl chloride (0.635 mmol) under inert atmosphere and cooled to -15°C . To a flame-dried 2 Dr vial was added **4-20** (200 mg, 0.577 mmol), freshly-distilled diisopropylethylamine (106 μ L, 78 mg, 0.606 mmol), and 2 mL anhydrous THF under inert atmosphere. The contents of this vial were added dropwise via syringe to the 10 mL round bottom flask, taking care to maintain the temperature at -15°C . The reaction was allowed to proceed for 2 hours at -15°C before slowly warming to room temperature. The mixture was then partitioned between water and DCM and the organic layer was collected. The aqueous layer was washed 3 additional times with DCM. The combined organic layers were dried with sodium sulfate and passed rapidly through a short (~3 cm) plug of silica gel. The plug was washed with a significant amount of DCM. Concentration under reduced pressure afforded the desired product (330 mg, 70%).

^1H NMR (500 MHz, Chloroform-*d*) δ 4.16 (q, $J = 7.1$ Hz, 6H), 3.89 (s, 2H), 3.62 (s, 4H), 3.44 (t, $J = 6.8$ Hz, 1H), 3.34 – 3.27 (m, 2H), 1.77 – 1.68 (m, 2H), 1.61 – 1.41 (m, 4H), 1.31 – 1.25 (m, 9H).

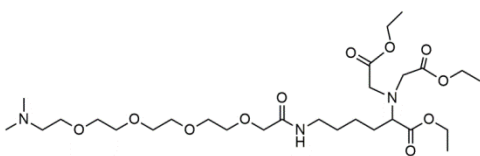
2-methyl-5,8,11-trioxa-2-azatridecan-13-ol (**4-22**)



To a flame-dried 50 mL round bottom flask equipped with a stir bar was added **4-4** (2.5 g, 7.2 mmol) and dimethylamine (18 mL, 2 M in THF, 36 mmol) under inert atmosphere. The flask was sealed with a septum and the mixture was heated to 40°C overnight. After cooling to room temperature, the solution was concentrated under reduced pressure. The residue was partitioned between ethyl acetate and water (pH = 3). The aqueous layer was collected and the organic layer was extracted with 3 more portions of water (pH = 3). The aqueous layers were combined and the pH was adjusted to pH = 11 before extracting with 5 portions of DCM. The combined organic layers were dried over sodium sulfate and concentrated under reduced pressure to afford the desired product (1.4 g, 88%).

¹H NMR (400 MHz, Methylene Chloride-*d*₂) δ 3.67 – 3.51 (m, 14H), 3.18 (s, 1H), 2.45 (t, *J* = 5.8 Hz, 2H), 2.20 (s, 6H).

ethyl 23-(2-ethoxy-2-oxoethyl)-22-(ethoxycarbonyl)-2-methyl-16-oxo-5,8,11,14-tetraoxa-2,17,23-triazapentacosan-25-oate (**4-23**)

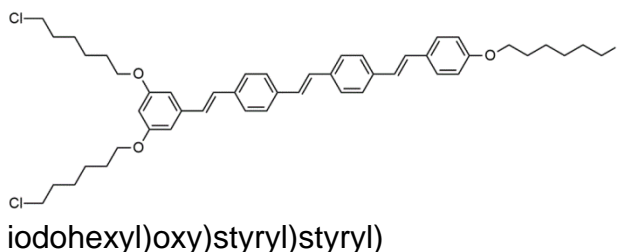


To a flame-dried 10 mL round bottom flask equipped with a stir bar was added sodium hydride (20.5 mg of 60 wt%, 0.513 mmol) and anhydrous THF (1 mL) under inert atmosphere. The heterogenous solution was cooled to 0°C. In a flame-dried 1 Dr vial, **4-22** (125 mg, 0.565 mmol) was dissolved in 2 mL anhydrous THF before slowly adding to the reaction vessel at 0°C via syring.

This solution was maintained at 0°C for 30 minutes before the slow addition of **4-21** (240 mg, 0.513 mmol) as a solution in THF (2 mL). The reaction mixture was maintained at 0°C for an additional 30 minutes before slowly allowing it to warm to room temperature. After 2 hours at room temperature, the mixture was diluted into ~25 mL of diethyl ether. The solution was triterated and the residual solid was washed with another portion of diethyl ether. After filtration to remove the remaining solids, the solution was concentrated under reduced pressure. The pure product (200 mg, 64%) was obtained following C18 reversed phase chromatography (water/methanol, 0-100% over 5 CVs followed by 2 CVs of methanol).

¹H NMR (500 MHz, Chloroform-*d*) δ 7.07 (s, 1H), 4.20 – 4.09 (m, 6H), 3.97 (s, 2H), 3.71 – 3.61 (m, 16H), 3.57 (t, *J* = 5.8 Hz, 2H), 3.40 (t, *J* = 7.5 Hz, 1H), 3.27 (q, *J* = 6.9 Hz, 2H), 2.51 (t, *J* = 5.7 Hz, 2H), 2.26 (s, 6H), 1.77 – 1.64 (m, 2H), 1.59 – 1.46 (m, 3H), 1.42 – 1.33 (m, 1H), 1.31 – 1.24 (m, 9H).

¹³C NMR (126 MHz, cdcl₃) δ 172.65, 171.36, 169.80, 70.89, 70.56, 70.53, 70.52, 70.30, 70.26, 69.15, 69.03, 64.84, 60.51, 60.42, 58.75, 52.69, 45.73, 38.68, 30.17, 29.32, 23.34, 14.27, 14.18.



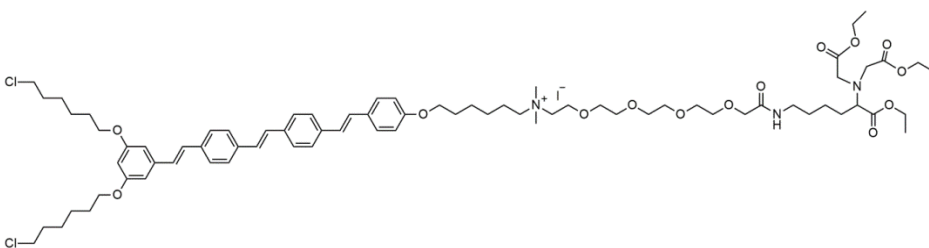
1,3-bis((6-chlorohexyl)oxy)-5-((E)-4-
((E)-4-((E)-4-((6-

iodohexyl)oxy)styryl)styryl)
styryl)benzene (**1-5**)

See Section 1-9

15% over 8 steps, yellow-green solid

N-(6-(4-((E)-4-((E)-4-((E)-3,5-bis((6-chlorohexyl)oxy)styryl)styryl)styryl)phenoxy)hexyl)-21-(2-ethoxy-2-oxoethyl)-20-(ethoxycarbonyl)-N,N-dimethyl-14,23-dioxo-3,6,9,12,24-pentaoxa-15,21-diazahehexacosan-1-aminium iodide (**4-24**)



To a 1 Dr vial equipped with a stir bar was added **4-23** (16

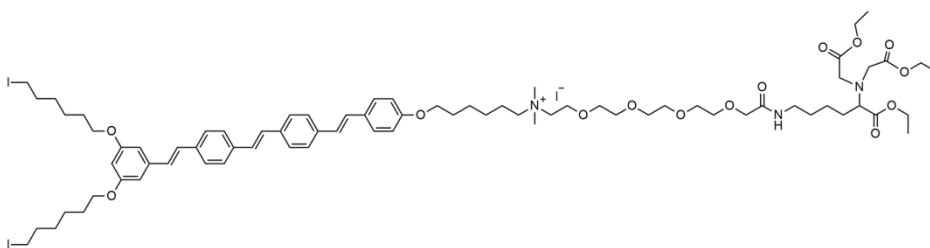
mg, 0.026 mmol), **1-5** (22 mg, 0.025 mmol), and anhydrous THF (0.2 mL). The mixture was stirred at 40°C for 2 days. After cooling to room temperature, the mixture was transferred to a 50 mL centrifuge tube containing 15 mL of cold diethyl ether. The semi-solid was collected by centrifugation before washing 2 additional times with diethyl ether. Residual volatiles were removed under reduced pressure to afford the pure product (36 mg, 95%).

¹H NMR (500 MHz, Chloroform-*d*) δ 7.56 – 7.41 (m, 10H), 7.15 – 6.84 (m, 8H), 6.67 (d, *J* = 2.2 Hz, 2H), 6.39 (t, *J* = 2.2 Hz, 1H), 4.18 – 4.12 (m, 7H), 4.03 – 3.98 (m, 8H), 3.87 (s, 2H), 3.73 – 3.60 (m, 20H), 3.57 (t, *J* = 6.7 Hz, 4H), 3.45 – 3.34 (m, 7H), 3.27 (q, *J* = 6.9 Hz, 2H), 1.88 – 1.32 (m, 30H), 1.29 – 1.26 (m, 9H).

¹³C NMR (126 MHz, cdcl₃) δ 172.64, 171.36, 160.43, 158.73, 139.28, 137.06, 136.84, 136.51, 136.29, 130.11, 128.67, 128.61, 128.28, 128.13, 127.90, 127.78, 126.92, 126.86, 126.83, 126.59, 126.17, 114.75, 105.16, 101.00, 70.85, 70.55, 70.51, 70.45, 70.43, 70.30, 67.83, 67.56, 66.24, 65.03, 64.73, 60.58, 60.50, 52.74,

52.07, 45.02, 38.67, 32.53, 30.13, 29.69, 29.27, 29.15, 28.97, 26.66, 25.93, 25.72, 25.45, 23.30, 22.84, 14.32, 14.22.

N-(6-(4-((E)-4-((E)-4-((E)-3,5-bis((6-iodohexyl)oxy)styryl)styryl)styryl)phenoxy)hexyl)-21-(2-ethoxy-2-oxoethyl)-20-(ethoxycarbonyl)-N,N-dimethyl-14,23-dioxo-3,6,9,12,24-pentaoxa-15,21-diazahexacosan-1-aminium iodide (**4-25**)



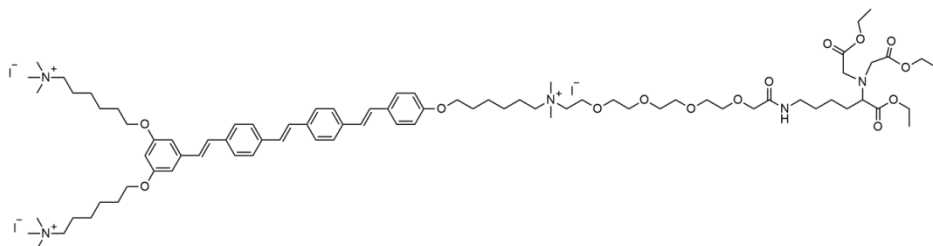
To a 5 mL gas-tight reaction vessel equipped with a stir bar

was added **4-24** (15 mg, 0.011 mmol), sodium iodide (17 mg, 0.11 mmol) and acetone (1 mL). The vessel was sealed and heated to 70°C for 2 days. After cooling to room temperature, the solids were removed by filtration before partitioning the solution between chloroform and water. The organic layer was collected and the aqueous layer washed with 2 more portions of chloroform. The combined organic layers were dried over sodium sulfate, filtered, and concentrated under reduced pressure to afford the pure product (16 mg, 99%).

^1H NMR (500 MHz, Chloroform-*d*) δ 7.57 – 7.42 (m, 10H), 7.13 – 6.87 (m, 8H), 6.67 (d, J = 2.2 Hz, 2H), 6.40 (t, J = 2.2 Hz, 1H), 4.15 (d, J = 7.1 Hz, 6H), 4.00 (t, J = 6.4 Hz, 6H), 3.96 – 3.92 (m, 2H), 3.83 – 3.79 (m, 2H), 3.78 – 3.59 (m, 20H), 3.44 – 3.37 (m, 8H), 3.33 – 3.27 (m, 2H), 3.23 (t, J = 7.0 Hz, 4H), 1.92 – 1.47 (m, 30H), 1.29 – 1.24 (m, 9H).

^{13}C NMR (126 MHz, cdCl_3) δ 172.77, 171.65, 170.31, 160.42, 158.75, 139.27, 137.07, 136.84, 136.50, 136.26, 130.05, 128.67, 128.60, 128.28, 128.15, 127.88, 127.78, 126.92, 126.86, 126.83, 126.60, 126.12, 114.79, 105.17, 101.00, 70.09, 67.83, 67.64, 66.14, 65.01, 64.49, 63.64, 60.80, 60.61, 52.96, 52.12, 38.90, 33.41, 31.92, 30.26, 29.80, 29.69, 29.36, 29.10, 28.98, 28.64, 27.22, 25.94, 25.72, 25.11, 23.02, 22.87, 22.69, 14.34, 14.22, 14.12, 6.99.

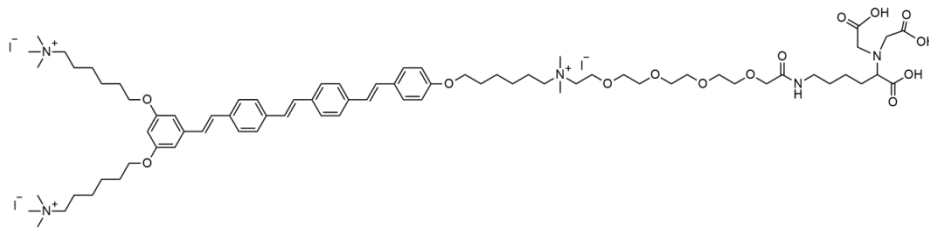
6,6'-((5-((E)-4-((E)-4-((E)-4-((6-(2-ethoxy-2-oxoethyl)-7-(ethoxycarbonyl)-27,27-dimethyl-4,13-dioxo-3,15,18,21,24-pentaoxa-6,12,27-triazatritriacontan-27-ium-33-yl)oxy)styryl)styryl)styryl)-1,3-phenylene)bis(oxy))bis(N,N,N-trimethylhexan-1-aminium) iodide (**4-26**)



To a 1 Dr vial equipped with a stir bar was added **4-25** (15 mg, 0.010 mmol), trimethylamine (0.03 mL, 3.2 M in methanol, 0.10 mmol), and THF (0.3 mL) under inert atmosphere. The mixture was stirred for 2 days at room temperature. During the course of the reaction, yellow solids were formed. These solids were dissolved by adding a drop of methanol before adding the entire solution to a 50 mL centrifuge tube containing 15 mL diethyl ether. The precipitate was collected by sequential centrifugation and wash steps with diethyl ether. 50/50 THF/diethyl ether was used as a final wash. Residual volatiles were removed under reduced pressure to afford the desired product as a yellowish solid (17 mg, 99%).

^1H NMR (400 MHz, $\text{DMSO-}d_6$) δ 7.70 – 7.51 (m, 10H), 7.34 – 7.04 (m, 6H), 6.94 (d, $J = 8.4$ Hz, 2H), 6.78 (d, $J = 2.1$ Hz, 2H), 6.39 (t, $J = 2.1$ Hz, 1H), 4.09 – 3.96 (m, 12H), 3.88 – 3.81 (m, 4H), 3.63 – 3.48 (m, 21H), 3.34 – 3.25 (m, 12H), 3.06 (s, 18H), 1.74 (dt, $J = 15.9, 9.3$ Hz, 8H), 1.52 – 1.16 (m, 31H).

6,6'-((5-((E)-4-((E)-4-((E)-4-((1,3-dicarboxy-2-(carboxymethyl)-23,23-dimethyl-9-oxo-11,14,17,20-tetraoxa-2,8,23-triazanonacosan-23-ium-29-yl)oxy)styryl)styryl)styryl)-1,3-phenylene)bis(oxy))bis(N,N,N-trimethylhexan-1-aminium) iodide (**4-27**)



To a 1 Dr vial equipped with a stir bar was added **4-26** (17

mg, 0.01 mmol) and a solution of lithium hydroxide (2.4 mg in 1 mL water, 0.1 M). The mixture was stirred under inert atmosphere overnight at room temperature. The solution was directly loaded on a C18 reverse phase column and flushed with 2 CVs of water before eluting the product with methanol. After concentration under reduced pressure, minimal methanol was used to dissolve the residue. This solution was added to a 50 mL centrifuge tube containing 15 mL diethyl ether and the precipitate was collected by centrifugation. Two subsequent wash and centrifuge steps with 50/50 diethyl ether/THF (anhydrous) afforded the desired product as a yellowish solid (14 mg/ 90%).

^1H NMR (400 MHz, $\text{DMSO-}d_6$) δ 7.71 – 7.46 (m, 10H), 7.33 – 7.03 (m, 6H), 6.91 (d, $J = 8.3$ Hz, 2H), 6.74 (d, $J = 2.1$ Hz, 2H), 6.35 (t, $J = 2.0$ Hz, 1H), 3.97 (t, $J = 6.4$ Hz,

6H), 3.86 – 3.79 (m, 4H), 3.58 – 3.45 (m, 18H), 3.33 – 3.20 (m, 9H), 3.19 – 3.11 (m, 6H), 3.02 (s, 18H), 1.80 – 1.14 (m, 30H).

Chapter 5: COEs as a Potential Novel Class of Antibiotic

5.1 Introduction

5.1.1 Antimicrobial Resistance and the Threat it poses to Humanity

According to the well-appreciated 2014 *Review on Antimicrobial Resistance*,³⁷ the world in 2050 could be one plagued by untreatable infections. In this review it was estimated that without a significant change in course, antimicrobial resistance (AMR) could result in 10 million deaths annually. Additionally, the financial burden of such a crisis could be expected to reach 100 trillion USD. A recent article in *The Economist*²¹⁰ made similar grim predictions of a future where surgeries that are routine today would become too risky due to the chance of contracting infections for which there is no cure. While there is still hope to avoid such a fate, there is a general consensus that we are currently losing the battle against drug-resistant bacteria. According to the latest CDC report on antibiotic resistance in the United States, 2.8 million people become infected with antibiotic-resistant bacteria per year and 35,000 die as a result.²¹¹

A number of factors have contributed to our struggle with AMR, not the least of which is an antibiotic pipeline that has long since stopped flowing. All major classes of antibiotics used today were developed by the 1960s.²¹²⁻²¹⁴ The predicted antibiotic development renaissance based on computational high-throughput screening never came to fruition, with most programs having nothing to show for their effort.^{215, 216}

Many of the major pharmaceutical companies have now left the antibiotic space due to the poor financial outlook.²¹⁷ Development of novel drugs to combat AMR (and potentially save our future) has been left up to academic researchers and small companies.

5.1.2 The Membrane as a Target for Antibiotics

Membrane-active antibiotics have been around since the 1940's following the discovery of polymyxins²¹⁸ and subsequent FDA-approval of colistin²¹⁹ but nature has a long history of using membrane disruption to combat microbes.^{28, 29} Natural AMPs were first isolated from *Bacillus brevis* in 1939 by Dubos,²²⁰ who subsequently demonstrated the ability of these AMPs to treat wound infections in guinea pigs.^{221,}
²²² A select few AMPs are currently in development as antibiotics but many more have unfortunately proved unsuitable as therapeutic agents.^{223, 224} These successes and failures have been chronicled in many recent reviews.³³⁻³⁵

Compared to the vast majority of antibiotics, which have protein targets, antibiotics that act on the bacteria membrane have a number of potential advantages: membranes are essential to survival and are present in all bacteria,^{225,}
²²⁶ disrupting the membrane has the potential to kill metabolically-inactive bacteria, and the opportunity for developing resistance is lower.^{28, 227} As such, AMPs generally possess broad-spectrum activity, including against strains which are multi-drug resistant (MDR).²²⁸ It is now understood that net-positive charge and hydrophobicity dictate the antimicrobial activity and selectivity of AMPs,^{229, 230} many

of which deactivate microbes directly through membrane disruption via a number of different mechanisms.²³¹⁻²³³

Guided in large part by the findings of AMP research, membrane-active small molecule antimicrobials are emerging as a potential means to combat MDR infections.³⁶ These compounds generally contain cationic groups and a hydrophobic core that can be derived from a vast number of structures including arylamides,²³⁴⁻²³⁷ arylureas,²³⁸ phenylene ethynylene,^{239, 240} cholic acid,²⁴¹ and various aryl or heteroaryl units.²⁴²⁻²⁴⁵ Similar to AMPs, a number of potential mechanisms of action have been identified such as pore formation¹⁵² or the remodeling of lipid domains.^{246, 247} In addition to potential mechanisms and selectivity towards bacteria, many of these compounds also share with AMPs the ability to evade resistance.³⁶

The ability of COEs to interact with microbial membranes has been well-established in this dissertation. This chapter will outline our preliminary efforts to develop COEs as membrane-active antibiotics. Much of the content of this chapter was included in a patent filing (UC Case No. 2018-423) and other pertinent data has been omitted for the protection of potential subsequent filings.

5.2 Design of a COE antibiotic – our initial “hit” compound

Previous work in our group, as well as the project described in Chapter 2, identified COE “length” as a key contributing factor for antimicrobial activity. The analysis detailed in Chapter 2 allowed us to explicitly define this parameter as the distance

between ammonium groups on opposite ends of the structure. It was found in both studies, however, that reducing this length will eventually result in a loss of cell affinity and thus poor antimicrobial activity. A visiting student in our group, Zichao Zhang, began synthesizing new COEs with increased hydrophobicity in an attempt to recover activity by restoring affinity for membranes. After a period of mixed results, our collective pool of design ideas became thin. Then, following a discussion with my former undergraduate labmate (Dr. Roscoe Linstadt of Prof. Bruce Lipshutz's lab) about a quaternization reaction he was working on, serendipity struck. Roscoe provided a small portion of N,N-dimethylhexylamine and Zichao synthesized a new COE, now called "COE2-2hexyl", which became our "hit" compound and marked the inception of our antibiotics effort.

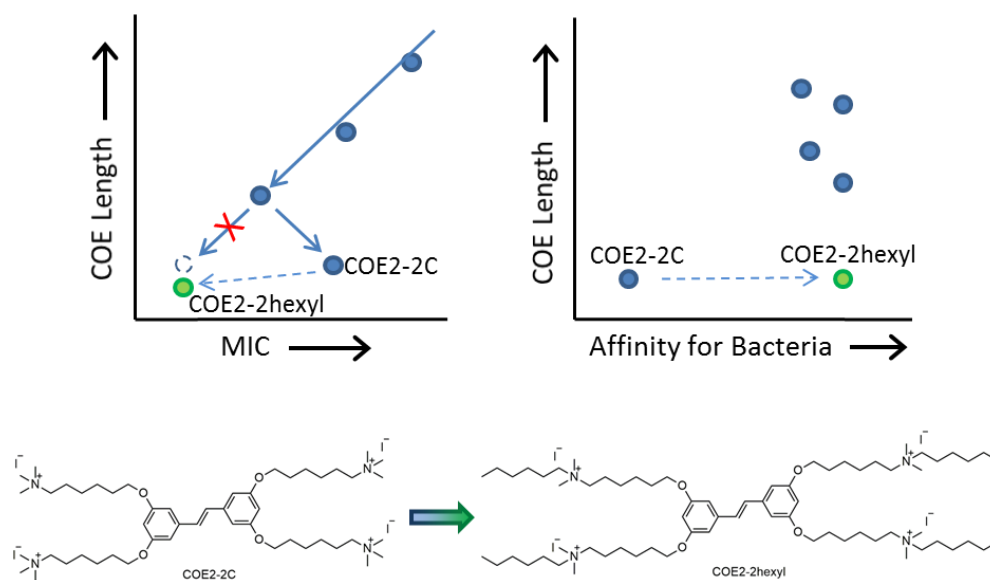


Figure 5-1 Derivatization of COE2-2C to produce a COE with improve antimicrobial activity through increased affinity for bacteria – COE2-2hexyl.

As shown schematically in Figure 5-1, COE2-2C had a higher-than-expected MIC which was attributed to its low affinity for bacteria. Substitution of one of the methyl

groups for a hexyl group on the terminal ammoniums provided increased affinity for cells without increasing the distance between opposite ammonium groups. Increasing the number of aromatic rings in the core or methylenes in the pendant chains would have also increased bacterial affinity but it was already shown in Chapter 2 that these modifications would also reduce antimicrobial activity. Introducing the additional hydrophobic domain beyond the ammonium groups in COE2-2hexyl allowed us to leverage both the hydrophobicity-affinity and length-antimicrobial activity trends.

Table 5-1 Comparison of antimicrobial activity of COE2-2hexyl and azithromycin.

Pathogen	MIC values (mg/mL)	
	Azithromycin	COE2-2hexyl
<i>S. Typhimurium</i>	4	2
<i>E. coli</i>	4	2
<i>P. aeruginosa</i>	128	8
<i>K. pneumoniae</i> (CRE)*	256	4
<i>S. flexneri</i>	2	2
<i>Y. pseudotuberculosis</i>	8	1
<i>A. baumannii</i>	64	4
<i>N. gonorrhoeae</i>	0.03	0.5
<i>S. pneumoniae</i>	8	8
<i>S. aureus</i> (MRSA)*	128	1

*clinical isolates from expired patients

Following the observation that COE2-2hexyl possessed good antimicrobial activity (MIC = 4 μ M for *E. coli* K12), we initiated a collaboration with Dr. Michael Mahan (UCSB) to help with the process of investigating COEs as antimicrobial agents. The Mahan lab tested COE2-2hexyl, along with a number of other COEs, against a broad panel of pathogenic bacteria. Their results, summarized in Table 5-

1, indicate that COE2-2hexyl has a broad spectrum of activity (i.e. functions against many strains of both gram-positive and gram-negative varieties). Even multi-drug resistant (MDR) bacteria were found to be susceptible to COE2-2hexyl. In fact, no strain that the Mahan Lab tested had an MIC > 8 µg/mL and most were more susceptible to COE2-2hexyl than the control antibiotic, azithromycin.

The positive MIC results prompted the Mahan Lab to test COE2-2hexyl in a mouse model for bacteremia. Mice were inoculated with the two clinical isolates (separately) indicated in Table 5-1 and it was confirmed that both strains were able to cause infection. Groups of five infective mice received either COE2-2hexyl (2 mg/kg, IV bolus, tail vein, once daily for 3 days) or vehicle control. All untreated mice expired as a result of the infection while all treated mice survived. This experiment was repeated and the initial results were confirmed – COE2-2hexyl was able to protect against 100 % lethal infections without causing overt toxicity in mice.

Table 5-2 IC₅₀ values for COE2-2hexyl against various cell lines. Asterisks (*) indicate test that were conducted at Eurofins Discovery Services.

	NIH 3T3	J774	Hep G2	Hep G2*	Primary Human Hepatocytes*	HRPTEpiC*
IC ₅₀ (µg/uL)	10.4	2.5	7.3	5.6	13.2	2.6

Although COE2-2hexyl was found to be non-toxic at a dose of 2 mg/kg, cytotoxicity results indicated that there is a potential risk of damage to mammalian cells. A postdoc in our group, Dr. Chenyao Nie, tested the cytotoxicity of COE2-2hexyl against various cell lines using the standard MTT assay. Her results were also confirmed by contracting Eurofins Discovery Services (St. Charles, MO) to

conduct similar tests. The results are summarized in Table 5-2. As suggested for membrane-active antimicrobials in general,³⁶ COE2-2hexyl appears to cause significant cytotoxicity. The remainder of this chapter will focus on our group's efforts to optimize COE structure to achieve low MIC, low cytotoxicity, and other positive attributes.

5.3 The effect of pendant and terminal alkyl chain lengths on antimicrobial and cytotoxic properties

In a similar manner as outlined in Chapter 2, a homologous series of COEs was developed specifically to investigate how structure impacts MIC and cytotoxicity. As the intent was to retain high antimicrobial activity, the distance between ammonium groups was kept short. Conjugated cores were limited to stilbene and distyrylbenzene. For the stilbene core, only pendant chains of 6 carbons were investigated. For the distyrylbenzene core, pendants from 2 to 4 carbons were utilized. The primary modification site in this homologous series was the terminal alkyl chain, which was varied from 1 to 6 carbons. A general structure encompassing this series of COEs is shown in Figure 5-2. All compounds for which there is no detailed synthetic method in Section 5.6 were prepared by Jakkarin Limwongyut. Certain intermediates were synthesized by Luana Llanes. Most of the MIC and cytotoxicity experiments were conducted by Dr. Chenyao Nie. Our cumulative results using this series of COE are shown in Table 5-3.

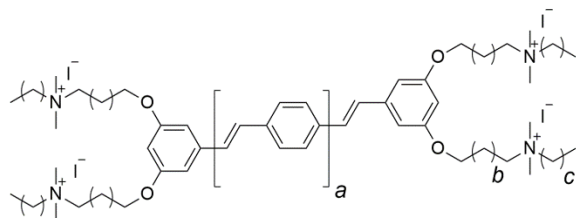


Figure 5-2 Generic structure of COEs used for preliminary antimicrobial/cytotoxicity SAR studies. Selectivity for bacteria was assessed as a function of parameters “a”, “b”, and “c”.

Two major trends can be observed from the data presented below. First, it appears that distyrylbenzene-based COEs perform better than their closest stilbene analogues. For example, all three distyrylbenzene derivatives containing “butyl” terminal chains show markedly better selectivity than COE2-2butyl. While we do not yet have an explanation for this trend, this observation does serve to narrow the scope of structures to investigate in future optimization efforts.

Table 5-3 Antimicrobial activity, cytotoxicity, and selectivity of thirteen COEs containing variable parameters “a”, “b”, and “c”.

parameter			Name	<i>E. coli</i> K12 MIC (µg/mL)	Hep G2 IC ₅₀ (µg/mL)	Selectivity IC ₅₀ /MIC
a	b	c				
0	4	5	COE2-2hexyl	4	7	2
0	4	4	COE2-2pentyl	4	41	10
0	4	3	COE2-2butyl	4	>128 (57%)	>32
1	2	5	COE2-3C-C4hexyl	4	15	4
1	2	4	COE2-3C-C4pentyl	4	321	80
1	2	3	COE2-3C-C4butyl	4	>1024 (85%)	>256
1	2	2	COE2-3C-C4propyl	8	>128 (91%)	>16
1	2	0	COE2-3C-C4	32	>1024 (100%)	>32
1	1	5	COE2-3C-C3hexyl	8	15	2
1	1	3	COE2-3C-C3butyl	4	637	160
1	1	1	COE2-3C-C3ethyl	32	>1024 (61%)	>32
1	0	5	COE2-3C-C2hexyl	4	13	3
1	0	3	COE2-3C-C2butyl	4	>1024 (85%)	>256

The second and more profound observation is the dependence on the terminal alkyl chain. All four COEs with “hexyl” terminal chains have low selectivity (~2-3). Reducing the length to “pentyl” results in an increase in selectivity of roughly an order-of-magnitude. Further reduction to “butyl” provides another order-of-magnitude increase in selectivity. Within this set of COEs, “butyl” represents an optimal terminal chain length as further reductions begin to have significant negative impacts on antimicrobial properties.

In order to assess the spectrum of activity of these new COEs, we contracted Emery Pharma (Alameda, CA) to conduct MIC measurements on a panel of the so-called “ESKAPE” pathogens. “ESKAPE” is an acronym coined by Rice²⁴⁸ in 2008 for the most serious antibiotic-resistant nosocomial pathogens - *Enterococcus faecium*, *Staphylococcus aureus*, *Klebsiella pneumoniae*, *Acinetobacter baumannii*, *Pseudomonas aeruginosa*, and *Enterobacter* species. These bacteria also occur near the top of the lists of priority pathogens published by the World Health Organization^{249, 250} and the CDC.²¹¹ The data are summarized in Table 5-4 below. Somewhat unexpectedly, the MIC values for *E. coli* K12 did not accurately predict the MICs against other strains (this may be common for many antibiotics but was not anticipated for COEs based on the data for COE2-2hexyl against a broad panel of pathogens in Table 5-1). In general, the compounds with the highest selectivity (IC₅₀/MIC) in our tests with *E. coli* K12 also had the highest selectivity towards other strains. Unlike *E. coli* K12, though, certain strains showed significantly reduced susceptibility to COEs with shortened terminal alkyl chains. In particular, *P. aeruginosa* showed limited susceptibility to anything shorter than a “hexyl” pendant

chain. While many of the MIC values did not reach desirable levels, this test did demonstrate that structural modifications can be used to improved selectivity for bacteria over mammalian cells. Additionally, it was found that COEs with low cytotoxicity were still highly effective against gram-positive bacteria, suggesting that gram-positive-specific COE antibiotics are well within reach.

Table 5-4 MIC values (in µg/mL) for ten COEs against ESKAPE pathogens tested at Emery Pharma as well as two *E. coli* strains.

	Gram positive			Gram negative								
	<i>E. faecium</i> 1674620	<i>S. aureus</i> ATCC 33591	<i>S. aureus</i> ATCC BAA-1717	<i>K. pneumoniae</i> ATCC BAA-2473	<i>K. pneumoniae</i> CDC0010	<i>A. baumannii</i> 1674627	<i>A. baumannii</i> CDC0290	<i>P. aeruginosa</i> 1674623	<i>P. aeruginosa</i> CDC0248	<i>E. cloacae</i> 1744299	<i>E. coli</i> ATCC 25922	<i>E. coli</i> K12
COE2-2hexyl	0.25	0.5	0.5	2	4	4	4	8	8	2	1	4
COE2-2butyl	0.5	0.5	0.5	16	32	>64	>64	>64	>64	16	4	4
COE2-3C-C4hexyl	0.25	0.5	1	4	4	2	4	16	32	2	2	4
COE2-3C-C4butyl	0.5	0.5	1	8	16	32	32	64	64	8	4	4
COE2-3C-C4propyl	1	1	1	8	32	64	64	>64	>64	8	4	8
COE2-3C-C4ethyl	4	1	2	16	32	64	64	>64	>64	8	8	16
COE2-3C-C4	8	2	2	32	64	64	64	>64	>64	8	8	32
COE2-3C-C3hexyl	0.25	2	0.5	2	2	2	2	16	32	2	1	8
COE2-3C-C3butyl	0.25	0.5	1	4	16	16	16	64	32	4	1	4
COE2-3C-C2butyl	1	1	2	4	16	32	32	64	64	4	1	4

Given the apparent (but not equivalent) dependence of MIC and cytotoxicity on the terminal chain length, we next set out to understand how the specific composition of the terminal group affects this trend. More precisely, we designed COEs with multiple, shorter terminal chains rather than a single long chain (Figure 5-3).

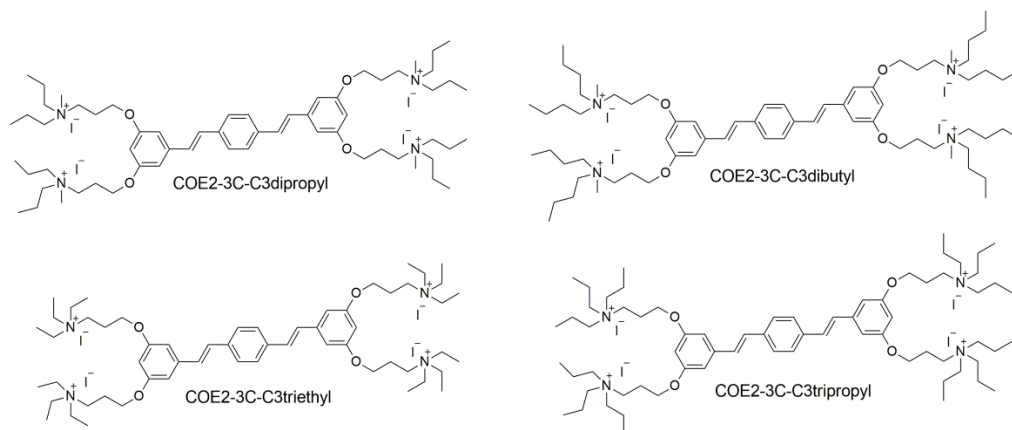


Figure 5-3 Four COEs designed to test the effects of multiple short terminal chains relative to a single long terminal chain.

The MIC and IC₅₀ values for these four COEs, as well as seven which contain single terminal chains, are presented in Table 5-5. Additionally, the sp³-carbon content of each COE is listed. “Terminal” refers to the number of carbons that occur beyond a single nitrogen atom (i.e. not between the core and the ammonium). “Total” refers to the total number of carbons in a single appendage (i.e. “terminal” plus the carbons between the core and ammonium). “Longest” refers to the longest continuous terminal alkyl chain.

Considering first the structures with single extended terminal chains, it appears that cytotoxicity is highly dependent on the length of the longest chain (reflected in either “terminal” or “longest”). For example, COE2-3C-C4butyl contains the same “total” as COE2-3C-C2hexyl (10) yet has a significantly-higher IC₅₀. This effect results in differential selectivity of these compounds, as described earlier in this section. It is unclear, however, whether MIC depends on the same structural parameter. Analysis of antimicrobial activity as a function of sp³-carbon content

indicates a minimum necessary hydrophobic character but the specific structural parameter cannot be identified.

Table 5-5 Antimicrobial activity and cytotoxicity of COEs as a function of pendant chain structure.

	<i>E. coli</i> K12 MIC ($\mu\text{g/mL}$)	Hep G2 IC ₅₀ ($\mu\text{g/mL}$)	sp ³ -carbon content		
			terminal	total	longest
----- Single Long Terminal Chains -----					
COE2-3C-C3ethyl	32	>1024 (61%)	4	7	2
COE2-3C-C3propyl	8	>1024 (87%)	5	8	3
COE2-3C-C3butyl	4	637	6	9	4
COE2-3C-C4pentyl	4	128	7	11	5
COE2-3C-C3hexyl	8	15	8	11	6
COE2-3C-C2hexyl	4	13	8	10	6
COE2-3C-C4butyl	4	>1024(85%)	6	10	4
----- Multiple Short Terminal Chains -----					
COE2-3C-C3dipropyl	2	>128 (92%)	7	10	3
COE2-3C-C3dibutyl	8	32	9	12	4
COE2-3C-C3triethyl	16	>128 (100%)	6	9	2
COE2-3C-C3tripropyl	64	-	9	12	3

The MIC values for the two structures containing three extended terminal chains (COE2-3C-C3triethyl and COE2-3C-C3tripropyl) were found to be unexpectedly high. This result may be attributable to excessive steric screening of the positive charge which could result in reduced affinity for negatively-charged membranes or lead to aggregation in solution. The two structures with one methyl group and two extended chains (COE2-3C-C3dipropyl and COE2-3C-C3dibutyl), as well as COE2-3C-C3triethyl, proved less-cytotoxic than would have been expected based on total hydrophobic content. This result supports the hypothesis that the length of terminal chains has more impact on cytotoxicity than does the cumulative number of “terminal” carbons (or “total” carbons). In the case of COE-3C-C3dipropyl and

COE2-3C-C3dibutyl, it was also found that replacing a single long chain with two shorter chains had less impact on MIC than cytotoxicity (i.e. increased selectivity for bacteria). In fact, the MIC of COE2-3C-C3dipropyl against *E. coli* K12 (2 µg/mL) was the lowest of any COE tested to this point. This suggests that while cytotoxicity is dependent mainly on the length of the terminal chains, MIC depends more heavily on the total hydrophobic content. The design of future compounds with improved selectivity will incorporate these important findings.

Given the promising results, COE2-3C-C3dipropyl was sent to Emery Pharma for evaluation against the ESKAPE panel. However, it was found that the improved MIC against *E. coli* K12 did not translate to other microbes. COEs with high MICs against *E. coli* K12 (>8 µg/mL) always showed poor activity against other gram-negative bacteria while good activity against *E. coli* K12 did not seem predictive of broad spectrum activity. To determine if this conclusion was warranted, the correlation (R) and significance (p) were calculated for MIC values of eight COEs between pairs of *E. coli* and gram-negative members of the ESKAPE panel. The R-values (calculated in MATLAB R2016b, academic license) for all pairs of bacteria are shown in Figure 5-4 and three representative comparisons are highlighted in Figure 5-5.

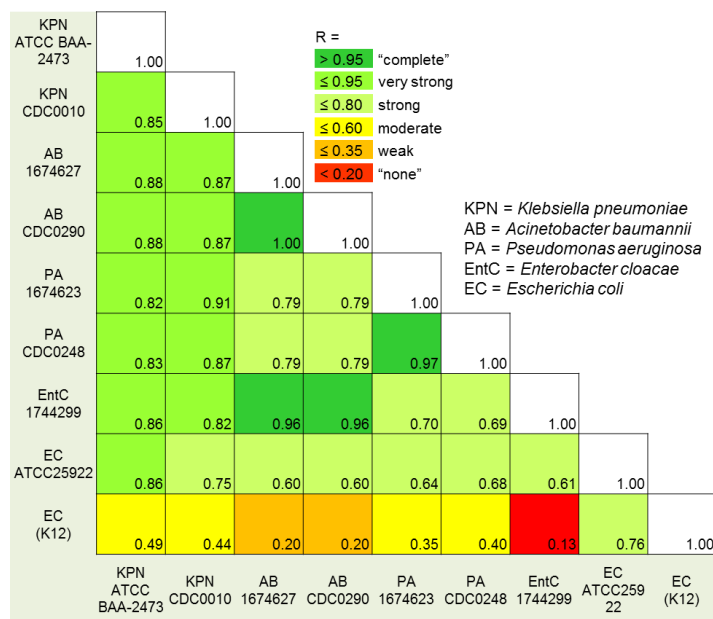


Figure 5-4 Correlation of MIC values for COEs against various gram-negative strains

Excluding *E. coli* K12, correlation between different strains is high (0.6-1.0). Correlation between *E. coli* K12 and any other strain is much weaker ($R < 0.5$) with the exception of *E. coli* ATCC 25922 ($R = 0.76$). In the plot of MIC values for *A. baumannii* and *E. cloacae* (Figure 5-5a), the values of one strain are highly predictive of the other despite the relatively higher MIC values for *A. baumannii*. The plot comparing *A. baumannii* with *P. aeruginosa* (Figure 5-5b), which have similar COE susceptibilities, shows a weaker, yet still predictive correlation. In contrast, the plot comparing *A. baumannii* and *E. coli* K12 (Figure 5-5c) highlights the poor correlation of the latter with other strains. For example, the plot shows that COEs with an MIC of 4 $\mu\text{g/mL}$ against *E. coli* K12 have MICs against *A. baumannii* ranging from 4-128 $\mu\text{g/mL}$. The obvious conclusion is that *E. coli* K12 is not a suitable model organism for MIC studies involving COEs but a more subtle observation can be

made as well – the fact that all other strains are well-correlated suggests a general mechanism of action (MOA) for COE antimicrobials.

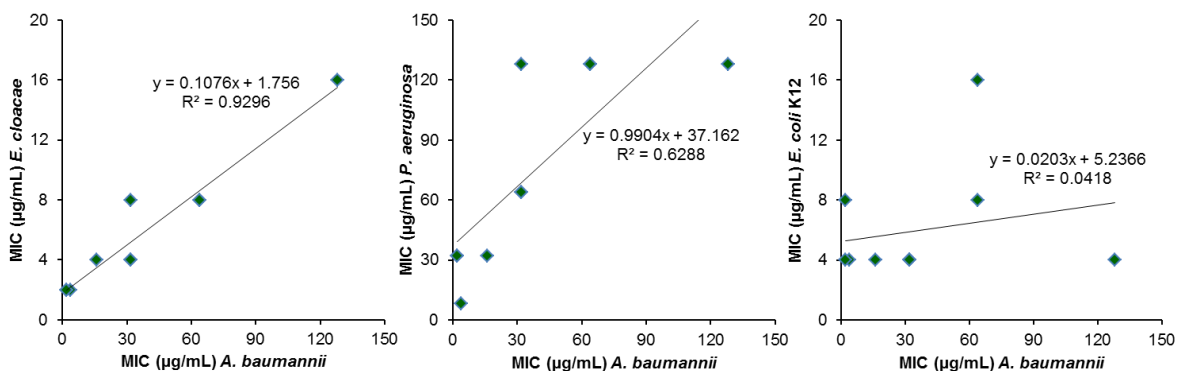


Figure 5-5 Comparison of MIC values against *A. baumannii* vs. *E. cloacae*, *P. aeruginosa*, and *E. coli* K12

5.4 Multi-functional end groups and their effect on COE antimicrobial activity

To further investigate the function of the terminal groups, we synthesized a series of COEs which contained end groups bearing multiple functional units (i.e. not simple alkyl chains). The six target COEs depicted below in Figure 5-6 are based on the same general scaffold of three aromatic rings with a pendant chain of three carbons. Five of these compounds have terminal groups comprised of propyl chains with various substitutions (alcohol, diol, sulfate, primary amine, quaternary amine) and the sixth contains N-methyl-DABCO. It was expected that alterations in the hydrophobic/hydrophilic balance, as well as changes in net charge, would affect the selectivity for microbes. We previously found that COEs with a net negative charge

do not associate with negatively-charged membranes²⁵¹ and thus we only included compounds with a formal charge greater than or equal to 0 in this study.

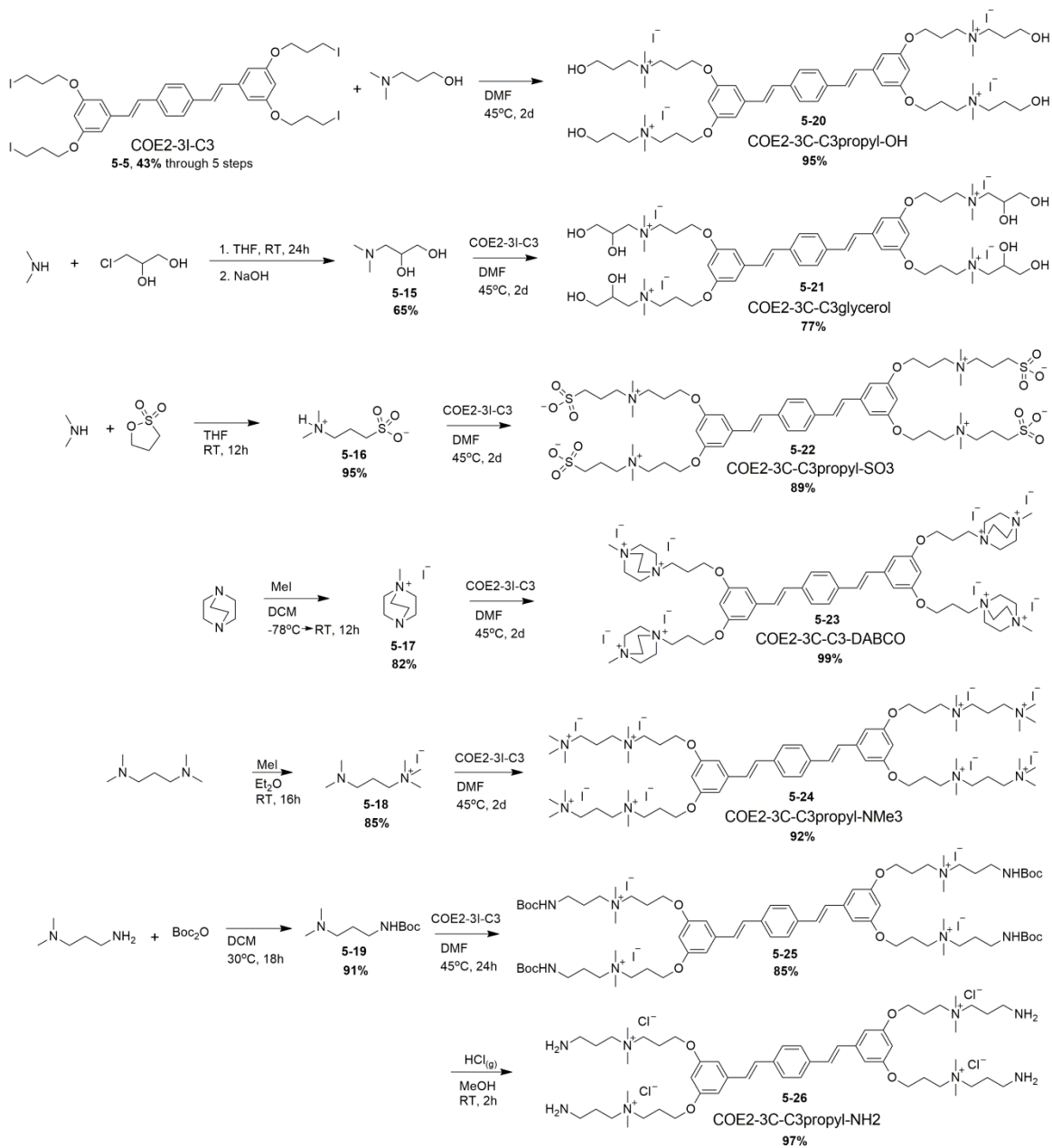


Figure 5-6 Synthetic routes used to access COEs with complex end groups.

In general, the synthesis of these COEs involved forming the appropriate amine and subsequent quaternization with the neutral intermediate, COE2-3I-C3. In the case of COE2-3C-C3propyl-OH, commercially available 3-dimethylamino-1-propanol was purchased and used directly in the quaternization reaction. For the other COEs, amine intermediates were prepared as follows: 3-dimethylamino-1,2-propanediol was prepared from dimethylamine and 3-chloro-1,2-propanediol, 3-(dimethylamino)propane-1-sulfonic acid was prepared by ring-opening of 1,3-propanesultone with dimethylamine, 1-methyl-1,4-diazabicyclo[2.2.2]octan-1-ium iodide was prepared by quaternizing DABCO with a single equivalent of methyl iodide, 3-(dimethylamino)-*N,N,N*-trimethylpropan-1-aminium iodide was prepared by quaternizing tetramethylpropane-1,3-diamine with a single equivalent of methyl iodide, and *tert*-butyl (3-(dimethylamino)propyl)carbamate was prepared from *N,N*-dimethylpropane-1,3-diamine and di-*tert*-butyl dicarbonate. In the case of COE2-3C-C3propyl-NH₂, the boc protecting group was removed in the final step with hydrochloric acid.

Table 5-6 Antimicrobial susceptibility tests of COEs containing complex terminal chains

	MIC values (µg/mL)	
	<i>E. coli</i> K12	<i>S. epidermidis</i>
COE2-3C-C3butyl	4	2
COE2-3C-C3propyl	8	16
COE2-3C-C3propyl-OH	>128	64
COE2-3C-C3glycerol	>128	>64
COE2-3C-C3propyl-SO ₃	>128	32
COE2-3C-C3DABCO	64	16
COE2-3C-C3propyl-NMe ₃	>128	32
COE2-3C-C3propyl-NH ₂	32	16

The MICs against *E. coli* K12 and *S. epidermidis* of these six COEs, along with COE2-3C-C3butyl and COE2-3C-C3propyl for reference, are shown in Table 5-6. In all cases, derivatization of the terminal alkyl chain resulted in reduced antimicrobial activity. The effect was less pronounced with *S. epidermidis*, suggesting that affinity for gram-positive bacteria is less sensitive to these particular structural modifications. In general, addition of negatively-charged moieties reduced the antimicrobial activity more than the addition of positively-charged groups (although it is interesting to note that COE2-3C-C3propyl-SO₃ and COE2-3C-C3propyl-NMe₃ have identical MIC profiles). This may be attributed to weakened coulombic interactions between cells and COEs bearing alcohol, diol, or sulfate groups. Hence, all six COEs may have reduced membrane-affinity due to increased hydrophilic content and the three COEs with negatively-charged moieties may suffer further reduction due to coulombic effects.

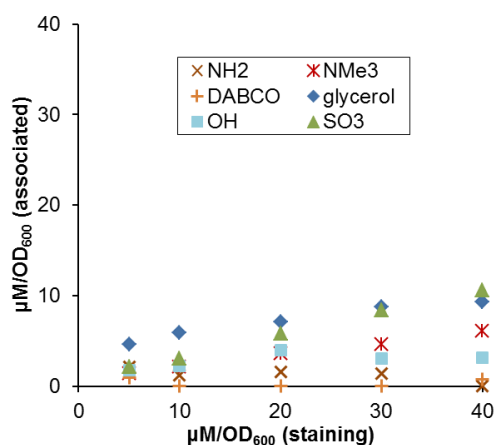


Figure 5-7 Association of “COE2-3C-C3propyl-“ family of COEs with *E. coli* K12.

To determine if reduced affinity for bacteria was responsible for the increased MICs, the association of these six compounds with *E. coli* K12 was measured. As shown in Figure 5-7, all six COEs displayed limited association. For comparison, the associated amounts of COE2-3C-C3butyl and COE2-3C-C3hexyl at a staining concentration of 40 $\mu\text{M}/\text{OD}_{600}$ are ~ 20 and ~ 40 $\mu\text{M}/\text{OD}_{600}$, respectively. Surprisingly, COE2-3C-C3glycerol and COE2-3C-C3propyl-SO₃, the two COEs with the least positive character, showed the greatest affinity for *E. coli* K12. The two compounds with the lowest association, COE2-3C-C3DABCO and COE2-3C-C3propyl-NH₂, both have net charges of +8 at neutral pH. The low affinity of these two COEs was particularly unexpected given that they had higher antimicrobial activity than the other four structures against both *E. coli* K12 and *S. epidermidis*.

Table 5-7 Comparison of antimicrobial activity and cytotoxicity/hemolysis of COE2-3C-C3butyl and COE2-3C-C3propyl-NH₂.

	Gram +		Gram -					mammalian	
	<i>E. faecium</i> 1674620	<i>S. aureus</i> ATCC 33591	<i>K. pneumoniae</i> CDC0010	<i>A. baumannii</i> CDC0290	<i>P. aeruginosa</i> CDC0248	<i>E. cloacae</i> 1744299	<i>E. coli</i> ATCC 25922	Viability at 128 $\mu\text{g}/\text{mL}$ (Hep G2)	Hemolysis at 1024 $\mu\text{g}/\text{mL}$ (CD-1 Mouse RBCs)
COE2-3C-C3butyl	0.25	0.5	16	16	32	4	1	75%	2.7%
COE2-3C-C3propyl-NH ₂	8	8	16	8	16	8	4	103%	0.3%

Although our preliminary MIC tests with the COEs containing terminal chains with multiple functional units did not provide promising results, we decided to test COE2-3C-C3propyl-NH₂ against the ESKAPE panel. Surprisingly, COE2-3C-C3propyl-NH₂

showed reasonable activity against all the strains in the panel, despite having a relatively high MIC against *E. coli* K12 (32 µg/mL). As shown in Table 5-7, COE2-3C-C3propyl-NH₂ has comparable MICs to the close analogue, COE2-3C-C3butyl. Additionally, COE2-3C-C3propyl-NH₂ appears to be less cytotoxic and hemolytic. These promising results have prompted us to investigate COE2-3C-C3propyl-NH₂ further and use this general framework for continuing optimization efforts.

5.5 Conclusions

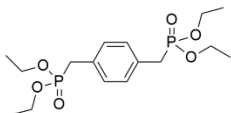
In conclusion, we leveraged our understanding of COE structural parameters on antimicrobial activity to begin investigating COEs as a novel class of antibiotics. The low affinity of short COEs for microbial membranes was overcome by increasing hydrophobic content. Our initial “hit” structure, COE2-2hexyl, showed broad-spectrum activity *in vitro* and was demonstrated to be protective in a murine bacteremia model. While COE2-2hexyl caused no overt signs of toxicity *in vivo* at relevant doses, we observed a high level of cytotoxicity (*in vitro*) which compelled us to design new structures with increased selectivity for microbes. Modulation of the terminal chain composition led to a significant improvement in selectivity (IC₅₀/MIC) from ~2 to >256. It was found that new derivatives with better selectivity retained their broad-spectrum activity against the ESKAPE pathogens. Through these studies we determined that *E. coli* K12 is not an appropriate model organism for screening our compounds and an effort is now being made to identify a better model which can provide predictive antimicrobial activity information for new derivatives. Finally, a

new “lead” framework was developed through the inclusion of heteroatoms in the pendant chains. COE2-3C-C3propyl-NH, in particular, shows promise as a scaffold for future optimization. Specifically, this structure possesses reasonable antimicrobial activity and negligible cytotoxic- or hemolytic- activity. Efforts to develop COEs as a novel class of antibiotics to fight the impending AMR crisis are ongoing.

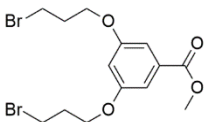
5.6 Synthetic Methods

Phosphonate **P1** was prepared according to literature.³⁹

tetraethyl (1,4-phenylenebis(methylene))bis(phosphonate) (P1)

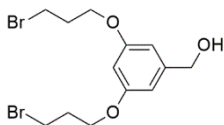


methyl 3,5-bis(3-bromopropoxy)benzoate (5-1)



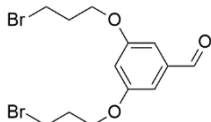
Methyl 3,5-dihydroxybenzoate (3 g, 17.8 mmol), 1,3-dibromopropane (54 g, 268 mmol), potassium carbonate (7.4 g, 53.5 mmol), and acetone (30 mL) were added to a flame-dried 100 mL two-neck flask equipped with a stir bar and reflux condenser. The mixture was maintained at 70°C for two days. After cooling to room temperature, the reaction mixture was partitioned between 200 mL of ethyl acetate and 100 mL of brine. The aqueous layer was removed and extracted with an additional 100 mL of ethyl acetate. The organic layers were combined, washed two additional times with brine, dried over MgSO₄, filtered, and concentrated by under reduced pressure (a significant amount of the excess 1,3-dibromopropane was distilled out of the mixture during concentration). The resulting oil was purified by flash chromatography (hexanes – 1 CV, 1:9 ethyl acetate/hexanes – 1CV, 1:8 ethyl acetate/hexanes – 3 CVs). The product was isolated as a clear oil (5.2 g, 71%).

(3,5-bis(3-bromopropoxy)phenyl)methanol (**5-2**)



To a flame-dried 50 mL round-bottomed flask equipped with a stir bar was added **5-1** (2 g, 4.88 mmol) under inert atmosphere. Anhydrous THF (25 mL) was added via cannula. After cooling the reaction mixture to -78°C , diisobutylaluminum hydride (2.2 mL, 12.2 mmol) was added via syringe. The mixture was allowed to slowly warm to room temperature and left overnight. The solution was cooled to 0°C and quenched by the sequential, slow addition of 50 mL Et_2O , 0.1 mL H_2O , 0.2 mL 2 M NaOH, and 1 mL H_2O . The mixture was again allowed to warm to room temperature and MgSO_4 was slowly added. Stirring was continued for 15 minutes before solids were removed over a pad of celite. Concentration of the filtrate afforded pure **5-2** as a clear oil which was used without further purification.

3,5-bis(3-bromopropoxy)benzaldehyde (**5-3**)



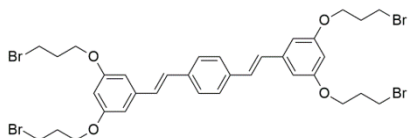
The entire sample of **5-2** (theoretical 4.88 mmol) was transferred to a 50 mL round bottom flask equipped with a stir bar. Manganese(IV) dioxide (6.36 g, 73.2 mmol) and dichloromethane (25 mL) were added. The resulting heterogeneous mixture was heated to 45°C for 8 hours. After cooling to room temperature, the reaction mixture was filtered through a pad of celite and concentrated under reduced pressure to yield the pure product as a clear oil (1.8 g, 97% through two steps).

^1H NMR (500 MHz, Chloroform-*d*) δ 9.90 (s, 1H), 7.02 (d, $J = 2.3$ Hz, 2H), 6.72 (t, $J = 2.3$ Hz, 1H), 4.15 (t, $J = 5.8$ Hz, 4H), 3.60 (t, $J = 6.4$ Hz, 4H), 2.33 (p, $J = 6.1$ Hz,

4H).

^{13}C NMR (126 MHz, cdCl_3) δ 191.76, 160.34, 138.45, 108.05, 107.90, 65.75, 32.13, 29.72.

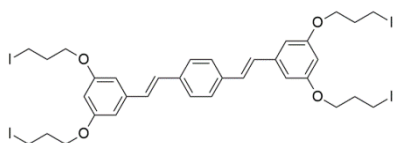
1,4-bis((E)-3,5-bis(3-bromopropoxy)styryl)benzene (**5-4**)



P1 (630 mg, 1.66 mmol) was added to a flame-dried 25 mL two-neck flask equipped with a stir bar under inert atmosphere. Anhydrous THF (1 mL) was added and the solution was cooled to 0°C. In a separate flask, sodium *tert*-butoxide (320 mg, 3.32 mmol) was dissolved in anhydrous THF (10 mL) under inert atmosphere and slowly transferred to the reaction vessel via syringe. The reaction mixture was maintained at 0°C for 15 minutes, at which point **5-3** (1.2 g, 3.16 mmol) was added as a solution in THF (4 mL). The mixture was allowed to warm to room temperature and left for an additional 12 hours under inert atmosphere. Following the complete consumption of **3** (monitored by TLC), the mixture was portioned between dichloromethane and water. The aqueous layer was removed and the organic layer was washed an additional 2 times with water. The organic layer was dried over sodium sulfate, filtered, and concentrated under reduced pressure. Following purification by flash chromatography (1:8 ethyl acetate/hexane – 4 CVs), it was found that a small amount of **3** remained (by NMR). Pure **5-4** was afforded as a slightly greenish-yellow solid (850 mg, 65 %) by recrystallization from 1:1 dichloromethane/hexanes.

^1H NMR (500 MHz, Chloroform-*d*) δ 7.52 (s, 4H), 7.14 – 7.02 (m, 4H), 6.71 (d, J = 2.2 Hz, 4H), 6.43 (t, J = 2.2 Hz, 2H), 4.16 (t, J = 5.8 Hz, 8H), 3.64 (t, J = 6.5 Hz, 8H), 2.36 (p, J = 6.1 Hz, 9H).

1,4-bis((E)-3,5-bis(3-iodopropoxy)styryl)benzene (**5-5**, “**COE2-3I-C3**”)



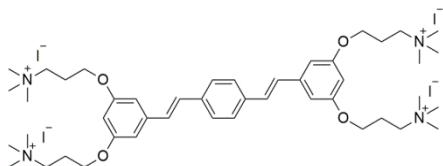
5-4 (700 mg, 0.84 mmol) and sodium iodide (1.9 g, 12.6 mmol) were combined in a 25 mL round bottomed flask equipped with a stir bar and reflux condenser.

Acetone (15 mL) was added and the mixture was refluxed for 2 days. After cooling to room temperature, the reaction was partitioned between DCM and saturated sodium thiosulfate. The aqueous layer was removed and the organic layer was washed 3 times with water. The organic layer was dried over sodium sulfate, filtered, and concentrated under reduced pressure to afford the pure product (830 mg, 97%) as a slightly greenish-yellow solid.

^1H NMR (500 MHz, Chloroform-*d*) δ 7.52 (s, 4H), 7.14 – 7.02 (m, 4H), 6.71 (d, J = 2.3 Hz, 4H), 6.42 (t, J = 2.2 Hz, 2H), 4.09 (t, J = 5.8 Hz, 8H), 3.41 (t, J = 6.7 Hz, 8H), 2.31 (p, J = 6.2 Hz, 8H).

3,3',3'',3'''-((((1E,1'E)-1,4-phenylenebis(ethene-2,1-diyl))bis(benzene-5,3,1-triyl))

tetrakis(oxy))tetrakis(N,N,N-trimethylpropan-1-aminium) iodide (**5-6**, “**COE2-3C-C3**”)



5-5 (30 mg, 0.03 mmol) was added to a 1 Dr vial equipped with a stir bar and a Teflon cap-liner. Anhydrous DMF (0.5 mL) was added and the

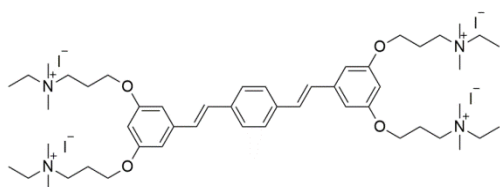
solution was stirred under inert atmosphere until no solids were visible. Trimethylamine (0.44 mmol) was added as a solution in methanol (3.2 M, 0.14 mL) and the mixture was stirred for 2 days at room temperature under inert atmosphere. The crude product was precipitated in diethyl ether, redissolved in methanol, and again precipitated in diethyl ether. The pure product (33 mg, 89%) was afforded following C18 reversed-phase chromatography (methanol/water, gradient from 0% to 50%).

^1H NMR (600 MHz, DMSO- d_6) δ 7.63 (s, 4H), 7.27 (dd, J = 30.9, 15.9 Hz, 4H), 6.85 (s, 4H), 6.48 (s, 2H), 4.11 (t, J = 6.0 Hz, 8H), 3.56 – 3.50 (m, 8H), 3.14 (s, 36H), 2.20 (dq, J = 11.9, 6.0 Hz, 8H).

^{13}C NMR (151 MHz, DMSO- d_6) δ 160.02, 139.75, 136.82, 129.23, 128.72, 127.43, 105.98, 101.56, 65.37, 63.47, 63.45, 63.43, 52.87, 52.84, 52.82, 23.09.

HRMS (ESI): ($[\text{M}-2\text{I}]^{2+}$) calcd: 500.1900, found: 500.1905

3,3',3'',3'''-((((1E,1'E)-1,4-phenylenebis(ethene-2,1-diyl))bis(benzene-5,3,1-triyl))tetrakis(oxy))tetrakis(N-ethyl-N,N-dimethylpropan-1-aminium) iodide
(5-7, "COE2-3C-C3ethyl")



5-5 (30 mg, 0.03 mmol) was added to a 1 Dr vial equipped with a stir bar and a Teflon cap-liner. Anhydrous DMF (0.5 mL) was added and

the solution was stirred under inert atmosphere until no solids were visible. N,N-dimethylethylamine (32 mg, 0.44 mmol) was added and the mixture was stirred for 2 days at 45°C under inert atmosphere. The crude product was precipitated in diethyl

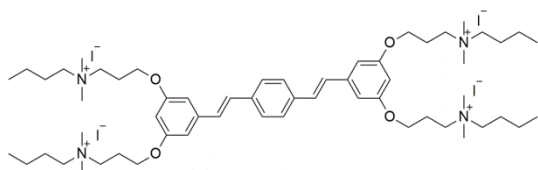
ether, redissolved in methanol, and again precipitated in diethyl ether. The pure product (31 mg, 80%) was afforded following C18 reversed-phase chromatography (methanol/water, gradient from 0% to 50%).

^1H NMR (600 MHz, $\text{DMSO-}d_6$) δ 7.63 (s, 4H), 7.28 (dd, $J = 30.0, 16.4$ Hz, 4H), 6.85 (s, 2H), 6.47 (t, $J = 2.2$ Hz, 1H), 4.12 (t, $J = 6.0$ Hz, 8H), 3.52 – 3.44 (m, 8H), 3.42 (q, $J = 7.2$ Hz, 8H), 3.07 (s, 24H), 2.21 – 2.13 (m, 8H), 1.28 (t, $J = 7.2$ Hz, 13H).

^{13}C NMR (151 MHz, $\text{DMSO-}d_6$) δ 160.01, 139.75, 136.83, 129.22, 128.73, 127.43, 105.98, 101.58, 65.33, 60.38, 59.11, 50.16, 22.68, 8.36.

HRMS (ESI): ($[\text{M}-2\text{I}]^{2+}$) calcd: 528.2213, found: 528.2213

N,N',N'',N'''-((((1E,1'E)-1,4-phenylenebis(ethene-2,1-diyl))bis(benzene-5,3,1-triyl))tetrakis(oxy))tetrakis(propane-3,1-diyl))tetrakis(N,N-dimethylbutan-1-aminium) iodide (**5-8**, “**COE2-3C-C3butyl**”)



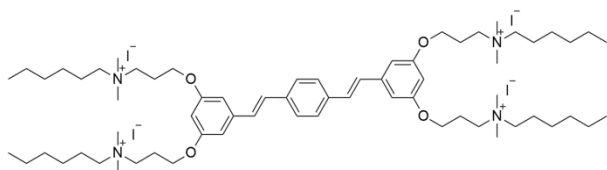
Same procedure as above for **COE2-3C-C3ethyl** with the substitution of N,N-dimethylbutylamine (45 mg, 0.44 mmol). (30 mg, 72%).

^1H NMR (600 MHz, $\text{DMSO-}d_6$) δ 7.63 (s, 4H), 7.27 (dd, $J = 26.7, 16.3$ Hz, 4H), 6.85 (d, $J = 2.3$ Hz, 4H), 6.47 (d, $J = 1.7$ Hz, 4H), 4.11 (t, $J = 6.0$ Hz, 8H), 3.53 – 3.44 (m, 8H), 3.09 (s, 24H), 2.24 – 2.11 (m, 8H), 1.72 – 1.64 (m, 8H), 1.33 (h, $J = 7.4$ Hz, 8H), 0.95 (t, $J = 7.4$ Hz, 12H).

^{13}C NMR (151 MHz, $\text{DMSO-}d_6$) δ 159.98, 139.75, 136.83, 129.22, 128.73, 127.43, 105.98, 101.61, 65.31, 63.34, 60.91, 50.72, 24.19, 22.71, 19.63, 14.05, 13.98.

HRMS (ESI): ([M-2I]2+) calcd: 584.2839, found: 584.2831

N,N',N'',N'''-((((1E,1'E)-1,4-phenylenebis(ethene-2,1-diyl))bis(benzene-5,3,1-triyl))tetrakis(oxy))tetrakis(propane-3,1-diyl)tetrakis(N,N-dimethylhexan-1-aminium) iodide (**5-9**, "COE2-3C-C3hexyl")



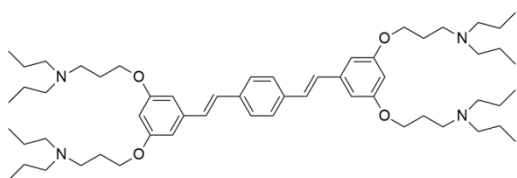
Same procedure as above for **COE2-3C-C3ethyl** with the substitution of N,N-dimethylhexylamine (57 mg, 0.44 mmol). (31 mg, 67%).

¹H NMR (600 MHz, DMSO-*d*₆) δ 7.63 (s, 4H), 7.27 (dd, *J* = 28.2, 16.5 Hz, 4H), 6.85 (d, *J* = 2.1 Hz, 4H), 6.47 (t, *J* = 2.1 Hz, 2H), 4.11 (t, *J* = 5.9 Hz, 8H), 3.51 – 3.45 (m, 8H), 3.09 (s, 24H), 2.22 – 2.13 (m, 8H), 1.73 – 1.64 (m, 8H), 1.32 – 1.27 (m, 24H), 0.88 (t, *J* = 6.7 Hz, 8H).

¹³C NMR (151 MHz, DMSO-*d*₆) δ 159.98, 139.76, 136.82, 129.21, 128.73, 127.41, 105.98, 101.61, 65.29, 63.50, 60.86, 50.72, 31.12, 25.86, 22.70, 22.34, 22.14, 14.29.

HRMS (ESI): ([M-2I]2+) calcd: 640.3465, found: 640.3469

3,3',3'',3'''-((((1E,1'E)-1,4-phenylenebis(ethene-2,1-diyl))bis(benzene-5,3,1-triyl))tetrakis(oxy))tetrakis(N,N-dipropylpropan-1-amine) (**5-10**)



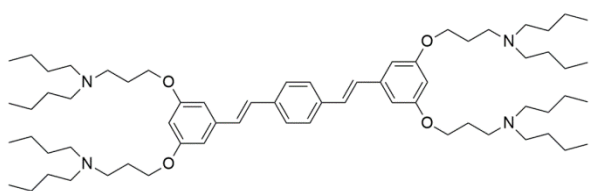
5-5 (60 mg, 0.06 mmol) was added to a 1 Dr vial equipped with a stir bar and a Teflon cap-liner. Anhydrous DMF (0.8 mL) was added and

the solution was stirred under inert atmosphere until no solids were visible. Dipropylamine (120 mg, 1.18 mmol) was added and the mixture was stirred for 2 days at room temperature under inert atmosphere. The crude product was precipitated in diethyl ether (20 mL) and 4 N HCl/dioxane (0.5 mL). The solid was centrifuged and washed once with diethyl ether before dissolving in water. Sodium hydroxide (1 M) was added until pH=12 was reached. The aqueous layer was extracted 5 times with diethyl ether. The combine organic portions were washed with pH=12 water 5 times, dried over sodium sulfate, and concentrated under reduced pressure. The pure product was afforded as a slightly yellowish oil (40 mg, 74%).

¹H NMR (500 MHz, Chloroform-*d*) δ 7.49 (s, 4H), 7.11 – 7.00 (m, 4H), 6.66 (d, *J* = 2.2 Hz, 4H), 6.40 (t, *J* = 2.2 Hz, 2H), 4.04 (t, *J* = 6.4 Hz, 8H), 2.60 (t, *J* = 7.1 Hz, 8H), 2.43 – 2.36 (m, 16H), 1.92 (p, *J* = 6.6 Hz, 8H), 1.52 – 1.41 (m, 16H), 0.88 (t, *J* = 7.3 Hz, 24H).

¹³C NMR (126 MHz, cdcl₃) δ 160.48, 139.15, 136.65, 128.77, 128.53, 126.87, 105.16, 101.07, 66.47, 56.35, 50.69, 27.26, 20.38, 12.00.

N,N',N'',N'''-((((1E,1'E)-1,4-phenylenebis(ethene-2,1-diyl))bis(benzene-5,3,1-triyl))tetrakis(oxy))tetrakis(propane-3,1-diyl))tetrakis(N-butylbutan-1-amine) (**5-11**)



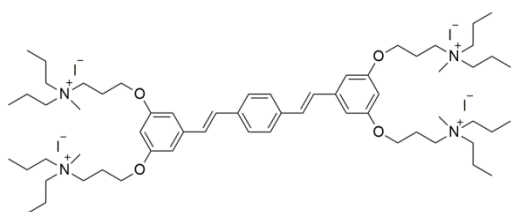
mg, 86%).

Same procedure as above for **5-10** using **COE2-3I-C3** (40 mg, 0.04 mmol) and dibutylamine (102 mg, 0.786 mmol). (35

^1H NMR (500 MHz, DMSO- d_6) δ 7.50 (s, 4H), 7.13 – 7.02 (m, 4H), 6.64 (d, $J = 2.2$ Hz, 4H), 6.31 (t, $J = 2.2$ Hz, 2H), 3.99 (t, $J = 6.2$ Hz, 8H), 2.34 (t, $J = 7.2$ Hz, 16H), 1.80 (p, $J = 6.6$ Hz, 8H), 1.40 – 1.30 (m, 16H), 1.31 – 1.20 (m, 16H), 0.84 (t, $J = 7.3$ Hz, 24H).

^{13}C NMR (126 MHz, cdCl_3) δ 160.47, 139.15, 136.65, 128.77, 128.52, 126.87, 105.18, 101.08, 66.48, 54.05, 50.63, 29.39, 27.21, 20.77, 14.13.

3,3',3'',3'''-((((1E,1'E)-1,4-phenylenebis(ethene-2,1-diyl))bis(benzene-5,3,1-triyl))tetrakis(oxy))tetrakis(N-methyl-N,N-dipropylpropan-1-aminium) iodide
(5-12, "COE2-3C-C3dipropyl")



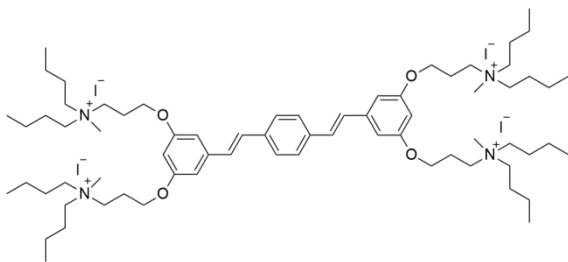
5-10 (16 mg, 0.016 mmol) and methyl iodide (20 mg, 0.14 mmol) were combined in a 1 Dr vial equipped with a stir bar and a Teflon cap-liner. Anhydrous DMF (0.3 mL) was added and

the solution was stirred under inert atmosphere at room temperature for 2 days. The crude product was precipitated in diethyl ether, redissolved in methanol, and again precipitated in diethyl ether. The pure product (20 mg, 77%) was afforded following C18 reversed-phase chromatography (methanol/water, gradient from 0% to 40%).

^1H NMR (500 MHz, DMSO- d_6) δ 7.63 (s, 4H), 7.35 – 7.21 (m, 4H), 6.85 (d, $J = 2.2$ Hz, 4H), 6.46 (t, $J = 2.2$ Hz, 2H), 4.12 (t, $J = 5.9$ Hz, 8H), 3.48 – 3.41 (m, 8H), 3.30 – 3.23 (m, 16H), 3.04 (s, 12H), 2.21 – 2.11 (m, 8H), 1.76 – 1.65 (m, 16H), 0.93 (t, $J = 7.2$ Hz, 24H).

^{13}C NMR (126 MHz, DMSO- d_6) δ 159.99, 139.76, 136.85, 129.22, 128.75, 127.45, 105.99, 101.62, 65.29, 62.69, 58.54, 48.29, 22.39, 15.63, 11.00.

N,N',N'',N'''-((((1E,1'E)-1,4-phenylenebis(ethene-2,1-diyl))bis(benzene-5,3,1-triyl))tetrakis(oxy))tetrakis(propane-3,1-diyl))tetrakis(N-butyl-N-methylbutan-1-aminium) iodide (**5-13**, "COE2-3C-C3dibutyl")



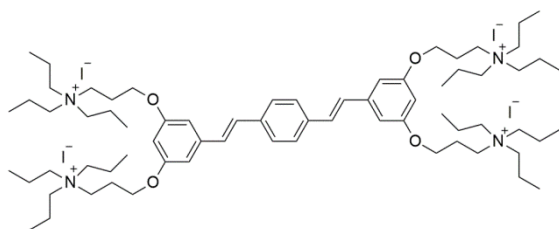
5-11 (30 mg, 0.03 mmol) and methyl iodide (33 mg, 0.23 mmol) were combined in a 1 Dr vial equipped with a stir bar and a Teflon cap-liner. Anhydrous DMF (0.4 mL)

was added and the solution was stirred under inert atmosphere at room temperature for 2 days. The crude product was precipitated in diethyl ether, redissolved in methanol, and again precipitated in diethyl ether. The pure product (24 mg, 53%) was afforded following C18 reversed-phase chromatography (methanol/water, gradient from 0% to 40%).

^1H NMR (500 MHz, DMSO- d_6) δ 7.63 (s, 4H), 7.27 (q, J = 16.3 Hz, 4H), 6.85 (d, J = 2.2 Hz, 4H), 6.46 (t, J = 2.2 Hz, 2H), 4.12 (t, J = 5.9 Hz, 8H), 3.47 – 3.40 (m, 8H), 3.32 – 3.27 (m, 16H), 3.04 (s, 12H), 2.19 – 2.10 (m, 8H), 1.71 – 1.61 (m, 16H), 1.32 (p, J = 7.4 Hz, 16H), 0.95 (t, J = 7.3 Hz, 24H).

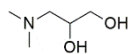
3,3',3'',3'''-((((1E,1'E)-1,4-phenylenebis(ethene-2,1-diyl))bis(benzene-5,3,1-triyl))
tetrakis(oxy))tetrakis(N,N,N-tripropylpropan-1-aminium) iodide

(5-14, "COE2-3C-C3tripropyl")



5-5 (20 mg, 0.02 mmol) was added to a 1 Dr vial equipped with a stir bar and a Teflon cap-liner. Anhydrous DMF (0.4 mL) was added and the solution was stirred under inert atmosphere until no solids were visible. Tripropylamine (28 mg, 0.20 mmol) was added and the mixture was stirred for 2 days at 45°C under inert atmosphere. The crude product was precipitated in diethyl ether, redissolved in methanol, and again precipitated in diethyl ether. The pure product (18 mg, 63%) was afforded following C18 reversed-phase chromatography (methanol/water, gradient from 0% to 50%).

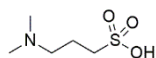
3-dimethylamino-1,2-propanediol (5-15)



To a 50 mL gas-tight flask equipped with a stir bar was added 3-chloro-1,2-propanediol (2 g, 18 mmol) and dimethylamine (27 mL, 2 M in THF, 54 mmol). The flask was sealed and heated to 60°C for 24 hours. After cooling to room temperature, an aqueous solution of sodium hydroxide (720 mg, 18 mmol, 5 mL water) was added slowly while stirring. The solution was transferred to a beaker along with 100 mL diethyl ether and sodium sulfate and stirred for 30 minutes. The solution was filtered and concentrated under reduced pressure to afford the desired product as a slightly yellow liquid (1.4 g, 65%).

^1H NMR (500 MHz, Chloroform-*d*) δ 3.81 – 3.76 (m, 2H), 3.75 (d, J = 3.8 Hz, 1H), 3.72 (d, J = 3.8 Hz, 1H), 3.52 (d, J = 4.6 Hz, 1H), 3.49 (d, J = 4.6 Hz, 1H), 2.56 (d, J = 9.6 Hz, 1H), 2.54 (d, J = 9.6 Hz, 1H), 2.30 (s, 12H), 2.24 (d, J = 3.9 Hz, 1H), 2.21 (d, J = 3.9 Hz, 1H). Note: apx 1:1.1 mixture of enantiomers.

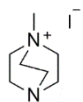
3-(dimethylamino)propane-1-sulfonic acid (**5-16**)



To a 50 mL gas-tight flask equipped with a stir bar was added 1,3-propanesultone (500 mg, 4.1 mmol) and dimethylamine (20 mL, 2 M in THF, 41 mmol). The flask was sealed and the mixture stirred overnight at room temperature. The cloudy solution was transferred to a 50 mL centrifuge tube containing 30 mL anhydrous diethyl ether and the resulting precipitate was collected by centrifugation. After decanting the supernatant, 20 mL of anhydrous diethyl ether was added, the centrifuge tube was sonicated briefly, and the solid was again collected by centrifugation. Residual volatiles were removed under reduced pressure, leaving the desired product as a hygroscopic white solid (650 mg, 95%).

^1H NMR (500 MHz, Deuterium Oxide) δ 3.16 (t, J = 7.6 Hz, 1H), 2.88 (t, J = 7.2 Hz, 1H), 2.78 (s, 1H), 2.05 (p, J = 8.1 Hz, 1H).

1-methyl-1,4-diazabicyclo[2.2.2]octan-1-ium iodide (**5-17**)

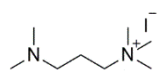


To a 50 mL round bottom flask was added DABCO (493 mg, 4.4 mmol) and dichloromethane (25 mL). The flask was cooled to -78°C under inert atmosphere before slowly adding methyl iodide (0.25 mL, 568 mg, 4 mmol) via syringe. The temperature was maintained at -78°C for 2 hours before slowly allowing

the solution to warm to 0°C. The resulting solid was collected by filtration and washed with ice cold dichloromethane. The solid was collected and dried under reduced pressure to afford the desired product was a hygroscopic white solid (833 mg, 82%)

¹H NMR (400 MHz, Chloroform-*d*) δ 3.26 – 3.19 (m, 6H), 3.06 – 2.99 (m, 6H), 2.88 (s, 3H).

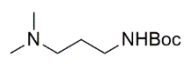
3-(dimethylamino)-*N,N,N*-trimethylpropan-1-aminium iodide (**5-18**)

 To a flame-dried 100 mL round bottom flask equipped with a stir bar was added tetramethylpropane-1,3-diamine (1.5 g, 11.5 mmol) and anhydrous diethyl ether (50 mL) under inert atmosphere. Methyl iodide (0.36 mL, 819 mg, 5.77 mmol) was added dropwise via syringe and the solution was allowed to stir at room temperature for an additional 2 hours. The resulting solid was collected by filtration and washed with ice cold anhydrous diethyl ether. The desired product (1.33 g, 85%, small amount of bis-quaternized byproduct) was obtained as a hygroscopic white solid after drying under reduced pressure.

¹H NMR (500 MHz, Methanol-*d*₄) δ 3.44 – 3.39 (m, 2H), 3.18 (s, 9H), 2.42 (t, *J* = 7.1 Hz, 2H), 2.29 (s, 6H), 2.01 – 1.94 (m, 2H).

¹³C NMR (126 MHz, cd₃od) δ 64.70, 55.39, 52.35, 44.02, 20.53.

tert-butyl (3-(dimethylamino)propyl)carbamate (**5-19**)

 To a 25 mL round bottom flask equipped with a stir bar was added *N,N*-dimethylpropane-1,3-diamine (1.00 g, 9.8 mmol), di-*tert*-butyl

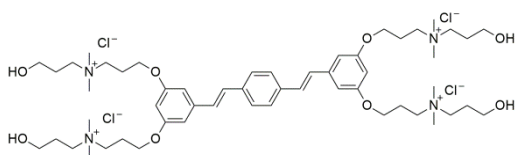
dicarbonate (2.03 g, 9.3 mmol), and dichloromethane (10 mL). The mixture was stirred at room temperature overnight under inert atmosphere. The contents were partitioned between water (pH = 11) and diethyl ether. The organic layer was collected and the aqueous layer was extracted 4 subsequent times with diethyl ether. The combined organic layers were dried over sodium sulfate, filtered, and concentrated under reduced pressure to afford the desired product as a slightly yellow oil (1.7 g, 91%)

$^1\text{H NMR}$ (500 MHz, Methylene Chloride- d_2) δ 3.15 (q, $J = 6.3$ Hz, 2H), 2.31 (t, $J = 6.8$ Hz, 2H), 2.20 (s, 6H), 1.62 (p, $J = 6.6$ Hz, 2H), 1.44 (s, 9H).

General procedure for quaternization:

The following quaternization reactions were all conducted in DMF at 45°C. Approximately 0.03 mmol of **5-5** “**COE2-3I-C3**” and 10 equivalents of the appropriate amine were stirred for 2 days before precipitation the desired product in diethyl ether.

3,3',3'',3'''-(((1E,1'E)-1,4-phenylenebis(ethene-2,1-diyl))bis(benzene-5,3,1-triyl))tetrakis(oxy))tetrakis(N-(3-hydroxypropyl)-N,N-dimethylpropan-1-aminium) chloride (**5-20**, “**COE2-3C-C3propyl-OH**”)

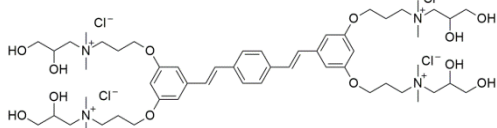


$^1\text{H NMR}$ (600 MHz, DMSO- d_6) δ 7.63 (s, 4H), 7.27 (dd, $J = 28.1, 16.4$ Hz, 4H), 6.85 (d, $J = 2.2$ Hz, 4H), 6.47 (t, $J = 2.2$ Hz, 2H), 4.80 (s,

4H), 4.11 (t, $J = 5.9$ Hz, 8H), 3.54 – 3.47 (m, 1H), 3.44 – 3.38 (m, 8H), 3.10 (s, 24H), 2.18 (m, 8H), 1.91 – 1.83 (m, 8H).

^{13}C NMR (151 MHz, DMSO- d_6) δ 160.02, 139.74, 136.83, 129.22, 128.73, 127.43, 105.97, 101.57, 65.32, 61.71, 60.91, 58.07, 50.85, 25.79, 22.71.

N,N',N'',N'''-((((((1E,1'E)-1,4-phenylenebis(ethene-2,1-diyl))bis(benzene-5,3,1-triyl))tetrakis(oxy))tetrakis(propane-3,1-diyl))tetrakis(2,3-dihydroxy-N,N-dimethylpropan-1-aminium) chloride (**5-21**, “**COE2-3C-C3glycerol**”)

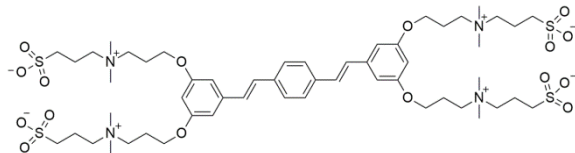


^1H NMR (600 MHz, DMSO- d_6) δ 7.61 (s, 4H), 7.25 (dd, $J = 31.4, 15.2$ Hz, 4H), 6.83 (d, $J = 2.2$ Hz, 4H), 6.44 (t, $J = 2.1$ Hz, 2H), 5.36 (d, $J = 5.1$

Hz, 4H), 4.99 (t, $J = 5.4$ Hz, 4H), 4.07 (qq, $J = 10.6, 5.8$ Hz, 12H), 3.58 (t, $J = 8.3$ Hz, 8H), 3.48 – 3.40 (m, 8H), 3.36 – 3.31 (m, 4H), 3.29 – 3.22 (m, 4H), 3.16 (s, 24H), 2.27 – 2.12 (m, 8H).

^{13}C NMR (151 MHz, DMSO- d_6) δ 160.04, 139.73, 136.83, 129.21, 128.74, 127.42, 105.93, 101.52, 66.65, 66.49, 65.42, 64.18, 62.22, 51.96, 51.91, 22.85.

3,3',3'',3'''-((((((1E,1'E)-1,4-phenylenebis(ethene-2,1-diyl))bis(benzene-5,3,1-triyl))tetrakis(oxy))tetrakis(propane-3,1-diyl))tetrakis(dimethylammonionediyl)) tetrakis(propane-1-sulfonate) (**5-22**, “**COE2-3C-C3propyl-SO3**”)

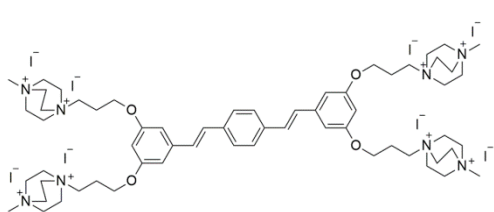


^1H NMR (500 MHz, DMSO- d_6) δ 7.61 (s, 2H), 7.31 (d, $J = 16.3$ Hz, 1H), 7.20 (d, $J = 16.3$ Hz, 1H), 6.83 (d, $J = 2.1$ Hz, 2H),

6.53 (d, $J = 2.0$ Hz, 1H), 4.09 (t, $J = 5.9$ Hz, 4H), 3.48 (dt, $J = 12.4, 6.5$ Hz, 8H), 3.16 (s, 2H), 3.08 (s, 12H), 2.52 (d, $J = 6.9$ Hz, 3H), 2.17 (dt, $J = 11.4, 5.0$ Hz, 4H), 2.08 – 1.98 (m, 4H).

^{13}C NMR (126 MHz, DMSO- d_6) δ 160.04, 139.70, 136.85, 128.71, 127.43, 106.03, 102.68, 65.25, 62.50, 60.60, 50.85, 49.05, 48.13, 22.67, 19.34.

4,4',4'',4'''-((((1E,1'E)-1,4-phenylenebis(ethene-2,1-diyl))bis(benzene-5,3,1-triyl))tetrakis(oxy))tetrakis(propane-3,1-diyl)tetrakis(1-methyl-1,4-diazabicyclo[2.2.2]octane-1,4-dium) iodide (**5-23**, “**COE2-3C-C3DABCO**”)

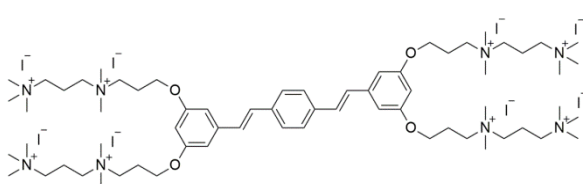


^1H NMR (600 MHz, DMSO- d_6) δ 7.64 (s, 4H), 7.39 – 7.19 (m, 4H), 6.88 (d, $J = 2.2$ Hz, 4H), 6.49 (t, $J = 2.1$ Hz, 2H), 4.15 (t, $J = 5.9$ Hz, 8H), 4.02 – 3.92 (m, 48H), 3.82 – 3.76 (m, 8H), 3.33 (s, 12H), 2.28 – 2.22 (m, 8H).

^{13}C NMR (151 MHz, DMSO- d_6) δ 159.93, 139.78, 136.83, 129.30, 128.68, 127.45, 106.06, 101.64, 65.12, 61.63, 52.90, 51.94, 50.96, 22.38.

HRMS (ESI): ($[\text{M}-3\text{I}]^3+$) calcd: 551.0978, found: 551.0976

N1,N1',N1'',N1'''-((((1E,1'E)-1,4-phenylenebis(ethene-2,1-diyl))bis(benzene-5,3,1-triyl))tetrakis(oxy))tetrakis(propane-3,1-diyl)tetrakis(N1,N1,N3,N3,N3-pentamethylpropane-1,3-diaminium) iodide (**5-24**, “**COE2-3C-C3propyl-NMe3**”)

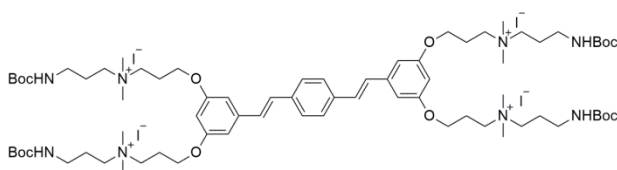


^1H NMR (600 MHz, DMSO- d_6) δ 7.64 (s, 4H), 7.29 (dd, $J = 41.7, 16.3$ Hz, 4H), 6.87 (d, $J = 2.2$ Hz, 4H), 6.51 (s, 2H),

4.15 (t, $J = 6.0$ Hz, 8H), 3.65 – 3.58 (m, 8H), 3.43 – 3.36 (m, 16H), 3.18 (s, 24H), 3.17 (s, 36H), 2.36 – 2.17 (m, 16H).

^{13}C NMR (151 MHz, DMSO- d_6) δ 160.01, 139.76, 136.83, 129.26, 128.67, 127.44, 106.02, 101.64, 65.35, 62.30, 61.57, 60.12, 53.14, 50.98, 22.77, 17.56.

3,3',3'',3'''-((((1E,1'E)-1,4-phenylenebis(ethene-2,1-diyl))bis(benzene-5,3,1-triyl))tetrakis(oxy))tetrakis(N-(3-((tert-butoxycarbonyl)amino)propyl)-N,N-dimethylpropan-1-aminium) iodide (**5-25**)

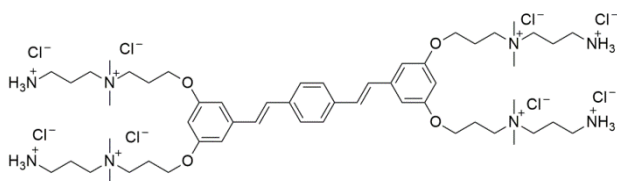


^1H NMR (500 MHz, DMSO- d_6) δ 7.63 (s, 4H), 7.34 – 7.22 (m, 4H), 6.96 (t, $J = 5.8$ Hz, 4H), 6.85 (d, $J = 2.1$ Hz, 4H),

6.47 (t, $J = 2.1$ Hz, 2H), 4.11 (t, $J = 6.0$ Hz, 8H), 3.55 – 3.46 (m, 8H), 3.36 – 3.31 (m, 8H), 3.10 (s, 24H), 3.05 – 2.99 (m, 8H), 2.22 – 2.14 (m, 8H), 1.89 – 1.82 (m, 8H), 1.38 (s, 36H).

^{13}C NMR (126 MHz, DMSO- d_6) δ 159.51, 155.59, 139.23, 136.32, 128.71, 128.24, 126.92, 105.46, 101.08, 77.82, 64.85, 61.20, 60.63, 50.29, 37.03, 30.74, 28.18, 22.65, 22.23.

N1,N1',N1'',N1'''-((((1E,1'E)-1,4-phenylenebis(ethene-2,1-diyl))bis(benzene-5,3,1-triyl))tetrakis(oxy))tetrakis(propane-3,1-diyl))tetrakis(N1,N1-dimethylpropane-1,3-diaminium) chloride (**5-26**, “**COE2-3C-C3propyl-NH2**”)



5-25 (35 mg, 0.02 mmol) and methanol

(2.5 mL) were combined in a 5 mL

round bottom flask equipped with a stir

bar. Hydrogen chloride (~10 mmol) gas was generated in a separate flask by the slow addition of sulfuric acid to sodium chloride and was bubbled through the reaction solution via teflon tubing. The solution was stirred for 3 hours at room temperature before transferring the contents to a 50 mL centrifuge tube containing 15 mL diethyl ether containing 0.1 M HCl. The precipitate was collected via centrifugation and the supernatant was decanted. The solid was redissolved in methanol and again precipitated by the addition of 10 mL diethyl ether containing 0.1 M HCl. The desired product was obtained after removing volatiles under reduced pressure (22 mg, 97%).

^1H NMR (500 MHz, DMSO- d_6) δ 8.65 (s, 12H), 7.62 (s, 4H), 7.39 – 7.12 (m, 4H), 6.85 (s, 4H), 6.51 (s, 2H), 4.11 (s, 8H), 3.69 – 3.43 (m, 16H), 3.13 (s, 24H), 2.95 – 2.81 (m, 8H), 2.28 – 2.05 (m, 16H).

^{13}C NMR (151 MHz, DMSO- d_6) δ 160.02, 139.72, 136.84, 129.26, 128.71, 127.42, 106.08, 101.69, 65.43, 61.58, 60.68, 50.75, 36.44, 22.73, 20.76.

Chapter 6: Additional Experiments and Supporting Information

6.1 Interactions of COEs with Lipopolysaccharide

Our group has demonstrated the ability of COEs to intercalate into microbial membranes and we have leveraged this ability to elicit desirable responses, such as those described in this dissertation. Specifics of COE-membrane interactions remain poorly understood, though. In particular, how LPS effects COE intercalation, and conversely, how COE intercalation affects LPS have not been studied to this point. This interaction may have important consequences in both biotech and medical applications of COEs. For example, LPS, which is also known as “endotoxin” in the medical field, can cause life-threatening immune responses when present in sepsis patients’ blood (these immune responses are responsible for many of the clinical symptoms of sepsis).²⁵²⁻²⁵⁴ In fact, a significant number of deaths of typhoid fever patients in the middle of the 20th century²⁵⁵ were later blamed on increased LPS levels following treatment with chloramphenicol.²⁵⁶ Similar consequences of antibiotic-induced LPS release were subsequently studied using other pathogens such as *E. coli*, *Haemophilus influenzae*, and *Pseudomonas aeruginosa*.²⁵⁷ It is now widely understood that antibiotic treatment can cause LPS release,^{258, 259} regardless of antibiotic class,²⁶⁰ and that this effect has clinical significance in sepsis patients.^{261, 262} In light of our recent effort to develop COEs as antibiotics, it seemed necessary to initiate studies into COE-LPS interactions as well as effects of COE intercalation on retention/release of LPS from living gram-negative bacteria.

Given the high degree of COE structure-property dependencies, three COEs were chosen for determining what effect intercalation has on the quantity of LPS released from *E. coli* K12 – DSBN, DSSN, and COE1-5C (shown in Figure 6-1). Ethylenediaminetetraacetic acid (EDTA) was used as a positive control for induced LPS release. EDTA is known to remove LPS from living cells^{83, 263} by chelating divalent cations (Ca^{2+} or Mg^{2+}) which normally stabilize LPS through ionic cross-linking.²⁶⁴

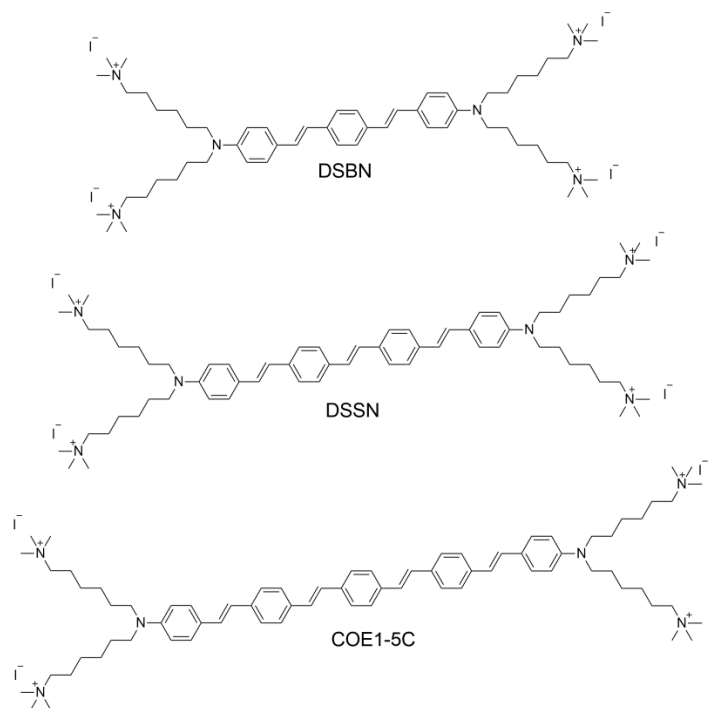


Figure 6-1 Structures of three COEs used to investigate the effects of COE-intercalation on the release of LPS from *E. coli* cells.

E. coli K12 cultures were grown from single colonies on agar plates for 6 hours in LB at 37°C. Cells were centrifuge, the supernatant was discarded, and cells were washed two times with 50 mM PBS before resuspending to $\text{OD}_{600} = 1.0$. Cell solutions were treated for 1 hour with 10 μM COE, 1 mM EDTA, or COE followed by

EDTA (EDTA added 15 minutes after COE). Cells were pelleted and the supernatants were transferred to new microfuge tubes. Supernatant samples were either freeze-dried directly or treated with proteinase K (0.1 mg/mL, 37°C, 1 hour) and then freeze-dried. Samples were dissolved in SDS-PAGE loading buffer at 5x the original concentration (i.e. 1/5 the original volume). Untreated control samples were prepared following the same procedure until the point where they were dissolved in loading buffer. These controls were concentrated 10x (instead of 5x) and then serially diluted in order to create a calibration curve. With the help of Dr. Kota Kaneshige from Dr. Stan Parson's lab (UCSB), 5 uL aliquots of all samples were loaded into wells of commercial SDS-PAGE gels. Components of the samples were separated by gel electrophoresis until the Bromophenol Blue from the loading buffer was approximately $\frac{3}{4}$ of the way down the gel. Bands were visualized using a silver-staining technique²⁶⁵ (stain and developer made in-house). The resulting gels are shown in Figure 6-2.

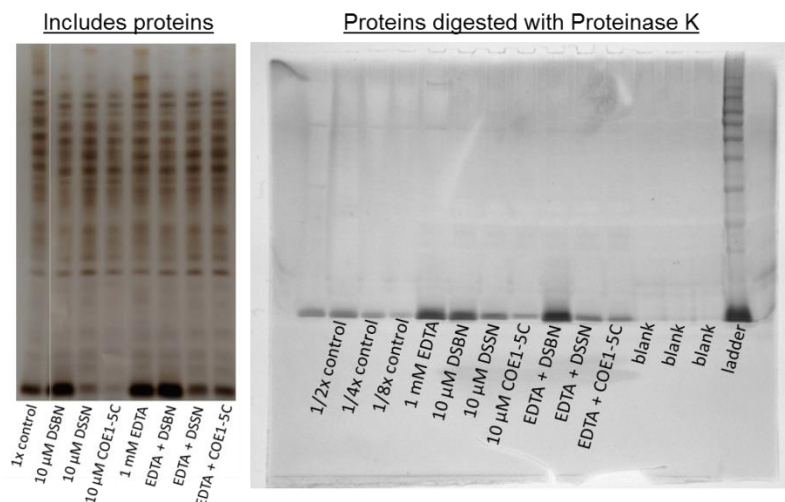


Figure 6-2 SDS-PAGE gels for quantification of LPS in *E. coli* K12 supernatants following treatment with COEs or EDTA – visualized using silver staining.

In both gels above, LPS concentration is indicated by the optical density of the band with the lowest retention (farthest towards the bottom of the images).²⁶⁶ This is confirmed by the fact that all other bands are no longer present in the gel using samples digested with proteinase K. It is clear that, as expected, EDTA caused a significant release of LPS relative to control. DSBN (the shortest of the 3 COEs) also caused LPS release, and the effect of EDTA plus DSBN was additive. The results were surprisingly different for DSSN and COE1-5C, as both COEs actually reduced the amount of LPS released. Furthermore, both DSSN and COE1-5C inhibited the action of EDTA. COE1-5C (the longest of the 3 COEs) was particularly effective at stabilizing LPS against EDTA treatment, with only ~38% release relative to control compared to 145% for EDTA alone. The optical densities for the bands on the gel using proteinase K treated samples are shown in Table 6-1.

Table 6-1 Quantitative comparison of the effects of three COEs and EDTA on the release of LPS from *E. coli* cells. Relative optical density of LPS bands in SDS-PAGE gels.

	Optical density
1/2x control	0.50
1/4x control	0.26
1/8x control	0.12
1 mM EDTA	1.45
10 μ M DSBN	1.24
10 μ M DSSN	0.67
10 μ M COE1-5C	0.27
EDTA + DSBN	1.92
EDTA + DSSN	0.56
EDTA + COE1-5C	0.38

The ability of COEs to either initiate or prevent LPS release is clearly dependent on structure, with the shortest COE causing release and the longer COEs inhibiting release. The observed LPS release caused by DSBN has ramifications for developing short COEs as antibiotics (recall that short COEs were found to have the highest antimicrobial activity in Chapter 2). Further investigation into this effect, as well as the underlying mechanism and subsequent events is warranted. For example, DSBN may cause LPS release by turning on a stress response in the bacteria or forcing LPS remodeling due to membrane “pinching”, both of which are known to promote the release of LPS in the form of outer membrane vesicles.^{267, 268}

The LPS stabilization by the longer COEs is equally profound. This effect may be partly responsible for the observation that COE1-5C was able to reduce the toxicity of butanol during bio-butanol production.²⁶⁹ Butanol is known to destabilize gram-negative outer membranes, in part, through the release of LPS.²⁷⁰ As COE1-5C can inhibit EDTA-mediated LPS removal, it is reasonable to assume that it may also have this effect with butanol. One potential explanation for COE-promoted LPS stabilization is the bridging of LPS molecules by the two terminal ammonium groups of each COE. In effect, the COEs may act as “pseudo-divalent cations” and fill the usual role of Ca^{2+} or Mg^{2+} . This hypothesis, along with the observation that longer COEs promote enhanced LPS-stabilization, was part of the initial inspiration for the design of an even longer COE bearing three pendant chains on either end to enhance protection against butanol toxicity in bioreactors. The resulting structure, COE-S6, was shown to protect bacteria against higher concentrations of butanol

than COE1-5C and this effect was linked, at least partially, to interactions with LPS.⁹⁶

Polymyxin B, a prototypical antimicrobial peptide, is known to cause LPS release²⁶⁰ but has also been shown to neutralize endotoxin,²⁷¹ presumably through aggregate formation.²⁷² When co-administered with LPS, Polymyxin B reduces endotoxin-related clinical markers in animal models.^{273, 274} While Polymyxin B is not a viable therapeutic agent due to high nephrotoxicity, many other compounds have been designed specifically to bind endotoxin and prevent it from eliciting severe immune response (either as therapeutic agents or as treatments for biologically-derived products that may contain endotoxin as an impurity).²⁷⁵⁻²⁷⁸ Given that our COEs, like Polymyxin B, have multiple positive charges, it was hypothesized that they may also be able to form aggregates with LPS. In addition to coulombic interactions, COE-LPS aggregation could be mediated by hydrophobic interactions between the COE core and lipid tails of LPS. As the phenylenevinylene core of our COEs is solvatochromic, such hydrophobic interactions would be expected to result in significant changes in COE photophysical properties.

To investigate the extent to which COEs are able to aggregate with LPS, changes in absorbance and fluorescence of DSSN were measured as a function of LPS concentration. The data shown in Figure 6-3 indicate that the local environment around DSSN becomes less polar in a concentration-dependent manner with the addition of LPS. A slight red-shift (from 412 nm to 424 nm) in absorbance was observed as the LPS/COE ratio was increased from 0 to 10. The effect is more apparent in the fluorescence spectra, where λ_{max} shifted from 594 nm in water to

~530 nm with the addition of 10 equivalents of LPS. Furthermore, the appearance of vibronic peaks is indicative of a nonpolar local environment. Similar spectral changes were observed previously when DSSN intercalated into DMPC liposomes.³⁹ The critical micelle concentration (CMC) from LPS is ~1.4 μM and no further aggregation is expected above this concentration.²⁷⁹ DSSN appears to be able to interact with free LPS (i.e. below its CMC) as well as promote further aggregation above the CMC. Additional experiments are required in order to truly understand COE-LPS interactions but the preliminary data are highly suggestive of COE-induced aggregation.

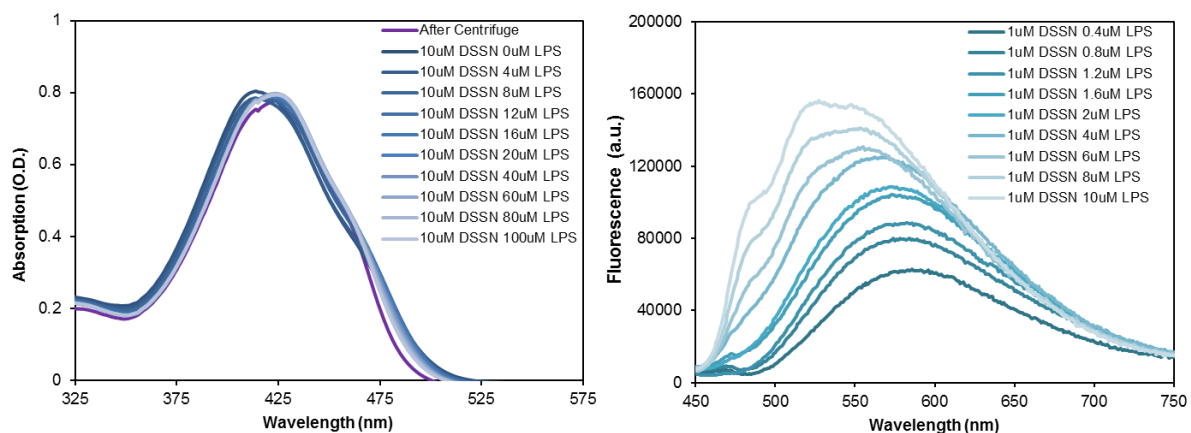


Figure 6-3 Absorbance and emission spectra of DSSN as a function of LPS concentration.

6.2 Effect of COEs on lipid phase transitions and lipid segregation as measured by differential scanning calorimetry

In addition to COE-LPS interactions described in the previous section, better understanding of the physical effects that COEs impart on lipid bilayers would serve to explain previous results and guide future design of novel COE structures. EPR

was used in Chapters 2 and 3 to investigate how COEs impact lipid order. Lipid ordering is highly dependent on temperature with most lipids exhibiting a gel-to-liquid crystal transition.²⁸⁰ The effects that exogenous compounds have on lipid bilayers can be investigated by measuring this transition temperature. Differential scanning calorimetry (DSC) is a routine and straightforward method for probing how T_m changes as a result of addition of other compounds to bilayers. In this case, DSC was used to monitor the T_m of DMPC liposomes as a function of added COE structure and concentration.

DMPC liposomes were prepared by extrusion¹⁰⁵ at 20 mM and stained with either DSBN or DSSN at concentrations from 1-6 mole %. 15 μ L aliquots were transferred to DSC pans and hermetically sealed. DSC scans were collected between 2-40°C at a ramp rate of 1°C/min (Figure 6-4). The main transition in the untreated DMPC liposomes was observed at ~24°C which is consistent with the literature.²⁸¹ Despite the similarity in structure of the two COEs tested, the effects on T_m were vastly different. It bears noting that both DSBN and DSSN are known to associate with DMPC liposomes in excess of 6 mol %, implying that the differences observed in this data cannot be explained by different degrees of association. Similar DSC results have been used to suggest differences in membrane affinity between different COEs²⁸² but it is my opinion that this is not the case and that these results suggest something entirely different and more profound.

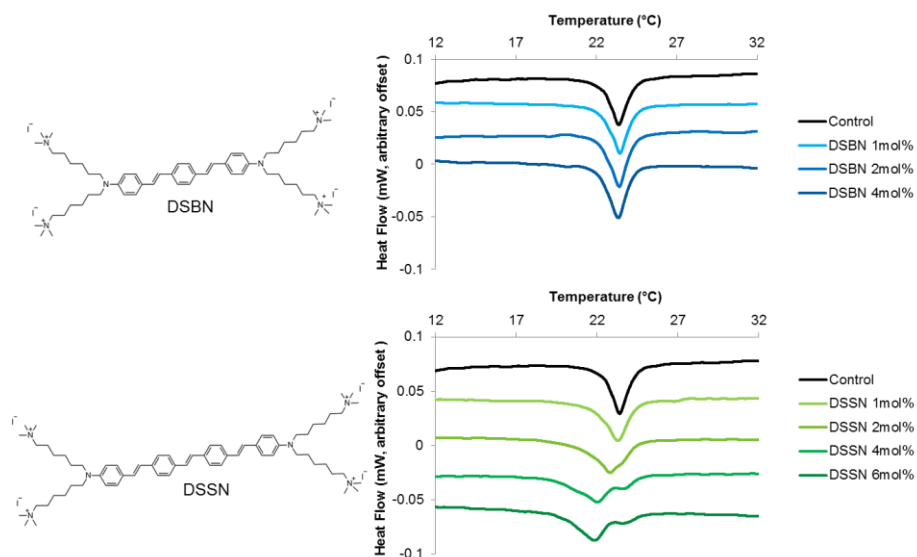


Figure 6-4 DSC traces of the gel-to-liquid transition in DMPC liposomes stained with different concentrations of DSBN and DSSN. No change is observed following the addition of up to 4 mole % DSBN. The addition of DSSN results in the formation of a second transition at a temperature below that of the control main transition.

Addition of DSBN to DMPC liposomes did not result in a significant change in T_m , even at the highest concentration tested (4 mole %). This result was not completely unexpected as COE2-3C-C6, a close structural analogue of DSBN, was found to negligibly impact lipid ordering in Chapter 2. Conversely, large changes in T_m were observed following the addition of DSSN, even at low concentrations. The structural analogue of DSSN, COE2-4C-C6, was shown in Chapter 2 to increase lipid ordering over roughly the same concentration range. At 1 mole %, DSSN slightly reduced T_m but the transition retained the uniform peak shape of the untreated control. When the concentration was increased to 2 mole %, a significant change in peak shape was observed – namely, the splitting of the peak into two components. As the concentration was increased further, the relative area under the lower-temperature transition increased. The position of the higher-temperature transition did not change

between 2-4 mole % and was comparable to that of the transition in the 1 mole % sample.

The observed effects of DSSN are consistent with the formation of COE-rich and COE-poor domains within the bilayer, as previously described for cholesterol.^{283, 284} The same observation was not made for DSBN which suggests that something about the slight difference in structure prevents DSBN from forming these COE-rich domains. One potential explanation is that the smaller conjugated core of DSBN is less prone to self-aggregation, although this theory is not supported by the analysis in the following paragraph. Another possibility is that the slight membrane thinning induced by DSBN precludes the formation of COE-rich domains. In other words, energy in the system may be minimized by distributing DSBN homogeneously rather than forming entire domains of thinned bilayer.

Computational models were previously used to predict COE aggregation following intercalation into bilayers.⁵² While the data presented here do support the notion of COE-rich and COE-poor domains, the characteristics of these domains are not consistent with the computational model. Instead of direct COE-COE interactions, the DSC results indicate that COE-rich domains are still primarily comprised of lipids. This conclusion can be derived from the following rationale: in the 2 mole % sample, the original peak (COE-poor domain) area was reduced by ~50%, indicating that half of the lipids remained in this domain. If all of the DSSN had partitioned into the COE-rich domains, an effective concentration of 4 mol % would have been achieved. Thus, the COE-rich domains in this particular case were comprised of a 1:25 COE:lipid mixtures. One potential explanation for the apparent

saturation at this ratio is coulombic repulsion of the COEs. As DMPC is zwitterionic, it does not provide any screening of the positive charges on DSSN. The results could be, and most likely would be, quite different in the case of anionic lipids. Future studies will employ other liposome systems as well as other COEs. Understanding COE-induced domain formation and lipid segregation may prove useful in explaining membrane permeabilizing and antimicrobial activities of COEs.

6.3 EPR order parameter and correlation time calculations

In chapters 2 and 3, EPR was used to determine the extent to which COEs affect the ordering of lipids. In both chapters, the nitoxide spin label 16-SASL functioned as the probe within large unilamellar vesicles. Experimental protocols can be found at the ends of the chapters but a description of the calculations (in MATLAB R2016b) is provided below per methods described in the literature.¹⁰⁶⁻¹¹⁰

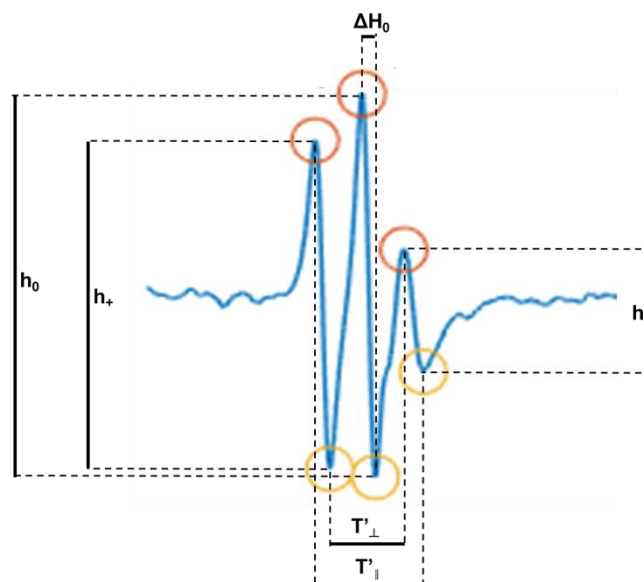


Figure 6-5 Values extracted from EPR spectra to calculate order parameter and effective correlation times.

Figure 6-5 shows an example EPR spectrum of 16-SASL in a DMPC:DMPG liposome system. The way in which the six necessary values are extracted from a spectrum is demonstrated. Order parameter is calculated using the following equations:

$$S = 0.5407 (T'_{\parallel} - T'_{\perp})/a_0 \quad \text{Equation 6-1}$$

$$a_0 = (T'_{\parallel} + 2T'_{\perp})/3 \quad \text{Equation 6-2}$$

where T'_{\parallel} and T'_{\perp} (in gauss) are extracted from EPR spectrum as shown in Figure 6-

5. The effective correlation times are calculated using the equations:

$$\tau_{2B} = 6.51 * 10^{-10} * \Delta H_0 [(h_0/h_-)^{1/2} - (h_0/h_+)^{1/2}]s \quad \text{Equation 6-3}$$

$$\tau_{2C} = 6.51 * 10^{-10} * \Delta H_0 [(h_0/h_-)^{1/2} + (h_0/h_+)^{1/2} - 2]s \quad \text{Equation 6-4}$$

where ΔH_0 (in gauss), h_0 , h_- , h_+ (arbitrary intensity units) are extracted from the spectrum.

To avoid the tedium of extracting values and calculating order parameter and correlation times for many spectra, a MATLAB script was written for batch-processing the data. The entire script is presented below and is followed by some guidance on use.

```

%Import data as *Numeric Matrix* and rename as "DataMatrix"
%note: column 1 = Gauss, column 2 = run #, column 3 = intensity

Max = max(DataMatrix(:,2));
ParsedData = cell(1,Max+1);% Data parsed into individual runs (if sequential runs were collected)
Output = zeros(4,Max+1);% S, Tau2b, Tau2c values in matrix as rows
figure; hold on % Visually inspect that maxima and minima were correctly identified
for i = 0:Max
    Set = ([DataMatrix(DataMatrix(:,2)==i,1),DataMatrix(DataMatrix(:,2)==i,3)]);
    ParsedData{i+1} = Set;
    X = Set(:,1);
    Yrough = Set(:,2);
    Y = tsmovavg(Yrough,'s',20,1); % smoothing function - only use if max/min were not properly identified
    % Adjust the level of smoothing by changing the 3rd input (it is 20 in this case)

    subplot(3,3,[i+1]) % define the # of subplots based on # of scans (3x3 for <9 subplots in this case)
    plot(X,Y); hold on;
    title(['scan ', num2str(i+1)]);

    [pks,locs] = findpeaks(Y,X);
    maxPeaks = horzcat(pks,locs);
    maxPeaksOrder = sortrows(maxPeaks,1);
    pksHighToLow = flipud(maxPeaksOrder);
    pks3High = pksHighToLow(1:3,1:2);
    scatter(pks3High(:,2),pks3High(:,1));
    Yinverse = Y*-1;
    [pksInv,locksInv] = findpeaks(Yinverse,X);
    minPeaks = horzcat(pksInv,locksInv);
    minPeaksOrder = sortrows(minPeaks,1);
    pksMinHighToLow = flipud(minPeaksOrder);
    pksMinHighToLowInv = horzcat(-1*pksMinHighToLow(:,1),pksMinHighToLow(:,2));
    pks3Min = pksMinHighToLowInv(1:3,1:2);
    scatter(pks3Min(:,2),pks3Min(:,1)); hold on
    maxAndMin = vertcat(pks3High,pks3Min);
    maxAndMinOrdered = sortrows(maxAndMin,2);
    spectralWidth = maxAndMinOrdered(5,2)-maxAndMinOrdered(1,2);
    amplitude1 = maxAndMinOrdered(2,1)*-1+maxAndMinOrdered(1,1);
    amplitude2 = maxAndMinOrdered(4,1)*-1+maxAndMinOrdered(3,1);
    amplitude3 = maxAndMinOrdered(6,1)*-1+maxAndMinOrdered(5,1);
    linewidth1 = maxAndMinOrdered(2,2)-maxAndMinOrdered(1,2);
    linewidth2 = maxAndMinOrdered(4,2)-maxAndMinOrdered(3,2);
    linewidth3 = maxAndMinOrdered(6,2)-maxAndMinOrdered(5,2);
    Tpar = (spectralWidth+linewidth3)/2;
    Tper = (spectralWidth-linewidth1)/2;
    a0 = (Tpar+(2*Tper))/3;
    orderParS = 0.5407*(Tpar-Tper)/a0;
    Tau2bSeconds = (6.51*10^(-10))*linewidth2*(((amplitude2/amplitude3)^0.5)-((amplitude2/amplitude1)^0.5));
    Tau2cSeconds = (6.51*10^(-10))*linewidth2*(((amplitude2/amplitude3)^0.5)+((amplitude2/amplitude1)^0.5)-2);
    Tau2b = Tau2bSeconds*10^9;
    Tau2c = Tau2cSeconds*10^9;
    Table = {'Order Parameter S',orderParS;'Tau2b (ns)',Tau2b;'Tau2c (ns)',Tau2c};
    Output(1,i+1) = i+1;
    Output(2,i+1) = orderParS;
    Output(3,i+1) = Tau2b;
    Output(4,i+1) = Tau2c;
end

```

```

...

OutputTransposed = Output.'; %Arrange values in columns

figure % plot of calculated order parameter vs. scan #
subplot(2,1,1)
scatter(OutputTransposed(:,1), OutputTransposed(:,2))
title('Order Parameter')

subplot(2,1,2) % plot of correlation times vs. scan #
scatter(OutputTransposed(:,1), OutputTransposed(:,3)); hold on;
scatter(OutputTransposed(:,1), OutputTransposed(:,4))
title('Correlation Time')

ColumnHeadings = [string('Scan Number');string('Order Parameter S');string('Tau2b (ns)');string('Tau2c (ns)')];
xlswrite('NameYourDataFile.xlsx',OutputTransposed) % write the data to an excel file - don't forget to rename!

```

The input data is arranged with the field strength (in gauss) in the first column, an index for the measurement number in the second column (for time-course experiments such as those presented in Chapter 3), and the measured intensity in the third column. After parsing by the index, the relevant values are extracted from each spectrum (as in Figure 6-5). Figure 6-6 shows an example of the first output plots which can be used to check that maxima and minima were correctly identified. A smoothing function is included (*tsmovavg*) for use in the event that noise in the spectra results in misidentification of peaks. Figure 6-7 shows an example of the output plots for order parameter and correlation time for sequential measurements. The data used to generate these plots is also written to an Excel file.

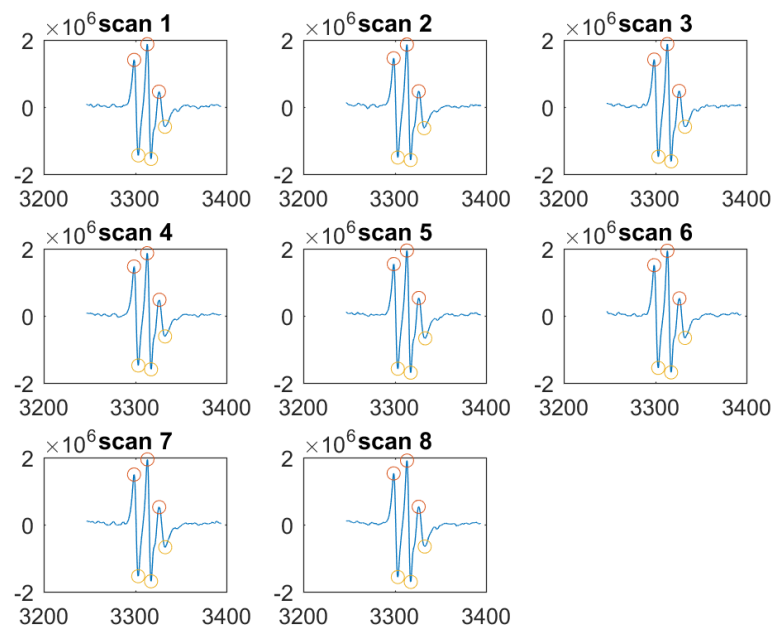


Figure 6-6 Example spectra from time-course EPR measurements with correctly identified maxima (red circles) and minima (yellow circles).

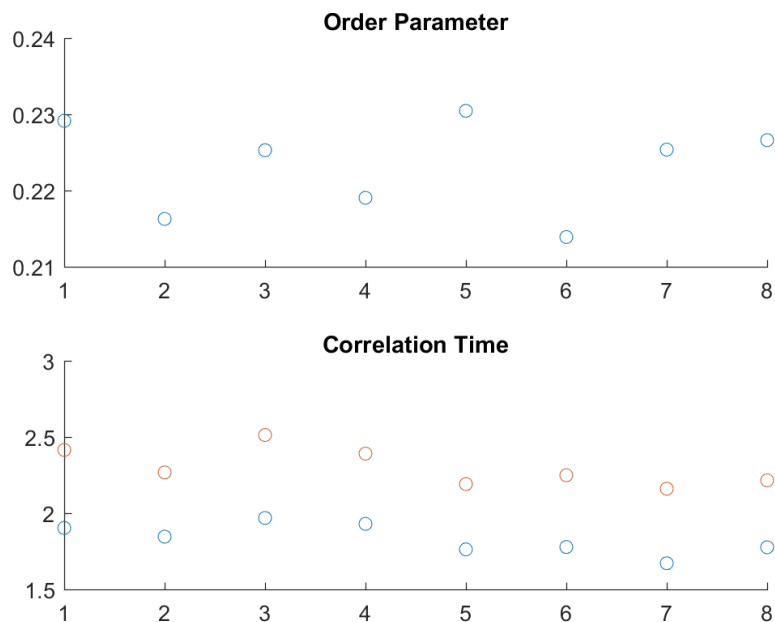


Figure 6-7 Example output of order parameter and correlation time from a time-course EPR experiment.

Summary and outlook

Through the strategic design of membrane-intercalating COEs, we have probed structure-activity relationships and prepared tailor-made COEs for specific effects on synthetic- and natural- membranes. The modular nature of COE chemical structures was leveraged to develop families of related structures or install particular functionalities at key positions. In Chapters 2 and 5, tuning individual structural elements allowed us to gain insights into how each structural module impacts affinity for microbial membranes, membrane permeability, lipid ordering, antimicrobial activity, and cytotoxicity. In Chapter 3, replacing the stilbene central core module of the previously-described COE2-4C with azobenzene yielded DSAzB, a COE with the ability to act as a photo-actuator for on-demand membrane permeabilization. In Chapters 1 and 4, asymmetry was introduced into the modular framework in order to incorporate a single occurrence of particular reactive functionalities. These reactive groups were used to produce COE monolayers for improved biotic-abiotic interfaces and to introduce chemical handles to the surface of cells.

Although certain aspects of COE-membrane interactions have been elucidated, future studies to understand the specifics of these interactions are warranted. For example, it appears that certain COEs are able to cause domain formation within bilayers but little is known about how these domains relate to permeabilization or antimicrobial action. Additionally, there is evidence for COE interactions with LPS (causing or preventing the release from living cells and aggregating in solution) but the implications of these interactions remain largely unexplored. A better

understanding of these phenomena and the COE structural parameters that govern them could guide future rafter design efforts.

Bibliography

1. Lombard, J., Once upon a time the cell membranes: 175 years of cell boundary research. *Biol Direct* **2014**, *9*.
2. Singer, S. J.; Nicolson, G. L., The Fluid Mosaic Model of the Structure of Cell Membranes. *Science* **1972**, *175* (4023), 720-+.
3. Hultgren, S. J.; Abraham, S.; Caparon, M.; Falk, P.; Stgeme, J. W.; Normark, S., Pilus and Nonpilus Bacterial Adhesins - Assembly and Function in Cell Recognition. *Cell* **1993**, *73* (5), 887-901.
4. Mitchell, P., Keilin's respiratory chain concept and its chemiosmotic consequences. *Science* **1979**, *206* (4423), 1148-59.
5. Deamer, D., The Role of Lipid Membranes in Life's Origin. *Life (Basel)* **2017**, *7* (1).
6. Barnett, J. A., A history of research on yeasts 2: Louis Pasteur and his contemporaries, 1850-1880. *Yeast* **2000**, *16* (8), 755-771.
7. Hesseltine, C. W., A Millennium of Fungi, Food, and Fermentation. *Mycologia* **1965**, *57* (2), 149-197.
8. Demain, A. L.; Lancini, G., Bacterial Pharmaceutical Products. *Prokaryotes: A Handbook on the Biology of Bacteria, Vol 1, Third Edition* **2006**, 812-833.
9. Xu, Z. H.; Lee, S. Y., Display of polyhistidine peptides on the Escherichia coli cell surface by using outer membrane protein C as an anchoring motif. *Appl Environ Microb* **1999**, *65* (11), 5142-5147.
10. Sousa, C.; Cebolla, A.; deLorenzo, V., Enhanced metalloadsorption of bacterial cells displaying poly-His peptides. *Nature Biotechnology* **1996**, *14* (8), 1017-1020.
11. Vaara, M., Agents That Increase the Permeability of the Outer-Membrane. *Microbiol Rev* **1992**, *56* (3), 395-411.
12. Wenzel, M.; Chiriac, A. I.; Otto, A.; Zweytick, D.; May, C.; Schumacher, C.; Gust, R.; Albada, H. B.; Penkova, M.; Kramer, U.; Erdmann, R.; Metzler-Nolte, N.; Straus, S. K.; Bremer, E.; Becher, D.; Brotz-Oesterhelt, H.; Sahl, H. G.; Bandow, J. E., Small cationic antimicrobial peptides delocalize peripheral membrane proteins. *P Natl Acad Sci USA* **2014**, *111* (14), E1409-E1418.
13. Fleming, J. T., Electronic Interfacing with Living Cells. *Adv Biochem Eng Biot* **2010**, *117*, 155-178.

14. Logan, B. E., Exoelectrogenic bacteria that power microbial fuel cells. *Nat Rev Microbiol* **2009**, 7 (5), 375-381.
15. Ajo-Franklin, C. M.; Noy, A., Crossing Over: Nanostructures that Move Electrons and Ions across Cellular Membranes. *Advanced Materials* **2015**, 27 (38), 5797-5804.
16. Malvankar, N. S.; Lovley, D. R., Microbial Nanowires: A New Paradigm for Biological Electron Transfer and Bioelectronics. *Chemsuschem* **2012**, 5 (6), 1039-1046.
17. Reguera, G.; McCarthy, K. D.; Mehta, T.; Nicoll, J. S.; Tuominen, M. T.; Lovley, D. R., Extracellular electron transfer via microbial nanowires. *Nature* **2005**, 435 (7045), 1098-1101.
18. Pham, T. H.; Boon, N.; Aelterman, P.; Clauwaert, P.; De Schampelaire, L.; Vanhaecke, L.; De Maeyer, K.; Hofte, M.; Verstraete, W.; Rabaey, K., Metabolites produced by *Pseudomonas* sp enable a Gram-positive bacterium to achieve extracellular electron transfer. *Appl Microbiol Biot* **2008**, 77 (5), 1119-1129.
19. Marsili, E.; Baron, D. B.; Shikhare, I. D.; Coursolle, D.; Gralnick, J. A.; Bond, D. R., *Shewanella* Secretes flavins that mediate extracellular electron transfer. *P Natl Acad Sci USA* **2008**, 105 (10), 3968-3973.
20. Tender, L. M.; Reimers, C. E.; Stecher, H. A.; Holmes, D. E.; Bond, D. R.; Lowy, D. A.; Pilobello, K.; Fertig, S. J.; Lovley, D. R., Harnessing microbially generated power on the seafloor. *Nature Biotechnology* **2002**, 20 (8), 821-825.
21. Reimers, C. E.; Tender, L. M.; Fertig, S.; Wang, W., Harvesting energy from the marine sediment-water interface. *Environ Sci Technol* **2001**, 35 (1), 192-195.
22. Donovan, C.; Dewan, A.; Heo, D.; Beyenal, H., Batteryless, Wireless Sensor Powered by a Sediment Microbial Fuel Cell. *Environ Sci Technol* **2008**, 42 (22), 8591-8596.
23. Shantaram, A.; Beyenal, H.; Raajan, R.; Veluchamy, A.; Lewandowski, Z., Wireless sensors powered by microbial fuel cells. *Environ Sci Technol* **2005**, 39 (13), 5037-5042.
24. Ghai, I.; Ghai, S., Understanding antibiotic resistance via outer membrane permeability. *Infect Drug Resist* **2018**, 11, 523-530.
25. Delcour, A. H., Outer membrane permeability and antibiotic resistance. *Biochim Biophys Acta* **2009**, 1794 (5), 808-16.
26. Seaton, R. A., Daptomycin: rationale and role in the management of skin and soft tissue infections. *J Antimicrob Chemoth* **2008**, 62, 15-23.

27. Zhanel, G. G.; Calic, D.; Schweizer, F.; Zelenitsky, S.; Adam, H.; Lagace-Wiens, P. R. S.; Rubinstein, E.; Gin, A. S.; Hoban, D. J.; Karlowsky, J. A., New Lipoglycopeptides A Comparative Review of Dalbavancin, Oritavancin and Telavancin. *Drugs* **2010**, *70* (7), 859-886.
28. Yeaman, M. R.; Yount, N. Y., Mechanisms of antimicrobial peptide action and resistance. *Pharmacol Rev* **2003**, *55* (1), 27-55.
29. Phoenix, D. A., Dennison, S. R. and Harris, F., Antimicrobial Peptides: Their History, Evolution, and Functional Promiscuity. *Antimicrobial Peptides* **2013**, 1-37.
30. Brogden, K. A., Antimicrobial peptides: Pore formers or metabolic inhibitors in bacteria? *Nat Rev Microbiol* **2005**, *3* (3), 238-250.
31. Zasloff, M., Magainins, a Class of Antimicrobial Peptides from *Xenopus* Skin - Isolation, Characterization of 2 Active Forms, and Partial Cdna Sequence of a Precursor. *P Natl Acad Sci USA* **1987**, *84* (15), 5449-5453.
32. Powers, J. P. S.; Hancock, R. E. W., The relationship between peptide structure and antibacterial activity. *Peptides* **2003**, *24* (11), 1681-1691.
33. Fjell, C. D.; Hiss, J. A.; Hancock, R. E. W.; Schneider, G., Designing antimicrobial peptides: form follows function. *Nat Rev Drug Discov* **2012**, *11* (1), 37-51.
34. Fox, J. L., Antimicrobial peptides stage a comeback. *Nature Biotechnology* **2013**, *31* (5), 379-382.
35. Mahlapuu, M.; Hakansson, J.; Ringstad, L.; Bjorn, C., Antimicrobial Peptides : An Emerging Category of Therapeutic Agents. *Front Cell Infect Mi* **2016**, *6*.
36. Ghosh, C.; Haldar, J., Membrane-Active Small Molecules: Designs Inspired by Antimicrobial Peptides. *Chemmedchem* **2015**, *10* (10), 1606-1624.
37. O'Neill, J., Review on antimicrobial resistance: tackling a crisis for the health and wealth of nations. In *Review on Antimicrobial Resistace.*, London, 2014.
38. Woo, H. Y.; Liu, B.; Kohler, B.; Korystov, D.; Mikhailovsky, A.; Bazan, G. C., Solvent effects on the two-photon absorption of distyrylbenzene chromophores. *J Am Chem Soc* **2005**, *127* (42), 14721-9.
39. Garner, L. E.; Park, J.; Dyar, S. M.; Chworos, A.; Sumner, J. J.; Bazan, G. C., Modification of the Optoelectronic Properties of Membranes via Insertion of Amphiphilic Phenylenevinylene Oligoelectrolytes. *J Am Chem Soc* **2010**, *132* (29), 10042-10052.
40. Garner, L. E.; Thomas, A. W.; Sumner, J. J.; Harvey, S. P.; Bazan, G. C., Conjugated oligoelectrolytes increase current response and organic contaminant

removal in wastewater microbial fuel cells. *Energ Environ Sci* **2012**, 5 (11), 9449-9452.

41. Du, J.; Catania, C.; Bazan, G. C., Modification of Abiotic-Biotic Interfaces with Small Molecules and Nanomaterials for Improved Bioelectronics. *Chem Mater* **2014**, 26 (1), 686-697.
42. Sivakumar, K.; Wang, V. B.; Chen, X. F.; Bazan, G. C.; Kjelleberg, S.; Loo, S. C. J.; Cao, B., Membrane permeabilization underlies the enhancement of extracellular bioactivity in *Shewanella oneidensis* by a membrane-spanning conjugated oligoelectrolyte. *Appl Microbiol Biot* **2014**, 98 (21), 9021-9031.
43. Wang, V. B.; Kirchhofer, N. D.; Chen, X. F.; Tan, M. Y. L.; Sivakumar, K.; Cao, B.; Zhang, Q. C.; Kjelleberg, S.; Bazan, G. C.; Loo, S. C. J.; Marsili, E., Comparison of flavins and a conjugated oligoelectrolyte in stimulating extracellular electron transport from *Shewanella oneidensis* MR-1. *Electrochem Commun* **2014**, 41, 55-58.
44. Hou, H.; Chen, X.; Thomas, A. W.; Catania, C.; Kirchhofer, N. D.; Garner, L. E.; Han, A.; Bazan, G. C., Conjugated oligoelectrolytes increase power generation in *E. coli* microbial fuel cells. *Adv Mater* **2013**, 25 (11), 1593-7.
45. Wang, V. B.; Du, J.; Chen, X. F.; Thomas, A. W.; Kirchhofer, N. D.; Garner, L. E.; Maw, M. T.; Poh, W. H.; Hinks, J.; Wuertz, S.; Kjelleberg, S.; Zhang, Q. C.; Loo, J. S. C.; Bazan, G. C., Improving charge collection in *Escherichia coli*-carbon electrode devices with conjugated oligoelectrolytes. *Phys Chem Chem Phys* **2013**, 15 (16), 5867-5872.
46. Kirchhofer, N. D.; Rengert, Z. D.; Dahlquist, F. W.; Nguyen, T. Q.; Bazan, G. C., A Ferrocene-Based Conjugated Oligoelectrolyte Catalyzes Bacterial Electrode Respiration. *Chem-US* **2017**, 2 (2), 240-257.
47. McCuskey, S. R.; Rengert, Z. D.; Zhang, M. W.; Helgeson, M. E.; Nguyen, T. Q.; Bazan, G. C., Tuning the Potential of Electron Extraction from Microbes with Ferrocene-Containing Conjugated Oligoelectrolytes. *Adv Biosyst* **2019**, 3 (2).
48. Catania, C.; Ajo-Franklin, C. M.; Bazan, G. C., Membrane permeabilization by conjugated oligoelectrolytes accelerates whole-cell catalysis. *Rsc Adv* **2016**, 6 (102), 100300-100306.
49. Wang, B.; Fronk, S. L.; Rengert, Z. D.; Limwongyut, J.; Bazan, G. C., Conjugated Oligoelectrolytes: Materials for Acceleration of Whole Cell Biocatalysis. *Chem Mater* **2018**, 30 (17), 5836-5840.
50. Limwongyut, J.; Liu, Y.; Chilambi, G. S.; Seviour, T.; Hinks, J.; Mu, Y. G.; Bazan, G. C., Interactions of a paracyclophane-based conjugated oligoelectrolyte with biological membranes. *Rsc Adv* **2018**, 8 (70), 39849-39853.

51. Yan, H. J.; Rengert, Z. D.; Thomas, A. W.; Rehermann, C.; Hinks, J.; Bazan, G. C., Influence of molecular structure on the antimicrobial function of phenylenevinylene conjugated oligoelectrolytes. *Chemical Science* **2016**, *7* (9), 5714-5722.
52. Hinks, J.; Wang, Y. F.; Poh, W. H.; Donose, B. C.; Thomas, A. W.; Wuertz, S.; Loo, S. C. J.; Bazan, G. C.; Kjelleberg, S.; Mu, Y. G.; Seviour, T., Modeling Cell Membrane Perturbation by Molecules Designed for Transmembrane Electron Transfer. *Langmuir* **2014**, *30* (9), 2429-2440.
53. Wang, B.; Wang, M.; Mikhailovsky, A.; Wang, S.; Bazan, G. C., A Membrane-Intercalating Conjugated Oligoelectrolyte with High-Efficiency Photodynamic Antimicrobial Activity. *Angew Chem Int Edit* **2017**, *56* (18), 5031-5034.
54. Wang, B.; Feng, G. X.; Seifrid, M.; Wang, M.; Liu, B.; Bazan, G. C., Antibacterial Narrow-Band-Gap Conjugated Oligoelectrolytes with High Photothermal Conversion Efficiency. *Angew Chem Int Edit* **2017**, *56* (50), 16063-16066.
55. Rabaey, K.; Verstraete, W., Microbial fuel cells: novel biotechnology for energy generation. *Trends Biotechnol* **2005**, *23* (6), 291-298.
56. Rabaey, K.; Rozendal, R. A., Microbial electrosynthesis - revisiting the electrical route for microbial production. *Nat Rev Microbiol* **2010**, *8* (10), 706-716.
57. Kim, B. H.; Chang, I. S.; Gil, G. C.; Park, H. S.; Kim, H. J., Novel BOD (biological oxygen demand) sensor using mediator-less microbial fuel cell. *Biotechnol Lett* **2003**, *25* (7), 541-545.
58. Zhang, A. Q.; Lieber, C. M., Nano-Bioelectronics. *Chem Rev* **2016**, *116* (1), 215-257.
59. Birmingham, K.; Gradinaru, V.; Anikeeva, P.; Grill, W. M.; Pikov, V.; McLaughlin, B.; Pasricha, P.; Weber, D.; Ludwig, K.; Famm, K., Bioelectronic medicines: a research roadmap. *Nat Rev Drug Discov* **2014**, *13* (6), 399-400.
60. Grill, W. M.; DeBerry, J. J., Innovative device illuminates the horizon of bioelectronic medicines. *Nat Rev Urol* **2019**, *16* (4), 209-210.
61. Kundu, M.; Krishnan, P.; Kotnala, R. K.; Sumana, G., Recent developments in biosensors to combat agricultural challenges and their future prospects. *Trends Food Sci Tech* **2019**, *88*, 157-178.
62. Zhao, F.; Slade, R. C. T.; Varcoe, J. R., Techniques for the study and development of microbial fuel cells: an electrochemical perspective. *Chem Soc Rev* **2009**, *38* (7), 1926-1939.

63. Yong, Y. C.; Dong, X. C.; Chan-Park, M. B.; Song, H.; Chen, P., Macroporous and Monolithic Anode Based on Polyaniline Hybridized Three-Dimensional Graphene for High-Performance Microbial Fuel Cells. *Acs Nano* **2012**, *6* (3), 2394-2400.
64. Jensen, H. M.; Albers, A. E.; Malley, K. R.; Londer, Y. Y.; Cohen, B. E.; Helms, B. A.; Weigele, P.; Groves, J. T.; Ajo-Franklin, C. M., Engineering of a synthetic electron conduit in living cells. *P Natl Acad Sci USA* **2010**, *107* (45), 19213-19218.
65. Goldbeck, C. P.; Jensen, H. M.; TerAvest, M. A.; Beedle, N.; Appling, Y.; Hepler, M.; Cambray, G.; Mutalik, V.; Angenent, L. T.; Ajo-Franklin, C. M., Tuning Promoter Strengths for Improved Synthesis and Function of Electron Conduits in *Escherichia coli*. *Acs Synth Biol* **2013**, *2* (3), 150-159.
66. Crittenden, S. R.; Sund, C. J.; Sumner, J. J., Mediating electron transfer from bacteria to a gold electrode via a self-assembled monolayer. *Langmuir* **2006**, *22* (23), 9473-9476.
67. Rahimnejad, M.; Najafpour, G. D.; Ghoreyshi, A. A.; Talebnia, F.; Premier, G. C.; Bakeri, G.; Kim, J. R.; Oh, S. E., Thionine increases electricity generation from microbial fuel cell using *Saccharomyces cerevisiae* and exoelectrogenic mixed culture. *J Microbiol* **2012**, *50* (4), 575-580.
68. Tanaka, K.; Tamamushi, R.; Ogawa, T., Bioelectrochemical Fuel-Cells Operated by the Cyanobacterium, *Anabaena-Variabilis*. *J Chem Technol Biot* **1985**, *35* (3), 191-197.
69. Park, D. H.; Kim, S. K.; Shin, I. H.; Jeong, Y. J., Electricity production in biofuel cell using modified graphite electrode with Neutral Red. *Biotechnol Lett* **2000**, *22* (16), 1301-1304.
70. Popov, A. L.; Kim, J. R.; Dinsdale, R. M.; Esteves, S. R.; Guwy, A. J.; Premier, G. C., The effect of physico-chemically immobilized methylene blue and neutral red on the anode of microbial fuel cell. *Biotechnol Bioproc E* **2012**, *17* (2), 361-370.
71. Amir, L.; Carnally, S. A.; Rayo, J.; Rosenne, S.; Yerushalmi, S. M.; Schlesinger, O.; Meijler, M. M.; Alfonta, L., Surface Display of a Redox Enzyme and its Site-Specific Wiring to Gold Electrodes. *Journal of the American Chemical Society* **2013**, *135* (1), 70-73.
72. Du, J.; Thomas, A. W.; Chen, X. F.; Garner, L. E.; Vandenberg, C. A.; Bazan, G. C., Increased ion conductance across mammalian membranes modified with conjugated oligoelectrolytes. *Chem Commun* **2013**, *49* (83), 9624-9626.

73. Yan, H.; Rengert, Z. D.; Thomas, A. W.; Rehermann, C.; Hinks, J.; Bazan, G. C., Influence of molecular structure on the antimicrobial function of phenylenevinylene conjugated oligoelectrolytes. *Chem Sci* **2016**, 7 (9), 5714-5722.
74. Hou, H. J.; Chen, X. F.; Thomas, A. W.; Catania, C.; Kirchhofer, N. D.; Garner, L. E.; Han, A.; Bazan, G. C., Conjugated Oligoelectrolytes Increase Power Generation in E. coli Microbial Fuel Cells. *Advanced Materials* **2013**, 25 (11), 1593-1597.
75. Radhakrishnan, C.; Lo, M. K. F.; Warriar, M. V.; Garcia-Garibay, M. A.; Monbouquette, H. G., Photocatalytic reduction of an azide-terminated self-assembled monolayer using CdS quantum dots. *Langmuir* **2006**, 22 (11), 5018-5024.
76. Walczak, M. M.; Popenoe, D. D.; Deinhammer, R. S.; Lamp, B. D.; Chung, C. K.; Porter, M. D., Reductive Desorption of Alkanethiolate Monolayers at Gold - a Measure of Surface Coverage. *Langmuir* **1991**, 7 (11), 2687-2693.
77. Brett, C. M. A.; Kresak, S.; Hianik, T.; Brett, A. M. O., Studies on self-assembled alkanethiol monolayers formed at applied potential on polycrystalline gold electrodes. *Electroanal* **2003**, 15 (5-6), 557-565.
78. Werner, W. S. M.; Tilinin, I. S., The Escape Probability of Auger and Photoelectrons from Solids. *Appl Surf Sci* **1993**, 70-1, 29-34.
79. Tanuma, S.; Powell, C. J.; Penn, D. R., Calculations of Electron Inelastic Mean Free Paths .5. Data for 14 Organic-Compounds over the 50-2000 Ev Range. *Surf Interface Anal* **1994**, 21 (3), 165-176.
80. Jette, E. R.; Foote, F., Precision Determination of Lattice Constants. *The Journal of Chemical Physics* **1935**, 3 (10), 605-616.
81. Funahara, Y.; Nikaido, H., Asymmetric localization of lipopolysaccharides on the outer membrane of Salmonella typhimurium. *J Bacteriol* **1980**, 141 (3), 1463-5.
82. Kamio, Y.; Nikaido, H., Outer membrane of Salmonella typhimurium: accessibility of phospholipid head groups to phospholipase c and cyanogen bromide activated dextran in the external medium. *Biochemistry* **1976**, 15 (12), 2561-70.
83. Nikaido, H.; Vaara, M., Molecular-Basis of Bacterial Outer-Membrane Permeability. *Microbiol Rev* **1985**, 49 (1), 1-32.
84. Nikaido, H., Molecular basis of bacterial outer membrane permeability revisited. *Microbiol Mol Biol R* **2003**, 67 (4), 593-+.

85. Rajagopal, K.; Singh, P. K.; Kumar, R.; Siddiqui, K. F., CTAB-mediated, single-step preparation of competent *Escherichia coli*, *Bifidobacterium* sp. and *Kluyveromyces lactis* cells. *Meta Gene* **2014**, *2*, 807-18.
86. Liu, J.; Qiao, Y.; Lu, Z. S.; Song, H.; Li, C. M., Enhance electron transfer and performance of microbial fuel cells by perforating the cell membrane. *Electrochem Commun* **2012**, *15* (1), 50-53.
87. Yong, Y. C.; Yu, Y. Y.; Yang, Y.; Liu, J.; Wang, J. Y.; Song, H., Enhancement of extracellular electron transfer and bioelectricity output by synthetic porin. *Biotechnol Bioeng* **2013**, *110* (2), 408-416.
88. Wachtmeister, J.; Rother, D., Recent advances in whole cell biocatalysis techniques bridging from investigative to industrial scale. *Curr Opin Biotechnol* **2016**, *42*, 169-177.
89. Lichtenberg, D.; Ahyayauch, H.; Alonso, A.; Goni, F. M., Detergent solubilization of lipid bilayers: a balance of driving forces. *Trends Biochem Sci* **2013**, *38* (2), 85-93.
90. Lichtenberg, D.; Ahyayauch, H.; Goni, F. M., The mechanism of detergent solubilization of lipid bilayers. *Biophys J* **2013**, *105* (2), 289-99.
91. Kozlov, M. M.; Lichtenberg, D.; Andelman, D., Shape of phospholipid/surfactant mixed micelles: Cylinders or disks? Theoretical analysis. *J Phys Chem B* **1997**, *101* (33), 6600-6606.
92. Elsayed, M. M.; Cevc, G., The vesicle-to-micelle transformation of phospholipid-cholesterol mixed aggregates: a state of the art analysis including membrane curvature effects. *Biochim Biophys Acta* **2011**, *1808* (1), 140-53.
93. Kragh-Hansen, U.; le Maire, M.; Moller, J. V., The mechanism of detergent solubilization of liposomes and protein-containing membranes. *Biophysical Journal* **1998**, *75* (6), 2932-2946.
94. Vanderwerf, M. J.; Hartmans, S.; Vandentweel, W. J. J., Permeabilization and Lysis of *Pseudomonas Pseudoalcaligenes* Cells by Triton X-100 for Efficient Production of D-Malate. *Appl Microbiol Biot* **1995**, *43* (4), 590-594.
95. Tufvesson, P.; Lima-Ramos, J.; Nordblad, M.; Woodley, J. M., Guidelines and Cost Analysis for Catalyst Production in Biocatalytic Processes. *Org Process Res Dev* **2011**, *15* (1), 266-274.
96. Zhou, C.; Chia, G. W. N.; Ho, J. C. S.; Moreland, A. S.; Seviour, T.; Liedberg, B.; Parikh, A. N.; Kjelleberg, S.; Hinks, J.; Bazan, G. C., A Chain-Elongated Oligophenylenevinylene Electrolyte Increases Microbial Membrane Stability. *Adv Mater* **2019**, *31* (18), e1808021.

97. Ortony, J. H.; Chatterjee, T.; Garner, L. E.; Chworos, A.; Mikhailovsky, A.; Kramer, E. J.; Bazan, G. C., Self-assembly of an optically active conjugated oligoelectrolyte. *J Am Chem Soc* **2011**, *133* (21), 8380-7.
98. Hubbell, W. L.; McConnell, H. M., Orientation and motion of amphiphilic spin labels in membranes. *Proc Natl Acad Sci U S A* **1969**, *64* (1), 20-7.
99. Qin, P. Z.; Warncke, K., METHODS IN ENZYMOLOGY Electron Paramagnetic Resonance Investigations of Biological Systems by Using Spin Labels, Spin Probes, and Intrinsic Metal Ions, Part A PREFACE. *Method Enzymol* **2015**, *563*, Xix-XX.
100. Borbat, P. P.; Costa-Filho, A. J.; Earle, K. A.; Moscicki, J. K.; Freed, J. H., Electron spin resonance in studies of membranes and proteins. *Science* **2001**, *291* (5502), 266-9.
101. Roessler, M. M.; Salvadori, E., Principles and applications of EPR spectroscopy in the chemical sciences. *Chem Soc Rev* **2018**, *47* (8), 2534-2553.
102. Rozantzev, E. G.; Neiman, M. B., Organic Radical Reactions Involving No Free Valence. *Tetrahedron* **1964**, *20* (1), 131-&.
103. Waggoner, A. S.; Kingzett, T. J.; Rottschaefer, S.; Griffith, O. H.; Keith, A. D., A Spin-Labeled Lipid for Probing Biological Membranes. *Chem Phys Lipids* **1969**, *3* (3), 245-+.
104. Griffith, O. H.; Waggoner, A. S., Nitroxide Free Radicals - Spin Labels for Probing Biomolecular Structure. *Accounts Chem Res* **1969**, *2* (1), 17-&.
105. Preparing Large, Unilamellar Vesicles by Extrusion (LUVET). <https://avantilipids.com/tech-support/liposome-preparation/luvet> (accessed August 23).
106. Subczynski, W. K.; Markowska, E.; Gruszecki, W. I.; Sielewiesiuk, J., Effects of Polar Carotenoids on Dimyristoylphosphatidylcholine Membranes - a Spin-Label Study. *Biochimica Et Biophysica Acta* **1992**, *1105* (1), 97-108.
107. Berliner, L. J., [18] Spin labeling in enzymology: Spin-labeled enzymes and proteins. In *Methods in Enzymology*, Academic Press: 1978; Vol. 49, pp 418-480.
108. Marsh, D., Electron spin resonance: spin labels. In *Membrane Spectroscopy*, Grell, E., Ed. Springer-Verlag: New York, 1981; pp 51-142.
109. Wisniewska, A.; Wolnicka-Glubisz, A., ESR studies on the effect of cholesterol on chlorpromazine interaction with saturated and unsaturated liposome membranes. *Biophys Chem* **2004**, *111* (1), 43-52.

110. Subczynski, W. K.; Markowska, E.; Sielewiesiuk, J., Spin-Label Studies on Phosphatidylcholine-Polar Carotenoid Membranes - Effects of Alkyl-Chain Length and Unsaturation. *Biochimica Et Biophysica Acta* **1993**, *1150* (2), 173-181.
111. Glover, R. E.; Smith, R. R.; Jones, M. V.; Jackson, S. K.; Rowlands, C. C., An EPR investigation of surfactant action on bacterial membranes. *Fems Microbiol Lett* **1999**, *177* (1), 57-62.
112. Kleinschmidt, J. H.; Mahaney, J. E.; Thomas, D. D.; Marsh, D., Interaction of bee venom melittin with zwitterionic and negatively charged phospholipid bilayers: a spin-label electron spin resonance study. *Biophys J* **1997**, *72* (2 Pt 1), 767-78.
113. Pistolesi, S.; Pogni, R.; Feix, J. B., Membrane insertion and bilayer perturbation by antimicrobial peptide CM15. *Biophys J* **2007**, *93* (5), 1651-60.
114. Kaur, P.; Li, Y.; Cai, J.; Song, L., Selective Membrane Disruption Mechanism of an Antibacterial gamma-AApeptide Defined by EPR Spectroscopy. *Biophys J* **2016**, *110* (8), 1789-1799.
115. Epanand, R. F.; Mowery, B. P.; Lee, S. E.; Stahl, S. S.; Lehrer, R. I.; Gellman, S. H.; Epanand, R. M., Dual mechanism of bacterial lethality for a cationic sequence-random copolymer that mimics host-defense antimicrobial peptides. *J Mol Biol* **2008**, *379* (1), 38-50.
116. Kaur, P.; Satyanarayana, T., Improvement in cell-bound phytase activity of *Pichia anomala* by permeabilization and applicability of permeabilized cells in soymilk dephytinization. *J Appl Microbiol* **2010**, *108* (6), 2041-2049.
117. Li, B.; Wang, L.; Su, L. Q.; Chen, S.; Li, Z. F.; Chen, J.; Wu, J., Glycine and Triton X-100 Enhanced Secretion of Recombinant alpha-CGTase Mediated by OmpA Signal Peptide in *Escherichia coli*. *Biotechnol Bioproc E* **2012**, *17* (6), 1128-1134.
118. Zhao, W. R.; Huang, J.; Peng, C. L.; Hu, S.; Ke, P. Y.; Mei, L. H.; Yao, S. J., Permeabilizing *Escherichia coli* for whole cell biocatalyst with enhanced biotransformation ability from L-glutamate to GABA. *J Mol Catal B-Enzym* **2014**, *107*, 39-46.
119. Trauble, H.; Overath, P., Structure of *Escherichia-Coli* Membranes Studied by Fluorescence Measurements of Lipid Phase-Transitions. *Biochimica Et Biophysica Acta* **1973**, *307* (3), 491-512.
120. Helander, I. M.; Mattila-Sandholm, T., Fluorometric assessment of Gram-negative bacterial permeabilization. *J Appl Microbiol* **2000**, *88* (2), 213-219.
121. Greenspan, P.; Mayer, E. P.; Fowler, S. D., Nile red: a selective fluorescent stain for intracellular lipid droplets. *J Cell Biol* **1985**, *100* (3), 965-73.

122. O'Brien, D. F.; Zumbulyadis, N.; Michaels, F. M.; Ott, R. A., Light-Regulated Permeability of Rhodopsin-Egg Phosphatidylcholine Recombinant Membranes. *P Natl Acad Sci USA* **1977**, *74* (12), 5222-5226.
123. Alvarez-Lorenzo, C.; Bromberg, L.; Concheiro, A., Light-sensitive Intelligent Drug Delivery Systems. *Photochem Photobiol* **2009**, *85* (4), 848-860.
124. Karimi, M.; Zangabad, P. S.; Baghaee-Ravari, S.; Ghazadeh, M.; Mirshekari, H.; Hamblin, M. R., Smart Nanostructures for Cargo Delivery: Uncaging and Activating by Light. *Journal of the American Chemical Society* **2017**, *139* (13), 4584-4610.
125. Zangabad, P. S.; Mirkiani, S.; Shahsavari, S.; Masoudi, B.; Masroor, M.; Hamed, H.; Jafari, Z.; Taghipour, Y. D.; Hashemi, H.; Karimi, M.; Hamblin, M. R., Stimulus-responsive liposomes as smart nanoplatfoms for drug delivery applications. *Nanotechnol Rev* **2018**, *7* (1), 95-122.
126. Shin, D. H.; Koo, M. J.; Kim, J. S.; Kim, J. S., Herceptin-conjugated temperature-sensitive immunoliposomes encapsulating gemcitabine for breast cancer. *Arch Pharm Res* **2016**, *39* (3), 350-358.
127. Kono, K., Thermosensitive polymer-modified liposomes. *Adv Drug Deliver Rev* **2001**, *53* (3), 307-319.
128. Drummond, D. C.; Zignani, M.; Leroux, J. C., Current status of pH-sensitive liposomes in drug delivery. *Prog Lipid Res* **2000**, *39* (5), 409-460.
129. Karanth, H.; Murthy, R. S. R., pH-sensitive liposomes - principle and application in cancer therapy. *J Pharm Pharmacol* **2007**, *59* (4), 469-483.
130. Sirsi, S. R.; Borden, M. A., State-of-the-art materials for ultrasound-triggered drug delivery. *Adv Drug Deliver Rev* **2014**, *72*, 3-14.
131. Hussein, G. A.; Pitt, W. G., Micelles and nanoparticles for ultrasonic drug and gene delivery. *Adv Drug Deliver Rev* **2008**, *60* (10), 1137-1152.
132. Golovin, Y. I.; Gribanovsky, S. L.; Golovin, D. Y.; Klyachko, N. L.; Majouga, A. G.; Master, A. M.; Sokolsky, M.; Kabanov, A. V., Towards nanomedicines of the future: Remote magneto-mechanical actuation of nanomedicines by alternating magnetic fields. *J Control Release* **2015**, *219*, 43-60.
133. Mathiyazhakan, M.; Yang, Y. X.; Liu, Y. B.; Zhu, C. G.; Liu, Q.; Ohl, C. D.; Tam, K. C.; Gao, Y.; Xu, C. J., Non-invasive controlled release from gold nanoparticle integrated photo-responsive liposomes through pulse laser induced microbubble cavitation. *Colloid Surface B* **2015**, *126*, 569-574.

134. Jiang, J. Q.; Qi, B.; Lepage, M.; Zhao, Y., Polymer micelles stabilization on demand through reversible photo-cross-linking. *Macromolecules* **2007**, *40* (4), 790-792.
135. Bao, C. Y.; Zhu, L. Y.; Lin, Q. N.; Tian, H., Building Biomedical Materials using Photochemical Bond Cleavage. *Advanced Materials* **2015**, *27* (10), 1647-1662.
136. Pidgeon, C.; Hunt, C. A., Light Sensitive Liposomes. *Photochem Photobiol* **1983**, *37* (5), 491-494.
137. Ohya, Y.; Okuyama, Y.; Fukunaga, A.; Ouchi, T., Photo-sensitive lipid membrane perturbation by a single chain lipid having terminal spiropyran group. *Supramol Sci* **1998**, *5* (1-2), 21-29.
138. Lei, Y. B.; Hurst, J. K., Photoregulated potassium ion permeation through dihexadecyl phosphate bilayers containing azobenzene and stilbene surfactants. *Langmuir* **1999**, *15* (10), 3424-3429.
139. Kano, K.; Tanaka, Y.; Ogawa, T.; Shimomura, M.; Kunitake, T., Photoresponsive Artificial Membrane - Regulation of Membrane-Permeability of Liposomal Membrane by Photoreversible Cis-Trans Isomerization of Azobenzenes. *Photochem Photobiol* **1981**, *34* (3), 323-329.
140. Bisby, R. H.; Mead, C.; Morgan, C. G., Photosensitive liposomes as 'cages' for laser-triggered solute delivery: the effect of bilayer cholesterol on kinetics of solute release. *Febs Lett* **1999**, *463* (1-2), 165-168.
141. Bisby, R. H.; Mead, C.; Morgan, C. C., Wavelength-programmed solute release from photosensitive liposomes. *Biochem Biophys Res Co* **2000**, *276* (1), 169-173.
142. Morgan, C. G.; Thomas, E. W.; Sandhu, S. S.; Yianni, Y. P.; Mitchell, A. C., Light-Induced Fusion of Liposomes with Release of Trapped Marker Dye Is Sensitized by Photochromic Phospholipid. *Biochimica Et Biophysica Acta* **1987**, *903* (3), 504-509.
143. Liu, X. M.; Yang, B.; Wang, Y. L.; Wang, J. Y., Photoisomerisable cholesterol derivatives as photo-trigger of liposomes: effect of lipid polarity, temperature, incorporation ratio, and cholesterol. *Biochim Biophys Acta* **2005**, *1720* (1-2), 28-34.
144. Shi, S. X.; Yin, T. X.; Tao, X. Y.; Shen, W. G., Light induced micelle to vesicle transition in an aqueous solution of a surface active ionic liquid. *Rsc Adv* **2015**, *5* (92), 75806-75809.

145. Wildes, P. D.; Pacifici, J. G.; Irick, G.; Whitten, D. G., Solvent and Substituent Effects on Thermal Isomerization of Substituted Azobenzenes - Flash Spectroscopic Study. *Journal of the American Chemical Society* **1971**, 93 (8), 2004-&.
146. Kraske, W. V.; Mountcastle, D. B., Effects of cholesterol and temperature on the permeability of dimyristoylphosphatidylcholine bilayers near the chain melting phase transition. *Bba-Biomembranes* **2001**, 1514 (2), 159-164.
147. Hays, L. M.; Crowe, J. H.; Wolkers, W.; Rudenko, S., Factors affecting leakage of trapped solutes from phospholipid vesicles during thermotropic phase transitions. *Cryobiology* **2001**, 42 (2), 88-102.
148. Morgan, C. G.; Bisby, R. H.; Johnson, S. A.; Mitchell, A. C., Fast Solute Release from Photosensitive Liposomes - an Alternative to Caged Reagents for Use in Biological-Systems. *Febs Lett* **1995**, 375 (1-2), 113-116.
149. Boulos, L.; Prevost, M.; Barbeau, B.; Coallier, J.; Desjardins, R., LIVE/DEAD BacLight : application of a new rapid staining method for direct enumeration of viable and total bacteria in drinking water. *J Microbiol Methods* **1999**, 37 (1), 77-86.
150. Sweeney, D. C.; Rebersek, M.; Dermol, J.; Rems, L.; Miklavcic, D.; Davalos, R. V., Quantification of cell membrane permeability induced by monopolar and high-frequency bipolar bursts of electrical pulses. *Biochim Biophys Acta* **2016**, 1858 (11), 2689-2698.
151. Wang, M.; Zhang, Y.; Cai, C.; Tu, J.; Guo, X.; Zhang, D., Sonoporation-induced cell membrane permeabilization and cytoskeleton disassembly at varied acoustic and microbubble-cell parameters. *Sci Rep* **2018**, 8 (1), 3885.
152. Yang, L.; Gordon, V. D.; Trinkle, D. R.; Schmidt, N. W.; Davis, M. A.; DeVries, C.; Som, A.; Cronan, J. E., Jr.; Tew, G. N.; Wong, G. C., Mechanism of a prototypical synthetic membrane-active antimicrobial: Efficient hole-punching via interaction with negative intrinsic curvature lipids. *Proc Natl Acad Sci U S A* **2008**, 105 (52), 20595-600.
153. Matsuzaki, K., Magainins as paradigm for the mode of action of pore forming polypeptides. *Bba-Rev Biomembranes* **1998**, 1376 (3), 391-400.
154. Epanand, R. M.; Rotem, S.; Mor, A.; Berno, B.; Epanand, R. F., Lipid Domains in Bacterial Membranes as a Predictor of Antimicrobial Potency. *Biophysical Journal* **2009**, 96 (3), 450a-450a.
155. Shai, Y., Mode of action of membrane active antimicrobial peptides. *Biopolymers* **2002**, 66 (4), 236-248.

156. Kalia, J.; Raines, R. T., Advances in Bioconjugation. *Curr Org Chem* **2010**, *14* (2), 138-147.
157. Valcourt, D. M.; Harris, J.; Riley, R. S.; Dang, M.; Wang, J. X.; Day, E. S., Advances in targeted nanotherapeutics: From bioconjugation to biomimicry. *Nano Res* **2018**, *11* (10), 4999-5016.
158. Medintz, I. L.; Uyeda, H. T.; Goldman, E. R.; Mattoussi, H., Quantum dot bioconjugates for imaging, labelling and sensing. *Nat Mater* **2005**, *4* (6), 435-446.
159. Spicer, C. D.; Pashuck, E. T.; Stevens, M. M., Achieving Controlled Biomolecule-Biomaterial Conjugation. *Chem Rev* **2018**, *118* (16), 7702-7743.
160. Patterson, D. M.; Nazarova, L. A.; Prescher, J. A., Finding the Right (Bioorthogonal) Chemistry. *Acs Chem Biol* **2014**, *9* (3), 592-605.
161. Bertozzi, C. R., GUEST EDITORIAL A Decade of Bioorthogonal Chemistry. *Accounts Chem Res* **2011**, *44* (9), 651-653.
162. McKay, C. S.; Finn, M. G., Click Chemistry in Complex Mixtures: Bioorthogonal Bioconjugation. *Chem Biol* **2014**, *21* (9), 1075-1101.
163. Mahal, L. K.; Bertozzi, C. R., Engineered cell surfaces: Fertile ground for molecular landscaping. *Chem Biol* **1997**, *4* (6), 415-422.
164. Georgiou, G.; Stathopoulos, C.; Daugherty, P. S.; Nayak, A. R.; Iverson, B. L.; Curtiss, R., 3rd, Display of heterologous proteins on the surface of microorganisms: from the screening of combinatorial libraries to live recombinant vaccines. *Nat Biotechnol* **1997**, *15* (1), 29-34.
165. Daugherty, P. S.; Chen, G.; Olsen, M. J.; Iverson, B. L.; Georgiou, G., Antibody affinity maturation using bacterial surface display. *Protein Eng* **1998**, *11* (9), 825-832.
166. Wu, C. H.; Mulchandani, A.; Chen, W., Versatile microbial surface-display for environmental remediation and biofuels production. *Trends Microbiol* **2008**, *16* (4), 181-188.
167. Fan, S. Q.; Hou, C. T.; Liang, B.; Feng, R. R.; Liu, A. H., Microbial surface displayed enzymes based biofuel cell utilizing degradation products of lignocellulosic biomass for direct electrical energy. *Bioresour Technol* **2015**, *192*, 821-825.
168. Schuurmann, J.; Quehl, P.; Festel, G.; Jose, J., Bacterial whole-cell biocatalysts by surface display of enzymes: toward industrial application. *Appl Microbiol Biot* **2014**, *98* (19), 8031-8046.

169. Jose, J.; Park, M.; Pyun, J. C., E-coli outer membrane with autodisplayed Z-domain as a molecular recognition layer of SPR biosensor. *Biosens Bioelectron* **2010**, *25* (5), 1225-1228.
170. Becker, S.; Michalczyk, A.; Wilhelm, S.; Jaeger, K. E.; Kolmar, H., Ultrahigh-throughput screening to identify E-coli cells expressing functionally active enzymes on their surface. *Chembiochem* **2007**, *8* (8), 943-949.
171. Mahal, L. K.; Yarema, K. J.; Bertozzi, C. R., Engineering chemical reactivity on cell surfaces through oligosaccharide biosynthesis. *Science* **1997**, *276* (5315), 1125-1128.
172. Li, P. Y.; Fan, Z.; Cheng, H., Cell Membrane Bioconjugation and Membrane-Derived Nanomaterials for Immunotherapy. *Bioconjug Chem* **2018**, *29* (3), 624-634.
173. Csizmar, C. M.; Petersburg, J. R.; Wagner, C. R., Programming Cell-Cell Interactions through Non-genetic Membrane Engineering. *Cell Chem Biol* **2018**, *25* (8), 931-940.
174. Dutta, D.; Pulsipher, A.; Luo, W.; Mak, H.; Yousaf, M. N., Engineering Cell Surfaces via Liposome Fusion. *Bioconjugate Chem* **2011**, *22* (12), 2423-2433.
175. Elahipanah, S.; Radmanesh, P.; Luo, W.; O'Brien, P. J.; Rogozhnikov, D.; Yousaf, M. N., Rewiring Gram-Negative Bacteria Cell Surfaces with Bio-Orthogonal Chemistry via Liposome Fusion. *Bioconjugate Chem* **2016**, *27* (4), 1082-1089.
176. Sletten, E. M.; Bertozzi, C. R., Bioorthogonal chemistry: fishing for selectivity in a sea of functionality. *Angew Chem Int Ed Engl* **2009**, *48* (38), 6974-98.
177. Jewett, J. C.; Bertozzi, C. R., Cu-free click cycloaddition reactions in chemical biology. *Chem Soc Rev* **2010**, *39* (4), 1272-9.
178. Huisgen, R., 1,3-Dipolar Cycloadditions. Past and Future. *Angewandte Chemie International Edition in English* **1963**, *2* (10), 565-598.
179. Rostovtsev, V. V.; Green, L. G.; Fokin, V. V.; Sharpless, K. B., A stepwise huisgen cycloaddition process: copper(I)-catalyzed regioselective "ligation" of azides and terminal alkynes. *Angew Chem Int Ed Engl* **2002**, *41* (14), 2596-9.
180. Tornøe, C. W.; Christensen, C.; Meldal, M., Peptidotriazoles on solid phase: [1,2,3]-triazoles by regiospecific copper(i)-catalyzed 1,3-dipolar cycloadditions of terminal alkynes to azides. *J Org Chem* **2002**, *67* (9), 3057-64.
181. Gaetke, L. M.; Chow, C. K., Copper toxicity, oxidative stress, and antioxidant nutrients. *Toxicology* **2003**, *189* (1-2), 147-63.
182. Wittig, G.; Krebs, A., Zur Existenz niedergliedriger Cycloalkine, I. *Chemische Berichte* **1961**, *94* (12), 3260-3275.

183. Agard, N. J.; Prescher, J. A.; Bertozzi, C. R., A strain-promoted [3 + 2] azide-alkyne cycloaddition for covalent modification of biomolecules in living systems. *J Am Chem Soc* **2004**, *126* (46), 15046-7.
184. Besanceney-Webler, C.; Jiang, H.; Zheng, T. Q.; Feng, L.; del Amo, D. S.; Wang, W.; Klivansky, L. M.; Marlow, F. L.; Liu, Y.; Wu, P., Increasing the Efficacy of Bioorthogonal Click Reactions for Bioconjugation: A Comparative Study. *Angew Chem Int Edit* **2011**, *50* (35), 8051-8056.
185. Wang, W.; Hong, S. L.; Tran, A.; Jiang, H.; Triano, R.; Liu, Y.; Chen, X.; Wu, P., Sulfated Ligands for the Copper(I)-Catalyzed Azide-Alkyne Cycloaddition. *Chem-Asian J* **2011**, *6* (10), 2796-2802.
186. Neef, A. B.; Schultz, C., Selective fluorescence labeling of lipids in living cells. *Angew Chem Int Ed Engl* **2009**, *48* (8), 1498-500.
187. del Amo, D. S.; Wang, W.; Jiang, H.; Besanceney, C.; Yan, A. C.; Levy, M.; Liu, Y.; Marlow, F. L.; Wu, P., Biocompatible Copper(I) Catalysts for in Vivo Imaging of Glycans. *Journal of the American Chemical Society* **2010**, *132* (47), 16893-16899.
188. Porath, J.; Carlsson, J.; Olsson, I.; Belfrage, G., Metal Chelate Affinity Chromatography, a New Approach to Protein Fractionation. *Nature* **1975**, *258* (5536), 598-599.
189. Hochuli, E.; Bannwarth, W.; Dobeli, H.; Gentz, R.; Stuber, D., Genetic Approach to Facilitate Purification of Recombinant Proteins with a Novel Metal Chelate Adsorbent. *Bio-Technol* **1988**, *6* (11), 1321-1325.
190. Hochuli, E.; Dobeli, H.; Schacher, A., New Metal Chelate Adsorbent Selective for Proteins and Peptides Containing Neighboring Histidine-Residues. *J Chromatogr* **1987**, *411*, 177-184.
191. Sulkowski, E., Immobilized metal-ion affinity chromatography: imidazole proton pump and chromatographic sequelae. II. Chromatographic sequelae. *J Mol Recognit* **1996**, *9* (5-6), 494-8.
192. Dorn, I. T.; Eschrich, R.; Seemuller, E.; Guckenberger, R.; Tampe, R., High-resolution AFM-imaging and mechanistic analysis of the 20 S proteasome. *J Mol Biol* **1999**, *288* (5), 1027-1036.
193. Schmitt, L.; Dietrich, C.; Tampe, R., Synthesis and Characterization of Chelator-Lipids for Reversible Immobilization of Engineered Proteins at Self-Assembled Lipid Interfaces. *Journal of the American Chemical Society* **1994**, *116* (19), 8485-8491.

194. Dietrich, C.; Schmitt, L.; Tampe, R., Molecular organization of histidine-tagged biomolecules at self-assembled lipid interfaces using a novel class of chelator lipids. *Proc Natl Acad Sci U S A* **1995**, *92* (20), 9014-8.
195. Chikh, G. G.; Li, W. M.; Schutze-Redelmeier, M. P.; Meunier, J. C.; Bally, M. B., Attaching histidine-tagged peptides and proteins to lipid-based carriers through use of metal-ion-chelating lipids. *Bba-Biomembranes* **2002**, *1567* (1-2), 204-212.
196. Benhabbour, S. R.; Luft, J. C.; Kim, D.; Jain, A.; Wadhwa, S.; Parrott, M. C.; Liu, R.; DeSimone, J. M.; Mumper, R. J., In vitro and in vivo assessment of targeting lipid-based nanoparticles to the epidermal growth factor-receptor (EGFR) using a novel Heptameric ZEGFR domain. *J Control Release* **2012**, *158* (1), 63-71.
197. Oh, K. J.; Barbuto, S.; Pitter, K.; Morash, J.; Walensky, L. D.; Korsmeyer, S. J., A membrane-targeted BID BCL-2 homology 3 peptide is sufficient for high potency activation of BAX in vitro. *J Biol Chem* **2006**, *281* (48), 36999-37008.
198. Cho, E. Y.; Ryu, J. Y.; Lee, H. A. R.; Hong, S. H.; Park, H. S.; Hong, K. S.; Park, S. G.; Kim, H. P.; Yoon, T. J., Lecithin nano-liposomal particle as a CRISPR/Cas9 complex delivery system for treating type 2 diabetes. *J Nanobiotechnol* **2019**, *17*.
199. Colletier, J. P.; Chaize, B.; Winterhalter, M.; Fournier, D., Protein encapsulation in liposomes: efficiency depends on interactions between protein and phospholipid bilayer. *BMC Biotechnol* **2002**, *2*, 9.
200. Santafe, A. A. M.; Blum, L. J.; Marquette, C. A.; Girard-Egrot, A. P., Chelating Langmuir-Blodgett Film: A New Versatile Chemiluminescent Sensing Layer for Biosensor Applications. *Langmuir* **2010**, *26* (3), 2160-2166.
201. Lauer, S. A.; Nolan, J. P., Development and characterization of Ni-NTA-bearing microspheres. *Cytometry* **2002**, *48* (3), 136-145.
202. Bazzill, J. D.; Stronsky, S. M.; Kalinyak, L. C.; Ochyl, L. J.; Steffens, J. T.; van Tongeren, S. A.; Cooper, C. L.; Moon, J. J., Vaccine nanoparticles displaying recombinant Ebola virus glycoprotein for induction of potent antibody and polyfunctional T cell responses. *Nanomed-Nanotechnol* **2019**, *18*, 414-425.
203. Bilek, G.; Matscheko, N. M.; Pickl-Herk, A.; Weiss, V. U.; Subirats, X.; Kenndler, E.; Blaas, D., Liposomal Nanocontainers as Models for Viral Infection: Monitoring Viral Genomic RNA Transfer through Lipid Membranes. *J Virol* **2011**, *85* (16), 8368-8375.
204. Kuruvilla, S. P.; Tiruchinapally, G.; Kaushal, N.; ElSayed, M. E. H., Effect of N-acetylgalactosamine ligand valency on targeting dendrimers to hepatic cancer cells. *Int J Pharm* **2018**, *545* (1-2), 27-36.

205. Li, C.; Wu, G.; Ma, R. J.; Liu, Y.; Liu, Y.; Lv, J.; An, Y. L.; Shi, L. Q., Nitriolotriacetic Acid (NTA) and Phenylboronic Acid (PBA) Functionalized Nanogels for Efficient Encapsulation and Controlled Release of Insulin. *Acs Biomater Sci Eng* **2018**, *4* (6), 2007-2017.
206. Lin, Y. C.; Liang, M. R.; Lin, Y. C.; Chen, C. T., Specifically and Reversibly Immobilizing Proteins/Enzymes to Nitriolotriacetic-Acid-Modified Mesoporous Silicas through Histidine Tags for Purification or Catalysis. *Chem-Eur J* **2011**, *17* (46), 13059-13067.
207. Dong, H.; Sarkes, D. A.; Rice, J. J.; Hurley, M. M.; Fu, A. J.; Stratis-Cullum, D. N., Living Bacteria-Nanoparticle Hybrids Mediated through Surface-Displayed Peptides. *Langmuir* **2018**, *34* (20), 5837-5848.
208. Rice, J. J.; Schohn, A.; Bessette, P. H.; Boulware, K. T.; Daugherty, P. S., Bacterial display using circularly permuted outer membrane protein OmpX yields high affinity peptide ligands. *Protein Sci* **2006**, *15* (4), 825-36.
209. Rice, J. J.; Daugherty, P. S., Directed evolution of a biterminal bacterial display scaffold enhances the display of diverse peptides. *Protein Eng Des Sel* **2008**, *21* (7), 435-42.
210. Attack of the superbugs: July 2041 - What if antibiotics stop working? The Economist: Geneva and New York, 2019.
211. Antibiotic Resistance Threats in the United States 2019, Centers for Disease Control and Prevention. <https://www.cdc.gov/drugresistance/biggest-threats.html>.
212. Walsh, C., Where will new antibiotics come from? *Nat Rev Microbiol* **2003**, *1* (1), 65-70.
213. Gould, K., Antibiotics: from prehistory to the present day. *J Antimicrob Chemoth* **2016**, *71* (3), 572-575.
214. Aminov, R. I., A brief history of the antibiotic era: lessons learned and challenges for the future. *Front Microbiol* **2010**, *1*.
215. Payne, D. J.; Gwynn, M. N.; Holmes, D. J.; Pompliano, D. L., Drugs for bad bugs: confronting the challenges of antibacterial discovery. *Nat Rev Drug Discov* **2007**, *6* (1), 29-40.
216. Tommasi, R.; Brown, D. G.; Walkup, G. K.; Manchester, J. I.; Miller, A. A., ESKAPEing the labyrinth of antibacterial discovery. *Nat Rev Drug Discov* **2015**, *14* (8), 529-542.
217. Barrett, J. F., Can biotech deliver new antibiotics? *Current Opinion in Microbiology* **2005**, *8* (5), 498-503.

218. Ainsworth, G. C.; Brown, A. M.; Brownlee, G., Aerosporin, an Antibiotic Produced by *Bacillus-Aerosporus Greer*. *Nature* **1947**, *160* (4060), 263-263.
219. Koyama, Y., A new antibiotic 'colistin' produced by spore-forming soil bacteria. *J. Antibiot.* **1950**, *3*, 457-458.
220. Kang, H. K.; Kim, C.; Seo, C. H.; Park, Y., The therapeutic applications of antimicrobial peptides (AMPs): a patent review. *J Microbiol* **2017**, *55* (1), 1-12.
221. Dubos, R. J., Studies on a Bactericidal Agent Extracted from a Soil Bacillus : li. Protective Effect of the Bactericidal Agent against Experimental Pneumococcus Infections in Mice. *J Exp Med* **1939**, *70* (1), 11-7.
222. Dubos, R. J., Studies on a Bactericidal Agent Extracted from a Soil Bacillus : I. Preparation of the Agent. Its Activity in Vitro. *J Exp Med* **1939**, *70* (1), 1-10.
223. Butler, M. S.; Blaskovich, M. A.; Cooper, M. A., Antibiotics in the clinical pipeline in 2013. *J Antibiot* **2013**, *66* (10), 571-591.
224. Butler, M. S.; Blaskovich, M. A. T.; Cooper, M. A., Antibiotics in the clinical pipeline at the end of 2015. *J Antibiot* **2017**, *70* (1), 3-24.
225. Hurdle, J. G.; O'Neill, A. J.; Chopra, I.; Lee, R. E., Targeting bacterial membrane function: an underexploited mechanism for treating persistent infections. *Nat Rev Microbiol* **2011**, *9* (1), 62-75.
226. Zhang, Y. M.; Rock, C. O., Membrane lipid homeostasis in bacteria. *Nat Rev Microbiol* **2008**, *6* (3), 222-233.
227. Bechinger, B.; Gorr, S. U., Antimicrobial Peptides: Mechanisms of Action and Resistance. *J Dent Res* **2017**, *96* (3), 254-260.
228. Pfalzgraff, A.; Brandenburg, K.; Weindl, G., Antimicrobial Peptides and Their Therapeutic Potential for Bacterial Skin Infections and Wounds. *Front Pharmacol* **2018**, *9*.
229. Jenssen, H.; Hamill, P.; Hancock, R. E. W., Peptide antimicrobial agents. *Clinical Microbiology Reviews* **2006**, *19* (3), 491-+.
230. Aoki, W.; Ueda, M., Characterization of Antimicrobial Peptides toward the Development of Novel Antibiotics. *Pharmaceuticals (Basel)* **2013**, *6* (8), 1055-81.
231. Toke, O., Antimicrobial peptides: New candidates in the fight against bacterial infections. *Biopolymers* **2005**, *80* (6), 717-735.
232. Epand, R. M.; Vogel, H. J., Diversity of antimicrobial peptides and their mechanisms of action. *Bba-Biomembranes* **1999**, *1462* (1-2), 11-28.

233. Hancock, R. E.; Chapple, D. S., Peptide antibiotics. *Antimicrob Agents Chemother* **1999**, *43* (6), 1317-23.
234. Tew, G. N.; Liu, D. H.; Chen, B.; Doerksen, R. J.; Kaplan, J.; Carroll, P. J.; Klein, M. L.; DeGrado, W. F., De novo design of biomimetic antimicrobial polymers. *P Natl Acad Sci USA* **2002**, *99* (8), 5110-5114.
235. Liu, D. H.; Doerksen, R. J.; Chen, B.; Clements, D.; Klein, M. L.; DeGrado, W. F., De novo design and synthesis of non-hemolytic biomimetic antimicrobial polymers. *Abstr Pap Am Chem S* **2003**, *225*, U184-U184.
236. Choi, S.; Isaacs, A.; Clements, D.; Liu, D. H.; Kim, H.; Scott, R. W.; Winkler, J. D.; DeGrado, W. F., De novo design and in vivo activity of conformationally restrained antimicrobial arylamide foldamers. *P Natl Acad Sci USA* **2009**, *106* (17), 6968-6973.
237. Tang, H.; Doerksen, R. J.; Jones, T. V.; Klein, M. L.; Tew, G. N., Biomimetic facially amphiphilic antibacterial oligomers with conformationally stiff backbones. *Chem Biol* **2006**, *13* (4), 427-435.
238. Tang, H. Z.; Doerksen, R. J.; Tew, G. N., Synthesis of urea oligomers and their antibacterial activity. *Chem Commun* **2005**, (12), 1537-1539.
239. Arnt, L.; Nusslein, K.; Tew, G. N., Nonhemolytic abiogenic polymers as antimicrobial peptide mimics. *J Polym Sci Pol Chem* **2004**, *42* (15), 3860-3864.
240. Ishitsuka, Y.; Arnt, L.; Majewski, J.; Frey, S.; Ratajczek, M.; Kjaer, K.; Tew, G. N.; Lee, K. Y. C., Amphiphilic poly(phenyleneethynylene)s can mimic antimicrobial peptide membrane disordering effect by membrane insertion. *Journal of the American Chemical Society* **2006**, *128* (40), 13123-13129.
241. Li, C. H.; Lewis, M. R.; Gilbert, A. B.; Noel, M. D.; Scoville, D. H.; Allman, G. W.; Savage, P. B., Antimicrobial activities of amine- and guanidine-functionalized cholic acid derivatives. *Antimicrob Agents Ch* **1999**, *43* (6), 1347-1349.
242. Thaker, H. D.; Som, A.; Ayaz, F.; Lui, D. H.; Pan, W. X.; Scott, R. W.; Anguita, J.; Tew, G. N., Synthetic Mimics of Antimicrobial Peptides with Immunomodulatory Responses. *Journal of the American Chemical Society* **2012**, *134* (27), 11088-11091.
243. Thaker, H. D.; Sgolastra, F.; Clements, D.; Scott, R. W.; Tew, G. N., Synthetic Mimics of Antimicrobial Peptides from Triaryl Scaffolds. *J Med Chem* **2011**, *54* (7), 2241-2254.
244. Thaker, H. D.; Cankaya, A.; Scott, R. W.; Tew, G. N., Role of Amphiphilicity in the Design of Synthetic Mimics of Antimicrobial Peptides with Gram-Negative Activity. *Acs Med Chem Lett* **2013**, *4* (5), 481-485.

245. Fu, T. H.; Li, Y.; Thaker, H. D.; Scott, R. W.; Tew, G. N., Expedient Synthesis of SMAMPs via Click Chemistry. *Acs Med Chem Lett* **2013**, 4 (9), 841-845.
246. Epand, R. M.; Epand, R. F., Lipid domains in bacterial membranes and the action of antimicrobial agents. *Biochim Biophys Acta* **2009**, 1788 (1), 289-94.
247. Mileykovskaya, E.; Sun, Q.; Margolin, W.; Dowhan, W., Localization and function of early cell division proteins in filamentous Escherichia coli cells lacking phosphatidylethanolamine. *J Bacteriol* **1998**, 180 (16), 4252-7.
248. Rice, L. B., Federal funding for the study of antimicrobial resistance in nosocomial pathogens: No ESKAPE. *Journal of Infectious Diseases* **2008**, 197 (8), 1079-1081.
249. World Health Organization *WHO publishes list of bacteria for which new antibiotics are urgently needed*; 2017.
250. Tacconelli, E.; Carrara, E.; Savoldi, A.; Harbarth, S.; Mendelson, M.; Monnet, D. L.; Pulcini, C.; Kahlmeter, G.; Kluytmans, J.; Carmeli, Y.; Ouellette, M.; Outtersson, K.; Patel, J.; Cavalieri, M.; Cox, E. M.; Houchens, C. R.; Grayson, M. L.; Hansen, P.; Singh, N.; Theuretzbacher, U.; Magrini, N.; Group, W. H. O. P. P. L. W., Discovery, research, and development of new antibiotics: the WHO priority list of antibiotic-resistant bacteria and tuberculosis. *Lancet Infect Dis* **2018**, 18 (3), 318-327.
251. Thomas, A. W.; Catania, C.; Garner, L. E.; Bazan, G. C., Pendant ionic groups of conjugated oligoelectrolytes govern their ability to intercalate into microbial membranes. *Chem Commun* **2015**, 51 (45), 9294-9297.
252. Bone, R. C., The pathogenesis of sepsis. *Ann Intern Med* **1991**, 115 (6), 457-69.
253. Michie, H. R.; Manogue, K. R.; Spriggs, D. R.; Revhaug, A.; O'Dwyer, S.; Dinarello, C. A.; Cerami, A.; Wolff, S. M.; Wilmore, D. W., Detection of circulating tumor necrosis factor after endotoxin administration. *N Engl J Med* **1988**, 318 (23), 1481-6.
254. Suffredini, A. F.; Fromm, R. E.; Parker, M. M.; Brenner, M.; Kovacs, J. A.; Wesley, R. A.; Parrillo, J. E., The cardiovascular response of normal humans to the administration of endotoxin. *N Engl J Med* **1989**, 321 (5), 280-7.
255. Reilly J Fau - Compagnon, A.; Compagnon A Fau - Tournier, P.; Tournier P Fau - Bastin, R.; Bastin R Fau - Du Buit, H.; Du Buit, H., [Accidents in the treatment of typhoid fever with chloromycetin; experimental study and therapeutic deductions]. (0366-1334 (Print)).

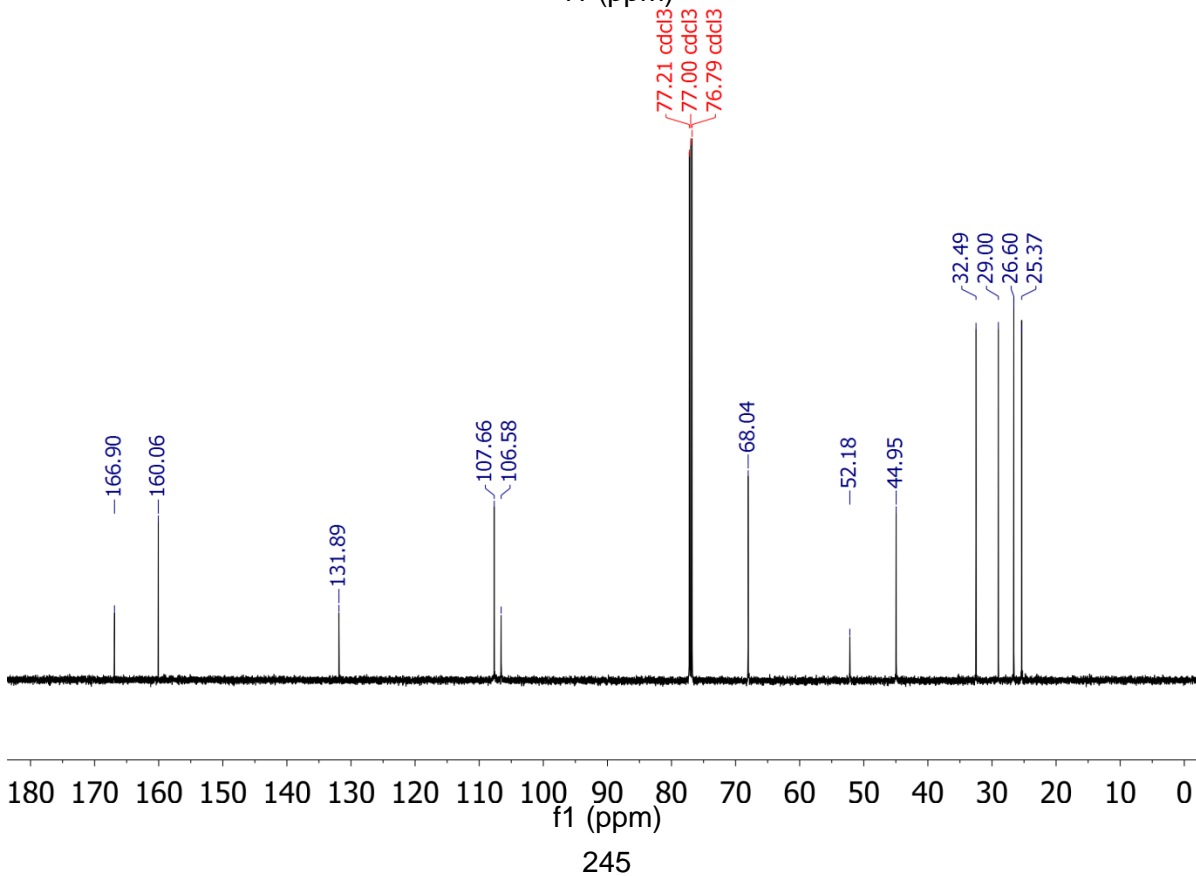
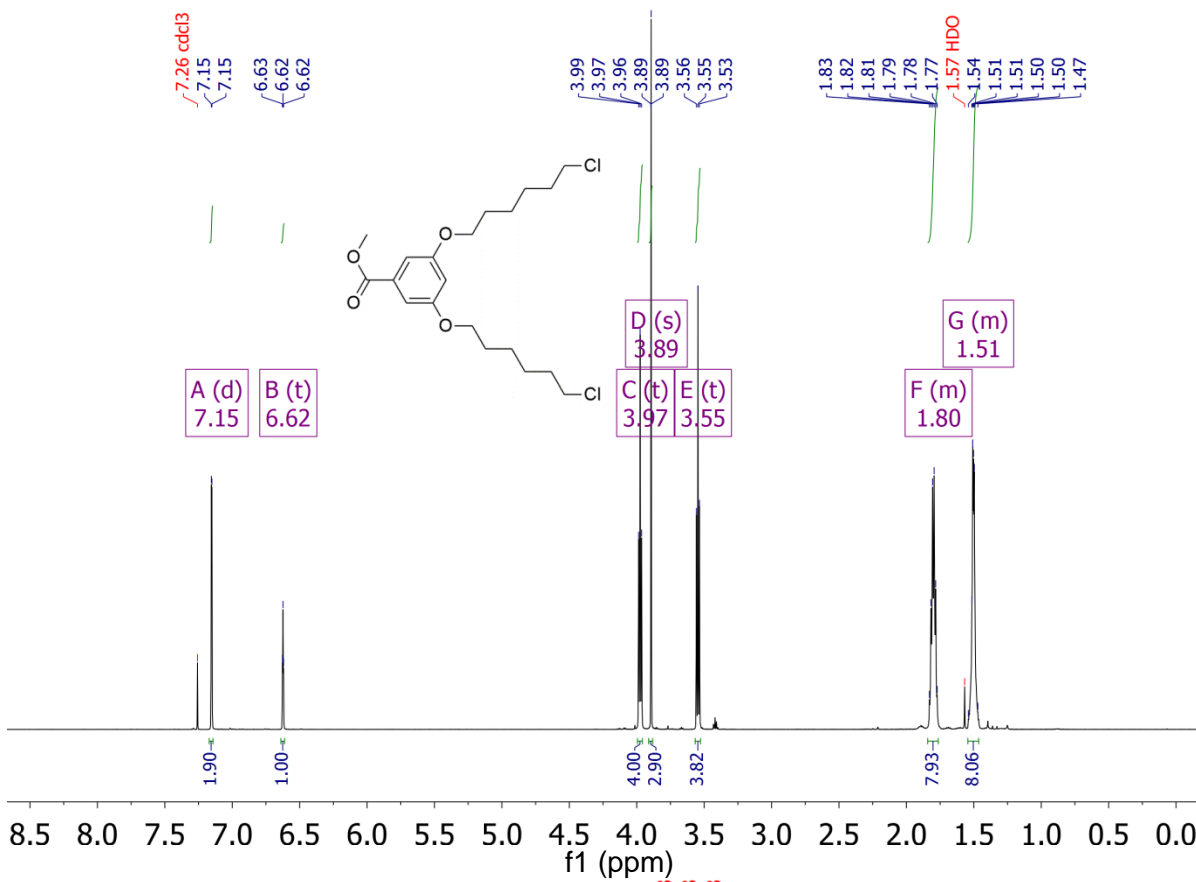
256. Hopkin, D. A., Frapper fort ou frapper doucement: a gram-negative dilemma. (0140-6736 (Print)).
257. Hurley, J. C., Antibiotic-induced release of endotoxin: a reappraisal. *Clin Infect Dis* **1992**, 15 (5), 840-54.
258. Dofferhoff, A. S.; Nijland, J. H.; de Vries-Hospers, H. G.; Mulder, P. O.; Weits, J.; Bom, V. J., Effects of different types and combinations of antimicrobial agents on endotoxin release from gram-negative bacteria: an in-vitro and in-vivo study. *Scand J Infect Dis* **1991**, 23 (6), 745-54.
259. Jackson, J. J.; Kropp, H., beta-Lactam antibiotic-induced release of free endotoxin: in vitro comparison of penicillin-binding protein (PBP) 2-specific imipenem and PBP 3-specific ceftazidime. *J Infect Dis* **1992**, 165 (6), 1033-41.
260. Evans, M. E.; Pollack, M., Effect of antibiotic class and concentration on the release of lipopolysaccharide from Escherichia coli. *J Infect Dis* **1993**, 167 (6), 1336-43.
261. Nau, R.; Eiffert, H., Modulation of Release of Proinflammatory Bacterial Compounds by Antibacterials: Potential Impact on Course of Inflammation and Outcome in Sepsis and Meningitis. *Clinical Microbiology Reviews* **2002**, 15 (1), 95.
262. Kirikae, T.; Nakano, M.; Morrison, D. C., Antibiotic-induced endotoxin release from bacteria and its clinical significance. *Microbiol Immunol* **1997**, 41 (4), 285-94.
263. Hancock, R. E., Alterations in outer membrane permeability. *Annu Rev Microbiol* **1984**, 38, 237-64.
264. Labischinski, H.; Barnickel, G.; Bradaczek, H.; Naumann, D.; Rietschel, E. T.; Giesbrecht, P., High state of order of isolated bacterial lipopolysaccharide and its possible contribution to the permeation barrier property of the outer membrane. *J Bacteriol* **1985**, 162 (1), 9-20.
265. Tsai, C. M.; Frasch, C. E., A sensitive silver stain for detecting lipopolysaccharides in polyacrylamide gels. *Anal Biochem* **1982**, 119 (1), 115-9.
266. Helander, I. M.; Alakomi, H. L.; Latva-Kala, K.; Mattila-Sandholm, T.; Pol, I.; Smid, E. J.; Gorris, L. G. M.; von Wright, A., Characterization of the action of selected essential oil components on gram-negative bacteria. *J Agr Food Chem* **1998**, 46 (9), 3590-3595.
267. Macdonald, I. A.; Kuehn, M. J., Stress-induced outer membrane vesicle production by *Pseudomonas aeruginosa*. *J Bacteriol* **2013**, 195 (13), 2971-81.

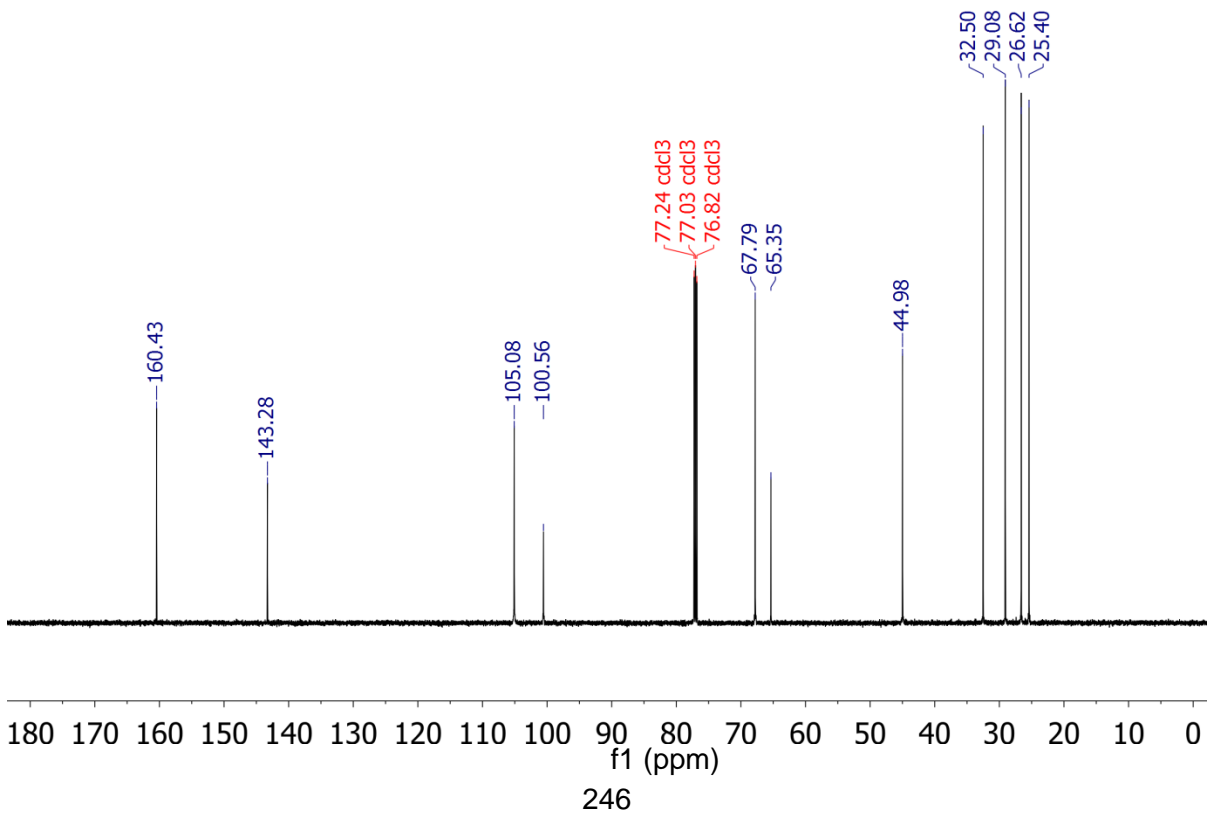
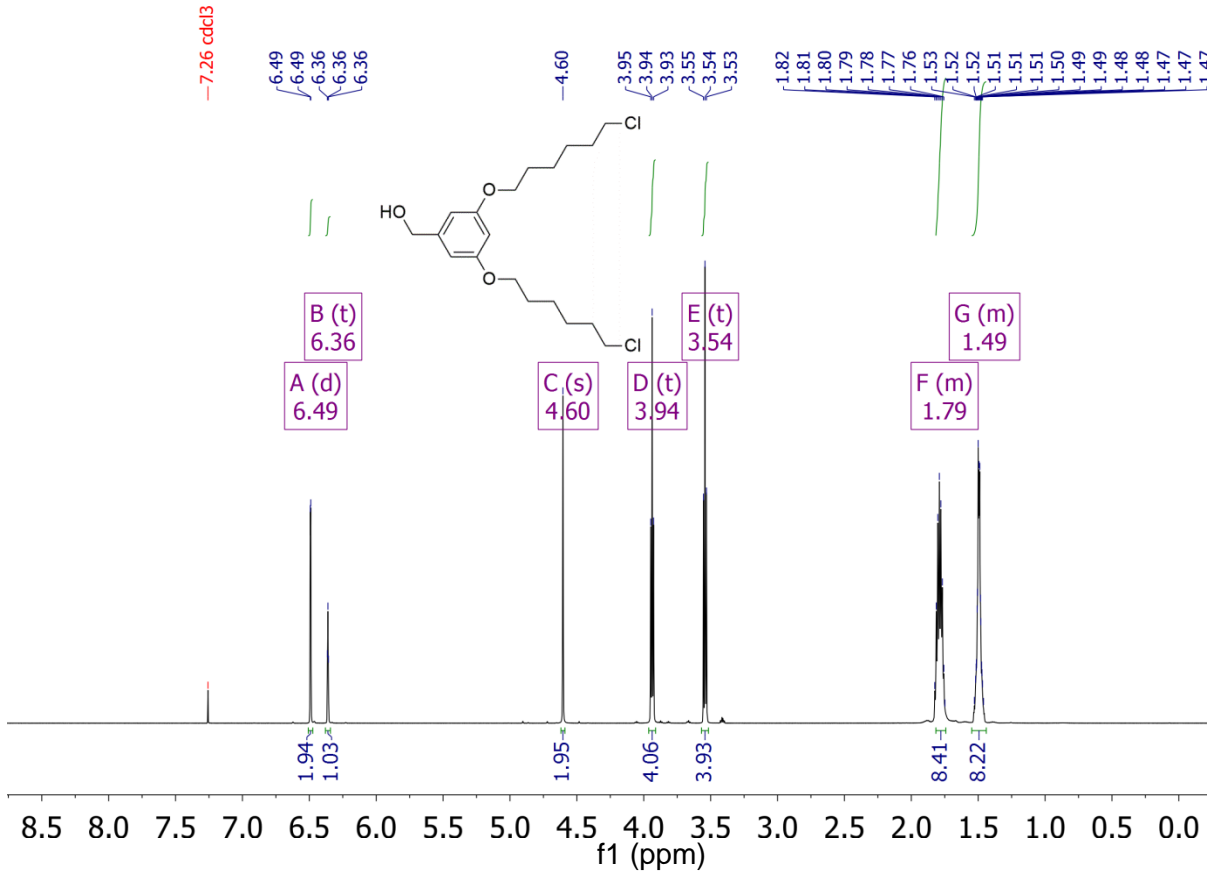
268. Elhenawy, W.; Bording-Jorgensen, M.; Valguarnera, E.; Haurat, M. F.; Wine, E.; Feldman, M. F., LPS Remodeling Triggers Formation of Outer Membrane Vesicles in Salmonella. *MBio* **2016**, *7* (4).
269. Hinks, J.; Wang, Y.; Matysik, A.; Kraut, R.; Kjelleberg, S.; Mu, Y.; Bazan, G. C.; Wuertz, S.; Seviour, T., Increased Microbial Butanol Tolerance by Exogenous Membrane Insertion Molecules. *ChemSusChem* **2015**, *8* (21), 3718-26.
270. Fletcher, E.; Pilizota, T.; Davies, P. R.; McVey, A.; French, C. E., Characterization of the effects of n-butanol on the cell envelope of E. coli. *Appl Microbiol Biotechnol* **2016**, *100* (22), 9653-9659.
271. Tsuzuki, H.; Tani, T.; Ueyama, H.; Kodama, M., Lipopolysaccharide: neutralization by polymyxin B shuts down the signaling pathway of nuclear factor kappaB in peripheral blood mononuclear cells, even during activation. *J Surg Res* **2001**, *100* (1), 127-34.
272. Domingues, M. M.; Inacio, R. G.; Raimundo, J. M.; Martins, M.; Castanho, M. A.; Santos, N. C., Biophysical characterization of polymyxin B interaction with LPS aggregates and membrane model systems. *Biopolymers* **2012**, *98* (4), 338-44.
273. Cooperstock, M. S., Inactivation of endotoxin by polymyxin B. *Antimicrob Agents Chemother* **1974**, *6* (4), 422-5.
274. Jandejsek, J.; Sourek, J., Inactivation by polymyxin B of the endotoxin-mediated interferon production in the rabbit. *Zentralbl Bakteriol Mikrobiol Hyg A* **1985**, *259* (3), 390-6.
275. David, S. A., Towards a rational development of anti-endotoxin agents: novel approaches to sequestration of bacterial endotoxins with small molecules. *J Mol Recognit* **2001**, *14* (6), 370-87.
276. Wood, S. J.; Miller, K. A.; David, S. A., Anti-endotoxin agents. 2. Pilot high-throughput screening for novel lipopolysaccharide-recognizing motifs in small molecules. *Comb Chem High Throughput Screen* **2004**, *7* (8), 733-47.
277. Wood, S. J.; Miller, K. A.; David, S. A., Anti-endotoxin agents. 1. Development of a fluorescent probe displacement method optimized for the rapid identification of lipopolysaccharide-binding agents. *Comb Chem High Throughput Screen* **2004**, *7* (3), 239-49.
278. Wood, S. J.; Miller, K. A.; Lushington, G. H.; Burns, M. R.; David, S. A., Anti-endotoxin agents. 3. Rapid identification of high-affinity lipopolysaccharide-binding compounds in a substituted polyamine library. *Comb Chem High Throughput Screen* **2006**, *9* (1), 27-36.

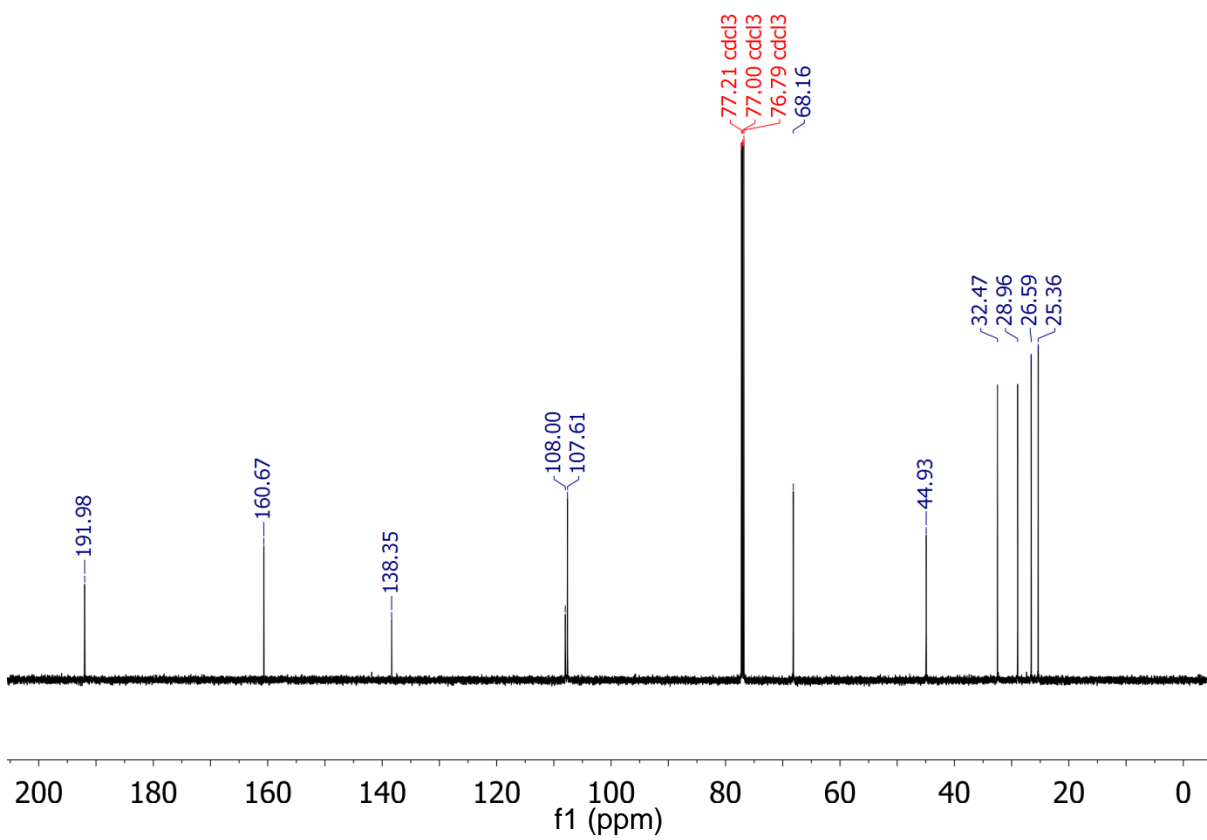
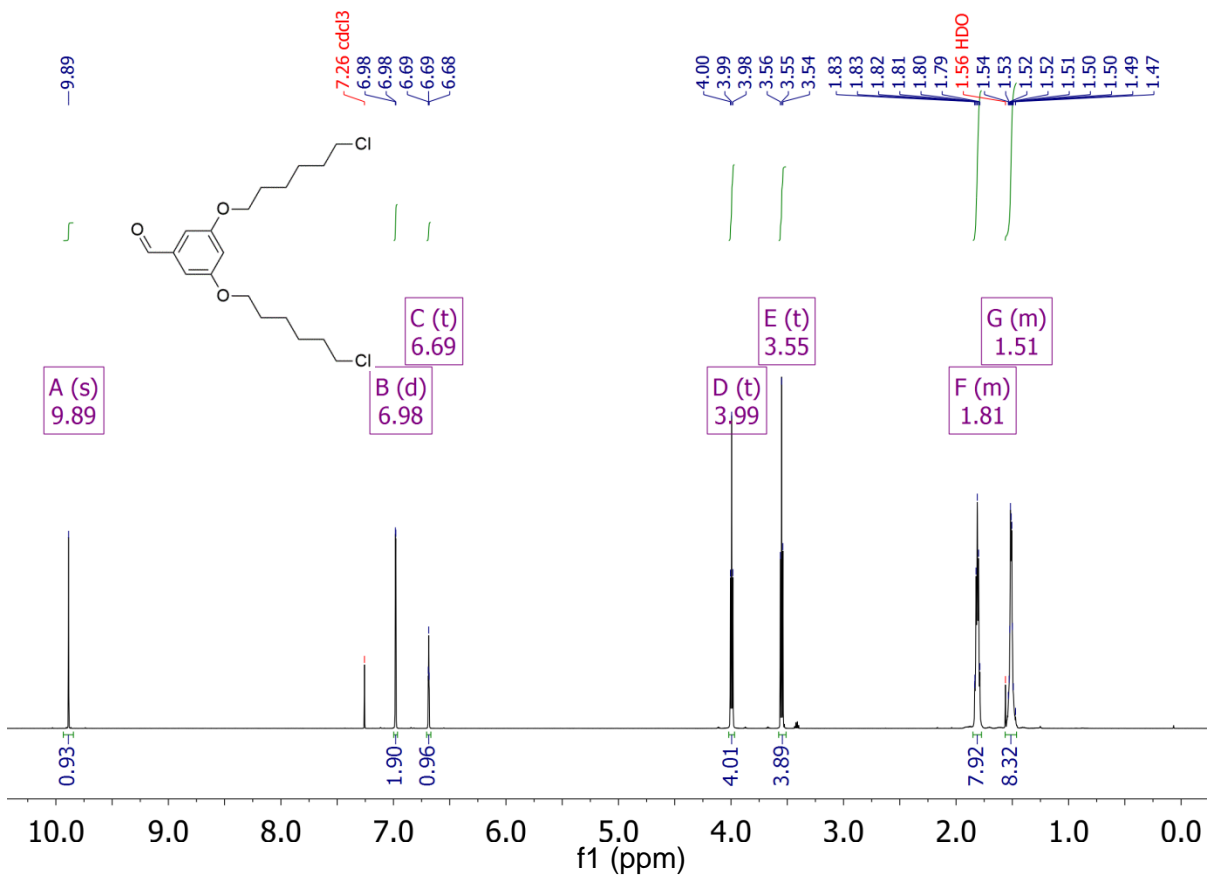
279. Yu, L.; Tan, M.; Ho, B.; Ding, J. L.; Wohland, T., Determination of critical micelle concentrations and aggregation numbers by fluorescence correlation spectroscopy: aggregation of a lipopolysaccharide. *Anal Chim Acta* **2006**, *556* (1), 216-25.
280. Pagano, R. E.; Cherry, R. J.; Chapman, D., Phase-Transitions and Heterogeneity in Lipid Bilayers. *Science* **1973**, *181* (4099), 557-559.
281. Prenner, E. J.; Lewis, R. N. A. H.; Kondejewski, L. H.; Hodges, R. S.; McElhaney, R. N., Differential scanning calorimetric study of the effect of the antimicrobial peptide gramicidin S on the thermotropic phase behavior of phosphatidylcholine, phosphatidylethanolamine and phosphatidylglycerol lipid bilayer membranes. *Bba-Biomembranes* **1999**, *1417* (2), 211-223.
282. Zhou, C.; Chia, G. W. N.; Ho, J. C. S.; Seviour, T.; Sailov, T.; Liedberg, B.; Kjelleberg, S.; Hinks, J.; Bazan, G. C., Informed Molecular Design of Conjugated Oligoelectrolytes To Increase Cell Affinity and Antimicrobial Activity. *Angew Chem Int Ed Engl* **2018**, *57* (27), 8069-8072.
283. McMullen, T. P.; Lewis, R. N.; McElhaney, R. N., Differential scanning calorimetric study of the effect of cholesterol on the thermotropic phase behavior of a homologous series of linear saturated phosphatidylcholines. *Biochemistry* **1993**, *32* (2), 516-22.
284. Malcolmson, R. J.; Higinbotham, J.; Beswick, P. H.; Privat, P. O.; Saunier, L., DSC of DMPC liposomes containing low concentrations of cholesteryl esters or cholesterol. *J Membrane Sci* **1997**, *123* (2), 243-253.

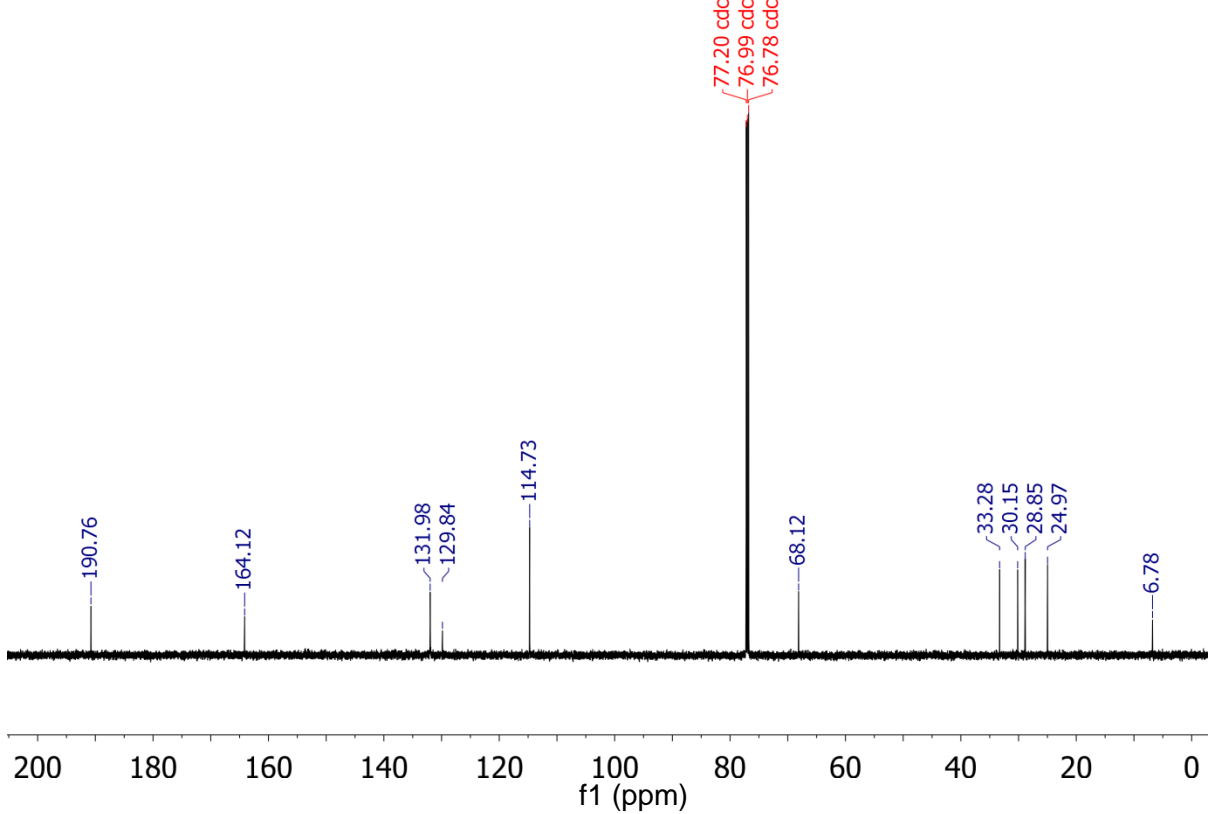
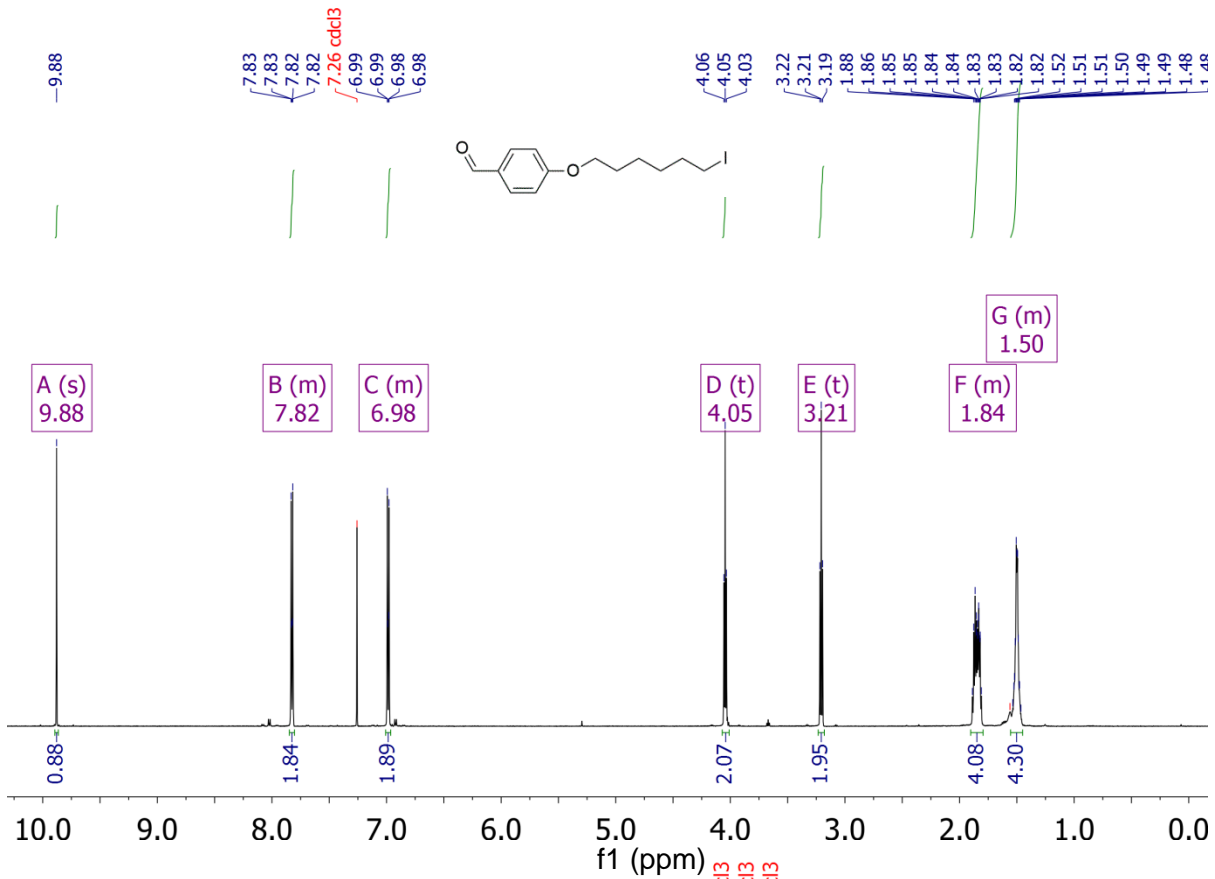
NMR Spectra

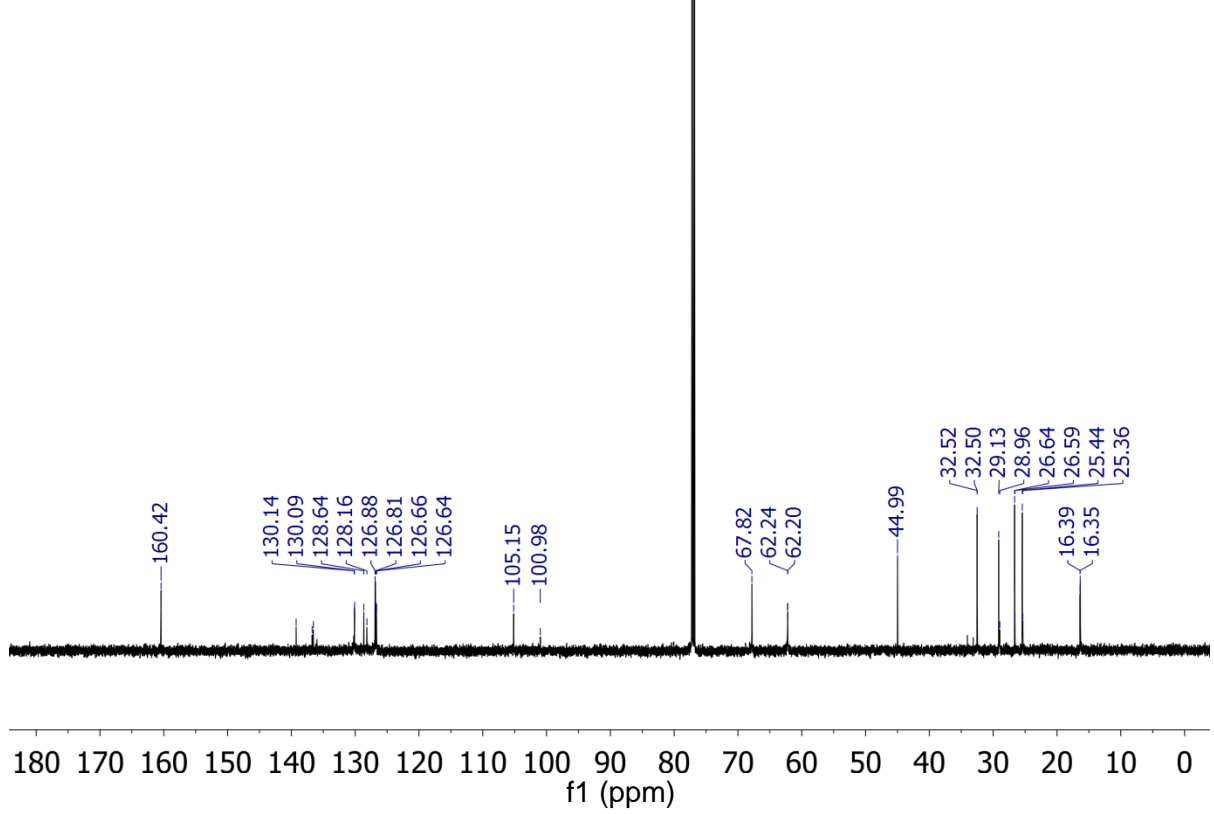
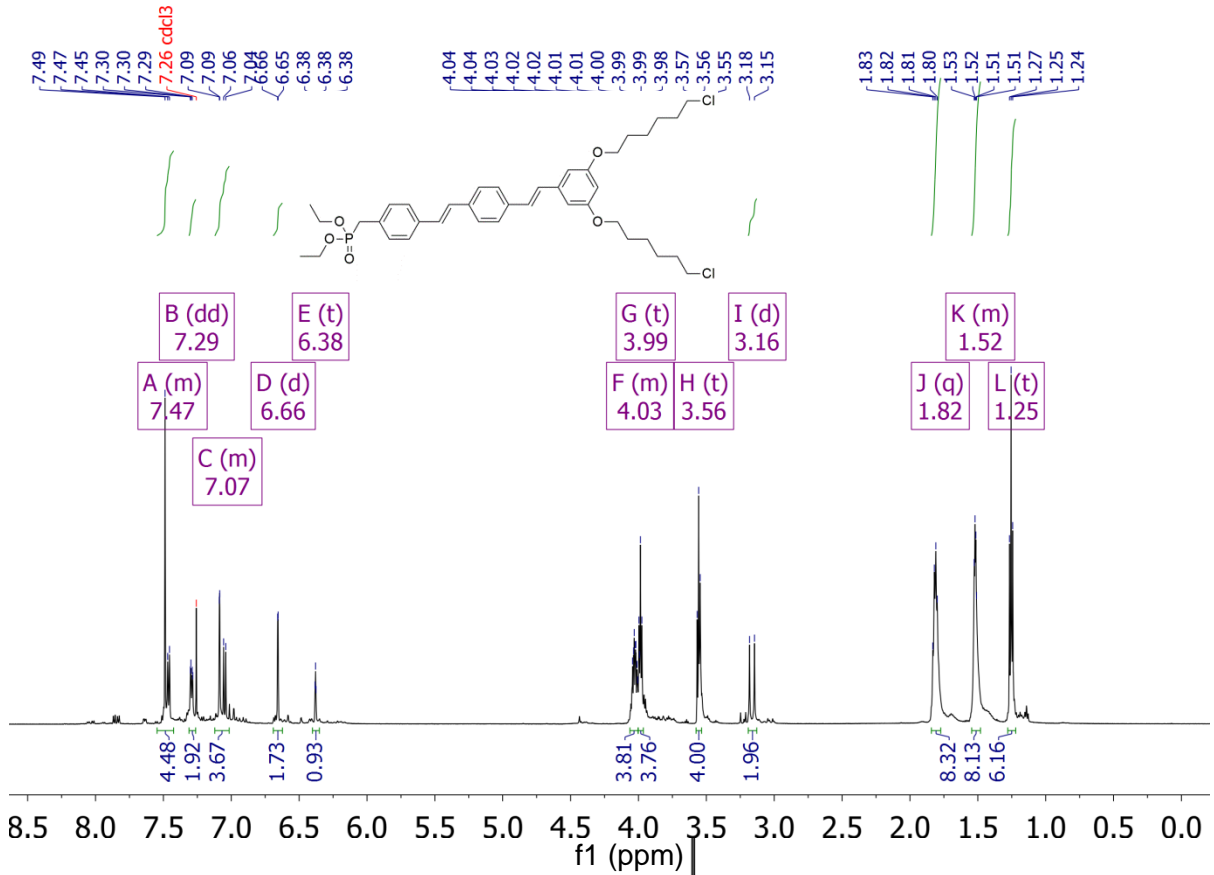
Chapter 1

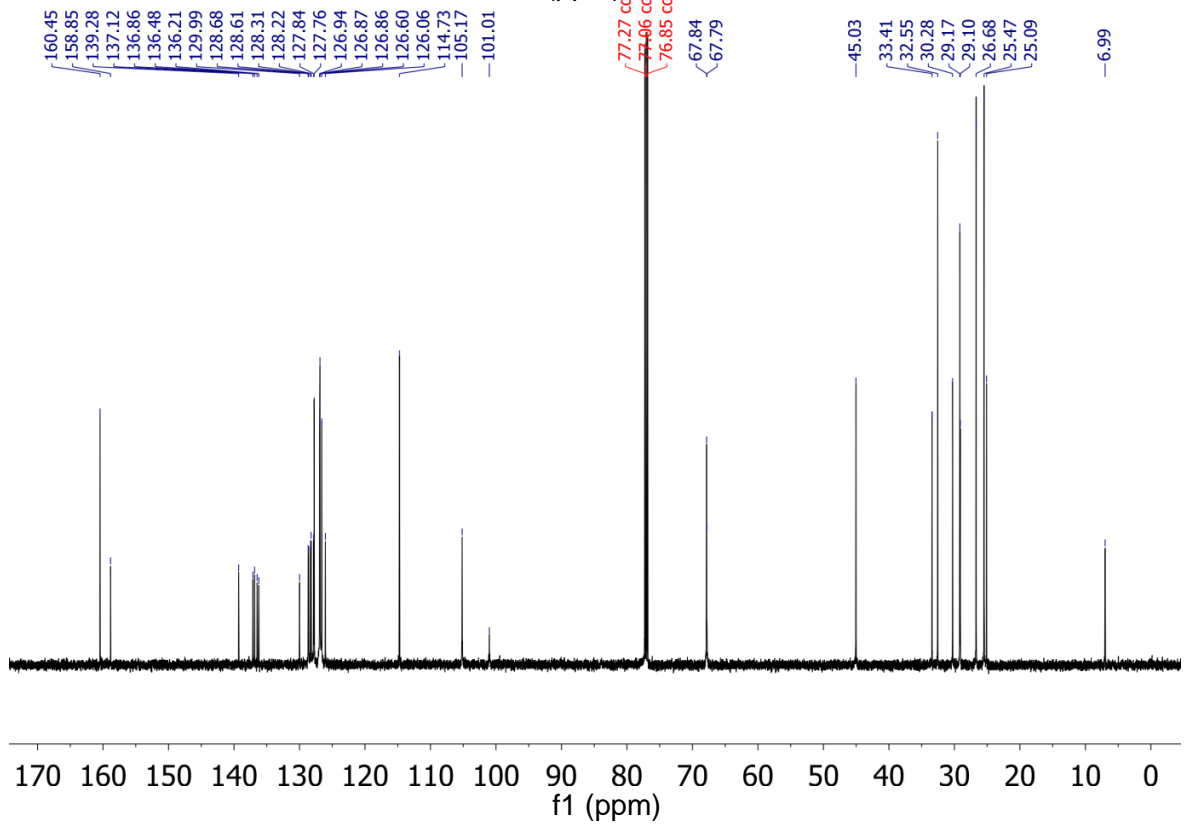
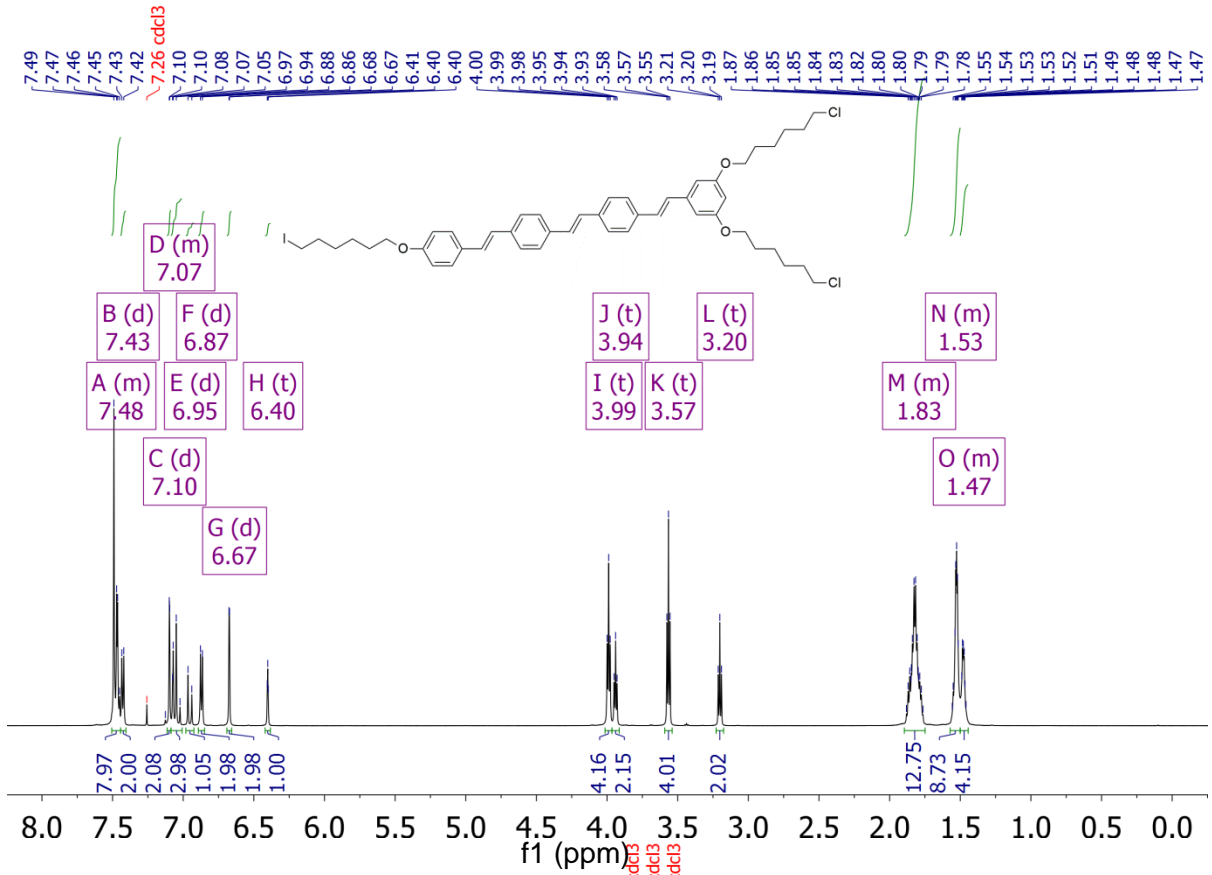


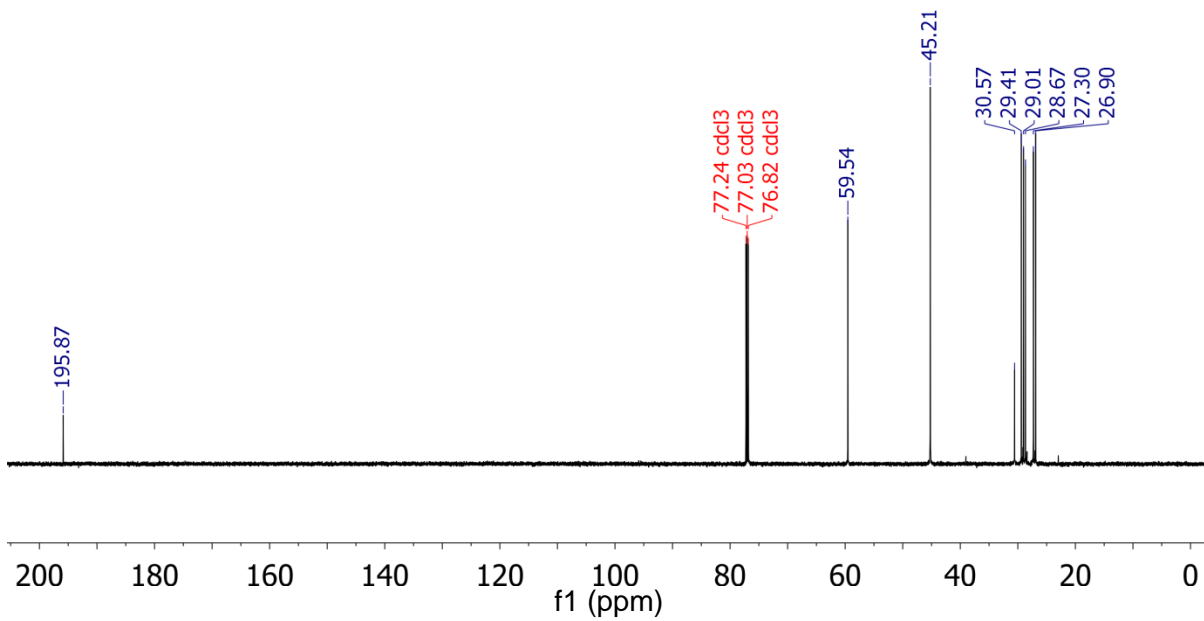
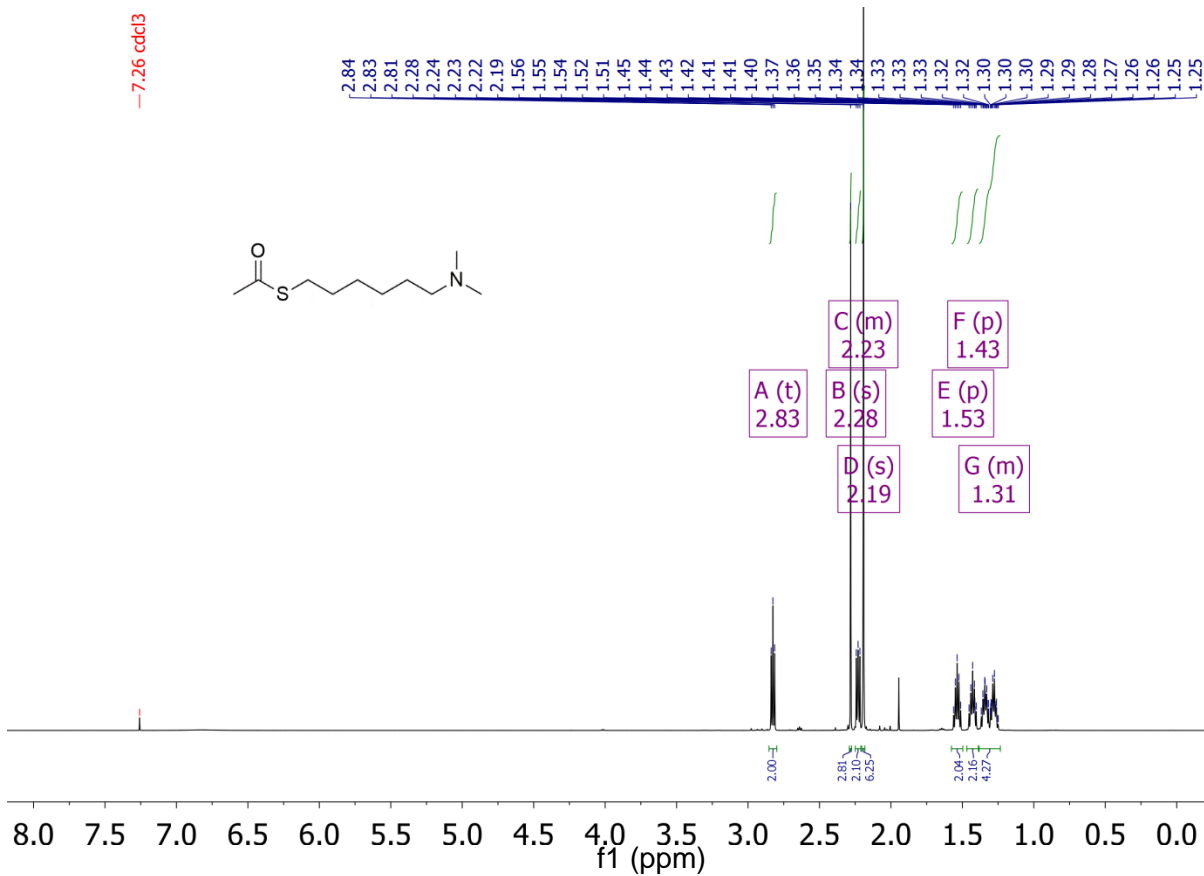


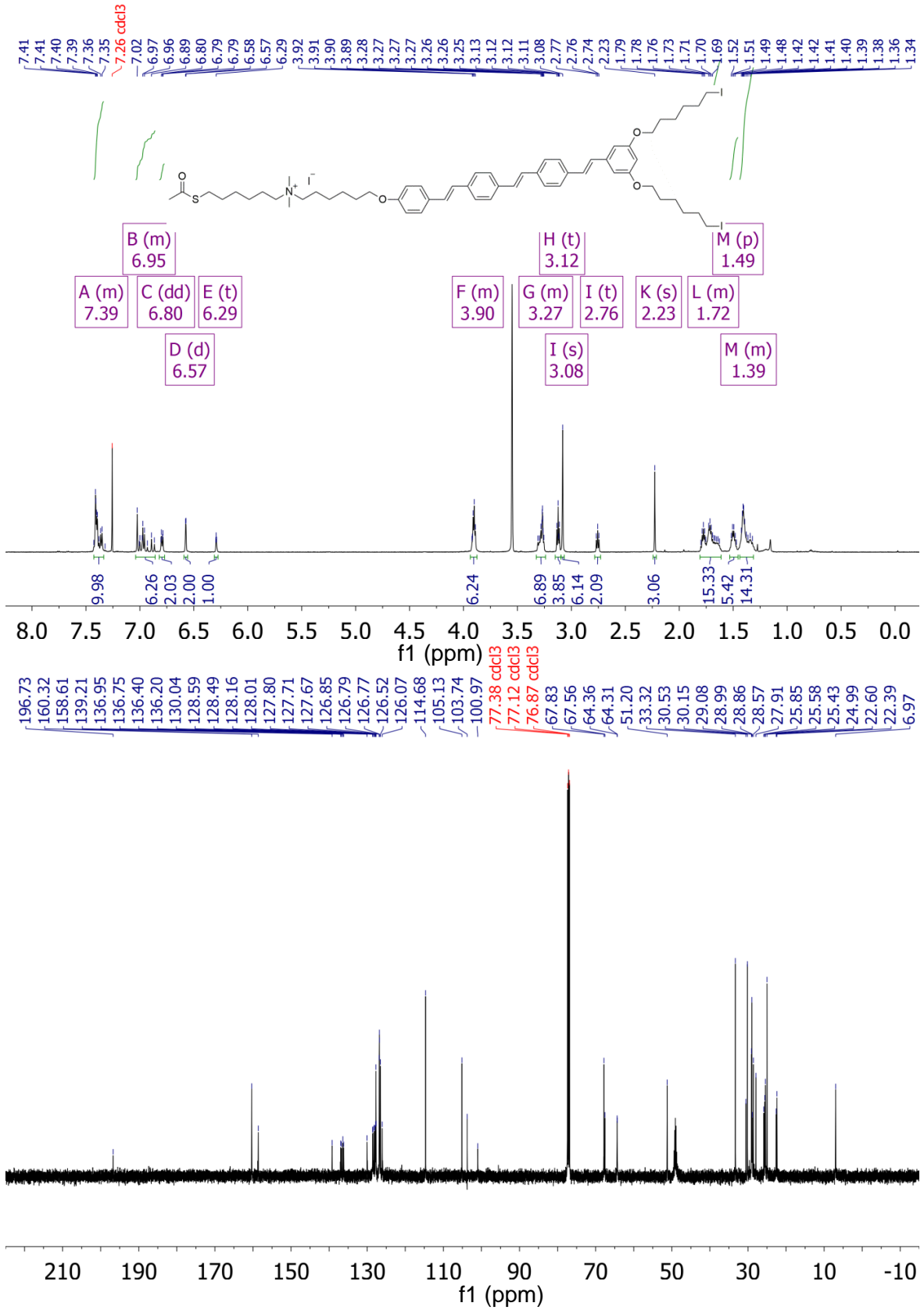


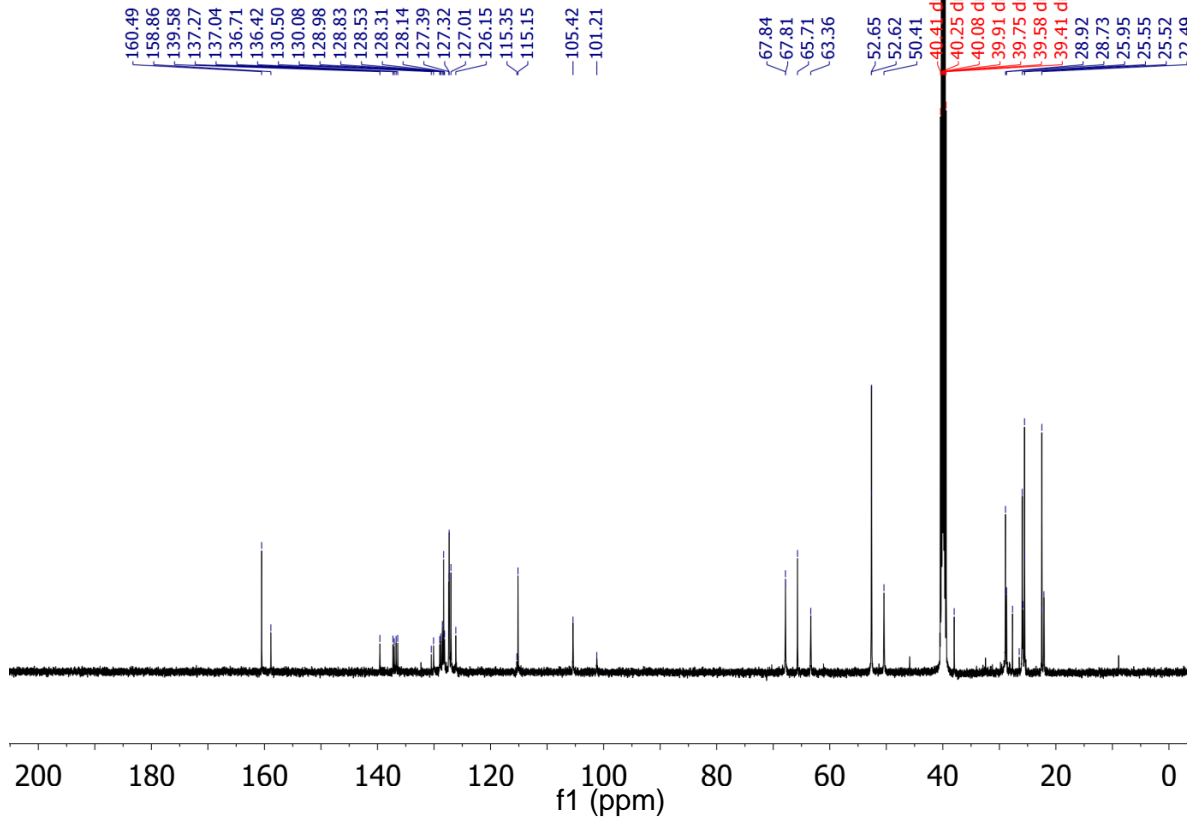
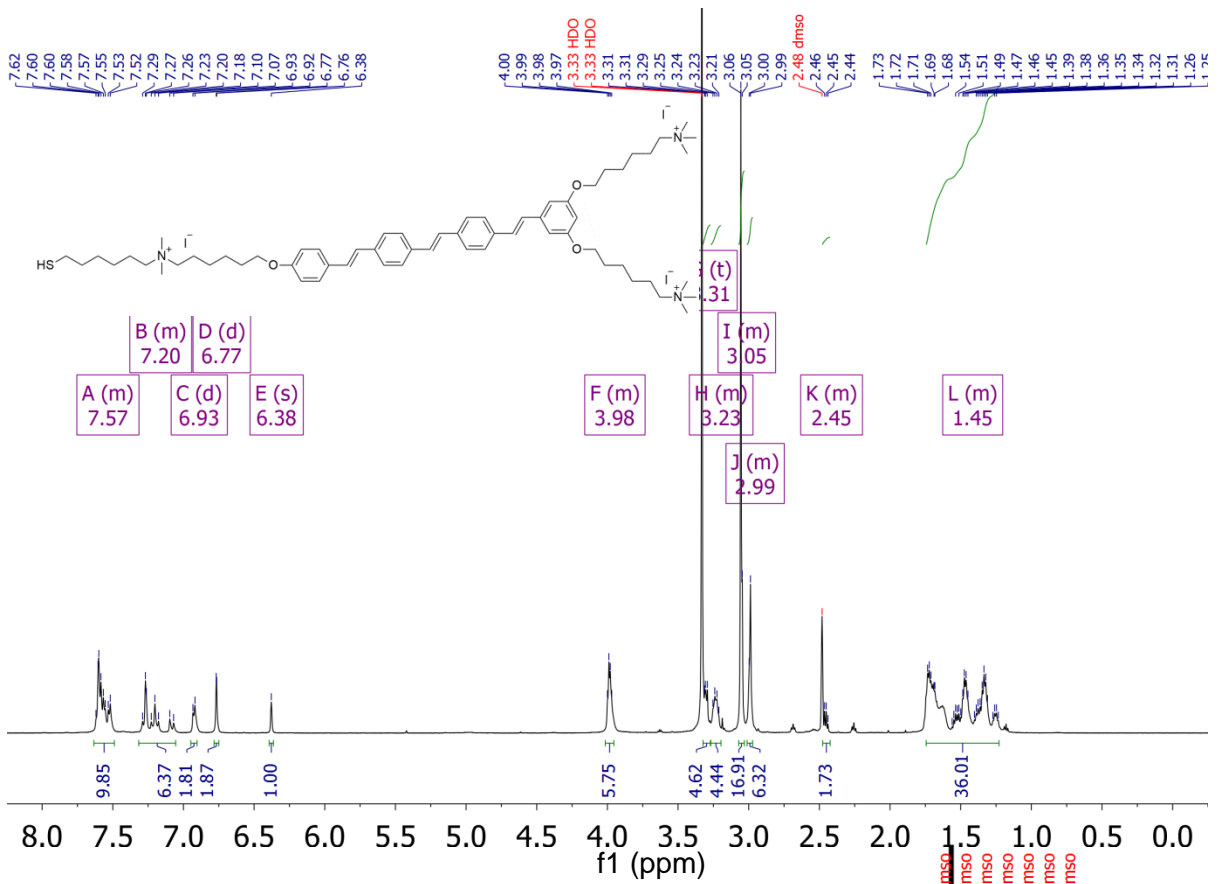




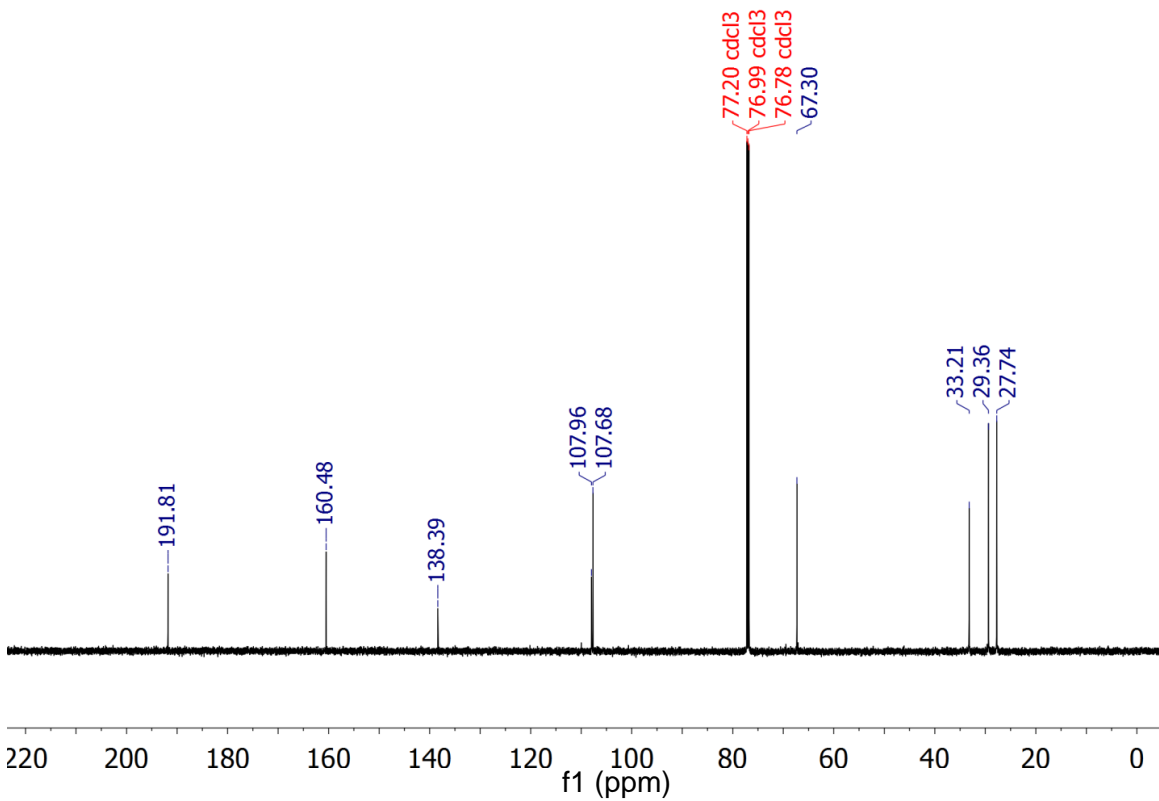
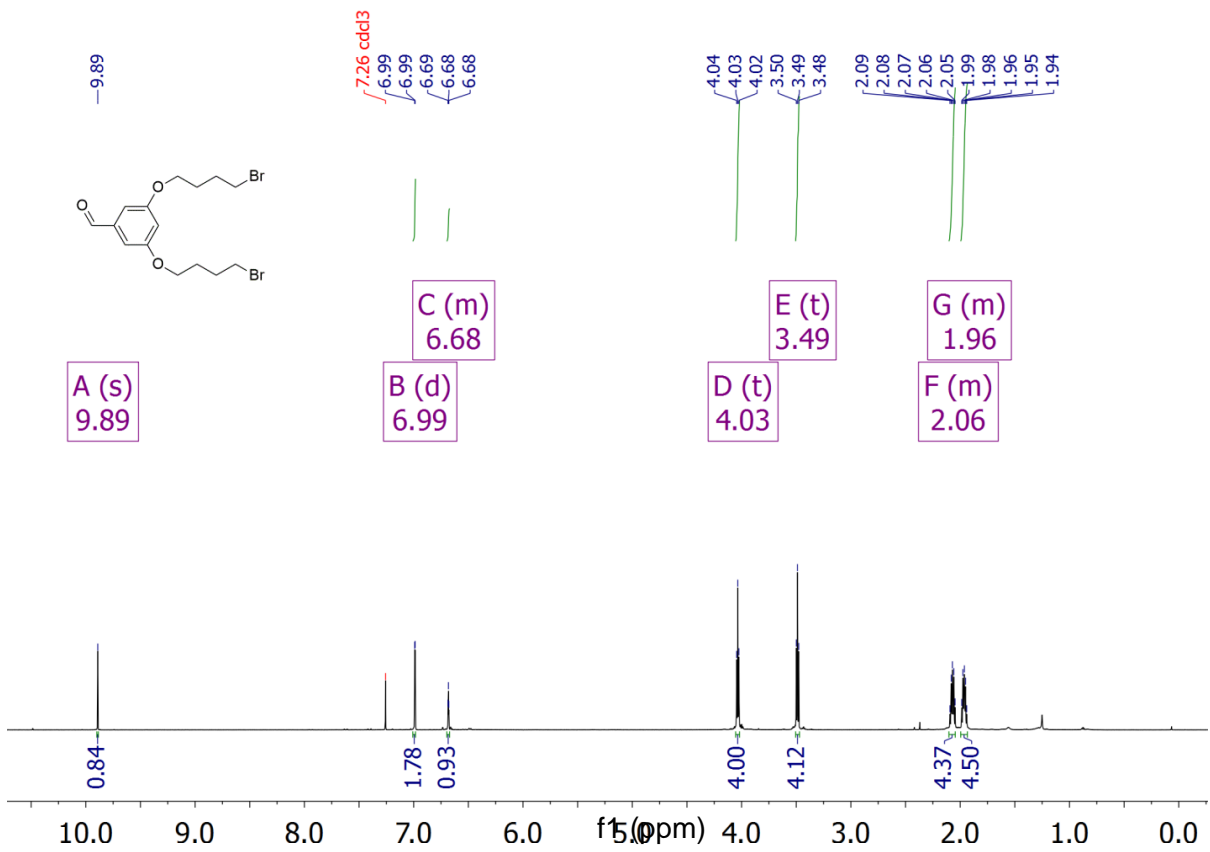


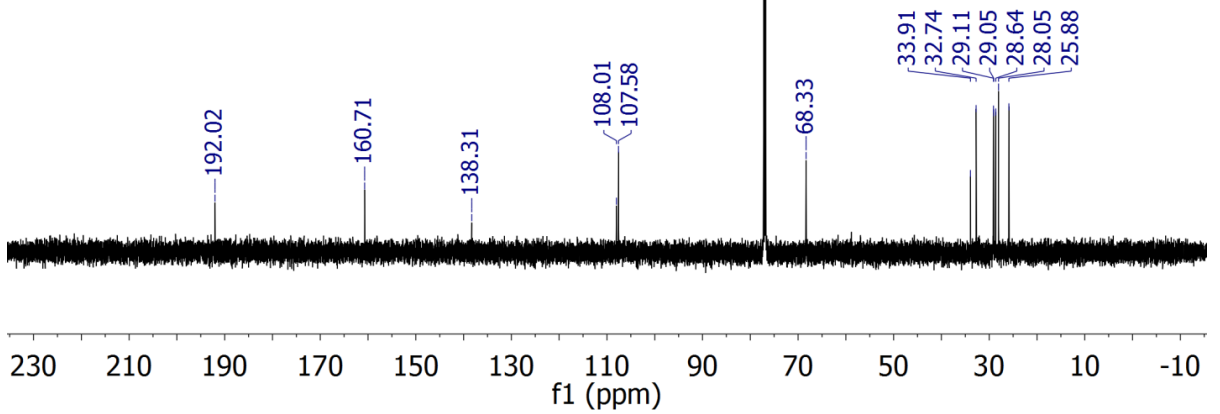
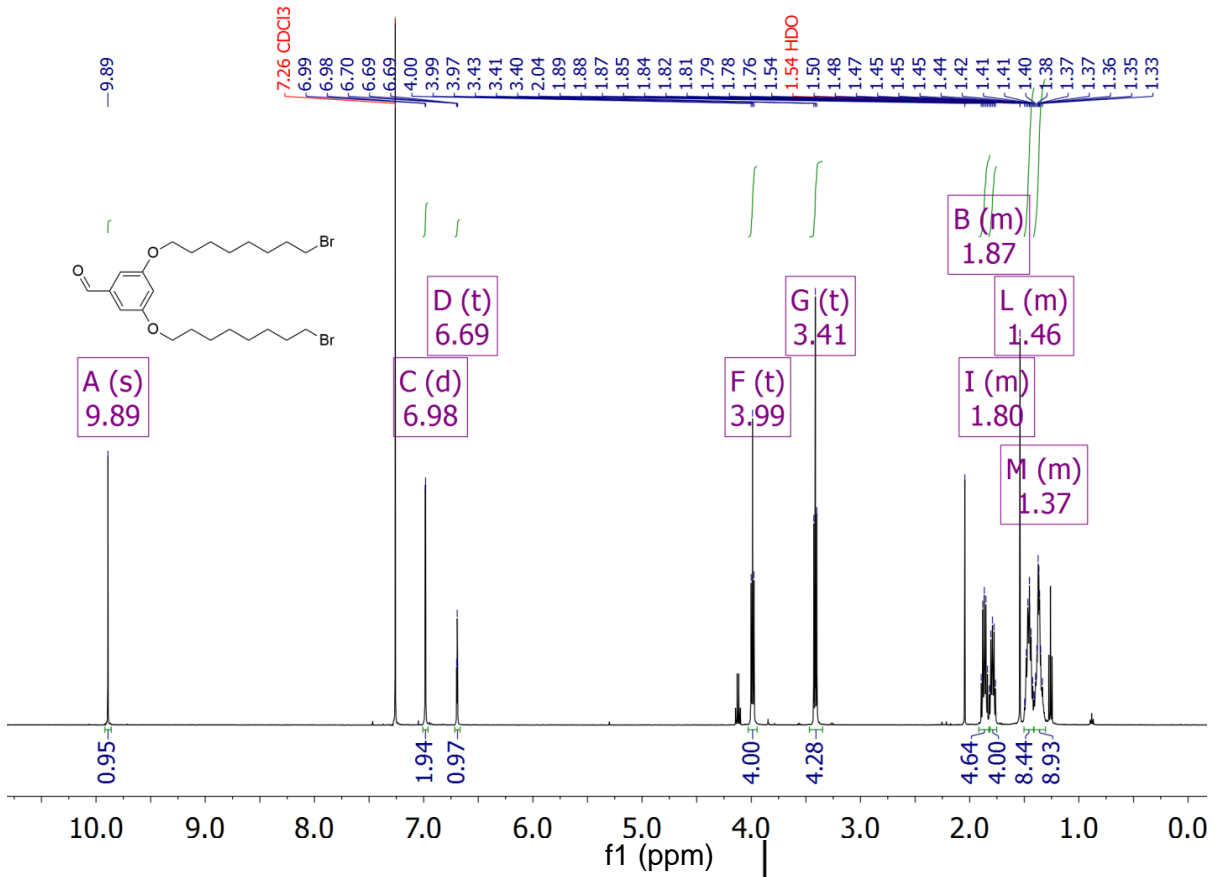


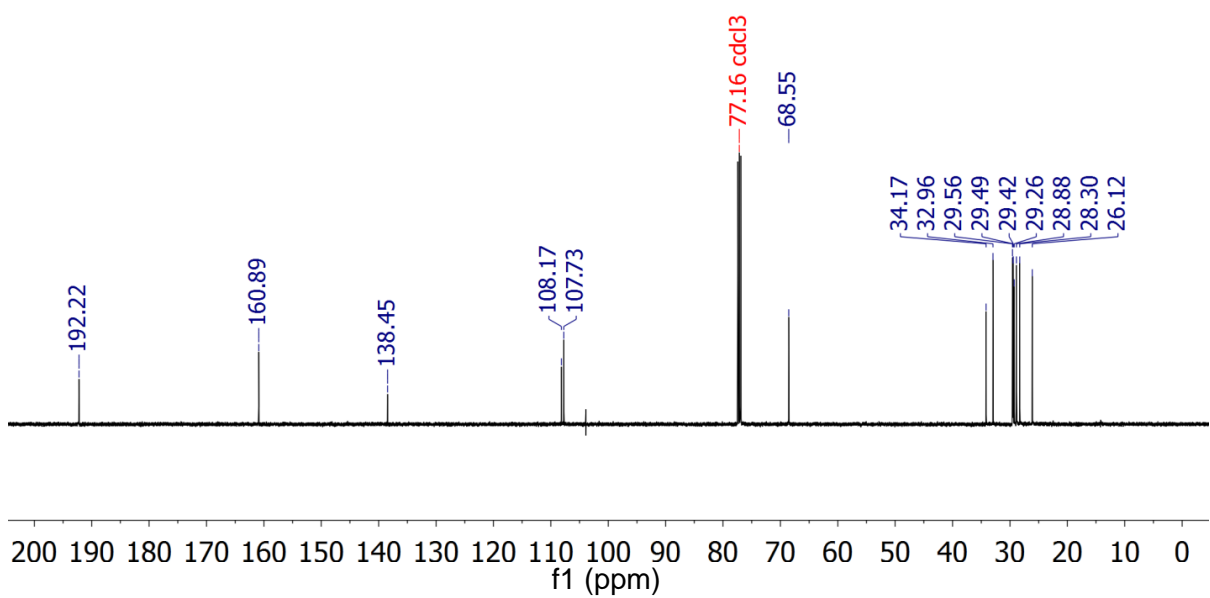
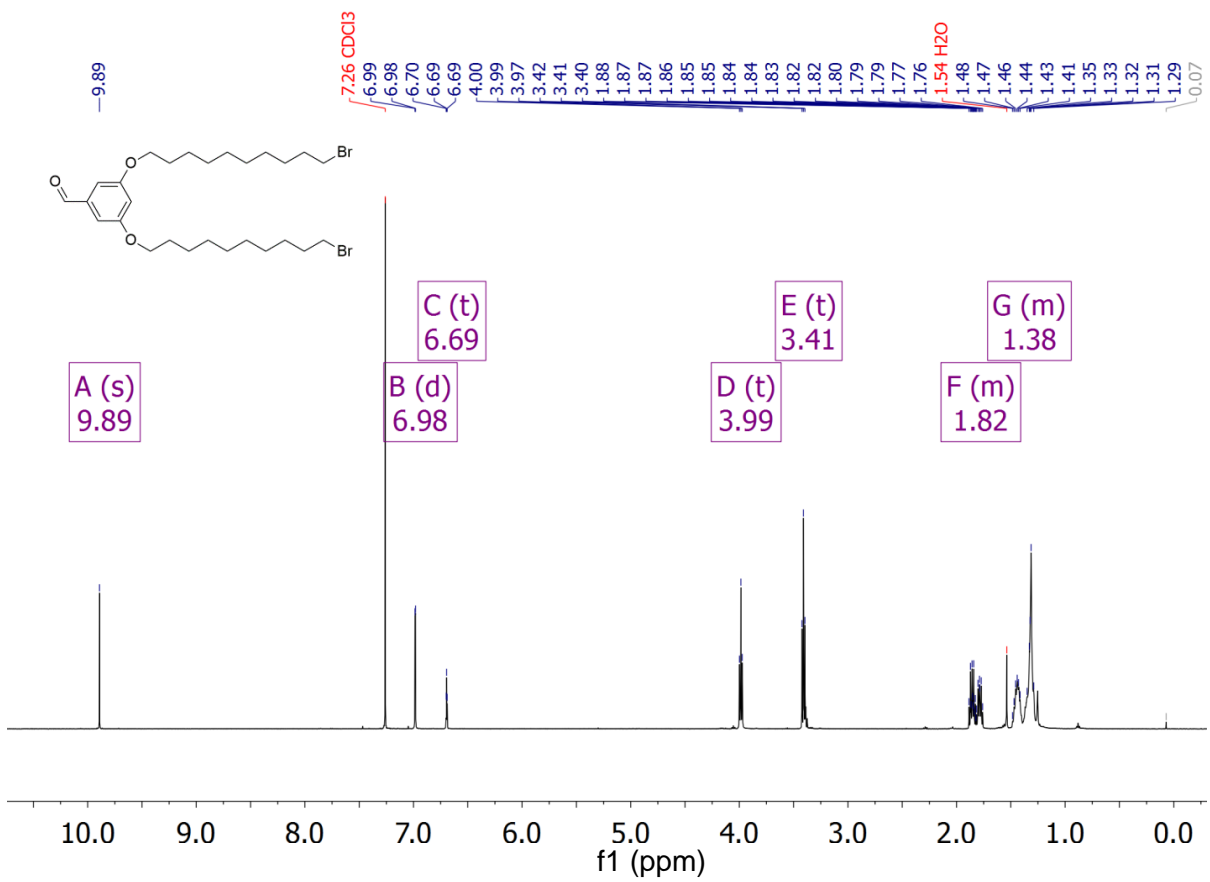


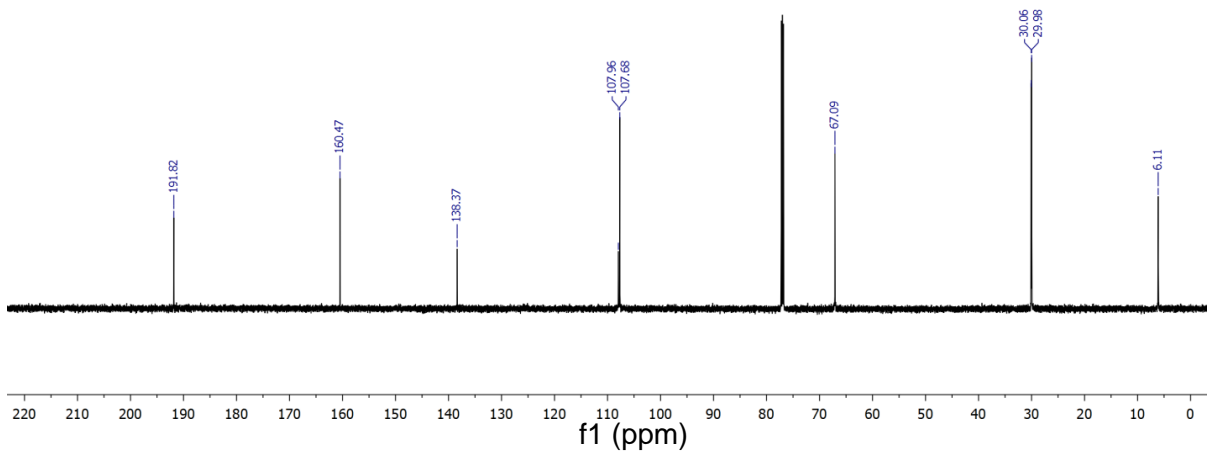
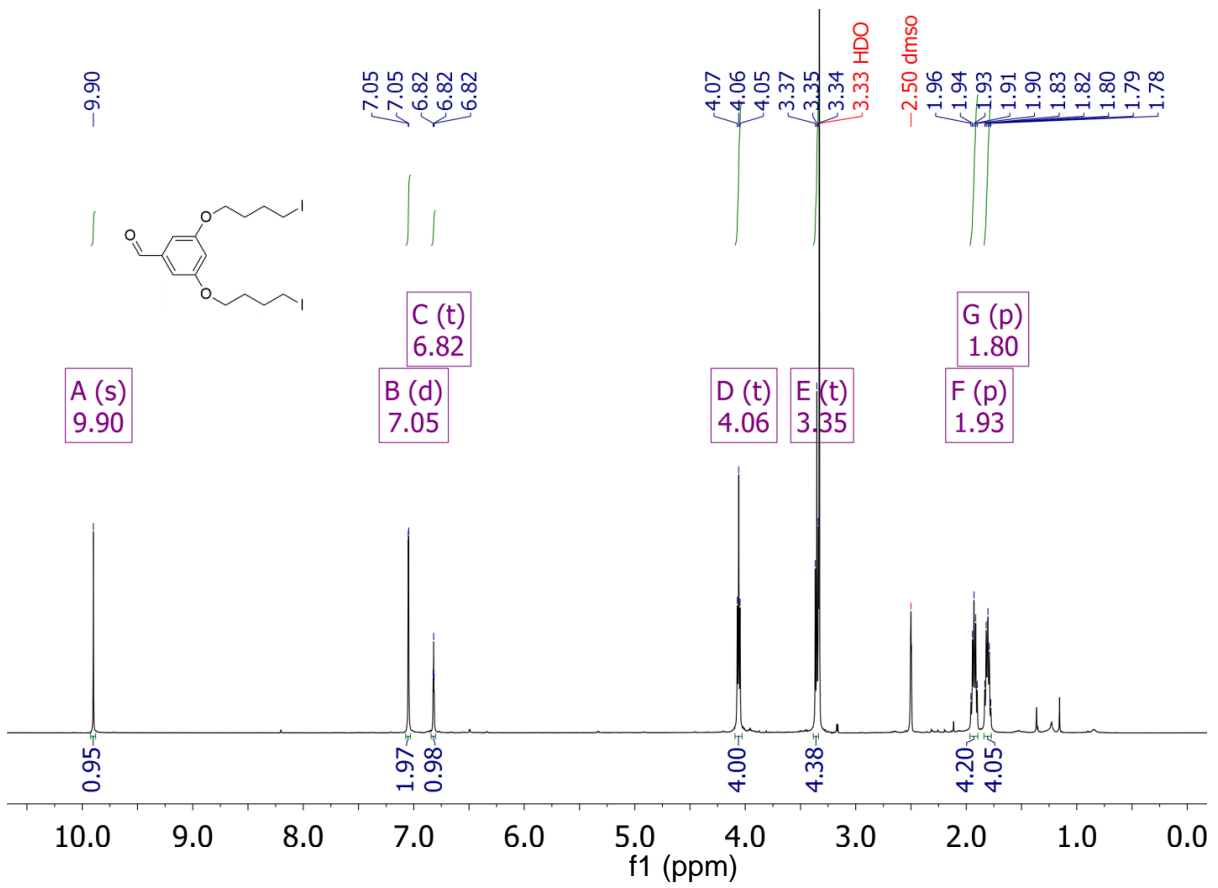


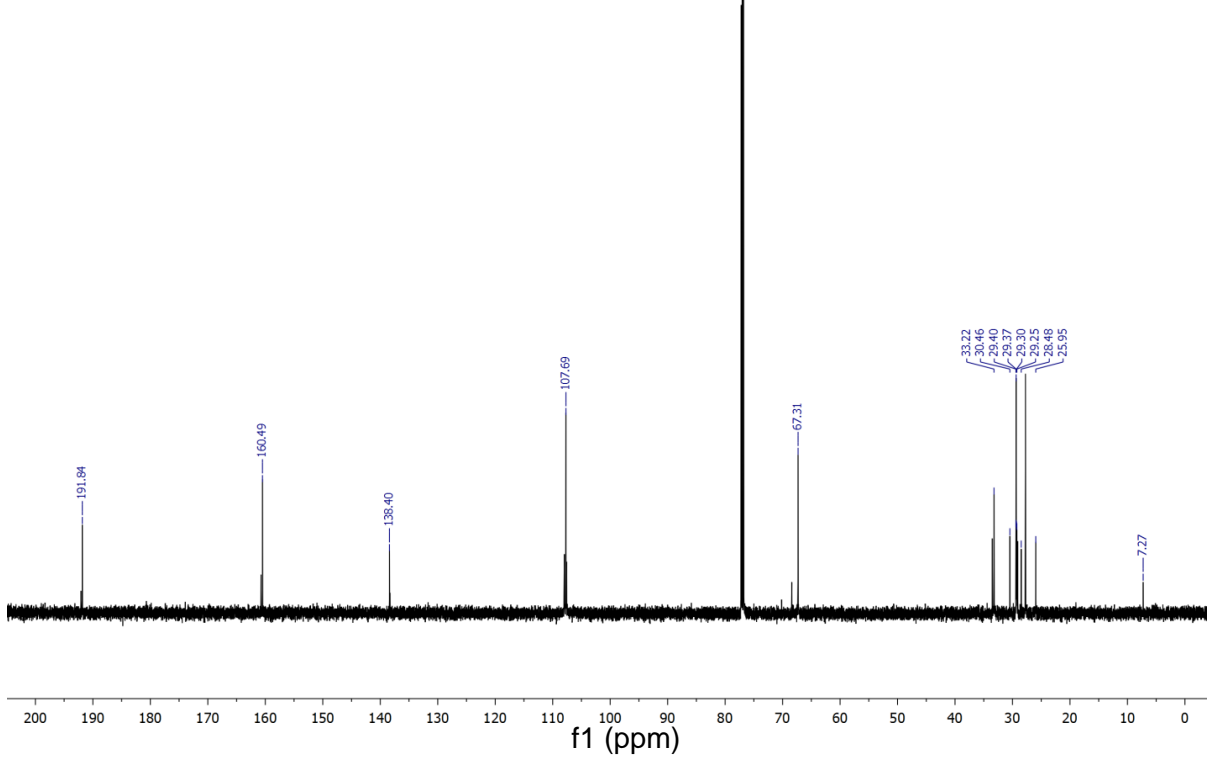
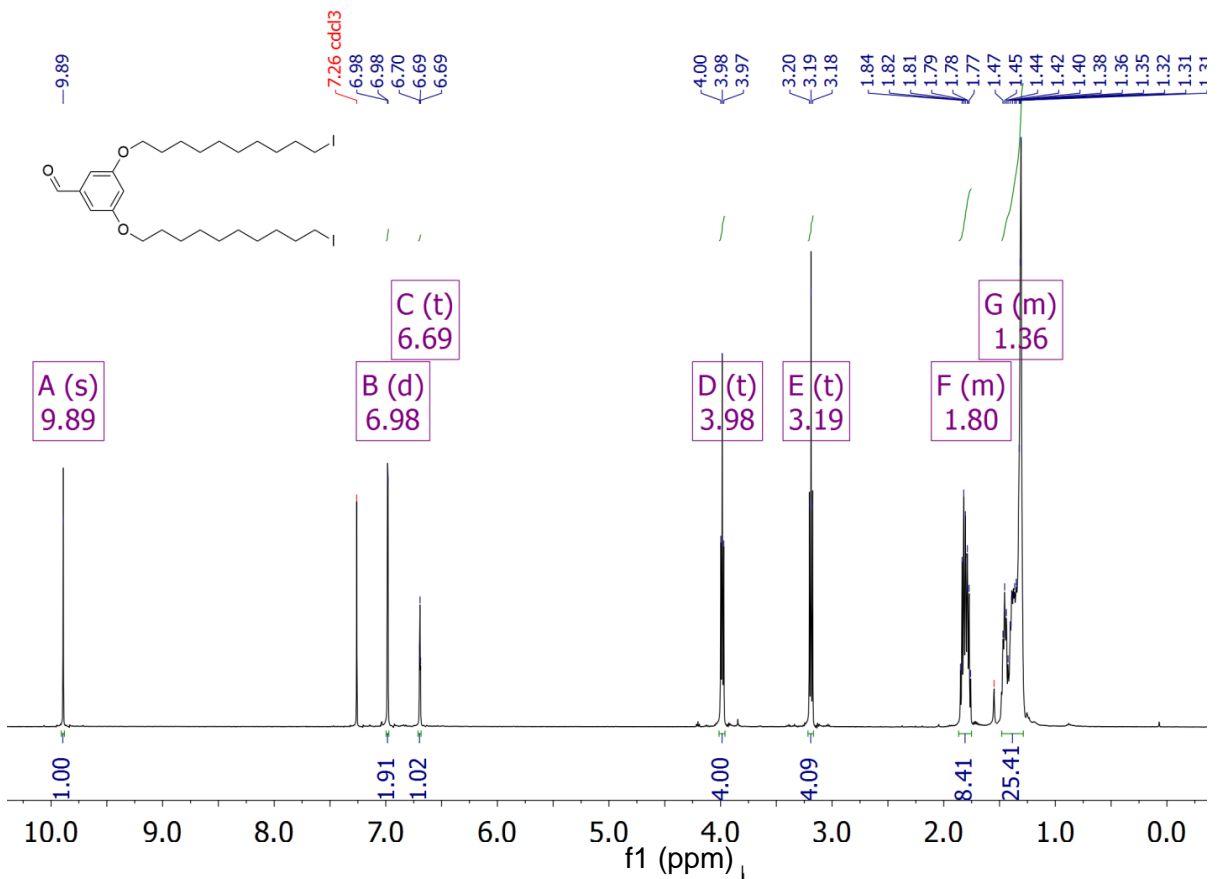
Chapter 2

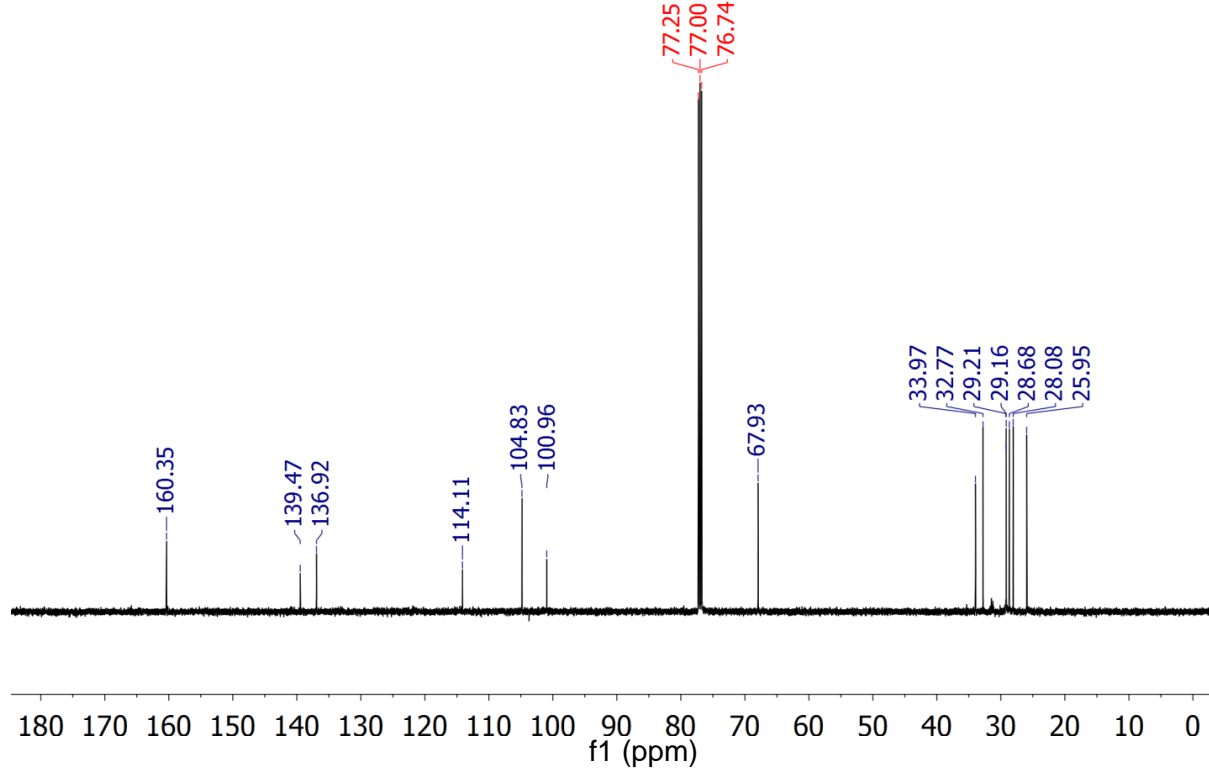
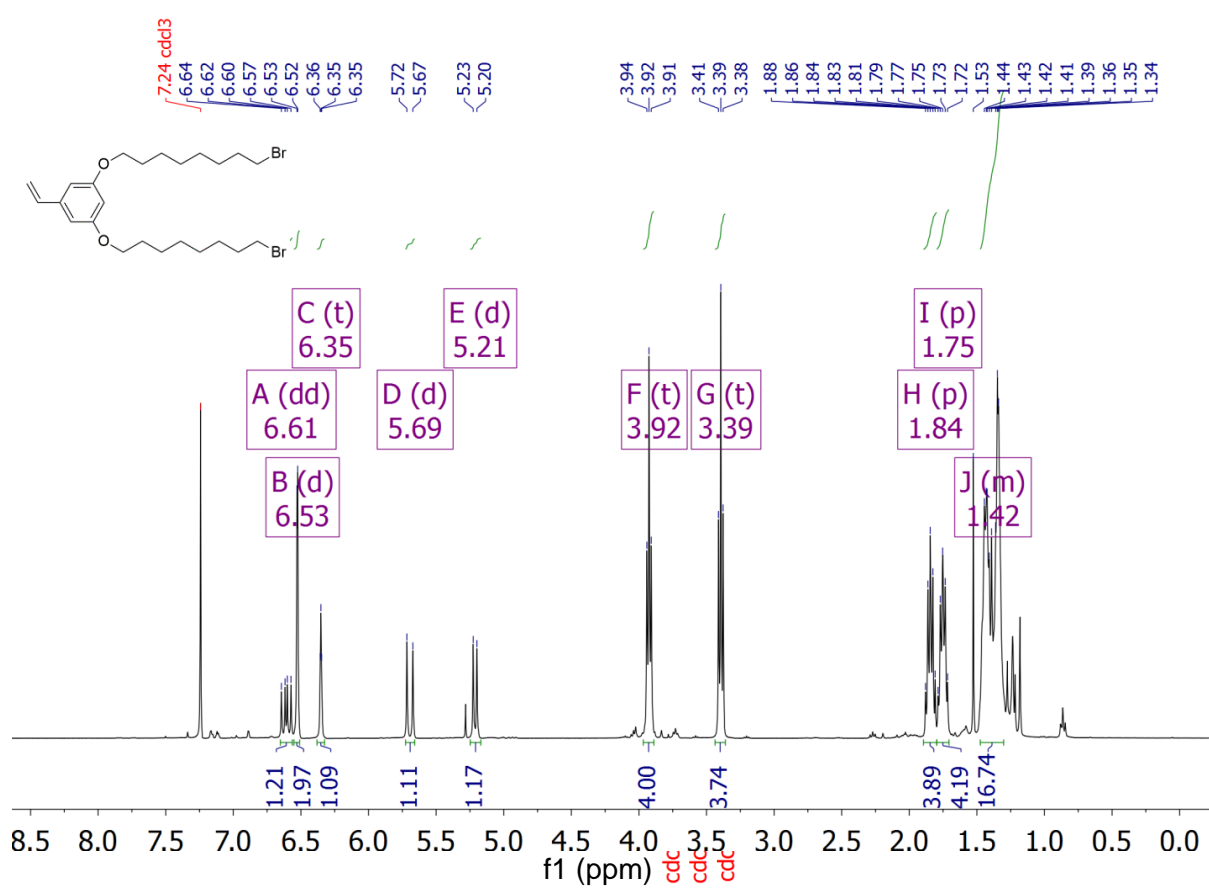


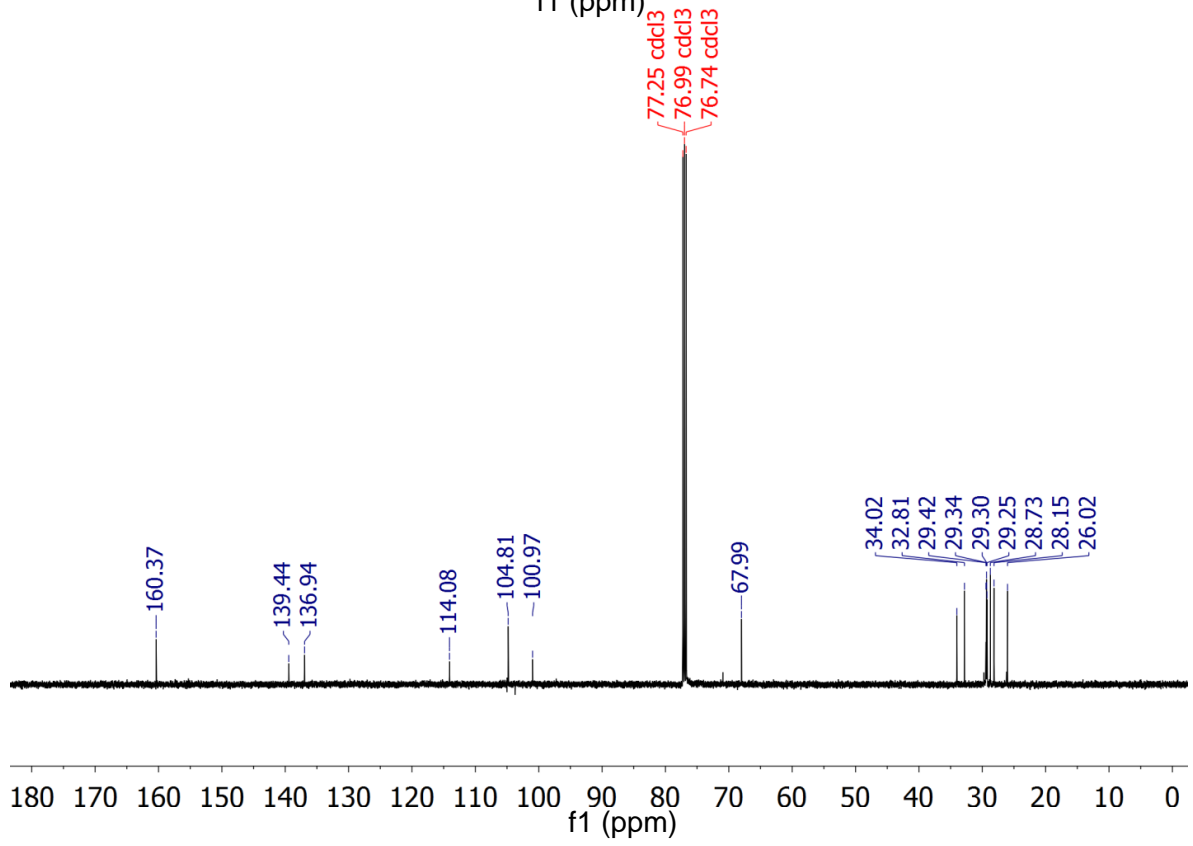
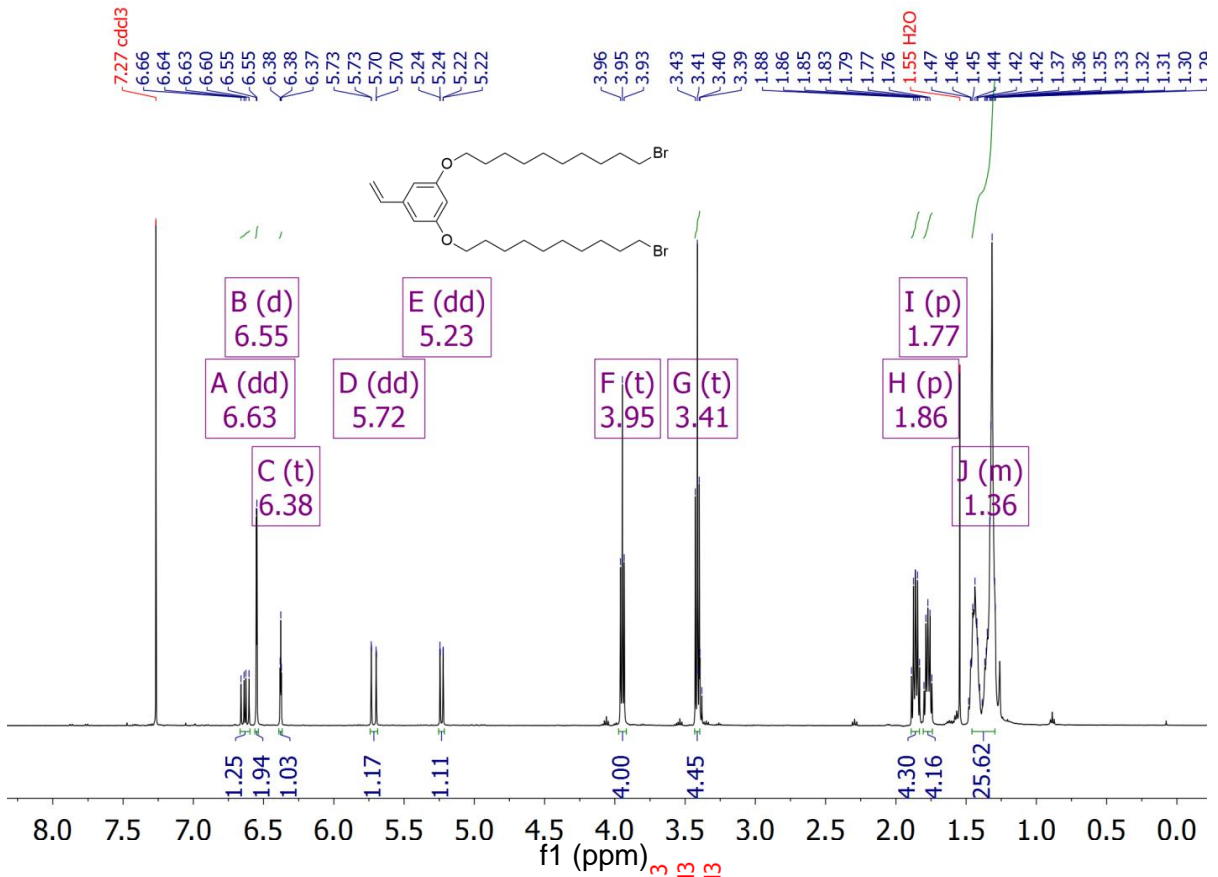


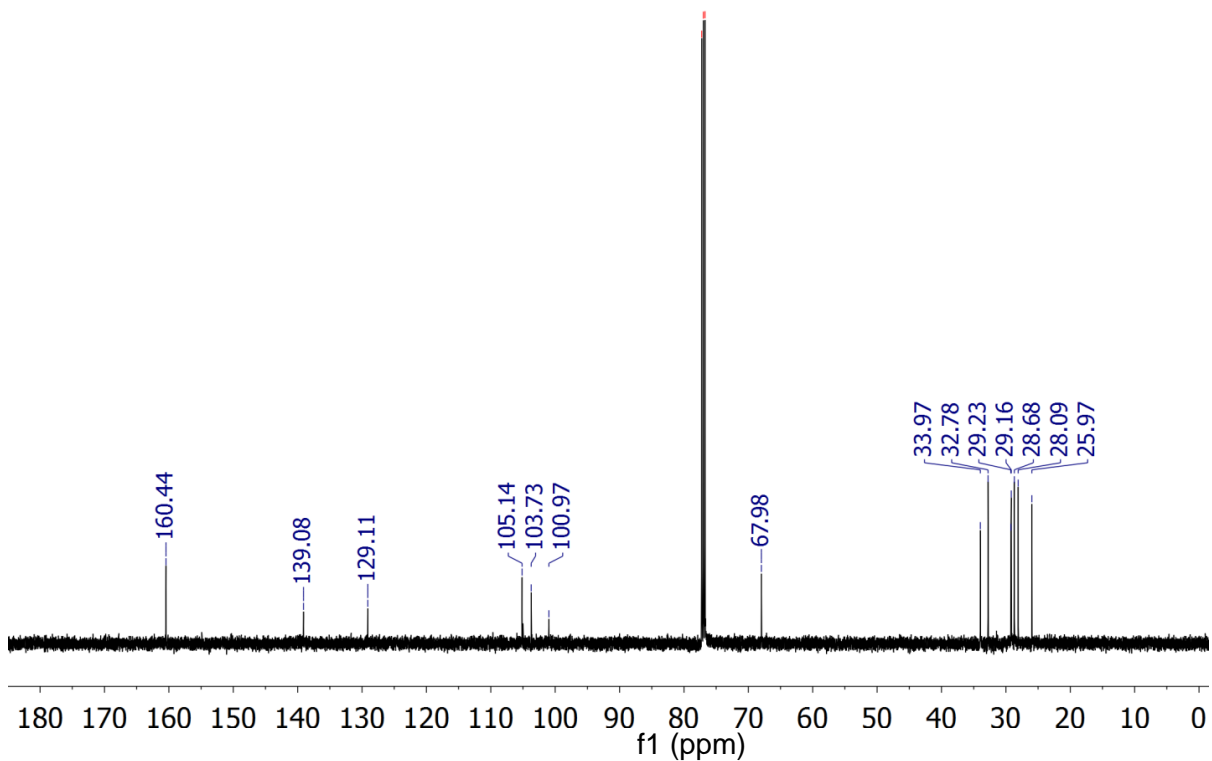
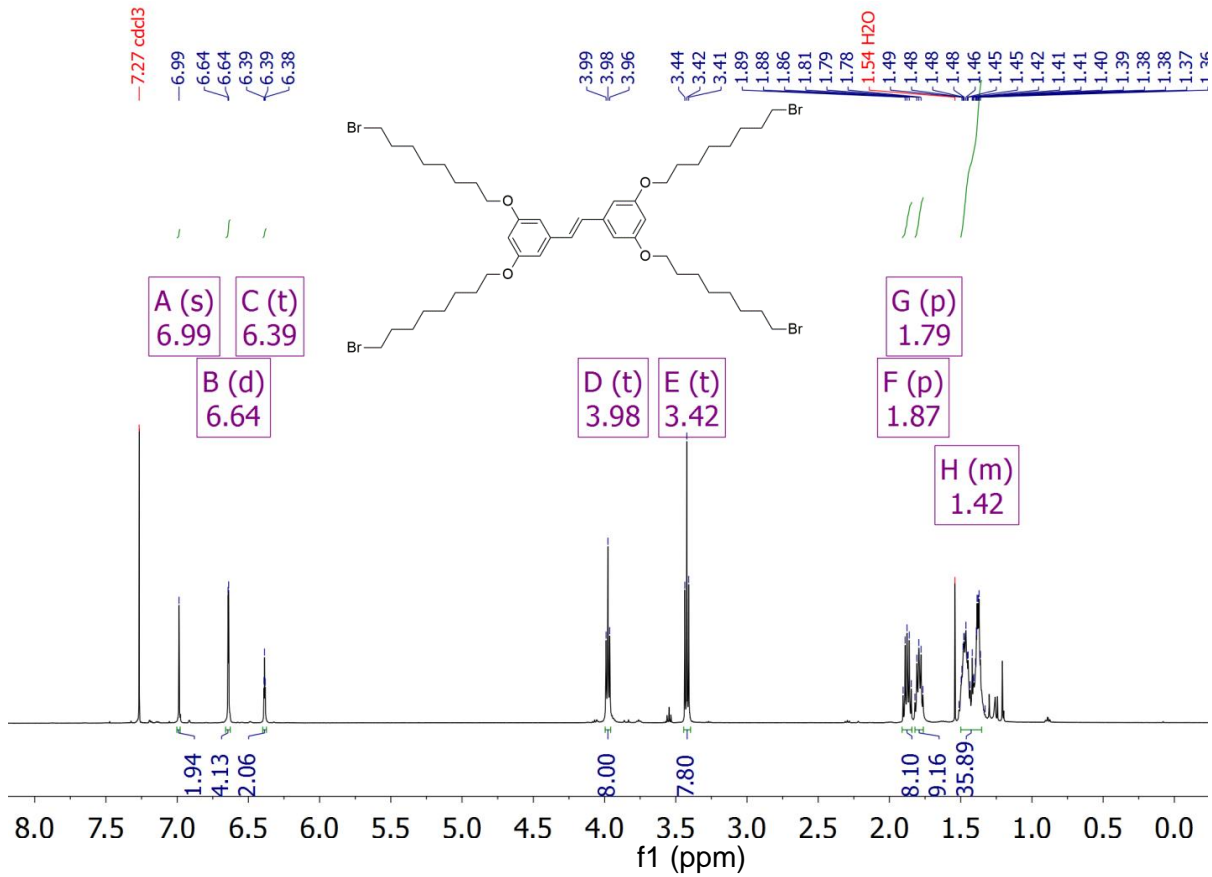


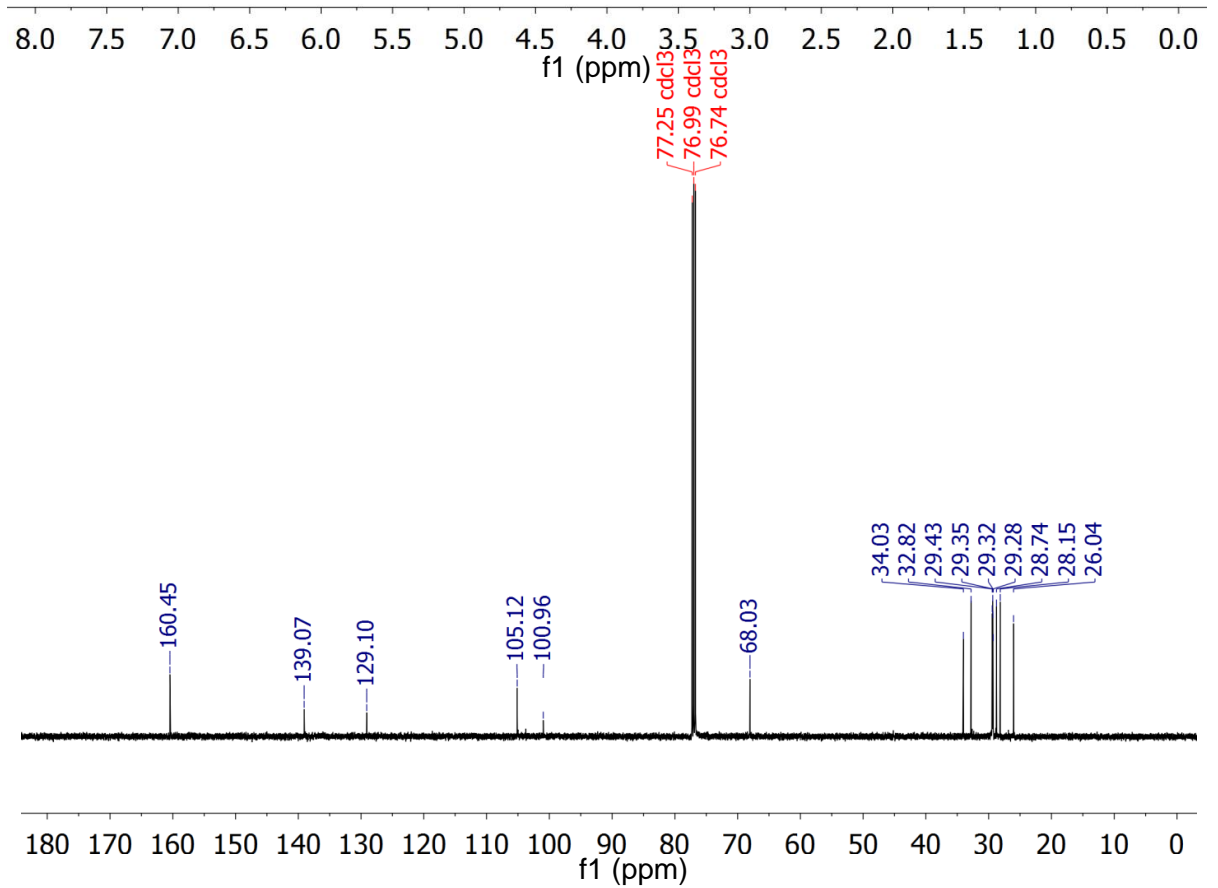
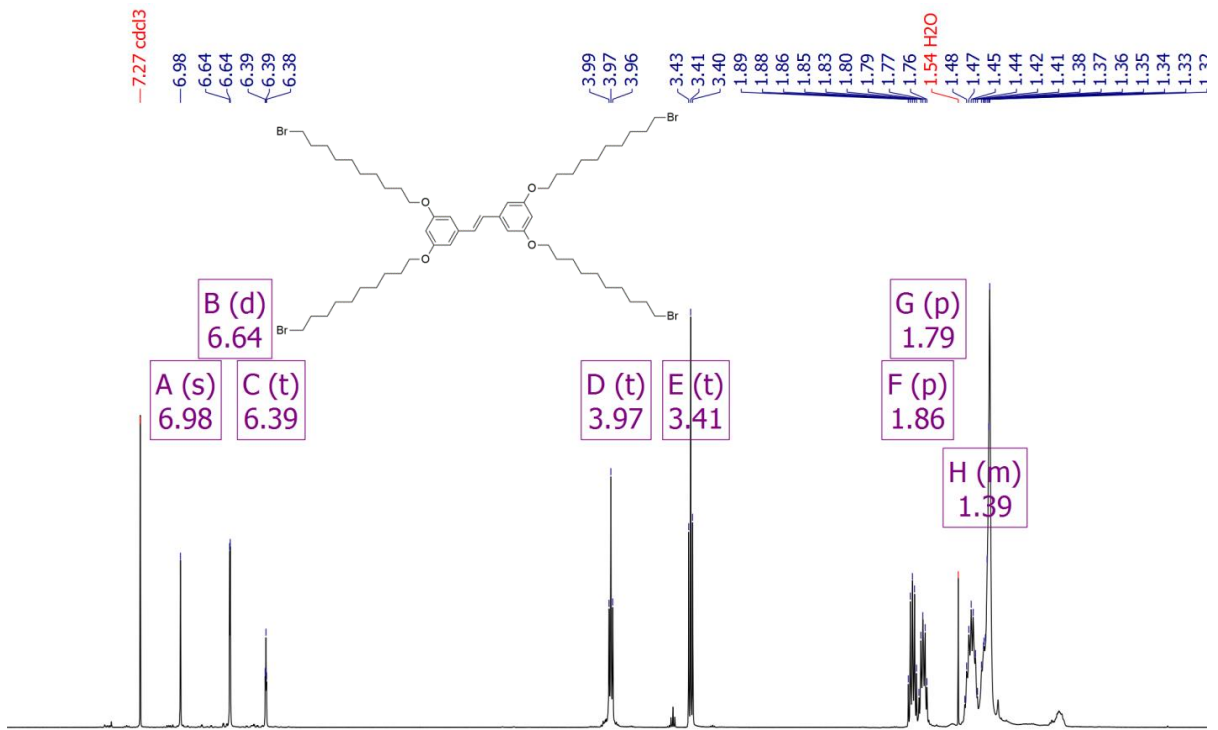


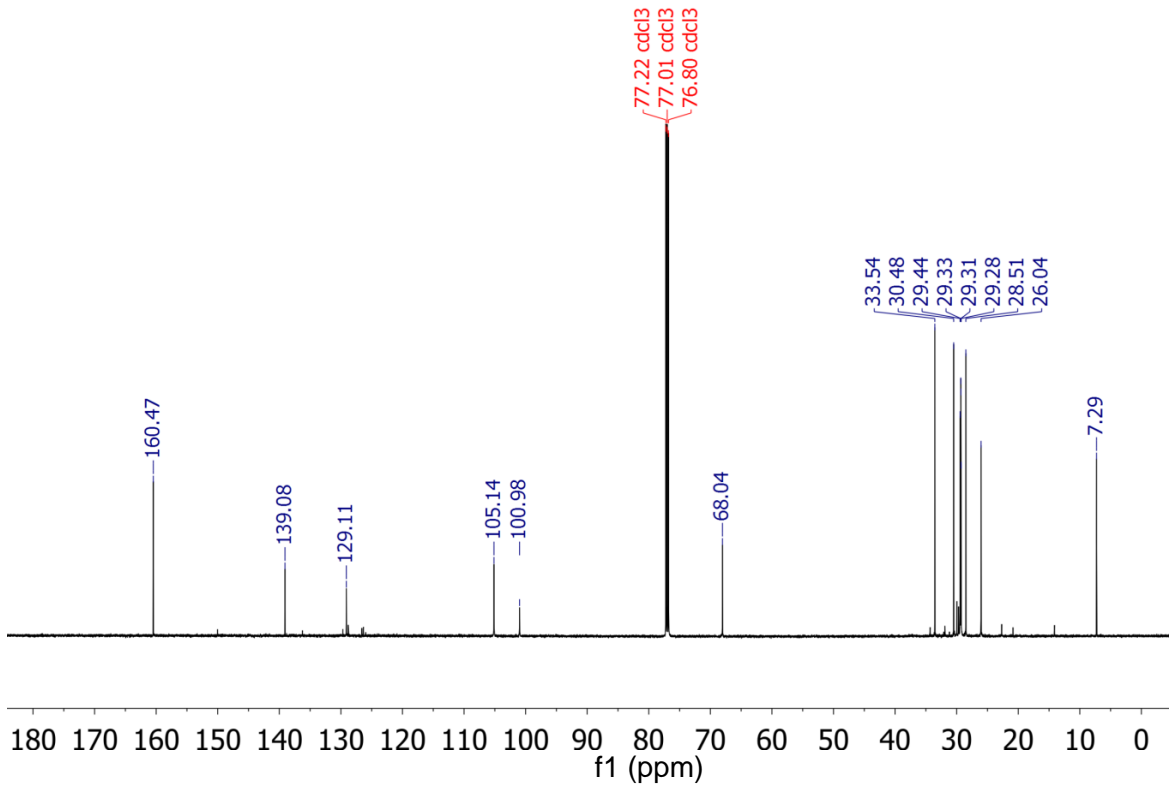
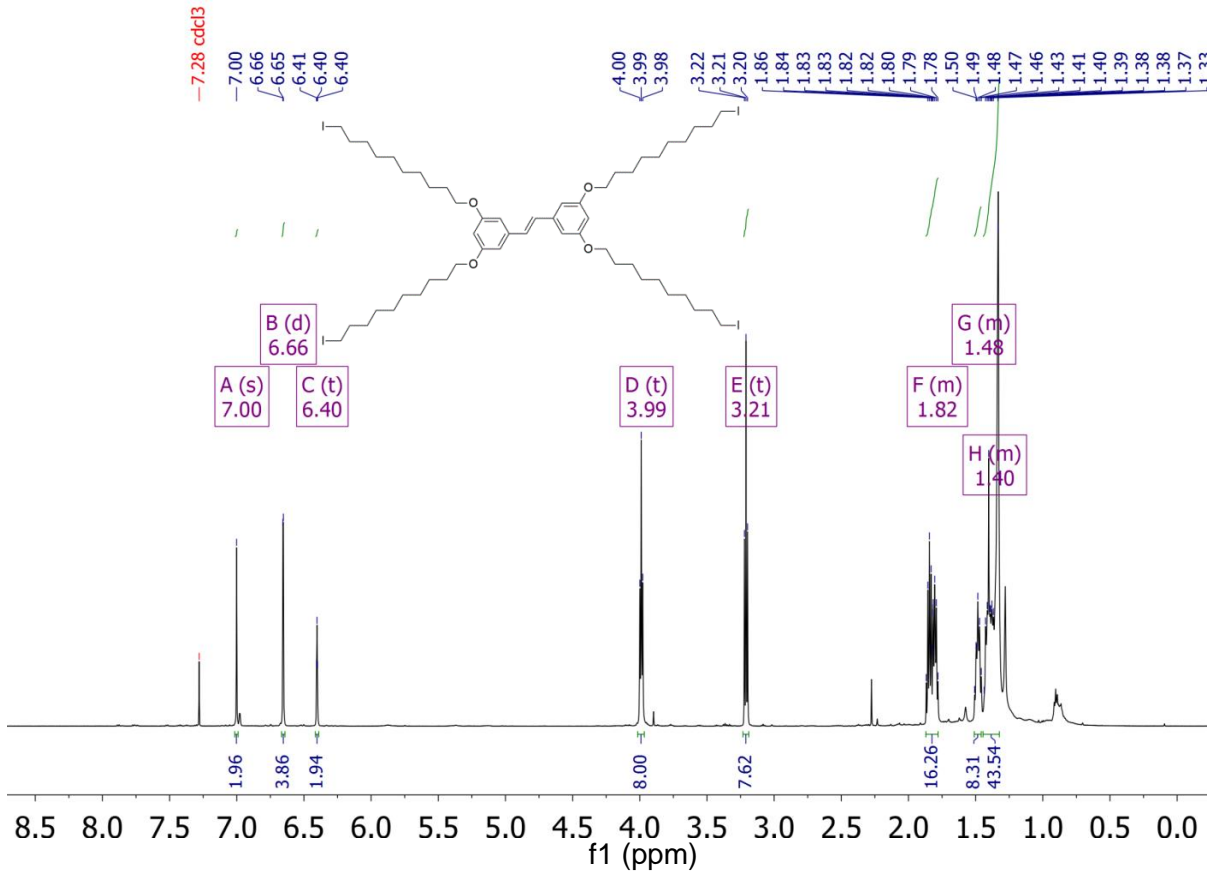


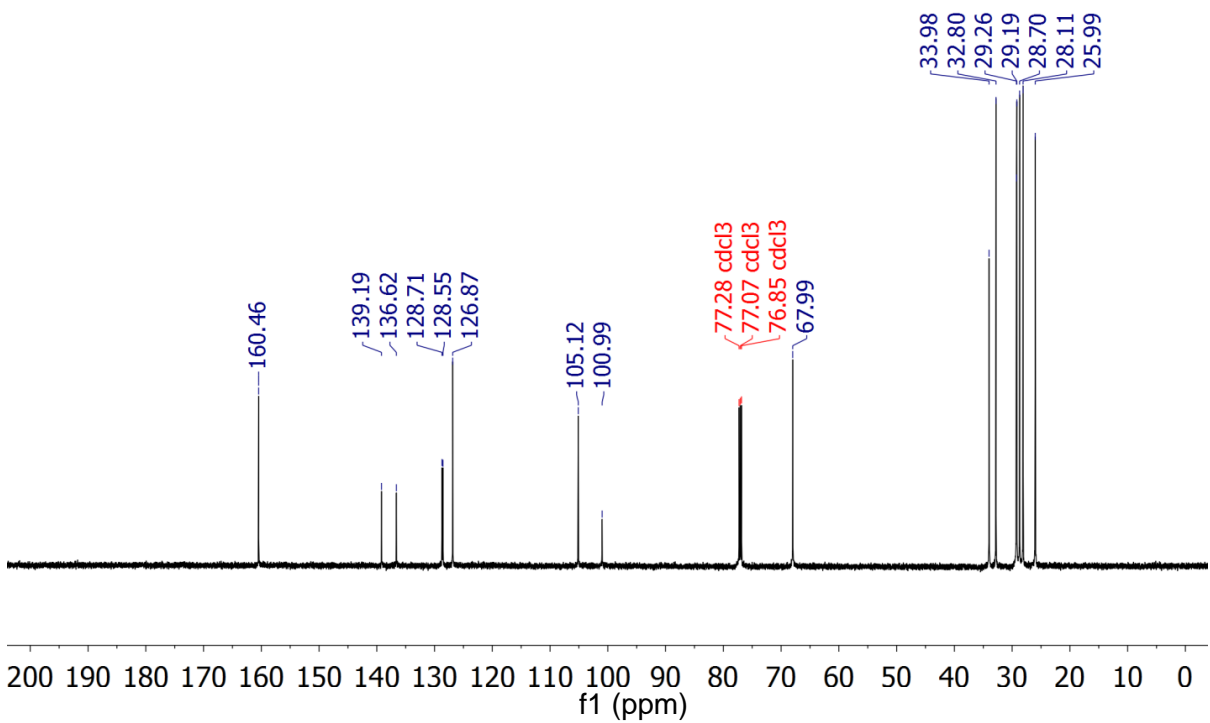
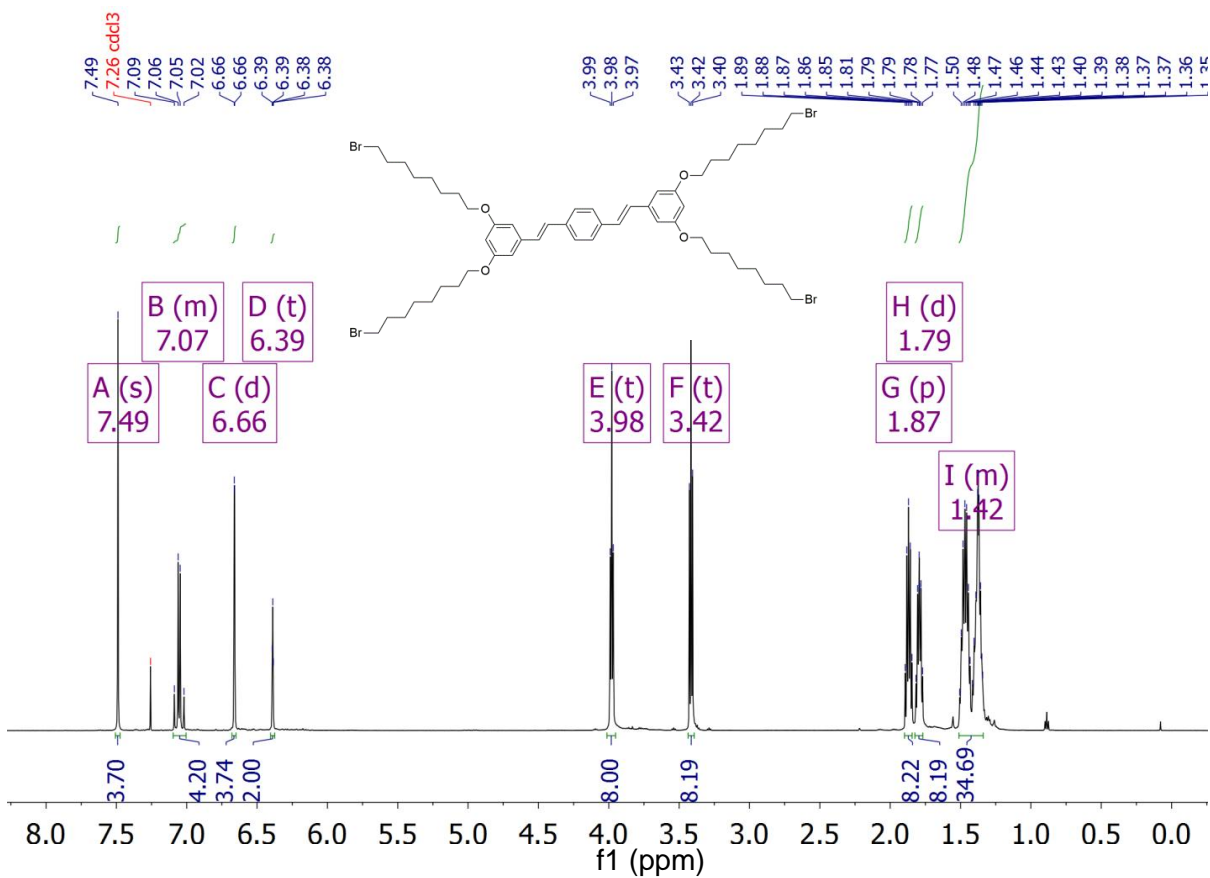


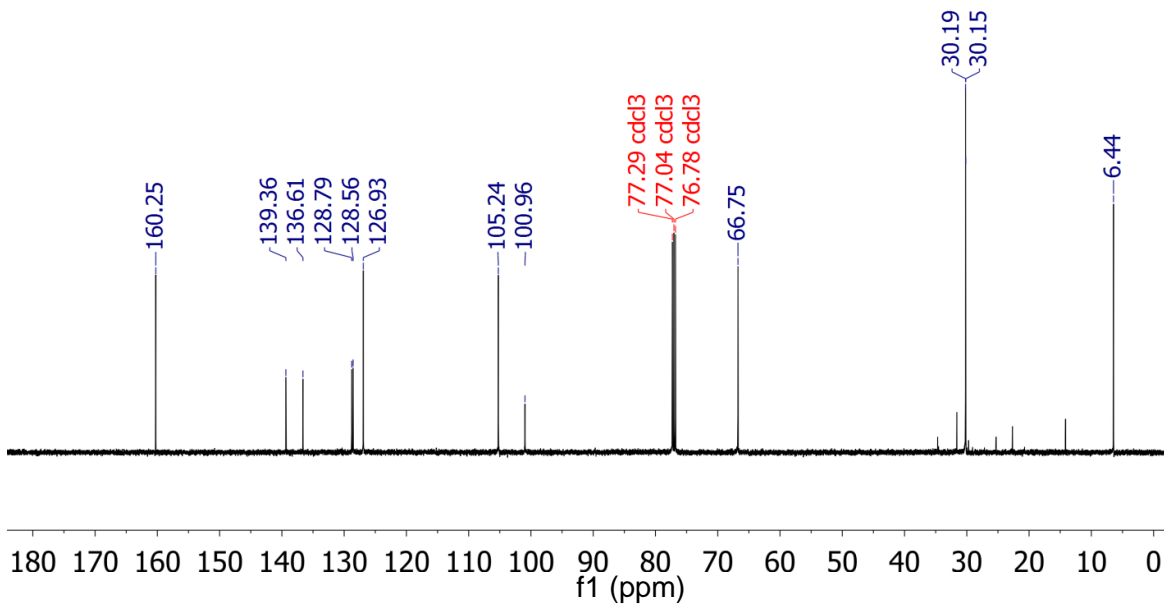
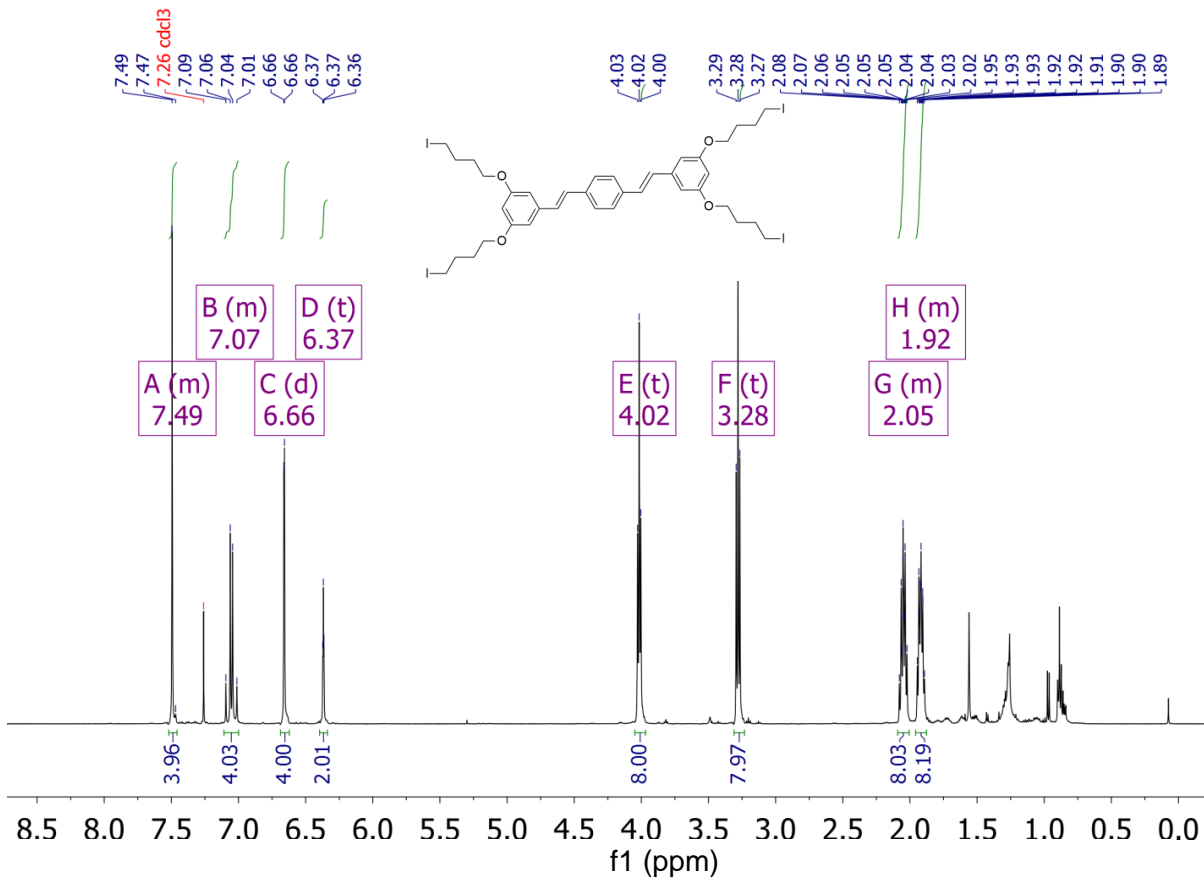


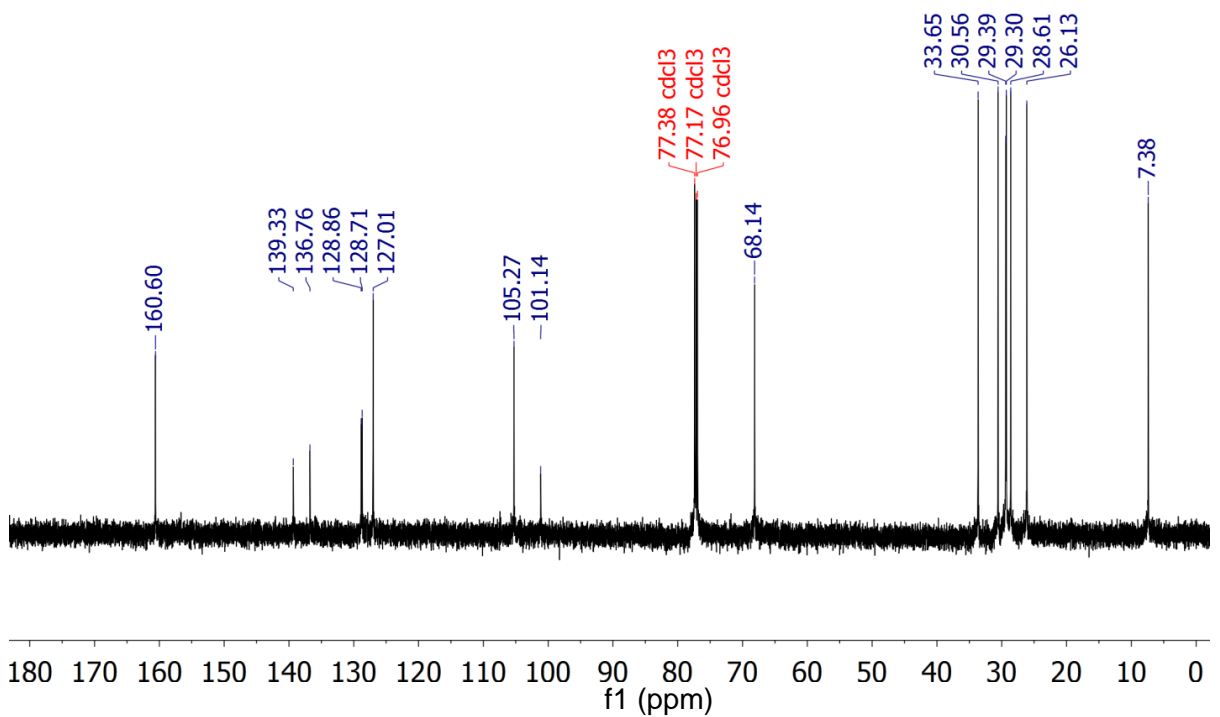
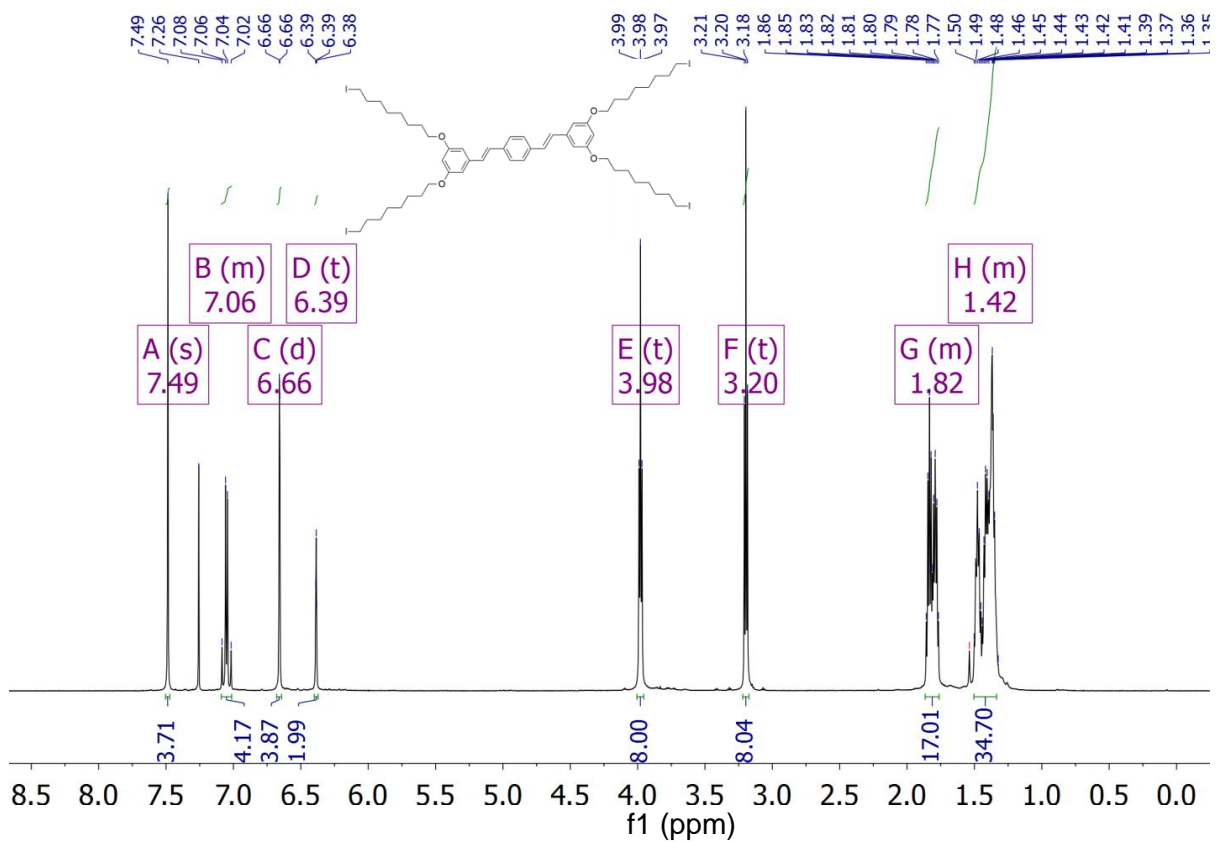


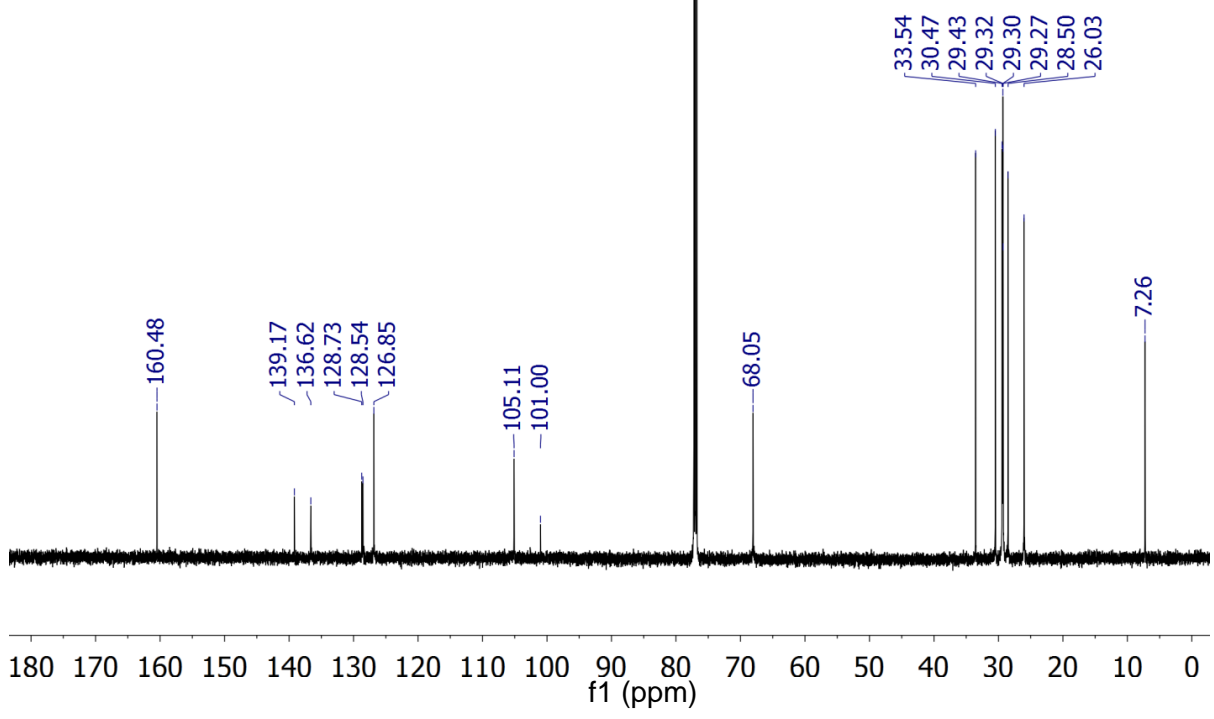
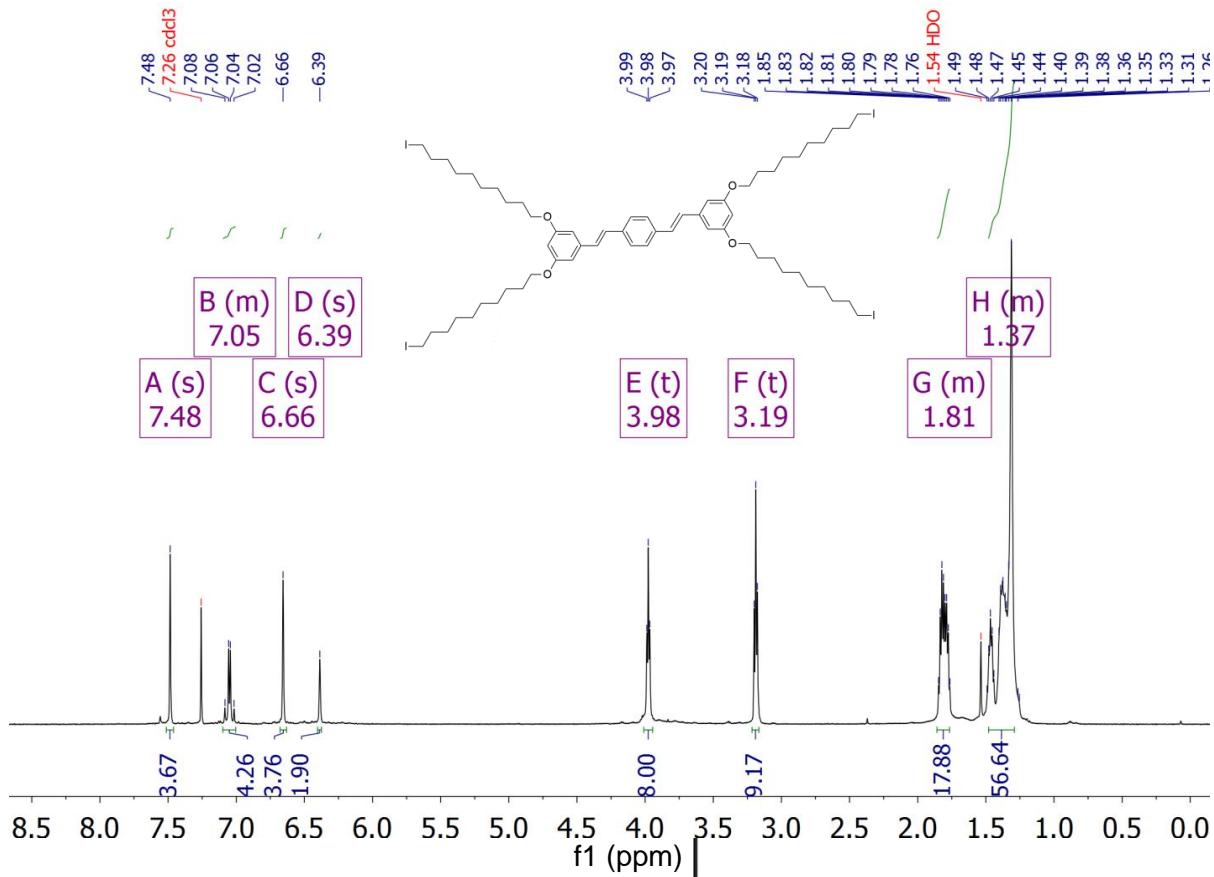


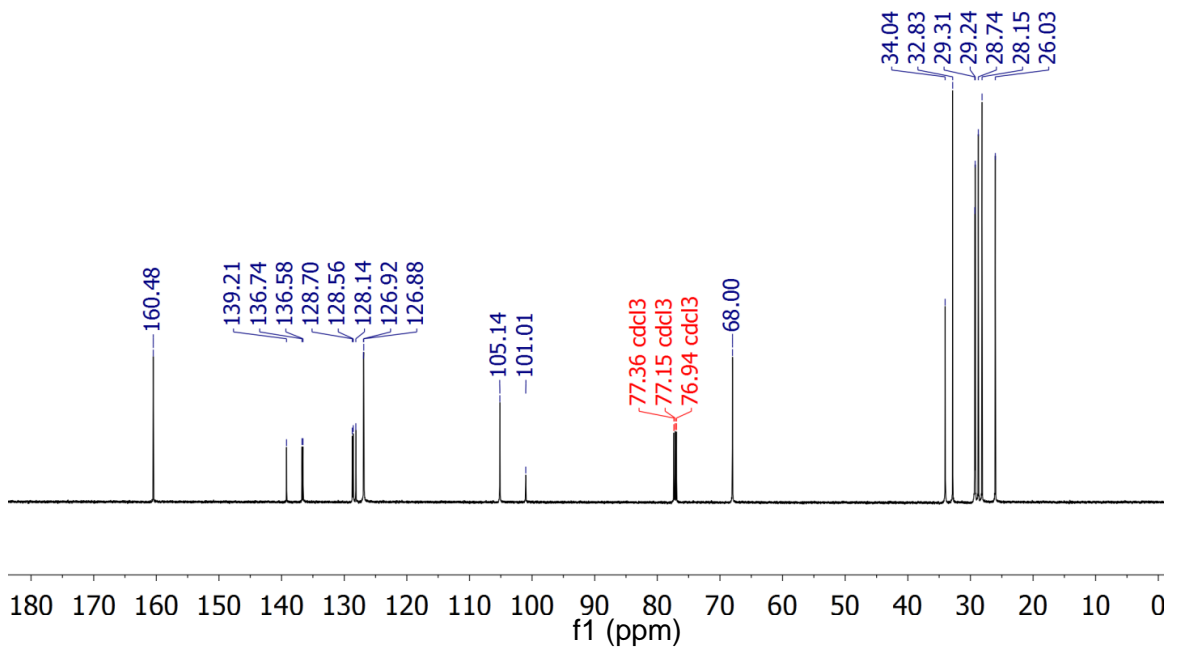
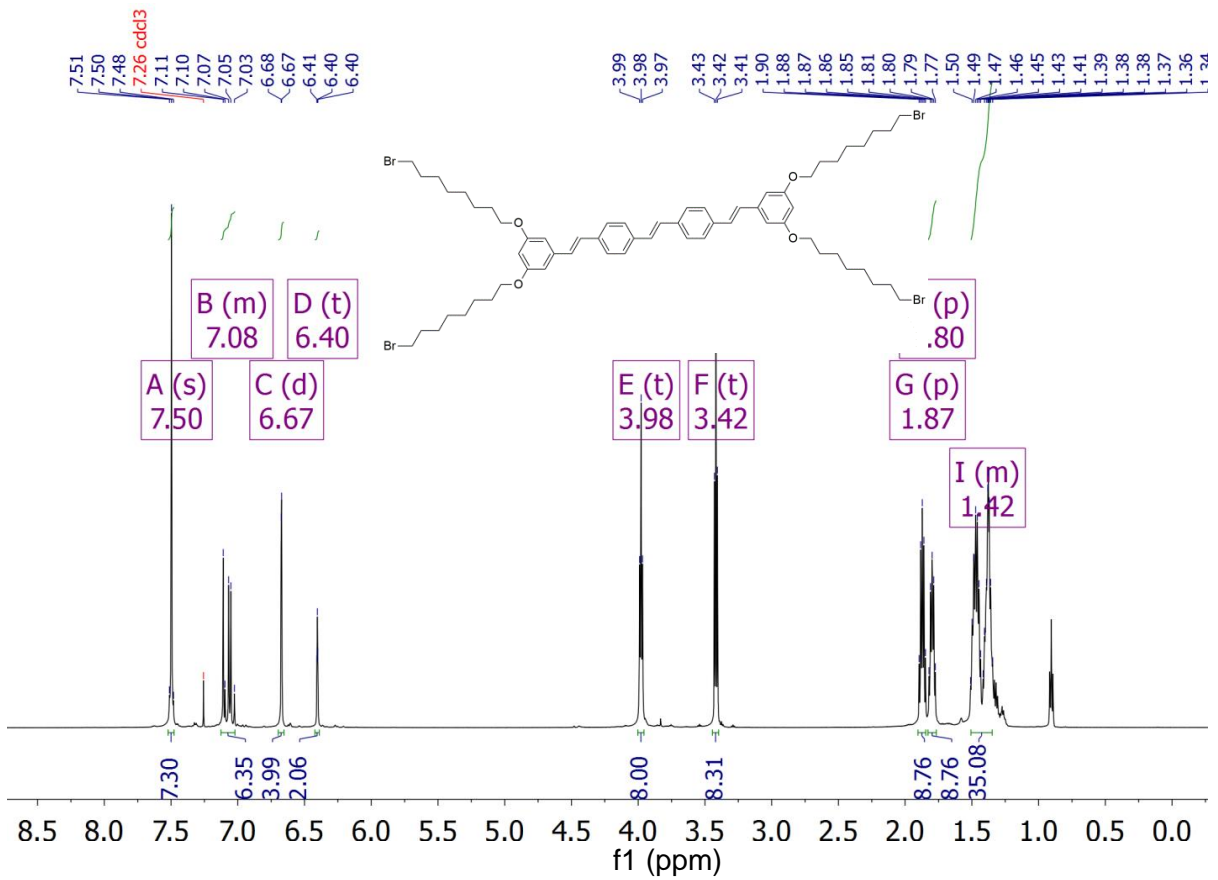


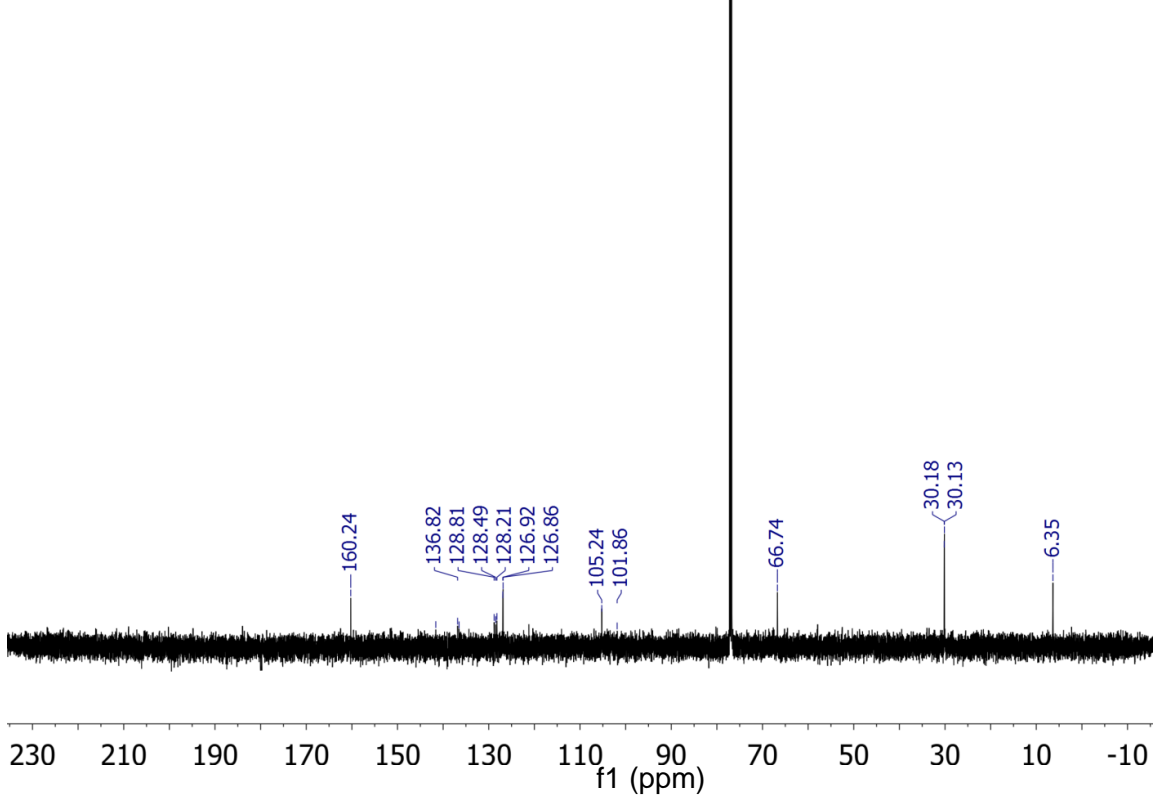
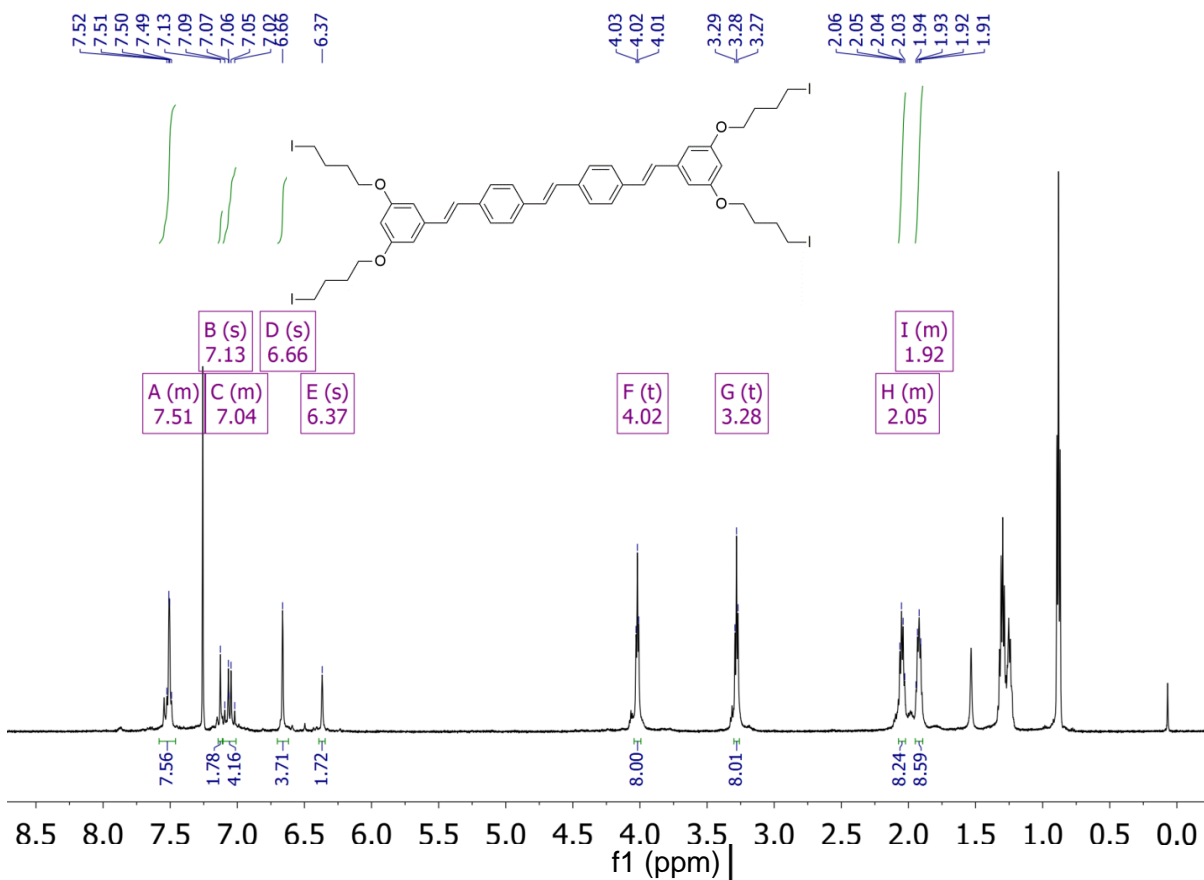


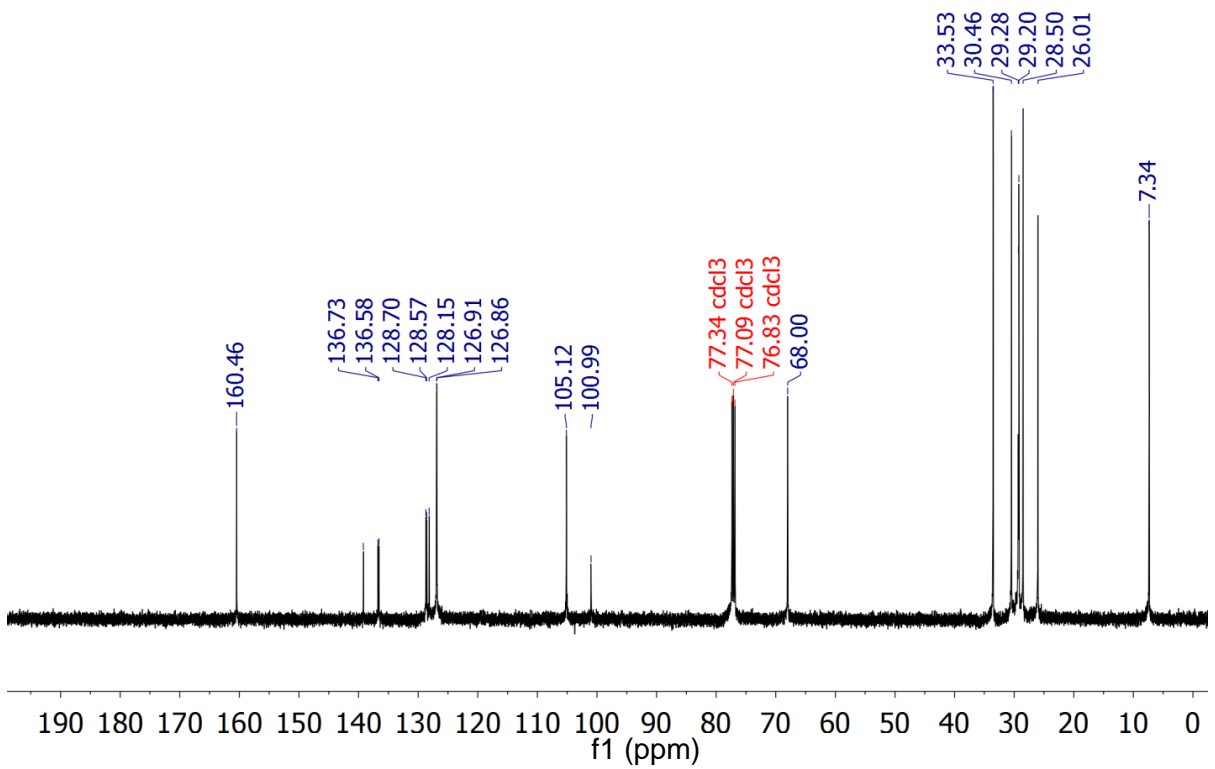
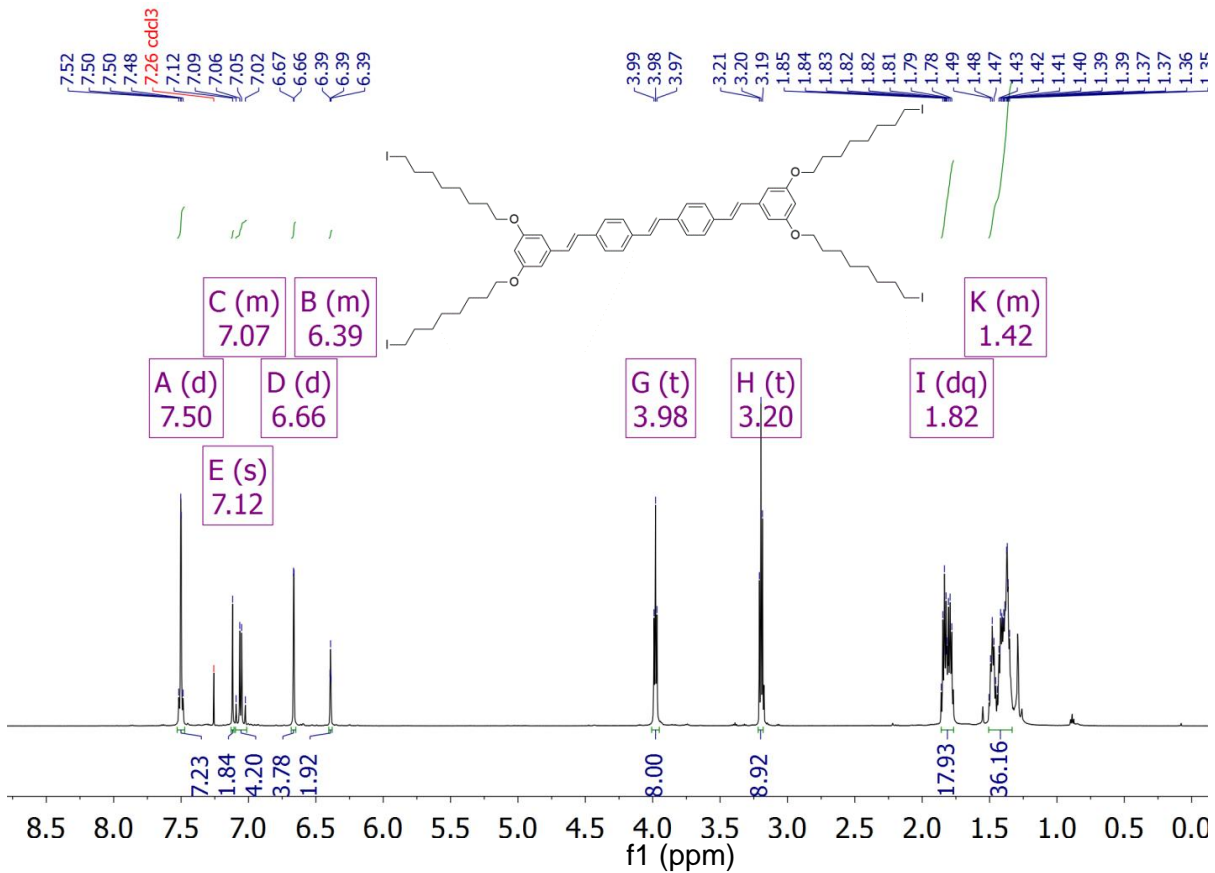


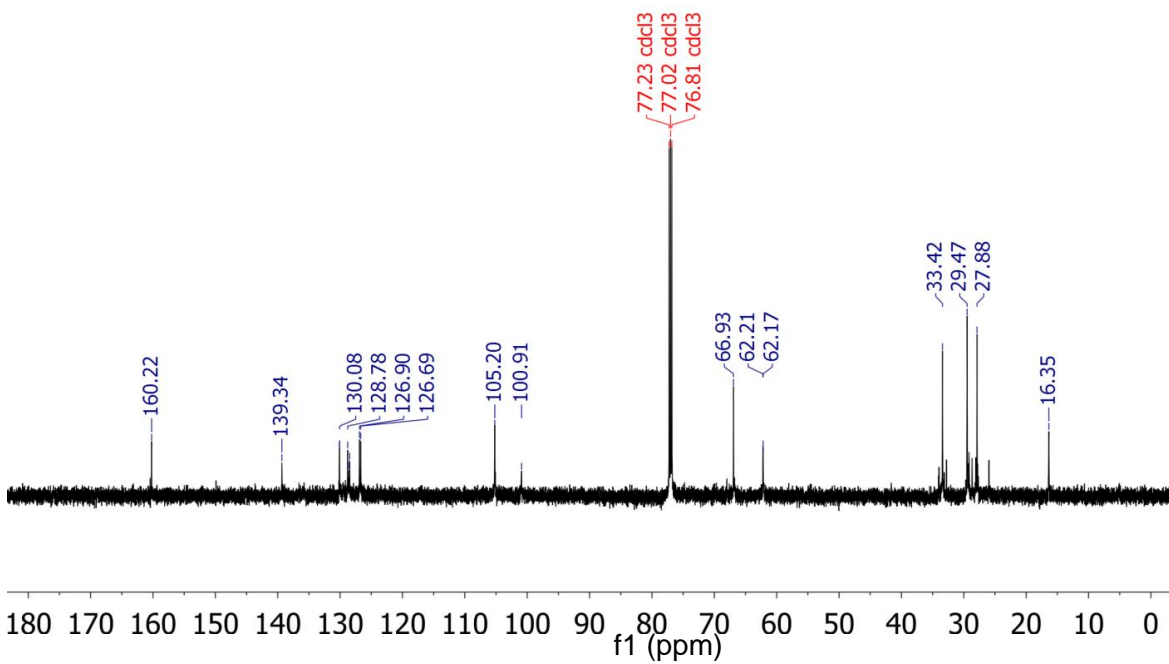
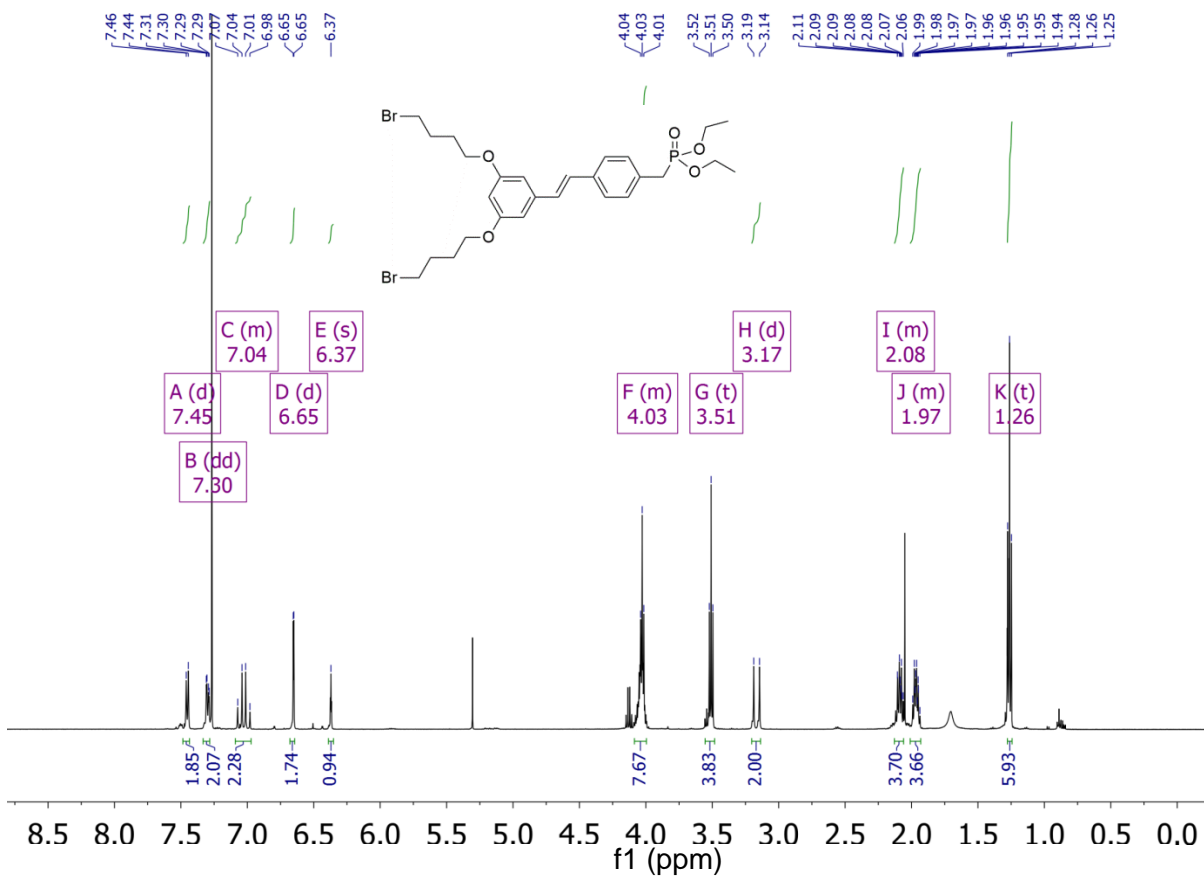


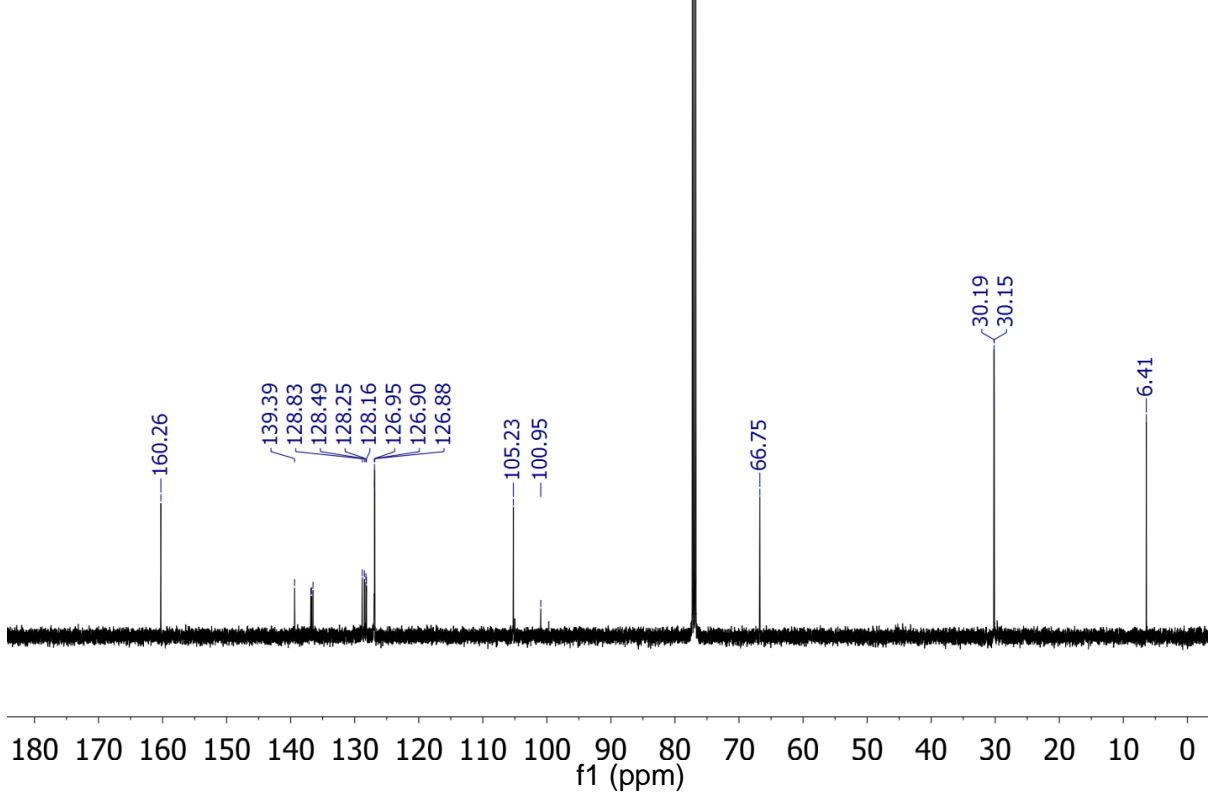
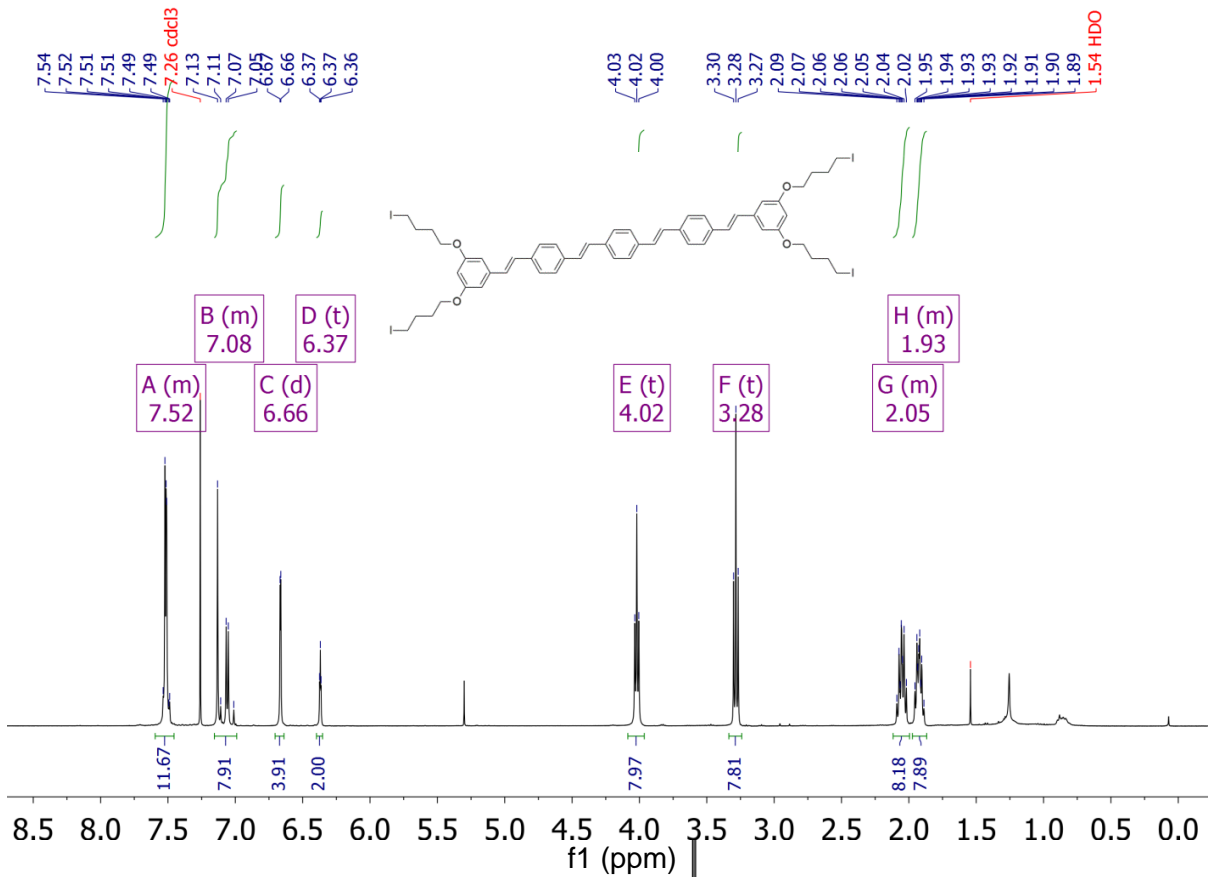


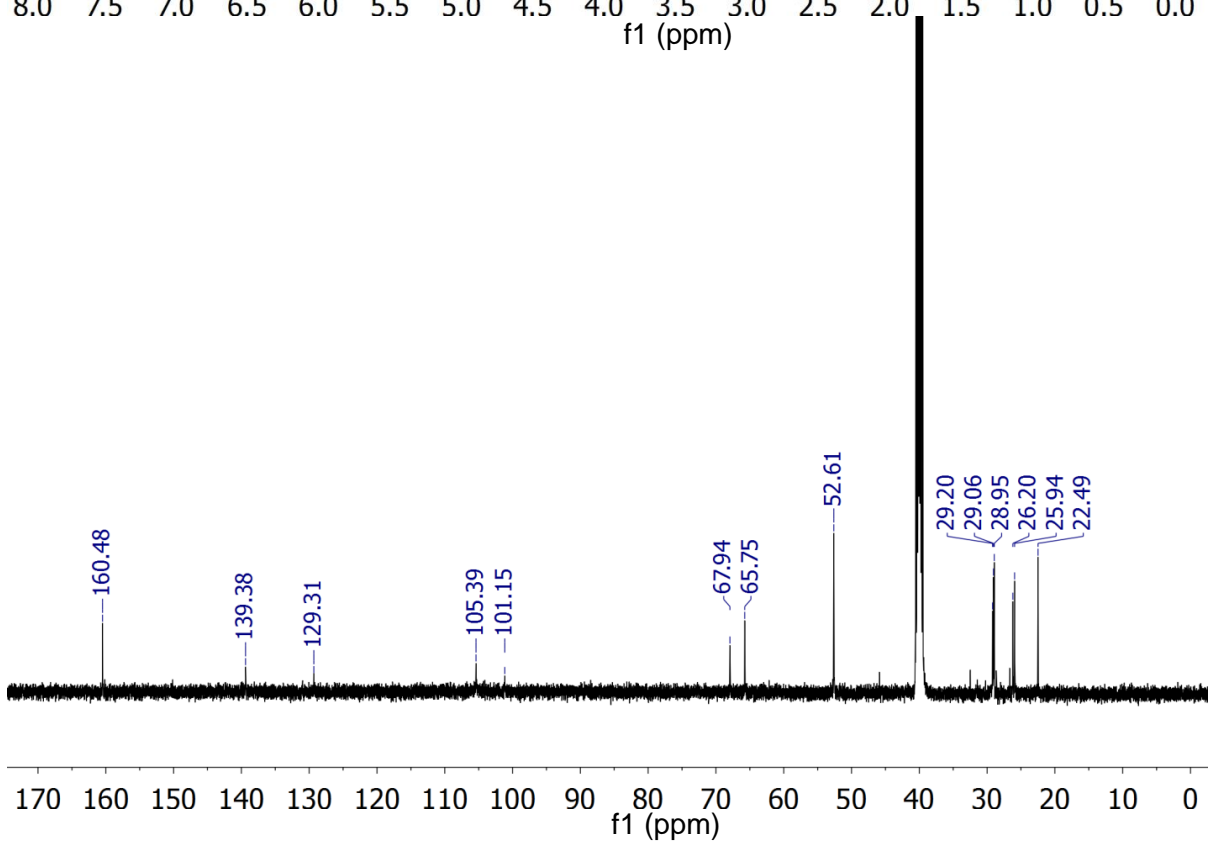
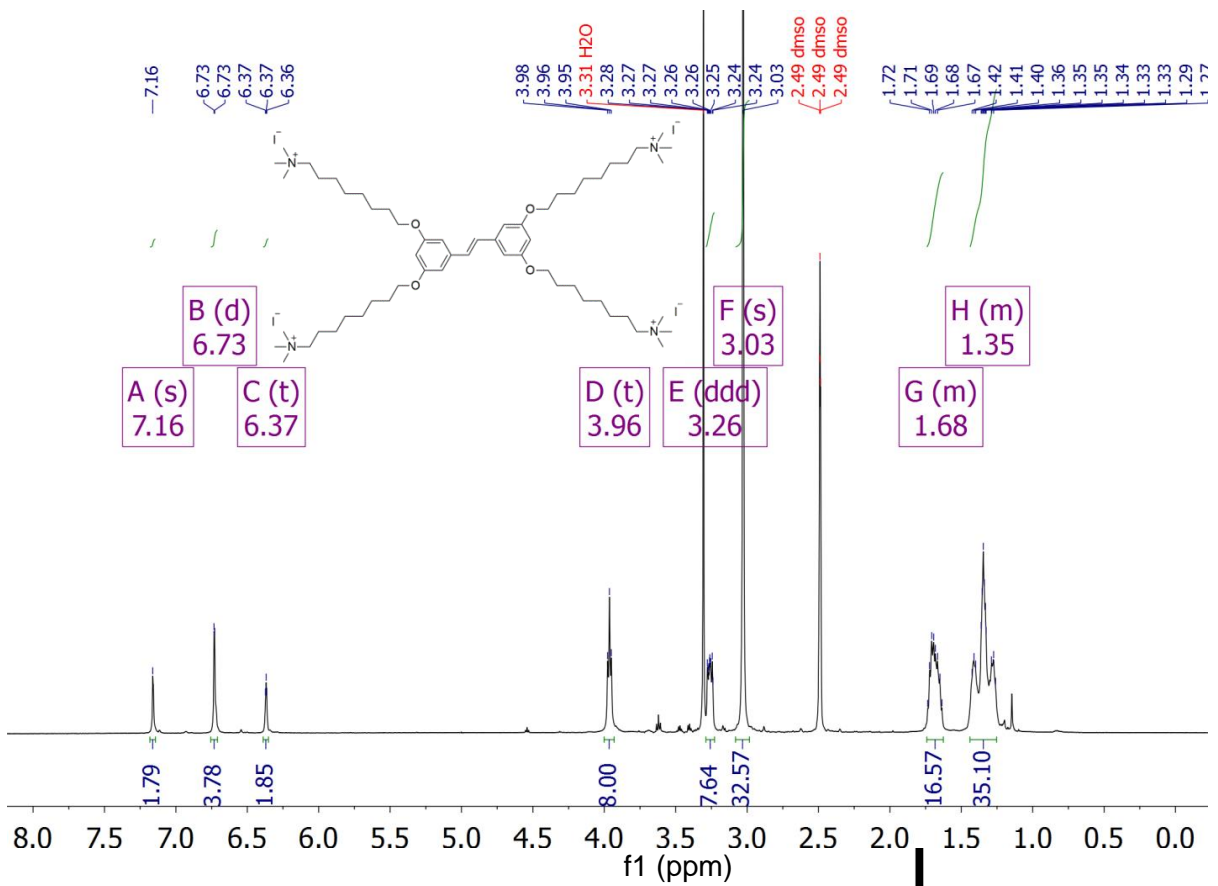


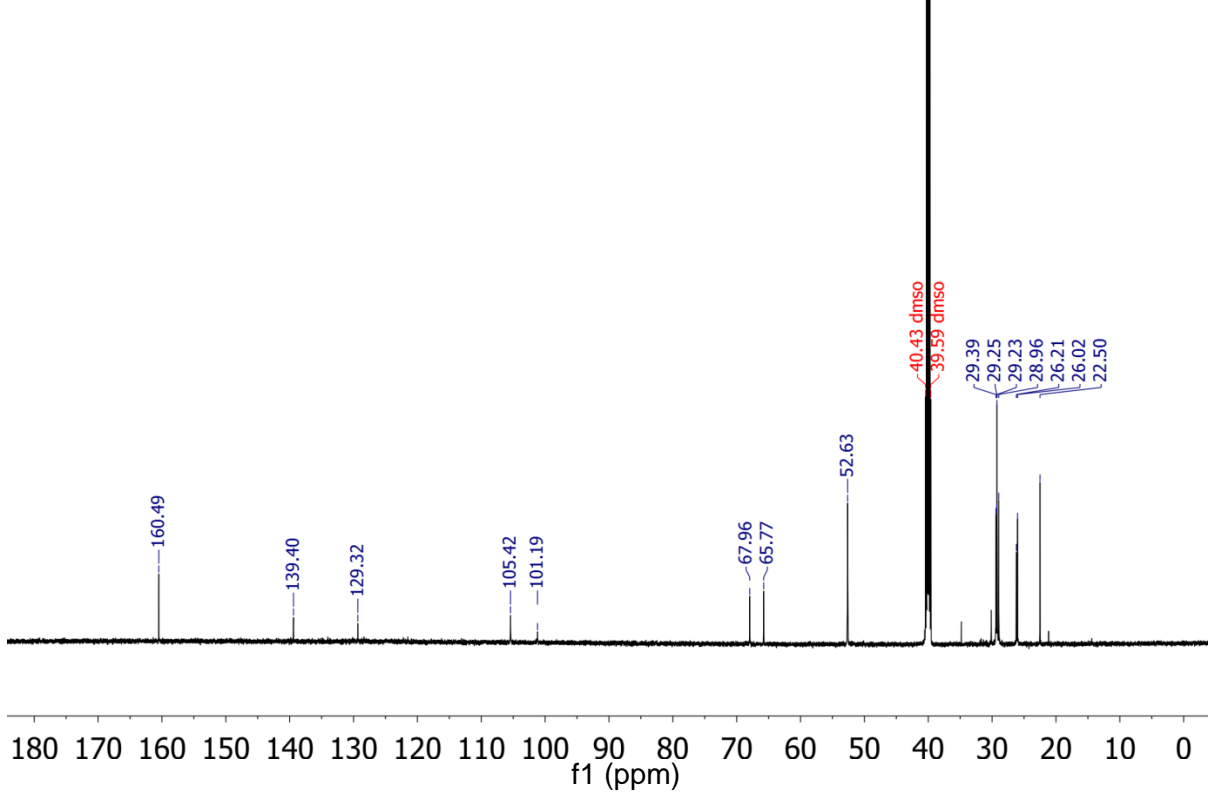
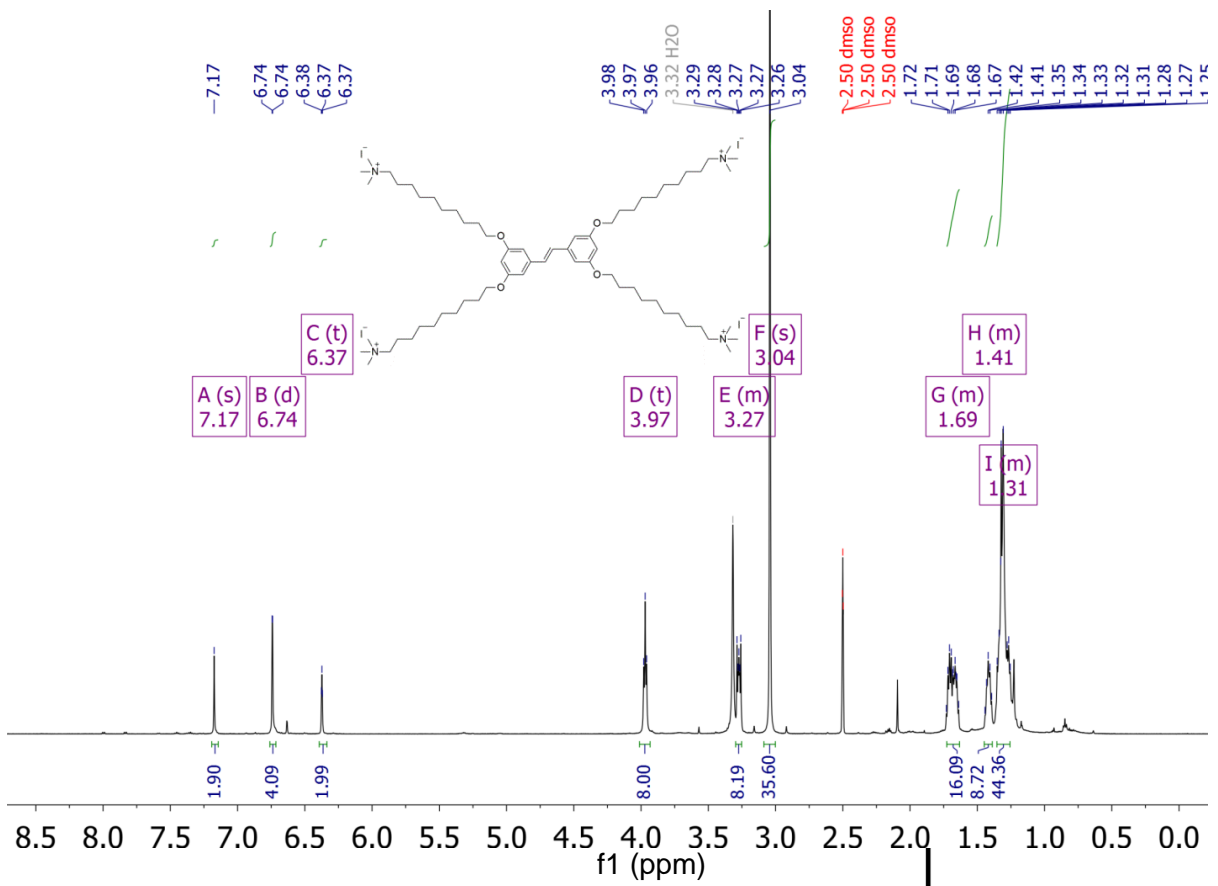


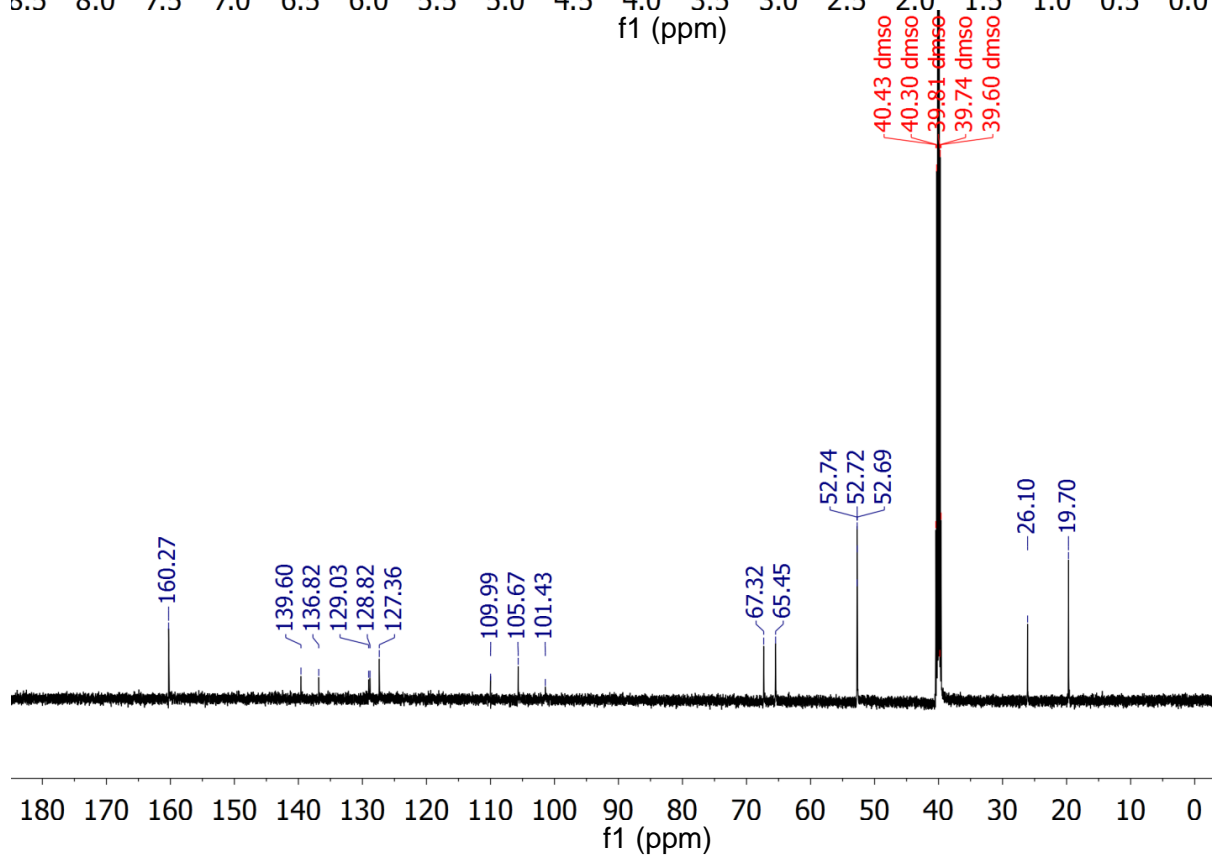
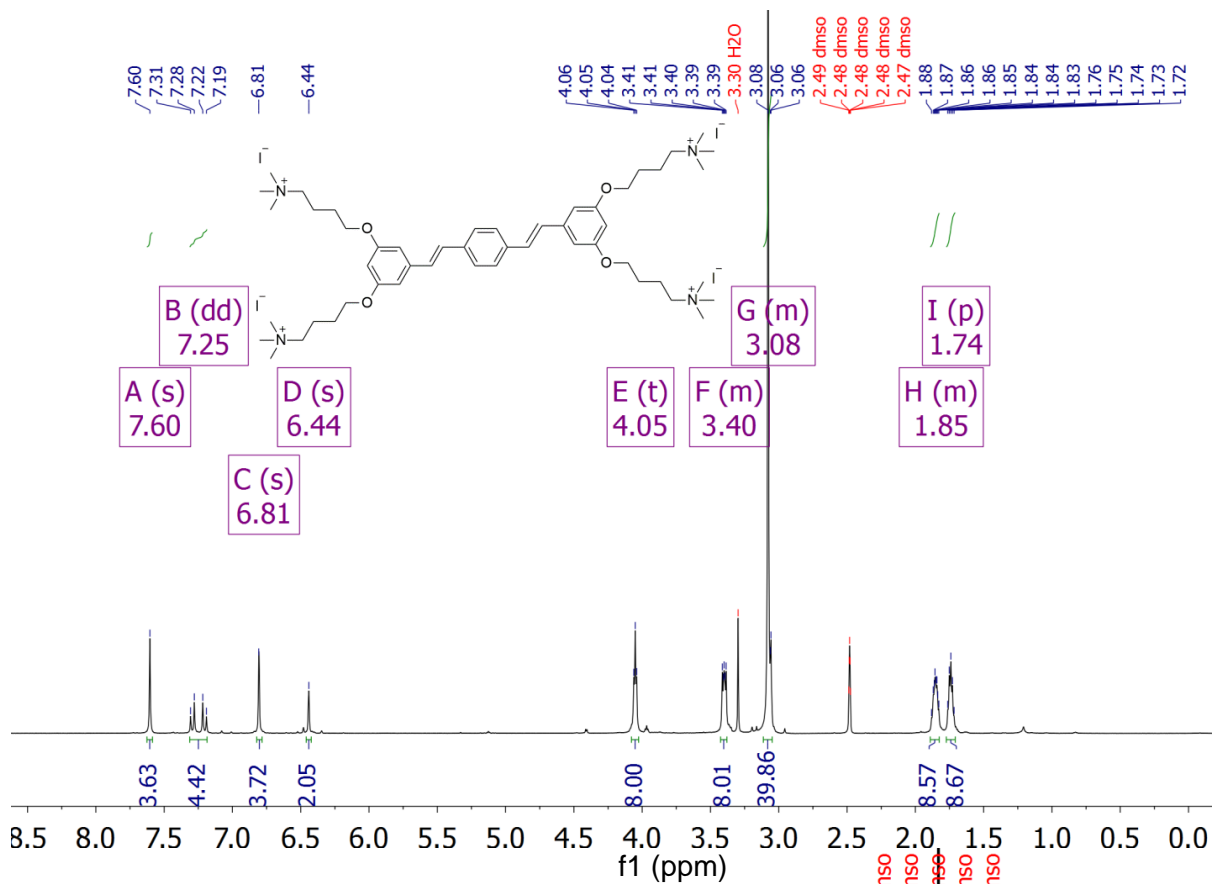


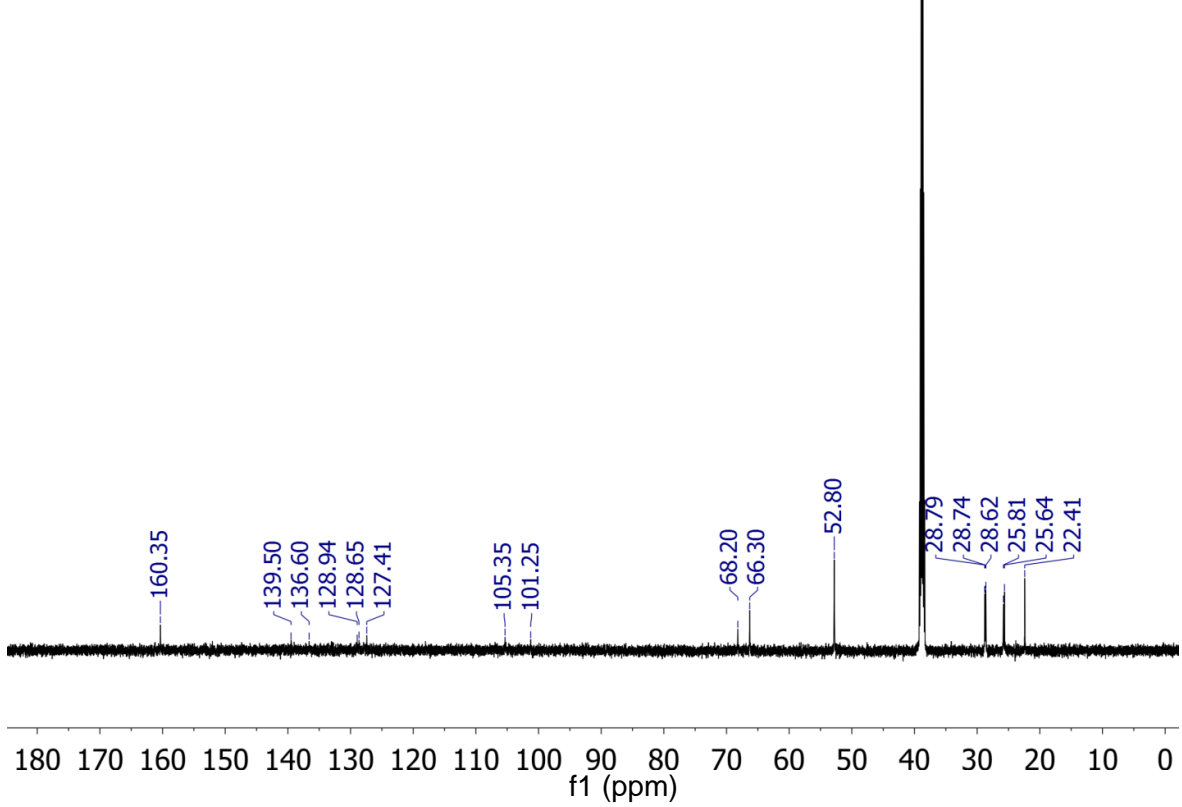
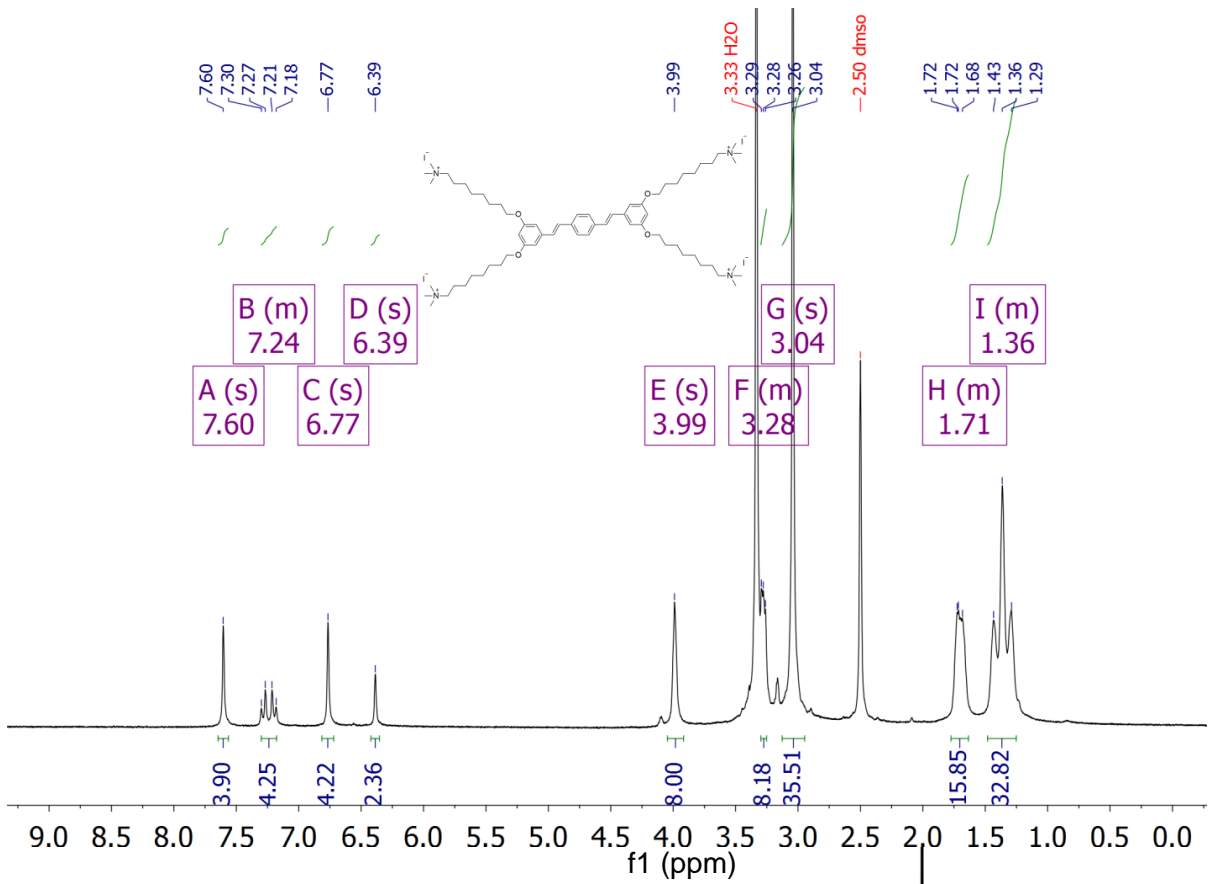


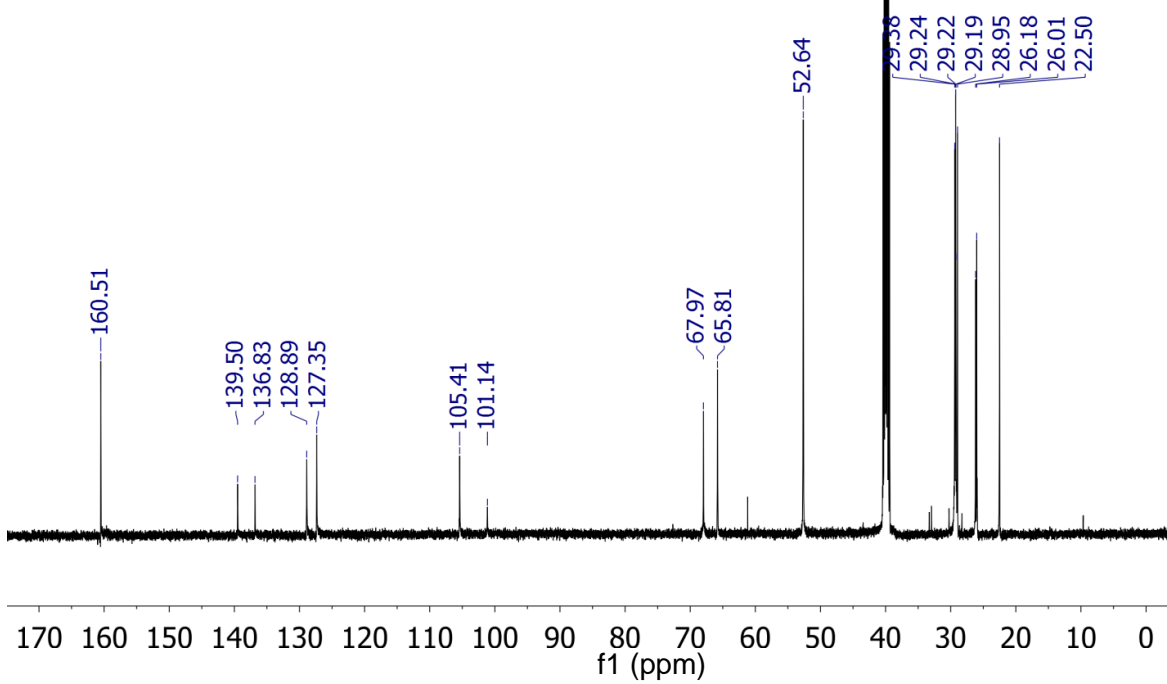
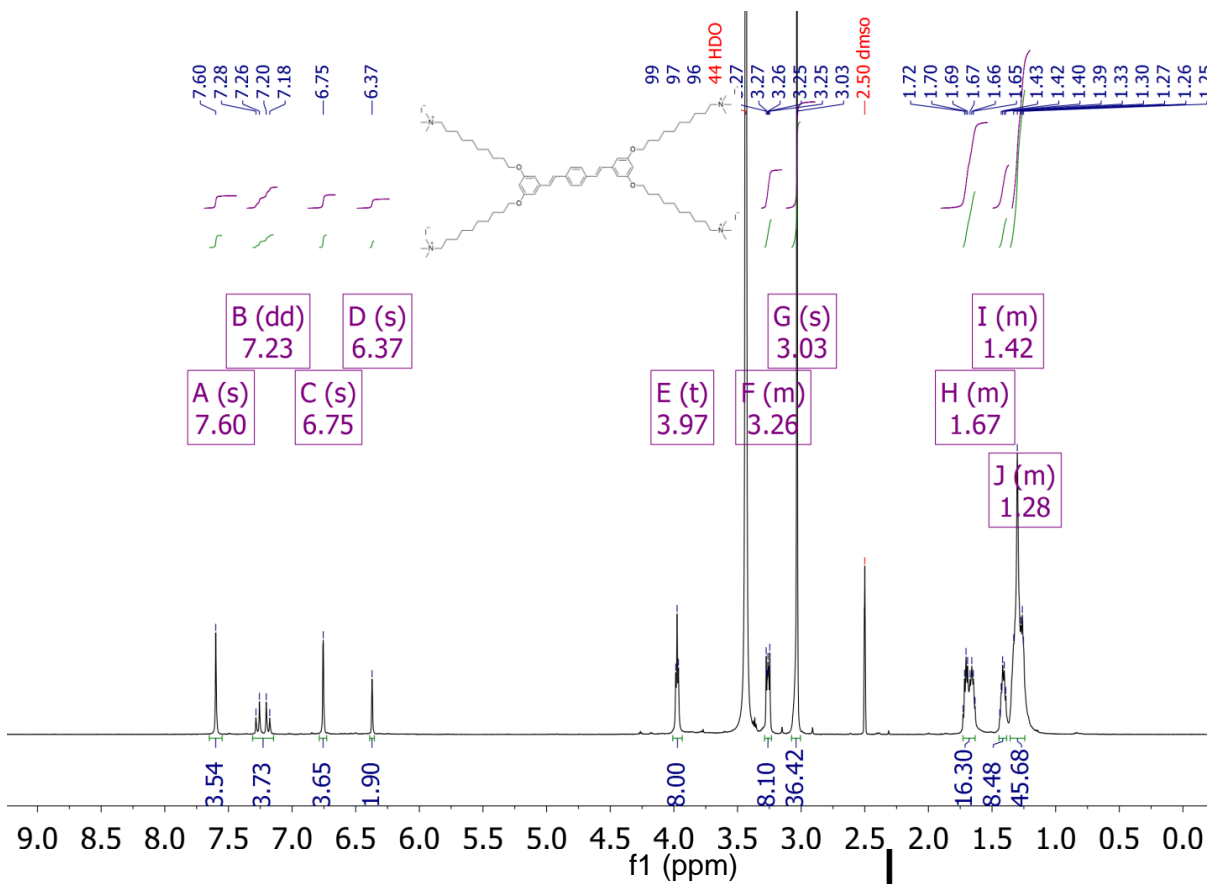


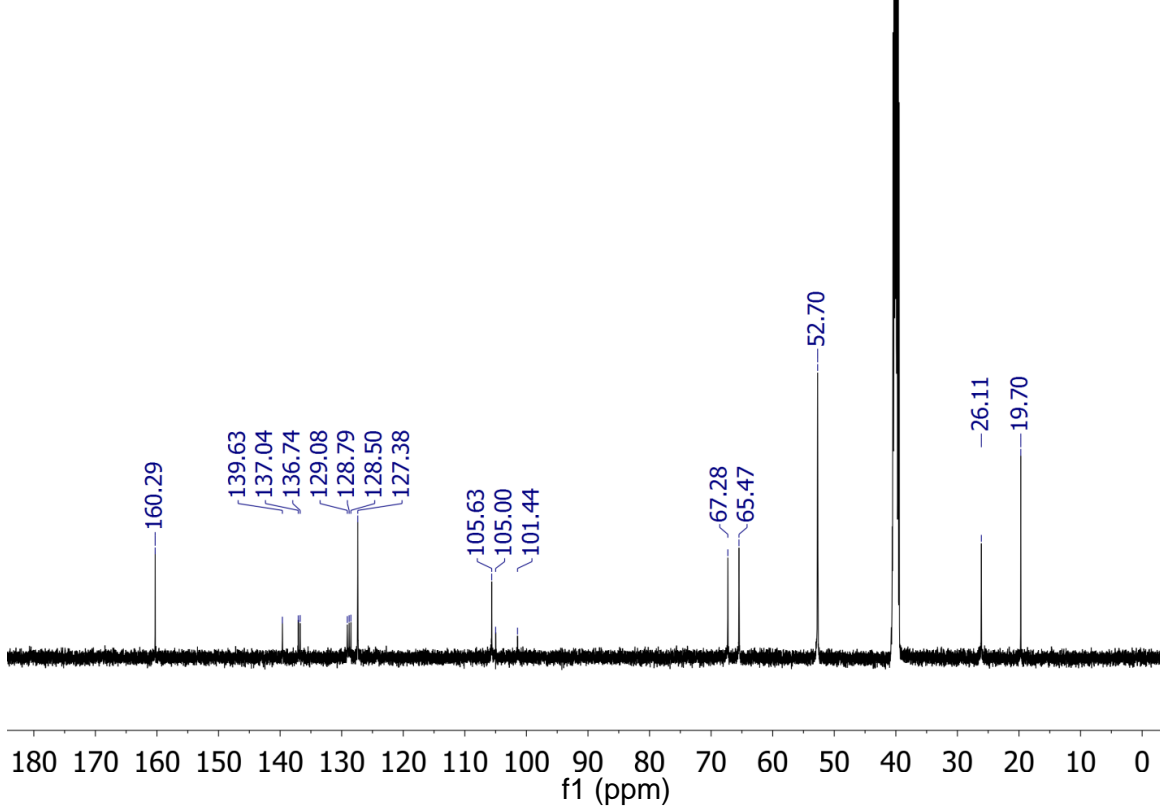
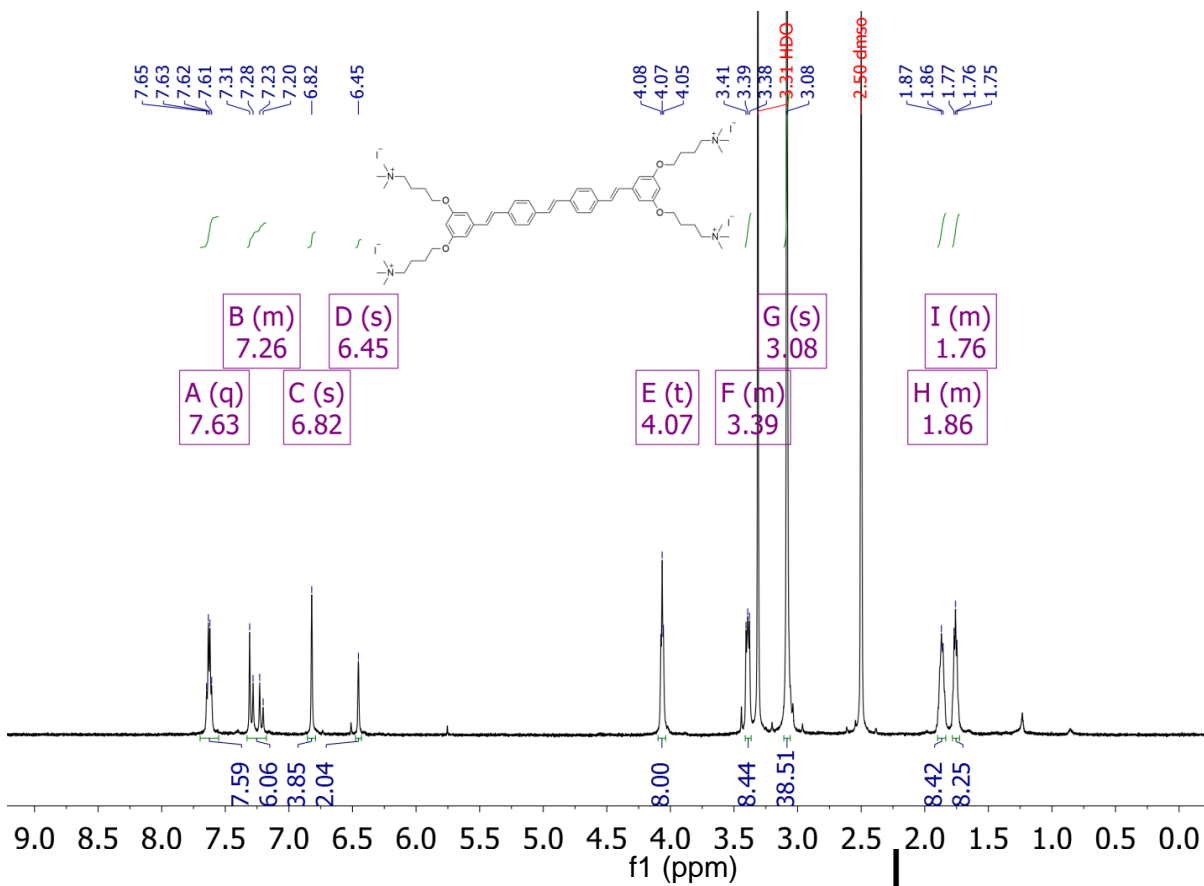


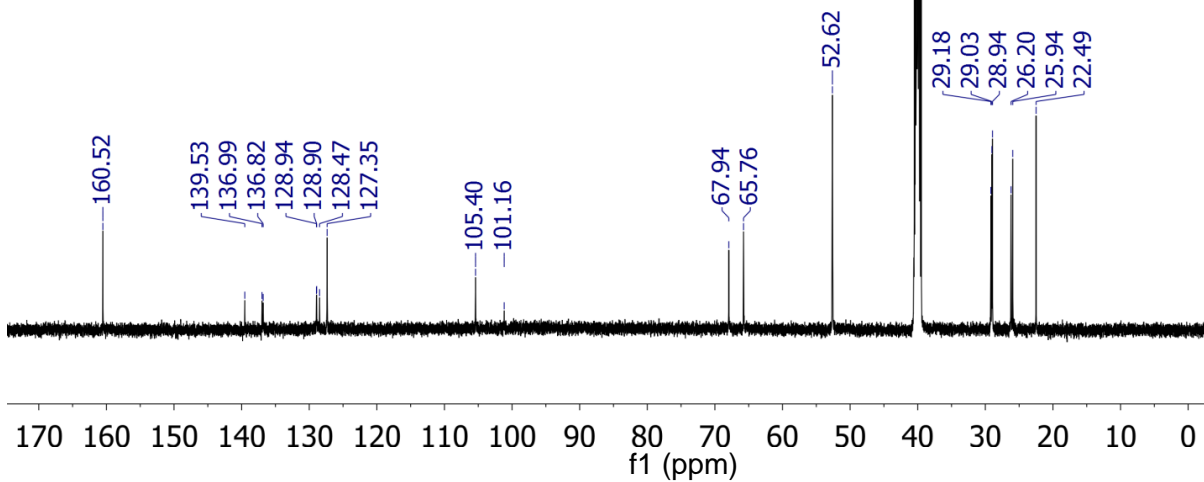
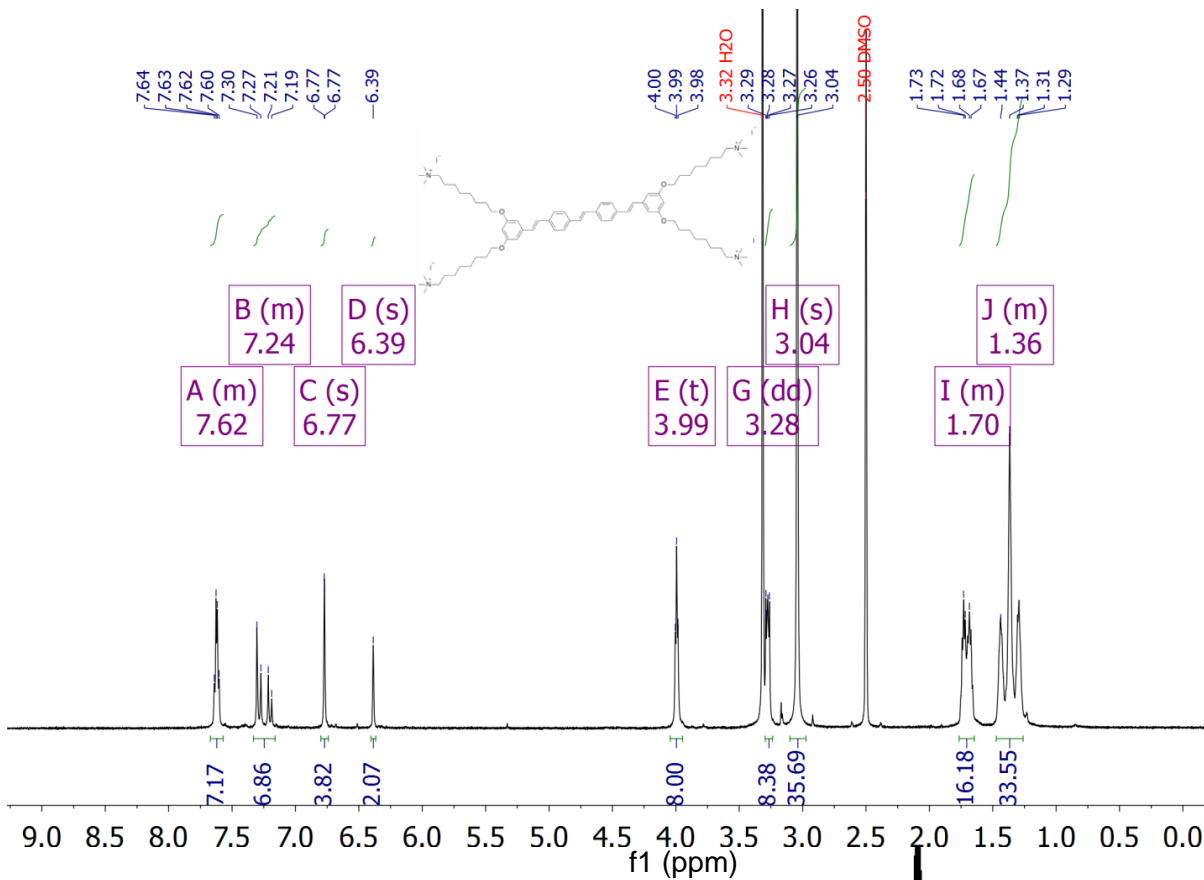


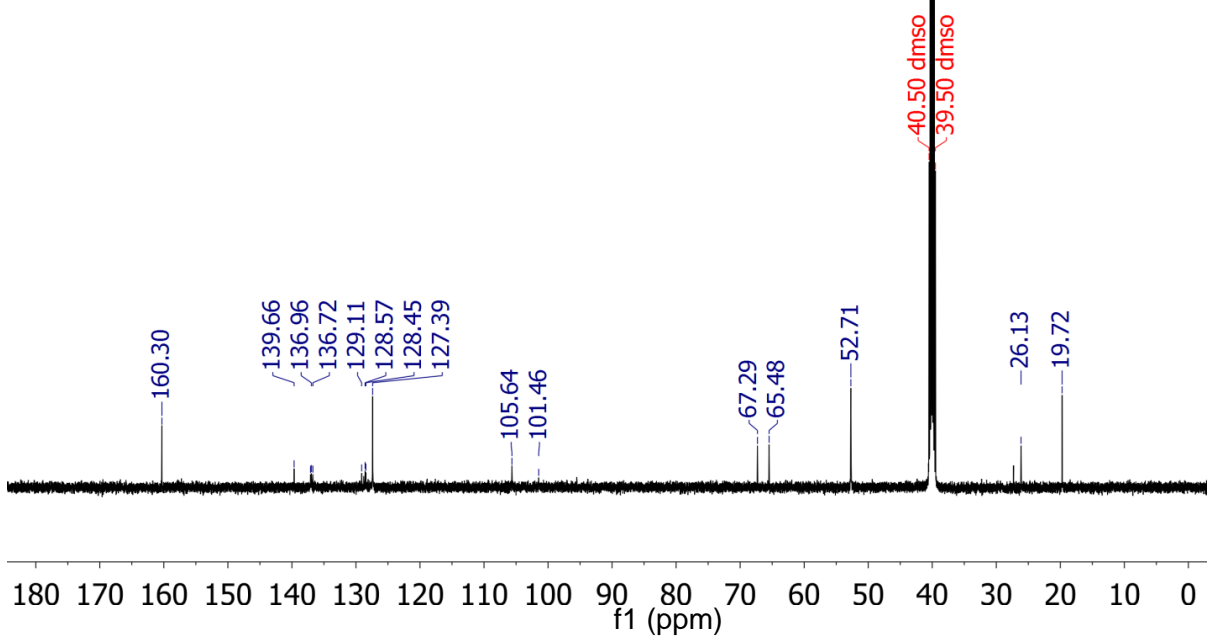
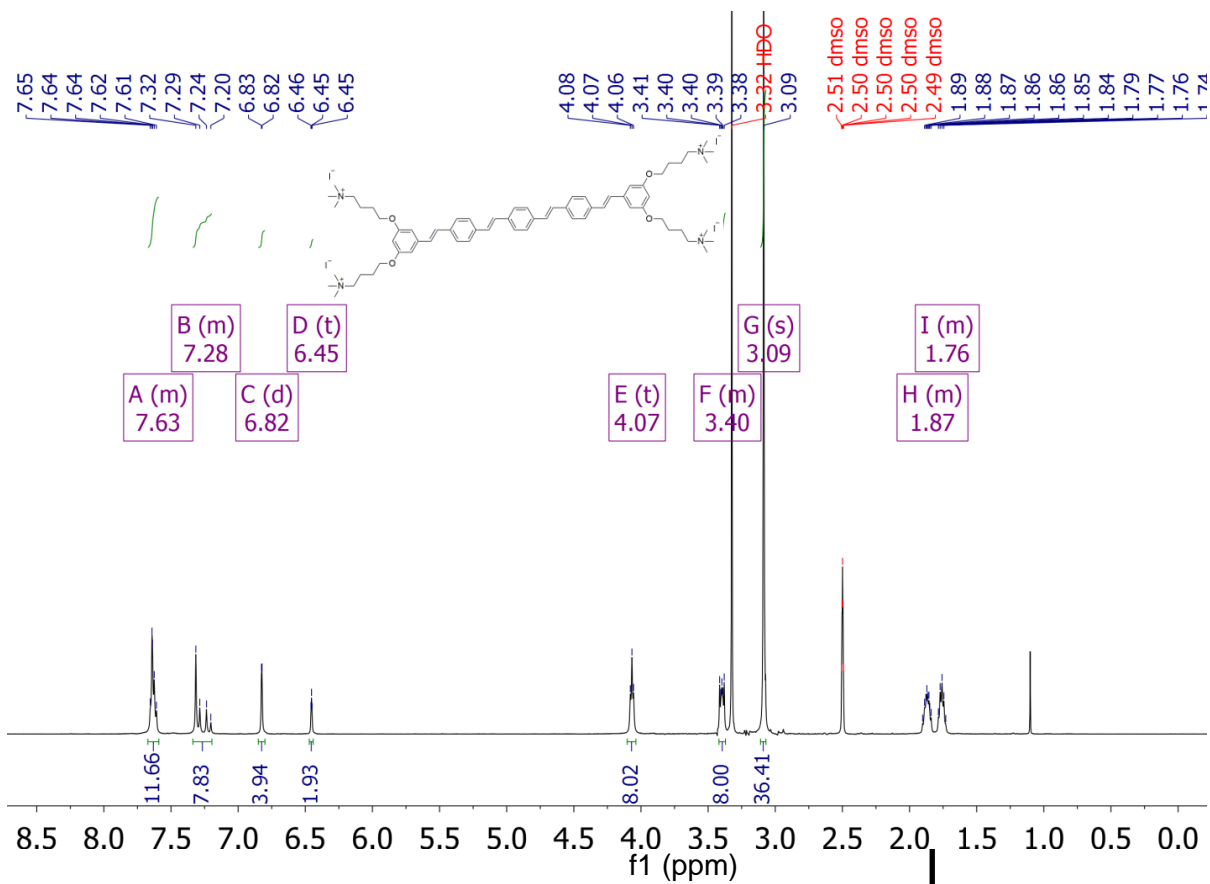




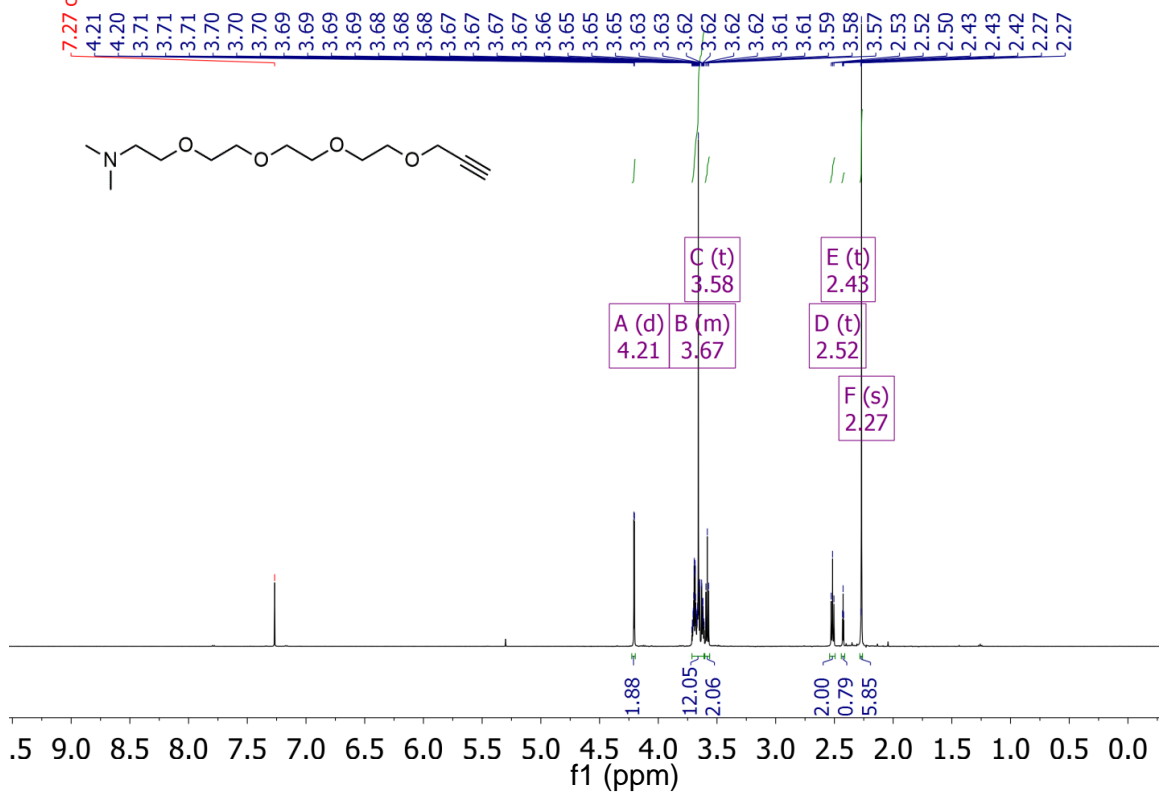
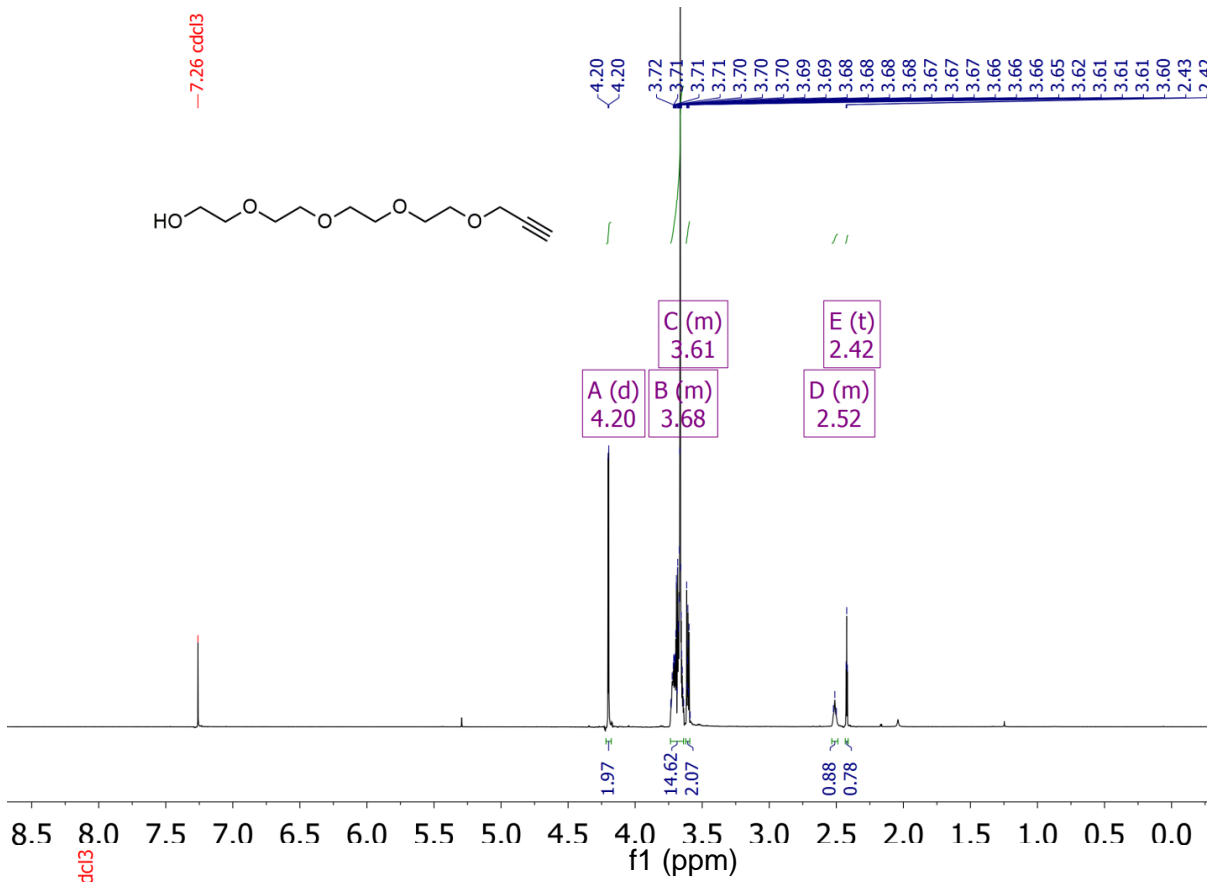


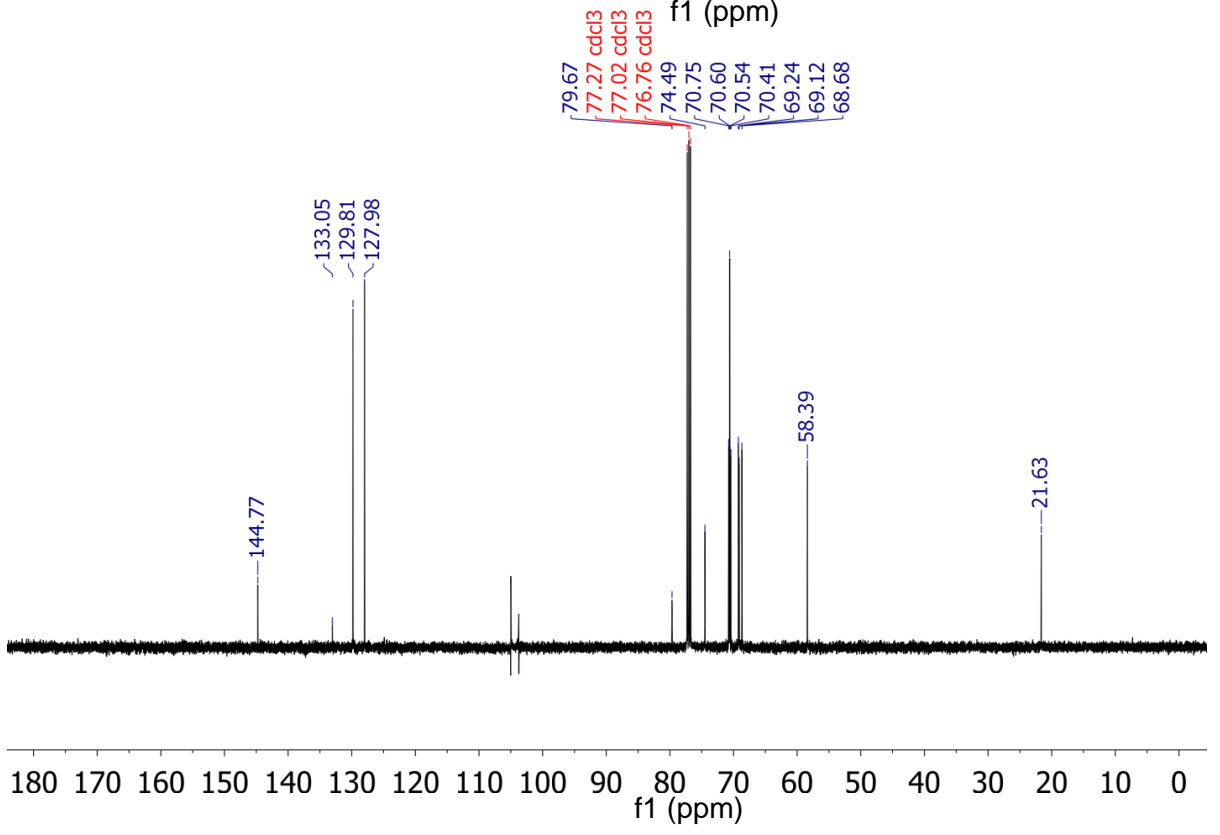
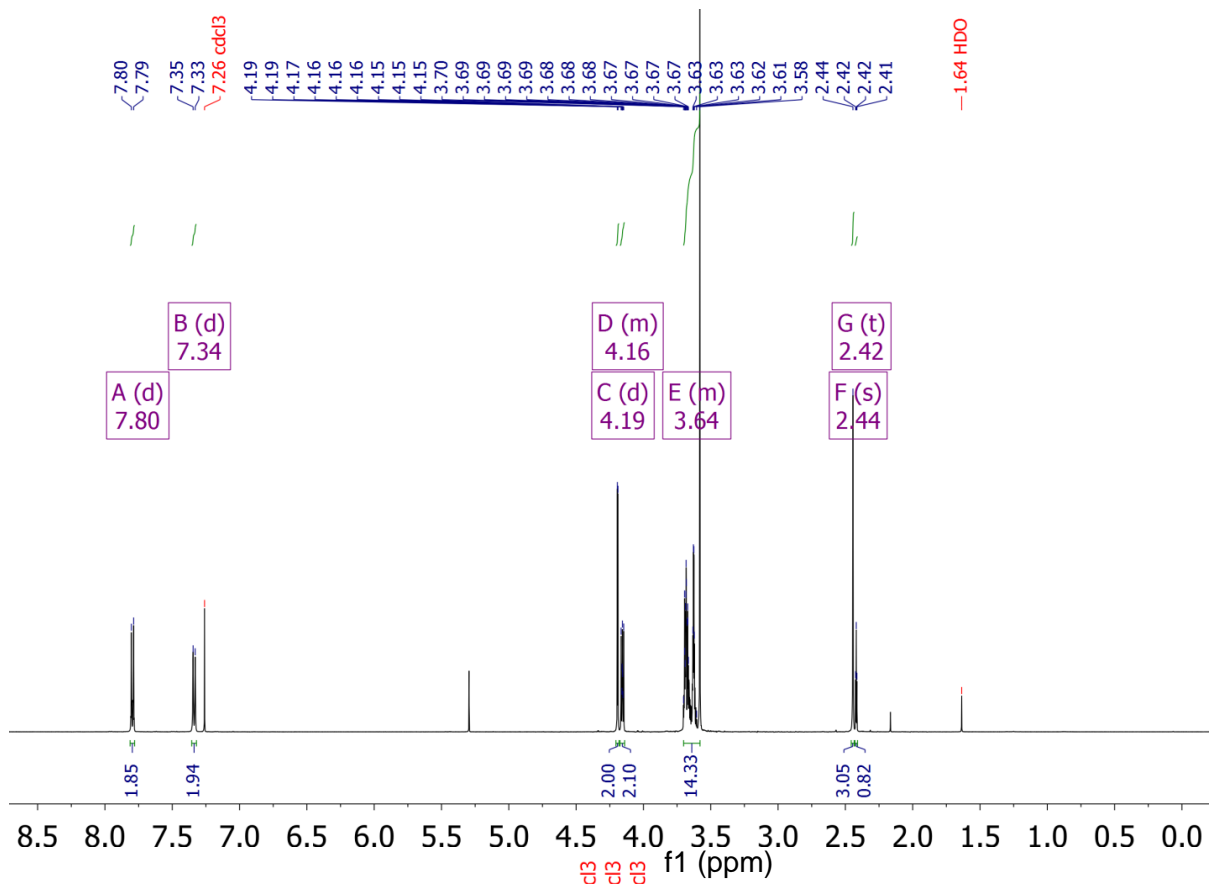


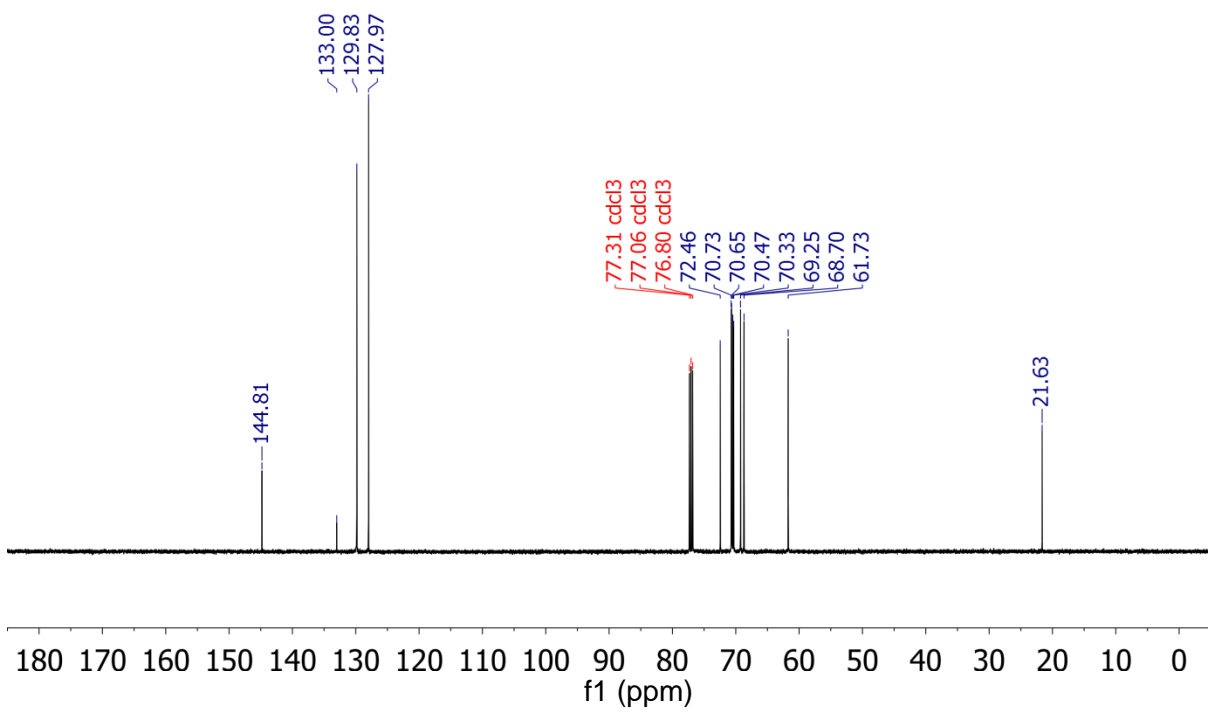
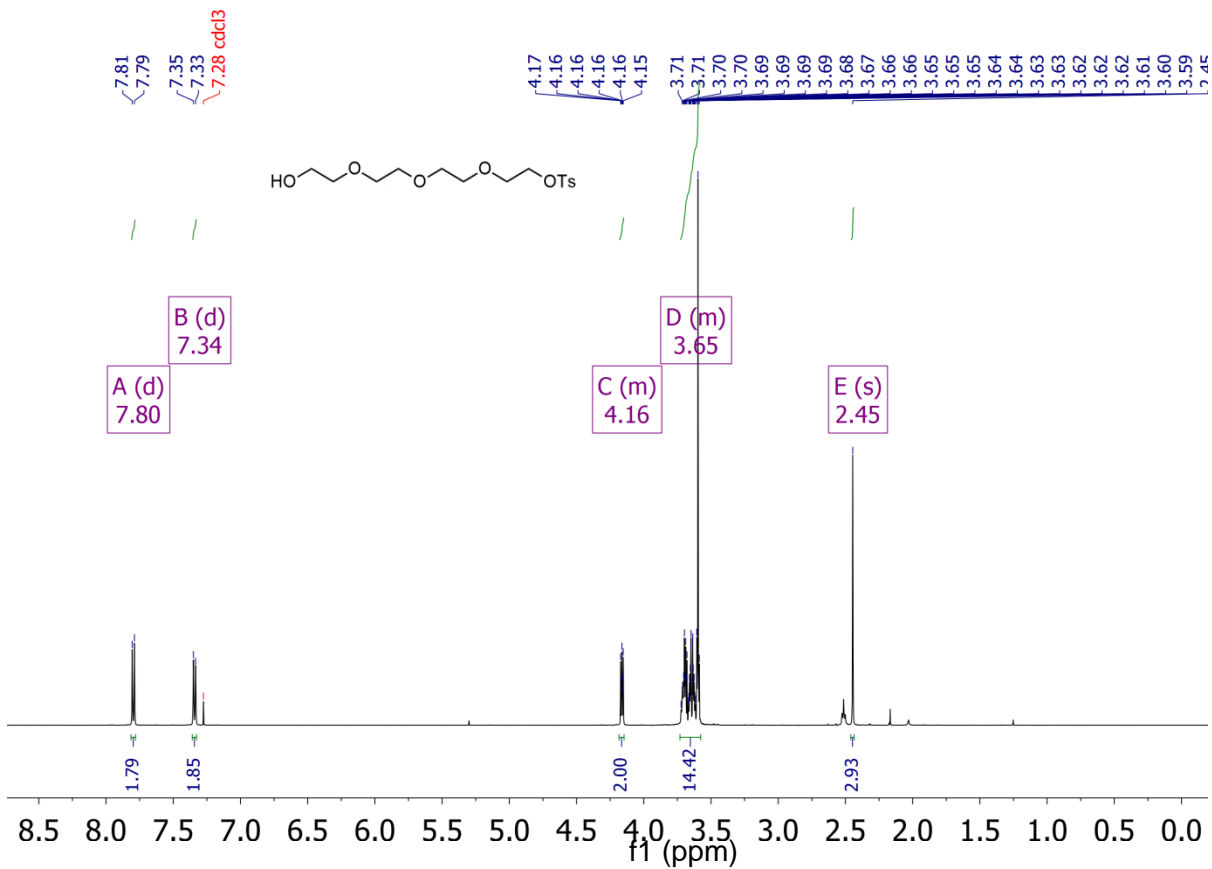


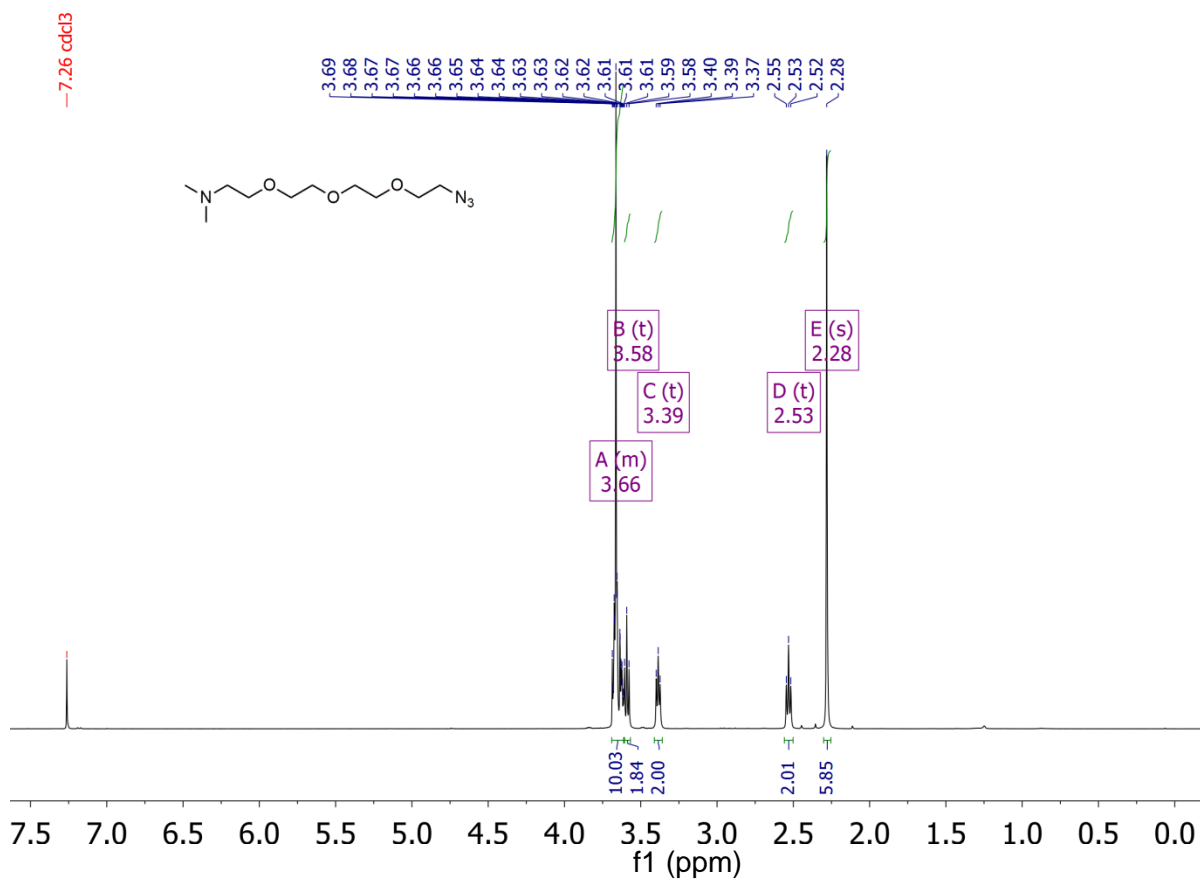


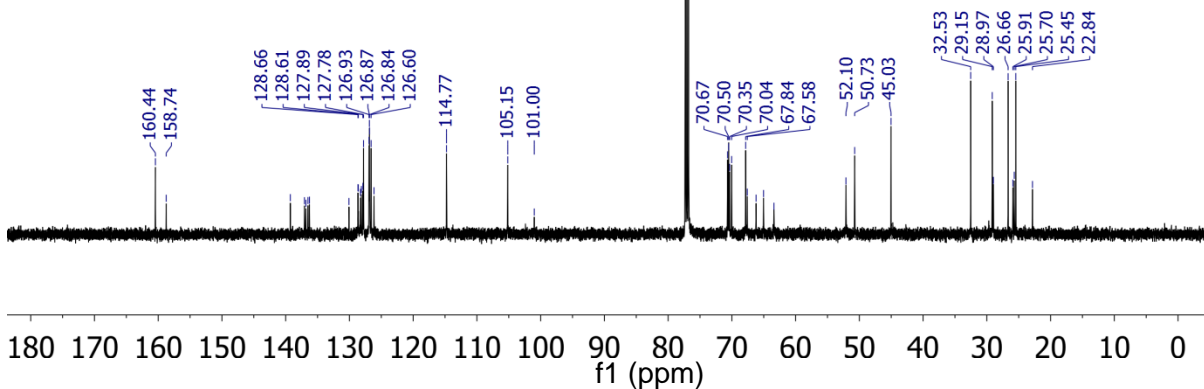
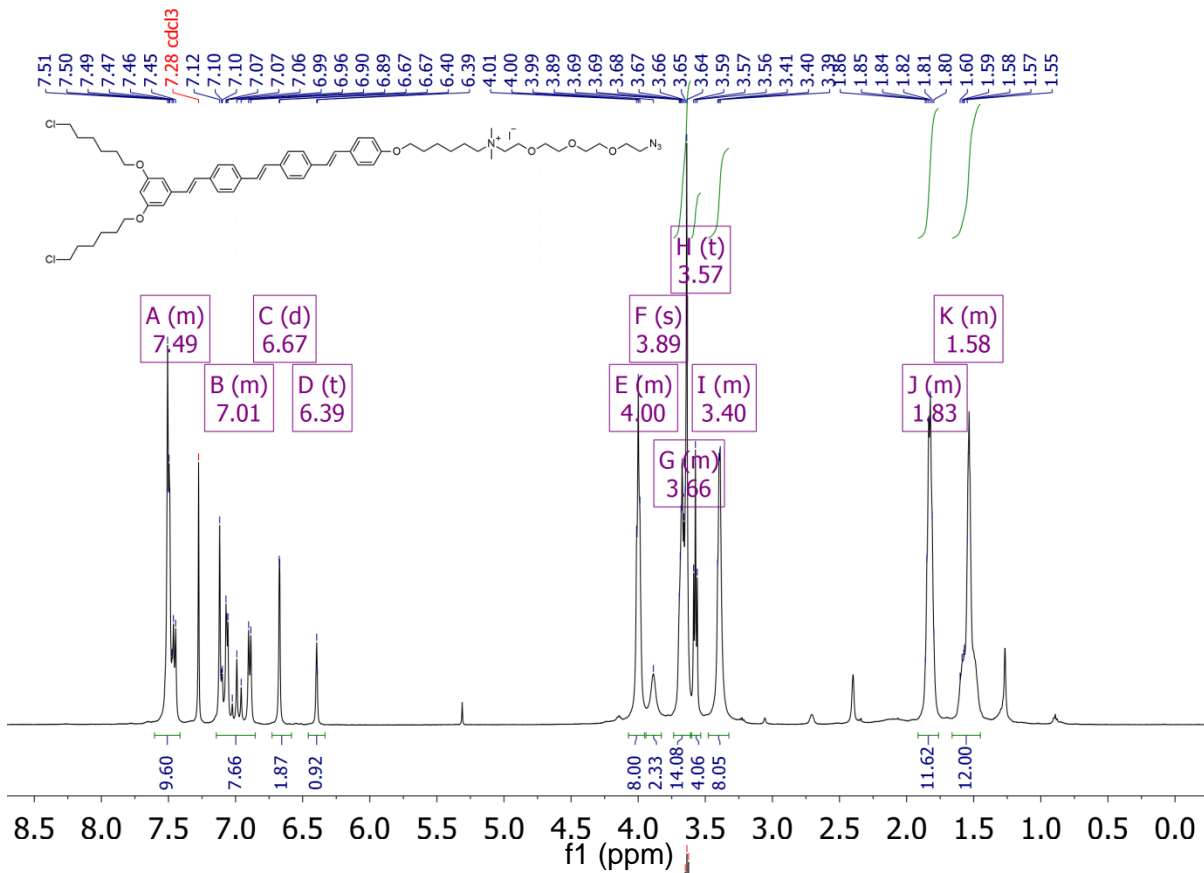
Chapter 4

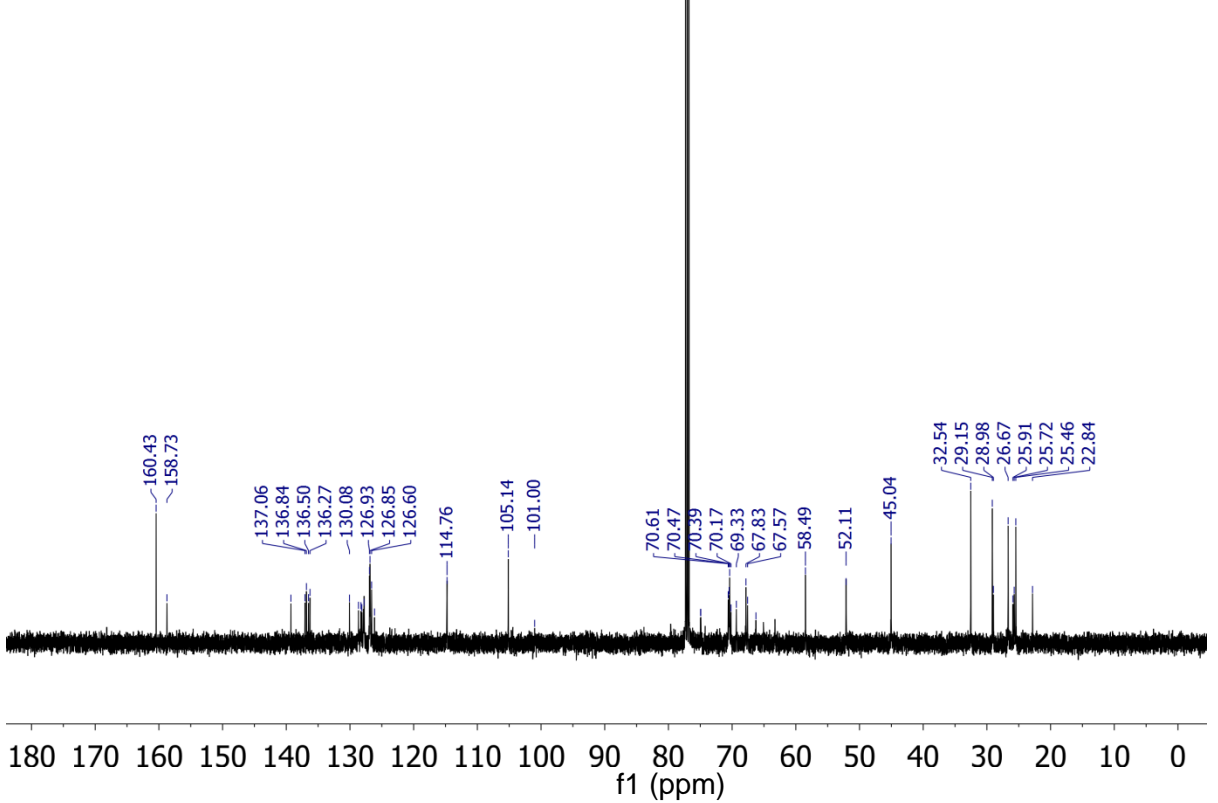
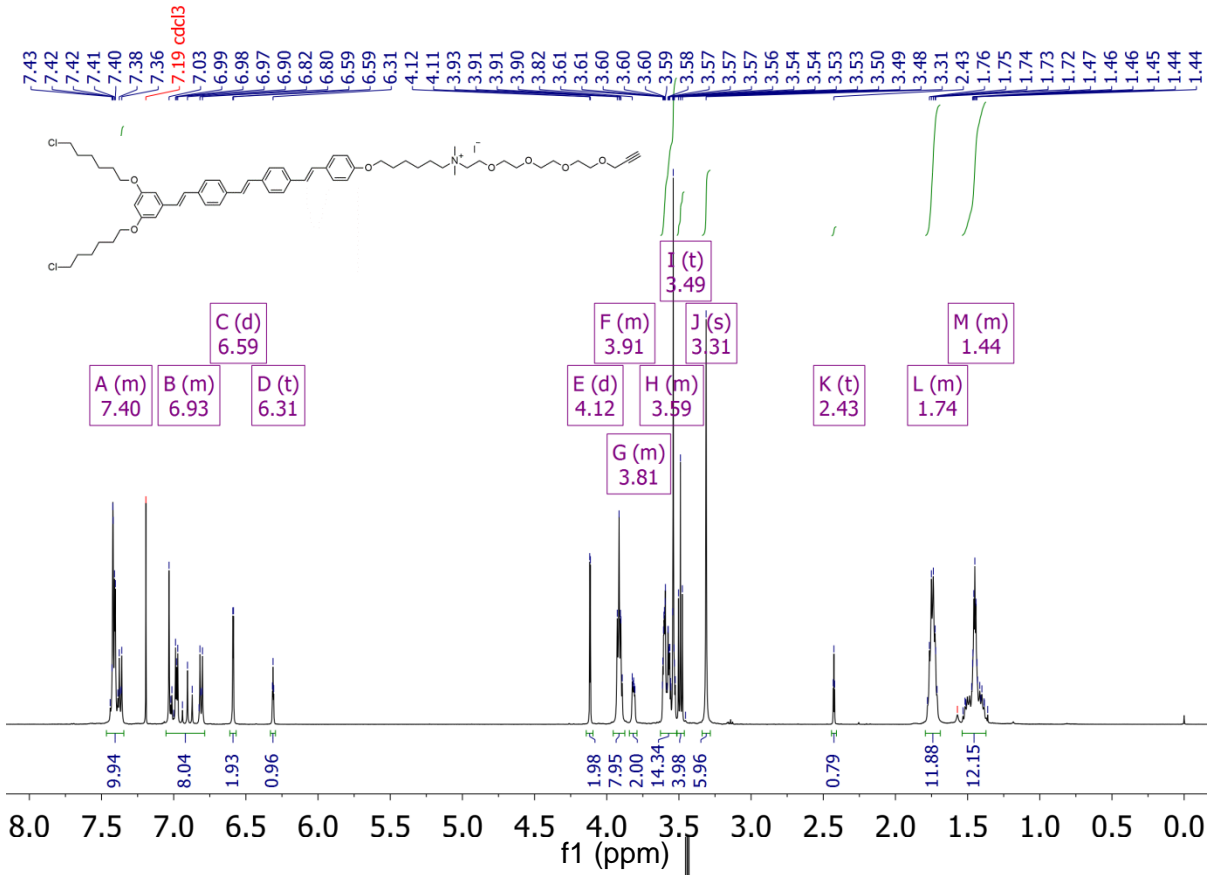


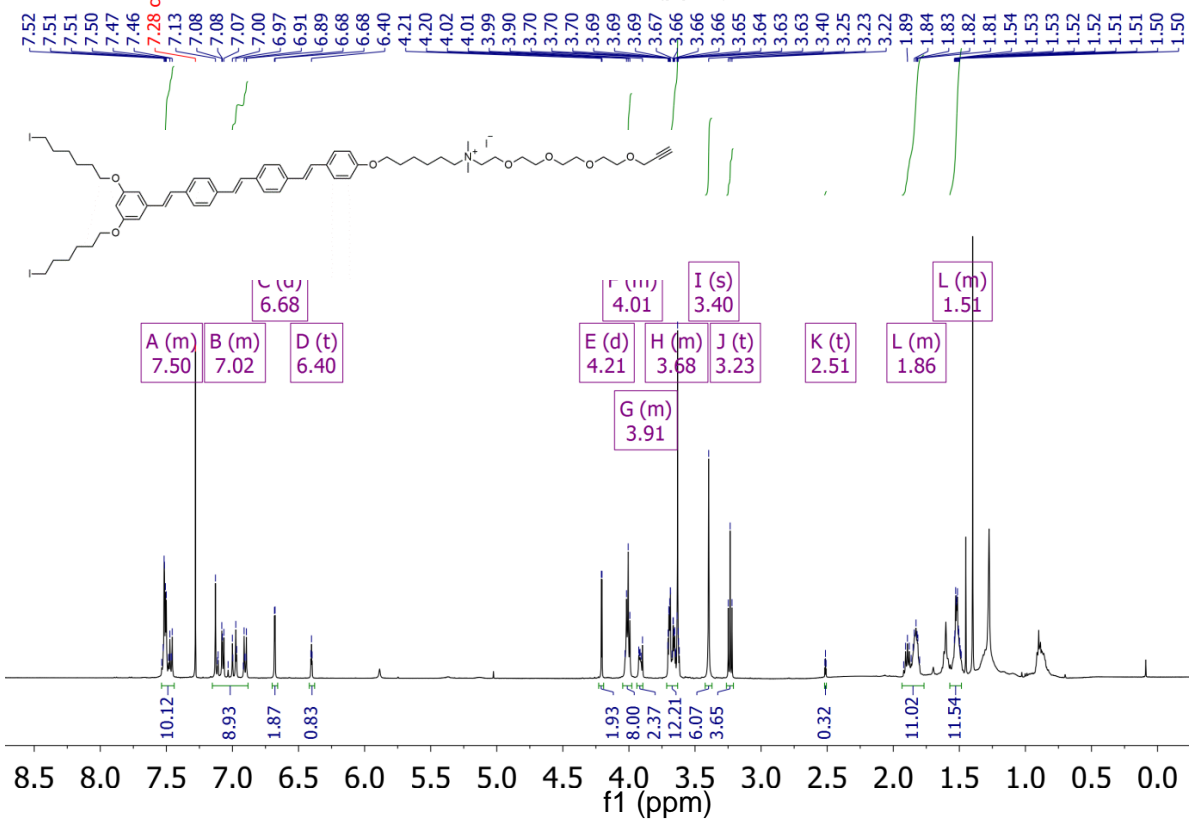
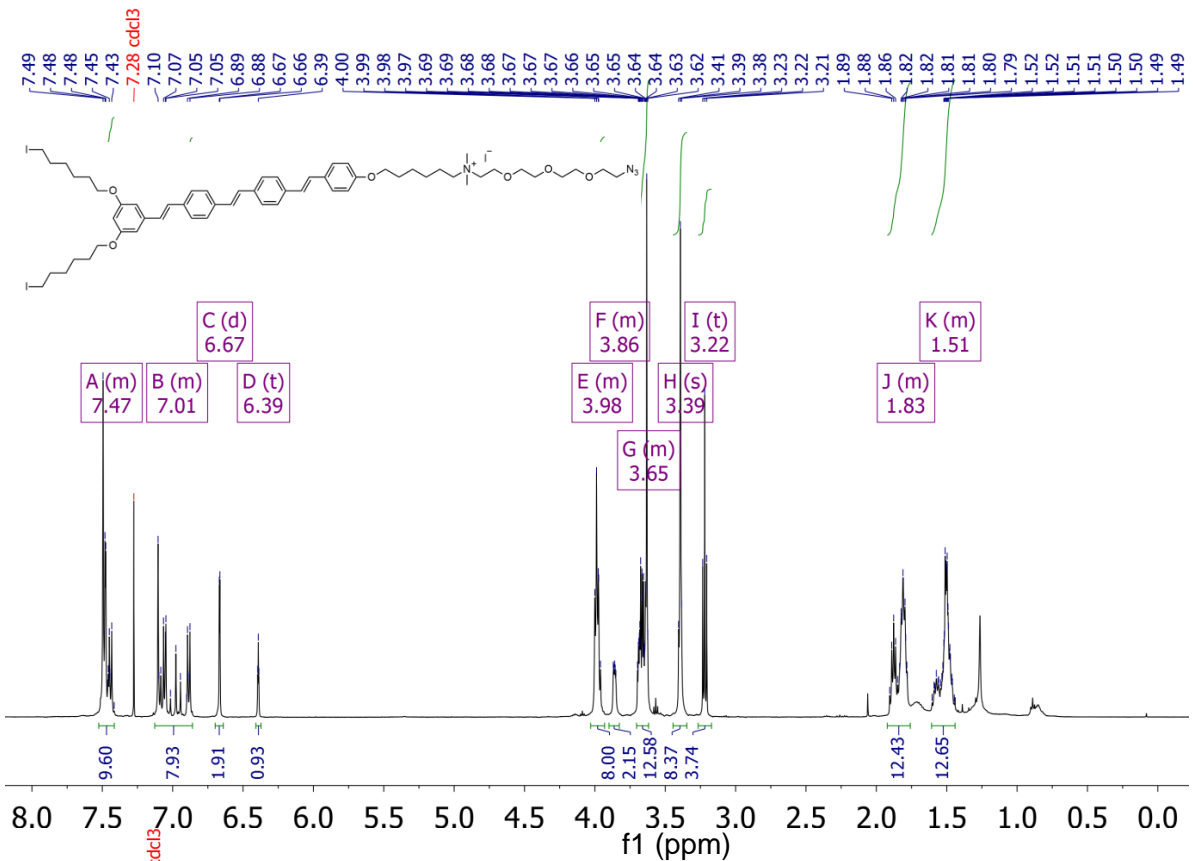


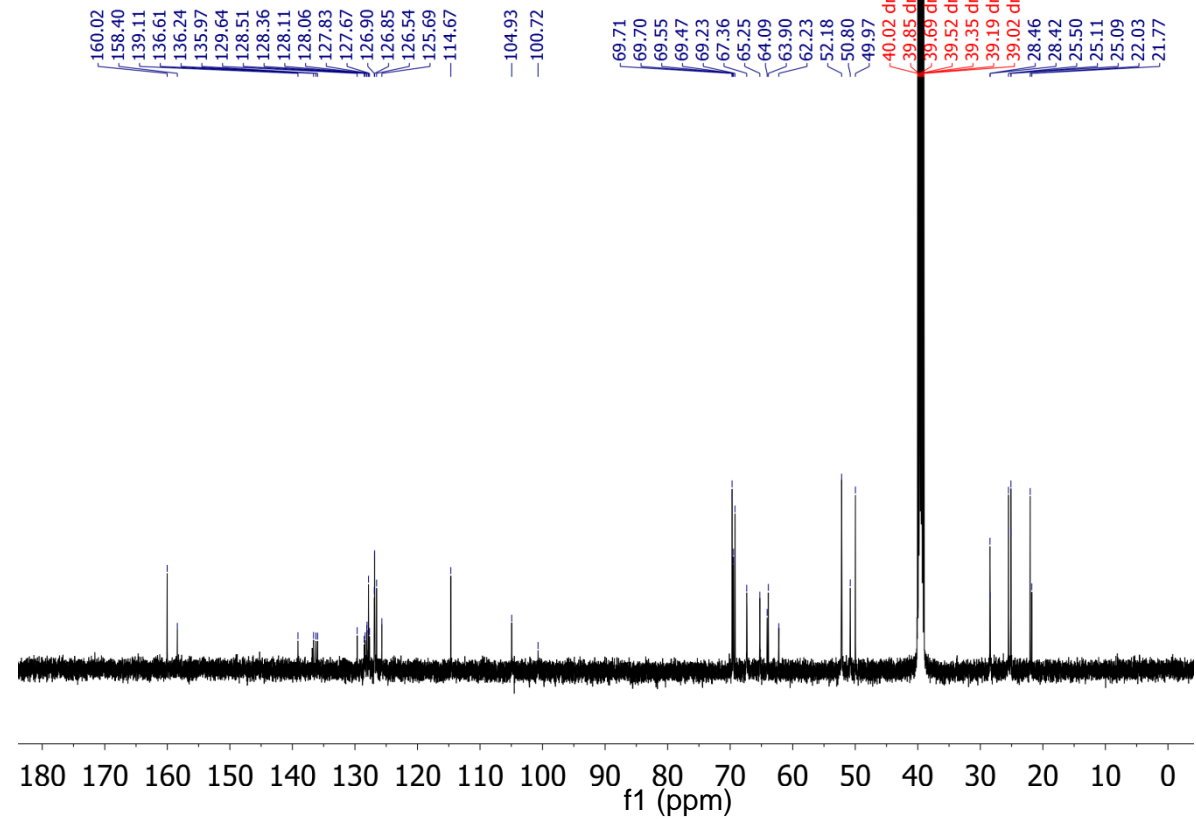
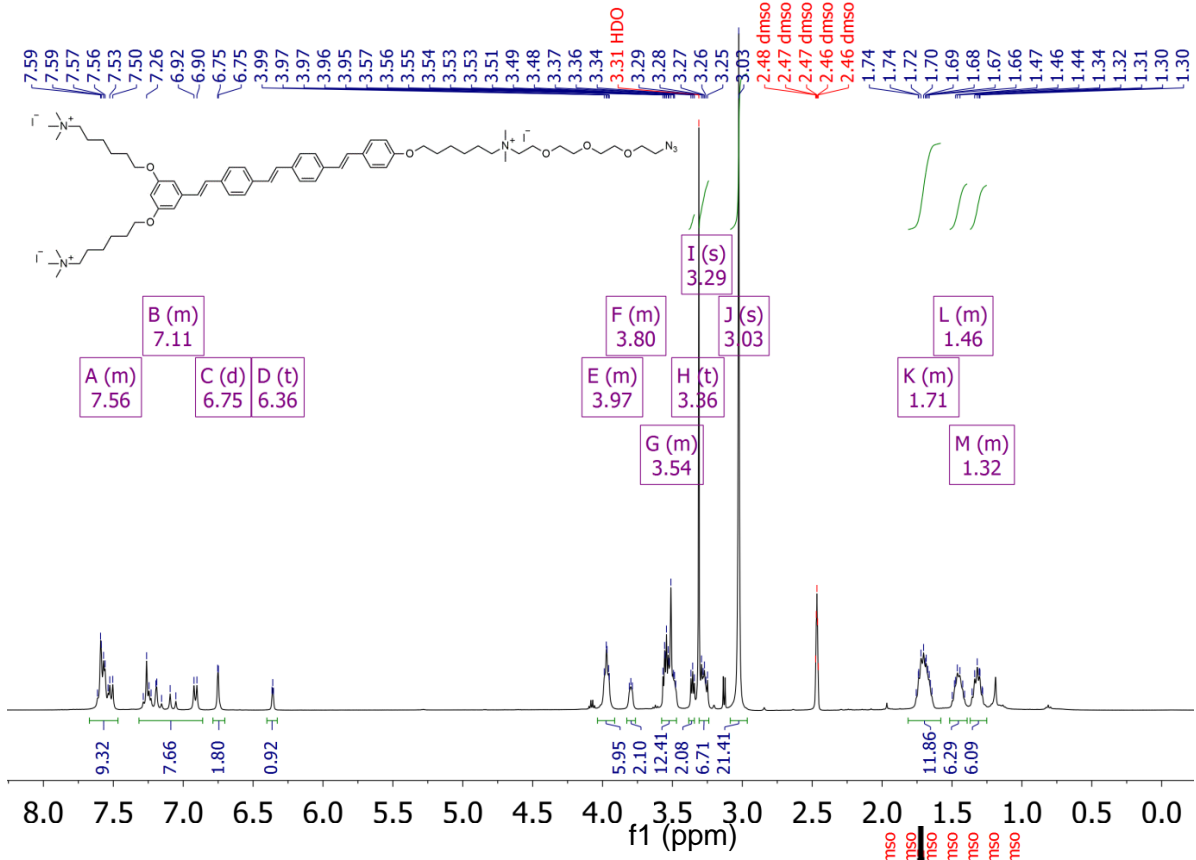


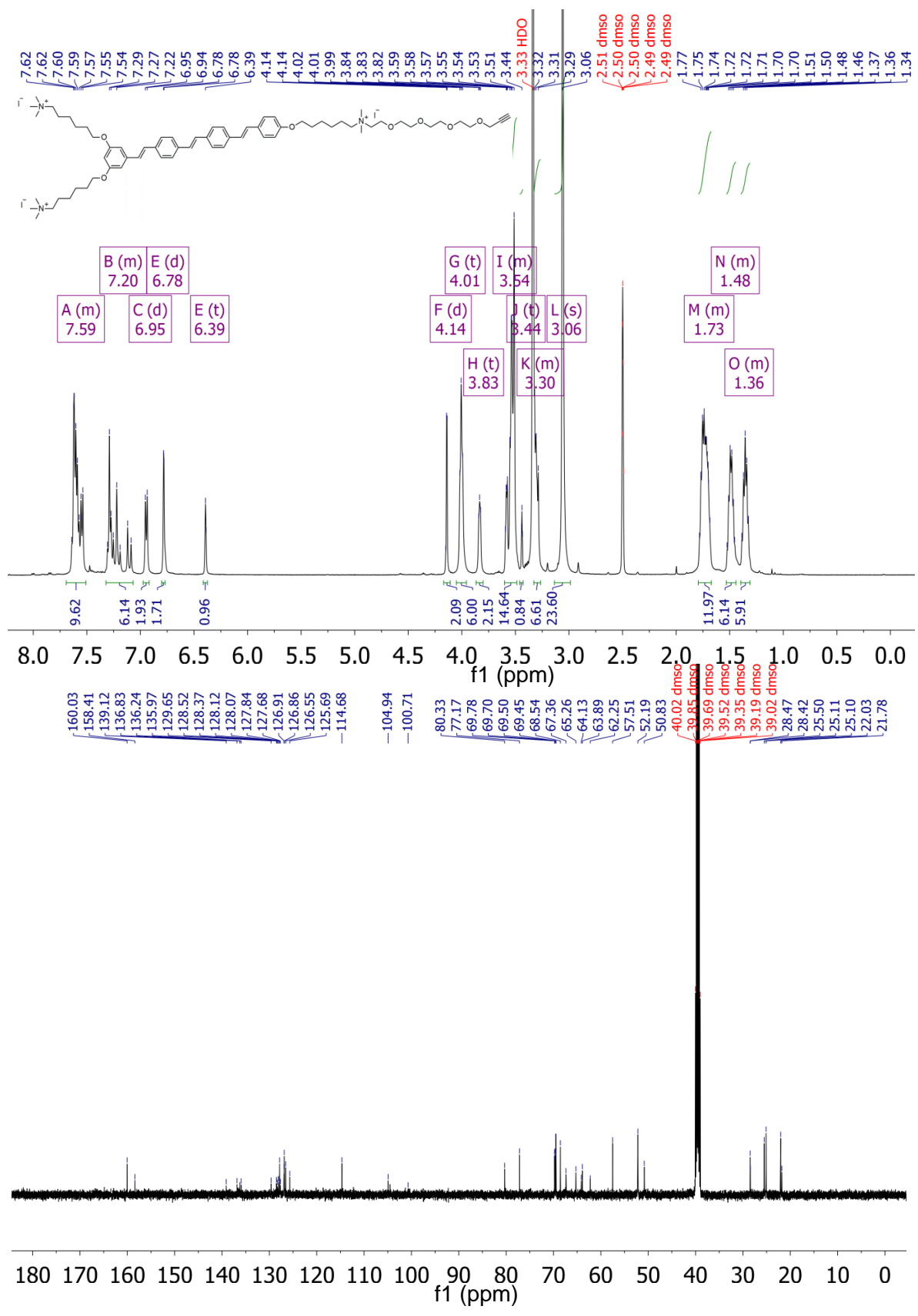


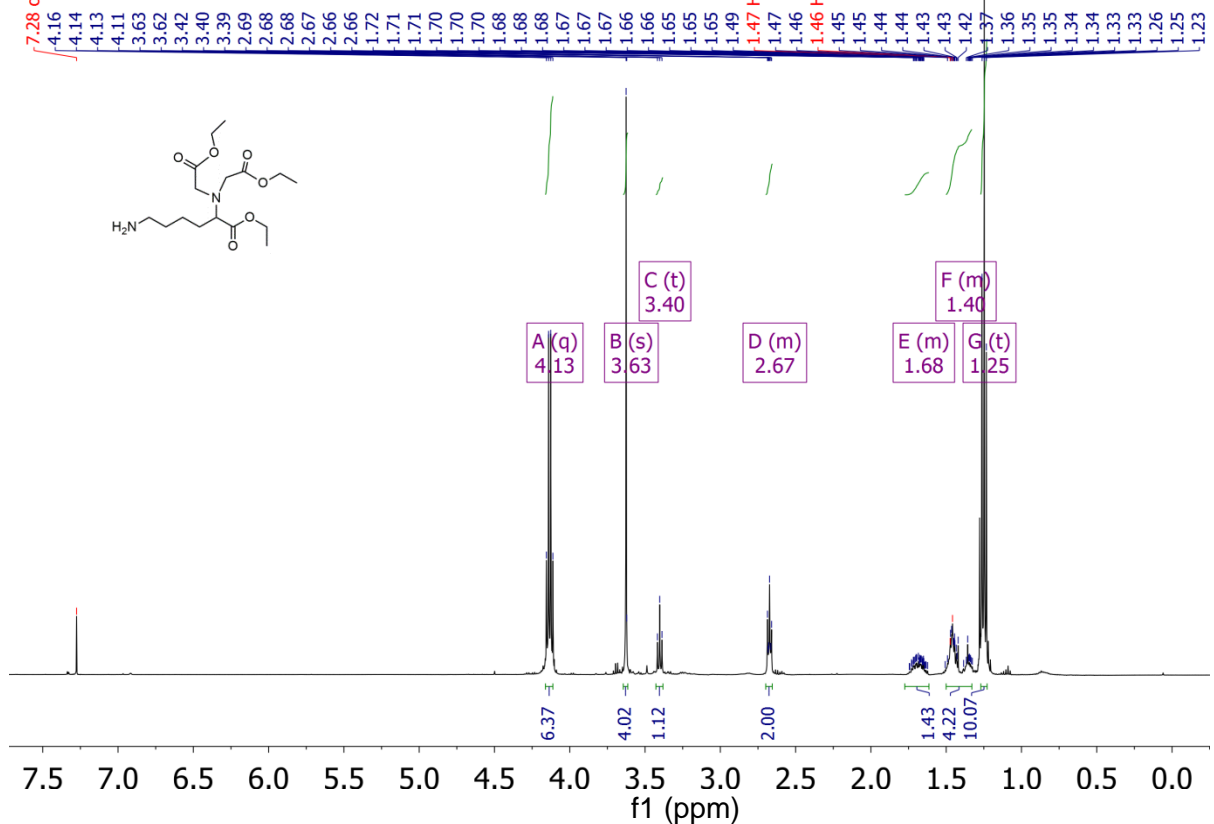
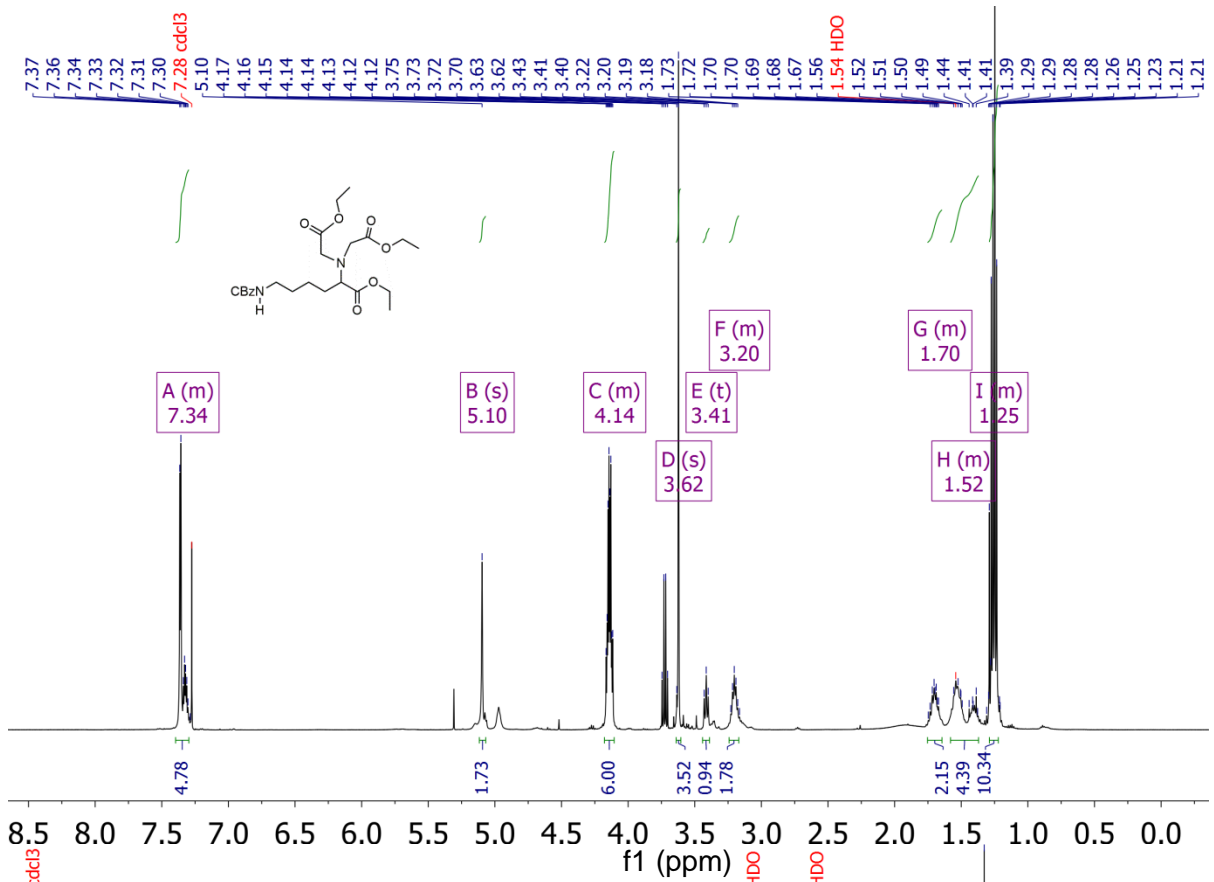


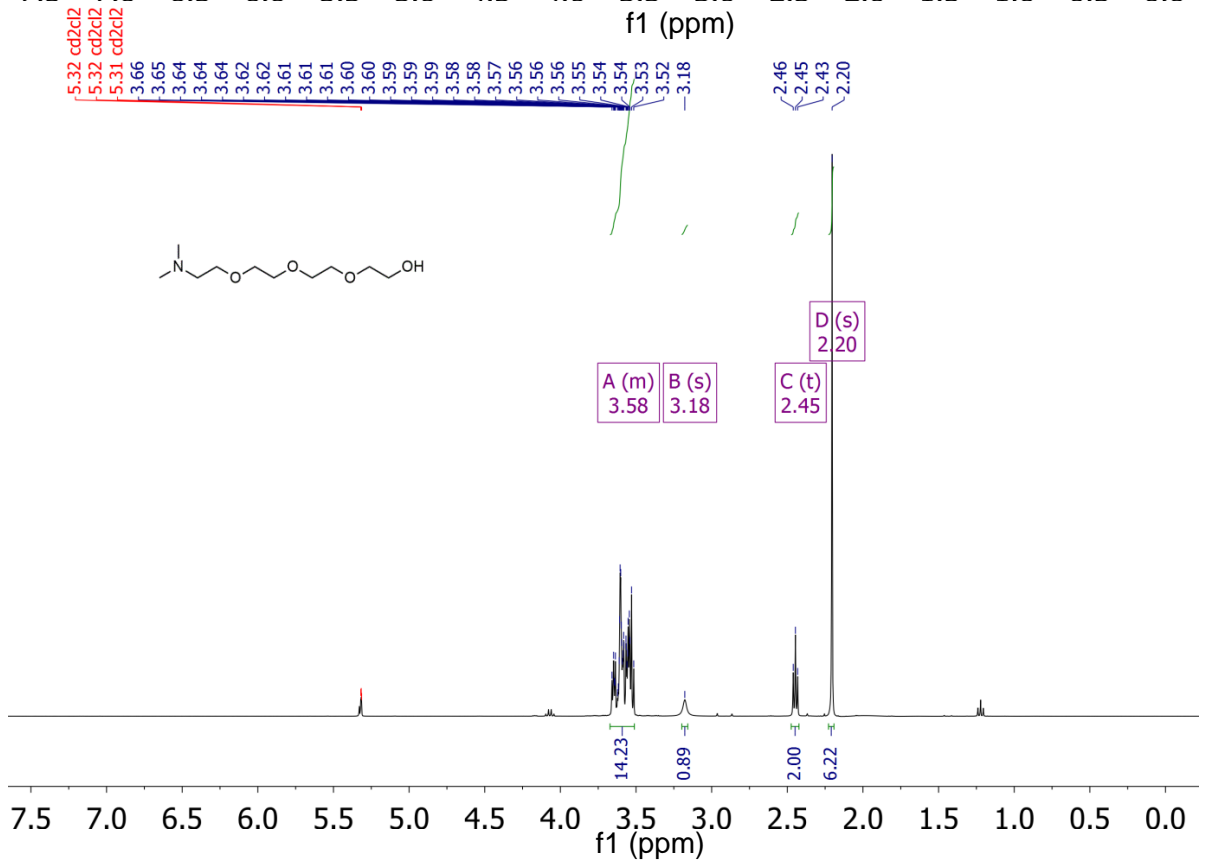
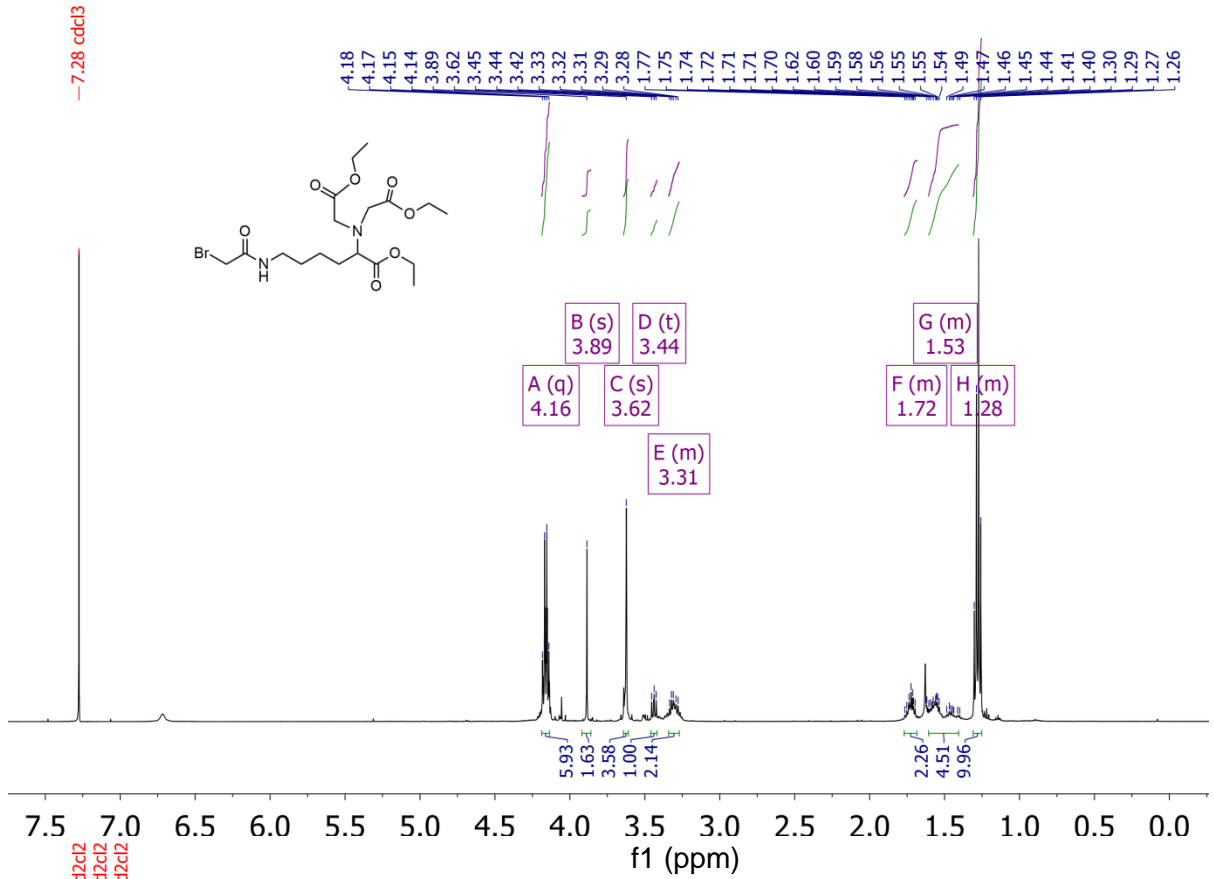


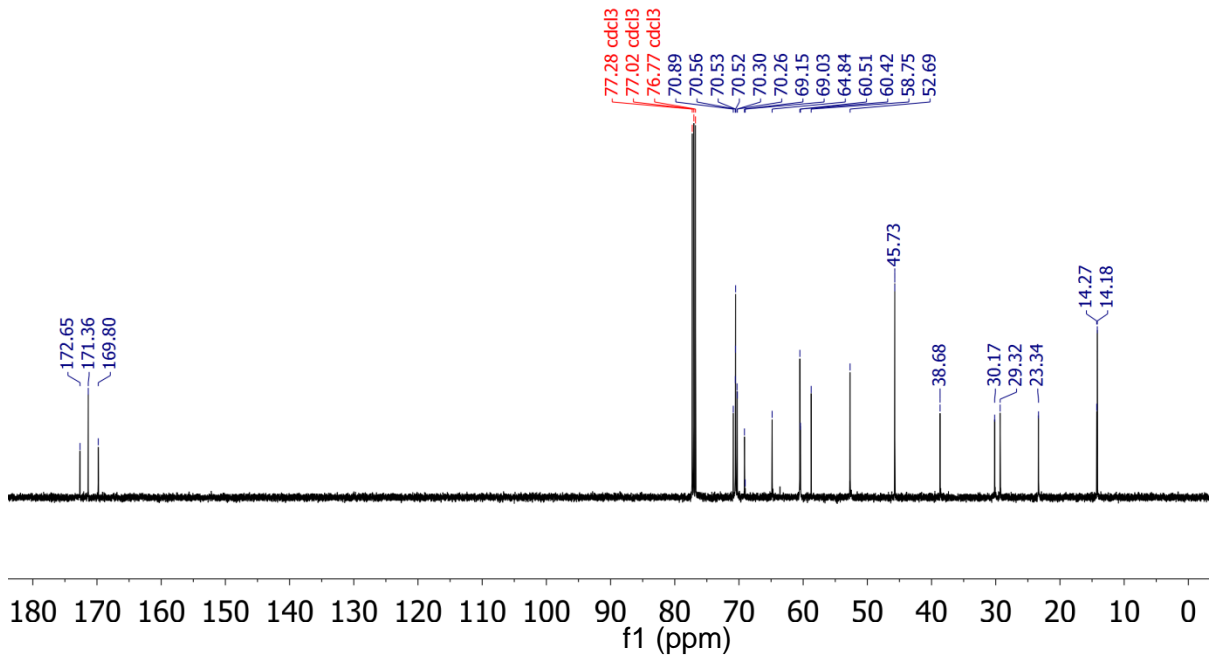
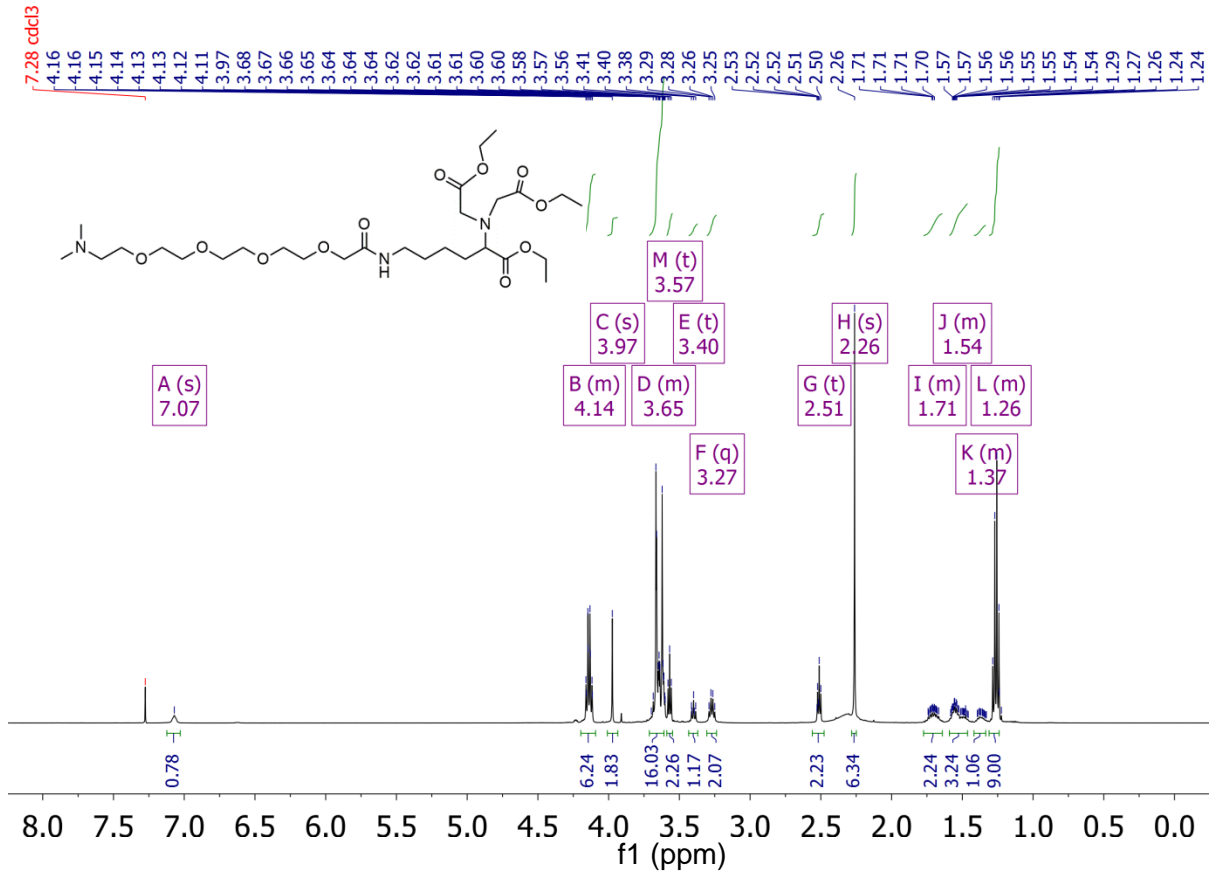


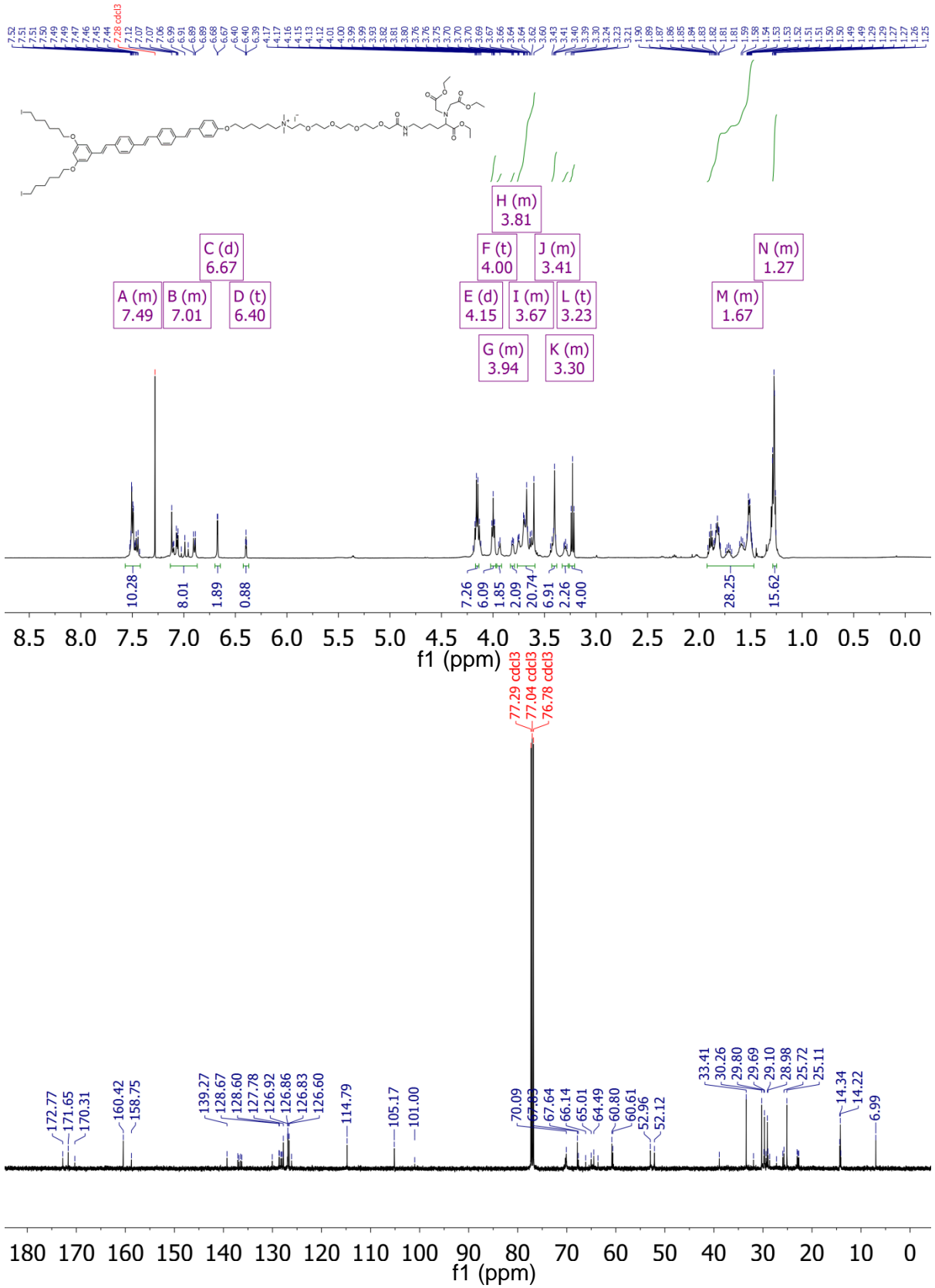


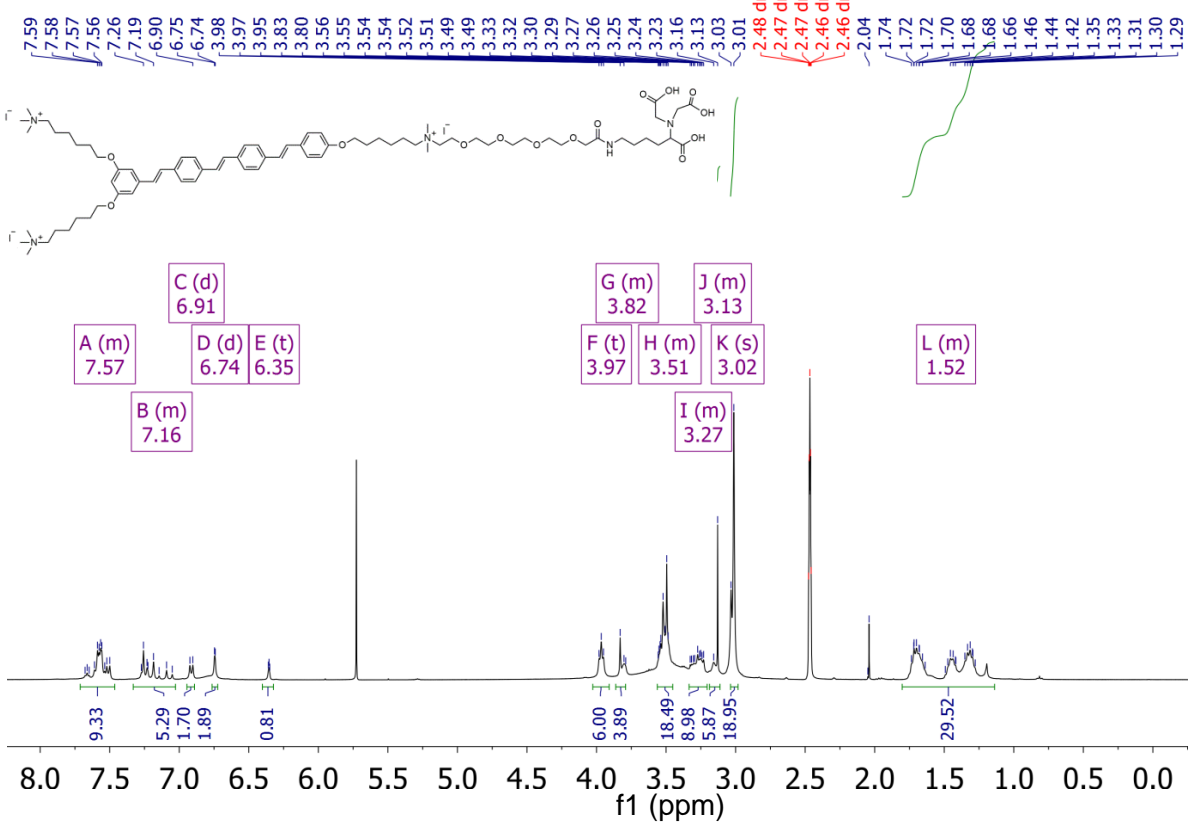
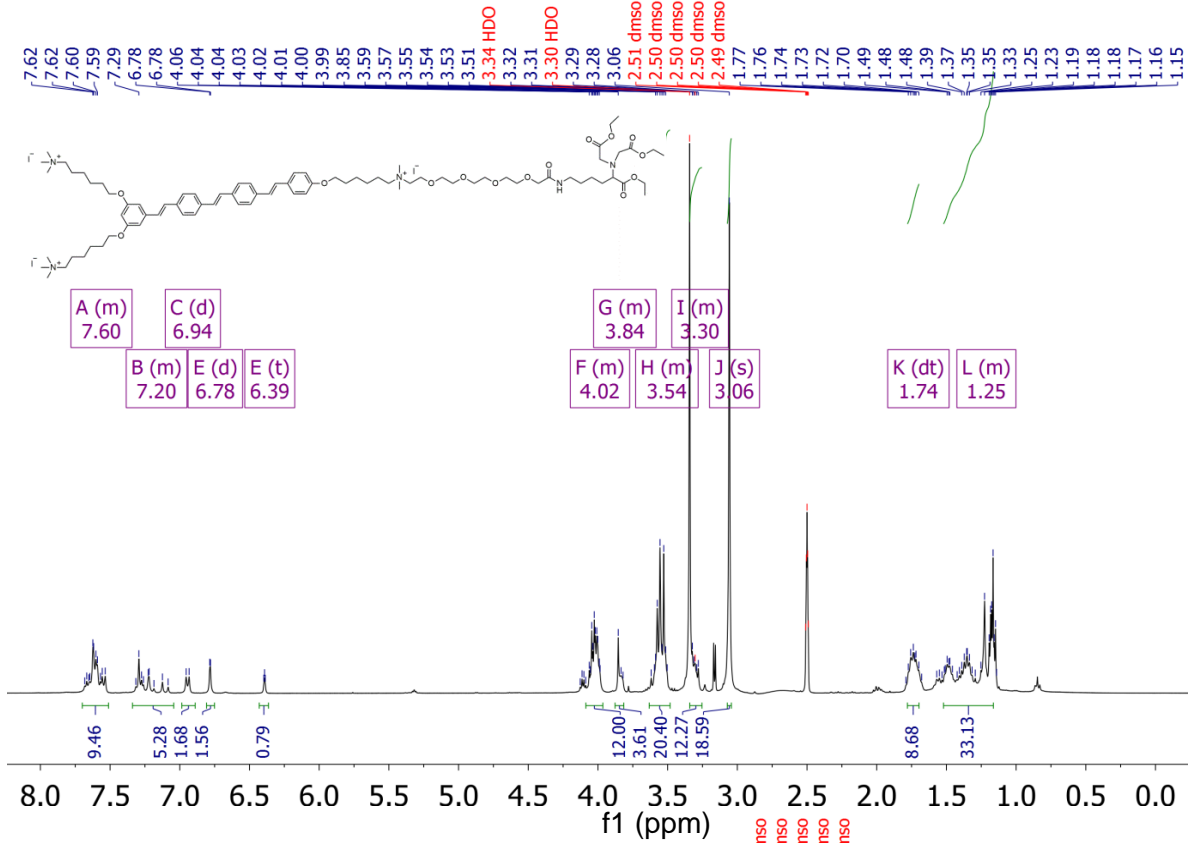




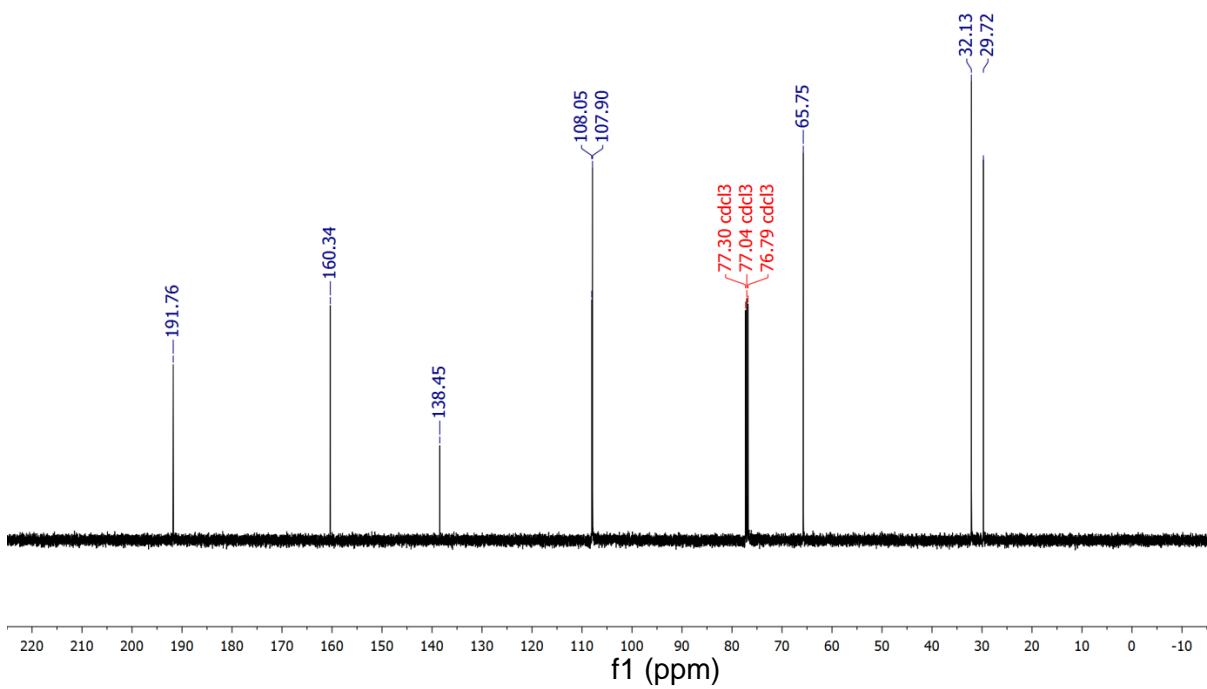
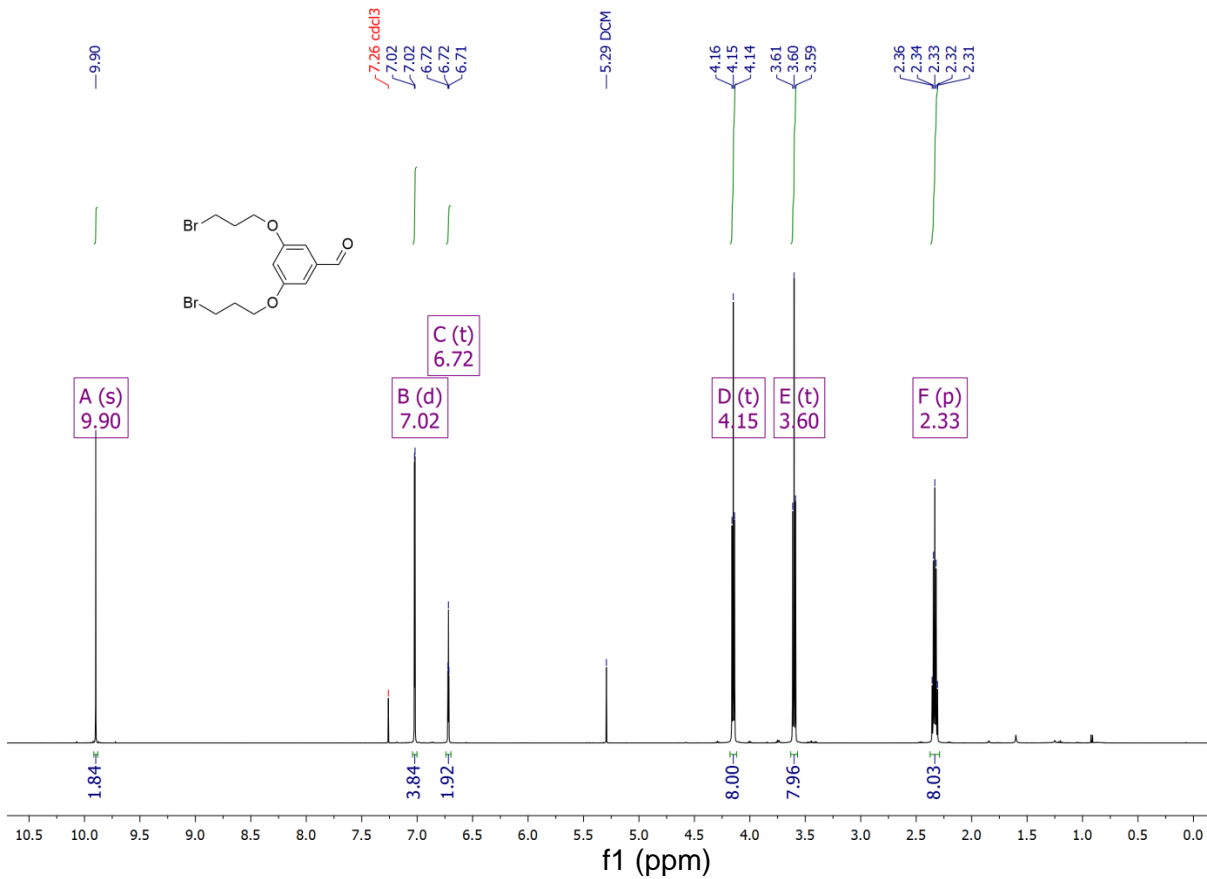


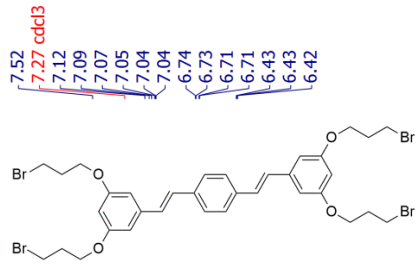




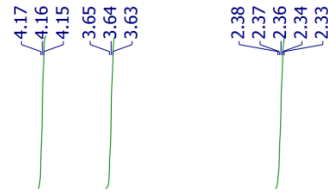


Chapter 5





7.52
7.27 cdd
7.12
7.09
7.07
7.05
7.04
6.74
6.73
6.71
6.71
6.43
6.43
6.42



C (d)
6.71

A (s)
7.52

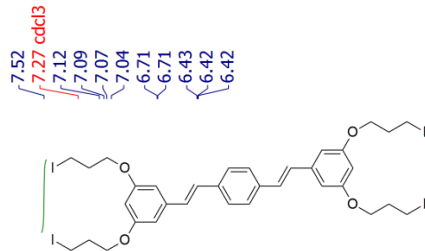
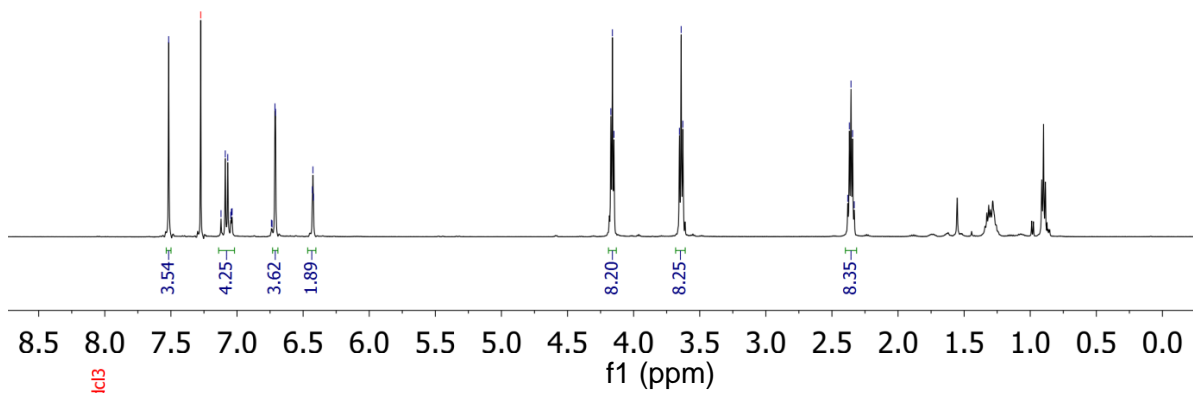
B (m)
7.08

D (t)
6.43

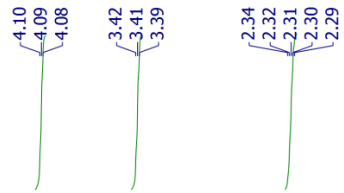
E (t)
4.16

F (t)
3.64

G (p)
2.36



7.52
7.27 cdd
7.12
7.09
7.07
7.04
6.71
6.43
6.42
6.42



C (d)
6.71

A (s)
7.52

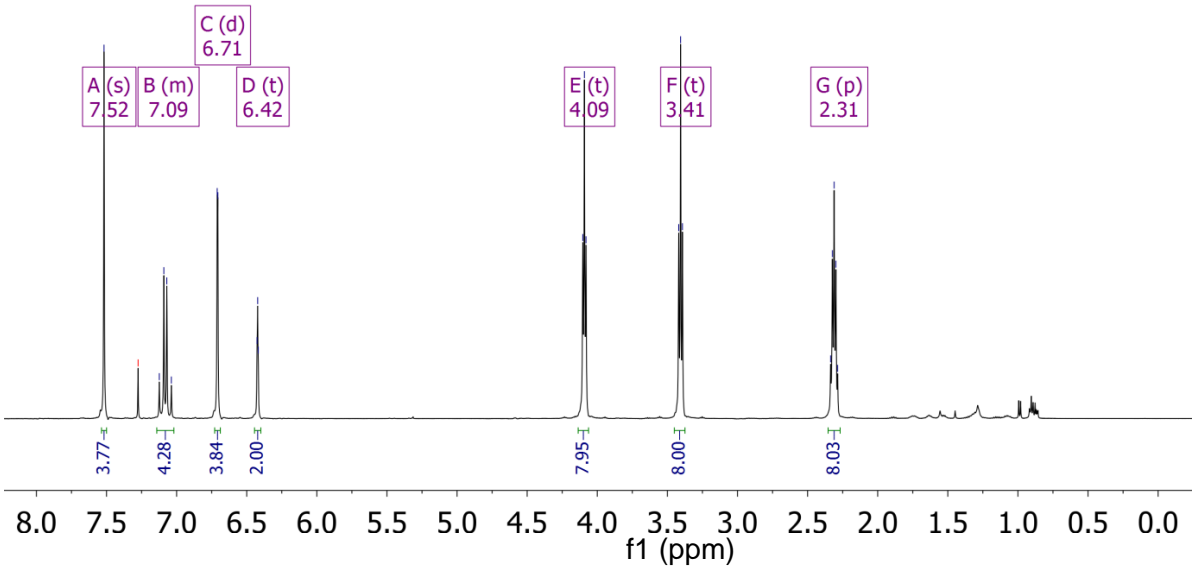
B (m)
7.09

D (t)
6.42

E (t)
4.09

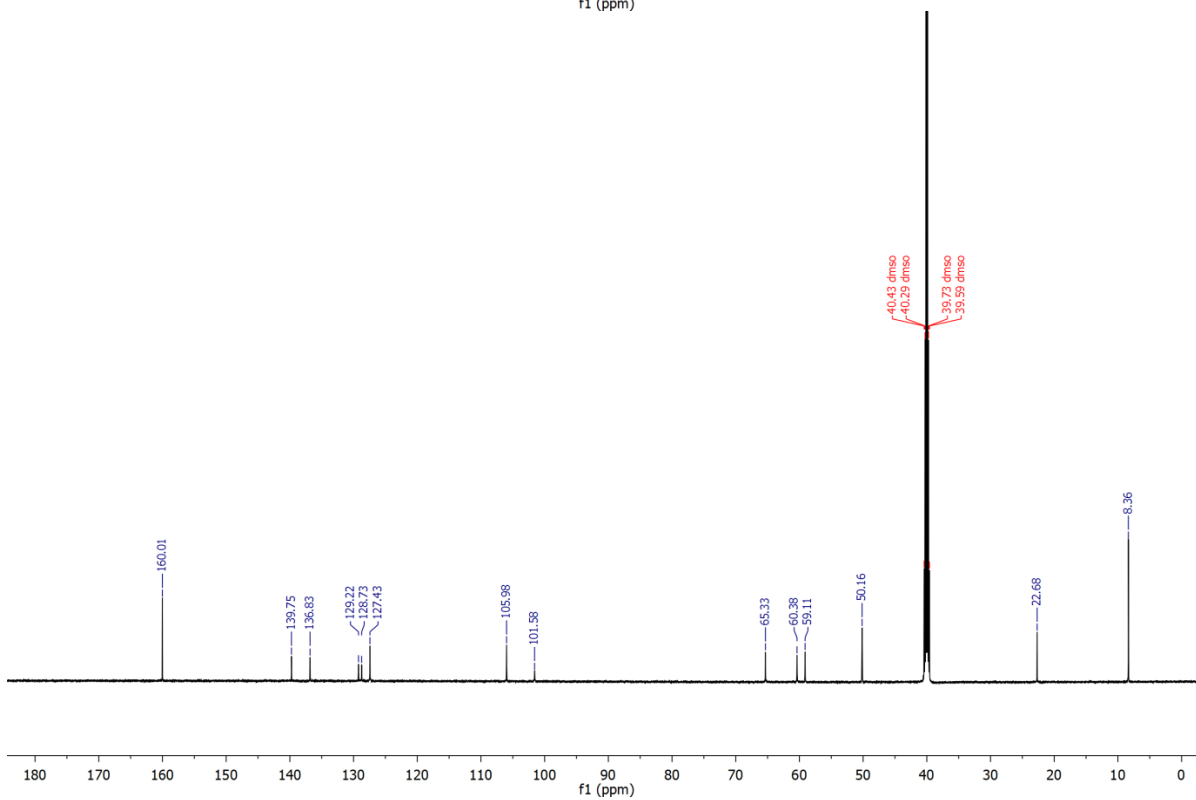
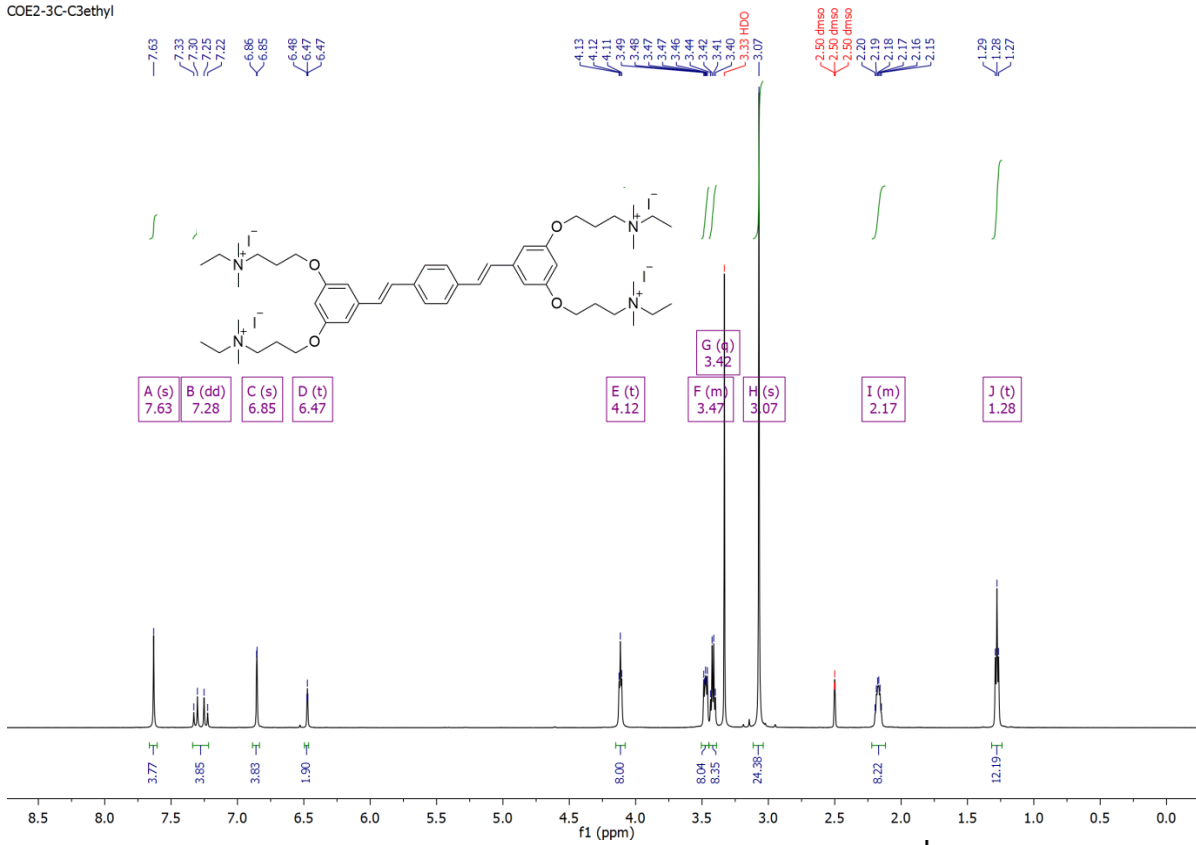
F (t)
3.41

G (p)
2.31

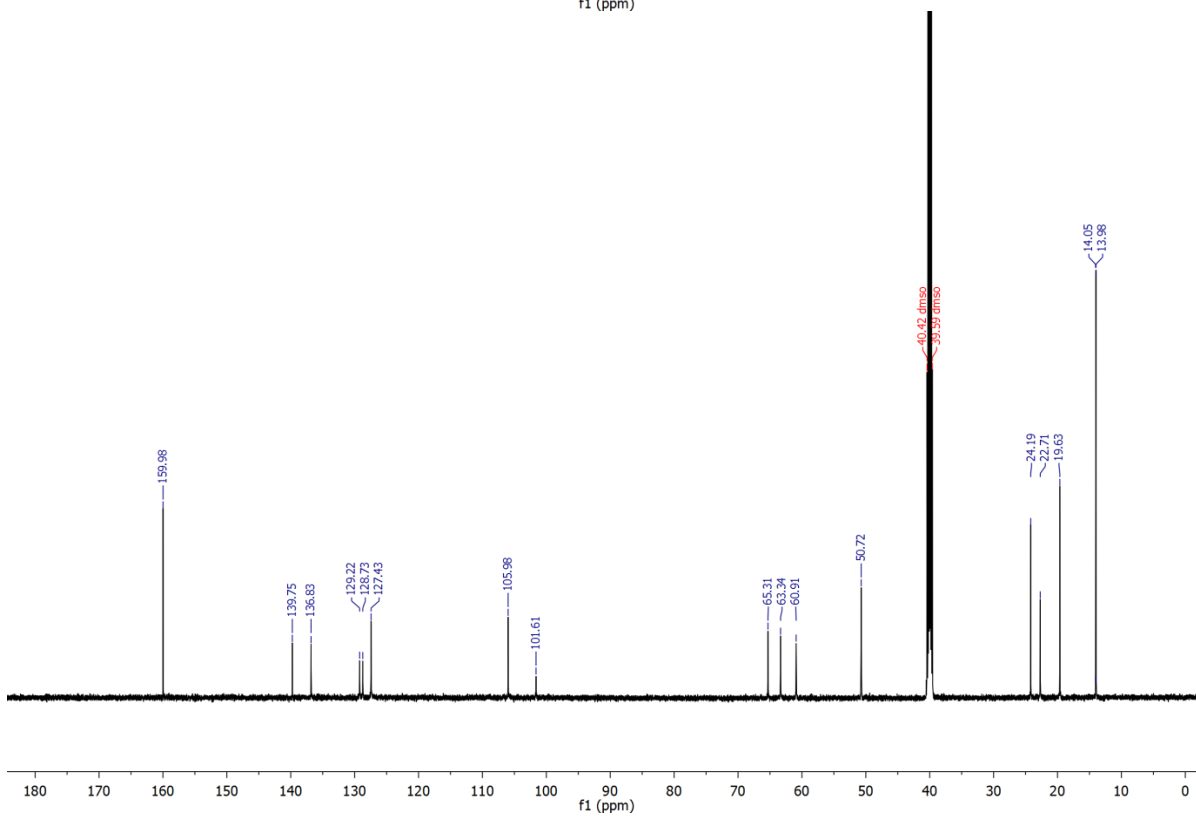
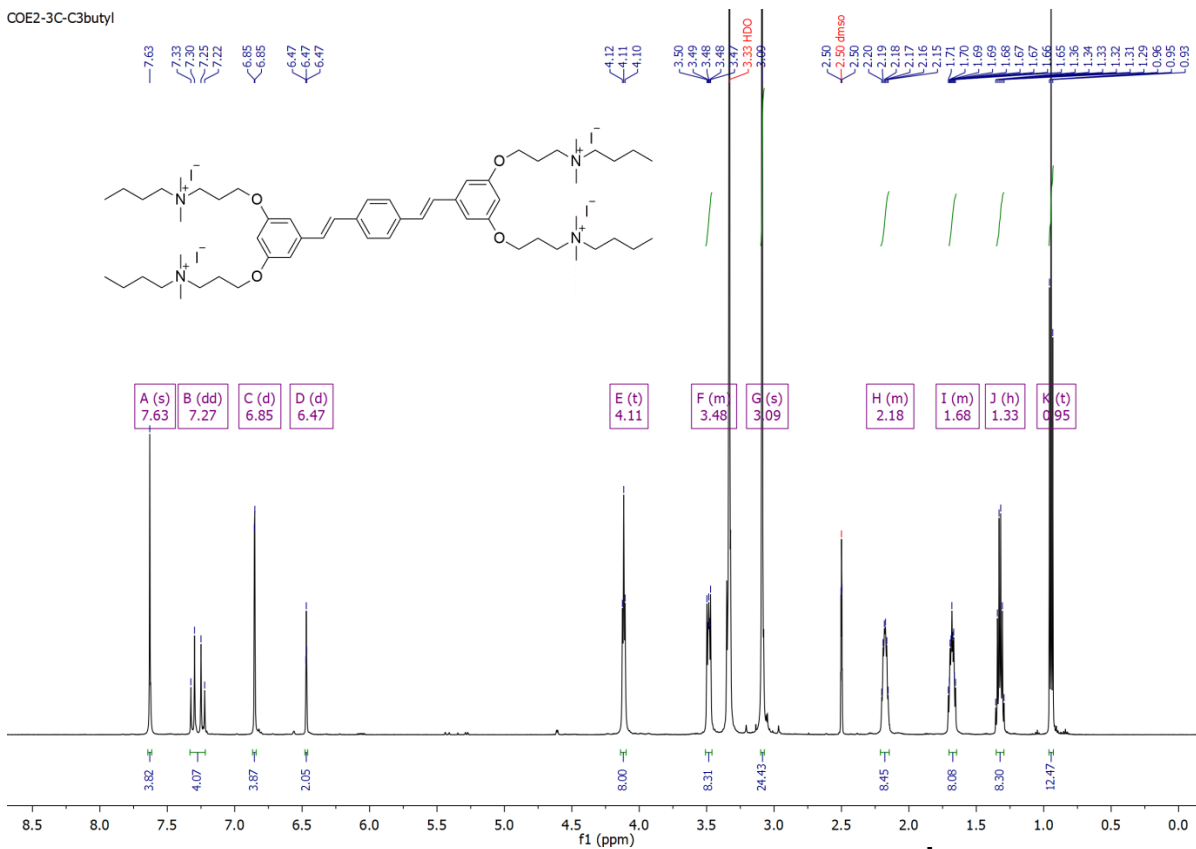


300

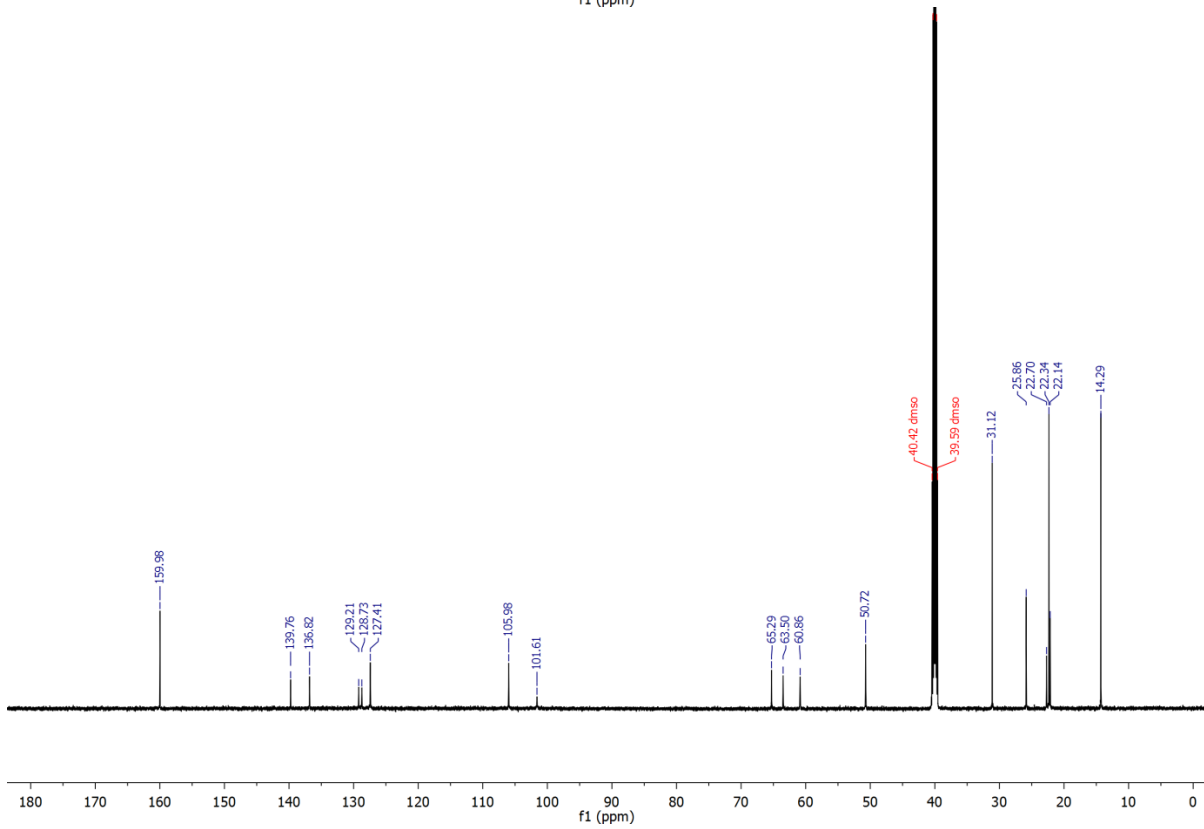
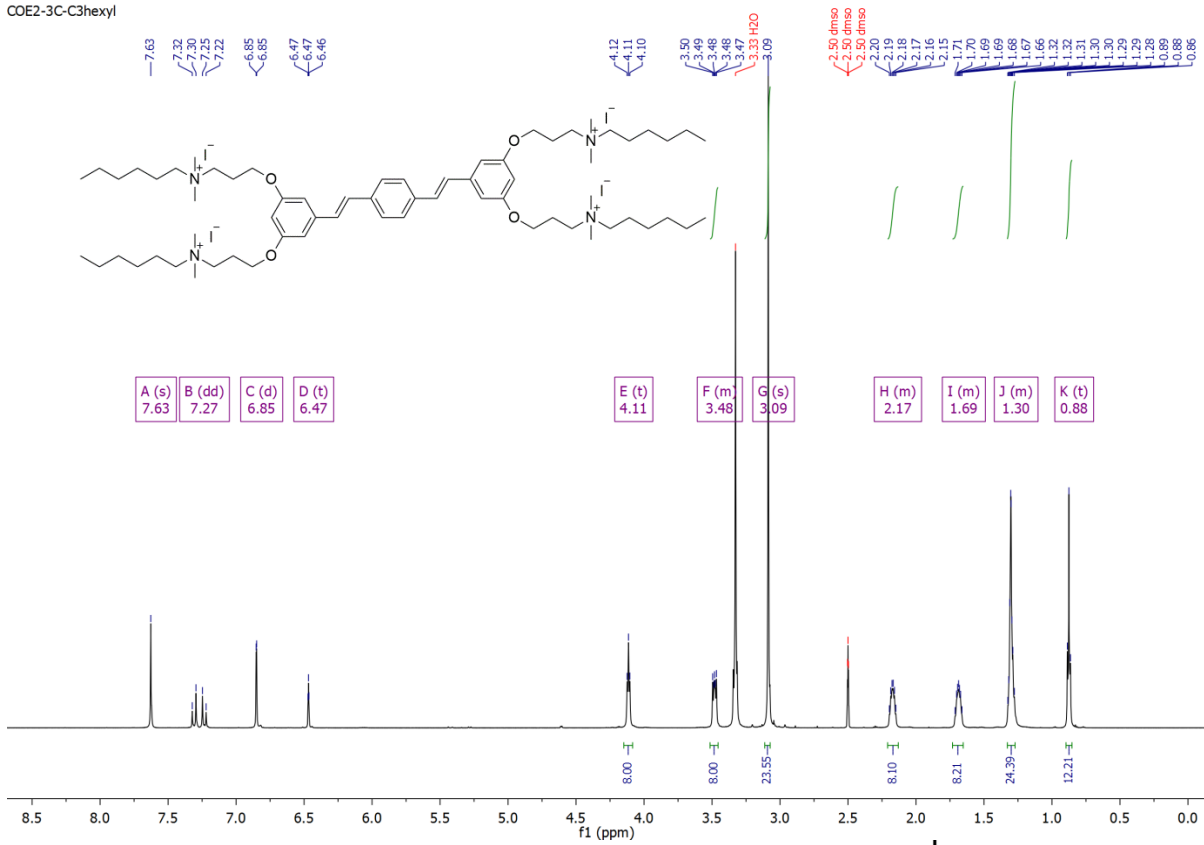
COE2-3C-C3ethyl

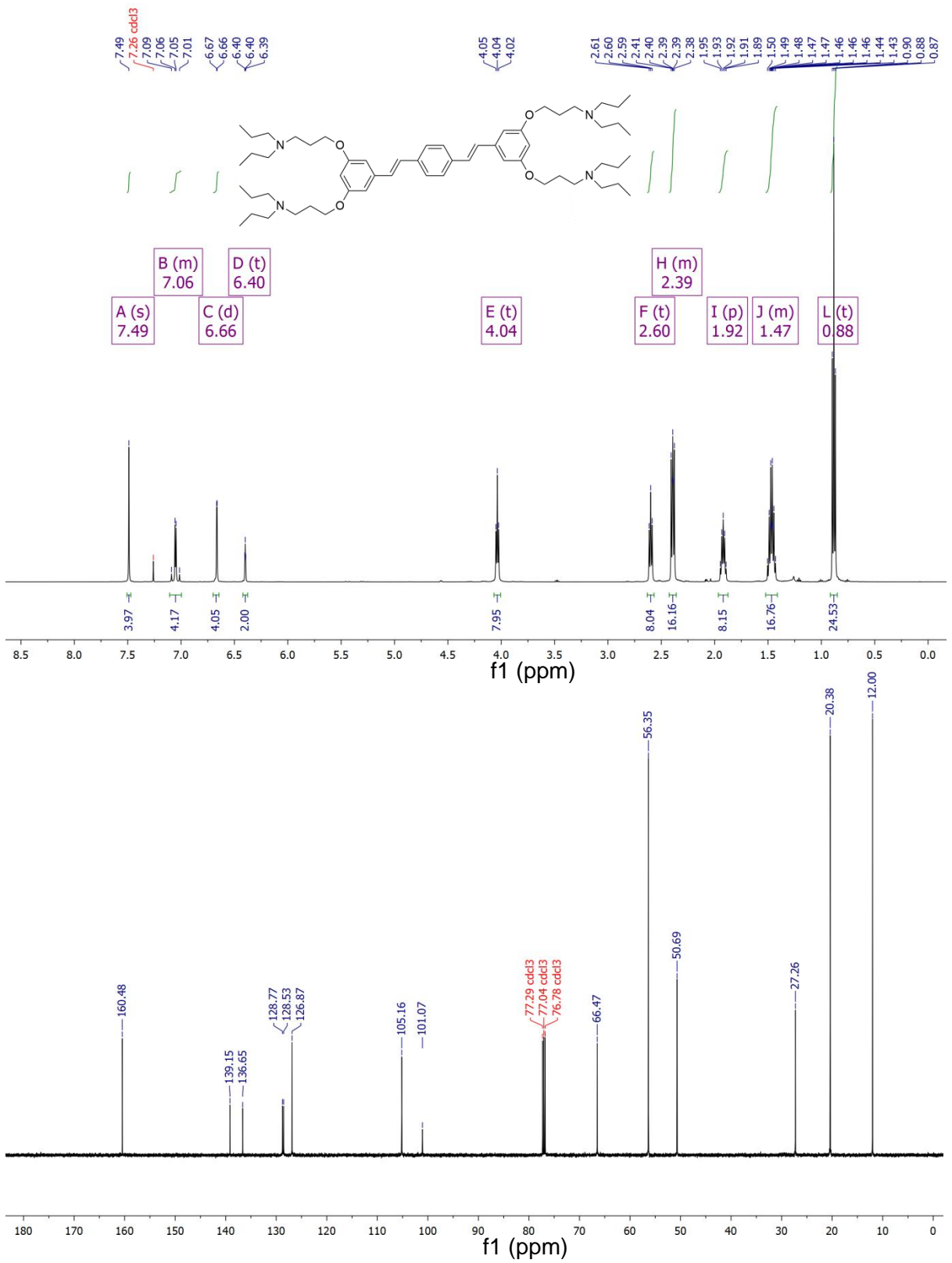


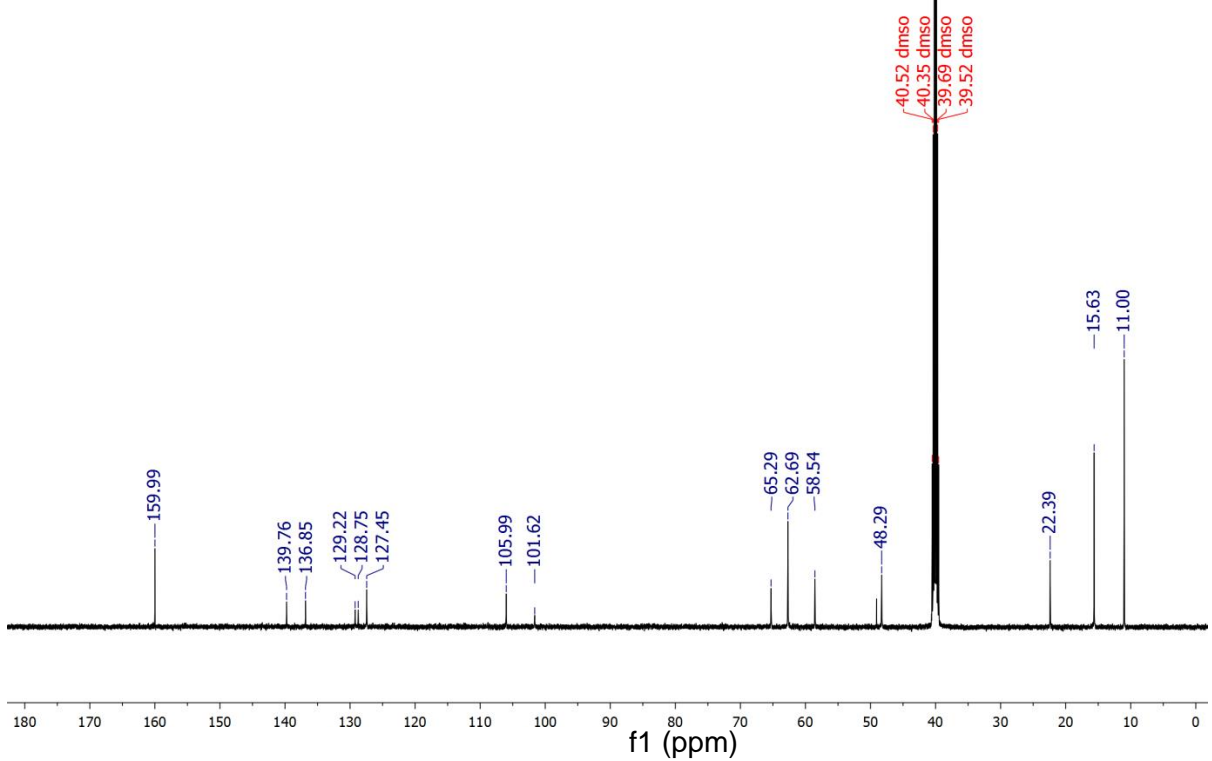
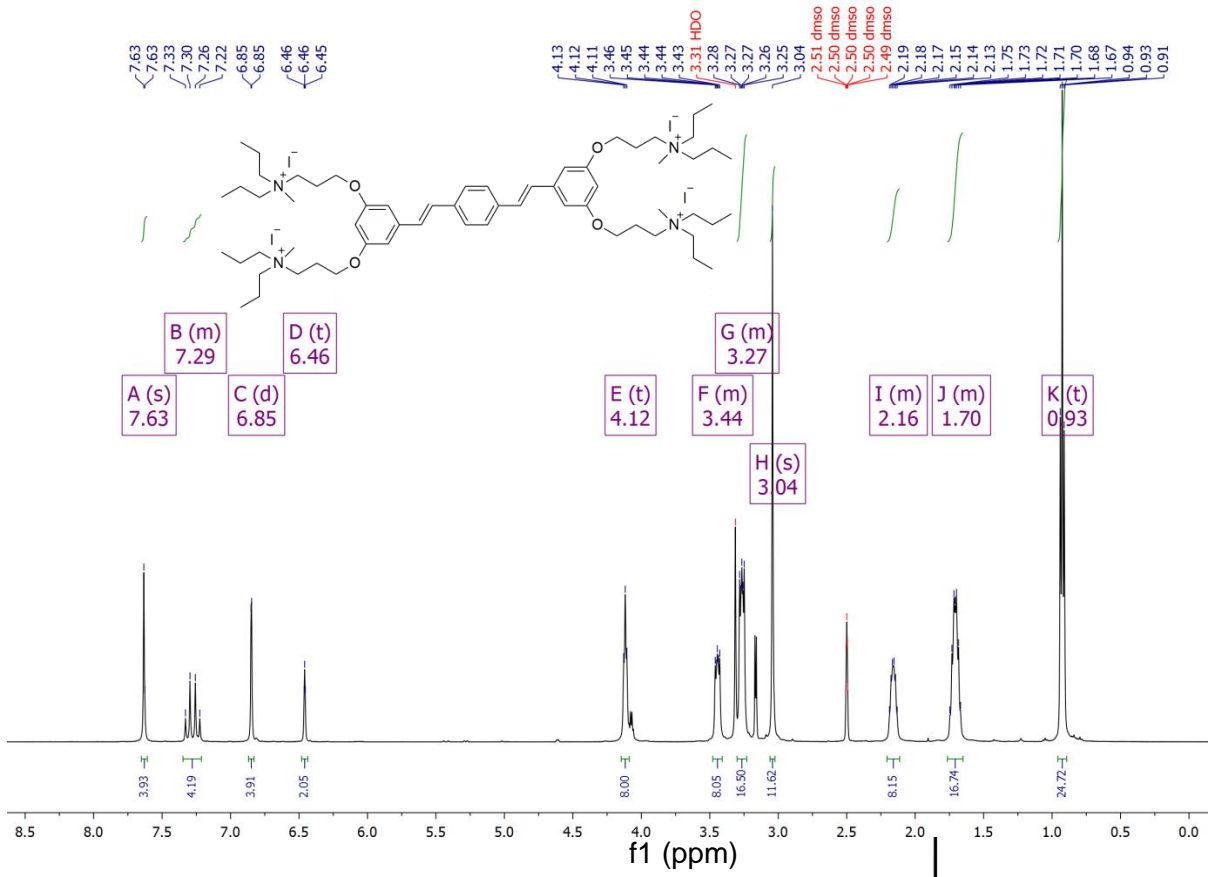
COE2-3C-C3butyl

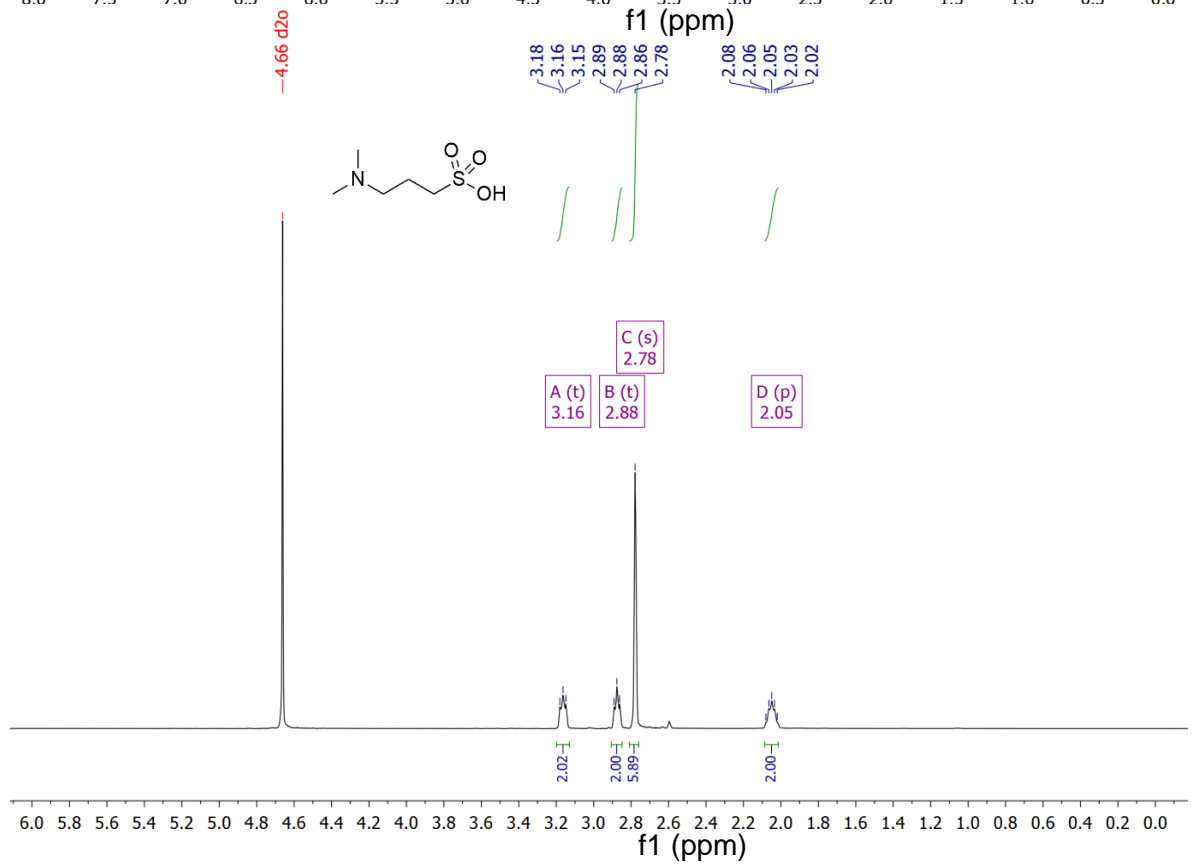
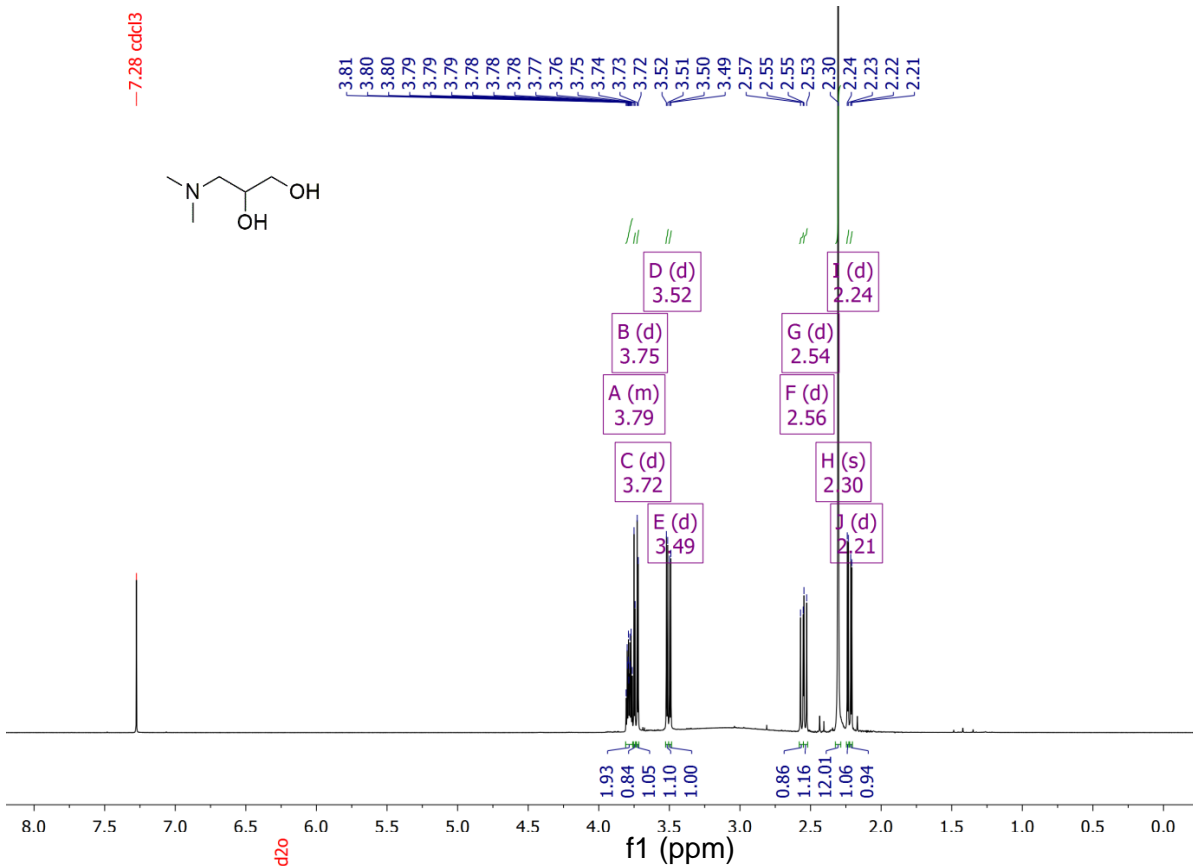


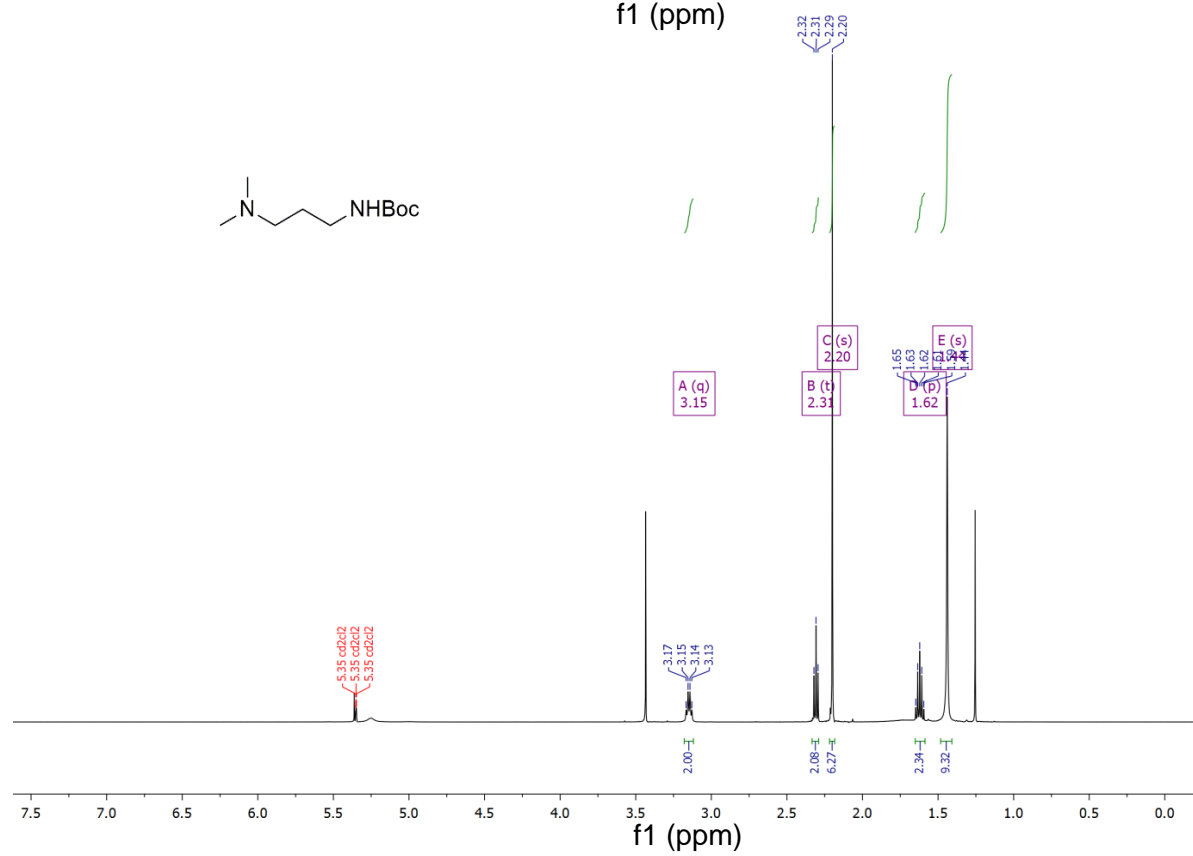
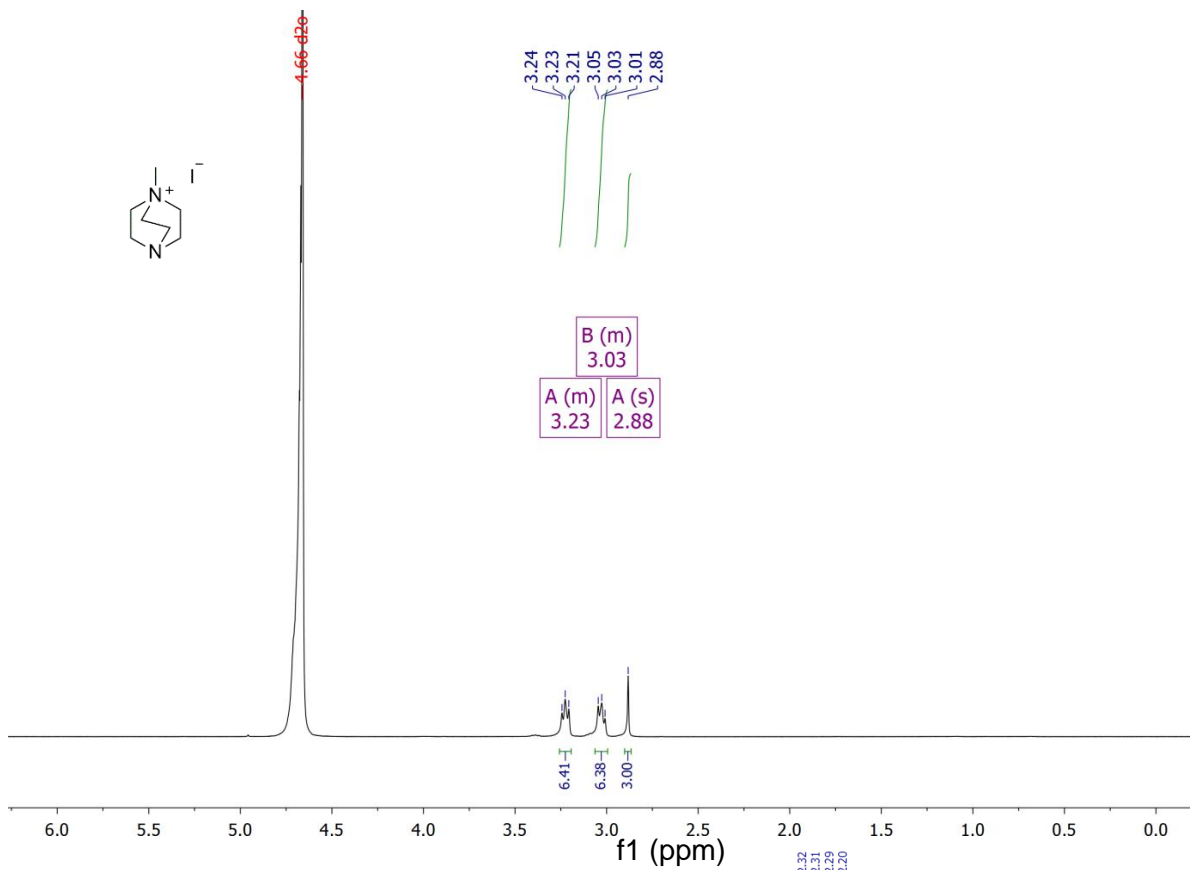
COE2-3C-C3hexyl

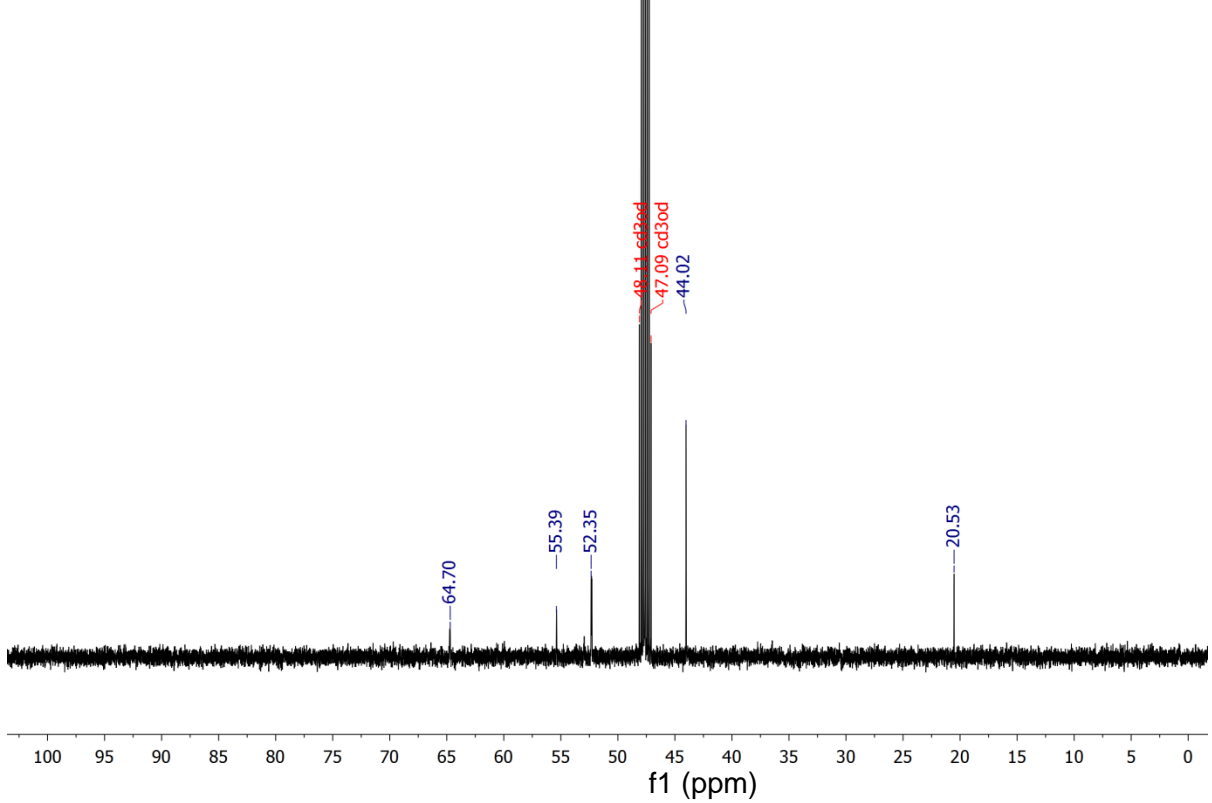
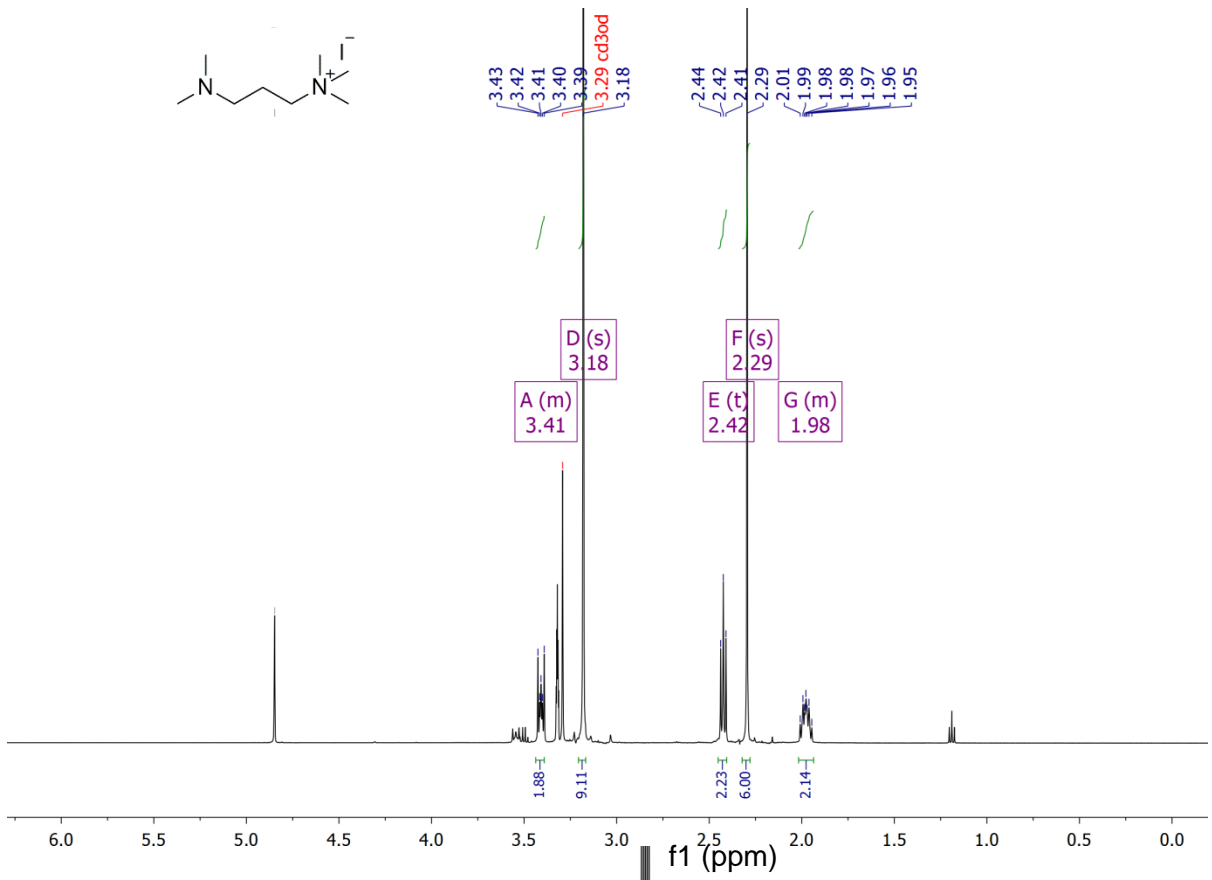
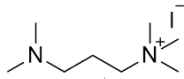




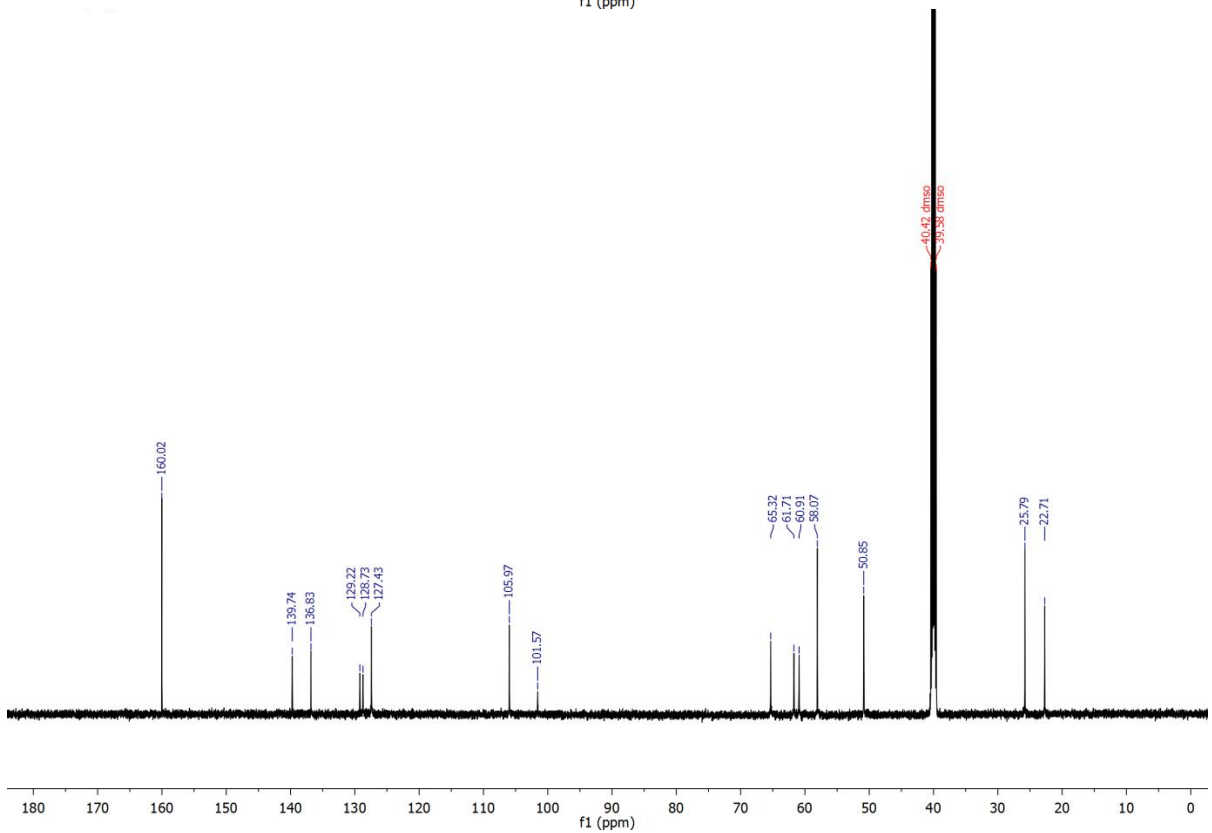
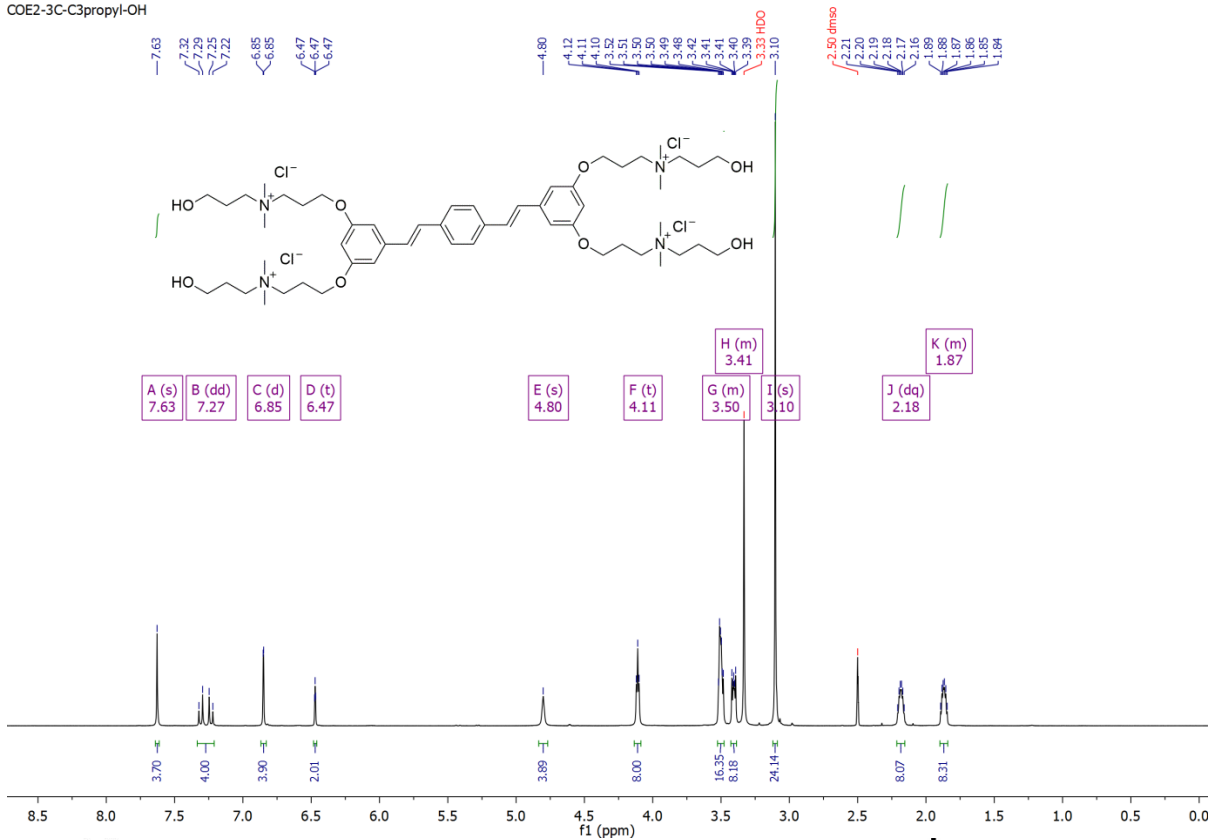




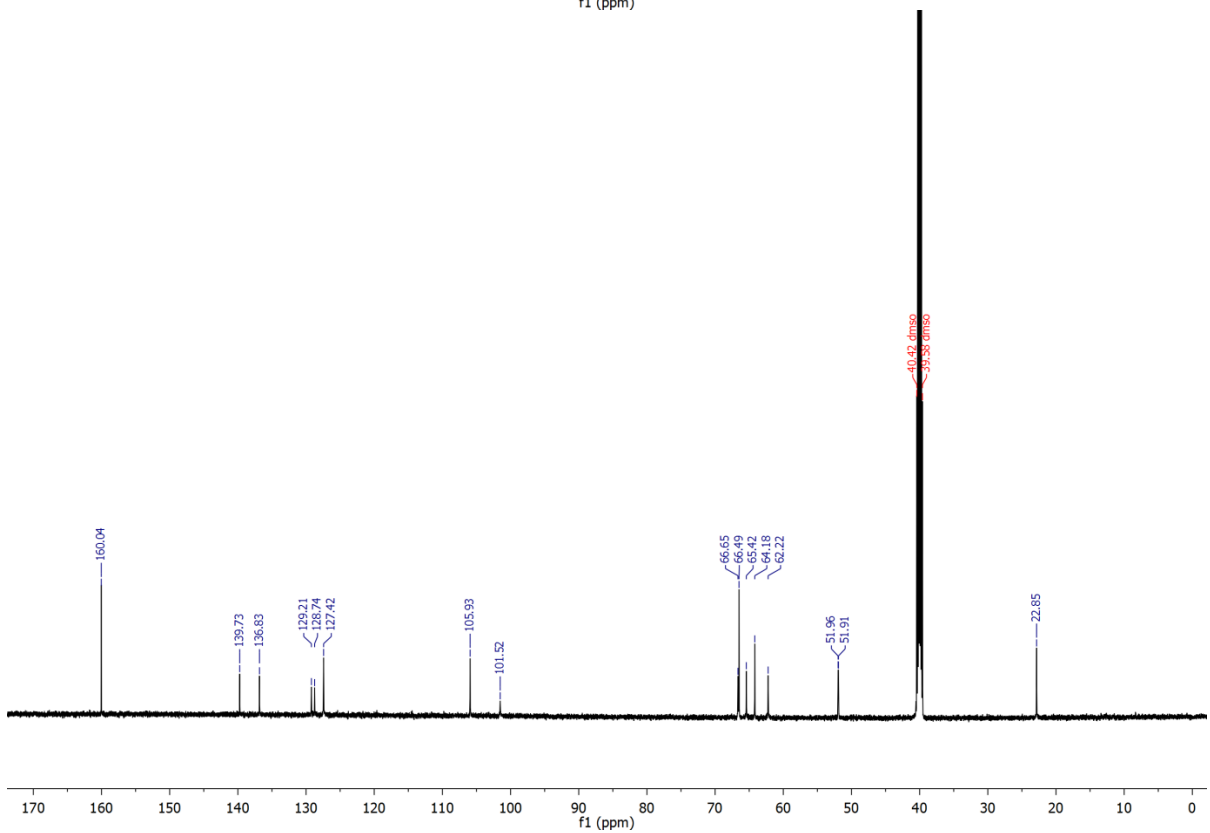
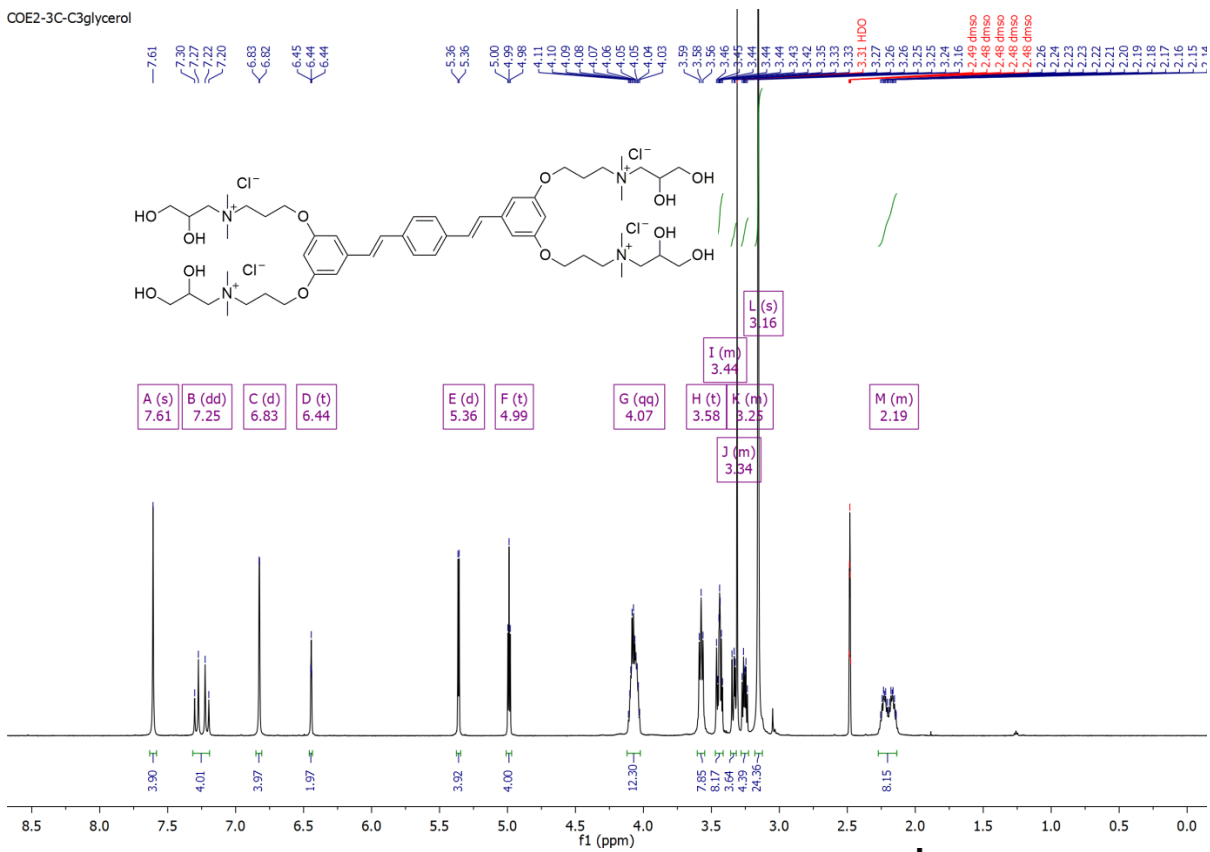




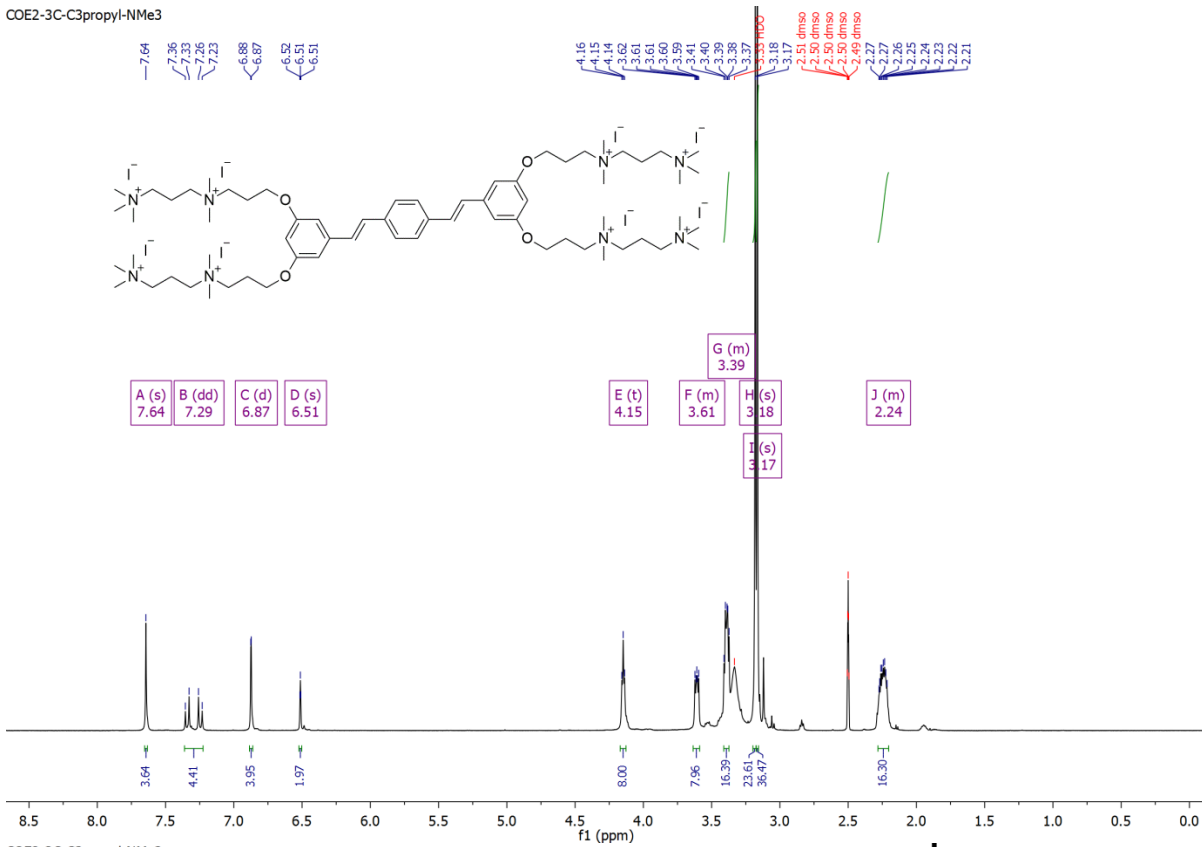
COE2-3C-C3propyl-OH



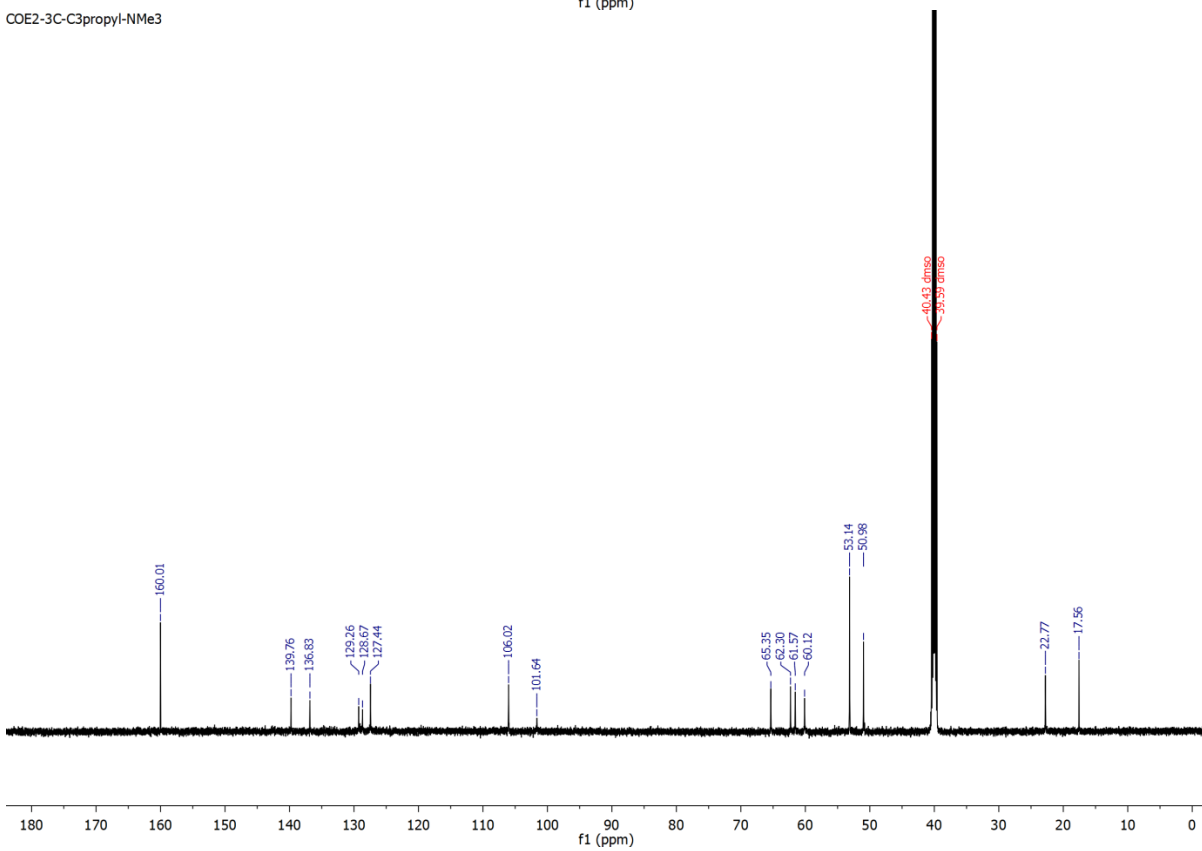
COE2-3C-C3glycerol

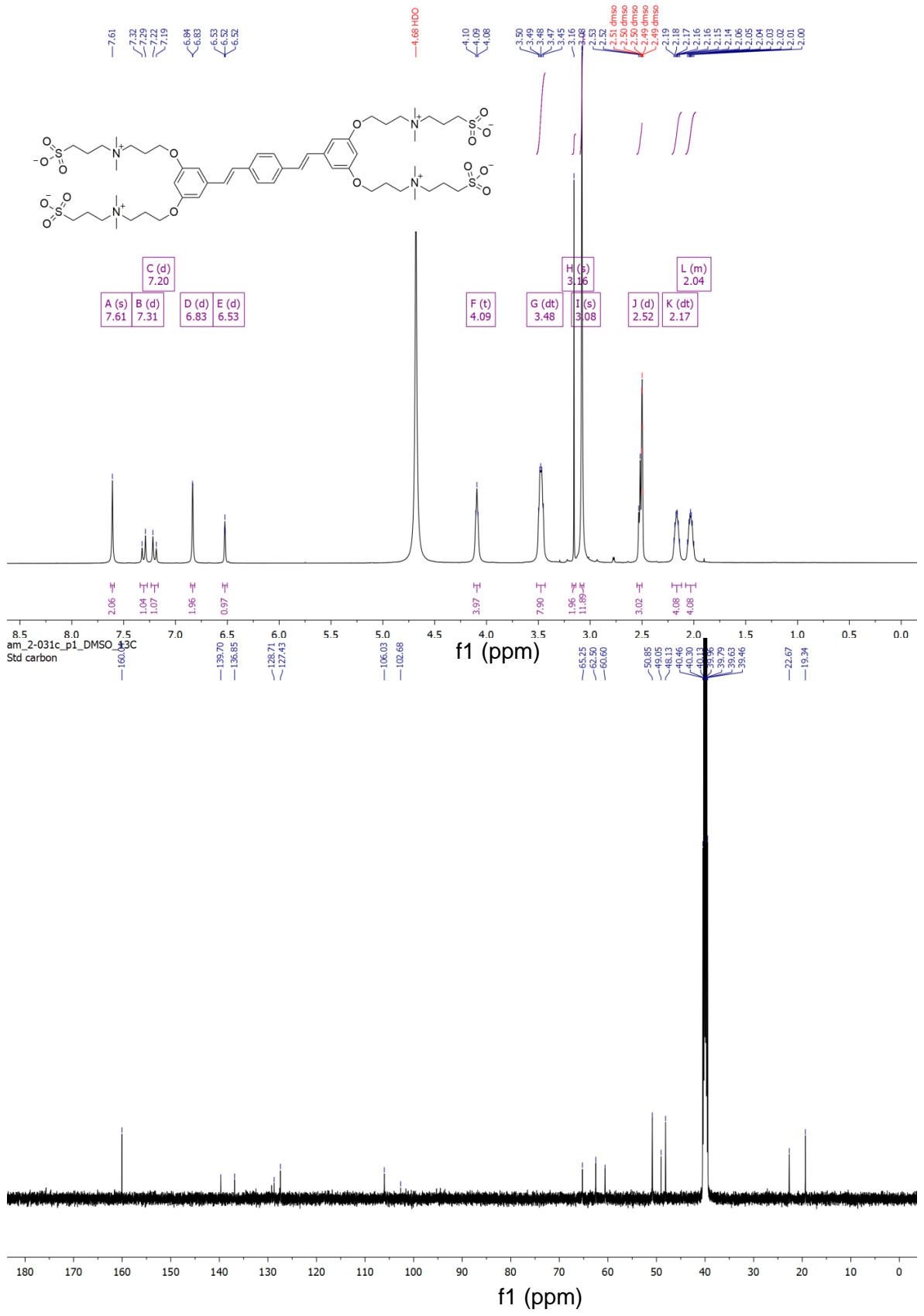


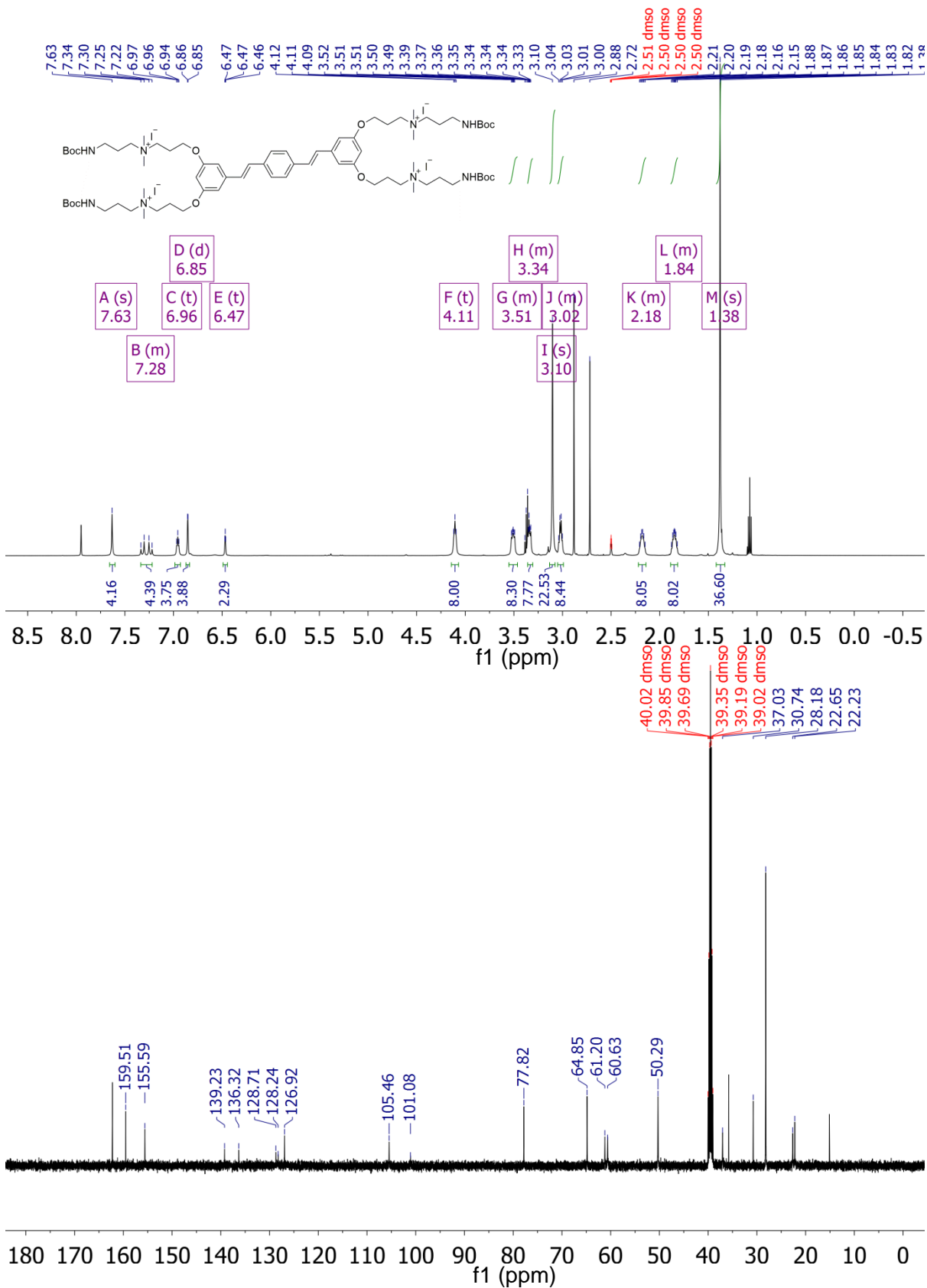
COE2-3C-C3propyl-NMe3



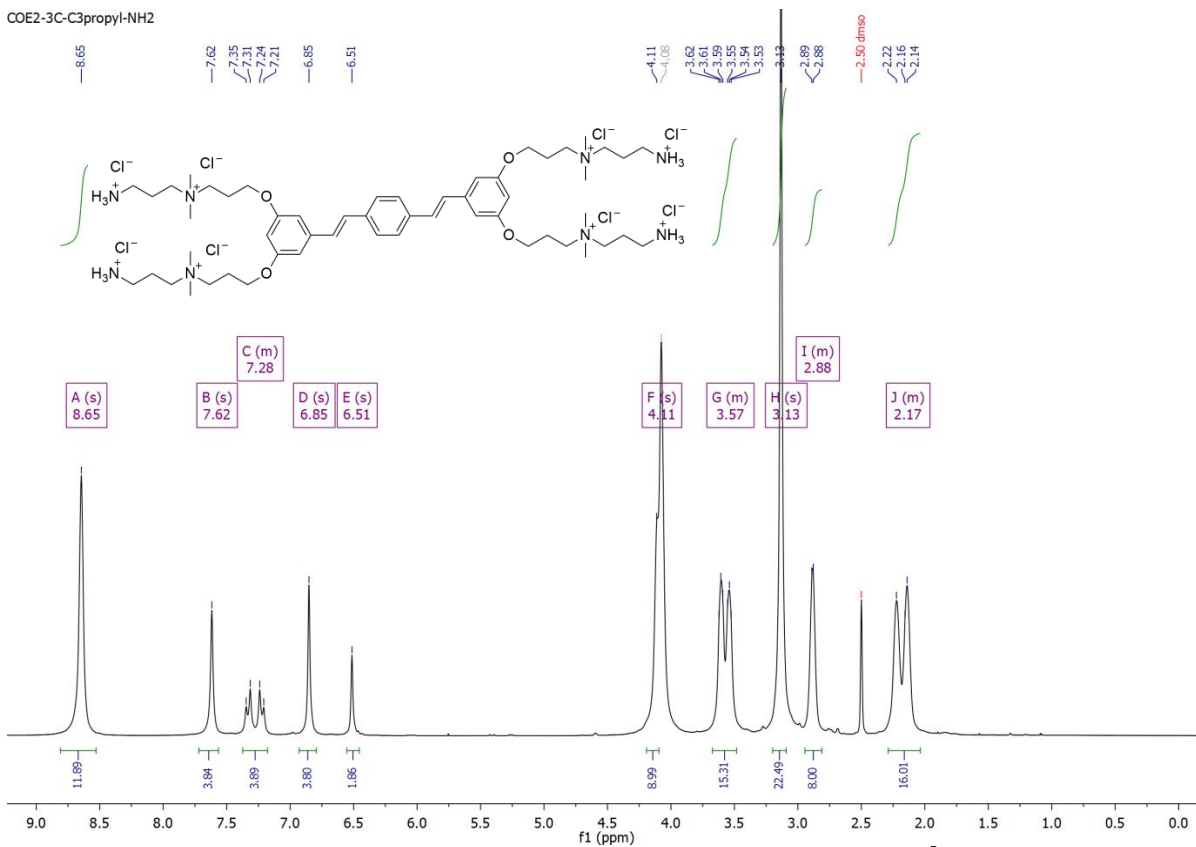
COE2-3C-C3propyl-NMe3







COE2-3C-C3propyl-NH2



COE2-3C-C3propyl-NH2

